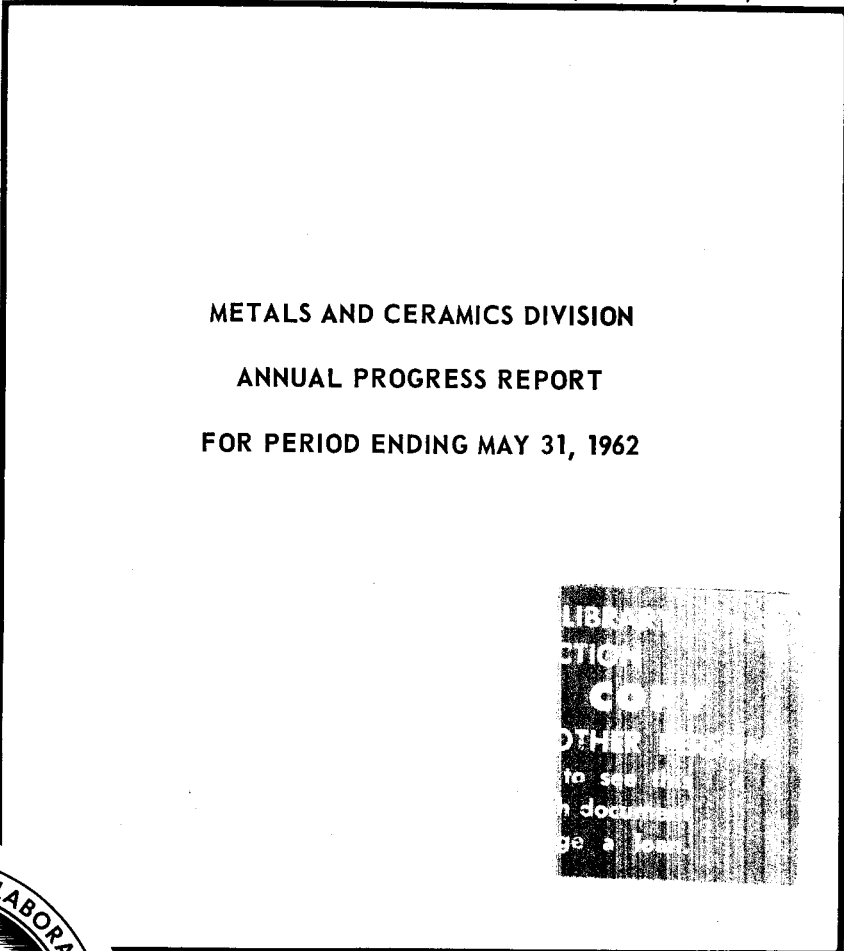


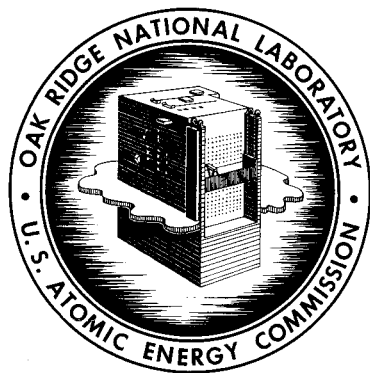
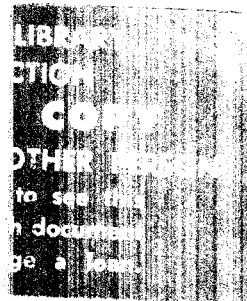


3 4456 0365196 5

ORNL-3313  
UC-25 - Metals, Ceramics, and Materials  
TID-4500 (17th ed., Rev.)



METALS AND CERAMICS DIVISION  
ANNUAL PROGRESS REPORT  
FOR PERIOD ENDING MAY 31, 1962



**OAK RIDGE NATIONAL LABORATORY**  
operated by  
**UNION CARBIDE CORPORATION**  
for the  
**U.S. ATOMIC ENERGY COMMISSION**

Printed in USA. Price \$3.50 Available from the  
Office of Technical Services  
U. S. Department of Commerce  
Washington 25, D. C.

LEGAL NOTICE

This report was prepared as an account of Government sponsored work. Neither the United States, nor the Commission, nor any person acting on behalf of the Commission:

- A. Makes any warranty or representation, express or implied, with respect to the accuracy, completeness, or usefulness of the information contained in this report, or that the use of any information, apparatus, method, or process disclosed in this report may not infringe privately owned rights; or
- B. Assumes any liabilities with respect to the use of, or for damages resulting from the use of any information, apparatus, method, or process disclosed in this report.

As used in the above, "person acting on behalf of the Commission" includes any employee or contractor of the Commission to the extent that such employee or contractor prepares, handles or distributes, or provides access to, any information pursuant to his employment or contract with the Commission.

ORNL-3313

Contract No. W-7405-eng-26

**METALS AND CERAMICS DIVISION ANNUAL PROGRESS REPORT**

for Period Ending May 31, 1962

J. H. Frye, Jr., Director  
J. E. Cunningham, Assistant Director

DATE ISSUED

APR 9 1962

OAK RIDGE NATIONAL LABORATORY  
Oak Ridge, Tennessee  
operated by  
UNION CARBIDE CORPORATION  
for the  
U. S. ATOMIC ENERGY COMMISSION



3 4456 0365196 5



## Summary

### PART I. REACTOR PROJECT ACTIVITIES

#### 1-10. Gas-Cooled Reactor, Molten-Salt Reactor, etc.

In support of the Laboratory's reactor projects and programs, the Metals and Ceramics Division was concerned with a diversity of problems involving the performance of fuel and structural materials in gaseous, aqueous, and molten-salt environments. Particular reactor projects and programs in which the Division exercised broad materials direction were related to the Gas-Cooled Reactor, Molten-Salt Reactor, High-Flux Isotope Reactor, Transuranium Program, Thermoneuclear Project, and Thorium Utilization Program. Programs involving the Division to a lesser extent (primarily fuel element development) include the Advanced Test Reactor, Army Power Reactor, Maritime Reactor, and Enrico Fermi Reactor. The outstanding developments on each project are reviewed.

### PART II. MATERIALS PROPERTIES

#### 11. Corrosion Engineering

Loop and capsule experiments were performed to investigate the nature of reactions occurring between contaminated helium and construction materials used in high-temperature gas-cooled reactors. Exposures of type 304 stainless steel in static helium containing impurities desorbed from graphite produced both iron and chromium oxidation products, the relative proportions depending on the CO:CO<sub>2</sub> ratios of the gas mixtures. Carburization of type 304 stainless steel occurred in all graphite-containing tests when the exposure temperatures were above 815°C. The presence of small quantities of CO<sub>2</sub> in these tests effected

relatively heavy oxidation of low-alloy steels at 593°C.

Compatibility problems arising from the juxtaposition of graphite and type 304 stainless steel surfaces were evaluated as a function of surface temperature and contact pressure. Diffusion couples of these materials became securely bonded during anneals at 650 and 750°C, and partial bonding occurred at anneals as low as 600°C. Carbide precipitation at stainless steel surfaces was evident only below bonded areas. Copper-plating or preoxidation of stainless steel surfaces effectively suppressed carburization and bonding even at relatively high contact loads (10,000 psi).

The corrosion rates of INOR-8 forced-convection systems under prolonged exposures to fluoride salt mixtures were measured as a function of service temperature. Weight losses of corrosion inserts exposed to LiF-BeF<sub>2</sub>-UF<sub>4</sub>-ThF<sub>4</sub> salt mixtures at 700 to 815°C did not increase measurably after 5000 hr and showed a relatively small temperature dependence. However, the nature of attack was noticeably affected by temperature.

Corrosion studies were initiated to evaluate the effects of HF and CF<sub>4</sub> on the attack of INOR-8 by fluoride salt mixtures. Additions of HF to INOR-8 loops containing the mixture NaF-ZrF<sub>4</sub> promoted rapid oxidation of nickel and the precipitation of NiF<sub>2</sub>. Exposure of INOR-8 to CF<sub>4</sub> vapor resulted in little attack up to 800°C; however, type 304 stainless steel, molybdenum, and Inconel specimens were heavily attacked under the same conditions.

#### 12. Fuels Evaluation

Neutron-activation techniques were used to study the fission-product-retention characteristics of graphite elements containing UC<sub>2</sub> particles coated

with pyrolytic carbon. When tested as unsupported particles, three types of coatings – laminar, columnar, and duplex – released on the order of  $10^{-4}\%$  of the  $Xe^{133}$  during postirradiation heating for 24 hr at temperatures below  $1800^{\circ}C$ . Duplicate batches of coated particles that had been fabricated into graphite fuel elements generally had release rates about 100 times higher, presumably as a result of coating rupture during fabrication or uranium migration through the coatings. The xenon-retention characteristics of a few elements were as good as those of the unsupported particles contained therein. These data led to the conclusion that satisfactory fuel elements can be fabricated with careful and proper techniques.

Release rate data on fission products other than xenon indicated rather surprisingly that the metallic species barium, strontium, and silver migrate through the coatings more rapidly than does xenon. Tests then made to confirm the suspicion that uranium might also migrate through the coatings showed that uranium migrates through  $100\text{-}\mu$ -thick laminar coatings in 20 hr at  $1700^{\circ}C$ .

### 13. Materials Compatibility

Selection of container materials compatible with alkali metals at elevated temperatures has been a continuing research program for several years. One area that received attention during the past year was an evaluation of methods for removing impurities from alkali metals.

The use of metals such as zirconium and titanium as getters was found to be the most practical and effective means of reducing the oxygen content. Research was initiated to determine the distribution coefficient of oxygen between potential getter materials and alkali metals.

Oxygen contamination of alkali metals has been observed to increase the corrosion of many container materials. In evaluating the accuracy of the existing analytical techniques for determining oxygen in the alkali metals, none of the analytical methods investigated gave satisfactory results. Therefore a program was initiated to develop a method for determining the oxygen content of potassium.

An investigation of the effect of oxygen concentration of refractory metals on their corrosion resistance to lithium at elevated temperatures

showed the pure metals niobium, tantalum, vanadium, and zirconium to exhibit excellent resistance at temperatures even in excess of  $800^{\circ}C$ . When small quantities of oxygen were added to either niobium or tantalum, lithium penetrated these metals very rapidly over a wide range of temperatures. No attack was observed when vanadium and zirconium were contaminated with oxygen to levels of 2000 and 4000 ppm, respectively.

A sample of grade CGB-X graphite was examined as part of the MSRE evaluation tests. Salt permeation tended to be restricted to a shallow penetration (less than 0.01 in.) below the external surface of the graphite with the salt pressure approximately three times that expected in the MSRE.

Tests on ten grades of graphite having porosities ranging from low to high indicated that a simple mercury-impregnation test at room temperature is suitable for quality control for various grades of graphite and can be related to molten fluoride salt permeation.

Twenty-hour-long purges with the thermal decomposition products of crystals of  $NH_4F \cdot HF$  in the range  $200$  to  $705^{\circ}C$  indicated that oxygen contamination can be removed from moderately permeable grades of graphite. During such purges, a slight reaction will occur between the  $NH_4F \cdot HF$  and INOR-8.

### 14. Mechanical Properties

The experimental work of this group was related to those areas in which significant problems exist in the various reactors under development at the Laboratory. Long-range research included studies of the effects of carburization in  $CO_2$  on the properties of stainless steels, of the effect of a hydrogen environment on creep and fracture of nickel-base alloys, and of means for solving deformation and fracture problems.

The strength and strain-fatigue properties of  $UO_2$ -stainless steel dispersion fuel plate developed for the Enrico Fermi Reactor core B were found to be consistent with what would be expected qualitatively for such a dispersion. The ductility of the plate in the transverse direction, however, was somewhat low.

The creep and tensile properties of the fuel plate and cladding materials for the Advanced

Test Reactor were investigated in the range 400 to 600°F. Aluminum alloys 6061-0 and X8001 in the annealed and cold-worked conditions were investigated.

A thorough evaluation of the properties of the EGCR fuel element under thermal-cycling conditions was completed and was begun for beryllium cladding and for type 304 stainless steel cladding having thicknesses smaller than the 0.020 in. planned for the EGCR. The brittleness of beryllium at low temperatures caused the finned beryllium tubing to fail under thermal cycling. The problems with thin stainless steel cladding are associated with the manner in which the tubes collapse onto the  $UO_2$  under external pressure.

The instantaneous collapse at elevated temperatures of type 304 stainless steel tubes under external pressure and the effects of tube ovality and wall-thickness variation were studied experimentally. The predictions of applied mechanical theories based on the stress-strain characteristics of the material correlated well with the experimental data. The ovality of the tubes was found to affect the critical pressure more significantly than did the variations in wall thickness, as was predicted by theory.

The stress-rupture properties of type 304 stainless steel and an Nb-1% Zr alloy were investigated in the useful temperature range for each material. Analysis of the data for type 304 stainless steel indicated that the stress-rupture properties may be successfully correlated by using the Dorn parameter.

The irradiation effects and mechanical properties of beryllium continued to be investigated. In-pile stress-rupture experiments at 520°C indicated the effect of irradiation on the stress-rupture strength to be small at this temperature. The room-temperature ductility of unirradiated beryllium tubing in the transverse direction was quite low, of the order of 0.2 to 0.3%.

The distribution of carbon in beryllium after exposure to  $CO_2$  was investigated to aid in the interpretation of corrosion phenomena in the material. With a  $C^{14}$  tracer technique, the carbon appeared to be concentrated in the surface reaction layer at temperatures between 600 and 800°C.

Study of the carburization of Fe-Ni-Cr alloys and type 304 stainless steel in  $CO_2$  and its effects on the mechanical properties was continued. The chromium content of the alloys

appears to be a major factor in determining the magnitude of carburization that occurs. The initial condition of the steel was found to be a significant factor in the effects of carburization on the strength and ductility. Cold working prior to carburization produces greater effects than those noted in annealed material.

The effect of a hydrogen environment on the creep and rupture properties of nickel-base alloys was investigated in detail. Several possible mechanisms of the observed weakening of these alloys at elevated temperatures in hydrogen were studied and some found to be unimportant to the effects observed.

In an internal-friction study of the aging reactions involving oxygen and nitrogen in Nb-1% Zr alloys, clustering of oxygen near zirconium atoms prevailed even at annealing temperatures as high as 1925°C and both oxygen and nitrogen precipitated at the aging temperatures.

An experimental technique was devised for evaluating the creep and stress-rupture properties of metallurgically stable alloys by use of a steadily increasing stress to fracture the material. The theoretical basis for correlating the results of such experiments with standard creep and stress-rupture tests was worked out, and experiments on types 304 and 309 stainless steels and Zircaloy-2 were performed. The correlation was good for the stress-rupture results for the stainless steels but not very satisfactory for the creep data. Interesting results were observed for Zircaloy-2 in that the strain-aging phenomenon in the alloy could be precisely evaluated at temperatures around 500°C.

Some deformation characteristics of Zircaloy-2 tubing at elevated temperatures under biaxial stress states were studied experimentally and related to analytical models developed for isotropic materials.

## 15. Nondestructive Test Development

Considerable effort was spent in developing new and adequate techniques for the various testing problems posed by nuclear technology, including studies on the use of ultrasonics, electromagnetics, and penetrating radiation.

Most of the ultrasonic development work involved behavior in thin sections so that this technique could be applied to the detection of nonbonding in

cladding structures. Through-transmission techniques were used for detection of nonbonding in flat fuel plates containing cores of  $\text{UO}_2$ -stainless steel dispersions, uranium-aluminum alloys, and  $\text{UO}_2$  or  $\text{U}_3\text{O}_8$ -aluminum dispersions. Local inhomogeneities were the limiting factors on sensitivity. New and versatile scanning equipment was designed and fabricated for fuel plate inspection development. Lamb-wave and ringing ultrasonic techniques were developed for the evaluation of brazed joints.

Electromagnetic or eddy-current studies included the development of prototype instrumentation and techniques for dual-coil, phase-sensitive measurements of thickness in restricted areas. This new system represents a marked improvement since it is relatively insensitive to coil-to-specimen spacing. Continued studies for the development of eddy-current techniques for space gaging included design of probes for a number of reactor fuel cores and extensive experimental studies to provide design criteria relative to coil size and shape and operating frequency. New probes were designed for the measurement of interrod spacing and tubing inner diameter.

Studies on low-voltage radiography were made on aluminum and steel of all applicable thicknesses and on beryllium up to 2.0 in. thick. A number of charts of exposure techniques, attainable sensitivities, and equivalence factors were prepared as aids to optimum radiography. The low-voltage system was applied to elementary micro-radiography on coated fuel particles, with viewing up to 500X being made of the finished high-resolution radiographic plates. Excellent detail was observed on many structural variables of the particles and coatings. Development of techniques for the evaluation of fuel homogeneity in rods and plates was begun. For fuel rods  $\text{Co}^{60}$  gamma rays are passed through the rod, and variations in fuel loading are detected as changes in transmitted beam intensity impinging upon a  $\text{NaI}(\text{TI})$  detector. For fuel plates a lower-energy x-ray machine is used as the radiation source. The purpose of this research is to develop appropriate standards and scanning techniques, so that fuel homogeneity can be monitored and recorded quantitatively.

Most of the development of nondestructive tests for the evaluation of problem materials was directed toward molybdenum and finned-beryllium tubing. The most useful techniques developed for

the finned-beryllium tubing involved low-voltage radiography, bobbin-coil eddy currents, and penetrants; those for molybdenum tubing involved penetrants, ultrasonics, and eddy currents.

Further remote ultrasonic measurements were made with modified mechanical fixtures on the core-vessel wall thickness of the HRT. Another important phase of remote inspection studies was the beginning of technique development for radiography in a radioactive background.

## 16. Physical Metallurgy

The two general problem areas of alloy stability and surface reactions were studied as related to the Gas-Cooled Reactor, the Enrico Fermi Reactor, the Fast Burst Reactor, and the Molten-Salt Reactor and the development of materials for high-temperature use.

The aging reaction, previously discovered in the Nb-1% Zr alloy, was found to be caused by the reduction in oxygen solubility in niobium when zirconium is added. The excess oxygen appears as precipitated  $\text{ZrO}_2$ . It was possible to predict the aging tendencies of a number of different heats of such an alloy based on the oxygen content and the solution annealing temperature. With this knowledge the alloy can be utilized for high-temperature use with more confidence.

Alloys based upon the Nb-V system are also under study for high-temperature applications. They possess superior yield and tensile strength over the Nb-1% Zr alloy up to 1090°C and in addition offer a more favorable density. A hot-hardness test was developed as a means of rapidly evaluating binary alloys in this system. This test proved to correlate very well with conventional tensile tests. The maximum tensile strength was found to occur between 30 and 50% V. Data from slow-bend tests, which were used as a substitute for creep tests, indicated the creep strength of the Nb-V system to be inferior to that of the Nb-1% Zr alloy at 1200°C.

It became desirable to determine more exactly the melting range of commercially produced INOR-8 as part of the study of factors leading to fissuring of weldments. The solidus temperatures were established as being between 2435 and 2480°F, and the liquidus temperatures between 2552 and 2559°F. Since the solidus temperatures range from 80 to 180°F above the corresponding nil-ductility

temperatures, it is doubtful that a liquid phase is responsible for the fissuring.

The creep resistance and thermal stability of U-Mo alloys containing 10 to 15 wt % Mo increased with the molybdenum content, but at the expense of increased notch sensitivity at low temperatures. A hydrogen absorption technique was developed which permits the transformation kinetics of the reaction  $\gamma \rightarrow \gamma' (U_2Mo) + \alpha$  (uranium) to be quantitatively determined.

The surface reactions of metals with their service environment are an important area of study. The behavior of structural alloys in high vacuum and with inert gases containing partial pressures of active gases is under investigation.

The evaporation characteristics of types 316, 304, and 446 stainless steels, INOR-8, Inconel, and Haynes alloy No. 25 were determined at 871 and 982°C at pressures of  $5 \times 10^{-7}$  torr. The alloying elements selectively evaporate in proportions that appear to be dependent upon the vapor pressure and the concentration of the elements. For example, it was determined that the evaporation rates increased with increasing chromium content of the alloy.

Studies of the reactions between type 304 stainless steel with CO and CO<sub>2</sub> were continued as part of the fuel element development program of the EGCR. From a study of numerous variables it was established that undesirable oxidation reactions could be avoided by atmospheres high in carbon monoxide content. These atmospheres promoted the formation of spinels and Cr<sub>2</sub>O<sub>3</sub> at rates dependent upon the  $P_{CO_2}/P_{CO}$  ratio and the temperature. Although increases in the proportion of carbon monoxide increased the extent of carburization up to a  $(P_{CO})^2/P_{CO_2}$  value of 0.227, further increases in this ratio thereafter resulted in less carburization. This effect was attributed to the presence of Cr<sub>2</sub>O<sub>3</sub> at the metal surface, which served as a barrier for carbon diffusion.

The oxidation resistance of types 316, 446, and 310 stainless steels, Haynes alloy No. 25, Inconel, and INOR-8 was determined at 927, 982, and 1038°C. The oxidation rates were lower for the nickel-base metals even though they contained less chromium than the other alloys did.

Attempts to clad niobium tubing with type 304 stainless steel to prevent contamination were partially successful when silver was used as an intermediate layer. Bond separation occurred at

the silver-type 304 stainless steel interface when the tubing was mechanically deformed subsequent to thermal cycling. Nickel coatings on a U-10 wt % Mo alloy for oxidation resistance were judged to be unreliable because the coated alloy exhibited an inconsistent and unpredictable oxidation behavior.

Gaseous contamination of niobium and its alloys between 850 and 1200°C was observed at pressures as low as  $3 \times 10^{-6}$  torr. With air as the impurity gas, niobium is contaminated with both oxygen and nitrogen in the proportions 100:1 even though the impurity gases are in the ratio 1:4. Since the permissible gas impurity levels in contact with the heated metal for extended exposure times were estimated to be in the range  $1 \times 10^{-7}$  torr, it was concluded that high-temperature tests should be conducted in vacua rather than in purified inert gases.

Preliminary results indicated that the oxidation characteristics of a Be-0.5 wt % Ba alloy in CO<sub>2</sub> depend upon the CO<sub>2</sub> pressure. This behavior is unlike that of unalloyed beryllium. However, the oxidation resistance was inferior to that of the unalloyed metal. Additional preliminary data showed that thin-walled molybdenum tubing can be made and that this metal is tolerant of high proportions of water vapor.

### PART III. METAL AND CERAMIC FABRICATION

#### 17. Ceramics Laboratory

Experimental studies were performed in the following general areas: (1) BeO and fueled BeO, (2) graphite and fueled graphite, (3) bulk UO<sub>2</sub> and ThO<sub>2</sub>, (4) thermal conductivity studies, and (5) Eu<sub>2</sub>O<sub>3</sub> and Sc<sub>2</sub>O<sub>3</sub>.

1. Techniques were developed for preparing approximately 900 cold-pressed and sintered BeO specimens for use in irradiation tests designed to systematically study the effects of grain size (approximately 20 to 70  $\mu$ ), density (90 to 97% of theoretical), pore structure, thermal stress, and temperature (approximately 100 to 1000°C) on the behavior of this material at high fast-neutron doses. The techniques were so designed that sintering to final dimensions was carried out at 1750°C in H<sub>2</sub> for all types of specimens. Techniques also were developed for preparing fueled BeO specimens of controlled density and microstructure; spheroidal UO<sub>2</sub> particles were prepared

by a method which promotes uniform densification during sintering. Phase studies using the porous collector technique showed that in the BeO-MgO-ZrO<sub>2</sub> system the eutectic temperature is 1720 ± 10°C and extensive solid solubility exists in the ZrO<sub>2</sub>-rich region of this system and that a eutectic reaction occurs at 2080 ± 10°C in the MgO-ZrO<sub>2</sub> system at a composition of 35 ± 2 mole % ZrO<sub>2</sub>. Studies in the O-U system showed that the weight loss of UO<sub>2+x</sub> at temperatures greater than 1200 to 1300°C is quantitatively consistent with the loss either of O<sub>2</sub> and UO<sub>3</sub> or of UO<sub>4</sub> as volatile species; pressure-temperature relationships for equilibrium between U<sub>3</sub>O<sub>8-y</sub> and UO<sub>2+x</sub> were determined.

2. Fueled graphite work was concerned primarily with the systems and configurations of interest to the Pebble-Bed Reactor Experiment. A variety of techniques were investigated for fabricating graphite spheres containing pyrolytic-carbon-coated fuel-carbide particles; a method involving pseudo-hydrostatic loading at room temperature was shown to hold major promise for this application. Evaluation of coated particle materials was continued on an expanded basis with emphasis on the correlation of measurable properties with performance during irradiation.

3. Approximately 1300 UO<sub>2</sub> specimens of various sizes, shapes, and grain sizes were prepared by cold pressing and sintering for use in irradiation tests, and methods were developed for activating nonsinterable, highly enriched UO<sub>2</sub> powders so as to increase the sintered bulk density from 66 to 95% of theoretical. Methods for optimizing particle properties, particle-size distributions, and fabrication variables were investigated for vibratorily compacted rods containing oxide fuels prepared both by arc fusing and by the sol-gel process. Uniform bulk densities of 89 to 91% of theoretical were achieved. The effect of measurable physical properties of pressed and sintered ThO<sub>2</sub> pellets on attrition resistance was investigated; it was shown that variations of bulk density per se in the range 92 to 97% of theoretical were not so significant as sintering time and therefore grain size.

4. The thermal conductivity of sintered UO<sub>2</sub> specimens was determined to a precision of ±1% between 27 and 875°C by the radial heat flow technique. A significant increase in the conductivity was observed at temperatures below 600°C after the material had been heated to 875°C;

this effect was attributed to a slight loss of oxygen during exposure of the specimens to the higher temperatures.

5. The swelling of certain Eu<sub>2</sub>O<sub>3</sub> compacts at 1350°C was eliminated by vacuum heat treatment of the Eu<sub>2</sub>O<sub>3</sub> powders at this temperature prior to compacting. The effect appears to be associated with the presence of a hydroxycarbonate phase in those compacts which exhibit swelling. The sintering characteristics of Sc<sub>2</sub>O<sub>3</sub> and the compatibility of this oxide with 13 other oxides were determined. The results were similar to those previously reported for Y<sub>2</sub>O<sub>3</sub>.

## 18. Metal Forming and Casting

The development of materials for potential application to low-temperature reactors (60 to 180°F), medium-temperature reactors (400 to 1100°F), and high-temperature systems (>1100°F) continued.

In the low-temperature reactor field, postirradiation examinations of high-investment aluminum-base fuels were completed. The excellent radiation performance of U<sub>3</sub>O<sub>8</sub> dispersions was revealed by the absence of swelling in miniature samples irradiated at 200°F to U<sup>235</sup> fission burnups of 77 at. %. The examination of a 19-plate prototype element containing 63 wt % U<sub>3</sub>O<sub>8</sub>-aluminum dispersions, which was irradiated in the lattice of the ORR to an average U<sup>235</sup> fission burnup of 41 at. %, further substantiated the excellent radiation stability of this system. Fuel plates from this element resisted swelling and blistering in postirradiation heat-treatment tests extended over the range 400 to 1000°F. X-ray diffraction studies on the dispersion fuels indicated that the U<sub>3</sub>O<sub>8</sub> particles had become amorphous under irradiation. A disordered form of UAl<sub>3</sub> was identified as one of the reaction products in the irradiated U<sub>3</sub>O<sub>8</sub>-bearing dispersion fuels. Similar studies on the 48 wt % U-3 wt % Si-Al alloy fuels showed a conversion of the ordered silicon-modified UAl<sub>3</sub> structure to a disordered UAl<sub>3</sub> formation in these samples as a result of irradiation.

The development of high-strength corrosion-resistant aluminum-base fuel plates for application in high-neutron flux reactors, such as the High-Flux Isotope Reactor (HFIR) and the Advanced Test Reactor (ATR), continued. The blistering initially associated with fabrication of the type 6061 aluminum-clad fuel plates for the HFIR was

drastically reduced by plate processing modifications. The feasibility of manufacturing the complex HFIR fuel units to close dimensional tolerances was further demonstrated by assembling both inner and outer annulus units. The close dimensional tolerances required in these assemblies dictate rigid control of the reproducibility of the involute curvatures in the formed plates. Although considerable progress was made in forming, the yield of reproducibly formed fuel plates is presently unsatisfactory.

The development of the more corrosion-resistant type X8001 aluminum-clad fuel plates for the ATR has provided a unique opportunity for investigating fabrication variables due to the long length and width range required in the fuel plates. Cross rolling and tandem core billet designs were used to develop procedures for fabricating to the required dimensional tolerances 19 fuel plates consisting of type X8001 aluminum cladding on a  $U_3O_8$  dispersion core. The technical feasibility of mechanically joining the fuel plates into the required fuel element design was demonstrated. Difficulty was encountered, however, in forming the fuel plates to meet the dimensional specifications of the water channel spacings in the assembled element.

Fabrication studies were continued on swaged  $UO_2$ -stainless steel fuel rods. To demonstrate the irradiation stability of such rods, 18 rods containing fused and ground  $UO_2$  were satisfactorily fabricated to manufacture an element for irradiation testing. The feasibility of fabricating Enrico Fermi type III spherical  $UO_2$ -stainless steel fuel plates with integral spacers was demonstrated. Fuel plates were fabricated with sufficient cladding thickness on one side to permit machining of the integral spacers. Difficulties encountered in maintaining plate flatness during fabrication were overcome by machining the spacers and subsequently annealing.

In the development of stainless steel-clad plate-type neutron absorbers, the postirradiation examination of 20, 30, and 40 wt %  $Eu_2O_3$  dispersions in elemental stainless steel continued to show good irradiation stability at neutron exposures up to  $2.9 \times 10^{21}$  nvt. Studies were continued on the boron-gradient concept and on advancing the fabrication technology. The feasibility of manufacturing an absorber which utilizes both the good irradiation behavior of  $Eu_2O_3$  and the economical advantages of boron

was demonstrated by fabricating plates with 37 wt %  $Eu_2O_3$ -elemental stainless steel tips and boron-gradient follower sections.

In the high-temperature materials field, Nb-V-base alloys with closely controlled compositions were satisfactorily melted by an argon atmosphere, tungsten-electrode, arc-melting process. Fabrication studies showed that the Nb-V alloys in the cast condition can be heavily cold-rolled without fracture. Investigations of zone melting in an electron-beam furnace demonstrated the feasibility of producing large, single crystals of niobium and possibly other refractory metals.

## 19. Powder Metallurgy

A volatile (removable) sintering-temperature depressant was used to fabricate an essentially all-uranium carbide fuel at temperatures as low as  $1300^\circ C$ , which is 600 degrees lower than the temperature required for sintering straight uranium monocarbide. With stoichiometric or slightly hyperstoichiometric UC and  $UAl_2$  in amounts of 5 to 10 wt % used as the sintering aid, monocarbide bodies of around 93% of theoretical density were achieved.

Preliminary results of hot-hardness tests indicated substantial dispersion hardening in hot-pressed and extruded compacts of Th-10 vol %  $AlO(OH)$ , Th-10 vol %  $ZrO_2$ , and thorium with  $ThO_2$  introduced by milling. Compatibility studies between thorium and fissile particles of  $UO_2$ , UC, and  $UC_2$  indicated the need for reaction barriers. Pyrolytic-carbon-coated UC and  $UC_2$  were the most resistant of the coated particles examined, giving protection to  $1100^\circ C$ .

Dense high-quality beryllide fuels having potential for breeder reactors were fabricated by both the hot-pressing method and the cold-pressing and sintering method. Preliminary dissolution tests in standard 4 M  $HNO_3$  showed that  $ThBe_{13}$ ,  $UBe_{13}$ , and  $(Th_9U_1)Be_{13}$  dissolve readily. Oxidation tests showed  $ThBe_{13}$  to have good oxidation resistance at  $700^\circ C$ .

Experimental studies showed that the duplex core required for the HFIR inner-annulus fuel plate can be produced in a single cold-pressing operation, greatly simplifying and reducing costs of fabrication. With this innovation, the serious blistering problem associated with the former hot-forging steps is eliminated. Special procedures

were evolved for cold pressing ATR fuel cores to extremely close thickness tolerances ( $\pm 0.0015$  in.), thereby mollifying the task of rolling plates to rigid straightness requirements.

In developing the target component of the HFIR, a blending procedure involving a rod-milling action was shown to be effective in mixing 10 to 25 vol % actinide oxide in aluminum. A technique was developed for pressing target pellets without spreading contamination. The actinide oxide-aluminum mix was completely enclosed in a primary aluminum containment, and the pellets then clad in a finned tube. Studies of the physical and mechanical properties of the target pellet and an evaluation of the adaptability of the fabrication sequence to remote operation are in progress.

## 20. Remote Fabrication Development

The efforts of the Remote Fabrication Group were directed toward designing and developing equipment and facilities for remotely fabricating reactor core components containing thorium,  $U^{233}$ ,  $Pu^{242}$ , or the transuranic elements. Criteria were established for the proposed Thorium Fuel Cycle Development Facility (TFCDF), which will be used for investigating the complete Th- $U^{233}$  fuel cycle. Fuel elements up to 12 ft in length can be disassembled, chemically processed, reconstituted, refabricated, and inspected in the proposed facility.

A Th- $U^{233}$  fuel rod facility is being built for use in extending fuel cycle technology through the development of techniques and equipment for the remote fabrication of Zircaloy-2-clad fuel rods containing Th-3 wt %  $U^{233}$  oxide. These elements will be used for critical experiments at the Brookhaven National Laboratory. Equipment is being provided for the following remote operations: comminution, screening, weighing, blending, and vibratory compaction of oxide powder and end capping, cleaning, and inspection of fuel rods. Construction of the facility structure is 20% complete, design of process equipment is 80% complete, and equipment fabrication and procurement are 30% complete.

Two lines of equipment for fabrication and inspection of target elements for the High-Flux Isotope Reactor (HFIR) are being designed and developed. One is for production of target elements containing  $Pu^{242}$ , which will be used for the first loadings of the HFIR target; the other is for manufacture of elements in the Transuranium Processing Plant

(TRU). The aluminum-clad elements will be processed in TRU both to remove the desired isotopes and to permit recycling of certain isotopes to the reactor. The fabrication and inspection procedures, which are essentially the same for both the plutonium-bearing element and the actinide-bearing element, involve calcination to form an oxide; powder-metallurgical steps to form an aluminum-clad pellet containing a pressed mixture of oxide and aluminum powder; pellet decontamination and mensuration; tube loading, end capping, and collapse steps to make a hermetically sealed element for containing pellets in intimate contact with the inside wall of the tube; and decontamination and inspection operations to ensure that the target element is radiologically safe and that it meets all specifications for weld integrity, dimensions, and distribution of target material. The equipment being developed for TRU will be semi-automatic in operation to allow completely remote handling of the process. The equipment for handling  $Pu^{242}$  will be installed in unshielded glove boxes and accordingly will be of simpler design than that for TRU. The design of the TRU equipment is approximately 20% complete. Procurement of equipment for the  $Pu^{242}$  work has commenced.

## 21. Welding and Brazing

The development of suitable procedures for fabricating various reactor components composed of materials ranging from aluminum and stainless steels to beryllium and niobium constituted a major portion of the work of the Welding and Brazing Laboratory.

Improved procedures for reducing shrinkage during welding were developed for fabricating prototype fuel elements for the HFIR program. Manual procedures were used successfully for welding the fuel plates on the inside and outside of the two annuli but in order to satisfy future production requirements, considerable emphasis is being placed on the development of automatic procedures. Procedures for fabricating the stainless steel-clad  $UO_2$  fuel element for core B of the Enrico Fermi Reactor to the tight dimensional tolerances required were completed.

A highly complex boiler assembly for a liquid-metal loop experiment was satisfactorily fabricated, as were several complex, instrumented, stainless steel, irradiation capsules with internal thermo-

couples. Methods for remotely brazing pipe joints for molten-salt service were devised, as were techniques for making the various thermocouple and burst-slug-detection tube penetrations through the pressure vessel of the EGCR.

Several very promising alloy compositions were formulated for brazing niobium, and the joints had excellent room- and elevated-temperature strengths. Procedures were developed for making end-closure welds in beryllium tubes with a strength of about 10,000 psi at 600°C. Experimental brazing alloy compositions were designed which readily flow on the oxide ceramics, and a demonstration compartmented fuel element of aluminum oxide was fabricated. Successful procedures were developed for joining ferritic steels to austenitic steels for high-temperature cyclic service.

## 22. Postirradiation Examination

Remote-replication techniques for macroscopic surface examinations were expanded to obtain replicas of sufficient quality for electron-microscope examinations. A total-body replication technique was developed for preparing nonradioactive duplicates of small objects such as 0.220-in.-diam irradiated ThO<sub>2</sub> spheres and 2½ × 8 × ⅜ in. sections of the HRE-2 core wall for detailed examination outside the hot cell. The surface topography produced had suitable detail for examination at up to 1000X.

Essentially all the metallographic equipment for use in the new PIE laboratory has been fabricated and tested. Supporting equipment such as manipulators, waste disposal canning and cleaning devices, optical equipment, and service plugs are in various stages of construction and testing. The remote scanning tank for use with ultrasonic inspection equipment is being slightly modified after an exhaustive mockup testing period. The shielded x-ray diffraction goniometer was completely assembled in a temporary location and on the basis of preliminary tests will provide satisfactory diffraction patterns.

## PART IV. APPLIED RESEARCH

### 23. Physical Properties of Ceramics Studies

The Physical Properties of Ceramics Group continued studies of methods of determining thermal

conductivity over temperatures ranging from 20 to 1000°C. The influence of the chemical and physical state of UO<sub>2</sub> on thermal conductivity is being studied in a thermal comparator apparatus that is operable to 400°C with a precision of ±3%. Measurements that were precise to ±1% and accurate to ±3% were made on UO<sub>2</sub> to 875°C in a radial heat flow apparatus. Equipment was constructed for measuring the thermal diffusivity to 1700°C by a quenching method. The total hemispherical emittance of INOR-8, Nb-1% Zr, and platinum was measured to 1000°C by electrically heating a strip specimen in a constant-temperature black-body vacuum chamber.

### 24. Sintering Studies

Heating thoria powder compacts to any given temperature gave a temperature-dependent densification end point free from influence of the heat-up cycle. An increase in densification rate of ThO<sub>2</sub> compacts between 1450 and 1600°C was observed which far exceeded the increase in rate of self-diffusion, suggesting that volume diffusion is not the dominant material transport mechanism. Several experiments gave densification characteristics that are compatible with a dislocation-movement transport mechanism. Weld necks formed between small crystals and the cleaved face of large CaF<sub>2</sub> crystals were surrounded by a high concentration of dislocations. Sintering of a CaF<sub>2</sub> pellet containing a small hole resulted in smaller grains around the hole. Preliminary data on self-diffusion of thorium and oxygen in ThO<sub>2</sub> were obtained.

### 25. Solid Reaction Studies

Diffusion coefficients of Al<sup>26</sup> and Mn<sup>54</sup> in aluminum were determined between 450 and 650°C. Reaction between hot-pressed beryllium and uranium monocarbide was found to occur throughout the range 700 to 1000°C, to result in a layer of UBe<sub>13</sub> with uniformly dispersed free carbon, and to be controlled by the diffusion of beryllium in UBe<sub>13</sub>. Diffusion coefficients of Zr<sup>95</sup> and Nb<sup>95</sup> in β-zirconium were determined over the range 900 to 1750°C. Preliminary experiments were performed in a study of the diffusion of Ti<sup>44</sup> in titanium. Preliminary data on the diffusion of niobium in both pressed and sintered UO<sub>2</sub> pellets and fused UO<sub>2</sub> indicated a diffusion coefficient

of  $1.46 \times 10^{-10}$  cm<sup>2</sup>/sec at 1505°C. A method for separating grain-boundary effects involving penetration plots obtained for polycrystalline materials was developed.

## 26. Metallurgy of Superconducting Materials

Microstructural examination of diffusion couples and as-cast ingots of the Nb-Sn system showed that there are at least three and probably five intermediate phases. Approximate melting points of some of the phases are, from the most niobium-rich side to the least-rich side, greater than 1000°C, 940°C, and 850°C for the first three phases.

Transformation kinetic studies of Zr-Nb alloys containing from 25 to 40 at. % Zr at temperatures from 500 to 950°C showed that a lamellar structure is produced sluggishly at 800 and 900°C, more rapidly at 600 and 700°C but too fine to be resolved optically, and not at all at 500°C in 24 hr; increasing the zirconium content increases the rate of reaction at all temperatures; the reactions at 500 and 600°C do not seem to produce  $\alpha$ -zirconium in the initial reaction; and the segregation during freezing is quite severe and an important problem. In tensile tests of as-fabricated Nb-25% Zr 0.010-in.-diam wire the ultimate tensile strength at 4.2°K was about 330,000 psi.

Purified technetium, Tc-Zr, and Tc-Mo ingots were arc-cast and hot-press-forged. The as-cast Tc-10 wt % Zr alloy consists of a primary body-centered cubic phase and a very small amount of divorced eutectic with a second cubic phase. A 50% Tc-50% Zr alloy is almost single-phase close-packed hexagonal. From resistance measurements, the critical temperature (in zero field) of purified technetium was found to be 8.26°K.

## 27. Zirconium Alloy Research

Studies of the formation of an  $\omega$  phase during aging of Zr-15% Nb-X alloys showed that decreasing the "betaizing" temperature and time, increasing the aging time at room temperature between beta quenching and elevated-temperature aging, and using slower quenching rates increase the incubation time and decrease the rate of formation of the  $\omega$  phase. The evidence indicated that the formation of  $\omega$  phase is affected by the vacancy concentration of the alloy at the time of aging at elevated tem-

perature. The validity of using aging curves determined by hardness measurements at room temperature after quenching from the aging temperature to show the correct transformation kinetics was confirmed by hot-hardness measurements during aging at 400°C.

The solubility of niobium in  $\alpha$ -zirconium as determined by metallographic examination disagrees considerably with that determined from resistivity measurements during heating and cooling. The redetermination of the solubility curve is continuing.

Continued study of the strain anisotropy in Zircaloy-2 disclosed that although the strain-strain equations derived from Hill's theory of anisotropy are experimentally verified, the theory, as developed, should not be applied to Zircaloy-2 since several of the essential assumptions are violated. It may be that the restrictive assumptions are not necessary. The room-temperature yield strength in compression was indicated to be as high, for certain textures, as 122,000 psi, while the yield strength in tension will be only 70,000 psi.

Oxidation-rate data for Zircaloy-2 obtained with a technique that permits determination of the time required to form a 20-A-thick layer of oxide to an accuracy of 5% or better showed that the oxidation rate is not smooth on a fine scale but has a cyclic variation in the rate. The oxidation process seems to be smoother at 600°C than at 450 or 500°C.

Thin-film oxides *in situ* (produced by anodizing zirconium) examined in a polarizing spectrometer appeared to absorb strongly at light wavelengths less than 2500 Å. X-ray diffraction measurements showed that the anodized film is essentially amorphous (give no x-ray diffraction maxima). No difference was observed in the optical properties of anodized films and those produced by water corrosion at 300°C.

## 28. Metallography

Transmission electron-microscope studies of niobium were used, with considerable promise, in helping to associate deformation bands, textures, and dislocation networks and to detect subgrains after low-temperature annealing. Preliminary studies were made on the interaction of impurities with dislocations during aging and recrystallization.

Hot-hardness testing was used as a quick survey method for preliminary evaluation of the strength of metals and alloys and for evaluating high-temperature deformation characteristics.

In support of the reactor projects both in general and radiation metallography, pyrolytic-carbon-coated uranium carbide fuels were examined in detail to appraise uniformity and homogeneity in both the coatings and the fuel. Various types of fuel elements were examined in the hot cells after extended fuel burnup to evaluate the integrity of the element and the condition of the fuel and contiguous matrix. In the SM-1 fuel element the maximum life seemed to be limited more by corrosion rates than by dimensional instability of the fuel. Uranium carbide particles compacted in graphite and irradiated in the MTR increased in volume in relation to void formation; however, no grain structure could be resolved by known techniques.

## PART V. FUNDAMENTAL RESEARCH

### 29. Crystal Physics

The program for developing methods for growing quality crystals of controlled purity was continued. A variety of crystal growth systems are being used in the attempt to synthesize large crystals of a large number of oxides, certain alkali metal halides, and some metals and intermetallic compounds.

### 30. Deformation of Crystalline Solids

The stored energy resulting from deformation of crystalline solids was measured for a series of Cu-Zr and Ni-Al alloys at 77 and 243°K. It was found that the rate of energy storage increases with strain for the first 20% elongation. Alloying increases the energy storage greatly while increasing the strength relatively less. A reduction in temperature increases the energy stored in pure metals significantly but has only a minor effect on the more concentrated alloys. Work was started on interpreting these results in terms of the changes produced inside the metal during deformation.

### 31. Reactions at Metal Surfaces

Studies of the fundamental mechanisms of oxidation of metals were continued, with particular emphasis placed on the role of mechanical stresses

in controlling the degree of protectiveness in oxide films. Evidence of large stresses in tantalum specimens resulting from the solution of oxygen in the tantalum lattice was provided by hot-stage microscopy techniques and by direct measurements of the flexure of tantalum specimens exposed to oxygen on one side only. Investigations of the nitridation and low-pressure oxidation of tantalum were initiated, and sulfidation studies revealed the occurrence of a maximum in the rate of sulfidation of tantalum between 700 and 800°C. Additional x-ray and optical studies of epitaxially induced strains in  $\text{Cu}_2\text{O}$  films were also undertaken.

### 32. Spectroscopy of Ionic Media

A high-temperature spectrophotometer of improved design was procured for the study of absorption spectra at 1000°C over the wavelength range 186 to 2600  $m\mu$ . A multispecies model was developed for the phenomenological light-absorbing behavior of solutions of bismuth metal in molten  $\text{BiCl}_3$ . Progress was made toward developing a code for calculating multicenter wave functions for molecules and molecule ions.

### 33. Structure of Metals

Mechanical twins were found in electron-beam-melted niobium deformed by high-speed impact at room temperature and by slow or fast compression at -196°C, and their crystallographic characteristics were determined. The addition of interstitial elements inhibited twinning and gave increased amounts of cleavage cracking on {100} planes. Theoretical expressions were developed for impurity-controlled and impurity-independent grain-boundary migration during recrystallization. These expressions were confirmed by data from alloys of 0.00021 to 0.0256 at. % Cu in zone-refined Al. A new treatment was developed for obtaining axis distributions from pole distributions. Deformation studies were initiated on the difference in behavior of grains in aggregates and single crystals and on the effect of reactor irradiation on subsequent preferred orientation in copper.

### 34. Theory of Alloying

The early transition metals Ti, Zr, Hf, V, Nb, Ta, Mo, and W and their alloys have been considered

in terms of electronic structure, alloy models, and crystalline defects. These metals and their alloys include high-field superconductors such as  $\text{Nb}_3\text{Zr}$ , which is under development in order to provide high fields for Fermi surface studies. Heat treatment of this superconductor at  $800^\circ\text{C}$  was found to give a tenfold increase in critical currents, apparently as a result of strains arising during the early stages of precipitation. The mechanism of the heat treatment was more closely understood when it was shown to be greatly enhanced by additions of oxygen and carbon. The precipitating phase is apparently a compound such as  $\text{ZrO}$  or  $\text{ZrC}$ . Size-effect studies of Nb-Zr superconductors showed that the main superconducting currents in small wires flow in a  $10^{-4}$ - to  $10^{-3}$ -cm depth on the surface. Critical current density was found to be greatly increased in small-diameter wires and to be inversely proportional to the diameter in wires with etched surfaces. The conventional insulation of superconducting magnets had shortened their lifetime because of a rapid transition time from the superconducting state to a normal state. The use of pure metal foils between layers of the magnet coils greatly extended the magnet lifetime. A study was made of transverse magnetoresistance in pure tungsten. With current flow in  $\langle 100 \rangle$  and  $\langle 110 \rangle$  directions, the magnetoresistance was anisotropic upon rotation of the magnetic field direction, while maintaining the field perpendicular to the current. Magnetoresistance increased in all directions quadratically with field strength, suggesting closed Fermi surfaces in tungsten with equal numbers of holes and

electrons. The low-temperature specific heats of  $\alpha$ -zirconium were completed for dilute additions of Ag, Cd, In, Sn, and Sb. The density of states increases linearly with these solutes in direct proportion to the solute valency. The Debye temperatures decrease linearly with each solute but the rates of change with valency are more complicated. New information was determined on the phase diagrams Zr-Ga and Zr-Pb.

### 35. X-Ray Studies of Crystalline Defects

Diffuse intensity measurements on the alloy Cu-16 at. % Al and their interpretation were completed. A model was found which convincingly reproduces the experimentally determined short-range-order parameters for this alloy.

A study of monochromators and their design and construction led to an improvement by more than a factor of 2 in the monochromatic x-ray intensity available for diffuse scattering studies.

### 36. X-Ray Diffraction

Service functions of the X-Ray Diffraction Group are summarized. Research programs were continued in the fields of radiation damage in beryllia, order-disorder phenomena in nonstoichiometric Cu-Au, and determinations of the crystal structure of several mixed oxides of fundamental and practical interest. Abstracts of publications on these subjects are given.

## Contents

SUMMARY .....	iii
PART I. REACTOR PROJECT ACTIVITIES	
1. GAS-COOLED REACTOR PROGRAM .....	3
EGCR Construction Support .....	3
Advanced Fuel Elements .....	5
Unclad Fuel Elements .....	6
2. MOLTEN-SALT REACTOR PROGRAM .....	8
3. HIGH-FLUX ISOTOPE REACTOR .....	10
4. TRANSURANIUM PROGRAM .....	12
5. THERMONUCLEAR PROJECT .....	13
6. THORIUM UTILIZATION PROGRAM .....	14
7. ADVANCED TEST REACTOR .....	15
8. ARMY POWER REACTOR PROGRAM .....	16
9. MARITIME PROGRAM .....	17
10. ENRICO FERMI REACTOR PROGRAM .....	18
PART II. MATERIALS PROPERTIES	
11. CORROSION ENGINEERING .....	21
Gas-Cooled Reactor Materials Compatibility Tests .....	21
Corrosion of Reactor Materials in Contaminated Helium .....	21
Graphite-Metal Compatibility Studies .....	22
Fluoride Salt Corrosion Studies .....	22
Forced-Convection Loops .....	22
Fluoride Salt Contamination Studies .....	23
Corrosion Effects of CF <sub>4</sub> .....	23
12. FUELS EVALUATION .....	26
Coated Particles .....	26
Uncoated Particles .....	27
13. MATERIALS COMPATIBILITY .....	28
Alkali-Metal Corrosion Studies .....	28
Alkali-Metal Purification .....	28
Corrosion of Refractory Metals by Lithium .....	29
Boiling-Potassium Studies .....	29

Graphite–Molten Fluoride Salt Studies .....	32
MSRE-Type Graphite .....	32
Ammonium Bifluoride as Oxygen-Purging Agent for Graphite .....	32
Permeation of Mercury and Molten Fluoride Salts .....	32
14. MECHANICAL PROPERTIES .....	33
Mechanical Properties of Type 347 Stainless Steel– $UO_2$ Cermet .....	33
Mechanical Properties of Aluminum Alloys 6061 and X8001 .....	34
Dimensional Studies of EGCR-Type Fuel Elements at Elevated Temperatures .....	34
Collapse of Cylinders Under External Pressure .....	35
Stress Rupture of Type 304 Stainless Steel Tubing .....	36
Stress Rupture of Nb–1% Zr Tubing .....	36
Beryllium Irradiation Effects .....	37
Mechanical Properties of Beryllium .....	37
Studies of the Distribution of Absorbed Carbon in Beryllium Exposed to Carbon Dioxide .....	38
Carburization of Fe–Ni–Cr Alloys in Flowing $CO_2$ .....	39
Effect of $CO_2$ on the Strength and Ductility of Type 304 Stainless Steel at Elevated Temperatures .....	39
Influence of Hydrogen on Nickel-Base Alloys .....	40
Aging of Nb–Zr Alloys .....	42
Stress-Rate Testing .....	44
Zircaloy-2 .....	45
15. NONDESTRUCTIVE TEST DEVELOPMENT .....	48
Ultrasonic Testing Methods .....	48
Fuel Plates .....	48
Brazed Joints .....	48
Eddy-Current Methods .....	49
Through-Transmission System .....	49
Space Gaging .....	49
Penetrating Radiation Methods .....	50
Low-Voltage Radiography .....	50
Homogeneity Studies .....	50
X-Ray Attenuation Coefficients .....	52
Problem Materials .....	52
Beryllium .....	52
Molybdenum .....	52
Remote-Inspection Development .....	52
Thickness of Core Vessel Wall .....	52
Radiography in Radiation Environs .....	53
16. PHYSICAL METALLURGY .....	54
Aging Phenomena in Dilute Niobium-Base Alloys .....	54
Dispersion-Strengthened Alloys .....	54
Uranium-Molybdenum Alloys .....	54
Oxidation Protection of a Cast U–10% Mo Alloy .....	56
Niobium-Base Alloy Studies .....	57
Melting Point of INOR-8 .....	58
Evaporation of Iron, Nickel, and Cobalt Alloys in High Vacua .....	59
Reactions of Type 304 Stainless Steel with Low-Pressure CO and $CO_2$ .....	60
Oxidation Studies .....	61
Cladding Studies .....	61

Contamination Studies of Refractory Metals .....	63
Molybdenum Research .....	63
Beryllium Corrosion Research .....	64
PART III. METAL AND CERAMIC FABRICATION	
17. CERAMICS TECHNOLOGY .....	67
BeO and Fueled BeO Studies .....	67
Fabrication Development of BeO .....	67
Fabrication Development of Fueled BeO .....	68
Phase Relationships in BeO–Metal Oxide Systems .....	68
Phase Relationships in the U-O System .....	69
Graphite and Fueled Graphite Studies .....	70
Coated Particle Fuel Element Development .....	70
Fueled-Graphite Fabrication .....	73
Uranium Oxide and Thorium Oxide Fabrication Development .....	73
Fabrication of $UO_2$ Pellets .....	73
Vibratory Compaction Studies .....	73
Thoria-Pellet Development .....	74
Thermal-Conductivity Studies .....	74
Europium Oxide Studies .....	76
Behavior During Sintering .....	76
Aqueous Corrosion Behavior .....	76
Scandium Oxide Studies .....	77
18. METAL FORMING AND CASTING .....	78
Irradiation Testing of Aluminum-Base Fuel Dispersions of $UAl_3$ , $U_3O_8$ , and $UC_2$ in Aluminum-Clad Plates .....	78
Aluminum-Base Fuel Element Fabrication .....	80
Fuel Plate Fabrication .....	83
Plate Forming and Assembly .....	85
Stainless Steel–Base Fuel Element Fabrication .....	87
Neutron Absorber Development .....	88
Irradiation Behavior of $Eu_2O_3$ Dispersions in Stainless Steel .....	88
Boron-Gradient Neutron Absorbers .....	89
Beryllium Fabrication Studies .....	89
Fabrication of Spiral-Finned Beryllium Tubing .....	89
Pressure Bonding of Beryllium .....	90
Fabrication of Refractory-Metal Alloys .....	90
Melting and Casting of Refractory Metals and Alloys .....	91
19. POWDER METALLURGY .....	94
Fabrication of Uranium Carbide with a Volatile Sintering-Temperature Depressant .....	94
Development of Dispersion-Hardened Thorium and Dispersion-Type Thorium Fuels .....	95
Beryllide Fuels .....	98
Aluminum Matrix Fuels .....	102
Transuranium HFIR Target Fabrication .....	103
20. REMOTE FABRICATION DEVELOPMENT .....	106
Thorium Fuel Cycle Development Facility .....	106
Th- $U^{233}$ Fuel Rod Facility .....	107
Transuranium Target Fabrication Equipment .....	108
Plutonium Target Fabrication Equipment .....	112

21. WELDING AND BRAZING .....	113
Component Fabrication Development .....	113
Aluminum Alloy Fuel Element Development .....	113
Fabrication of Stainless Steel Flat-Plate Fuel Elements .....	114
Loop Fabrication .....	116
Pressure Vessel Penetrations .....	116
Instrumented Fuel Capsule Fabrication .....	117
Solidified Metal Seal Development .....	118
Remote Brazing .....	118
Materials-Joining Development .....	119
Niobium .....	119
Beryllium .....	119
Ceramics .....	120
INOR-8 .....	121
Welding of Ferritic Steels to Stainless Steels .....	121
Graphite .....	122
22. POSTIRRADIATION EXAMINATION .....	123
Reactor Project Support Activities .....	123
Thorium Utilization Program .....	123
Hot-Cell Examination of In-Pile Slurry Autoclaves .....	124
Homogeneous Reactor Experiment .....	124
Experimental Gas-Cooled Reactor .....	124
Molten-Salt Reactor Experiment .....	127
Development of Postirradiation Examination Techniques .....	127
Remote Replication .....	127
Ultrasonic Cleaning .....	128
Development of Remote Equipment .....	128
Positioning Tank for Ultrasonic Testing .....	128
Metallography Mounting Equipment .....	129
Kentron Microhardness Tester, Cutoff Saw, and Metallographic Polishing Equipment .....	129
Stereomicroscopes and Stages .....	129
Master-Slave Manipulators .....	129
In-Cell Canner .....	129
In-Cell Sound Transmission System .....	130
X-Ray Diffraction Apparatus .....	130

## PART IV. APPLIED RESEARCH

23. PHYSICAL PROPERTIES OF CERAMICS .....	135
A Thermal Comparator Apparatus for Thermal Conductivity Measurements from 40 to 400°C .....	135
Further Studies on the Thermal Comparator Apparatus .....	135
A Radial Heat Flow Apparatus for Thermal Conductivity Measurements from 60 to 1600°C .....	136
Further Studies on the Radial Heat Flow Apparatus .....	136
Studies on a Quenching Apparatus for Measuring Thermal Diffusivity .....	136
Total Hemispherical Emittance of Pt, Cb-1% Zr, and Polished and Oxidized INOR-8 in the Range 100 to 1200°C .....	137

24. SINTERING STUDIES.....	138
Sintering Rates of Fluorite-Structure Materials .....	138
Dislocations Around Weld Necks .....	138
Microstructure Around Hole.....	140
Hot Pressing of Thorium Oxide .....	141
Diffusion of Thorium in Thorium Oxide.....	142
25. SOLID REACTION STUDIES.....	145
Diffusion of Al <sup>26</sup> and Mn <sup>54</sup> in Aluminum .....	145
Reaction Between Beryllium and Uranium Monocarbide .....	145
Diffusion of Zr <sup>95</sup> and Nb <sup>95</sup> in $\beta$ -Zirconium .....	145
Diffusion of Fission Products in UO <sub>2</sub> .....	146
Ti <sup>44</sup> Diffusion in Titanium .....	148
26. METALLURGY OF SUPERCONDUCTING MATERIALS.....	149
Niobium-Tin System .....	149
Zirconium-Niobium System .....	149
Technetium .....	150
Technetium-Zirconium System .....	151
Technetium-Molybdenum System.....	151
27. ZIRCONIUM ALLOY RESEARCH.....	152
Physical Metallurgy of Zirconium Alloys .....	152
Zr-15% Nb-X.....	152
Solubility of Niobium in $\alpha$ -Zirconium .....	154
Zirconium-Palladium System .....	156
Strain Anisotropy of Zircaloy-2 .....	156
Oxidation-Rate Measurements .....	157
Oxide Film Studies .....	157
28. METALLOGRAPHY .....	159
Specialized Metallographic Studies and Related Equipment Development.....	159
Electron Metallography .....	159
Elevated-Temperature Hardness Testing .....	163
Instrument for Determining Crushing Strength of Microparticles.....	166
New Metallographic Techniques.....	166
Identification of Carbides, Nitrides, and Oxides in Niobium by Electrolytic Staining.....	166
Etching Behavior of Grain Boundaries in Nickel .....	169
Reactor Project Support.....	169
Irradiation Studies on EGCR Prototype Fuel Elements .....	169
Advanced EGCR Irradiation Experiments.....	169
Examination of Irradiated Advanced Reactor Fuels .....	171
Examination of EGCR In-Pile Tube-Burst Specimens.....	171
Examination of UO <sub>2</sub> Meltdown Experiment No. 1 .....	173
Metallography of Pyrolytic Carbon-Coated and Uncoated Uranium Carbide Spheres.....	173
Unusual Etching Characteristics of UC-UC <sub>2</sub> Spherical Particles .....	174
Metallographic Examination of Uranium Sesquicarbide Bulk Sample .....	176
Examination of Heat Flux Corrosion Test Samples .....	177

## PART V. FUNDAMENTAL RESEARCH

29. CRYSTAL PHYSICS .....	181
30. DEFORMATION OF CRYSTALLINE SOLIDS.....	183
31. REACTIONS AT METAL SURFACES .....	185
Tantalum-Gas Reactions .....	185
Copper Oxidation Studies .....	186
32. SPECTROSCOPY OF IONIC MEDIA .....	187
High-Temperature Spectrophotometer.....	187
Optical Absorption in Bi-BiCl <sub>3</sub> Melts .....	187
Wave Function Calculations .....	187
33. STRUCTURE OF METALS.....	189
Twinning in Columbium .....	189
Effect of Interstitial Elements on Twinning and Fracture in Columbium.....	189
Mechanism of Boundary Migration in Recrystallization .....	189
Influence of Recovery on Recrystallization in Aluminum.....	190
Evaluation of Fiber Textures for Cubic Metals .....	190
Deformation Studies .....	191
Stability of <111> Fiber Texture .....	191
Inhomogeneous Deformation in Grains of Polycrystalline Aluminum .....	191
Texture of Irradiated Copper .....	193
34. THEORY OF ALLOYING.....	194
Increased Critical Currents in Nb-Zr Superconductors from Precipitation	
Heat Treatment.....	194
Interstitial Impurities and Size Effects in Nb-Zr Superconductors .....	195
Superconducting Magnets.....	197
Thin-Foil Electron Transmission Study of Nb-Zr Superconductors .....	197
Magnetoresistance of Tungsten .....	198
Specific Heats of Zirconium Alloys.....	200
The Zr-Pb Phase Diagram.....	202
The Zr-Ga Phase Diagram.....	202
35. X-RAY STUDIES OF CRYSTALLINE DEFECTS.....	204
Short-Range Structure of the Alloy Cu-16 at. % Al.....	204
Monochromator Design .....	206
36. X-RAY DIFFRACTION.....	207
Routine Analyses .....	207
Structural Changes in Irradiated BeO .....	207
High-Temperature X-Ray Diffraction Study of the Order-Disorder Transition	
in a Cu-32.2 at. % Gold Alloy .....	208
On the Crystal Structure of the Orthomanganites of the Heavy Lanthanides	
and Yttrium .....	208
PAPERS AND ORAL PRESENTATIONS GIVEN AT SCIENTIFIC AND	
TECHNICAL MEETINGS.....	211
PUBLICATIONS .....	217
ORGANIZATION CHART .....	223

# **Part I**

## **Reactor Project Activities**

P. Patriarca

---



# 1. Gas-Cooled Reactor Program<sup>1</sup>

J. H. Coobs

The materials effort under way in support of the overall gas-cooled reactor program at the Oak Ridge National Laboratory consists of EGCR construction support, experimental studies aimed at reducing fuel cycle costs associated with EGCR and GCR-3, an advanced gas-cooled power reactor, and development of unclad ceramic fuel elements for service in the Pebble-Bed Reactor Experiment (PBRE). Major activities in each of these support areas during the past year are presented below along with pertinent background information.

## EGCR CONSTRUCTION SUPPORT

The Experimental Gas-Cooled Reactor (EGCR) under construction at Oak Ridge is an outgrowth of conceptual design studies by Kaiser Engineers and ORNL and, when finished in early 1963, will represent the first gas-cooled reactor system built in the United States for civilian power. The nuclear plant of 84-Mw (thermal), 21-Mw (electrical) capacity will use stainless steel-clad, slightly enriched  $UO_2$  fuel in a graphite-moderated core structure contained in a carbon-steel pressure vessel, 24 ft in diameter and 45 ft high. The helium coolant exits the reactor at 1050°F and 315 psia, exchanges its heat to steam, and returns to the reactor core at 510°F. Plant construction is being performed by the H. K. Ferguson Company, and the Laboratory has the responsibility for procurement of critical nuclear components, such as the fuel and control rod assemblies.

The fuel assemblies for the EGCR consist of a seven-element cluster of  $UO_2$  pellets clad with 0.020-in.-thick type 304 stainless steel. The

cluster is supported within a 1-in.-thick graphite sleeve that has an outside diameter of 5 in., an inside diameter of 3 in., and a stacked length of 29 in. The  $UO_2$  pellets are 0.707-in. OD by 0.323-in. ID by 0.740-in. length. The hollow center in the pellets serves to reduce the buildup of fission-gas pressure and center-line temperatures within the element. The design lifetime of the elements is conservatively set at 10,000 Mwd/metric ton. The nominal peak operating temperature of the stainless steel cladding is about 1500°F.

Manufacture of the initial fuel loading for startup of the EGCR has been initiated at Westinghouse Electric Corporation, and all critical phases of work are being monitored to ensure compliance with the high-quality standards specified on materials and workmanship. Procedures were reviewed and approved for the control of moisture content in  $UO_2$ , the welding and radiographic examination of end closures on the fuel elements, the welding of end caps to the spiders, and the copper brazing of mid-plane spacers to the fuel element tubes. During the past year the fabrication of the  $UO_2$  pellets was completed, and all other components were purchased. Approximately 25% of the fuel element tubes were loaded and assembly of the clusters was initiated. The total cost associated with fabrication of the fuel assemblies will run \$55 per kilogram of contained uranium metal.

Reactor operating plans call for monitoring the temperature of the fuel, cladding, coolant, and graphite sleeves in four selected fuel channels. Hence, fabrication techniques were developed for installing swaged Chromel-Alumel thermocouples on the inner surfaces of the fuel element tubes. The thermocouples were held in place by a mandrel while being copper-brazed to the inner surface. As many as four thermocouples were attached to

<sup>1</sup>Reported in detail or referenced in Parts II and III, this report.

a single capsule by this method. Several such capsules were prepared and were successfully tested by irradiation in the ORR Poolside Facility and in GCR-ORR Loop No. 1. Using these techniques, a full-scale mockup of an instrumented fuel assembly was completed and the technical feasibility demonstrated.

The dimensional behavior of the fuel assemblies under the cyclic conditions expected in the EGCR was experimentally investigated to resolve uncertainties arising from differences in the mechanical properties between the cladding and the fuel pellets of hollow geometry. An apparatus has been built to simulate the thermal conditions during service. The dimensional behavior of the experimental fuel assemblies was determined both with a radial gap between the cladding and the fuel pellet and with the cladding collapsed onto the pellet by external pressure.

The element containing a radial gap between the cladding and the fuel pellet was found to respond to thermal cycling the same way that the individual components would react if subjected to the same thermal conditions and tested separately. When no radial gap existed between the fuel and the cladding, the behavior during thermal cycling was found to be a function of the fuel temperature, the cladding temperature, and the external pressure. Under such conditions, plastic axial strains were induced in the cladding during cycling; therefore methods were developed for predicting the amount of strain induced for a given set of conditions.

During this extensive series of thermal cycling tests, severe deformations were induced in the cladding without a single failure, and the fuel pellets fractured without the fuel being significantly redistributed. Consequently, it is predicted that the EGCR fuel elements will remain dimensionally stable under the proposed operating conditions.

The design of the control rods for the EGCR has been established: they will be 20 ft long and  $3\frac{1}{4}$  in. in outside diameter and have an absorber length of 15 ft. The rods will be made in 5-ft-long segments and be supported by a central stainless steel rod flexible enough to ensure its entry into the core even if the control rod channels are not straight. Each absorber segment will be made up of 3-in.-high annular rings of hot-pressed  $B_4C$  encased in copper-plated stainless steel tubing and will be vented to the primary coolant system through stainless steel filters. The design life

of the rods is greater than 20 years. These rods are now being procured from Dresser Products, Inc.

Selected mechanical properties of AGOT graphite were studied, as a function of temperature, to provide a basis for predicting the behavior of the moderator material in the EGCR. As initially loaded into the reactor, the graphite columns will be under compression; but after the reactor goes critical, the columns will undergo radiation-induced shrinkage. Because of the neutron-flux gradient from point to point within the reactor core, bending strains will be imposed on the graphite columns.

Specimens of AGOT taken from three blocks were examined by means of incrementally loaded short-time tensile, short-time bending, and creep tests under compressive, tensile, and bending loads. The test results showed that the mechanical properties of graphite are not affected by temperatures in the range 75 to 1100°F and, therefore, that the fracture stresses and strains are not temperature dependent. The fracture stresses calculated on the basis of elasticity theory for bending are greater than the experimental fracture stresses under tensile loads, but the fracture strains are very similar. Some initial creep was detected, but the creep rate decreased to less than  $5 \times 10^{-9}$  in. in.<sup>-1</sup> hr<sup>-1</sup> in a very short time. Wide variations exist in the mechanical properties, and the mechanical anisotropy is difficult to predict. It may be concluded, however, that as the section size of the graphite block increases the strength variation is also greater across the block.

Because of the low ductility of graphite, the tensile strains produced by the variable radiation dose will not be expected to be sustained during reactor operation without fracturing. Fracture may not occur, however, if the radiation-induced shrinkage is either inhibited or stopped by the occurrence of stress or if the effects of radiation permit the graphite to sustain greater tensile strains before fracturing. A program of irradiations is in progress to study the effects of irradiation on the creep ductility of graphite.

Welding procedures were developed for joining type 304 stainless steel to ASTM A-387, grade D, steel and to ASTM A-212, grade B, carbon steel. Large ducts of these materials will be subjected to cyclic temperature service in the EGCR, and joints between them will develop severe stresses because of differential thermal expansion. A newly developed commercial nickel-base welding rod

(BP-85) was used in the development of the welding procedures. Extensive tests of large welded specimens showed that the joints will perform satisfactorily.

Methods were developed for fabricating the joints at the penetrations of the stainless steel burst-slug-detection tubes and stainless steel-clad thermocouples through the carbon steel pressure shell of the EGCR. Both types of penetrations require the welding of relatively thin-walled components to thicker members under conditions of very limited accessibility. Suitable joint designs were developed, and fabrication and inspection procedures were established during the construction of prototype assemblies to demonstrate feasibility. Conventional welding and brazing equipment and joining procedures were used throughout. It is expected that personnel of the Metals and Ceramics Division will act in a consulting capacity during field fabrication of these components.

### ADVANCED FUEL ELEMENTS

In order to take advantage of the EGCR as a test bed for advanced fuel elements and of the extensive information gained from the design and construction of the EGCR, a study of an advanced clad-type 2000-Mw (thermal) reactor, GCR-3, was initiated. Cladding materials for advanced fuel assemblies are being studied which will promote increased efficiency as a result of higher outlet coolant temperatures, increased heat flux ratings, and/or reduced thermal neutron absorption in the core.

Beryllium is attractive as a nuclear reactor material for fuel cladding and as a moderator because of its high-neutron scattering cross section, its low-neutron capture cross section, and its high thermal conductivity. Consequently, batches of smooth-walled beryllium tubing were procured from all domestic and foreign sources for evaluating and testing its use as a cladding material in gas-cooled reactors. In addition, a supply of finned tubing was obtained as a product of a fabrication subcontract with Nuclear Metals, Inc. This tubing is approximately 0.5 in. in inside diameter with a 0.040-in. minimum wall thickness and has 12 equally spaced helical fins.

Nondestructive inspection techniques were developed for comparing the quality of beryllium tubing and for ensuring the integrity of test spec-

imens. Low-voltage radiography utilizing bare-film exposure techniques and a helium-atmosphere couple was found to be an excellent nondestructive tool to facilitate inspection. The presence of pitting on the inner surface or contamination from foreign materials was readily detected by this inspection. An eddy-current procedure using an internal bobbin coil was developed for detecting cracks in the finned tubing. The more conventional liquid-penetrant and ultrasonic techniques were adapted to supplement the radiographic inspection.

Joint designs and welding procedures were developed for the fabrication of test specimens and irradiation capsules. Welds in tubing submitted by several vendors all exhibit similar strengths at both room temperature and 1110°F, averaging 23,000 and 11,000 psi, respectively. Brazing alloys for joining beryllium were investigated through flowability tests.

The changes in the mechanical and physical properties resulting from neutron irradiation may be traced to the displacements produced by energetic neutrons or to the products from the  $(n, 2n)$  and  $(n, \alpha)$  reactions with beryllium and the effects produced by agglomeration of the gases produced by these transmutations. A program of irradiations was conducted in which beryllium specimens of various chemical compositions and fabrication histories were exposed at temperatures between 120 and 1435°F. Postirradiation bend tests and hardness measurements were made, and the density decreases during irradiation were determined. These data were compared with those obtained by postirradiation annealing of specimens irradiated at 120°F. Other small tubular specimens were pressurized and irradiated at temperatures between 930 and 1300°F to study the effects of irradiation on the mechanical properties.

The results indicated that slight hardening occurs upon irradiation or postirradiation annealing at temperatures below 1110°F. Dimensional measurements showed that beryllium swells more than 1% when irradiated to a fast ( $>1$  Mev) neutron exposure of  $3.6 \times 10^{20}$  neutrons/cm<sup>2</sup>. No significant swelling occurs during irradiation at lower temperatures or for lower exposures. The results of several in-pile stress-rupture experiments at 1110°F tests may be represented by the equation

$$\Delta_{100} = 5.37 \times 10^{-14} \phi_t^{0.628} ,$$

where  $\Delta_{100}$  is the fractional decrease in 100 hr of rupture strength after an exposure of  $\phi_I$  neutrons/cm<sup>2</sup>. Additional tests at 970°F showed that exposures as high as  $3.4 \times 10^{20}$  neutrons/cm<sup>2</sup> have little effect on the rupture time at this temperature.

The reactions of beryllium with potential coolants were also studied. The rate of reaction with wet and dry CO<sub>2</sub> was found to be parabolic in the range 550 to 1330°F for times up to 1000 hr. At 1340°F, a "breakaway" reaction was observed in wet CO<sub>2</sub> after 60 to 70 hr. The reaction products were found to be BeO and Be<sub>2</sub>C, and the amount of both increased with time and temperature.

The reaction between beryllium that contained carbon as an impurity and wet helium was initially rapid, but a protective oxide soon formed on the beryllium that was similar to that formed in dry CO<sub>2</sub>. This behavior is believed to be associated with decarburization during the early stages of the test. The products of the reaction of beryllium with water vapor were BeO and hydrogen gas. Methane was found to be a reaction product when Be<sub>2</sub>C was exposed to water vapor or hydrogen.

A series of tests was also run in static, dry CO<sub>2</sub> at 1380°F on a Be-0.5 wt % Ba alloy. This alloy was prepared for testing because of the excellent high-temperature stability of barium carbonate which could stabilize the protective oxide film on the alloy at a relatively low partial pressure of CO<sub>2</sub>. Three tests were run at CO<sub>2</sub> pressures of 6, 50, and 570 torr, respectively. Reaction rate curves determined from weight-gain data indicated that the reaction was pressure dependent.

Two simulated beryllium fuel elements consisting of hollow UO<sub>2</sub> pellets clad with the finned tubing were fabricated and were tested to failure by thermal cycling out-of-pile. A radial temperature gradient between 200 and 440°F was established during cycling. No permanent axial deformation of the beryllium was detected after testing. However, the beryllium tubing cracked both circumferentially and in an axial direction after 67 cycles between 480 and 1200°F. The axial cracking apparently resulted from the concentration of stresses between the fins.

### UNCLAD FUEL ELEMENTS

The pebble-bed reactor concept offers the advantages of simplicity of the fuel element design, ease

of fuel handling, suitability for high-temperature operation, and good neutron economy but suffers the disadvantage that some fission-product activity will enter the coolant system. A 5-Mw (thermal) Pebble-Bed Reactor Experiment (PBRE) has been designed which will assist in evaluating technical feasibility of the pebble-bed concept as well as make important contributions to the general development of all-ceramic gas-cooled reactors.

The core of the PBRE is a 2½-ft-diam, 4-ft-tall cylinder containing approximately 12,000 spherical graphite fuel elements 1½ in. in diameter. Fuel spheres are added to and removed from the core by gravity flow while the reactor is at power. Exposed fuel can be recycled to the top of the core.

Helium coolant at 500 psia enters the bottom of the core at 550°F and emerges from the top at 1250°F. Concentric ducting connects the reactor to a single heat exchanger. The entire pressure envelope is swept with helium at the temperature at which it emerges from the heat exchanger.

One of the primary objectives of the experiment is to investigate the behavior of graphite fuel elements, the development and procurement of which are the responsibility of the Metals and Ceramics Division.

In the past year pyrolytic-carbon-coated uranium carbide and uranium-thorium carbide particles were evaluated as fuel materials. Coatings applied at low temperatures exhibited a laminar structure, whereas those applied at high temperatures had a columnar or duplex structure. Metallographic techniques were developed for examination of such particles and of graphite-matrix fuel elements containing coated particles. These particles generally met a preliminary requirement for surface contamination of less than  $5 \times 10^{-3}$  % of the contained fuel. Leaching with 8 M nitric acid reduced the exposed fuel, as determined by alpha counting, while thermal cycling to 2730°F generally caused an increase in the leachable fuel and surface contamination. Techniques for contact microradiography of the particles were developed to permit measurement of the coating thickness and uniformity and to detect the presence of unfueled particles and uranium migration into the coating.

In an extensive series of neutron-activation tests the as-received particles exhibited good fission-gas retention properties at temperatures less than 2730°F. At higher temperatures, uranium migrated

into the carbon coatings and the coatings cracked. Indications are that these processes are dependent upon the microstructure of the carbon coatings.

Cylindrical bodies of fueled graphite consisting of dispersions of particles in a graphite matrix were obtained from two vendors and were tested extensively. Leaching and neutron-activation tests indicated that some phases of the fabrication procedures could damage the particles, resulting in poor retention of fission products. However, after a series of tests on several batches of fueled bodies, it was concluded that by proper control of the fabrication process satisfactory fueled graphite bodies could be produced. A specification defining the properties of fueled graphite spheres was thus developed and is being used in procuring prototype PBRE fuel elements for testing.

The fission products other than  $\text{Xe}^{133}$  that are released from fueled graphite were identified and were measured in a separate series of neutron-activation tests. Fueled graphite elements were lightly irradiated and heat-treated, and the released fission products were collected on a deposition tube near the specimen. The major species released at temperatures up to 2190°F were  $\text{I}^{131}$ ,  $\text{Te}^{132}$ , and  $\text{Ag}^{111}$ . The fractions of iodine and tellurium released were approximately the same as the  $\text{Xe}^{133}$  released, but the silver isotope was

detected in much greater amounts. Apparently  $\text{Ag}^{111}$  diffuses readily through the coatings at 1830 to 2190°F. The release of  $\text{Ba}^{140}$  by a similar mechanism was observed at temperatures of 2550°F and above.

Irradiation tests in both static and sweep capsules were performed to burnups as high as 15 at. % of uranium at temperatures between 1500 and 2600°F. It was observed that some of the pyrolytic carbon coatings cracked during irradiation; however, acceptable fission-gas retention with respect to the PBRE was observed in tests at the lower temperatures. Cracking of the coatings can be attributed to the combined effects of swelling of the fuel particles, uranium migration, radiation-induced shrinkage of the coatings, and pressure buildup of fission gases within the coated particles. The relative importance of each of these processes is not yet known.

During these irradiations, fueled graphite bodies were observed to shrink as much as 6% after exposures of between 3 and  $6 \times 10^{19}$  fissions/cm<sup>3</sup>. However, most of the bodies without unfueled graphite shells or siliconized-SiC coatings retained their integrity, while all those with shells or coatings developed cracks during irradiation. Additional experiments are in progress to determine the causes of this cracking.

## 2. Molten-Salt Reactor Program<sup>1</sup>

A. Taboada

Construction of a prototype reactor of 10-Mw (thermal) capacity is under way at ORNL to demonstrate the dependability, serviceability, and safety aspects of the molten-salt concept for civilian power application, and to acquire the engineering knowledge needed in scaling the system to large central-station power plants. The concept offers a number of attractive features, including high temperature, low pressure, good neutron economy, low fuel cycle cost, and high power density.

A molten-salt mixture of  $\text{LiF}\text{-BeF}_2\text{-ZrF}_4\text{-ThF}_4\text{-UF}_4$  in the mole percentage of 70-23-5-1-1 will be utilized in the Molten-Salt Reactor Experiment (MSRE) to serve as the fuel and primary coolant. After flow through vertical channels in the cylindrical, single-region, graphite-moderated core of  $4\frac{1}{2}$  ft diameter by  $5\frac{1}{2}$  ft height, the fluid will reach the shell side of a salt-to-salt heat exchanger at a maximum temperature and pressure of 1225°F and 50 psig. The container material is INOR-8, a nickel-base alloy developed at ORNL for service in contact with fluoride salts at elevated temperatures. In the experiment heat from the secondary loop containing a non-fuel-bearing molten salt will be discharged to the atmosphere through a secondary air-blast heat exchanger.

The nature and current status of major support activities during the past year are summarized below.

Procurement of all major INOR-8 components required in the construction of the MSRE is complete except for the heat exchanger. Product specifications on the nickel-base alloy containing 17 wt % Mo, 7 wt % Cr, and 5 wt % Fe were prepared for the purchase of the plate, sheet, bar, and wire,

while fabrication procedures were developed for procurement of castings, forgings, and formed heads. In addition, a weldability test was developed and successfully employed to ensure that each heat of INOR-8 was weldable and free of the microfissures frequently encountered in nickel-base materials.

Welding and brazing techniques were developed and incorporated into the final design of the MSRE heat exchanger to assure maximum integrity of the tube-to-sheet joints.

Brazing materials and techniques were developed for making remote pipe-joint attachments that will be utilized in the remote maintenance program for the MSRE. Inspection techniques for detecting nonbonds were established, and modifications are being developed which will permit remote application.

The dynamic corrosion-test loop program was completed, and out-of-pile corrosion rates for INOR-8 were established to be less than 1 mil/yr at 1300°F. A study to determine the corrosive effects of  $\text{CF}_4$  vapor in the molten salt was initiated, and preliminary results indicated very little attack to INOR-8 at temperatures up to 1472°F.

Additional mechanical properties data on INOR-8 weld metal and castings were obtained and incorporated into a design data submission to the ASME Boiler and Pressure Vessel Code Committee for codification approval.

Additional data on the constitutional diagram and physical properties of INOR-8 alloy were obtained. The solidus line of a number of commercially produced heats was found to lie in the range 2435 to 2480°F, while the liquidus line was observed to fall between 2552 and 2559°F. The total hemispherical emittance of INOR-8 as measured in a constant-temperature, black-body vacuum chamber at 1112°F was found to be 0.24.

<sup>1</sup>Reported in detail or referenced in Parts II and III, this report.

A graphite-moderator specification requiring low salt permeation was prepared, and materials initially procured to this specification appeared to be acceptable. Salt permeation was less than 1 vol %. Techniques involving the use of ammonium bifluoride as a gettering agent were developed for removal of oxygen from graphite.

During the coming year the major metallurgical effort in support of the MSRE will be directed toward the development and procurement of a central control rod and the planning and implementation

of a surveillance program aimed at determining the irradiation behavior of INOR-8 and graphite under MSRE conditions. A supporting irradiation study to determine the effects of irradiation on the mechanical properties of INOR-8 over a range of temperatures will also be initiated. The effect of impurities in the fuel salt on the corrosion of INOR-8 will be further established, as will the effects of time and temperature on permeation of graphite by salt compositions of potential use in the MSRE.

### 3. High-Flux Isotope Reactor<sup>1</sup>

R. J. Beaver

The main function of the High-Flux Isotope Reactor (HFIR) being constructed at ORNL is to provide an intense radiation source for the production of research quantities of the transplutonic elements. The design of this high-performance unit is based on the flux-trap principle and consists of a central cylindrical island surrounded by a light-water-moderated and -cooled annular fuel region, which in turn is encompassed by a thin control region and beryllium reflector. The unit will operate at a maximum power density of 4000 kw/liter in the active core and requires a maximum heat-transfer rate from the fuel surfaces of  $1.5 \times 10^6$  Btu hr<sup>-1</sup> ft<sup>-2</sup>. Heat removal will be accomplished by flowing water with an inlet temperature of 120°F and a pressure of 600 psig through a 0.05-in. coolant channel at a velocity of 40 fps. The compact reactor is designed to operate at a power level of 100 Mw and achieves an unperturbed thermal flux of about  $5 \times 10^{15}$  neutrons cm<sup>-2</sup> sec<sup>-1</sup> in the central trap region.

The fuel component has many interesting features which pose challenging fabrication problems to the materials people responsible for its development. The fuel distribution, for instance, must be contoured to flatten the power distribution in the radial direction. In addition, a burnable poison must be incorporated into the inner ring of the fuel annulus to help minimize reactivity variations during the lifetime of the core. The composite plates must be formed into the shape of an involute and assembled in a manner to maintain a constant water-gap thickness of 0.050 in. in the radial direction. The full core loading will actually consist of two annular rings sized in a manner to

fit concentrically with one another to form the 5.0-in.-ID  $\times$  17.0-in.-OD fuel annulus.

Previous work on the HFIR fuel element showed that significant problems existed in several areas: fabricating both the inner and outer fuel plates to ensure freedom from blisters and other unbonded regions; forming involute plates to acceptable tolerances; assembling plates into a fuel element array within rigid plate-spacing tolerances; and developing nondestructive techniques for precise detection of fuel segregation and nonbonds in small regions.

Intolerable concentrations of gases in the aluminum fuel plate materials led to the need for pre-treating the aluminum by vacuum degassing, which contributed significantly to the solution of the blister problem. In addition to this innovation, the type 6061 aluminum frame and cladding of the fuel plate were clad with type 1100 aluminum so that the mating surfaces during rolling would be the more readily bonded to type 1100 aluminum. As a result, the yield of blister-free outer-annulus plates was increased from 50 to 85%. Similarly, the yield of acceptable inner-annulus plates was increased from 5 to 95%.

Low-pressure Marforming was shown to be a satisfactory method for forming unfueled plates to within required tolerance levels, but difficulty arose in attempting to form composite plates in the same manner — a yield of only 26% was realized. However, the process yield was doubled when deviations in the fuel plate thickness were controlled to less than  $\pm 0.4$  mil. Since further significant improvements by low-pressure Marforming were questionable, work was initiated on two alternate methods — high-energy forming and high-pressure Marforming.

As a result of improvement in assembly and welding techniques, an unfueled element was

<sup>1</sup>Reported in detail or referenced in Parts II and III, this report.

assembled to very close tolerances, welded, and provided to a mockup facility for flow testing. Additional studies in assembling composite fuel plates showed that corrective spacing strips were necessary if fuel element spacings in the reference design were to be maintained within tolerance. Consequently, two alternative approaches with lower cost potential are being investigated for assembly. One consists of sliding plates between two grooved, concentric tubes and securing the

plates by circumferential welds uniformly spaced along the length of the element. The other scheme involves mechanically joining 16 to 20 plates between two segments of a tube and assembling a number of segments together to form the required fuel annulus.

It is expected that the first core loading of the HFIR will be of the reference design, with the majority of the subsequent loadings of the most economical of the alternate designs.

## 4. Transuranium Program<sup>1</sup>

W. C. Thurber

This ORNL program forms an integral part of the AEC transplutonic element program, which is aimed at production of research quantities of the very heavy elements such as Am<sup>243</sup>, Cm<sup>244</sup>, and Cf<sup>252</sup>. It involves the development of chemical separation processes for these actinide elements, development of methods for producing HFIR targets, and design and construction of the Transuranium Processing Plant (TRU). The role of the Metals and Ceramics Division in the program is primarily that of fabricating the HFIR target elements, including development of suitable equipment for remote processing of the target in the TRU facility.

The aluminum-clad HFIR target rods, containing 200 to 300 g of Pu<sup>242</sup>, must be of absolute integrity and must be fabricated by completely remote methods in order to contain the alpha, beta, gamma, and neutron activity associated with various actinide oxides — a requirement heretofore not encountered in the manufacture of reactor core components. Consequently, a process and equipment development program is being pursued to establish the technology required for fabrication of the HFIR target rods in the TRU facility.

In the past year, prototype fuel pellets containing simulated actinide oxides mixed with aluminum were produced in laboratory equipment, and pellet-cleaning schemes were studied. A welding problem

in producing the second end closure in the target tubes was uncovered. Although not yet resolved, it appears that the problem is less severe with type X8001 aluminum than with type 1100 aluminum.

The hydrostatic collapse of aluminum tubes, both finned and unfinned, was studied as a function of external pressure. It was demonstrated that the target-rod end closure welds could be inspected by x radiography, background activity from the rod notwithstanding.

Conceptual design and layout in the three fabrication cubicles of the TRU were accomplished for virtually all of the target-rod fabrication equipment. Detailed designs were completed on such key items as the pellet press, die magazine, target loading device, transfer arm, hydrostatic vessel, pellet-cleaning device, and inspection equipment. Construction of the pellet press, pellet-cleaning apparatus, and hydrostatic vessel was initiated.

Since the initial HFIR targets will contain only alpha-emitting plutonium, a separate simplified fabrication facility can be used. Process flow-sheets were devised for this fabrication line, and the suitability of the operation for conventional glove boxes was assured. Procurement of commercially available equipment and redesign of some items from the TRU equipment line were initiated.

It is expected that construction of the TRU facility will begin in the coming year and that the process and equipment development will continue in a hot-cell mockup.

---

<sup>1</sup>Reported in detail or referenced in Part III, this report.

## 5. Thermonuclear Project

R. E. Clausing

The ultimate purpose of the thermonuclear project is to produce electrical power from the energy release by fusion of deuterium or deuterium and tritium nuclei. The basic problems associated with the attainment and confinement of high-temperature plasmas are under investigation. Two principal experimental machines, DCX-1 and DCX-2, incorporate a high-energy injection scheme in which 600-keV molecular ions are injected into a highly evacuated tank in the presence of a magnetic field. The ions are dissociated by arcs, residual gases, or previously trapped ions and are retained as atomic ions within the magnetic field.

The success of these and future experiments has required expansion of existing vacuum technology, which is under study in the Metals and Ceramics Division. A large getter-pump-test apparatus was operated to further explore the use of vapor-deposited metal films as vacuum pumps.<sup>1</sup> The equipment

and techniques developed allow the accurate measurement of adsorption rates approaching the theoretical maximums. Film deposition procedures were developed which give pumping speeds for hydrogen of more than 85% of that possible with a perfect adsorber. This is 25 times the value obtained in commercial titanium pumps by means of the common methods of evaporation.

The pumping characteristics of several kinds of evaporated titanium films were determined for a variety of gases in the pressure range  $3 \times 10^{-9}$  to  $5 \times 10^{-5}$  torr.

As power-producing devices are developed, research and development will be required to develop a blanket to surround the reaction volume, to remove heat, to shield against radiation, and perhaps to breed new fuel. Future work will also involve the study of materials and fabrication methods for superconducting electromagnets capable of producing very high magnetic fields, thus promoting the utilization of thermonuclear power.

---

<sup>1</sup>R. E. Clausing, *A Large-Scale Getter Pumping Experiment Using Vapor Deposited Titanium Films*, ORNL-3217 (Oct. 24, 1961).

## 6. Thorium Utilization Program<sup>1</sup>

W. C. Thurber

The development of fuel systems which use thorium instead of  $U^{238}$  as the fertile material in thermal and intermediate reactors has the near-term objective of reducing fuel cycle costs through the better neutron properties of  $U^{233}$  as compared with those of plutonium. Moreover, these improved properties result in higher conversion ratios, longer reactivity lifetimes, and greater burnup of recycled fuels. The long-term objective is that of achieving Th- $U^{233}$  conversion ratios of 1.0 or greater. The attractive features of thorium-based fuel systems are offset somewhat by the fact that thorium and  $U^{233}$  are radioactive after discharge from a reactor and must be recycled remotely. More practical experience and information on remote handling are required before a worthwhile evaluation of the potential of the Th- $U^{233}$  fuel cycle can be made.

In support of the near-term objectives, emphasis in the past year was placed on developing a process by which metal-clad fuel rods can be remotely fabricated with relative ease. The method selected to produce fuel rods was to compact coarse, dense fuel particles of  $ThO_2 \cdot UO_2$  with vibrational energy. It has been demonstrated that a chemically derived oxide distributed into three controlled size fractions can be compacted to bulk densities in excess of 88% of the theoretical value by using

simple, inexpensive pneumatic equipment. Densities in excess of 90% can be achieved with more sophisticated pneumatic devices. Methods of fuel material preparation and compaction that were thoroughly studied yielded information that was used to design equipment which can be operated semiremotely to fabricate 1000  $U^{233}$ -bearing fuel rods for critical experiments at Brookhaven National Laboratory.

In conjunction with the Chemical Technology Division an integrated Th- $U^{233}$  fuel rod facility with appropriate alpha and gamma shielding for semiremote operation was designed and is being constructed in which  $ThO_2 \cdot U^{233}O_2$  fuel can be synthesized, sized, vibrated into fuel rods, sealed by welding, and inspected.

Gamma-scanning techniques are being developed which will permit measurement of axial density variation and the absolute density of vibratory compacted fuel rods. Excellent correlation was obtained between the bulk density as determined by gamma scanning and the density from volumetric measurement and fuel weight. The method appears to be sensitive to axial density variations of less than 1%.

In exploiting the long-term potential of the thorium materials, studies were conducted on methods of producing  $ThO_2$  spheres for possible application in the fertile blanket of the reactor. Sintering studies demonstrated the effects of grain size, density, and pore structure on attrition resistance of these spheroidal pellets.

---

<sup>1</sup>Reported in detail or referenced in Parts II and III, this report.

## 7. Advanced Test Reactor<sup>1</sup>

R. J. Beaver

The Advanced Test Reactor (ATR), under construction at National Reactor Test Station, was designed to provide additional experimental loop irradiation space for the AEC testing program. Perturbed neutron fluxes exceeding  $10^{15}$  thermal neutrons  $\text{cm}^{-2} \text{sec}^{-1}$  and  $1.5 \times 10^{15}$  epithermal neutrons  $\text{cm}^{-2} \text{sec}^{-1}$  will be produced. The core configuration provides for nine flux trap regions in a geometry similar to that of a four-leaf clover, with one flux trap in each leaf, one at the intersection of the leaves, and one between each pair of leaves. The nominal power level will be 250 Mw. ORNL is supporting the design effort and has the responsibility of developing the fuel element technology.

The fuel element consists of 19 composite fuel plates mounted between two side plates to form a  $45^\circ$  segment of a right circular cylinder. This concept requires that each fuel plate contain a fuel section of a different width and that each composite plate be formed to its specific radius of curvature. In order to control the excess reactivity, boron must be intimately mixed with the fuel. Powder metallurgical techniques are being

used to process fuel cores using a uranium oxide and a boron compound dispersed in aluminum.

A significant number of fuel plates clad with type X8001-0 aluminum, the structural material initially selected, and containing a dispersion of 34 wt %  $\text{U}_3\text{O}_8$  have been fabricated. It was demonstrated that these 49-in.-long plates could be roll-bonded to the dimensional tolerances specified and they could be mechanically joined into an ATR fuel element array by roll swaging. Several plate and fuel element specimens were provided for associated testing programs.

A nondestructive testing study has established standards for examination of segregation of the fissile phase by radiographic and gamma-scintillation counting. Standards for examination of unbonded areas by ultrasonic through-transmission techniques were also prepared and evaluated for this application.

Tensile and creep data for annealed types X8001 and 6061 aluminum, as well as 10% cold-worked type X8001 aluminum, were obtained at temperatures ranging from 70 to 600°F. These data were also supported with measurements of the modulus of elasticity for these materials. Type 6061 aluminum was recommended as the cladding for the fuel plate because of its superior strength properties.

---

<sup>1</sup>Reported in detail or referenced in Parts II and III, this report.

## 8. Army Power Reactor Program<sup>1</sup>

R. J. Beaver

In support in the materials field to the Army Power Reactor program, effort was directed toward advancing the technology of  $\text{UO}_2$ -stainless steel dispersion fuels, as well as burnable poison and neutron absorber materials, the major core constituents of typical Army Reactor plants.

The initial core loading for the first Army Reactor, designated SM-1, was fabricated by the Metals and Ceramics Division. The fuel element consists of 18 composite plates containing a dispersion of 26.16 wt %  $\text{UO}_2$  and 0.13 wt %  $\text{B}_4\text{C}$  in type 302B stainless steel.

In the past year a fuel element from this reactor was subjected to postirradiation examination after a burnup of 45% of the  $\text{U}^{235}$  atoms. No damage was found which could have impaired its performance, but transgranular cracking which could not be accounted for was observed in the cladding. Corrosion was prevalent at the brazed joints, but did not appear to be catastrophic.

Completion of studies on irradiation damage to stainless steel-clad specimens containing 3 wt %  $\text{B}^{10}$  dispersed in iron revealed that dimensional

integrity was acceptable up to a  $\text{B}^{10}$  atom burnup of 6%. The possibility of attaining 8% burnup of the  $\text{B}^{10}$  atoms was indicated.

Examination of irradiated stainless steel-clad specimens containing dispersions of  $\text{Eu}_2\text{O}_3$  showed that no dimensional or microstructural changes had occurred after an exposure estimated to be as high as  $2 \times 10^{21}$  *nvt*. Although both the irradiated and unirradiated specimens with dispersions of  $\text{Eu}_2\text{O}_3$  in stainless steel containing more than 20 wt %  $\text{Eu}_2\text{O}_3$  are prone to crack when exposed to 500°F pressurized water, the  $\text{Eu}_2\text{O}_3$  does not appear to escape from the sample into the water.

In the development of improved dispersions of  $\text{UO}_2$  in stainless steel containing borosilicate glass as a burnable poison, the difficulty experienced previously in the borosilicate particles stringing was overcome, and substitution of spherical  $\text{UO}_2$  resulted in a definite improvement in microstructural homogeneity. Boron losses during fabrication were found to be negligible.

A method was developed for producing monoclinic  $\text{Eu}_2\text{O}_3$ , which is stable when heated to 2200°F. Differential thermal analysis techniques were also developed to determine the acceptability of  $\text{Eu}_2\text{O}_3$  as a dispersoid in stainless steel.

<sup>1</sup>Reported in detail or referenced in Part III, this report.

## 9. Maritime Program<sup>1</sup>

W. C. Thurber

The main objective of the Maritime program has been to evaluate nonsintered bulk  $\text{UO}_2$  fuel rods for potential use in future core loadings of the NS "Savannah" reactor. For propulsion the ship uses a 69-Mw, 20,000-shp pressurized water plant, with the water coolant operating at 1750 psi and 500°F. Fuel for the initial cores is sintered  $\text{UO}_2$  pellets in type 304 stainless steel cladding.

Fabrication studies have centered on vibratory compaction of fused and crushed  $\text{UO}_2$  in 0.5-in.-OD  $\times$  0.035-in.-wall stainless steel tubes. It was demonstrated that densities of 87 to 88% of theoretical could be readily achieved. With developed techniques, fuel rods for five in-pile experiments in a pressurized water loop, were manufactured and successfully irradiated. Supporting studies included investigation of gas evolution of  $\text{UO}_2$ , measurements of the coefficient of thermal expansion of swaged  $\text{UO}_2$ , and determination of the burst strength of swaged fuel tubes.

---

<sup>1</sup>Reported in detail or referenced in Part III, this report.

## 10. Enrico Fermi Reactor Program<sup>1</sup>

W. C. Thurber

The materials assistance to the Enrico Fermi Reactor program is concerned with the development of an improved fuel element for future operation of this 300-Mw (thermal) power plant located near Detroit, Michigan. The plant was designed and constructed by the Power Reactor Development Company to investigate the economic potential of the fast reactor concept for nuclear power production. Initially, it will be fueled with zirconium-clad 10 wt % Mo-U alloy pins and blanketed with stainless steel-clad 2.75 wt % Mo-U alloy pins. Because these fuel components exhibit dimensional instability on exposure to radiation at elevated temperatures, a new fuel element with greater burnup capability for service in 900°F sodium is required for future loadings.

The fuel elements proposed for core B of the reactor are brazed bundles of 14 stainless steel-clad plates, each fueled with a dispersion of 35 wt % spheroidal UO<sub>2</sub> in a type 347 stainless steel

matrix. The responsibility for developing procedures to fabricate these elements has been assigned to this division, while the fuel element design and test responsibility resides with Atomic Power Development Associates.

Fuel bundle fabrication studies demonstrated that the complex, closely dimensioned assembly containing approximately 120 separate parts can be produced by a single brazing operation. Dimensional control of the coolant channels to an average spacing of  $\pm 4\%$  can be readily maintained.

Suitable nondestructive examination techniques to assess the UO<sub>2</sub> homogeneity, detect unbonded areas, and measure the cladding thickness in individual fuel plates were devised. Eddy-current devices were developed to measure coolant-channel spacings and linear dimensions in generally un-accessible locations.

Procedures were developed by which spheroidal UO<sub>2</sub> particles can be characterized as to their resistance to fragmentation and stringering during fuel plate rolling. These methods can be used in fuel procurement specifications to ensure proper oxide quality.

---

<sup>1</sup>Reported in detail or referenced in Parts II and III, this report.

**Part II**  
**Materials Properties**

D. A. Douglas, Jr.

---



## 11. Corrosion Engineering

J. H. DeVan

### GAS-COOLED REACTOR MATERIALS COMPATIBILITY TESTS

J. H. DeVan      B. Fleischer

Impurities in helium-cooled, graphite-moderated reactors are derived both from the desorption of gases from graphite and from leakage of air, steam, or lubricating oils into the coolant stream. Studies were made to evaluate the types and amounts of impurities arising from each of these sources and their effects on reactor construction materials, principally graphite and ferrous alloys. Tests were conducted in large-scale stainless steel containment vessels or dynamic loop systems to simulate service conditions.

An adjunct of this investigation is concerned with the reaction from mating stainless steel with graphite surfaces in the presence or absence of gaseous impurities. These studies are intended to clarify the mechanism of adsorption and migration of carbon at stainless steel surfaces.

### Corrosion of Reactor Materials in Contaminated Helium

J. H. DeVan

Loop and capsule experiments were performed to study gas-solid reactions occurring between contaminated helium and construction materials used in high-temperature gas-cooled reactors.<sup>1-3</sup> The principal contaminants investigated in this program comprised combinations of the gases CO<sub>2</sub>, CO, H<sub>2</sub>O, H<sub>2</sub>, and CH<sub>4</sub>. Test specimens included several types of austenitic stainless steels, medium-alloy steels, and graphite, data being collected over the temperature range 600 to 1000°C

and generally at relatively low impurity partial pressures.

All phases of this program, except studies dealing with the interaction of graphite and type 304 stainless steel, have been completed. Test results can be summarized as follows:

1. At least two distinct oxide types were identified in exposures of type 304 stainless steel in static tests containing impurities desorbed from graphite. In tests in which gas-metal reactions served to establish relatively high CO/CO<sub>2</sub> ratios, the oxides were composed chiefly of Fe<sub>3</sub>O<sub>4</sub>. In all the other tests, the oxides were composed of 2Cr<sub>2</sub>O<sub>3</sub>·Fe<sub>2</sub>O<sub>3</sub>, with small amounts of MnO<sub>2</sub> and Cr<sub>2</sub>O<sub>3</sub>.

2. In tests simulating the temperature and environmental conditions of the Experimental Gas-Cooled Reactor, specimens of type 304 stainless steel fuel cladding exhibited carbon increases at all temperatures between 815 and 981°C. Carburation rates were highest in association with environments effecting oxide films of the type Fe<sub>3</sub>O<sub>4</sub>.

3. Significant grain growth and limited intergranular oxidation of type 304 stainless steel fuel cladding were consistently observed at cladding temperatures of 926°C or above.

4. The oxidation resistance of steels containing less than 7% Cr tended to be poor in simulated reactor atmospheres at 593°C, but was generally

<sup>1</sup>J. H. DeVan, *GCR Quart. Progr. Rept. June 30, 1961*, ORNL-3166, pp 167-68.

<sup>2</sup>J. H. DeVan and H. Inouye, "Reactions of Reactor Materials with Gaseous Contaminants in Helium-Cooled Reactor Systems," paper presented at the US/UK (AGR) Gas-Coolant Compatibility Meeting, Culcheth, England, April 4-5, 1962.

<sup>3</sup>J. L. Scott, *GCR Quart. Progr. Rept. Sept. 30, 1961*, ORNL-3210, pp 59-61.

satisfactory at 760°C. Oxidation of these materials in helium containing as little as 100 ppm CO<sub>2</sub> effected corrosion losses of approximately 0.07 in./yr.

5. Additions of CO<sub>2</sub>, CO, and H<sub>2</sub>O to helium loops operating at a hot-leg temperature of 593°C and at a cold-leg temperature of 260°C produced no measurable effects on graphite specimens held for 1000 hr at 593°C. (Maximum concentrations of CO<sub>2</sub> and H<sub>2</sub>O in certain of these tests ranged up to 1.0 and 0.15 vol %, respectively.) Similarly, graphite specimens at 760°C showed no significant weight losses following a 1000-hr exposure in a forced-convection loop to which had been added 0.07 cm<sup>3</sup> (liquid) of H<sub>2</sub>O per hour. In neither test series was carbon detected at cold-leg surfaces.

### Graphite-Metal Compatibility Studies

#### B. Fleischer

Compatibility problems arising from juxtaposition of graphite and metal surfaces at high temperature are being investigated as a function of surface temperature and contact pressure.<sup>3-5</sup> Initial tests were conducted with graphite and type 304 stainless steel couples under vacuum at temperatures between 540 and 700°C and with contact pressures ranging from 0 to 10,000 psi. Stainless steel specimens were pretreated to provide three surface conditions: hydrogen-fired, preoxidized, and copper-plated.

Diffusion anneals of 1000-hr duration in vacuum resulted in complete bonding between the hydrogen-fired surfaces and graphite at 650 and 700°C with contact pressures as low as 500 psi. At 600°C, partial bonding occurred, the effective area increasing with increasing contact pressure. At 540°C, neither bonding nor carburization could be detected metallographically, although an increase in carbon concentration was shown by chemical analysis of the stainless steel specimens.

Carbide precipitation below the stainless steel surfaces was extensive in bonded areas but was virtually absent in the nonbonded areas. When bonding occurred, diffusion rates of carbon in

stainless steel were comparable with those reported for stainless steel in carbon-saturated sodium. However, phases produced in surface reactions between graphite and stainless steel were of higher order than those reported for the sodium carrier.

Bonding and carburization were completely suppressed at all test conditions by the presence of either an oxide film or a copper plate.

### FLUORIDE SALT CORROSION STUDIES

J. H. DeVan

Molten fluoride salts, since they afford exceptional stability under irradiation and can be fused with fluorides of uranium and thorium, offer important advantages as high-temperature fuel solutions for nuclear reactors and as fuel processing media. Both applications have stimulated experimental studies of the corrosion processes by which molten-salt mixtures attack potential reactor materials. Current studies are directed at corrosion problems associated with the Molten-Salt Reactor Experiment (MSRE) under construction at ORNL. Investigations centered around the alloy system 17 Mo-7 Cr-5 Fe-bal Ni (wt %) (designated INOR-8) and the salt system LiF-BeF<sub>2</sub>. Tests utilized both large-scale forced-convection loops and smaller static systems.

#### Forced-Convection Loops

The concluding phase of the MSRE forced-convection-loop program was concerned with the effects of temperature on the corrosion rate of INOR-8 systems containing mixtures of the type LiF-BeF<sub>2</sub>-UF<sub>4</sub>-ThF<sub>4</sub>.<sup>6,7</sup> Table 11.1 compares the corrosion rates of INOR-8 measured in pumped loops operating with maximum temperatures ranging from 700 to 815°C. Weight losses of corrosion inserts in these systems remained at essentially constant values after 5000 hr. When judged from the standpoint of total weight loss, the temperature dependence of the corrosion rates was relatively small. The

<sup>4</sup>B. Fleischer, *GCR Quart. Progr. Rept. Dec. 31, 1961*, ORNL-3254, p 53.

<sup>5</sup>*GCR Quart. Progr. Rept. Mar. 31, 1962*, ORNL-3302 (in press).

<sup>6</sup>*MSR Progr. Rept. Mar. 1 to Aug. 31, 1961*, ORNL-3215, p 96.

<sup>7</sup>*MSR Program, Semiann. Progr. Rept. Feb. 28, 1962*, ORNL-3282 (in press).

Table 11.1. Corrosion Rates of Inserts Located in the Hot Legs of INOR-8 Forced-Convection Loops as a Function of Operating Temperature

Loop temperature gradient: 200°C  
Flow rate: 2.0 gpm  
Reynolds No.: 3000

Loop Number	Salt Mixture <sup>a</sup>	Insert Temperature (°C) <sup>b</sup>	Time (hr)	Weight Loss Per Unit Area (mg/cm <sup>2</sup> )	Equivalent Loss in Wall Thickness (μ)
9354-4	130	700	5,000	1.8	2.0
			10,000	2.1	2.3
			15,140	1.8	2.0
MSRP-14	Bu-14	700	2,200	0.7	0.8
			8,460	3.8	4.3
			10,570	5.1	5.8
MSRP-15	Bu-14	760	8,770	11.2	12.7
			10,880	10.0 <sup>c</sup>	11.2
MSRP-16	Bu-14	815	5,250	9.6	10.9
			7,240	9.0 <sup>c</sup>	9.1

<sup>a</sup>Composition 130: LiF-BeF<sub>2</sub>-UF<sub>4</sub>, 62-37-1 mole %; composition Bu-14: LiF-BeF<sub>2</sub>-ThF<sub>4</sub>-UF<sub>4</sub>, 67-18.5-14-0.5 mole %.

<sup>b</sup>Same as maximum wall temperature.

<sup>c</sup>Average of two inserts.

metallographic appearance of specimen surfaces, however, was noticeably affected by the test temperature. At the highest test temperature (815°C) exposed surfaces underwent a depletion of chromium, as evidenced by the appearance of sub-surface voids (Fig. 11.1). At lower temperatures the surfaces were only slightly pitted and were lined with a thin surface film, shown in Fig. 11.2. The composition of this layer indicates a higher Ni/Mo ratio than was originally present in the base metal and suggests that the layer may constitute an intermetallic transformation product of the Ni-Mo system.

#### Fluoride Salt Contamination Studies

Experiments are in progress to examine the effects of oxidizing impurities on the corrosion behavior of molten fluoride fuels and to establish tolerances for such impurities in the MSRE cover gas.<sup>7,8</sup> Initial studies are concerned with the

impurity HF, which may be formed through the hydrolysis of residual moisture by fluoride melts.

Preliminary experiments, which utilized INOR-8 thermal-convection loops containing the mixture NaF-ZrF<sub>4</sub> and dissolved HF, were unsuccessful because of precipitation of the corrosion product NiF<sub>2</sub> and subsequent plugging of the systems. Accordingly, the program was revised to utilize static capsules rather than circulating loops. Test equipment has been completed, and studies of HF-containing salts are continuing.

#### Corrosion Effects of CF<sub>4</sub>

Postirradiation examination of in-pile test capsules<sup>7</sup> (ORNL-MTR-47-3) disclosed the presence of CF<sub>4</sub> in the cover gas above graphite boats containing MSRE fuel. The escape of CF<sub>4</sub> might constitute a serious problem because of chemical changes simultaneously produced in the fuel. To circumvent this condition, an overpressure of CF<sub>4</sub> on the primary system would be required. To evaluate this expedient, experiments are under

<sup>8</sup>MSR Progr. Rept. Mar. 1 to Aug. 31, 1961, ORNL-3215, pp 99-100.

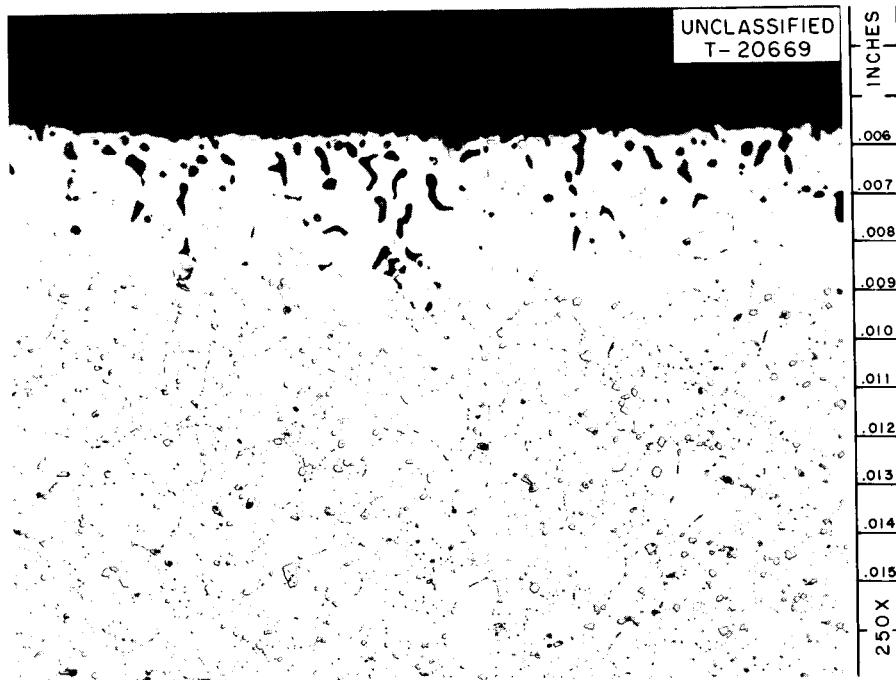


Fig. 11.1. Appearance of Specimen Removed from Point of Maximum Salt-Metal Interface Temperature ( $815^{\circ}\text{C}$ ) of INOR-8 Forced-Convection Loop MSRP-16. Operating time, 7240 hr; salt mixture,  $\text{LiF}-\text{BeF}_2-\text{ThF}_4-\text{UF}_4$ , 67-18.5-14-0.5 mole %.

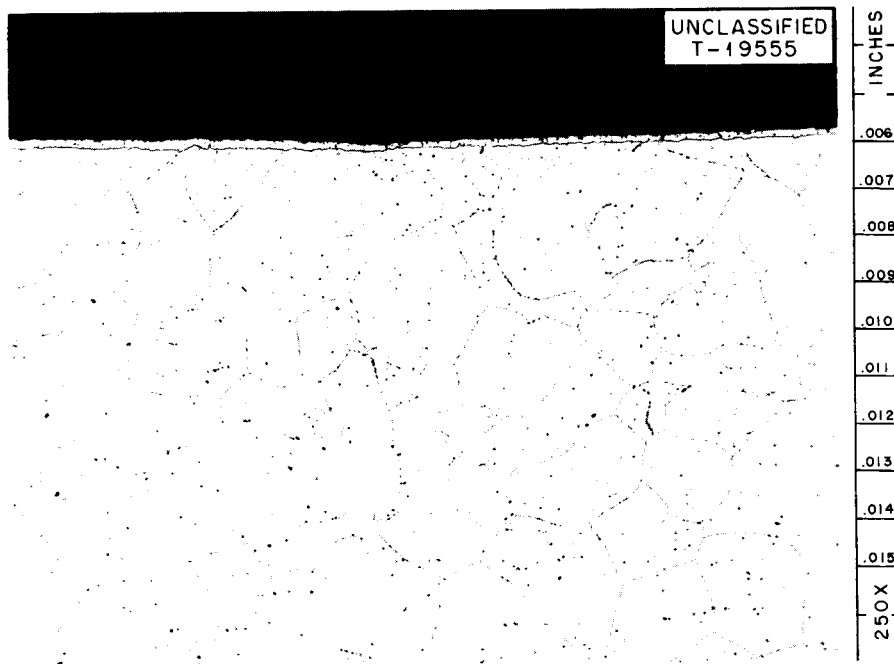


Fig. 11.2. Appearance of Metallographic Specimen from Point of Maximum Salt-Metal Interface Temperature ( $700^{\circ}\text{C}$ ) of INOR-8 Forced-Convection Loop 9354-4. Operating time, 15,140 hr; salt mixture,  $\text{LiF}-\text{BeF}_2-\text{UF}_4$ , 62-37-1 mole %.

way to determine the effects of  $\text{CF}_4$  exposure on MSRE core materials.

Tests carried out in the range 600 to 800°C showed little effect of  $\text{CF}_4$  vapor on INOR-8 graphite or nickel, although materials such as type 304 stainless steel, molybdenum, and Inconel

were heavily attacked. INOR-8 specimens at 800°C exhibit reaction films (identified as  $\text{NiF}_2$  and  $\text{CrF}_2$ ) less than 0.0001 in. in thickness following 500-hr exposures to  $\text{CF}_4$  vapor at 6 psig. Further tests of INOR-8 are being conducted in MSRE fuel salt saturated with  $\text{CF}_4$ .

## 12. Fuels Evaluation

J. L. Scott

R. E. Adams

R. A. Bowman

### COATED PARTICLES

Graphite elements containing  $UC_2$  particles coated with pyrolytic carbon are being evaluated in anticipation of their use in the Pebble Bed Reactor Experiment (PBRE), a 5-Mw experimental reactor proposed by ORNL for study of the essential features of this type of reactor concept. The rate of fission-product release is expected to be higher with the all-ceramic fuel elements proposed for the PBRE than with metal-clad fuel elements. Therefore a major phase of the evaluation program concerned the fission-product-retention characteristics of the particle coatings. Details of the neutron-activation technique used are given elsewhere.<sup>1</sup>

Small samples of unsupported  $UC_2$  particles coated with pyrolytic carbon obtained commercially were used in the experiments. The coatings varied from 50 to 100  $\mu$  in thickness and were of three characteristically different microstructures,<sup>2</sup> laminar, columnar, and duplex. X-ray diffraction patterns indicated all coatings to be of graphite of small crystallite size,<sup>3</sup> with the laminar coating showing as an apparently strained lattice.

To date, about 20 batches of coated particles have been examined,<sup>4-7</sup> and all three types of coatings were shown to be very retentive of fission-product gases when properly prepared: typical batches released only about  $1 \times 10^{-4}$  % of

$Xe^{133}$  in 3 hr at 1400°C. Some batches showed higher rates of  $Xe^{133}$  release, which, in general, resulted from either high uranium contamination on the surface or from fissures in the poorly prepared coatings. Those batches showing good fission-gas-retention properties at 1400°C also had excellent retention characteristics at 1800°C, but at 2000°C some of the coatings began to rupture. This rupturing is attributed to stresses resulting from differential thermal expansion between the  $UC_2$  core and the pyrolytic carbon coating. An exact correlation cannot be made, because information on the temperatures at which the coatings were applied to the particles has been withheld by the vendors.

Although the pyrolytic carbon coatings were very retentive with respect to xenon at 1800°C and below,  $Ba^{140}$  and  $Sr^{84}$  were released rapidly at 1400°C and above. Like  $Xe^{133}$ ,  $I^{131}$  and  $Te^{132}$  were released only when defective coatings were present. The more rapid diffusion of metallic fission products is attributed to the higher solubility of the metallic species in the carbon coatings, and causes concern that uranium might be somewhat soluble in the coatings and diffuse through them. This type of migration would not be detected by neutron-activation tests unless the diffusion anneals were done prior to the tests.

<sup>1</sup>D. F. Toner and J. L. Scott, *Am. Soc. Testing Materials, Spec. Tech. Publ. No. 306*, pp 86-99 (1961).

<sup>2</sup>C. K. H. DuBose and R. J. Gray, *Metallography of Pyrolytic Carbon Coated and Uncoated Uranium Carbide Spheres*, ORNL-TM-91 (Mar. 21, 1962).

<sup>3</sup>O. B. Cavin, X-Ray Diffraction Group.

<sup>4</sup>J. L. Scott *et al.*, *GCR Quart. Progr. Rept. June 30, 1961*, ORNL-3166, pp 86-89.

<sup>5</sup>D. F. Toner and J. L. Scott, *GCR Quart. Progr. Rept. Sept. 30, 1961*, ORNL-3210, pp 138-46.

<sup>6</sup>J. L. Scott *et al.*, *GCR Quart. Progr. Rept. Dec. 31, 1961*, ORNL-3254, pp 145-48.

<sup>7</sup>"Fuels Evaluation Section," *GCR Quart. Progr. Rept. Mar. 31, 1962*, ORNL-3302 (in press).

When the coated particles were incorporated into a fuel element, the rate of  $Xe^{133}$  release determined by neutron activation was, in general, much higher than that for the coated particles themselves.<sup>5</sup> One explanation for this anomaly was suggested by the correlation found between the pressures used in compacting the bodies and the release of  $Xe^{133}$ . This possibility was confirmed by metallographic examination<sup>8</sup> of one of the poorest elements, which contained about 1% of particles with defective coatings. In many other fuel elements, only one or two particles out of several thousand were broken, and one fuel element showed as good fission-gas-retention properties as the starting materials.<sup>6</sup>

To further substantiate the presence of particles with defective coatings, after the postirradiation anneals a number of the fuel elements were exposed at room temperature to helium containing 0.6% water vapor. In a number of instances xenon continued to be released because of the hydrolysis of the exposed  $UC_2$ , but in other instances fuel elements showing some  $Xe^{133}$  release on annealing showed no further release on exposure to the moist helium. The source of the xenon in these tests is thought to be uranium contamination in the graphite matrix.

Another explanation for the increased  $Xe^{133}$  release from the fuel elements is the possibility of uranium migration to the surface. Several fuel elements were annealed prior to neutron activation to test this idea. The results are incomplete, but good evidence was found for the migration of uranium through laminar coatings in 20 hr at 1700°C<sup>7</sup> and through duplex coatings in 24 hr at 2000°C. Long-time tests at lower temperatures are now in progress.

## UNCOATED PARTICLES

In an attempt to determine the mechanisms of xenon release from particles with defective coatings, neutron-activation tests were done on uncoated  $UC_2$  particles in the range 1000 to 2000°C. The so-called "uncoated" particles actually had a 10- to 15- $\mu$ -thick permeable coating of graphite on the external surfaces. This thin graphite coating forms, during the production of  $UC_2$ , from excess carbon. Some graphite and UC are also present in the  $UC_2$  matrix.

The release of  $Xe^{133}$  from the uncoated particles was characterized by an initial rapid release followed by diffusion-controlled release.<sup>7-9</sup> The initial release is probably due to the release of some of the recoils from the graphite shell. The diffusion-controlled release is thought to be due to combined diffusion from the coating and the  $UC_2$  in the range 1000 to 1800°C. At higher temperatures the graphite layer is depleted of xenon, and diffusion from  $UC_2$  is the rate-controlling step. The activation energy for the combined diffusion processes was found to be about 20 kcal/mole and that for diffusion from  $UC_2$  to be roughly 37 kcal/mole.

Other fission products<sup>7</sup> released from uncoated particles and the lowest temperature at which detectable amounts were found in samples containing a total of about  $10^{15}$  fissions were  $I^{131}$ , <1000°C;  $Te^{132}$ , <1000°C;  $Ba^{140}$ , 1050°C;  $Sr^{89}$ , <1000°C;  $Ru^{103}$ , 1600°C; and  $Nd^{147}$ , 2000°C. An isotope of particular importance,  $Cs^{137}$ , could not be detected, as a result of the low burnup of the neutron-activated fuel samples. A new apparatus is being developed for more carefully controlled studies of fission-product release, transport, and deposition from fueled graphite.

<sup>8</sup>E. L. Long, Jr., Metallography Group.

<sup>9</sup>J. L. Scott *et al.*, *GCR Quart. Progr. Rept. Dec. 31, 1961*, ORNL-3254, pp 151-53.

## 13. Materials Compatibility

E. E. Hoffman

### ALKALI-METAL CORROSION STUDIES

E. E. Hoffman

The physical properties of alkali metals make them highly desirable as nuclear coolants and heat-transfer media. Unfortunately, the hazards associated with any leakage of these fluids as well as their corrosive nature have curtailed their extensive use. In most cases, utilization has been limited to those systems in which no other heat-transfer fluid meets the requirements. For several years this group has been studying various facets of the corrosion problems inherent in containing flowing alkali metals at high temperatures. During the past year, investigations were conducted on the optimum techniques for removing nonmetallic impurities and the development of suitable analytical procedures for determining the purity of alkali metals, on the relation between oxygen distribution and corrosion of refractory metals in contact with lithium, and on the use of a nickel-base alloy for containing boiling potassium.

#### Alkali-Metal Purification

A. P. Litman

Impurities, such as oxygen, nitrogen, and carbon, in alkali metals may cause alteration of the properties of container materials, affect mass transfer, or cause plugging due to precipitation of alkali-metal impurity compounds. Studies of methods<sup>1</sup> for purifying the alkali metals have

<sup>1</sup>E. E. Hoffman, *Corrosion of Materials by Lithium at Elevated Temperatures*, ORNL-2924 (Oct. 3, 1960).

included low-temperature filtration, cold trapping, vacuum distillation, and gettering with active metals. Recent investigations by this group point to gettering, combined with low-temperature filtration in some cases, as the most practical and efficient method for lowering the oxygen content of the alkali metals. The gettering technique relies on the relative thermodynamic activity of the oxygen in the alkali metal vs that of the solid metal. Therefore an oxygen distribution coefficient exists between the getter and the alkali metal. The coefficient and the system kinetics are important factors in the purification process.

For purification, solubility, and corrosion studies, accurate analytical procedures are needed for several impurities. The lack of such procedures, especially for oxygen in the alkali metals, has seriously hampered progress in the areas of investigation mentioned above. For example, the correlation between the methods used in determining oxygen in potassium was poor, and when controlled oxygen additions were made, all the oxygen was not extracted from the potassium samples. A comprehensive review<sup>2</sup> of existing analytical methods verifies the need for better techniques. An improvement may result from forthcoming modifications to the analytical equipment, revision of present sampling procedures, and advanced studies on a gettering vacuum-fusion method investigated a few years ago.<sup>3</sup>

<sup>2</sup>C. R. F. Smith, *The Determination of Oxygen in Sodium - A Critical Review of Analytical Methods*, NAA-SR-Memo-2061 (April 1960).

<sup>3</sup>P. H. Goble, W. M. Albrecht, and M. W. Mallett, "Determination of Oxygen in Sodium," *Progress Relating to Civilian Applications During 1957*, BMI-1173, p 67 (February); BMI-1181, p 70 (April); BMI-1189, p 59 (May); BMI-1201, p 55 (June).

## Corrosion of Refractory Metals by Lithium

J. R. DiStefano

Lithium has long been under consideration for application as a heat-transfer fluid in nuclear reactors because of its attractive physical and nuclear properties. Early static corrosion test data<sup>4</sup> and solubility studies<sup>5</sup> indicated that the refractory metals are more resistant to dissolution and other types of liquid-metal corrosion than are the more conventional materials of reactor construction. In addition, extensive lithium studies<sup>1</sup> in both static and dynamic test systems on a wide variety of metals and alloys indicated that only the refractory metals would be suitable for application in dynamic, nonisothermal systems operating at temperatures in excess of 650°C.

More recent investigations have shown, however, that although the pure metals niobium, tantalum, vanadium, and zirconium exhibit excellent resistance to attack by lithium at temperatures even in excess of 800°C, the presence of small quantities of oxygen in either niobium or tantalum can lead to a very rapid penetration of these metals by lithium over a wide range of temperatures. Vanadium and zirconium, on the other hand, showed no attack when contaminated with oxygen to levels of 2000 and 4000 ppm, respectively.

In an effort to understand the mechanism of attack by lithium, studies were concentrated during the past year on the Nb-Li system. It was found that the interaction between molten lithium and oxygen-contaminated niobium results in the formation of a corrosion product most often found in grain boundaries or along {110} planes. The product was found to contain lithium and oxygen, but no further identification was made. The major variables affecting the extent of lithium penetration of niobium were found to be oxygen concentration and temperature. Time was a relatively insensitive variable in the sense that the maximum depth of corrosion generally occurred in from 1 to 5 hr.

In addition to lithium penetration, a transfer of oxygen was observed in all the refractory-metal-lithium systems investigated. Oxygen transfer

appears to occur according to Nernst's law of distribution of a solute between two immiscible solvents:  $K = a_A/a_B$ , where  $a_A$  is the activity of the solute in solvent A,  $a_B$  is the activity of the solute in solvent B, and  $K$  is a constant (at a given temperature), called the "distribution coefficient." The data are insufficient at this time to permit the calculation of the various distribution coefficients; however, the qualitative extent of gettering was observed to be in agreement with that predicted by the standard free energies of formation for the various oxides of the solid metals and lithium oxide.

The results presented in this section will be reported in considerable detail.<sup>6</sup>

## Boiling-Potassium Studies

E. E. Hoffman

D. H. Jansen

The use of a boiling alkali metal as the working fluid in a Rankine cycle turbogenerator power system has been proposed as a method of producing electrical power for use in space systems. Potassium has been judged to be one of the more attractive fluids for this application. Current research is directed toward a correlation of compatibility information developed in the past in single-phase (liquid) test systems with the corrosion phenomena observed in two-phase (liquid-vapor) systems.

The studies were begun with a nickel-base alloy, Inconel, as the container material because considerable sodium corrosion data are available on this alloy. The test loop, Fig. 13.1, was operated for 1500 hr under the temperature conditions indicated. Examination of the boiling-liquid loop after test indicated the same types of corrosion observed previously in circulating-liquid tests: dissolution of the container, mass-transfer crystal deposition, and carbon transfer. The principal difference noted was the concentration of some of these effects in localized areas. A much greater concentration of carbon occurred in certain regions of the two-phase loop than had

<sup>4</sup>A. de S. Brasunas, *Interim Report on Static Liquid-Metal Corrosion*, ORNL-1647, pp 32-44 (May 11, 1954).

<sup>5</sup>U. F. Bychkov, A. N. Rozanov, and V. P. Yakobleva, *Atomnaya Energ.* 7(6), 531-36 (1959).

<sup>6</sup>J. R. DiStefano and E. E. Hoffman, "Relation Between Oxygen Distribution and Corrosion in Some Refractory Metal-Lithium Systems," paper to be presented at the International Conference on the Corrosion of Reactor Materials, Salzburg, Austria, June 4-9, 1962; transactions to be published by International Atomic Energy Agency.

been noted in the single-phase loops. A typical example of the degree to which this occurred is shown in Fig. 13.2. Concentration of mass-transfer products was localized as illustrated by the weight-change profile in Fig. 13.3. The sharp temperature gradient in the potassium just below the liquid-vapor interface in the subcooler section resulted in a more localized concentration of

deposits than is usually noted in single-phase loops. Some metal crystal deposition also occurred on the boiler wall as a result of solute element buildup caused by the concentrating effects of the distillation process. Thus, although no new phenomenon was uncovered, it is apparent that some of the corrosion mechanisms will tend to be aggravated in a boiling system.

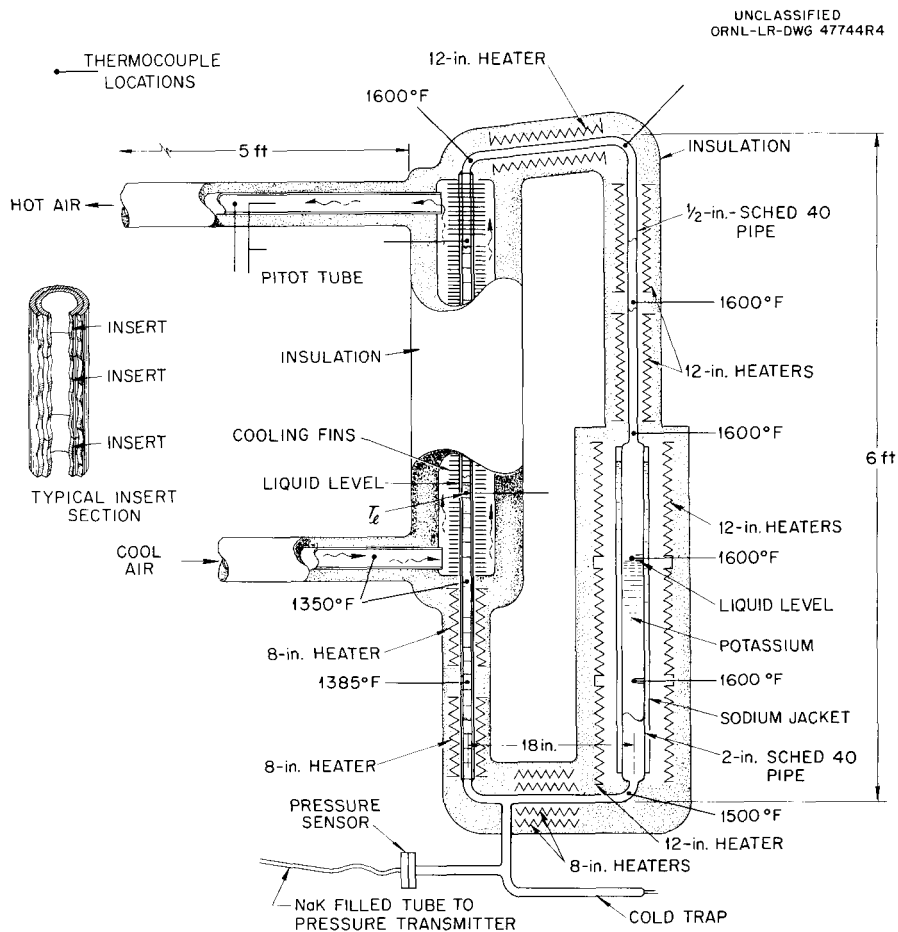


Fig. 13.1. Boiling-Potassium Loop.

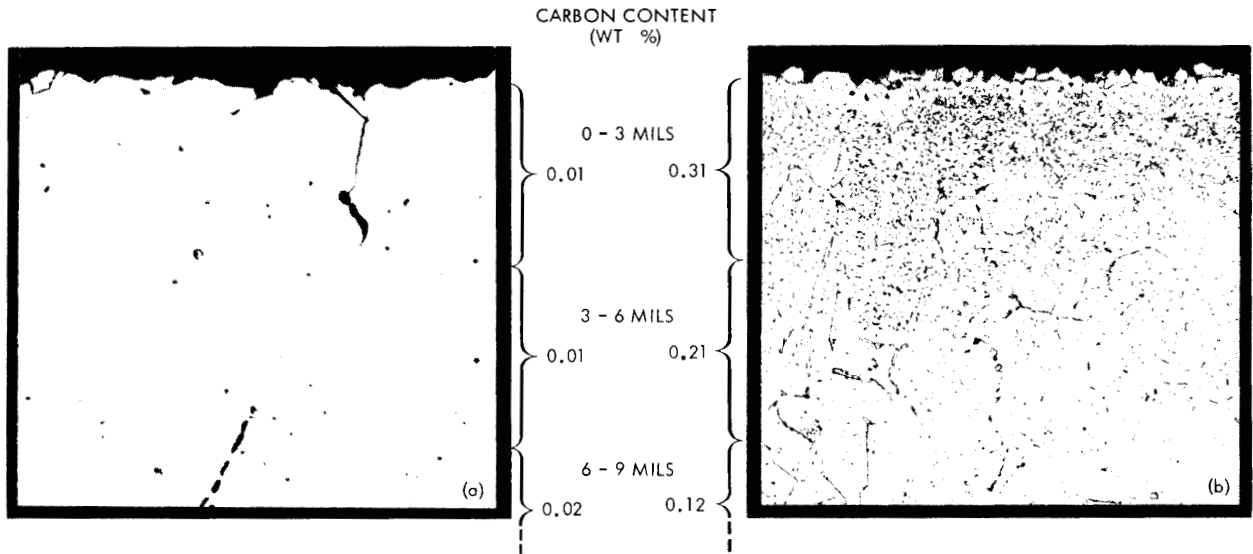


Fig. 13.2. Inconel Inserts from (a) Condensing Region and (b) Subcooled Liquid Region of Condenser from Inconel-Boiling-Potassium Loop Showing Carbon Gradient in the Two Regions. Loop test conditions: time, 1500 hr; boiler temperature, 1600°F.

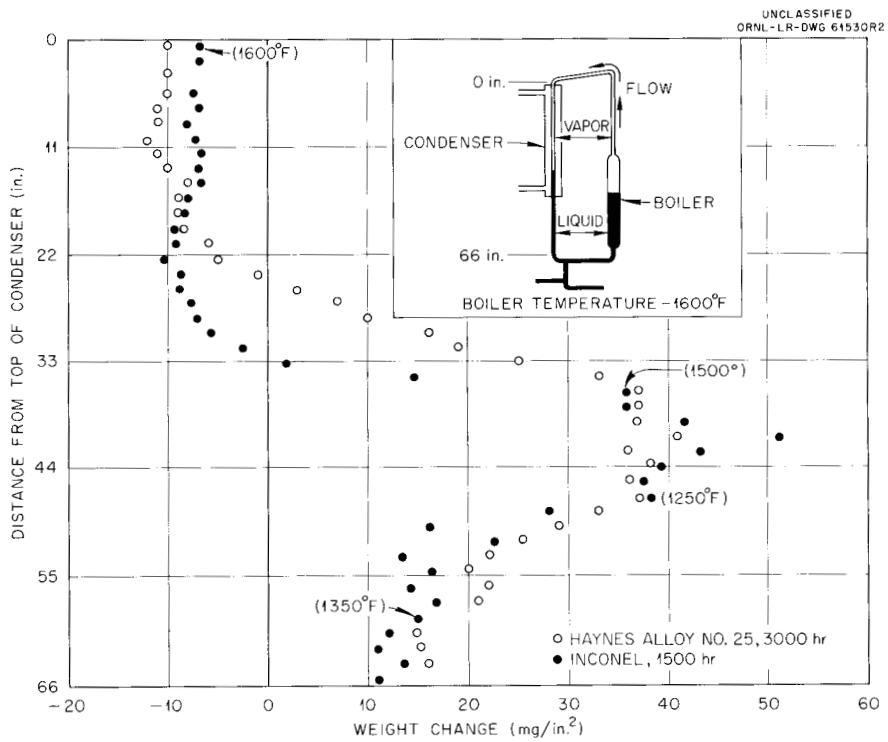


Fig. 13.3. Profile of Weight Change of Inconel Inserts in Condenser Leg of Inconel-Boiling-Potassium Loop.

## GRAPHITE-MOLTEN FLUORIDE SALT STUDIES

W. H. Cook

### MSRE-Type Graphite

A  $2\frac{1}{2} \times 2\frac{1}{2} \times 15$ -in. sample cut from a treated and fully graphitized 4-in.-diam graphite cylinder was evaluated with respect to the MSRE<sup>7</sup> and met or approached essentially all the requirements. The graphite, grade CGB-X, was found to be deficient only in that it had an average bulk density of 1.83 g/cc, whereas the requirement for the MSRE graphite bars is 1.87 g/cc, minimum. The requirements of chemical purity,<sup>8</sup> oxygen contamination, and permeation by mercury and by molten fluoride salts<sup>8</sup> were met. In two tests the graphite developed an average equilibrium pressure with 28 cc (STP) of CO per 100 cc of graphite when heated to 1800°C in a system initially evacuated to  $<10^{-3}$  torr at room temperature. The limit set for the MSRE graphite bars is 30 cc (STP) of CO under these conditions.

Pertinent findings<sup>8</sup> exclusive of specifications were that the pore structure tended to be heterogeneous but that 98% of the accessible porosity had pore-entrance diameters of less than 0.35  $\mu$ . The smallness of these pore-entrance diameters kept the nonwetting molten-fluoride salt from permeating the graphite. In general, the salt permeation tended to be restricted to a shallow penetration, less than 0.01 in., below the surfaces in contact with the molten salt under a pressure approximately three times that expected in the MSRE. An isolated penetration to a depth of 0.18 in. was found in a random sample of a test specimen that had the largest salt permeation.

<sup>7</sup>H. G. MacPherson *et al.*, ORNL CF-57-4-27 (Apr. 29, 1957) (classified).

<sup>8</sup>MSR Program Semiann. Progr. Rept. Feb. 28, 1962, ORNL-3282 (in press).

The graphite bars fabricated for the MSRE should equal or surpass the properties of grade CGB-X graphite.

### Ammonium Bifluoride as Oxygen-Purging Agent for Graphite

**Removal of Oxygen from Graphite.** – Oxygen contamination of graphite has been observed to cause precipitation of  $UO_2$  in some graphite-fluoride salt systems.<sup>9,10</sup> Tests have indicated<sup>8</sup> that oxygen can be removed from moderately permeable grades of graphite by exposing them for 20 hr to the thermal decomposition products of crystals of ammonium bifluoride,  $NH_4F \cdot HF$ , at temperatures as low as 200°C. Purging tests were conducted at 200, 400, 500, 600, and 705°C.

**Reactions and Effects on INOR-8.** – Reaction layers formed on 0.040-in.-thick tensile specimens that were included in the purging tests at 500, 600, and 705°C. The thickest layer was approximately 0.005 in. and was formed at the highest purging temperature. This reaction layer did not alter the tensile properties at room temperature or at 675°C.<sup>11</sup>

### Permeation of Mercury and Molten Fluoride Salts

Tests on ten grades of graphite having porosities ranging from low to high indicated that a simple mercury-impregnation test at room temperature is suitable for quality control for various grades of graphite because it can be related to the standard molten-fluoride-salt permeation screening test.<sup>8</sup>

<sup>9</sup>MSRP Quart. Progr. Rept. Jan. 31, 1959, ORNL-2684, p 80.

<sup>10</sup>W. H. Cook, *Met. Div. Ann. Progr. Rept.* July 1, 1960, ORNL-2988, p 227.

<sup>11</sup>MSRP Progr. Rept. Mar. 1 to Aug. 31, 1961, ORNL-3215, p 115.

## 14. Mechanical Properties

J. R. Weir

### MECHANICAL PROPERTIES OF TYPE 347 STAINLESS STEEL-UO<sub>2</sub> CERMET

J. T. Venard      R. W. Swindeman

A program is in progress to determine certain mechanical properties of the type 347 stainless steel-UO<sub>2</sub> cermet that is to comprise the Enrico Fermi core B fuel. To date, the investigation has covered the elastic modulus vs temperature, tensile properties vs temperature, and strain cycling at 1150°F and 120 cpm.

Figure 14.1 is a plot of the elastic modulus of type 347 stainless steel and type 347 stainless steel-UO<sub>2</sub> vs temperature. Since the UO<sub>2</sub> comprises approximately 20 vol %, it is interesting that a line corresponding to 80% of the elastic modulus for type 347 stainless steel fits well with values for the cermet. The tensile properties of this material are shown in Fig. 14.2. Metallography has shown the UO<sub>2</sub> dispersion particles to be interconnected somewhat by a complex network in the type 347 stainless steel matrix. The UO<sub>2</sub> would be expected to act as a brittle boundary aligned normal to the stress applied (in the transverse direction) and would be expected to fracture at low strains. The load is therefore transferred almost entirely to the type 347 stainless steel matrix. Further deformation of the matrix results in high localized stresses (and therefore strains) at particle-matrix interfaces. The end result of these effects is that the tensile strength, yield strength, and ductility are lower than those of type 347 stainless steel.

Strain-cycling tests run at 120 cpm and 1150°F indicated that the strain-fatigue curve can be represented by

$$N^{1/2} \epsilon_p = C,$$

where  $N$  is the number of cycles to failure,  $\epsilon_p$  is the plastic strain range, and  $C$  is a constant equal to approximately 0.19. Further work in this area is in progress.

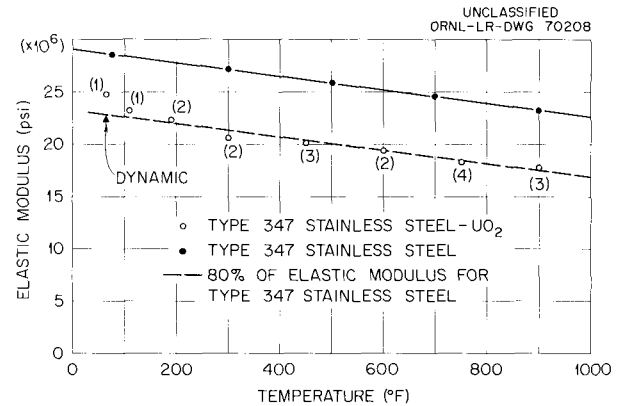


Fig. 14.1. Comparison of Modulus of Type 347 Stainless Steel and UO<sub>2</sub>-Dispersed Stainless Steel.

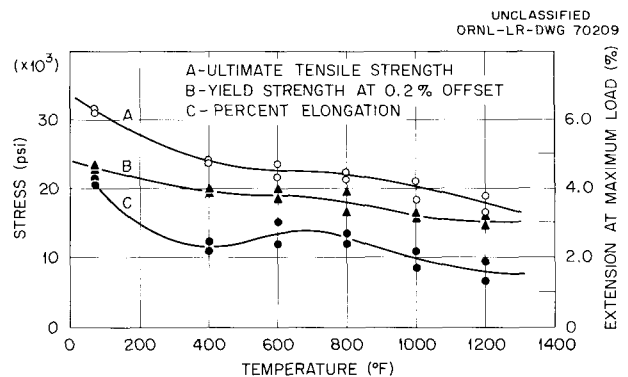


Fig. 14.2. Tensile Properties of 20 vol % UO<sub>2</sub>-Type 347 Stainless Steel Bare Plate Transverse to Rolling Direction. Annealed at 1150°C for 1 hr in hydrogen and then furnace-cooled.

## MECHANICAL PROPERTIES OF ALUMINUM ALLOYS 6061 AND X8001

W. R. Martin

Selection of a suitable cladding material for the fuel element plates of the Advanced Test Reactor (ATR) required the determination of the mechanical properties of several aluminum alloys at elevated temperatures.

Two aluminum alloys, 6061-0 and X8001, were chosen for mechanical property tests after consideration of fabrication, corrosion, and strength requirements of the fuel elements. The tensile properties, elastic moduli, and isochronous stress-strain curves in the strain range 0 to 1% were generated for both alloys in the annealed condition at 400, 500, and 600°F. A cursory examination was made of the creep properties of 10 and 15% cold-worked aluminum X8001 (approx H14 to H16) at 400 and 500°F.

The results, as summarized in Table 14.1, indicate that the time-dependent deformation properties of alloy 6061-0 in the range 400 to 600°F are superior to those of alloy X8001. The tensile and short-time-creep strengths of alloy X8001 were increased by cold working in the range 10 to 15% compared with those of the annealed material, but were significantly less than those of alloy 6061-0. The recovery of the cold-worked alloy X8001 during creep testing at the lowest temperature investigated, 400°F, was sufficient to reduce the 100-hr isochronous stress-strain data to values within experimen-

tal error for the same material in the annealed condition. These experiments complete the mechanical property program on testing of ATR cladding alloys.

## DIMENSIONAL STUDIES OF EGCR-TYPE FUEL ELEMENTS AT ELEVATED TEMPERATURES

W. R. Martin

The dimensional studies of fuel elements during thermal cycling are being investigated at thermal and pressure conditions predicted for the Experimental Gas-Cooled Reactor (EGCR). Previous studies showed that plastic deformation of the cladding can occur as a result of cycling. These studies of the fuel elements consisting of cored UO<sub>2</sub> fuel pellets clad with 0.020-in. type 304 stainless steel did not result in a single event that could be interpreted as a fuel element failure.

In advanced concepts of gas-cooled reactor fuel elements, beryllium may be used as the cladding material or the thickness of the stainless steel cladding may be decreased. Experimental programs related to these two areas are in progress. The results obtained thus far indicate the following:

1. The low ductility of the finned beryllium tubing at temperatures below 500°F requires that a radial clearance exist between cladding and fuel to prevent the introduction of strain in the clad by the fuel. An example of a finned beryllium-clad fuel element failure due to fuel-cladding interaction is shown in Fig. 14.3.

Table 14.1. Typical Isochronous Stress-Strain Data for Aluminum Alloys 6061 and X8001 at Elevated Temperatures

Type of Material	Stress (psi) Necessary To Produce 0.1% Strain in a Given Time at Various Temperatures					
	400°F		500°F		600°F	
	100 hr	450 hr	100 hr	450 hr	100 hr	450 hr
X8001-0	1325	1050	750	620	325	200
X8001, 10% cold-worked	1650	1100	850			
X8001, 15% cold-worked	1650	1100	750			
6061-0	5200	4600	2900	2300	1500	1150

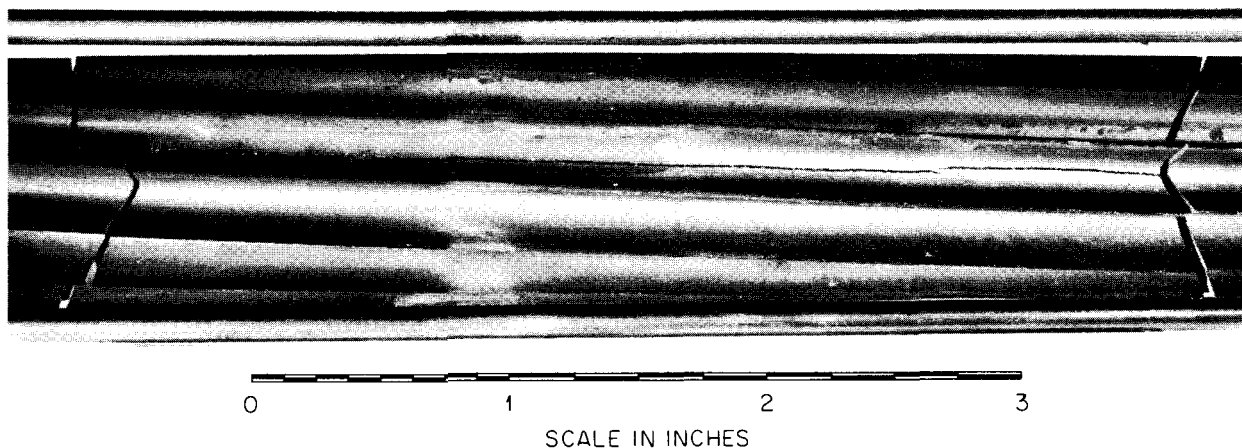


Fig. 14.3. Finned Beryllium-Clad  $\text{UO}_2$  Fuel Element Fractured Due to Thermal Expansion of Fuel During Thermal Cycling.

2. Reduction in the thickness of stainless steel cladding does not greatly increase the axial plastic deformation of the cladding during cycling. However, one of the problems associated with the thin-wall tubing is instability under external pressure at elevated temperatures. With an initial radial clearance of 0.004 in., stainless steel claddings 0.005 and 0.010 in. in thickness buckled in a nonuniform manner under external pressure. As a result, the metal failed in subsequent thermal cycling. Thus the diametral clearance between fuel and cladding must be reduced below some critical value to ensure a uniform collapse.

These data indicate that in all concepts of beryllium-clad fuel elements interaction of fuel and cladding must be prevented until the basic problem of low-temperature ductility is solved. If the thickness of stainless steel cladding is reduced, a material less embrittled by irradiation will be required. The lower limit of cladding thickness will depend upon the smallest diametral clearances that will allow loading of the fuel into the cladding and yet prevent nonuniform buckling of the tube under reactor conditions.

## COLLAPSE OF CYLINDERS UNDER EXTERNAL PRESSURE

J. T. Venard      C. R. Kennedy

The problem of the possible collapse of reactor piping subjected to periods of external pressure loading has led to an investigation of the tube collapse phenomenon.

A graphical solution developed to simplify inelastic collapse design problems was shown to agree with test results. The von Karman reduced modulus was used in the graphical solution to correct for the stress redistribution due to yielding. The effects of the geometric imperfections of ovality and wall-thickness variations on collapse pressure were shown to be related to the stress-strain behavior of the material.

Figure 14.4 is representative of the excellent correlation of the stress-strain behavior with experimental collapse data. These data and a discussion of the concept of "critical time" in creep-buckling behavior are presented in detail elsewhere.<sup>1</sup>

<sup>1</sup>C. R. Kennedy and J. T. Venard, *Collapse of Tubes by External Pressure*, ORNL-TM-166 (April 1962).

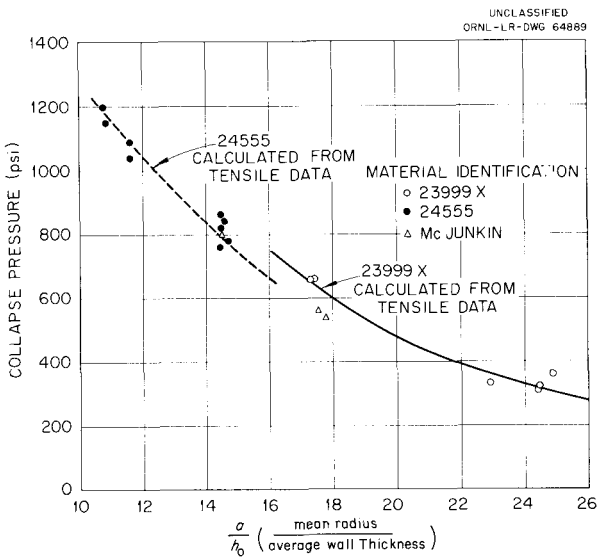


Fig. 14.4. Instantaneous Collapse Pressure vs  $a/b_0$ . Curves calculated from tensile data.

### STRESS RUPTURE OF TYPE 304 STAINLESS STEEL TUBING

J. T. Venard

The use of the Dorn parameter in correlating stress-rupture results of type 304 stainless steel was reported previously.<sup>2</sup> This correlation, along with experimental results, is shown in Fig. 14.5 for 1100, 1200, 1300, 1400, 1500, 1600, and 1800°F.

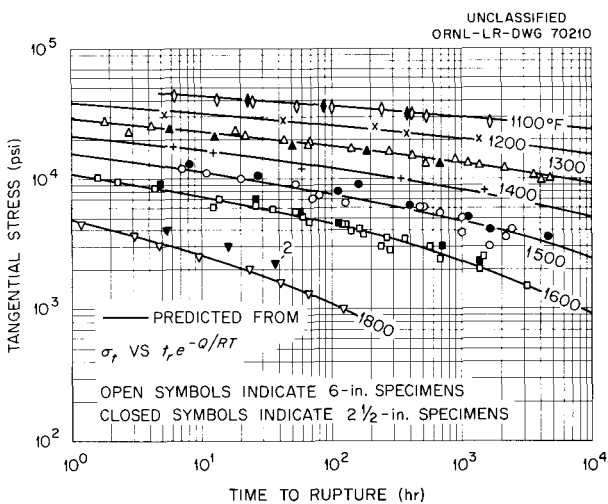


Fig. 14.5. Type 304 Stainless Steel Tube-Burst Data for As-Received Specimens Tested in Air Compared with Data Predicted from  $\sigma_t$  vs  $t_r e^{-Q/RT}$ .

No size effect is seen except at 1800°F, where increased ductility of the material causes end effects to become appreciable in the 2½-in.-long specimens.

The ex-pile testing of specimens from heat 23999X is essentially complete and will be reported in detail in a topical report.

### STRESS RUPTURE OF Nb-1% Zr TUBING

R. L. Stephenson

The ex-pile tube-burst properties of Nb-Zr alloys are being studied to provide control data for comparison with the results of in-pile tube-burst studies. Thus far, the stress-rupture curves for specimens from two heats of Nb-1% Zr alloy tubing have been determined. Figures 14.6 and 14.7 give the stress-rupture curves at 1800 and 2000°F for heats T-25 and PGVE, respectively.

<sup>2</sup>J. T. Venard, *GCR Quart. Progr. Rept. Sept. 30, 1961*, ORNL-3210, p 177.

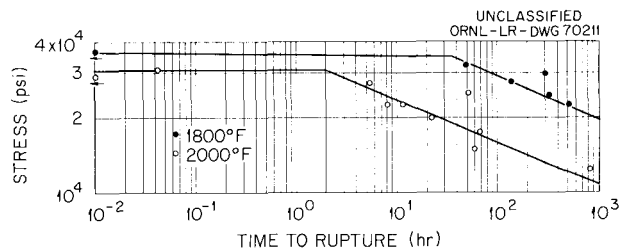


Fig. 14.6. Tube-Burst Strength of Nb-1% Zr Alloy (Heat T-25).

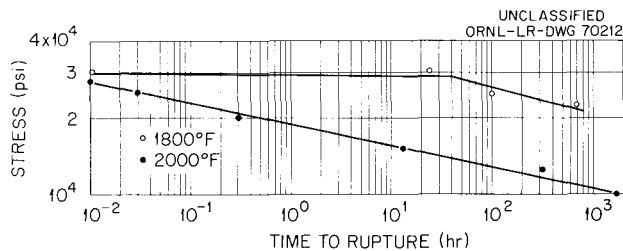


Fig. 14.7. Tube-Burst Strength of Nb-1% Zr Alloy (Heat PGVE).

## BERYLLIUM IRRADIATION EFFECTS

J. R. Weir      J. W. Woods

Radiation effects in beryllium that produce changes in its mechanical properties at temperatures above room temperature are due primarily to the helium generated in the beryllium by the  $(n, 2n)$  and  $(n, \alpha)$  reactions. Experiments performed previously to determine some of the effects on certain mechanical properties have been reported.<sup>3</sup>

A few in-pile stress-rupture experiments were performed during the past year on beryllium having a fabrication history differing from that of material tested previously. These experiments showed that the effects in warm-extruded tubing are smaller than those observed in tubing produced by hot pressing and hot extrusion. The latter tubing showed a 20% decrease in stress-rupture strength at a fast flux of  $2 \times 10^{20}$  *nv*, whereas the decrease exhibited in a few in-pile tests of warm-extruded tubing under similar conditions was of the order of 10%.

In-pile stress-rupture experiments conducted at 520°C on tubing produced by hot pressing and by warm extrusion showed no effect of irradiation to integrated fast flux in the range 1 to  $3.4 \times 10^{20}$  *nv*. Although the strength at 520°C appeared to be unaffected by irradiation, the fracture strains observed in the hot-pressed tubes after irradiation were 0.5 to 2.5% as compared with values of 1.0 to 4.0% in unirradiated tubes. The warm-extruded tubing exhibited fracture strains of 2.0 to 3.6% in irradiated tubes and values of 1.5 to 3.5% in unirradiated tubes. It appears that only small effects on the stress-rupture ductility at 520°C are produced by irradiation to these levels of neutron exposure.

<sup>3</sup>J. R. Weir, "The Effect of High-Temperature Reactor Irradiation on Some Physical and Mechanical Properties of Beryllium," paper presented at the Institute of Metals Conference on the Metallurgy of Beryllium held at the Royal Commonwealth Society, London, October 16-18, 1961; proceedings to be published by the Institute of Metals, London.

## MECHANICAL PROPERTIES OF BERYLLIUM

J. W. Woods

The proposed use of beryllium-clad fuel elements in gas-cooled reactors presents a serious problem because of the low-fracture ductility in the transverse direction in tubing at low temperatures. This problem is increased by the differences in coefficients of thermal expansion of beryllium and of uranium dioxide. Upon cooling or during nuclear heating of the fuel elements, the cladding may be subjected to tensile strains of the order of the fracture strain.

Extrusion of tubes results in unfavorable alignment of the (0001) and (1120) fracture planes with respect to the transverse direction. Thus, when tested in the transverse direction, low ductility would be expected. Hot-pressed block, on the other hand, exhibits a random orientation, and tubes machined from this material would not be expected to have directional properties.

In order to examine the effects of fabrication history on the room-temperature ductility of beryllium tubing, burst tests were performed on tubing manufactured by Pechiney, Imperial Chemical Industries, and Brush Beryllium Company. The tubing from Pechiney and Imperial was produced by hot extrusion, and that from Brush by machining from a hot-pressed block. The results of the tube-burst testing are shown in Table 14.2. The tangential strain obtained from tubing machined from a hot-pressed block, while extremely small, was greater than that obtained from extruded tubing. British investigators<sup>4</sup> have reported that the ductility, as determined at 600°C in the longitudinal direction, may be increased by a factor of 2 or 3 by overaging at temperatures above 575°C. The effects of annealing and overaging on the room-temperature ductility of beryllium tubing fabricated by the various manufacturers are being investigated.

<sup>4</sup>A. Moore, F. Morrow, V. D. Scott, and D. A. Cheer, "Precipitation-Aging and Improved Mechanical Properties in Commercially Pure Beryllium and Beryllium Alloys," paper presented at the Institute of Metals Conference on the Metallurgy of Beryllium held at the Royal Commonwealth Society, London, October 16-18, 1961; proceedings to be published by the Institute of Metals, London.

Table 14.2. Room-Temperature Burst Properties of As-Machined Beryllium Tubing

Fabricator	Specification Length (in.)	Tangential Stress at Fracture (psi)	Tangential Strain at Fracture (%)	Modulus in Tangential Direction
				$\times 10^6$
Brush	3	48,340	0.22	45.5
Brush	3	52,890	0.55	46.8
Brush	3	50,860	0.25	46.5
Brush	2	49,300	0.39	37.5
Brush	2	45,400	0.18	42.6
Brush	2	49,400	0.27	49.2
Imperial	3	53,400	0.18	54.5
Imperial	3	50,300	0.19	52.8
Imperial	3	41,400	0.85	38.6
Imperial	2	61,230	0.20	53.4
Imperial	2	54,600	0.14	76.0
Pechiney	3	49,600	0.11	52.2
Pechiney	2	44,700	0.10	52.6
Pechiney	2	58,180	0.19	43.4

### STUDIES OF THE DISTRIBUTION OF ABSORBED CARBON IN BERYLLIUM EXPOSED TO CARBON DIOXIDE

H. E. McCoy, Jr.

Studies by Werner *et al.*<sup>5</sup> have shown that beryllium is carburized as a result of exposure to CO<sub>2</sub> and have demonstrated that a correlation exists between the carbon concentration and breakaway oxidation in wet CO<sub>2</sub>. In an effort to better understand these observations, experiments involving C<sup>14</sup> were performed to determine the location of absorbed carbon in beryllium exposed to CO<sub>2</sub>.

The experimental apparatus used for these studies is a nonmetallic loop through which is pumped CO<sub>2</sub>. A special pump that was developed for this application is described in detail in another report.<sup>6</sup>

<sup>5</sup>W. J. Werner *et al.*, *GCR Quart. Progr. Rept. Mar. 31, 1961*, ORNL-3102, pp 136-39.

<sup>6</sup>B. McNabb and H. E. McCoy, Jr., *A Laboratory Gas-Circulating Pump*, ORNL-TM-75 (Nov. 30, 1961).

The CO<sub>2</sub> is obtained by the thermal decomposition of BaCO<sub>3</sub> in which 5% of the carbon atoms have mass No. 14. Any CO formed as a reaction product is oxidized to CO<sub>2</sub> by a column of cupric oxide at 500°C in series with the test specimen.

The material used for these studies was Pechiney Super Purity Flake, which had been hot extruded. The details of a series of tests over the range 1100 to 1500°F are presented elsewhere.<sup>7</sup> The important observations based upon these experiments may be summarized as follows:

1. Oxidation seems to progress along the inclusions that are present in the starting material. This observation implies strongly that some impurity concentrated in the inclusions may be influential in oxidation.

2. The surface-reaction layer is composed of interdispersed oxide and metallic particles. The metallic particles appear to be of the same composition as the matrix.

<sup>7</sup>*GCR Quart. Progr. Rept. Mar. 31, 1962*, ORNL-3302 (in press).

3. The absorbed carbon is concentrated in the reaction layer, as evidenced by the sharp drop in activity at the metal-reaction layer interface. Surface sectioning and counting techniques indicate further that the carbon is concentrated in the oxide particles present in the reaction layer.

### CARBURIZATION OF Fe-Ni-Cr ALLOYS IN FLOWING CO<sub>2</sub>

H. E. McCoy, Jr.

It was pointed out previously<sup>8</sup> that type 304 stainless steel is carburized as a result of exposure to flowing CO<sub>2</sub> at elevated temperatures. Significant observations were that carburization occurred over the range 1200 to 1700°F and that the quantity of carbon absorbed increased with time at a given temperature. Recent studies disclosed additional factors relative to the carburization of type 304 stainless steel by flowing CO<sub>2</sub>:

1. The presence of chromium is apparently necessary for carburization to occur. The importance of alloy composition is demonstrated by Table 14.3.

2. Metallographic studies, involving both standard techniques and C<sup>14</sup>, show that the carbon is added

uniformly. There are no indications that carbon penetration occurred exclusively along grain boundaries or through areas in the proximity of breaks in the surface oxide.

3. The rate of carburization is not very sensitive to temperature nor is a carburized case evident metallographically in specimens exposed at temperatures above 1300°F. This implies that the carburization reaction is kinetically controlled at temperatures less than 1300°F and controlled by the carburizing potential of the gas at higher temperatures.

### EFFECT OF CO<sub>2</sub> ON THE STRENGTH AND DUCTILITY OF TYPE 304 STAINLESS STEEL AT ELEVATED TEMPERATURES

W. R. Martin

In determining the usefulness of stainless steels as cladding materials in high-temperature gas-cooled reactors it is important to know the effect that their reactions with the coolant have on their strength and ductility. The mechanisms by which the coolant (CO<sub>2</sub> in this investigation) affects the strength properties of type 304 stainless steel are being investigated in the range 1300 to 1700°F.

The creep strength of type 304 stainless steel when tested in an environment of CO<sub>2</sub> is greater

<sup>8</sup>H. E. McCoy *et al.*, *Met. Div. Ann. Progr. Rept. May 31, 1961*, ORNL-3160, pp 85-86.

Table 14.3. Effect of Alloy Composition on the Carburization of Metals in Flowing CO<sub>2</sub> at 1000 and 1500°F

Test Conditions		Alloy Composition (wt %)	Carbon Content (wt %)	
Temperature (°F)	Time (hr)		Original	Final
1500	67.0	Nickel	0.0100	
	64.0	Ni-5 Fe	0.0100	<0.001
	118.4	Ni-5 Fe	0.0100	<0.001
	70.3	Ni-15 Cr	0.0150	<0.021
	64.1	Ni-15 Cr-5 Fe	0.0160	<0.028
1000	75	Iron	0.007	<0.017
		Fe-1 Cr	0.006	0.011
		Fe-3 Cr	0.008	0.026
		Fe-10 Cr	0.007	0.124

than for the same material tested in an inert environment of argon. The chemistry and metallurgical structure of the steel tested in  $\text{CO}_2$  differ from those of the steel tested in an inert environment. Typical microstructures for the steel creep-tested in  $\text{CO}_2$  are shown in Fig. 14.8. Although oxygen analyses of the metal substrate are not significantly different from those for the as-received material, the average carbon content of the metal substrate was increased by 0.3 wt % in 1200 hr at  $1500^\circ\text{F}$ . In a specimen exposed for 5000 hr at  $1500^\circ\text{F}$  the carbon content at the oxide-metal surface was 0.33% compared with 0.45% at the middle of the specimen. This carbon gradient could be caused by redistribution of the carbon within the sample or could be due to decarburization.

The question of whether the strengthening observed in  $\text{CO}_2$  is due to oxidation or carburization was investigated. Experiments on the effect of various partial pressures of oxygen in argon showed that the creep rate was minimum at approximately 10 ppm. The creep rate in  $\text{CO}_2$  at equivalent stress and temperature was lower by a factor of 3 than the minimum rate observed in oxygen-argon mixtures. From this evidence it was concluded that the strengthening observed in  $\text{CO}_2$  is primarily due to carburization.

Creep ductilities of material annealed prior to testing were not affected by testing in  $\text{CO}_2$  at temperatures of 1300 to  $1700^\circ\text{F}$ . However, the addition of 5 to 20% strain into specimens prior to creep testing greatly reduced the creep-fracture ductility of specimens tested in  $\text{CO}_2$  compared with that for specimens tested in argon. Fracture ductilities of specimens tested in  $\text{CO}_2$  in uniaxial tension were as low as 1.5%. The microstructure of these low-ductility specimens showed a fine precipitate along slip lines. These tests point out that the level of carbon is not necessarily the criterion upon which high or low ductility can be related but that the distribution of carbides may be more important. Further studies, possibly by means of electron-transmission microscopy, are needed to resolve the low-ductility problem.

## INFLUENCE OF HYDROGEN ON NICKEL-BASE ALLOYS

H. E. McCoy, Jr.

The deleterious effect that hydrogen has on the creep strength of nickel-base alloys at elevated temperatures was pointed out previously.<sup>9</sup> The important characteristics of this environmental effect are that (1) the influence of hydrogen is manifested through an increase in the secondary creep rate and a decrease in the time for the initiation of tertiary creep, (2) the magnitude of the effect becomes greater as the strain rate decreases, and (3) the rupture ductility is not significantly reduced. Recent studies have been directed toward developing a plausible mechanism to account for the experimental observations.

One possible mechanism, which was proposed for low-temperature hydrogen embrittlement,<sup>10</sup> is that hydrogen may be segregated in the metal and be influential in causing crack nuclei to propagate. The high-diffusion rate of hydrogen in nickel<sup>11</sup> makes the possibility of hydrogen segregation seem very questionable at elevated temperatures. To further check this point, an experiment involving diffusion of hydrogen into and out of an Inconel specimen was conducted. The results indicated that hydrogen very rapidly permeates the metal and can be easily removed.

A more plausible mechanism is that the presence of hydrogen increases the rate of void growth in the metal. The mechanism of creep by void growth as a result of vacancy condensation has been demonstrated by McLean<sup>12</sup> and Greenwood<sup>13</sup> to be important under conditions of high temperatures

<sup>9</sup>H. E. McCoy *et al.*, *Met. Div. Ann. Progr. Rept. May 31, 1961*, ORNL-3160, pp 85-90.

<sup>10</sup>R. Troiano, *Trans. ASM* **52**, 54 (1960).

<sup>11</sup>M. L. Hill and E. W. Johnson, *Acta Met.* **3**, 566 (1955).

<sup>12</sup>D. McLean, *J. Inst. Metals* **85**, 468 (1956-57).

<sup>13</sup>J. N. Greenwood *et al.*, *Acta Met.* **2**, 250 (1954).

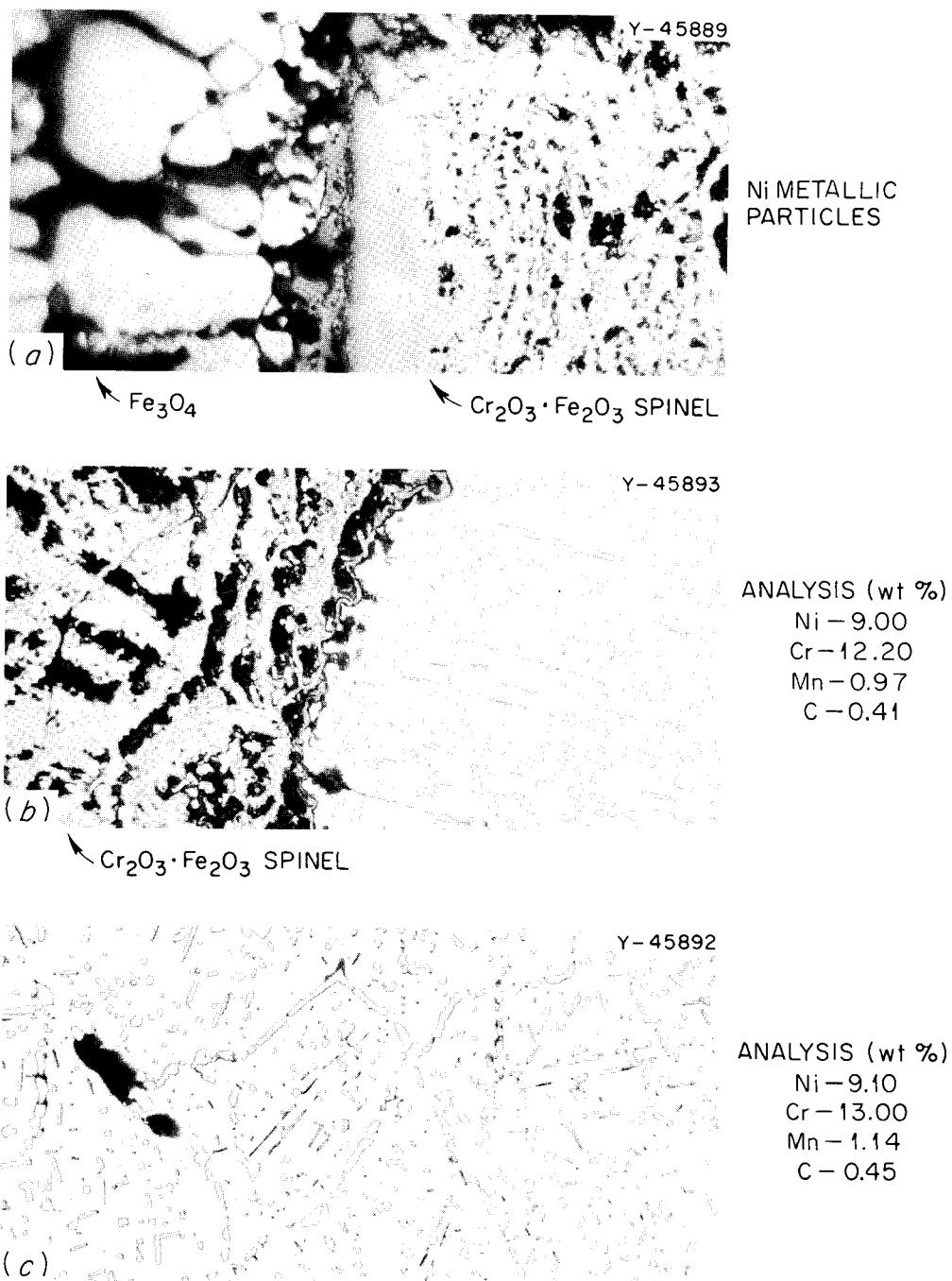


Fig. 14.8. Typical Photomicrographs of Type 304 Stainless Steel Creep-Tested for 5000 hr in Carbon Dioxide at 1500°F. (a) Oxide-oxide interface; (b) oxide-metal interface; (c) metal substrate 0.025 in. from original metal surface. Etchant, aqua regia. 500X. Vendor's analysis of as-received material: 9.55 Ni-18.30 Cr-1.18 Mn-0.07 C (wt %).

and low-strain rates. The rate of growth of voids could conceivably be increased by the presence of hydrogen, resulting in an increase in the concentration of vacancies or an increase in their mobility. The vacancy-atom interchange mechanism (which currently seems the most realistic) for self-diffusion in a pure metal predicts a dependence of the rate of self-diffusion on the energies of formation and transport of vacancies. Hence, studies of self-diffusion in pure nickel should indicate whether the number or mobility of vacancies is increased by hydrogen being present in solution. For experimental reasons, the approach used was that of measuring the rate of diffusion of  $\text{Co}^{60}$  into nickel. Pairs of specimens were annealed in argon and in hydrogen at equivalent temperatures. The specimens were then sectioned (by J. F. Murdock of the Solid Reaction Studies Group) and the penetration plots determined. The details of this investigation have been reported.<sup>14</sup> The significant conclusion is that the rates of self-diffusion are equivalent for both environments. This in turn means that neither the concentration of vacancies nor their mobility is significantly different in the two environments.

A factor shown by Balluffi and Seigle<sup>15</sup> to be of importance in the growth of voids in stressed specimens is the surface energy of the void, which creates a driving force for the void to collapse. If sufficient stress is applied, the voids will grow. If the presence of hydrogen decreases the surface energy of nickel, the stress required for void growth is reduced. Sintering studies showed that the sintering rate (rate of collapse of voids) of nickel powders is greater in vacuum than in hydrogen. This is indirect evidence that hydrogen does decrease the surface energy of nickel. Experiments are in progress to measure directly the surface energy of nickel in argon and in hydrogen.

### AGING OF Nb-Zr ALLOYS

R. L. Stephenson

H. E. McCoy

The existence of an aging reaction in Nb-1% Zr alloys involving significant mechanical property changes has been demonstrated.<sup>16</sup> Oxygen is currently thought to be involved in this reaction.<sup>17</sup> Internal friction is recognized as a useful tool for studying the precipitation of interstitial solutes from supersaturated solid solutions in body-centered cubic metals<sup>18-20</sup> and is therefore being

used to study the observed aging. The results of preliminary experiments were described previously.<sup>21</sup> The development of a device for automatically sensing and recording vibrational amplitude as a function of time has also been published.<sup>22</sup> Recent experiments have been devoted to identifying the observed peaks and making preliminary observations as to the nature and kinetics of the aging reaction itself.

Figure 14.9 shows the internal friction spectra of pure niobium containing various levels of oxygen after annealing at 1925°C. It is known<sup>23</sup> that (at 1 cps) peaks due to the stress-induced ordering of oxygen and nitrogen atoms are found at 160 and 285°C, respectively. The broadening and apparent shifting of the oxygen peak at high contents are thought to be caused by interactions between oxygen atoms similar to those observed<sup>24</sup> in tantalum. Figure 14.10 shows the internal friction spectrum of an Nb-0.16% Zr specimen containing 1070 ppm  $\text{O}_2$ . The peak at approximately 220°C is observed only when both zirconium and oxygen are present and cannot be produced by large additions of oxygen to pure niobium. It is therefore concluded that this peak is caused by the stress-induced motion of oxygen atoms in the neighborhood of a zirconium atom. Similar observations have been

<sup>14</sup>H. E. McCoy, Jr., and J. F. Murdock, *Influence of Argon and Hydrogen Environments on the Rate of Diffusion of Cobalt-60 in Nickel*, ORNL-TM-235 (to be published).

<sup>15</sup>R. W. Balluffi and L. L. Seigle, *Acta Met.* 5, 449 (1957).

<sup>16</sup>D. O. Hobson, *A Preliminary Study of the Aging Behavior of Wrought Columbium-1% Zirconium Alloys*, ORNL-2995 (Jan. 6, 1961).

<sup>17</sup>D. O. Hobson, "Aging Phenomenon in Columbium-Base Alloys," paper presented at the AIME High Temperature Materials Conference, Cleveland, Ohio, April 26-27, 1961.

<sup>18</sup>C. Wert, *Thermodynamics in Physical Metallurgy*, American Society of Metals, Cleveland, Ohio, 1950.

<sup>19</sup>P. M. Robinson and R. Rawlings, *Iron and Steel* 31, 65 (1958).

<sup>20</sup>A. S. Nowich, *Progr. in Metal Phys.* 4, 37 (1953).

<sup>21</sup>H. E. McCoy et al., *Metal Div. Ann. Progr. Rept. May 31, 1961*, ORNL-3160, p 86.

<sup>22</sup>R. L. Stephenson and H. E. McCoy, *J. Sci. Instr.* 39(2), 54-55 (1962).

<sup>23</sup>R. W. Powers and M. V. Doyle, *J. Metals, Trans. AIME* 209, 1285 (October 1957).

<sup>24</sup>R. W. Powers and M. V. Doyle, *Acta Met.* 4, 233 (1956).

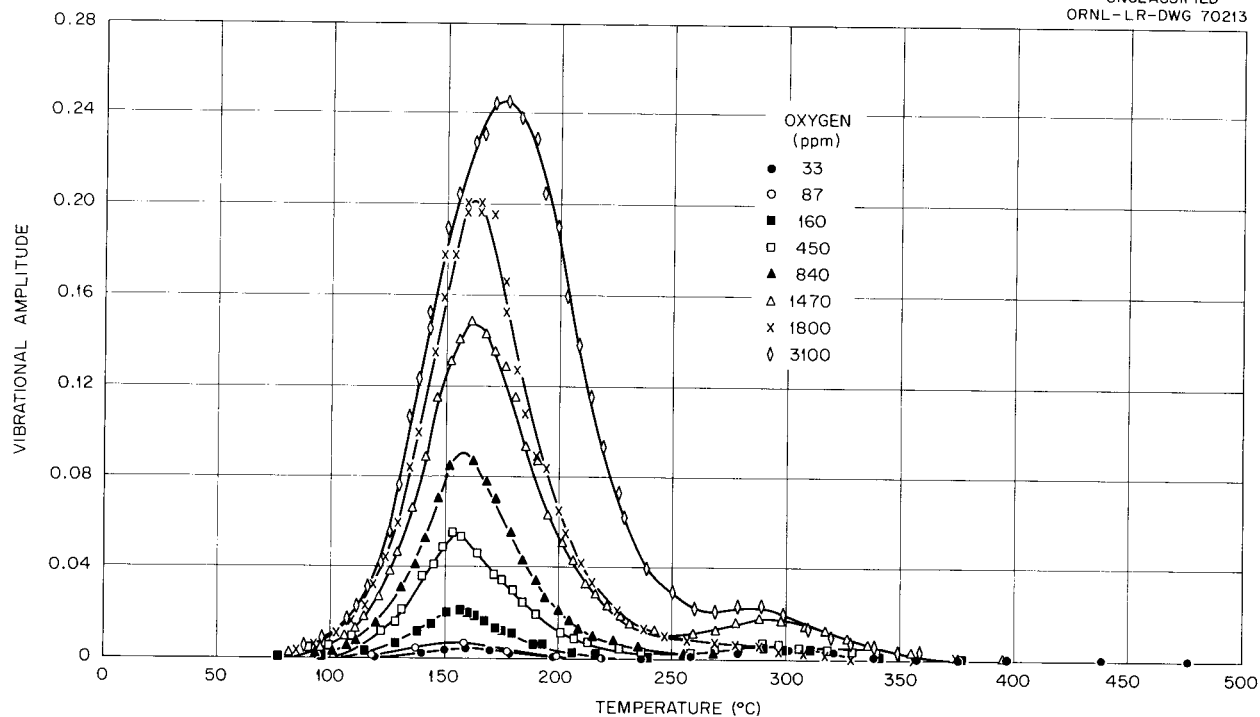
UNCLASSIFIED  
ORNL-LR-DWG 70213

Fig. 14.9. Internal Friction Spectrum of Niobium Containing Various Levels of Oxygen.

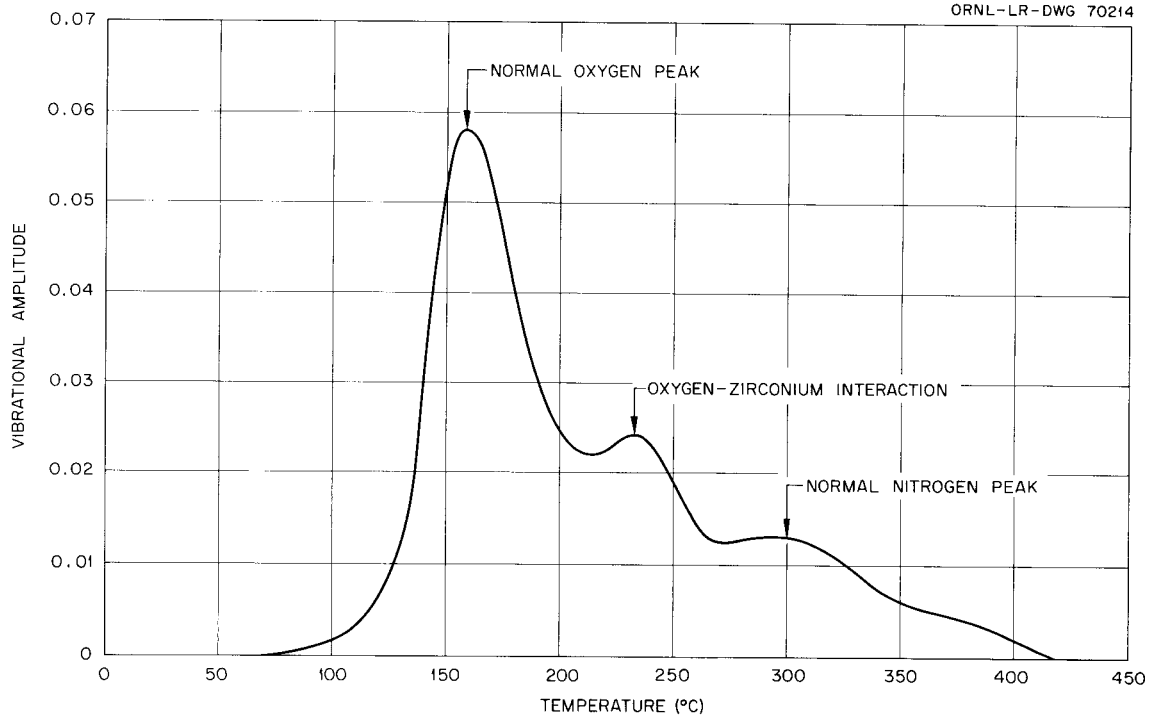
UNCLASSIFIED  
ORNL-LR-DWG 70214

Fig. 14.10. Internal Friction Spectrum of Nb-0.16% Zr Alloy Annealed at 1925°C.

made concerning nitrogen in the Fe-Mn, Fe-Cr, Fe-Mo, and Fe-V systems.<sup>25</sup> Figure 14.11 shows the internal friction spectrum of an Nb-1.09% Zr alloy and the effect of aging. The 220°C peak is readily observable upon the addition of only 0.16% Zr (Fig. 14.10) and is seen (Fig. 14.11) to predominate at low oxygen contents upon the addition of 1.09% Zr. Thus it is concluded that oxygen is preferentially "clustered" about zirconium atoms even after an annealing treatment at temperatures up to 1925°C. Preliminary experiments indicate that the peaks at approximately 380 and 480°C are due to the presence of nitrogen. It can also be seen from Fig. 14.11 that all these peaks decrease in height upon aging, indicating that both nitrogen and oxygen precipitate upon aging. Experiments are in progress to determine whether oxygen or nitrogen or both are important in causing the observed mechanical property changes.<sup>26</sup>

<sup>25</sup>L. J. Dijkstra and R. J. Sladek, *Trans. Am. Inst. Mining Met. Petrol. Engrs.* 197, 69 (1953).

<sup>26</sup>D. O. Hobson, *A Preliminary Study of the Aging Behavior of Wrought Columbium-1% Zirconium Alloys*, ORNL-2995 (Jan. 6, 1961).

## STRESS-RATE TESTING

C. R. Kennedy

The constant-load creep-rupture test is used, in general, to generate high-temperature-strength design data. However, it is obvious that under realistic service conditions the load does not remain constant but varies considerably. The general method of obtaining lifetime expectancies under varying loads has involved a summation of rupture-life fraction:

$$\frac{\Delta t_1}{t_{r1}} + \frac{\Delta t_2}{t_{r2}} + \frac{\Delta t_3}{t_{r3}} + \dots = 1, \quad (1)$$

where  $\Delta t_1, \Delta t_2, \Delta t_3, \dots$  are the times under stresses  $\sigma_1, \sigma_2, \sigma_3, \dots$  and  $t_{r1}, t_{r2}, t_{r3}, \dots$  are the rupture lives for stresses  $\sigma_1, \sigma_2, \sigma_3, \dots$ . This method has been relatively successful for predicting failure of a wide range of materials varying from aluminum alloys at low temperatures to "super alloys" at very high temperatures. It is proposed that the method be extended to provide an analytical model for the stress-rupture characteristics of a material. In this manner it should be

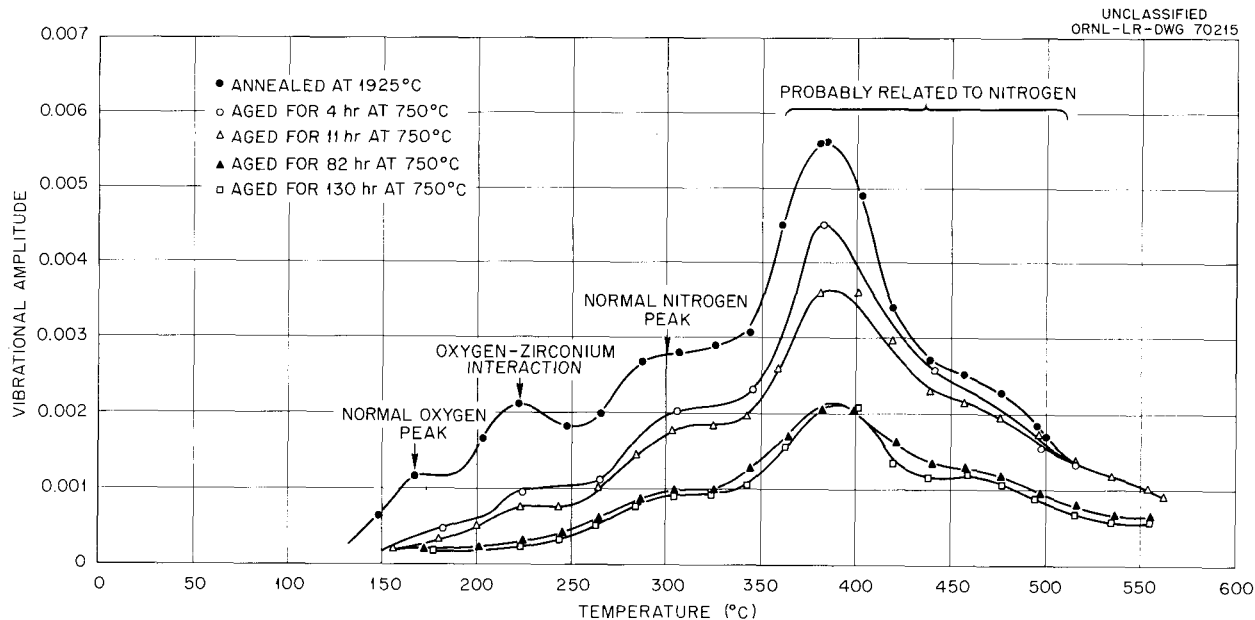


Fig. 14.11. Effect of Aging on the Internal Friction Spectrum of Nb-1.09% Zr Alloy Containing 3100 ppm O.

possible to obtain a fairly close approximation of the creep-rupture strength of a material by programming several simple short-time tests.

The stress-rupture characteristics of most materials can be fairly well represented by the expression

$$t_r = \left( \frac{A}{\sigma} \right)^n, \quad (2)$$

where  $t_r$  is the rupture life under applied stress  $\sigma$ , and  $A, n$  are constants. Rearrangement of Eq. (2) to

$$t_r \sigma^n = A^n \quad (3)$$

states that the time to rupture times the stress to some power ( $n$ ) is a constant for a given temperature. Equation (1) implies that the sum of  $\Delta t_i \sigma_i^n$  can never be greater than the constant  $A^n$ .

Thus

$$\sum_{t_i} \Delta t_i \sigma_i^n = A^n, \quad (4)$$

which is of the form

$$A^n = \int_0^{t^1} dt_i \sigma_i^n, \quad (5)$$

where  $t^1$  is the total rupture time for the variable stress conditions. The type of test to be programmed requires that the stress be applied at a constant rate and that the final stress and total test time be recorded:

$$\frac{d\sigma}{dt} = \dot{\sigma} = \text{constant}, \quad (6)$$

$$\sigma = t \dot{\sigma}. \quad (7)$$

By substituting Eq. (7) into Eq. (5),

$$A^n = \dot{\sigma}^n \int_0^{t^1} dt_i t_i^n, \quad (8)$$

which integrates to

$$A^n = \dot{\sigma}^n \frac{t^{n+1}}{n+1}. \quad (9)$$

Using Eq. (7) again, Eq. (9) becomes

$$t_f = (A/\dot{\sigma})^n (1+n), \quad (10)$$

where  $t_f = t^1$  and  $\sigma_f$  is the stress at  $t_f$ . Thus, by performing several tests with different stress rates ( $\dot{\sigma}$ ), the constants  $A$  and  $n$  can be obtained.

Thus, by performing several tests with different stress rates ( $\dot{\sigma}$ ), the constants  $A$  and  $n$  can be obtained.

The accuracy of Eq. (10) is demonstrated in Fig. 14.12, giving the results of 11 stress-rate tube-burst tests on type 304 stainless steel specimens from heat 23999X from 1100 to 1700°F. Also included in this figure are the standard testing results plotted in Fig. 14.5 which show that the agreement is within 5%. A similar test series with type 309 stainless steel from 1100 to 1500°F also demonstrated the accuracy of Eq. (10).

Stress-rate testing is also being applied in determining creep constants with limited success. The type 309 stainless steel test series was successful in producing creep data at the higher temperatures. However, the material behavior did not follow the analytical model at the lower test temperatures.

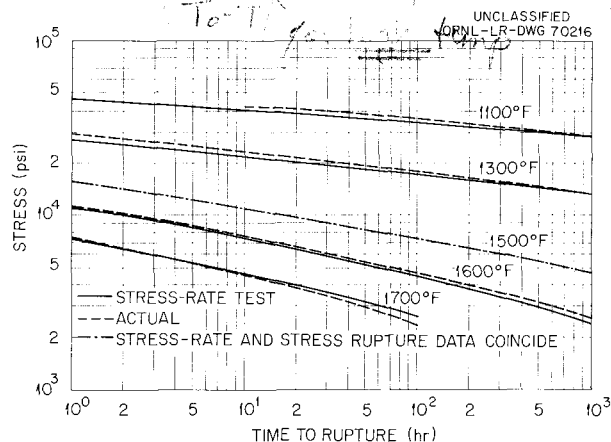


Fig. 14.12. Comparison of Actual Stress-Rupture Properties of Type 304 Stainless Steel and Those Predicted by Stress-Rate Testing.

## ZIRCALOY-2

C. R. Kennedy

The deformation and fracture characteristics have been described fairly completely for isotropic materials, even under complex stress conditions, but not for the close-packed hexagonal zirconium-base alloys, such as Zircaloy-2, which exhibits strong preferred orientations. Therefore these characteristics of Zircaloy-2 will be investigated not only at room temperature but also under creep conditions.

A combination of axial load and internal pressure was used to produce biaxial stress states from pure axial tension to pure tangential tension. The tubing was tested in the annealed condition for  $\frac{1}{2}$  hr at 1450°F, and was found to exhibit a strong intensity of  $\{10\bar{1}0\}$  poles in the axial direction, strong intensity of  $\{0001\}$  poles with an absence of  $\{10\bar{1}0\}$  or  $\{11\bar{2}0\}$  poles in the tangential direction, and a moderate intensity of  $\{11\bar{2}0\}$  poles in the radial direction.

In accordance with the basal pole concentration and the lack of  $\{10\bar{1}0\}$  or  $\{11\bar{2}0\}$  poles in the tangential direction, room-temperature tensile properties reported last year<sup>27</sup> demonstrated the greater resistance to deformation in this direction. The high-temperature fracture characteristics shown in Fig. 14.13 follow this general behavior

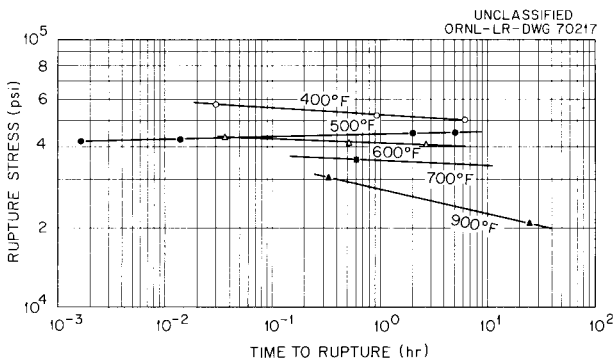


Fig. 14.13. Stress-Rate Test Results for Zircaloy-2.

except for the short-time fracture results. Apparently, the high stress applied to produce the short-time rupture also causes twinning to allow for greater ease of slip in the tangential direction. This will also cause a greater resistance to deformation in the radial direction; thus, the axial direction is forced to accommodate greater strains than normally expected. For example, when the tangential to axial stress ratio is 2:1, no axial strain should occur. This was observed in the long-time tube-burst tests, but when the time to rupture was short, negative strains were observed.

<sup>27</sup>C. R. Kennedy, *Metal. Div. Ann. Progr. Rept.* May 31, 1961, ORNL-3160, pp 92-93.

It is important to recognize this phenomenon since short-time tests at high temperatures may be deceiving in demonstrating the effect of the anisotropy.

The effect of the mechanical anisotropy is described by the Hill constants in the general equation

$$1 = H(\sigma_Z - \sigma_\theta)^2 + F(\sigma_\theta - \sigma_R)^2 + G(\sigma_Z - \sigma_R)^2, \quad (11)$$

where  $F$ ,  $G$ ,  $H$  are anisotropy constants and  $\sigma_Z$ ,  $\sigma_\theta$ ,  $\sigma_R$  are axial, tangential, and radial stresses.

The constants for fracture vary with time as described above, but they approach values equal to those determined from creep for times greater than 1000 hr:  $H = F$  and  $G = 2.1H$ , which compares with the room-temperature values of  $H = F$  and  $G = 3.7H$ . The lower values for creep and rupture indicate a less-pronounced mechanical anisotropy at the elevated temperatures.

Zircaloy-2 also exhibits the phenomenon of strain aging that produces a pronounced effect on the creep-rupture characteristics over an intermediate temperature range. The temperature range of greatest sensitivity begins when thermal diffusion of interstitials is sufficient to cause aging during deformation. As the temperature is increased, the effect diminishes to the point that the thermal energy allows the interstitials to randomize. The temperature range in which aging occurs is characterized by very flat stress-rupture curves which sometimes indicate higher stress-rupture strength than at lower temperatures. The new stress-rate test provides a simple and fast way of determining the temperature range in which aging occurs and the magnitude of the effect. The results of testing tubes between 400 and 900°F are shown in Fig. 14.13. The results for the tests at 700 and 900°F agree very closely with the standard test data given in Fig. 14.14. The positive slope at 500°F illustrates the significance of strain aging at approximately this temperature and predicts that in standard stress-rupture tests a specimen will either fail on loading or last indefinitely. The magnitude of the stress level required to cause failure will be determined by the rate of loading. Thus, it is quite obvious that in performing standard constant-load creep-rupture tests at approximately 500°C great care must be given to the rate of load application or inconsistencies will result.

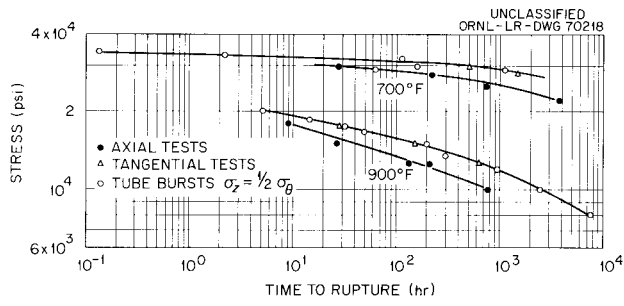


Fig. 14.14. Stress-Rupture Properties of Zircaloy-2 Tubes.

## 15. Nondestructive Test Development

R. W. McClung

### ULTRASONIC TESTING METHODS

K. V. Cook      R. W. McClung

Most of the emphasis in the ultrasonic development program has been on studies of ultrasonic behavior in thin sections and particularly on application of ultrasound for the detection of nonbonding in cladding structures.

#### Fuel Plates

Studies<sup>1</sup> were continued on the through-transmission ultrasonic detection of nonbonding in flat fuel plates, including  $\text{UO}_2$  dispersed in stainless steel (proposed for core B of the Enrico Fermi Reactor), uranium clad with aluminum (used for Oak Ridge Research Reactor and High-Flux Isotope Reactor plates), and  $\text{UO}_2$  and  $\text{U}_3\text{O}_8$  dispersed in aluminum (proposed for Advanced Test Reactor and HFIR fuel elements). A number of each type of fuel plates were examined with varying conditions of ultrasonic frequency and beam collimation to determine the optimum for maximum sensitivity. Results thus far indicate that, in general, smaller nonbonds can be detected in the alloy cores than in the dispersion cores, the sensitivity being limited by the localized inhomogeneities of dispersion cores. For example,  $\frac{1}{16}$ -in. nonbonds were readily detected in uranium-aluminum cores with the background transmission variables giving much smaller responses. In some cases,  $\frac{1}{16}$ -in. nonbonds were detectable in  $\text{U}_3\text{O}_8$ -aluminum cores, but on other,

similar, plates the core variations created transmission intensity variations as great as that from a  $\frac{1}{16}$ -in. nonbond. Thus, the plate could have been erroneously rejected. In such instances, the  $\frac{3}{32}$ - or  $\frac{1}{8}$ -in. nonbonds could still be discriminated, however. It may be possible with further fabrication experience on cermet cores and more ultrasonic investigation to overcome some of these difficulties.

A new and versatile scanner was designed and fabricated. This unit will be incorporated on the existing tube-scanning tank and will be usable for automatic scanning of plate as well as for extensive development work on other techniques such as Lamb waves for plate inspection.

#### Brazed Joints

Lamb-wave and ringing ultrasonic techniques were developed and applied to the detection of nonbonds in brazed areas for a liquid-metal boiler<sup>2</sup> consisting basically of a concentric arrangement of a stainless steel tube, copper disks, and a stainless steel can. Other efforts included development of techniques for the evaluation of a brazed tube-to-sleeve joint<sup>3</sup> which has been proposed for reactor remote-maintenance operation. Extensive development will be required before these techniques can be adapted for remote application.

<sup>1</sup>R. W. McClung and K. V. Cook, *Met. Div. Ann. Progr. Rept. May 31, 1961*, ORNL-3160, pp 135-36.

<sup>2</sup>K. V. Cook and R. W. McClung, "Development of Ultrasonic Techniques for the Evaluation of Brazed Joints," submitted to the *Welding Journal*.

<sup>3</sup>MSR Program Semiann. Progr. Rept. Feb. 28, 1962, ORNL-3282 (in press).

## EDDY-CURRENT METHODS

C. V. Dodd      R. W. McClung

### Through-Transmission System

One phase of the recent eddy-current investigations was the development of new techniques and instrumentation for making thickness measurements of various reactor components and materials. The system being studied uses a two-coil, through-transmission principle: the phase of the received signal is monitored relative to the transmitted signal. This method is sensitive primarily to the amount of electrically conducting material through which the electromagnetic wave passes and consequently is relatively insensitive to the coil-to-specimen spacing, a problem that generally plagues eddy-current testing. Therefore it is very applicable for thickness measurements in locations where limited access reduces confidence in the inspection probe being in intimate contact with the specimen.

A difficult problem in the measurement of small phase shifts in the presence of large amplitude variations caused by changes in coil spacing was largely overcome through the use of two new "zero-crossover" trigger circuits which actuate a high-speed flip-flop circuit. The direct-current output of the flip-flop is proportional to the shift and the specimen thickness.

This system will be applicable for the measurement of fillet thickness in finned tubing, for the end-spacer thicknesses of flat-plate fuel elements such as the Fermi core B element, for wall-thickness measurements on graphite tubing, and for numerous other difficult measurements. Further studies in this prototype system are being directed toward single probes containing both transmitter and receiver coils for measurements from one side of a specimen and toward application of the phase-sensitive technique for flaw detection.

### Space Gaging<sup>4</sup>

A major part of the eddy-current program has been directed toward the development of techniques for

<sup>4</sup>C. V. Dodd and R. W. McClung, *Fuel Element Coolant Channel and Other Spacing Measurements by Eddy-Current Techniques*, ORNL-TM-129 (Mar. 20, 1962).

the measurement of space between components such as fuel plates and rods. Most of the work has utilized the probe configuration (Fig. 15.1) that was developed for measuring the interplate channel spacing in fuel elements for the HFIR, ATR, Fermi Reactor, and Army Power Package Reactor (APPR). Tests are in progress to relate the changes in coil impedance with variation in the spacing and to provide quantitative design criteria. A number of coils were constructed to specified diameters, lengths, and number of turns. Their impedance was measured in a balanced-bridge network as a function of driving frequency and coil-to-specimen spacing. Fairly accurate relationships were noted between frequency and coil diameter, and approximate relationships were observed between coil length and the impedance per change in unit spacing.

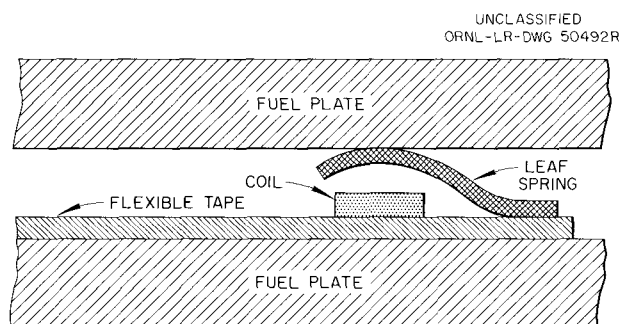


Fig. 15.1. Probe for Measuring Interplate Channel Spacing.

The probe designed to measure the spacing between tubular fuel elements is shown in Fig. 15.2. The modified V shape of the probe holds the coil equidistant from the measured rods and controls the amount of coil insertion between the rods as a function of rod spacing. This latter movement will cause an impedance change which can be calibrated in terms of interrod spacing. Figure 15.3 shows the type of probe designed to measure the inner diameter of tubing. As the probe is moved longitudinally or circumferentially through the tube, inner-diameter variations cause the spring-loaded ferromagnetic feeler to move laterally, which will be reflected as impedance changes in the solenoid coil surrounding the feeler.

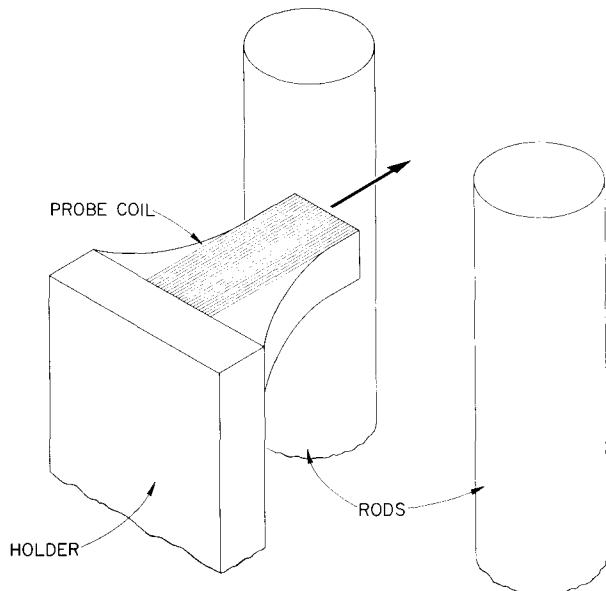
UNCLASSIFIED  
ORNL-LR-DWG 58763

Fig. 15.2. Probe for Measurement of Interrod Spacing.

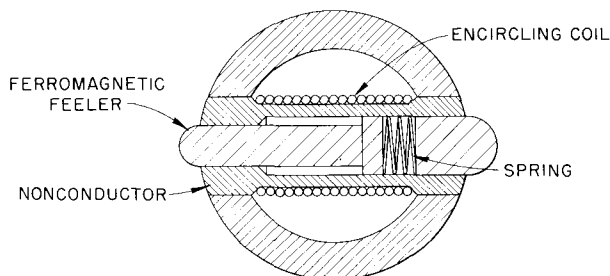
UNCLASSIFIED  
ORNL-LR-DWG 56398

Fig. 15.3. Probe for Measuring Inner Diameter of Tubing.

## PENETRATING RADIATION METHODS

### Low-Voltage Radiography

R. W. McClung

An extensive study was made of low-voltage radiographic conditions to determine optimum techniques and the capabilities and limitations of such radiography for thin sections of aluminum, steel, and beryllium.<sup>5</sup> The test variables were the input

<sup>5</sup>R. W. McClung, *Techniques for Low-Voltage Radiography*, ORNL-3252 (Feb. 14, 1962).

kilovoltage (energy of the x-ray beam), the specimen thickness, and the intermediate atmosphere between the x-ray tube head and the specimens.

The system was used for examining approximately 1/2-in.-thick aluminum, 2-in.-thick beryllium, and 0.037-in.-thick steel specimens and other materials in a wide variety of shapes. Considerable advantage in both the sensitivity and the required exposure time was realized through the use of intermediate helium atmospheres and darkroom, bare-film-exposure techniques. Contrast sensitivities as low as 0.1% were obtained, which is far superior to the normal 2% sensitivity. A number of exposure technique charts were constructed as aids to optimum radiography.

More recently, emphasis has been directed toward the application of low-voltage microradiographic techniques for the nondestructive evaluation of graphite-coated uranium carbide particles.<sup>6,7</sup> The radiographs were recorded by several different detectors and then viewed at high magnifications to reveal the core and coatings of the carbide particles. Type M radiographic film was successfully viewed at magnifications of up to about 60X before the grain size of the emulsion became very evident. Nuclear track plates, which seem to have about the same exposure speed as type M film, can be magnified up to approximately 200X before the grain size becomes excessive. The highest magnifications were obtained with high-resolution plates having very fine-grained emulsions (grain size, about 0.1  $\mu$ ). The particle and coating images were very sharp even at 500X. Since such excellent detail could be obtained, it is possible to detect low-density core sections, unfueled particles, and high-density material in the coatings. Figure 15.4 is a microradiograph of a number of particles illustrating these conditions.

### Homogeneity Studies

B. E. Foster

S. D. Snyder

**Fuel Rods.** — A system comprised of an NaI(Tl) crystal, a photomultiplier tube, a high-voltage supply, and a modified Brown recorder with 21-mv suppression circuit was used to detect and measure fuel-loading variations in vibratory-compacted fuel

<sup>6</sup>E. S. Bomar *et al.*, *GCR Quart. Progr. Rept. Dec. 31, 1961*, ORNL-3254, pp 141-43.

<sup>7</sup>*GCR Quart. Progr. Rept. Mar. 31, 1962*, ORNL-3302 (in press).

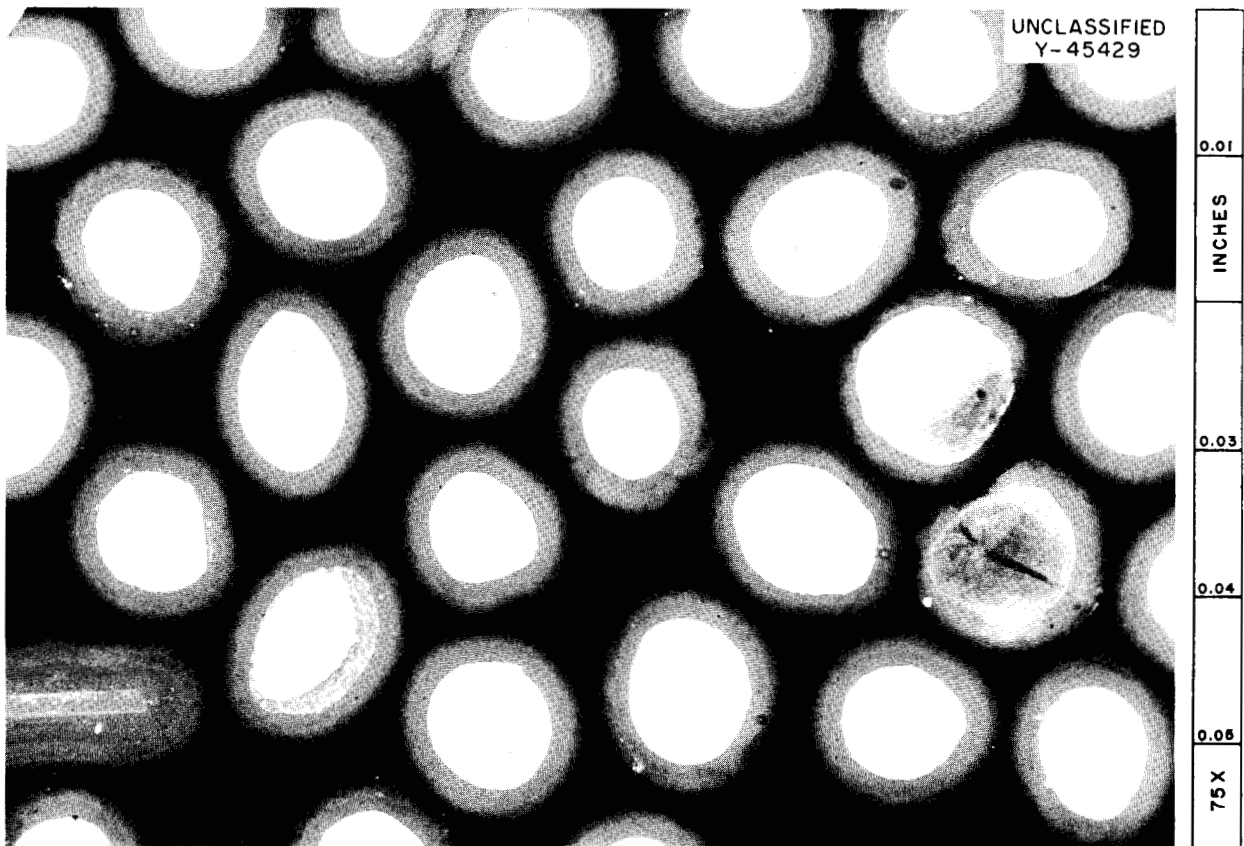


Fig. 15.4. Microradiograph of  $UC_2$  Particle Coated with Pyrolytic Graphite. 75X.

rods. The technique is based on the measurement of the attenuation of gamma rays transmitted from a 1-curie  $Co^{60}$  source and collimated to a  $\frac{1}{8}$ -in.-diam beam. The rods are driven longitudinally through the gamma-ray beam, and the variations of attenuation transmitted through a specimen are recorded as a function of rod length. Based on the limited number of fuel rods thus far examined, the predicted density agreed to within 1% with the known bulk density. A more accurate calibration will be realized when better density standards have been obtained. This technique is being used to evaluate the homogeneity of the BNL kilorod fuel elements and should be applicable for any element manufactured by vibratory compaction or swaging.

**Fuel Plates.** — Radiation-attenuation measurement techniques for the nondestructive evaluation of homogeneity in flat fuel plates and realistic calibration standards are being developed. X rays

in the range 50 to 150 kvp and both x-ray film and NaI(Tl) scintillators are used.

The homogeneity of the  $UO_2$ -stainless steel dispersion plates for core B of the Enrico Fermi Reactor was recorded on radiographs and compared with those of known standards.<sup>8</sup> In recent studies an attempt is being made to use scintillation for detecting inhomogeneities in thin fuel plates for the ORR, HFIR, and ATR. Satisfactory standards have been difficult to obtain because of the lower uranium content and thinner plate sections. Several approaches to this problem are under study, including uranium foil with aluminum sheet, U-Al alloys with aluminum sheet,  $U_3O_8$  dispersed in aluminum, and equivalent-absorption thicknesses of nonfissionable material.

<sup>8</sup>R. W. McClung, *Feasibility Studies — Nondestructive Testing of the Enrico Fermi Reactor Core B Fuel Element*, ORNL-3221, pp 21-30 (Dec. 21, 1961).

## X-Ray Attenuation Coefficients

B. E. Foster

The study of x-ray attenuation coefficients by scintillation spectrometry was concluded for the range 50 to 150 kvp and for the materials Zircaloy-2, type 1100 aluminum, types 304 and 347 stainless steels, and enriched U-Al alloys.<sup>9</sup> Curves derived from experimental and calculated coefficients were compared, and good agreement was found except for the uranium-bearing samples, which did not agree with NBS low-energy values.<sup>10</sup> The uranium values obtained by other experimenters<sup>11</sup> are in agreement with ours.

## PROBLEM MATERIALS

R. W. McClung

Considerable effort was spent in developing non-destructive tests for the evaluation of materials that are unusually difficult to inspect, such as beryllium and molybdenum tubing.

### Beryllium

Techniques involving fluorescent penetrants, low-voltage radiography, and eddy-currents were used to evaluate 0.500-in.-ID beryllium tubing with 12 identical external helical fins.<sup>12</sup> The fluorescent-penetrant method was demonstrated to be capable of revealing pits, pinholes, and cracks in the outer surface of the tubing. Because of the very large changes in section thickness necessitated by the fins, the radiographic technique was used to examine only the root areas between the fins. Three successive radiographs at 60° rotational intervals were adequate to achieve 85% coverage

<sup>9</sup>B. E. Foster and J. W. Evans, "X-Ray Mass Attenuation Coefficients in the Range 50 to 150 kvp," to be published in the *Journal of the Society for Non-Destructive Testing*.

<sup>10</sup>G. W. Grodstein, *X-Ray Attenuation Coefficients from 10 KEV to 100 MEV*, NBS-583 (Apr. 30, 1957).

<sup>11</sup>R. E. Connally et al., *Uranium Analysis by Gamma Absorptiometry*, p 15, HW-54438 (May 20, 1958).

<sup>12</sup>R. W. McClung and C. V. Dodd, *GCR Quart. Progr. Rept. June 30, 1961*, ORNL-3166, pp 114-15; R. W. McClung, *GCR Quart. Progr. Rept. Dec. 31, 1961*, ORNL-3254, pp 185-86; *Mar. 31, 1962*, ORNL-3302 (in press).

of this thin area; the remaining 15% was obscured by a projected fin image transversing a projected groove image. (The radiograph is made through both welds simultaneously.) The most common discontinuities detected were pitting and high-density particles.

The eddy-current technique required the design of a special bobbin-type coil to fit the inside of the tube bore. The signals generated could be recorded on slightly modified commercial equipment. Through the use of machined, longitudinal reference notches, the sensitivity was determined for both inner and outer surface defects. As with the radiographic technique, emphasis was placed on inspecting the areas of the thin-wall section between the fins. The eddy-current technique was demonstrated to be capable of revealing cracks 0.004 in. deep on the inner surface or at the groove portion of the outer surface.

### Molybdenum

Tentative techniques were developed for the evaluation of 0.500 × 0.020 in. molybdenum tubing. Pits, pinholes, gouges, and longitudinal cracks were revealed by the penetrant examination, and elongated pits and high-density material by the radiographic technique. A number of inner and outer surface transgranular cracks, the deepest being about 90% through the wall, were detected by both the ultrasonic and eddy-current inspections.

## REMOTE-INSPECTION DEVELOPMENT

R. W. McClung

K. V. Cook

### Thickness of Core Vessel Wall<sup>13</sup>

The thickness of the HRT core vessel wall was measured by a remote pulse-reflection ultrasonic technique. A mechanical rig was designed to permit measurements in both the 90 and 30° conical sections and the spherical section of the vessel. The rig located the transducer near the axis of the pear-shaped vessel, which simplified the operation

<sup>13</sup>R. W. McClung and K. V. Cook, *Development of Ultrasonic Techniques for the Remote Measurement of the HRT Core Vessel Wall Thickness*, ORNL-TM-103 (Mar. 15, 1962).

and permitted measurements to be taken in roughened areas that could not be measured previously. But even more important, these measurements are believed to be the most accurate ones that have been taken. The largest number of measurements were made in the spherical section, with values being taken at approximately 30° longitudinal intervals and 20° latitudinal intervals. Apparently, no significant change had occurred in the wall thickness since the last series of measurements.<sup>14</sup>

#### Radiography in Radiation Environs

A brief investigation<sup>15</sup> was made into the possibility of using radiography on HFIR target rod weldments in a background of approximately 300 rads/hr at 0.1-Mev gamma irradiation. The energy level of the image-forming x irradiation was 48 kvp,

and 8 sec was required to obtain a reasonable radiograph of the sample weld. Duplicate films were then subjected to varying exposures of 100-kvcp (kilovoltage constant potential) x irradiation to superimpose the fogging background on the image of the weld. This energy would have somewhat more effect on the film blackening than would 0.1-Mev gamma irradiation. An irradiation of approximately 1 r did not seriously degrade the image quality. Thus if the total exposure time to the background can be kept to very nearly that of the image-forming exposure, useful radiography can be performed on the proposed target rod weldments in fields of this energy and intensity.

---

<sup>14</sup>R. W. McClung, *Mel. Div. Ann. Progr. Rept. July 1, 1960*, ORNL-2988, pp 416-17.

<sup>15</sup>*Transuranium Quart. Progr. Rept. Feb. 28, 1962*, ORNL-3290 (in press).

## 16. Physical Metallurgy

H. Inouye

### AGING PHENOMENA IN DILUTE NIOBIUM-BASE ALLOYS

D. O. Hobson<sup>1</sup>

The lack of agreement on the mechanical properties of different heats of an Nb-1% Zr alloy (commercial designation FS-80) was found to be due mainly to an aging reaction involving zirconium and oxygen. A detailed study of the aging phenomena showed that zirconium restricts the oxygen solubility in the alloy and results in the precipitation of a phase which ultimately forms  $ZrO_2$ .

It was concluded that the aging tendencies of numerous heats of this alloy containing various concentrations of oxygen, nitrogen, and carbon impurities could be predicted on the basis of the oxygen content and the solution annealing temperature. Similar aging phenomena were predicted for other alloys of niobium, provided an element was present that formed a more stable oxide than niobium.<sup>2</sup>

### DISPERSION-STRENGTHENED ALLOYS<sup>3</sup>

Blake King

The high-temperature strength of pure metals can be improved spectacularly by dispersement of a fine array of hard particles, provided that these particles are insoluble in the metal at the service temperatures. The chemical and physical properties of the pure metal, on the other hand, are

altered only slightly in comparison since these properties depend upon the matrix properties.

Dispersion-strengthened pure metals, therefore, lack the corrosion resistance of alloys and have a weaker matrix. To overcome these deficiencies, an investigation was initiated to strengthen an Fe-5% Cr-7% Al-1% Nb-0.5% Ti alloy which possessed exceptional resistance to several oxidizing gases but lacked the desired strength. Mathematical expressions were derived from existing theories of dispersion strengthening for the optimum matrix-particle relationships. It was concluded that the dispersed phase should be  $Al_2O_3$  at a concentration of less than 10 vol % of the alloy and of such a size to give an interparticle spacing between 2 to 3  $\mu$ .

Experiments demonstrated that pure  $Al_2O_3$  could be formed on the matrix alloy by oxidation at about 982°C. Thus the technique selected to introduce the particles into the alloy was to preoxidize master alloy powders prepared from melts and to dilute the required levels with pure elemental powders during consolidation. Promising master alloys which were suitable for mechanical fragmentation to powders contained 60 to 70 wt % Fe, 20 to 38 wt % Al, and 4 to 12 wt % Cr. One group of alloy melts was found to be self-pulverizing at room temperature due to the spontaneous reaction of aluminum carbide with the moisture in the air. Typical compositions of master alloys in this class contained 45 to 62 wt % Fe, 45 to 50 wt % Al, 4 wt % Cr, and 1 to 1.5 wt % C.

### URANIUM-MOLYBDENUM ALLOYS

H. Inouye

Uranium containing 10 to 15 wt % Mo has been considered as a metallic fuel for fast reactors on

<sup>1</sup>Now with Metal Forming and Casting Group.

<sup>2</sup>D. O. Hobson, *Aging Phenomena in Columbium-Base Alloys*, ORNL-3245 (Mar. 16, 1962).

<sup>3</sup>Work done under subcontract with the University of Miami.

the basis of its superior resistance to transformation below 563°C and superior creep resistance above this temperature. Between 400 and 700°C, these two material properties are considered to be the controlling factors which determine the extent of swelling of this alloy during neutron irradiation at subcritical fluxes. It was therefore the purpose of this investigation to determine the alloy composition possessing the greatest resistance to transformation of the metastable  $\gamma$  phase to  $\gamma'$  ( $U_2Mo$ ) and  $\alpha$  ( $\alpha$ -uranium) and the composition possessing the greatest creep strength.

Creep tests were conducted on standard 0.505-in.-diam tensile specimens machined from 1-in.-diam extruded rod, gamma-heat-treated (annealed for 24 hr at 900°C, water-quenched), and tested at 485, 550, and 600°C. A creep rate of  $8.2 \times 10^{-4}\%$ /hr was measured for the U-10% Mo alloy at a stress of 10,000 psi and at 485°C. Data were not obtained for U-13.5% Mo and U-15% Mo alloys, because the specimens ruptured in the threads upon loading.

Comparative creep results obtained for several alloys at a stress of 5000 psi and at 550°C, shown in Fig. 16.1, indicated that the U-13% Mo alloy was the strongest alloy under the test conditions. The specimens tested at 600°C did not exhibit a well-defined second-stage creep and thus did not permit a calculation of the minimum creep rates;

however, data at two stress levels are given in Table 16.1. It appears that the U-15% Mo alloy is the strongest of the alloys tested at this temperature.

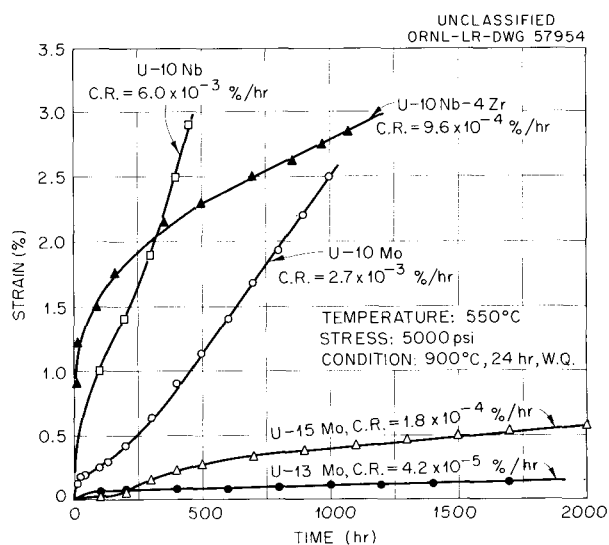


Fig. 16.1. Creep Curves of Uranium-Base Alloys at 550°C.

Table 16.1. Creep Results for Gamma-Heat-Treated U-Mo Alloys Tested at 600°C

Alloy	Time (hr) to a Given Strain					Rupture Life (hr)	Elongation (%)
	0.2%	0.5%	1%	2%	5%		
At 5000 psi							
U-10% Mo				6		180	25.5
U-13.5% Mo	90	350	610	1030		Discontinued at 1082 hr <sup>a</sup>	
U-15% Mo	290	920				Discontinued at 1196 hr <sup>b</sup>	
At 10,000 psi							
U-13% Mo			143	198	293	331	7.5
U-15% Mo			360	540		Discontinued at 763 hr <sup>c</sup>	

<sup>a</sup>3.4% strain.

<sup>b</sup>0.65% strain.

<sup>c</sup>3.83% strain.

Hydrogen absorption occurs in the  $\alpha$  phase at 225°C but not in the  $\gamma$  and  $\gamma'$  (U<sub>2</sub>Mo) phases. This principle was used to determine quantitatively the transformation kinetics of the reaction  $\gamma \rightleftharpoons \gamma' + \alpha$ . The conventional techniques based on hardness, x-ray, metallographic, and resistivity determinations, on the other hand, give only a qualitative measure of this reaction. The results of the experiments are summarized in Table 16.2. Transformation was promoted by cold work and the transformation time, the most stable alloy appeared to be the U-15% Mo alloy, and the effect of stress on the transformation could not be ascertained.

It was concluded from this investigation that the U-15% Mo alloy was the most promising alloy from both the standpoint of creep resistance and the thermal stability in the range 500 to 600°C. Further studies of U-Mo alloys are not planned.

## OXIDATION PROTECTION OF A CAST U-10% Mo ALLOY

H. Inouye

The Fast Burst Reactor, which consists of a critical arrangement of segmented U<sup>235</sup>-10% Mo alloy parts, experiences thermal cycles from room temperature to 800°F in air. The thermal history includes tests as long as 1 hr at 800°F, during which time oxidation of this alloy will cause a serious contamination problem. Therefore the protective properties of various types of nickel coatings on the alloy when thermally cycled (1 hr at 800°F, 15 min at room temperature) were evaluated.

A characteristic feature of all coatings studied was their inconsistent and unpredictable behavior in protecting the uranium alloy. As an example, a

Table 16.2. Transformation Kinetics for the Reaction  $\gamma \rightleftharpoons \gamma' + \alpha$

Alloy	Temperature (°C)	Time (hr)	H <sub>2</sub> (STP) Absorbed per Gram of Alloy (cc)	Amount of Transformation (%)	Amount of $\alpha$ -U in Alloy (wt %)
U-10% Mo	500	48	0.275	0.46	0.172
	500	48 <sup>a</sup>	32.2	53.7	20.15
	500	252	15.7	26.2	9.82
	550 <sup>b</sup>	820	28.2	47.0	17.6
U-13.5% Mo	500	500	0.238	0.795	0.149
	500	500 <sup>c</sup>	1.80	6.0	1.13
	500	2000	0.785	2.62	0.49
	550 <sup>b</sup>	3600	3.36	11.2	2.1
U-15% Mo	500	500			
	500	500 <sup>d</sup>	0.295	4.7	0.298
	500	1000	0.245	4.1	0.256

<sup>a</sup>Cold worked 58% before transforming.

<sup>b</sup>Gage section of creep specimen stressed at 5000 psi.

<sup>c</sup>Cold worked 21% before transforming.

<sup>d</sup>Cold worked <10% before transforming.

0.003-in.-thick nickel plate protected the alloy for 200 cycles, while an alloy coated with a 0.0035-in.-thick layer failed in less than 10 cycles. Furthermore, doubling the plate thickness (0.007 in.) resulted in failure within 60 cycles. Vacuum annealing the coating prior to testing improved the tenacity of the plates somewhat. The uncoated alloy oxidized at a rate of 0.43 mg/cm<sup>2</sup> per cycle.

## NIObIUM-BASE ALLOY STUDIES

T. K. Roche

Niobium-base alloys are of interest as structural materials for systems operating at temperatures greater than 2000°F, which is beyond the maximum useful temperature for the conventional iron-, nickel-, and cobalt-base alloys. An alloy of Nb-1% Zr has been extensively studied. Inadequate strength properties limit its use to temperatures below 2200°F. As a result, an investigation of other niobium-base alloys was initiated with the aim of selecting a composition that will exhibit increased strength above this temperature.

The alloys selected for study were based on the Nb-V system. Hot-hardness and slow-bend tests were used to qualitatively rate the strength of the alloys.

Results of the fabricability tests are included in "Fabrication of Refractory-Metal Alloys," Chap. 18, this report. Data obtained by Armour Research Foundation<sup>4</sup> on Nb-V binary alloys in the composition range of about 25 to 50% V show these alloys to have better short-time strength properties at room temperature and 2000°F than the Nb-1% Zr alloy. Hot-hardness measurements up to 1832°F carried out at ORNL on as-cast samples of alloys containing 1, 10, 20, 30, and 50% V-bal Nb and on a wrought sample of a 60% V-bal Nb alloy confirmed the strengthening effect of vanadium in niobium, with peak strength reached in the 30-50% V range. The hot-hardness data are shown in Fig. 28.9, Chap. 28, this report.

Aging studies were performed on Nb-40% V, Nb-50% V, and Nb-40% V-1% Zr alloys to which had been added 350, 290 and 520 ppm O<sub>2</sub>, respectively. Samples were solution-heat-treated at 2900°F and aged for times up to 500 hr at 1700°F. No indication of aging was noted for the alloys containing 40 and 50% V either metallographically or by room-temperature hardness measurements. How-

ever, the Nb-40% V-1% Zr composition showed the precipitation of a pepper-like phase, presumed to be ZrO<sub>2</sub>, which increased in amount with time. Room-temperature hardness evaluation of this alloy after aging did not show a pronounced hardness peak with increasing aging time as might have been expected.

Recent data were obtained which indicate that Nb-V binary alloys lack creep resistance for long-time high-temperature service. A slow-bend test apparatus was constructed to qualitatively assess materials for their creep resistance. The entire apparatus is under vacuum, and a small specimen of rectangular cross section is suspended as a cantilever beam, loaded to a preselected fiber stress after reaching the test temperature, and then measured for deflection as a function of time. To date, the alloys Nb-1% Zr and Nb-40% V have been tested, under the conditions and with the results shown in Table 16.3. A quantitative comparison of the data cannot be made, because the alloys differed widely in interstitial content and the Nb-40% V alloy test was run under conditions of better vacuum. Nevertheless, a lack of creep resistance by the Nb-40% V alloy is indicated. Similar results were also obtained by Armour Research Foundation<sup>5</sup> in their stress-rupture tests on a series of alloys of base composition V-1% Ti-60% Nb at 2000°F and a stress of 10,000 psi. Rupture times were relatively short, varying from 13 hr for the alloy V-1% Ti-60% Nb to 47.7 hr for the alloy V-1% Ti-10% Ta-60% Nb. Several of the compositions showing intermediate rupture times were alloys with carbon, oxygen, nitrogen, and boron added singly up to 500 ppm and tungsten added singly at the 5 wt % level to the base composition.

At the present time, the available strength data do not favor the use of Nb-V alloys for long-time, high-temperature (>2000°F) application. However, this system does appear attractive at lower temperatures (<1800°F).

A program is being formulated to evaluate selected high-strength alloys. The alloys of interest have already been through a laboratory development stage and include the following compositions: Ta-8% W-2% Hf; Nb-5% Mo-5% V-1% Zr; Nb-10% W-1% Zr-0.1% C; Nb-27% Ta-10% W-1% Zr; Nb-5% W-1% Zr-0.2% Y-0.06% C; Ta-30% Nb-7.5% V.

<sup>4</sup>Improved Vanadium-Base Alloys (Bimonthly Report No. 2), ARF-2210-2.

<sup>5</sup>Improved Vanadium-Base Alloys (Final Report), ARF-2210-6.

Table 16.3. Conditions and Results of Slow-Bend Tests

Temperature: 2200°F  
Fiber stress: 8000 psi

Alloy	Analysis (ppm)			Test Duration (hr)	Sample Deflection (in.)	Pressure (mm)	Remarks
	O <sub>2</sub>	N <sub>2</sub>	C <sub>2</sub>				
Nb-1% Zr	950	180	190	221	0.122	> 10 <sup>-5</sup> during heatup  10 <sup>-5</sup> at beginning of test  2.2 × 10 <sup>-6</sup> at end of test	Specimen discolored after test
Nb-40% V	350	130	140	13	0.543	≤ 10 <sup>-5</sup> during heatup  5 × 10 <sup>-6</sup> at beginning of test  1.5 × 10 <sup>-6</sup> at end of test	Specimen bright after test

Table 16.4. Comparison of Nil-Ductility Temperature with Melting-Temperature Range for Various Heats of INOR-8

Heat Number	Vendor	Nil-Ductility Temperature (°F)	Melting-Temperature Range (°F)	
			Liquidus Temperature	Solidus Temperature
Y-8488	INCO	2300		2480 ± 18
NI-5055	Haynes	2245		2435 ± 9
SP-19	Haynes	2400		2480 ± 18
SP-26	Haynes		2559 ± 2	
M-1666	Westinghouse		2552	

### MELTING POINT OF INOR-8

T. K. Roche

The observance of base-metal cracking in certain heats of INOR-8 when welded under restraint prompted a more accurate determination of its temperature range of melting.<sup>6</sup> The cooling curve method and the tension-fracture method were used

for determining the liquidus and solidus temperatures, respectively. These data served as the basis for comparing the nil-ductility temperatures of the various heats of INOR-8. The nil-ductility temperatures were determined by Rensselaer Polytechnic Institute in their hot-ductility apparatus and the ductility was found to be inferior at high temperatures.

Typical data are presented in Table 16.4. Although no definite conclusions are yet possible, the solidus temperatures appear to be somewhat higher than the nil-ductility temperatures, thereby creating

<sup>6</sup>MSRP Progr. Rept. Mar. 1-Aug. 31, 1961, ORNL-3215, p 102.

some doubt that liquid phases are the cause of the elevated-temperature brittleness reported.

## EVAPORATION OF IRON, NICKEL, AND COBALT ALLOYS IN HIGH VACUA

D. T. Bourgette

Conventional high-temperature alloys are being considered for use in vacua less than  $10^{-6}$  torr. The vapor pressures of the elements will cause these alloys to evaporate if they are heated to high temperatures under these vacuum conditions. The selective alloy depletion that is expected could lead to compositional changes which would affect their mechanical properties. It was the purpose of this investigation to determine the evaporation characteristics and the resultant effect on the mechanical properties of several alloys and to investigate methods of minimizing evaporation.

Experimental techniques were developed and evaporation rates determined for types 316, 304, 446 stainless steels, Inconel, INOR-8 (17% Mo-7% Cr-bal Ni), and Haynes alloy No. 25 at 871 and

982°C and at pressures of  $5 \times 10^{-7}$  torr. The evaporation rates as determined from weight-loss measurements are summarized in Table 16.5. A study of these data shows that the evaporation rates increase with the chromium content of the alloys, as would be expected from vapor pressure considerations. The rates are, however, between one or two orders of magnitude less than those predicted for evaporation of the component elements into free space. Presently, it is speculated that this difference is due to the test conditions and not to the interacting effects of the alloying elements on each other.

The selective loss of alloying elements was confirmed by analysis of the vaporized metal deposits. As an example, the analysis of the deposit vaporized from type 304 stainless steel (Table 16.6) showed that the proportional silicon, manganese, and chromium losses were greater than either iron or nickel. With the exception of silicon, these values are in proportion to their vapor pressures. The evaporation rates of oxidized specimens were lower by factors of between 2 and 10. Metal losses decrease the tensile and yield strengths and increase the ductility of the alloys.

Table 16.5. Evaporation Rates of Alloys at  $5 \times 10^{-7}$  Torr

Alloy	Initial Chromium Content (wt %)	Evaporation Rate ( $\text{mg cm}^{-2} \text{hr}^{-1}$ ) <sup>a</sup>			
		At 871°C		At 982°C	
		Initial	Final	Initial	Final
INOR-8	6.78			$2.5 \times 10^{-3}$	$2.0 \times 10^{-3}$
Inconel	14.81	$5.7 \times 10^{-4}$	$2.8 \times 10^{-4}$	$6.0 \times 10^{-3}$	$3.0 \times 10^{-3}$
Type 316 stainless steel	15.86	$4.5 \times 10^{-3}$	$6.7 \times 10^{-4}$	$11.3 \times 10^{-3}$	$6.7 \times 10^{-3}$
Type 304 stainless steel	18.04	$2.1 \times 10^{-3}$	$2.7 \times 10^{-4}$	$8.3 \times 10^{-3}$	$3.5 \times 10^{-3}$
Haynes alloy No. 25	19.40	$6.8 \times 10^{-3}$	$4.6 \times 10^{-3}$	$12.5 \times 10^{-3}$	$5.7 \times 10^{-3}$
Type 446 stainless steel	24.70	$7.5 \times 10^{-3}$	$1.0 \times 10^{-3}$	$1.3 \times 10^{-2}$	$1.1 \times 10^{-2}$

<sup>a</sup>Initial rates based on first 30 hr of test; final rates based on the rates between 500 to 600 hr.

Table 16.6. Analysis of Deposits Evaporated from Type 304 Stainless Steel at 982°C and  $5 \times 10^{-7}$  Torr.

Element	Analysis of Original Alloy (wt %)	Analysis of Vapor Deposit (wt %)	Ratio (wt %): Deposit/Original	Vapor Pressure of Element (torr)
Manganese	1.63	6.00	3.68	$5 \times 10^{-3}$
Chromium	18.30	41.25	2.26	$2 \times 10^{-5}$
Silicon	0.050	0.939	18.75	$5 \times 10^{-8}$
Iron	~69.6	49.75	0.715	$2 \times 10^{-7}$
Nickel	10.44	2.01	0.192	$7 \times 10^{-8}$

### REACTIONS OF TYPE 304 STAINLESS STEEL WITH LOW-PRESSURE CO AND CO<sub>2</sub>

H. Inouye

The fuel elements of the EGCR will be clad with type 304 stainless steel and will be exposed to helium at 315 psia for periods up to 25,000 hr (3 yr) at estimated temperatures between 200 to 1000°C. The helium will contain small amounts of impurity gases such as CO, CO<sub>2</sub>, H<sub>2</sub>, H<sub>2</sub>O, and CH<sub>4</sub>, and the coolant is therefore expected to react with the cladding to cause oxidation, carburization, and decarburization. The purpose of this investigation was to determine the permissible limits of CO and CO<sub>2</sub>, the nature of the surface reactions, and an indication of the degree of control attainable over these reactions by controlling the gas composition.

It was found that by varying the  $P_{\text{CO}_2}/P_{\text{CO}}$  ratio numerous types of oxides could be formed, some being protective and others nonprotective. The presence of the nonprotective oxides was evidenced by an accelerated rate of oxidation and was due to the formation of Fe<sub>3</sub>O<sub>4</sub> and FeO. This could constitute a problem, since, in addition to being nonprotective, Fe<sub>3</sub>O<sub>4</sub> is not adherent when the oxidation exceeds 0.3 mg/cm<sup>2</sup>. Thus it might, during a reactor temperature excursion, introduce abrasive particles into the high-velocity helium stream and carry radioactive particles to various parts of the gas system.

The initiation of the accelerated oxidation rates, commonly called the "breakaway" phenomenon, was extended to longer times as the  $P_{\text{CO}_2}/P_{\text{CO}}$  ratio was decreased. The critical gas ratio below

which this phenomenon was not observed was experimentally determined to be between 0.45 and 0.67 at 982°C. To control this undesirable reaction, it was concluded that the reaction  $\text{Fe} + \text{CO}_2 \rightarrow \text{FeO} + \text{CO}$  should be prevented. The equilibrium  $P_{\text{CO}_2}/P_{\text{CO}}$  ratio for this reaction at 982°C is 0.40 and increases as the temperature decreases.

As the  $P_{\text{CO}_2}/P_{\text{CO}}$  ratio was further decreased below 0.40, combinations of NiO, FeO, and MnO with Cr<sub>2</sub>O<sub>3</sub> which had spinel structures developed and then gradually disappeared at the lowest gas ratios, leaving only Cr<sub>2</sub>O<sub>3</sub> detectable. Under these conditions ( $P_{\text{CO}_2}/P_{\text{CO}}$  values between 0.018 to 0.45), the reactions obeyed the parabolic growth rate and were insensitive to the concentrations of these gases.

Carburization of the metal occurred concurrently with oxidation for gas compositions studied above about 600°C. The carburization increased uniformly with temperature, reaching maxima between 800 to 900°C and then decreasing with further increase in temperature. The variables that determined the carbon content of the alloy for a given time were the oxidation reaction, the carbon potential  $(P_{\text{CO}})^2/P_{\text{CO}_2}$ , and the reaction temperature.

These interacting effects led to the occurrence of another carbon maxima at a  $(P_{\text{CO}})^2/P_{\text{CO}_2}$  value of 0.227 for all temperatures above 700°C.

Of the above controlling variables, it was concluded that the overriding factor influencing the carbon content of the alloy was the ability of the oxide layer to act as a barrier for carbon diffusion. The most desirable oxides were Cr<sub>2</sub>O<sub>3</sub>, the spinels, and the oxides of iron, in that order.

On the basis of this investigation, it was concluded that both the oxidation and the carburizing reactions can be controlled by maintaining gas conditions which favor the formation of  $\text{Cr}_2\text{O}_3$  as a surface layer. The details of this investigation have been reported.<sup>7</sup>

### OXIDATION STUDIES

T. K. Roche      H. Inouye

It was the purpose of this investigation to evaluate the oxidation resistance of numerous conventional high-temperature alloys since many of the present testing programs employ these alloys in the range 700 to 1050°C.

The results of oxidation runs at 927, 982, and 1038°C are shown in Table 16.7. With the exception of the stainless steels, all the alloys oxidized at a rate which decreased with time, indicating that protective oxides were being formed on the surface and therefore that the alloys would be suitable for long-time tests. Contrary to the accepted belief that oxidation rates decrease as the chromium content is increased, the weight-gain data indicated that the oxidation rates increased with the chromium content of the alloys tested. This behavior tentatively is attributed to the formation of nitrides in addition to the oxide.

Type 316 stainless steel exhibited a sharp breakaway oxidation at all temperatures for a short period of about 20 hr. Thereafter the oxidation decreased to a very slow rate. The rate curve for the oxidation of type 446 stainless steel consisted of consecutive series of jogs of a parabolic shape. Apparently, the intermittent periods of rapid weight gain occurred when there were ruptures in the protective oxide film. Type 310 stainless steel showed an increasing rate of oxidation after about 200 hr above 982°C, indicating the onset of accelerated oxidation or breakaway oxidation. These data demonstrate that the usually recommended oxidation-resistant alloys such as types 446 and 310 stainless steels are not so desirable as some containing less chromium.

An aluminum bronze alloy, although not a high-strength metal, was tested merely to show its superiority over the conventional alloys. In fact,

<sup>7</sup>GCR Quart. Progr. Rept. Mar. 31, 1962, ORNL-3302 (in press); H. Inouye, GCR Quart. Progr. Repts. Dec. 31, 1961, ORNL-3254, pp 48-50; Sept. 30, 1961, ORNL-3210, pp 47-52; and June 30, 1961, ORNL-3166, pp 104-6.

the oxidation rate at 7°C below its melting point of 1021°C was not significantly different from that at 982°C.

### CLADDING STUDIES

T. K. Roche

Refractory metals must be coated or clad with oxidation-resistant materials when intended for elevated-temperature service if vacua or inert gases are not employed. The cladding of niobium with conventional oxidation-resistant alloys results in the formation of brittle reaction layers at the composite interface which fracture when thermally cycled due to the wide difference in their expansion coefficients.<sup>8</sup> This investigation was for the purpose of developing suitable metal composites for service in oxidizing environments up to about 1000°C. Two approaches were evaluated, both of which were designed to eliminate the brittle reaction layer at the composite interface. One method depended upon use of a ductile transition layer which would not react with the cladding or the niobium. Silver was used for this purpose in a type 304 stainless steel-niobium composite. Metallurgical bonds that withstood severe flattening and bending tests were achieved by vacuum brazing the component parts. Thermal cycling a 6-in.-long specimen of such a composite between room temperature and 780°C over a period of 13 days (11 cycles) resulted in a 1/2% increase in the length of the stainless steel cladding. Subsequent bending and flattening tests caused a separation of the composite at the stainless steel-silver interface.

In the other approach, several layers differing in composition were inserted between the stainless steel and the niobium in an attempt to develop a transition layer with a graded expansion coefficient. Furthermore, the transition layers were fabricated from metal powders so as to control the distribution of the brittle reaction phases. Metallographic examination of representative reaction zones indicated that the distribution of the brittle phases can be changed by this method. Service tests under transient thermal conditions have not been completed.

<sup>8</sup>T. K. Roche, *Met. Div. Ann. Progr. Rept. May 31, 1961, ORNL-3160, p 145.*

Table 16.7 Oxidation Rates of High-Temperature Alloys Tested in Air at 927, 982, and 1038°C

Test Time (hr)	Weight Gain (mg/cm <sup>2</sup> )						
	Type 316 Stainless Steel	Haynes Alloy No. 25	Type 310 Stainless Steel	Type 446 Stainless Steel	Inconel	INOR-8	94% Cu-6% Al
At 927°C							
10	0.17	1.0	0.28	0.20	0.05	0.04	0.10
25	0.28	1.29	0.49	0.37	0.22	0.07	0.12
50	2.77	1.33	0.59	0.52	0.33	0.10	0.13
100	4.26	1.55	0.64	1.05	0.44	0.18	0.15
200	4.30	1.74	0.83	1.38	0.62	0.29	0.17
300	4.35	1.89	0.97	1.52	0.74	0.35	0.18
At 982°C							
10	0.8	0.36	0.50	0.47	0.42	0.10	0.21
25	6.8	0.69	0.73	0.71	0.53	0.21	0.26
50	7.2	1.01	0.95	0.95	0.67	0.31	0.30
100	7.3	1.36	1.22	1.34	0.88	0.45	0.31
200	7.5	1.84	1.58	1.89	1.15	0.64	0.32
300	7.6	2.21	1.97	2.42	1.35	0.77	0.33
At 1038°C							
10	15.5	0.9	1.07	0.85	0.67	0.50	
25	26.0	1.25	1.72	1.55	0.92	0.68	
50	28.3	1.7	2.52	2.20	1.17	0.85	
100	28.3	2.27	3.77	3.95	1.50	1.13	
200	28.3	3.15	5.82	4.80	2.07	1.58	
300	28.3	3.72	7.62	5.55	2.47	1.97	

## CONTAMINATION STUDIES OF REFRACTORY METALS

H. Inouye

Refractory metals are easily contaminated by gases at high temperatures, which affects their mechanical and chemical properties. The gas-metal reactions lead to material failure or to test results that are not representative of the metal under investigation. Because the extent of the gas-metal reactions depends upon the concentration of the active gas species, the usual precaution taken to minimize contamination is to heat the metal under vacuum or in inert gases. The purpose of this investigation is to determine which environment should be used for extended exposure times of the metal at temperatures up to 1200°C and the permissible concentrations of the active gases when the metal of interest is niobium and its alloys.

The methods that were explored to assess the extent of gaseous contamination were based on weight change, hardness, analysis of the metal after test, and tensile properties. Of these various methods, analysis of the metal was considered to be the most reliable measure of the extent of contamination.

Hardness and tensile property changes were observed to correlate with the weight changes only when the metal did not age and when there was a weight gain. At 1000°C weight gains were observed at  $1 \times 10^{-5}$  torr and weight losses at  $3 \times 10^{-6}$  torr. It is suspected that the weight losses at the lower pressure were due to evaporation since oxidation has been demonstrated to occur at this pressure.<sup>9</sup>

The rate of the chemisorption of gases on the surface of the metal was found to be the controlling variable during the initial stages of contamination below  $1 \times 10^{-4}$  torr and the diffusion rates of the contaminant within the metal to be rate-controlling thereafter. Thus niobium alloys that contain elements which form oxides more stable than niobium are contaminated with oxygen at a higher than normal rate since such elements serve as a sink for the dissolved gas.<sup>10</sup>

In gaseous mixtures such as air at 1000 and 1200°C and at pressures between 1 and  $5 \times 10^{-4}$  torr, niobium is contaminated with both oxygen and nitrogen in the ratio of about 100:1, respectively, even though the gas concentrations are in the ratio 1:4. This behavior was concluded to be due to the diffusion rate of oxygen in the metal being higher than that of nitrogen. For equivalent oxygen pressures, the reaction rates in gas mixtures were lowered by an order of magnitude when nitrogen was present.<sup>10</sup> This indicates that chemisorption of nitrogen on the metal surface was responsible for the observation.

Although highly purified argon or helium in a thoroughly outgassed system (baked for 72 hr at approx 900°C) was demonstrated to provide protection equivalent to a vacuum of  $1 \times 10^{-5}$  torr, it was concluded that high-temperature tests of refractory metals should be conducted in vacua for the following reasons: The permissible gas impurity levels are estimated to be in the range  $1 \times 10^{-7}$  torr (1 part/10 billion), which is beyond the analytical sensitivity of all instruments except the mass spectrometer. Furthermore, an immediate response occurs in vacuum systems when the impurity concentration changes since the vacuum gages and the mass spectrometer measure only the impurities of interest.

## MOLYBDENUM RESEARCH

W. J. Werner

The potential value of molybdenum in high-temperature devices relies on its use in atmospheres that are not oxidizing. Suitable environments appear to be vacua, liquid metals, and gases that are reducing toward its oxides. Preliminary experiments confirmed that molybdenum is tolerant of high proportions of water vapor. This tolerance can be further increased by the presence of hydrogen.

Although the brittleness of molybdenum near room temperature, and hence its lack of fabricability, is an obstacle to its use as a material of construction, techniques have been developed for the fabrication of thin-walled tubing. The tubing made to date has not been of the high quality required in reactors.

<sup>9</sup>J. E. Spruiell, "The Oxidation of Columbium at 850°C in Oxygen at Low Pressures," Masters degree thesis, Department of Chemical and Metallurgical Engineering, University of Tennessee, June 1960.

<sup>10</sup>H. Inouye, *Met. Div. Ann. Progr. Rept.* May 31, 1961, ORNL-3160, p 144.

## BERYLLIUM CORROSION RESEARCH

W. J. Werner

One obstacle which prevents the use of beryllium in  $\text{CO}_2$  environments above  $600^\circ\text{C}$  is its lack of corrosion resistance when water vapor is also present. This investigation is a continuation of a research program directed toward an understanding of the factor(s) leading to the occurrence of an accelerated rate of oxidation commonly referred to as the "breakaway" phenomenon. As was previously reported,<sup>11</sup> it was theorized that the reaction observed between  $\text{Be}_2\text{C}$  and water vapor initiated the breakaway phenomenon in beryllium of commercial purity.

The solution to the problem during this period was approached by using ultrapure metal, in the belief that impurities concentrated at the grain boundaries were responsible for the lack of corrosion resistance, and by alloying beryllium. Corrosion tests of a Be-0.5% Ba alloy were conducted in dry  $\text{CO}_2$  with the hope that barium would form a protective carbonate layer. Preliminary results indicated that the reaction rates of the alloy decrease with increases in the  $\text{CO}_2$  pressure, which is not observed in unalloyed beryllium. The corrosion rate of the alloy was greater than that of the unalloyed metal. A zone-refined single crystal of beryllium was obtained for further studies.

---

<sup>11</sup>W. J. Werner, *Met. Div. Ann. Progr. Rept. May 31, 1961*, ORNL-3160, p 143.

**Part III**  
**Metal and Ceramic Fabrication**

G. M. Adamson, Jr.

---



## 17. Ceramics Technology

W. O. Harms

### BeO AND FUELED BeO STUDIES

#### Fabrication Development of BeO

R. L. Hamner

High-purity BeO specimens with carefully controlled properties were fabricated for irradiation experiments in the Engineering Test Reactor (ETR). These experiments were designed to evaluate BeO as a moderator material for reactors in which large fast neutron doses would be accumulated. Cold pressing and sintering techniques were used to fabricate the specimens to dimensional tolerances of  $\pm 0.002$  in. without machining. Fabrication procedures were based on studies of the effect of green density and sintering time on the shrinkage characteristics and sintered densities of the specimens. Grain size was controlled by the time of heat treatment at 1750°C.

Approximately 900 specimens were prepared to density, dimensional, and microstructural specifications.<sup>1-5</sup> These experiments were statistically designed for studying the effects of density, grain size, and temperature on BeO bodies irradiated at fast neutron ( $>1$  Mev) doses of greater than  $10^{21}$  neutrons/cm<sup>2</sup>. The specimens were of two sizes and of four types: high-density specimens, 97%

of theoretical density, composed of two groups varying in grain size by a factor of 3 (average grain diameters of 24 and 70  $\mu$ ), and low-density specimens, 90% of theoretical density, composed of two groups varying in grain size by a factor of 2 (average grain diameters of 17 and 34  $\mu$ ). The high-density specimens were prepared without the use of binders; the low-density specimens were sintered under the same conditions, but an epoxy resin was used as a fugitive organic material to provide high porosity. Specimens with small grain size were sintered for 1 hr at 1750°C and those having larger grain size were heat-treated for 60 hr at 1750°C. All heat treatments were carried out in a hydrogen atmosphere.

It was observed that the bulk density of BeO bodies was affected markedly when the rate of heating to the sintering temperature in a hydrogen atmosphere was widely varied. The final bulk density obtained for a material pressed to a given green density decreased from 96 to 64% of theoretical when the time to reach the sintering temperature was increased from 2 to 24 hr.<sup>1</sup> These results are directly opposite to those reported by Livey *et al.*<sup>6</sup> based on sintering studies of BeO conducted in an air atmosphere. They are consistent, however, with results obtained recently by Morize.<sup>7</sup> The effect observed may be attributed to the prolonged exposure of the BeO to trace amounts of moisture in the hydrogen atmosphere during sintering,<sup>8</sup> or simply to the activity of the powder being reduced during long exposure to temperatures lower than that necessary for satisfactory sintering.

<sup>1</sup>R. L. Hamner, *GCR Quart. Progr. Rept. Sept. 30, 1961*, ORNL-3210, pp 233-34.

<sup>2</sup>R. L. Hamner, *Mel. Div. Ann. Progr. Rept. May 31, 1961*, ORNL-3160, p 63.

<sup>3</sup>R. L. Hamner, *GCR Quart. Progr. Rept. June 30, 1961*, ORNL-3166, pp 83-84.

<sup>4</sup>R. L. Hamner, *GCR Quart. Progr. Rept. Dec. 31, 1961*, ORNL-3254, pp 263-64.

<sup>5</sup>*GCR Quart. Progr. Rept., Mar. 31, 1962*, ORNL-3302 (in press).

<sup>6</sup>D. T. Livey *et al.*, *Nucl. Energy [IV]* 3, 111-34 (1960).

<sup>7</sup>P. Morize, Centre d'Etudes Nucléaires de Saclay, private communication.

<sup>8</sup>C. A. Aitken, *J. Am. Ceram. Soc.* 43(12), 630 (1960).

### Fabrication Development of Fueled BeO

A. T. Chapman      R. L. Hamner  
R. E. Meadows      A. J. Taylor

Studies of large-particle (100 to 500  $\mu$ ) dispersions of  $\text{UO}_2$  and  $(\text{U}, \text{Th})\text{O}_2$  solid solutions in BeO were continued<sup>9,10</sup> as part of a long-range development program for advanced gas-cooled power reactors. The fabrication procedures used in cold pressing and sintering were essentially the same as those described previously.<sup>9,10</sup>

Prototype specimens containing 30 vol % of depleted  $\text{UO}_2$  were fabricated for high-temperature irradiation experiments designed to investigate the effect of a controlled void volume around the fuel particles on the dimensional and structural integrity and on fission-gas release during irradiation. The void volume was obtained by incorporating fuel particles which exhibited a higher shrinkage than the BeO matrix. Calculations based on experimentally determined linear shrinkages of 19% for the BeO matrix and 23% for the  $\text{UO}_2$  fuel particles indicated that void gaps of 2.0 to 2.5  $\mu$  had been obtained in the specimens. The incorporation of voids of this size in the sintered specimen results in a decrease in the final density from 95 to approximately 92% of theoretical.

Several techniques for producing spheroidal fuel particles were experimentally evaluated.<sup>11</sup> Satisfactory spheroidal fuel particles for the experiment were made by tumbling irregularly shaped granules of a selected green density in a high-velocity air stream. By continuously removing the fines instead of allowing them to accumulate on the particles, uniform densification of the particles during sintering was obtained. This feature reduced the tendency for internal voids and laminations to form and offers the economically attractive possibility of reprocessing the fines for subsequent spheroidization.

<sup>9</sup>R. L. Hamner, *GCR Quart. Progr. Rept. Dec. 31, 1960*, ORNL-3049, pp 196-201.

<sup>10</sup>R. L. Hamner, *Met. Div. Ann. Progr. Rept. May 31, 1961*, ORNL-3160, p 64.

<sup>11</sup>*GCR Quart. Progr. Rept. Mar. 31, 1962*, ORNL-3302 (in press).

### Phase Relationships in BeO-Metal Oxide Systems

A. T. Chapman      R. E. Meadows

Phase studies were continued in BeO-metal oxide systems by using the porous collector technique.<sup>12</sup> The temperature of first liquid formation was determined for a number of compositions in the ternary system  $\text{BeO-MgO-ZrO}_2$ . These data are presented in Fig. 17.1 and establish the ternary eutectic plane at  $1720 \pm 10^\circ\text{C}$ . The contour of the temperature-composition surface indicates an extensive area of solid solubility in the  $\text{ZrO}_2$ -rich portion of the system. However, this region of solid solubility was not unequivocally substantiated by x-ray diffraction, petrography, and metallography of quenched and furnace-cooled specimens.

The eutectic temperature and composition for the BeO-MgO and BeO- $\text{ZrO}_2$  systems were reported previously.<sup>12</sup> The third binary side, MgO- $\text{ZrO}_2$ , of this ternary system was examined with the porous collector technique, and the eutectic temperature and composition were established at  $2080 \pm 10^\circ\text{C}$  and  $35 \pm 2$  mole %  $\text{ZrO}_2$ , respectively.

<sup>12</sup>A. T. Chapman, R. A. Potter, and R. E. Meadows, *Met. Div. Ann. Progr. Rept. May 31, 1961*, ORNL-3160, pp 62-63.

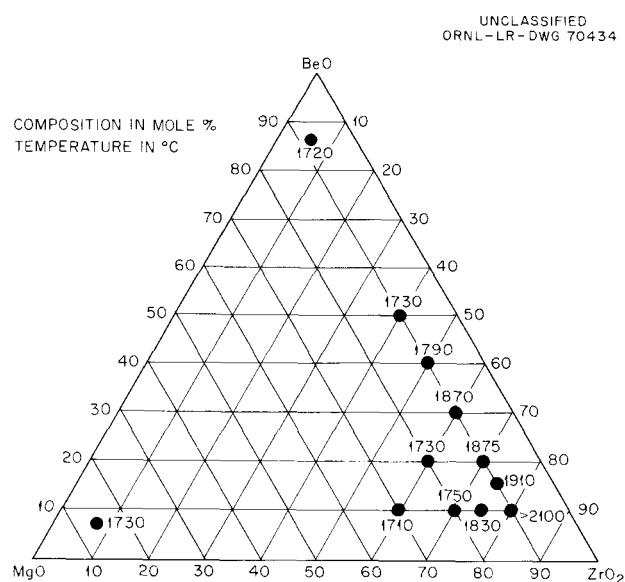


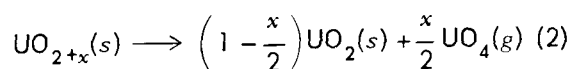
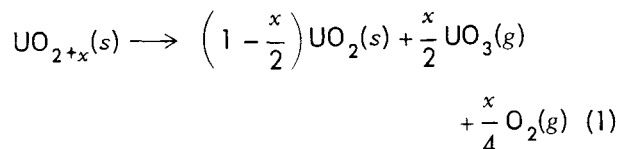
Fig. 17.1. Temperature of First Melting in the Ternary System  $\text{MgO-ZrO}_2\text{-BeO}$ .

## Phase Relationships in the U-O System

A. T. Chapman      R. E. Meadows

A program was designed to evaluate the potential of fueled BeO for use in gas-cooled power reactors having all-ceramic fuel elements. The effects of temperature and oxygen pressure on the phase relationships in the uranium-oxygen system are of interest in connection with the migration or loss of fuel and with the compatibility of coolant and BeO-UO<sub>2</sub> and BeC-(U, Th)O<sub>2</sub> fuel elements that are not sealed in a metallic can.

Thermogravimetric equipment was designed and constructed for use at temperatures as high as 1800 to 2000°C in vacuum or 1400 to 1600°C in various gases. Preliminary results showed that above 1200 to 1300°C at a pressure of 10<sup>-5</sup> to 10<sup>-6</sup> torr, UO<sub>2+x</sub> (0 < x < 0.2) loses weight; the magnitude of this loss indicates that a volatile uranium species is present. Experiments at 1500 to 1700°C showed that this process was essentially complete after the O/U ratio reached 2.02 to 2.04. Two reactions which could explain this behavior are given below:



Both reactions indicate that UO<sub>2+x</sub> under the described environmental conditions produces a volatile component (or components) with a "composite" O/U ratio of 4. The theoretical amount of weight lost, which is also the same for both reactions, can be calculated by knowing the O/U ratio of the starting material and final residue.

The theoretically predicted weight losses and O/U ratio of the volatile phase based on reactions 1 and 2 are compared with experimental values in Table 17.1. These data show that the proposed reactions adequately describe the experimental results; however, the experimental method does not provide a distinction between UO<sub>4</sub> and UO<sub>3</sub> plus O<sub>2</sub> as the gas-phase components. Since other investigators have identified UO<sub>3</sub> as a gas, reaction 1 is probably the correct one to use in the interpretation of these data.

These findings indicate that the loss of uranium as a volatile phase can readily occur from cubic UO<sub>2+x</sub> and suggest that equilibrium studies in the uranium-oxygen system should include UO<sub>3</sub> and UO<sub>4</sub> as well as oxygen as possible gas-phase components.

During additional experiments it was possible to detect the relatively rapid weight changes accompanying the loss or gain of oxygen from powdered UO<sub>2+x</sub>, U<sub>3</sub>O<sub>8-y</sub>, or a mixture of both, as the materials were cycled across the two-phase region in which the orthorhombic U<sub>3</sub>O<sub>8-y</sub> and the cubic UO<sub>2+x</sub> are in equilibrium. (This region is represented as a line on an oxygen pressure-temperature diagram.) The specimens were successively heated and cooled in a fixed oxygen pressure, and the

Table 17.1. Comparison of Experimental Data Obtained by Heating UO<sub>2+x</sub> Powders to 1600 to 1700°C at 10<sup>-5</sup> to 10<sup>-6</sup> Torr with Theoretical Predictions Based on Reactions 1 and 2

Experiment No.	O/U Ratio of Starting Material		O/U Ratio of Volatile Material		Weight Loss (%)	
	Initial	Final	Theoretical	Experimental	Theoretical	Experimental
VF-4	2.186	2.031	4.0	4.2	8.4	8.7
VF-7	2.186	2.022	4.0	4.0	8.8	9.1
VF-8	2.003	2.003				
VF-13	2.081	2.026	4.0	4.1	3.0	2.7

weight change was noted as a function of temperature. It was necessary to compensate for the continual loss of gaseous  $\text{UO}_3$  or  $\text{UO}_4$ ; however, the rate of oxidation or oxygen depletion as the sample crossed the two-phase region was rapid enough to permit positive recognition of the event.

The data obtained are presented in Fig. 17.2. The high-temperature (1550°C) experimental point was reported earlier<sup>13</sup> and was obtained during quenching studies in air. No attempt was made to investigate the stability region of  $\text{U}_4\text{O}_{9-y}$ ; the technique used, at least at present, cannot distinguish  $\text{U}_4\text{O}_{9-y}$  from  $\text{UO}_{2+x}$ . In addition, the experimental conditions are such that gaseous  $\text{UO}_3$  or  $\text{UO}_4$  is continually removed from the sample and deposited in cooler regions of the furnace. The influence of  $\text{UO}_3$  or  $\text{UO}_4$  on the equilibrium oxygen pressure is unknown, and the representation in Fig. 17.2 may be valid only when the pressure of the volatile species is low.

<sup>13</sup>A. T. Chapman, R. A. Potter, and R. E. Meadows, *Met. Div. Ann. Progr. Rept. May 31, 1961*, ORNL-3160, p 63.

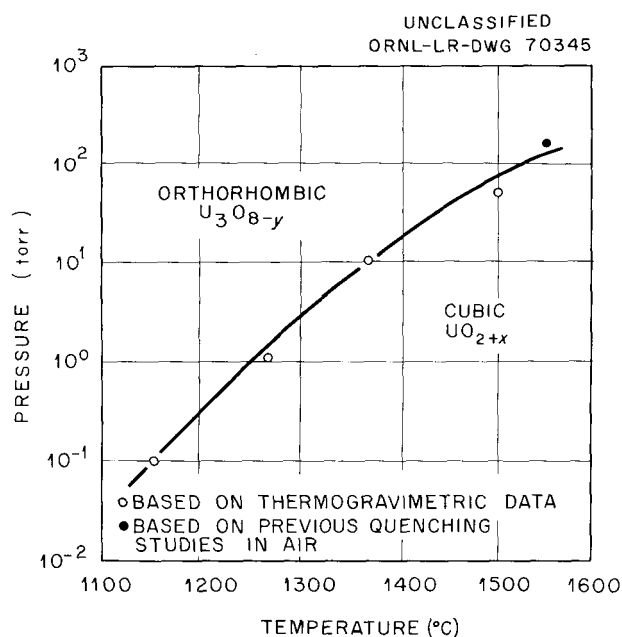


Fig. 17.2. Experimentally Determined Oxygen Pressures and Temperatures at Which  $\text{UO}_{2+x}$  and  $\text{U}_3\text{O}_{8-y}$  Are in Equilibrium.

## GRAPHITE AND FUELED GRAPHITE STUDIES

### Coated Particle Fuel Element Development<sup>14</sup>

R. L. Beatty

F. L. Carlsen, Jr.

E. S. Bomar

J. L. Cook

In the development of fuel elements based on the coated particle concept the Ceramics Laboratory specifies and prepares, or procures, the fuel particles and fuel bodies, performs the necessary pre-irradiation examinations, specifies the conditions for and assists in the design of the irradiation tests, and assists in the postirradiation examinations.

The out-of-pile properties and the behavior of materials under irradiation are being correlated by examining samples of both coated particles and fueled bodies containing coated particles which have been or will be exposed in various research reactors. Coated-particles and fueled-graphite bodies were procured from several sources and a number of their preirradiation properties measured.<sup>15-18</sup> Forty-two lots of particles have been received and are in varying stages of examination.

If a relatively clean reactor system is to result from use of fuel elements utilizing the coated particles, close control over exposed fuel is required. The exposed fuel may result from either surface contamination or from defective coatings. Surface contamination is measured by counting the alpha particles emitted from the surface of the coated particle. Defective coatings are detected by leaching with 8 M  $\text{HNO}_3$ . With a few exceptions, the various lots of coated particles from commercial sources have met the requirement of the total exposed fuel not exceeding  $5 \times 10^{-3}\%$  of the contained fuel.

<sup>14</sup>T. Hikido, J. M. Kerr, and F. L. Carlsen, Jr., *Met. Div. Ann. Progr. Rept. May 31, 1961*, ORNL-3160, p 58.

<sup>15</sup>J. M. Kerr, *GCR Quart. Progr. Rept. June 30, 1961*, ORNL-3166, pp 84-86.

<sup>16</sup>J. M. Kerr, F. L. Carlsen, Jr., and T. Hikido, *GCR Quart. Progr. Rept. Sept. 30, 1961*, ORNL-3210, pp 133-38.

<sup>17</sup>E. S. Bomar et al., *GCR Quart. Progr. Rept. Dec. 31, 1961*, ORNL-3254, pp 137-45.

<sup>18</sup>*GCR Quart. Progr. Rept. Mar. 31, 1962*, ORNL-3302 (in press).

Samples have been thermally cycled to 1450 to 1500°C to test the resistance of the coatings to stresses caused by differential thermal expansion and the ability of the coatings to prevent migration of the fuel. Sixteen lots of particles from each of four sources showed both good and poor performance; the reasons for the failures were not determined.

Contact radiography techniques were developed in conjunction with Nondestructive Testing (Chap. 15, this report) and with Metallography<sup>19</sup> and proved to be an effective means of detecting migration of fuel in the coating, as shown in Fig. 17.3. Radiography was also used to check on the contour of the core particles, as shown in Fig. 17.4, to measure the core diameter and cladding thickness, and to

<sup>19</sup>C. K. H. DuBose and R. J. Gray, *Metallography of Pyrolytic Carbon Coated and Uncoated Uranium Carbide Spheres*, ORNL TM-91 (Mar. 21, 1962).

detect the presence of high-density inclusions, such as fuel fragments, in the coating layer.

Microscopic examinations supplemented by x-ray diffraction showed that  $UC_2$ , UC, and graphite are the principal constituents of the uranium carbide fuel particles. Pyrolytic carbon coatings were found to range in microstructure from lamellar or onion-type to columnar.

The crushing strengths of various lots of particles were determined in order to serve as a possible index of the mechanical integrity and uniformity of the coated particles. The equipment for determining these crushing strengths is described in Chap. 28 of this report.

Four types of irradiation facilities are being used in this program: the LITR static capsules, the ORR-C1 and B9 instantaneous fission-gas release facilities, the ORR poolside sweep capsules, and the ORNL-MTR-48 sweep capsules. During the

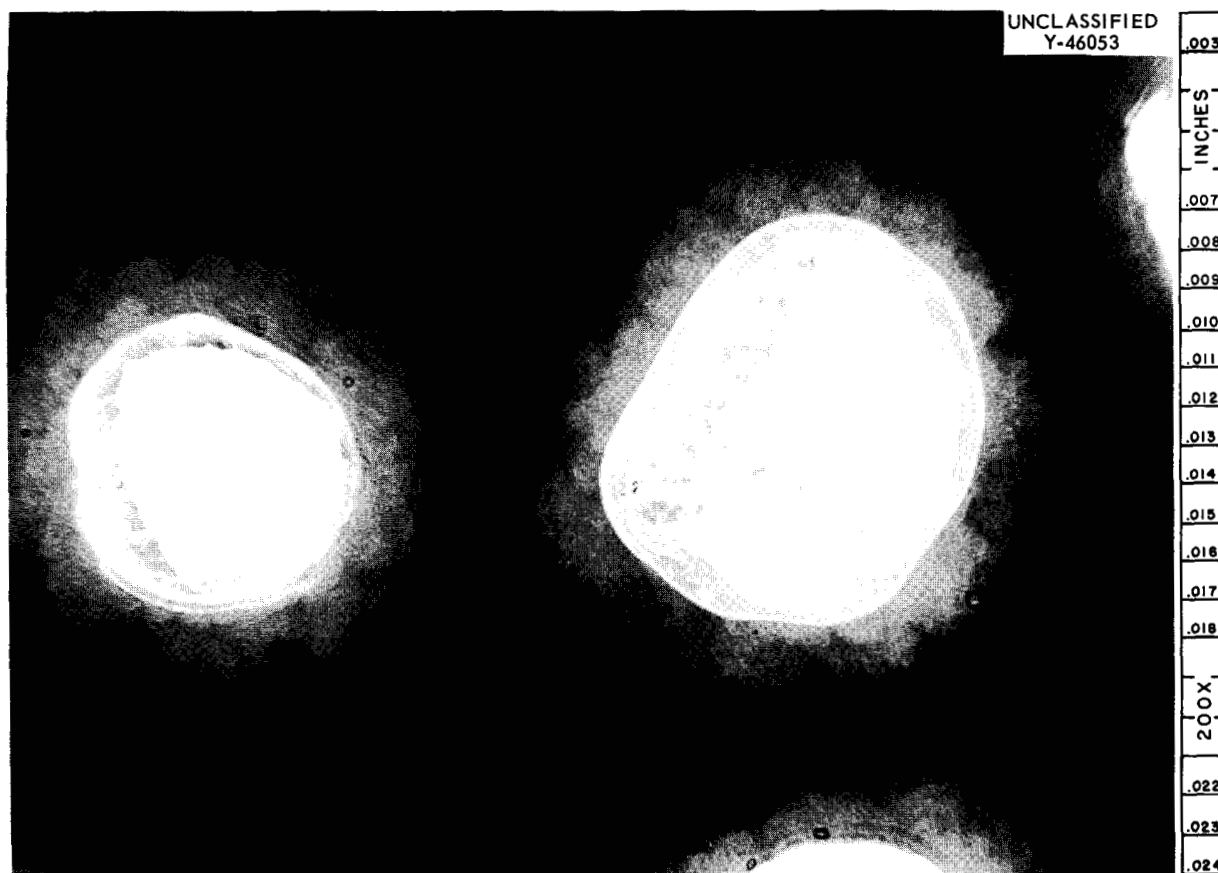


Fig. 17.3. Contact Radiograph of Pyrolytic-Carbon-Coated Uranium Carbide Particle. Halo effect around dense fuel particles is the result of fuel migration into coating.

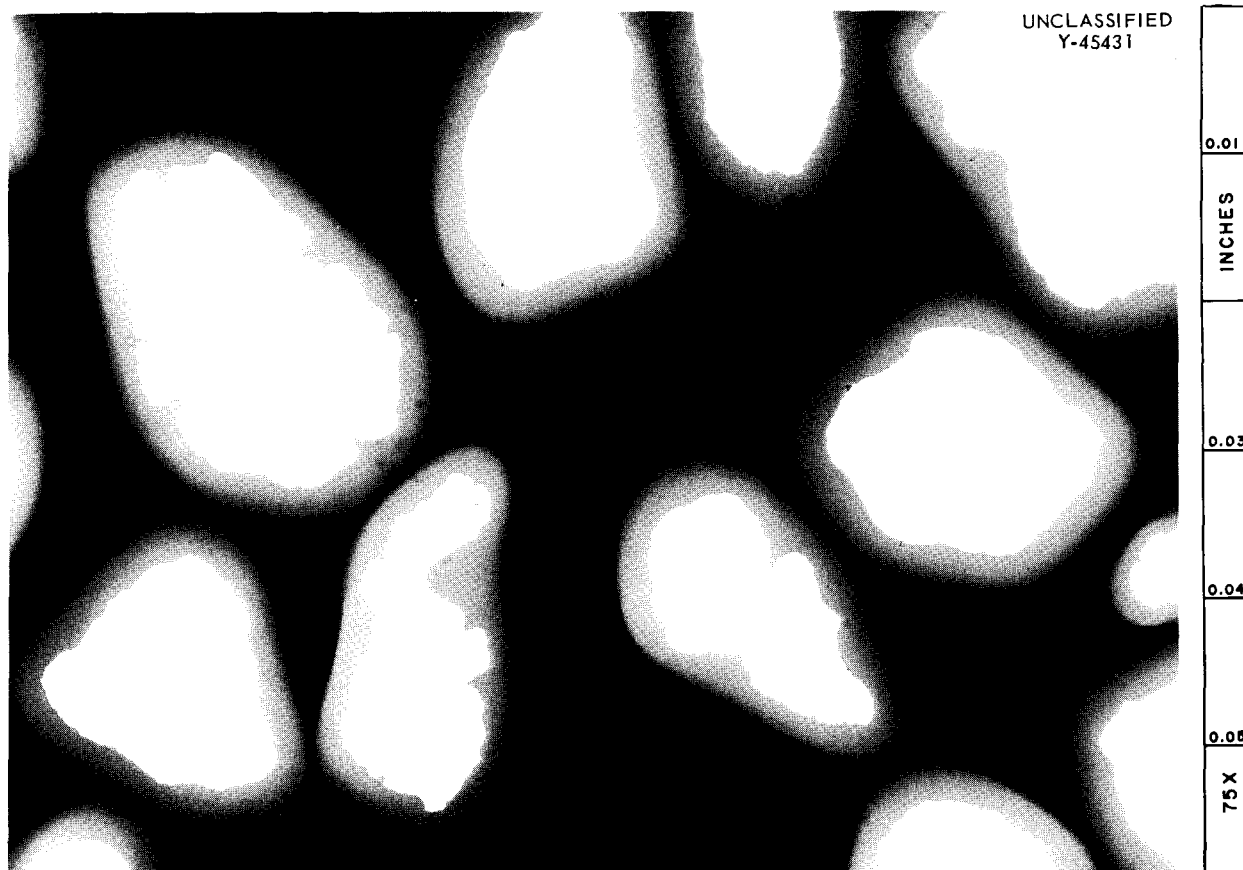


Fig. 17.4. Contact Radiograph of Pyrolytic-Graphite-Coated Thorium-Uranium Carbide (Th-U) $C_2$ . The high-density core exhibits an irregular shape which is filled in by the less dense graphite coating.

past year the Ceramics Laboratory assisted in the preparation of some 15 irradiation experiments, which are in various stages of completion. Only three capsules were examined in the hot cells; therefore, only preliminary results are available.

Results of the irradiation experiments and the hot-cell examinations were reported regularly during the past year,<sup>20-23</sup> and are summarized here. At temperatures of approximately 1500°F the release behavior of pyrolytic-carbon-coated uranium carbide particles was quite erratic. For example,

<sup>20</sup>F. R. McQuilken and W. E. Thomas, *GCR Quart. Progr. Rept. June 30, 1961*, ORNL-3166, pp 123-25.

<sup>21</sup>F. R. McQuilken and W. E. Thomas, *GCR Quart. Progr. Rept. Sept. 30, 1961*, ORNL-3210, pp 158-63.

<sup>22</sup>J. G. Morgan *et al.*, *GCR Quart. Progr. Rept. Dec. 31, 1961*, ORNL-3254, pp 54-57, 161-69.

<sup>23</sup>*GCR Quart. Progr. Rept. Mar. 31, 1962*, ORNL-3302 (in press).

the release rate divided by the birth rate,  $R/B$ , for  $Kr^{88}$  ranged from approximately  $10^{-5}$  to  $3 \times 10^{-4}$ , but there was no observable effect of burnup up to 15 at. % of uranium. In higher temperature tests the fission-gas release rates increased with burnup. For example, in a test on similar pyrolytic-carbon-coated uranium carbide particles at 2600°F, the  $R/B$  for  $Kr^{88}$  showed a steady increase with burnup from an initial value of  $5 \times 10^{-4}$  to  $1.8 \times 10^{-2}$  at 7 at. % burnup of uranium. In hot-cell examinations it was observed that some of the pyrolytic carbon coatings had cracked, ranging from 2 to 100%, depending upon the irradiation temperature and environment, and, tentatively, the microstructure of the pyrolytic carbon coating; for example, unsupported coated particles irradiated under static conditions at approximately 2500°F to burnups of 6 at. %, 2% cracked, but in a helium sweep test of a fueled-graphite specimen containing coated particles, 100% of the coatings cracked

after an irradiation to 15 at. % at a maximum temperature of 2600°F. The mechanisms responsible for the cracking have not yet been clearly established, and further experiments are in progress.

#### Fueled-Graphite Fabrication

A. J. Taylor      J. M. Robbins

A program was initiated to investigate the variables associated with producing fueled-graphite spheres of the type required for the Pebble-Bed Reactor Experiment.<sup>24</sup> Basically, the reference fuel element for the PBRE is a  $1\frac{1}{2}$ -in.-diam graphite sphere containing approximately 60,000 uniformly dispersed pyrolytic-carbon-coated (U, Th)C<sub>2</sub> particles with a  $\frac{1}{16}$ -in.-thick unfueled outer shell. The purpose of the fabrication studies is to systematically investigate variables which bear on the mechanical, chemical, and thermal stability of the fuel sphere with particular reference to the effects of irradiation.

The preliminary work consisted in characterizing various graphite flours and binders and fabricating shapes from blends of these materials. Natural and synthetic graphite powders and mixtures of both were used to fabricate cylindrical and spherical shapes. The binders, which include coal tar pitches, vegetable pitches, and a furan resin, were characterized primarily with respect to coking value (the percentage by weight of the binder which after baking remains as a carbonaceous residue). Preheating the pitch binders at 130 to 180°C to drive off certain highly volatile components improved the coking values. The furan resin with a coking value of 42% was selected for future studies.

The forming techniques investigated were (1) cold pressing at room temperature followed by baking at 1000°C, (2) warm pressing at 150°C followed by baking at 1000°C, and (3) hot molding at 800°C. Both uniaxial and isostatic types of loading methods were used. For the spherical product under consideration, some form of isostatic pressing at room temperature appeared to hold the most promise as an initial forming step and to offer the following advantages over conventional uniaxial loading: damage to coated particles is minimized, laminar strains which result in cracks in the baked

product are eliminated, and the equatorial flash or rim is eliminated or at least minimized. The initial shaping procedure adopted consists in forming the graphite-base body in a soft polyvinyl chloride mold in a steel jacket by using conventional uniaxial loading techniques. With the proper mold design, the forces transmitted to the body under these conditions are essentially hydrostatic.

#### URANIUM OXIDE AND THORIUM OXIDE FABRICATION DEVELOPMENT

##### Fabrication of UO<sub>2</sub> Pellets

A. J. Taylor      J. M. Robbins

Approximately 1300 UO<sub>2</sub> specimens of various sizes, shapes, grain size, and enrichment were fabricated by cold pressing and sintering during this report period for use in irradiation experiments for the Gas-Cooled Reactor program.<sup>25</sup>

An activation procedure was developed for two types of highly enriched UO<sub>2</sub> powders of relatively low sinterability in order to achieve a required bulk density of greater than 88% of theoretical. In the as-received condition, the highest density obtainable was 66% of theoretical. The activation procedure consisted in oxidizing and reducing the powders at 650°C in air and in hydrogen, respectively. After five oxidation-reduction cycles, a density of approximately 95% of theoretical was attained. A 5 wt % solution of camphor in acetone was used as binder and lubricant in these studies.

##### Vibratory Compaction Studies

W. S. Ernst      R. L. Beatty

Evaluation of ThO<sub>2</sub>-3 wt % UO<sub>2</sub> produced by the Chemical Technology Division utilizing the sol-gel process continued. Crushing yields of the crude sol-gel product and vibrated bulk densities of processed materials were correlated with the sol-gel process parameters. The resulting improvements in material characteristics obtained from these studies increased the utilization of crude sol-gel material and the bulk density obtained by vibratory compaction.

<sup>24</sup> *Conceptual Design of the Pebble Bed Reactor Experiment*, ORNL TM-201, pp 185-92 (May 17, 1962).

<sup>25</sup> A. J. Taylor and J. M. Robbins, *GCR Quart. Progr. Rept. Mar. 31, 1961*, ORNL-3102, p 91; *June 30, 1961*, ORNL-3166, pp 77-78; *Sept. 30, 1961*, ORNL-3210, pp 174-75; *Dec. 31, 1961*, ORNL-3254, pp 187-88.

Development studies designed specifically for the fabrication of fuel rods containing  $\text{ThO}_2$ -3 wt %  $\text{UO}_2$  constituted the major effort during this period. These studies are in support of the large-scale demonstration of remote fabrication which will produce fuel rods for a zero-power critical assembly at the Brookhaven National Laboratory employing  $\text{ThO}_2$ - $\text{UO}_2$  containing  $\text{U}^{233}$ . As a result of these studies, equipment was specified for processing oxide from the sol-gel process into a product suitable for vibratory compaction. In addition, the operating parameters of this equipment are currently being optimized. The results indicate that more than 95% of the crude sol-gel feed can be processed into a product which will yield vibrated bulk densities between 89 and 91% of theoretical in 45-in.-long  $\times$  0.500-in.-diam tubes having wall thicknesses of 0.035 in.

Studies of the axial distribution of bulk fuel density showed that in general the bulk density at any given point varied less than  $\pm 1\%$  about the average value. However, small regions of fuel were found for which the bulk density was from 3 to 5% less than the average value. Instrumentation developed in the Nondestructive Testing Group based on the gamma-ray attenuation properties of  $\text{ThO}_2$  and  $\text{UO}_2$  was used for these studies.

Irradiation specimens of various sizes, containing enriched  $\text{ThO}_2$ -5 wt %  $\text{UO}_2$  made by the arc-fusion or the sol-gel process, were fabricated and are presently being irradiated in the NRX reactor, the ORR, and the MTR. These specimens range in bulk density from 83 to 89% of theoretical.

Vibratory compaction of arc-fused  $\text{UO}_2$  was considered for the advanced core development of the NS "Savannah." This work was concerned primarily with fabrication of irradiation specimens for the Maritime Loop in the ORR. Vibrated bulk densities between 87 and 88% of theoretical were obtained in these specimens.<sup>26</sup> Studies to optimize the particle-size distribution and establish specifications for purchasing arc-fused  $\text{UO}_2$  were also performed.

<sup>26</sup>J. T. Lamartine, W. S. Ernst, Jr., and J. W. Tackett, *Maritime Reactor Program, Ann. Progr. Rept. Nov. 30, 1961, ORNL-3238, pp 86-94.*

### Thoria-Pellet Development

A. J. Taylor      R. A. McNees<sup>27</sup>  
R. A. Potter

The development of techniques was continued for preparing and characterizing  $\text{ThO}_2$  pellets suitable for use in fluidized-blanket systems where high attrition resistance is required.<sup>28</sup> The studies were designed to establish a correlation between measurable and controllable physical properties and attrition resistance. The effects studied were bulk density, grain size, surface-connected porosity, and macrostructure as affected primarily by the fabrication procedure.

Sintered cylinders with domed ends formed during pressing were, in many instances, severely laminated and exhibited large internal voids. During spouted bed tests the pellets exhibited poor attrition resistance, and attack was pronounced in the areas of defects. However, rounded-edged cylindrical pellets and spheroidal pellets, made by tumbling right cylinders in the first instance and cubes in the second,<sup>28</sup> were found to be more satisfactory.

The spouted bed tests of pellets designed to furnish information concerning the effects of grain size and bulk density on attrition resistance indicated that variations of bulk density per se in the range 92 to 97% of theoretical were not as significant as sintering time and, therefore, grain size.

### THERMAL-CONDUCTIVITY STUDIES

T. G. Godfrey      D. L. McElroy<sup>29</sup>

Thermal-conductivity measurements on  $\text{UO}_2$  pressed and sintered to 93.4% of theoretical density were made at 27 to 875°C in the previously described radial heat flow apparatus.<sup>30</sup> In the

<sup>27</sup>Now with the Director's Department.

<sup>28</sup>R. A. McNees and A. J. Taylor, *Met. Div. Ann. Progr. Rept. May 31, 1961, ORNL-3160, pp 61-62.*

<sup>29</sup>Physical Properties Group.

<sup>30</sup>T. G. Godfrey and D. L. McElroy, *Met. Div. Ann. Progr. Rept. May 31, 1961, ORNL-3160, pp 64-65.*

higher regions of the test temperature range (generally at around 650°C), electrical difficulties hindered the measurements. A procedure which involves the isothermal intercomparison of all meas-

uring thermocouples prior to each thermal-conductivity determination was used to obtain data reproducible to  $\pm 1\%$  and accurate to  $\pm 3\%$ . The reported results<sup>31</sup> agree well with the results of Howard and Gulvin<sup>32</sup> and are plotted in Fig. 17.5.

<sup>31</sup>T. G. Godfrey and D. L. McElroy, *GCR Quart. Progr. Rept. Sept. 30, 1961, ORNL-3210, pp 175-76; Dec. 31, 1961, ORNL-3254, pp 264-66; Mar. 31, 1962, ORNL-3302 (in press).*

<sup>32</sup>V. C. Howard and T. F. Gulvin, *Thermal Conductivity Determinations on UO<sub>2</sub> by a Radial-Flow Method, IG Rept.-51 (RD/C) (1961).*

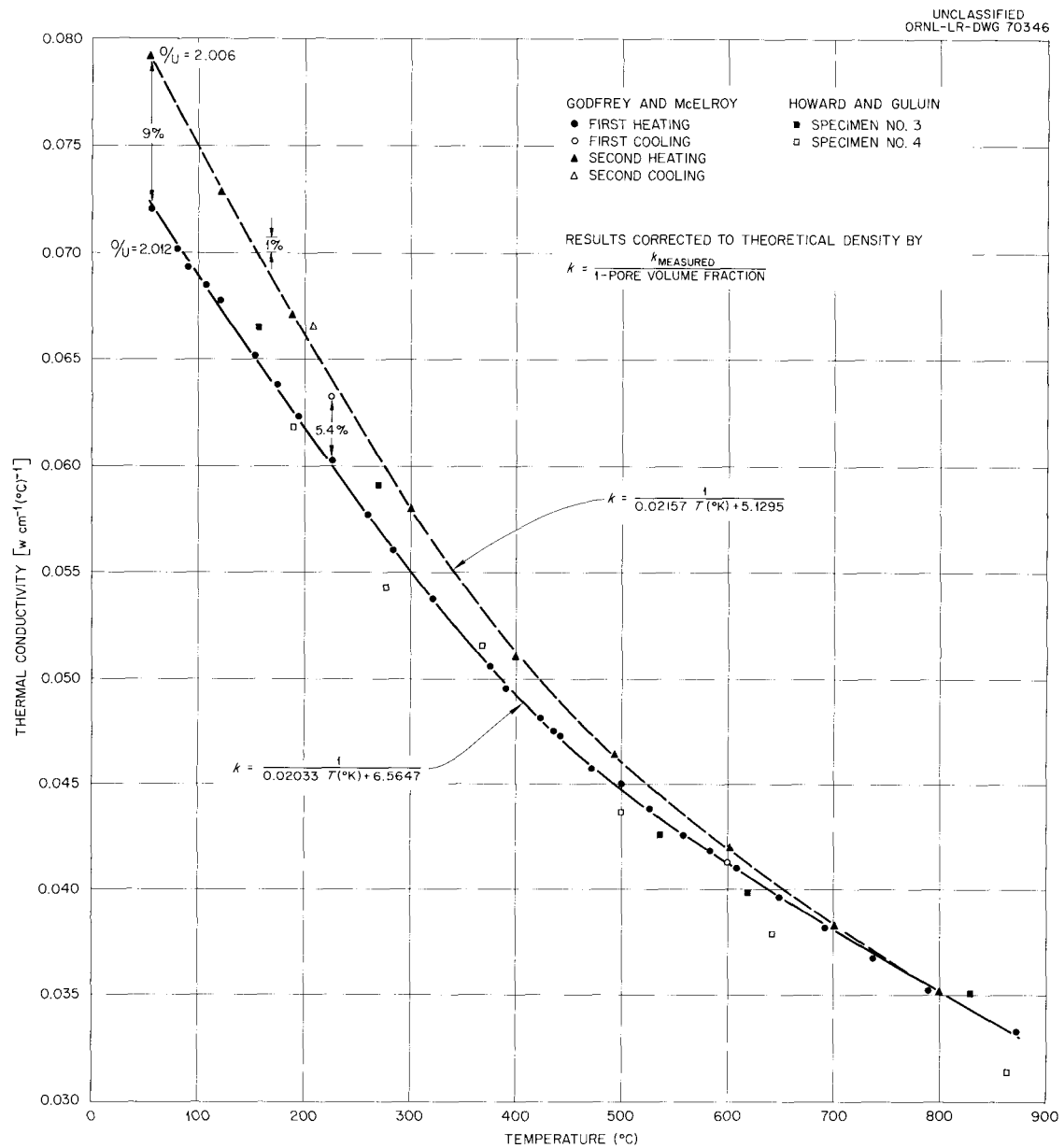


Fig. 17.5. The Effect of Temperature and Stoichiometry on the Thermal Conductivity of UO<sub>2+x</sub> Pressed and Sintered to 93.4% of Theoretical Density.

The first heating curve shown in Fig. 17.5 may be fitted to  $\pm 1\%$  by  $k = \rho/[6.5647 + 0.02033 T]$ , where  $\rho$  is the ratio of the measured bulk density to the theoretical density,  $k$  is the thermal conductivity in  $\text{w cm}^{-1} (\text{C})^{-1}$ , and  $T$  is the temperature in degrees Kelvin. Data taken at  $600^\circ\text{C}$  on cooling from  $875^\circ\text{C}$  were the same as those obtained on heating; however, the value of  $k$  obtained at  $223^\circ\text{C}$  was 5.4% higher than that obtained earlier. Upon opening the apparatus, it was observed that the tantalum shields which surrounded the specimen had oxidized to  $\beta\text{-Ta}_2\text{O}_5$ . Subsequent analysis of the oxygen-to-uranium ratio of the specimen yielded a value of 2.006, as compared with the original value of 2.012. The change in thermal conductivity may be due to this change in composition. Second-heating thermal conductivity values to  $800^\circ\text{C}$  confirmed the data obtained at  $223^\circ\text{C}$  and were within 1% of the first heating curve above  $600^\circ\text{C}$ . The second heating curve may be fitted to  $\pm 1\%$  by  $k = \rho/[5.1295 + 0.02157 T]$ . The variation in  $k$  with composition appears to be more pronounced at lower temperatures and to be small at  $600^\circ\text{C}$  or higher. These data indicate that the large ( $\pm 30\%$ ) differences reported in the literature for the thermal conductivity of  $\text{UO}_2$  at room temperature may be due to subtle differences in oxygen concentration in specimens used by various investigators.

Modifications to the radial heat flow apparatus were initiated in an attempt to avoid the electrical difficulties encountered above  $650^\circ\text{C}$  and to thus extend the measurements on  $\text{UO}_2$  to at least  $1400^\circ\text{C}$ .

## EUROPIUM OXIDE STUDIES

R. A. Potter      R. A. McNees<sup>27</sup>

Experimental studies of europium oxide were continued in order to provide information useful in the fabrication and performance of  $\text{Eu}_2\text{O}_3$ -bearing stainless steel neutron absorber plates for the Army Package Power Reactor Program.<sup>33,34</sup> Two major problems were investigated: (1) the swelling of cold-pressed powder compacts during the initial sintering operation at  $1350^\circ\text{C}$  and (2) the insta-

<sup>33</sup>R. A. Potter and R. A. McNees, *Met. Div. Ann. Progr. Rept.* May 31, 1961, ORNL-3160, p 65.

<sup>34</sup>R. A. McNees and R. A. Potter, *Army Reactor Program Progress Report*, ORNL-3231, pp 16-22 (Jan. 31, 1962).

bility of defected plates in contact with water at  $250^\circ\text{C}$ .

## Behavior During Sintering

The behavior of cold-pressed  $\text{Eu}_2\text{O}_3$  compacts during heating at  $1350^\circ\text{C}$  was established as being similar to that for metal-ceramic compacts used in the standard absorber-plate fabrication procedure.<sup>35</sup> These compacts were prepared by cold pressing various batches of  $\text{Eu}_2\text{O}_3$  powder at 10,000 psi, using material derived from crushing and grinding of pellets which had been sintered at 1700 to  $1750^\circ\text{C}$ . On heating to  $1350^\circ\text{C}$  for 1 hr in air or in hydrogen, some compacts exhibited swelling and others did not.

X-ray diffraction analyses of materials which underwent swelling revealed the presence of a second (unidentified) phase in addition to monoclinic  $\text{Eu}_2\text{O}_3$ . When these powders were subjected to thermogravimetric analysis (TGA), weight losses up to 8.4% were recorded during heating to  $1350^\circ\text{C}$  at a pressure of  $10^{-5}$  torr. It was also noted that, on differential thermal analysis (DTA) of these powders, a pronounced endothermic effect occurred in the range 940 to  $1285^\circ\text{C}$ , depending upon heating rate. Material which had been treated in the TGA apparatus no longer contained the second phase and behaved satisfactorily on subsequent compacting and heating to  $1350^\circ\text{C}$ . Analysis by infrared spectroscopy showed that the powders which had swelled contained significant amounts of  $\text{CO}_2$  and  $\text{H}_2\text{O}$ , and as much as 0.4 wt % carbonate was detected by wet chemical analysis.

In view of these observations, it was postulated that some  $\text{Eu}_2\text{O}_3$  powders may be sufficiently activated during processing to result in reaction with or adsorption of  $\text{CO}_2$  and  $\text{H}_2\text{O}$ , which may combine with the oxide to form an europium hydroxycarbonate. This undesirable phase can be detected readily by DTA and subsequently eliminated by heat treatment to  $1350^\circ\text{C}$  at a pressure of  $10^{-5}$  torr.

## Aqueous Corrosion Behavior

Compacts made from  $\text{Eu}_2\text{O}_3$  powders of different origins were found to be severely attacked by water

<sup>35</sup>C. F. Leitten, R. J. Beaver, and J. E. Cunningham, *Specification and Fabrication Procedures on Europium Bearing Absorber Rods for Reactivity Control in Core II of SM-1*, ORNL-2733, pp 28-31 (July 29, 1959).

at 100°C within 5 hr of exposure regardless of the process history of the powders. X-ray diffraction analyses of powder taken from each of the compacts after the corrosion test showed that a second phase, tentatively identified as  $\text{Eu}(\text{OH})_3$ , was present in addition to monoclinic  $\text{Eu}_2\text{O}_3$ .

## SCANDIUM OXIDE STUDIES

C. E. Curtis<sup>36</sup>

The effects of temperature and environment on the sintering behavior of  $\text{Sc}_2\text{O}_3$  and the compatibility of  $\text{Sc}_2\text{O}_3$  with 13 other oxides at 1600°C were studied. The  $\text{Sc}_2\text{O}_3$  powder used was at least 99% pure, with Ce, Ba, Ca, and Si being the major impurities. Pellets which had been dry-pressed without binder at 20,000 psi were heated at 1500, 1600, and 1700°C in air, oxygen, or hydrogen for 2 hr. The sintered densities achieved were approximately 88% of theoretical at 1500°C and approximately 96% of theoretical at 1600 and 1700°C for all environments used, the white oxide turned

to dark gray in all cases, and the sintered  $\text{Sc}_2\text{O}_3$  pellets exhibited no gross reaction with laboratory air over a period of several months.

In the compatibility tests equimolar mixtures of  $\text{Sc}_2\text{O}_3$  with 13 selected oxides were heated for 2 hr in air at 1600°C, and the products were examined by means of the x-ray diffractometer technique. All mixtures were dry-pressed at 20,000 psi prior to the heat treatments. Compound formation occurred for those mixtures containing  $\text{Al}_2\text{O}_3$ ,  $\text{BeO}$ ,  $\text{CaO}$ ,  $\text{Fe}_2\text{O}_3$ ,  $\text{Gd}_2\text{O}_3$ ,  $\text{SiO}_2$ ,  $\text{Sm}_2\text{O}_3$ ,  $\text{TiO}_2$ , and  $\text{Y}_2\text{O}_3$ ; solid solutions were formed with  $\text{HfO}_2$ ,  $\text{ZrO}_2$ , and  $\text{MgO}$ ; and no reaction occurred with  $\text{ThO}_2$ . Destructive reaction occurred only in the  $\text{Sc}_2\text{O}_3$ - $\text{Fe}_2\text{O}_3$  pellet; pellets of all the other compositions were merely sintered. Under the conditions used, compound formation was complete for mixtures containing  $\text{Gd}_2\text{O}_3$ ,  $\text{Sm}_2\text{O}_3$ , and  $\text{Y}_2\text{O}_3$ , indicating equimolar compound formation in these systems; in all other mixtures showing compound formation, one or both of the original components remained.

The results obtained in this investigation are similar to those reported for  $\text{Y}_2\text{O}_3$  under comparable conditions.<sup>37</sup>

<sup>36</sup>Consultant.

<sup>37</sup>C. E. Curtis, *J. Am. Ceram. Soc.* 40(8), 274-79 (1957).

## 18. Metal Forming and Casting

C. F. Leitten, Jr.

### IRRADIATION TESTING OF ALUMINUM-BASE FUEL DISPERSIONS OF $UAl_3$ , $U_3O_8$ , AND $UC_2$ IN ALUMINUM-CLAD PLATES

C. F. Leitten, Jr.      A. E. Richt<sup>1</sup>  
R. J. Beaver

The evaluation of irradiation effects in aluminum-clad dispersions of  $UAl_3$  and  $U_3O_8$  in aluminum was continued. The initial results of the postirradiation examination of a series of miniature test specimens containing dispersions of 64 wt %  $UAl_3$ , 63 wt %  $U_3O_8$ , and 60 wt %  $UC_2$  in aluminum were reported previously.<sup>2</sup> Additional specimens irradiated to higher burnups showed no major deviations from the data previously reported, with the exception that at  $U^{235}$  fission burnups in excess of 60 at. % the  $U_3O_8$ -bearing aluminum samples appear to be decreasing slightly in density. However, the densities resulting from irradiating the samples to  $U^{235}$  fission burnups as high as 77 at. % are still significantly greater than the preirradiation densities. Increased reaction between the  $U_3O_8$  particles and the aluminum matrix was also apparent at these higher burnup levels.

The  $UAl_3$ -bearing aluminum specimens continued to show density decreases with increasing fission burnup. The reactions noted previously in the matrix of this type of plate were again apparent in the specimens irradiated to  $U^{235}$  fission burnups as high as 70 at. %.

Paralleling the irradiation testing of the miniature specimens, a 19-plate prototype fuel element

containing 63 wt %  $U_3O_8$ -aluminum dispersions was irradiated in the lattice of the ORR to an average  $U^{235}$  fission burnup of 41 at. % with a maximum peak burnup of 57 at. %. The fuel dispersions had been prepared by standard powder metallurgy techniques and were bonded with type 1100 aluminum by roll cladding. The uranium was 20% enriched in the  $U^{235}$  isotope. After irradiation the visual appearance of the element was excellent. Dimensional measurements on the fuel assembly revealed no evidence of gross dimensional changes. Fuel plate spacing measurements were well within the  $0.116 \pm 0.012$  in. fabrication specification except for the minimum clearance of 0.090 in. in the channel between the top two fuel plates. This decrease in channel height resulted from a slight rippling of the top outer fuel plate during irradiation. Postirradiation thickness measurements of fuel plates were all within the nominal  $0.050 \pm 0.001$  in. preirradiation thickness specification.

Results of the metallographic examination of various sections from the fuel element were consistent with the results obtained from the miniature  $U_3O_8$ -Al dispersion specimens. As illustrated in Fig. 18.1, significant reaction between the  $U_3O_8$  and the aluminum matrix occurred in regions of high burnup. As was noted in the miniature specimens, the reaction is predominantly associated with the finer  $U_3O_8$  particles.

In order to evaluate the effect of postirradiation heat treatment on the dimensional stability of the fuel plates, two fuel plates having maximum  $U^{235}$  fission burnups of approximately 57 at. % were heat-treated for 24 hr in 100°F increments from 400 to 1000°F. Between each successive increment of heat treatment the plates were visually inspected and measured for dimensional changes.

<sup>1</sup>Metallography Group.

<sup>2</sup>R. J. Beaver and A. E. Richt, *Met. Div. Ann. Progr. Rept. May 31, 1961*, ORNL-3160, pp 95-99.

No indication of fuel plate blistering or measurable swelling was noted even after the 1000°F heat treatment. Metallographic examination of the heat-treated plates indicated that no gross microstructural changes had occurred, although cracking had appeared in the fuel particles as a result of heat treating. However, as shown in Fig. 18.2, propagation of the cracks through the aluminum matrix was not sufficient to cause blistering or swelling.

Powder samples were obtained from irradiated  $U_3O_8$ ,  $UAl_3$ , and  $UC_2$  dispersions in aluminum and submitted to BMI for x-ray diffraction analyses in order to identify the reaction products observed in these fuel samples after irradiation.

The results of this x-ray study are summarized in Table 18.1. It was interesting to find that  $UAl_3$  was identified as a reaction product in the irradiated  $U_3O_8$ -Al specimen. Although previous studies<sup>3</sup> had revealed the formation of  $UAl_3$  in this system after long exposure at 1112°F, it was always accompanied by a volume increase. No such volume increase was observed in this system. The absence of  $U_3O_8$  and  $UO_2$  in the x-ray pattern for the irradiated sample indicates that these oxides had become amorphous. The  $UAl_3$ -Al

<sup>3</sup>R. C. Waugh, *The Reaction and Growth of Uranium Dioxide-Aluminum Fuel Plates and Compacts*, ORNL-2701 (Mar. 9, 1959).

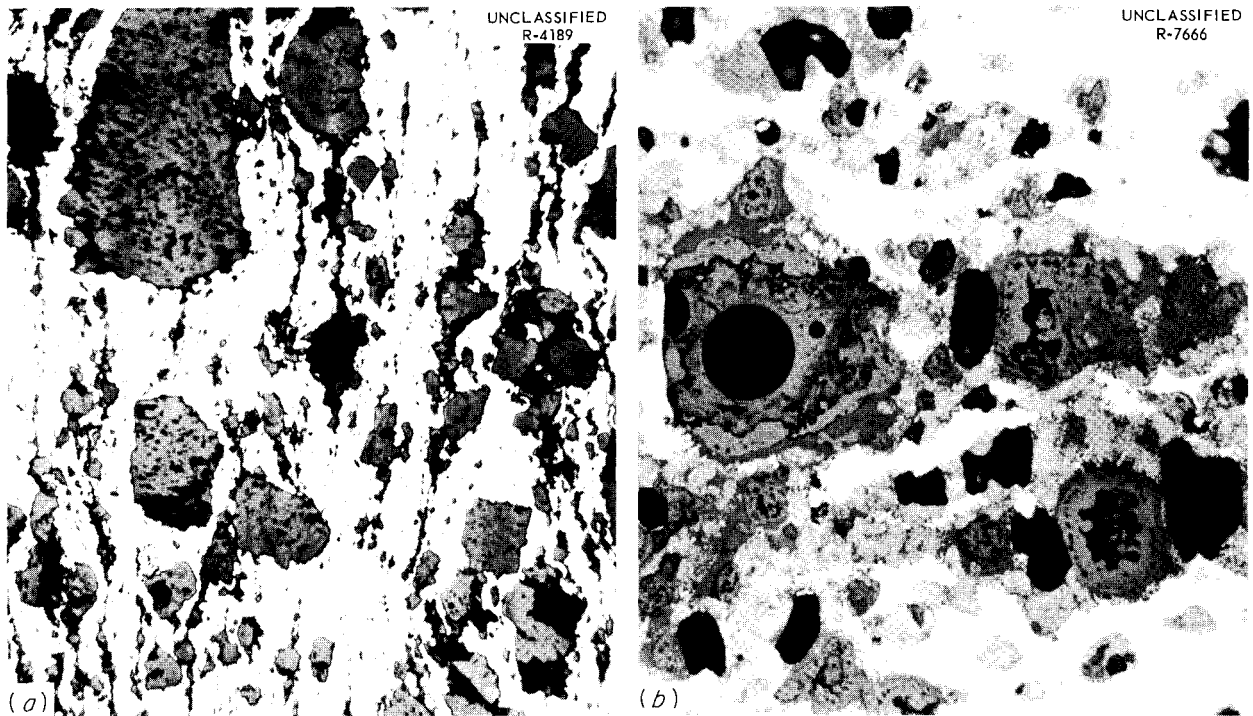


Fig. 18.1. Microstructure of a 63 wt %  $U_3O_8$ -Al Dispersion. (a) Preirradiated; unetched; (b) irradiated to a  $U^{235}$  fission burnup of 57 at. %; etched with 10%  $H_2SO_4$ , 10%  $H_2O_2$ . 500X. Reduced 20%.

Table 18.1. Results of X-Ray Diffraction Studies on Irradiated  $U_3O_8$ ,  $UAl_3$ , and  $UC_2$  Dispersions in Aluminum

Type of Dispersion	Identified Constitutents	
	Preirradiation	Postirradiation
$U_3O_8$ -Al	$U_3O_8$ , $UO_2$ -Al	$UAl_3$ (disordered) + Al
$UC_2$ -Al	$UC_2$ , UC-Al	$UC_2$ -UC-Al-Al <sub>4</sub> C <sub>3</sub> (possible)
$UAl_3$ -Al (48 wt % U-3 wt % Si-bal Al)	$UAl_3$ (ordered)-Al	$UAl_3$ (disordered) + Al

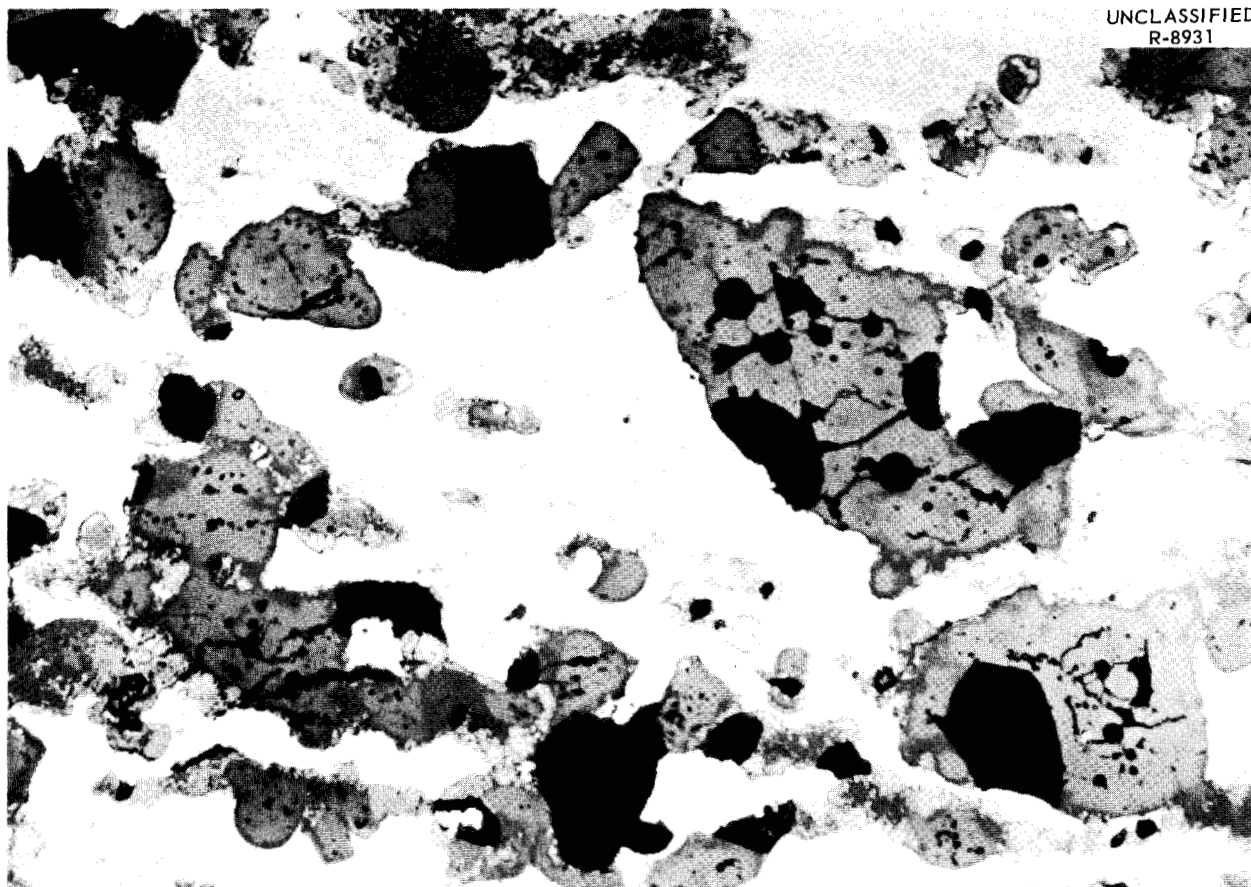
UNCLASSIFIED  
R-8931

Fig. 18.2. Microstructure of a 63 wt %  $U_3O_8$ -Al Dispersion Irradiated to a  $U^{235}$  Fission Burnup of 57 at. % and Subsequently Heat-Treated for 24 hr in  $100^\circ F$  Increments from  $400$  to  $1000^\circ F$ . Etchant: 10%  $H_2SO_4$ , 10%  $H_2O_2$ , 500X.

dispersions showed no indication of the expected reaction product  $UAl_4$ . However, the  $UAl_3$  appeared to have undergone an ordered-disordered transformation as a result of irradiation.

### ALUMINUM-BASE FUEL ELEMENT FABRICATION

C. F. Leittin, Jr.

During the past year emphasis was placed on advancements in aluminum-base fuel element technology aimed at high-flux high-performance reactors. Of particular concern were the strength, irradiation stability, and corrosion resistance of the aluminum-base fuel elements in reactors of this type which can operate at elevated central fuel temperatures ( $400$  to  $475^\circ F$ ), at high neutron

fluxes ( $>2 \times 10^{15}$  neutrons  $cm^{-2} sec^{-1}$ ), and at heat fluxes of approximately  $1.5 \times 10^6$  BTU  $ft^{-2} hr^{-1}$ .

Development of the fuel element for the High Flux Isotope Reactor, a joint effort of the Powder Metallurgy, Welding and Brazing, Metal Forming and Casting, and Reactor Projects Groups, continued. In addition, work began on the fuel element for the Advanced Test Reactor.<sup>4</sup>

The design<sup>5</sup> of the HFIR fuel element is illustrated in Fig. 18.3. Design specifications were reported last year.<sup>5</sup> Manufacturing of the two fuel

<sup>4</sup>D. R. deBoisblanc *et al.*, *The Advanced Test Reactor (ATR) Fuel Conceptual Design*, IDO-16667 (Nov. 1, 1960).

<sup>5</sup>R. J. Beaver and A. E. Richt, *Met. Div. Ann. Progr. Rept.* May 31, 1961, ORNL-3160, p 101.

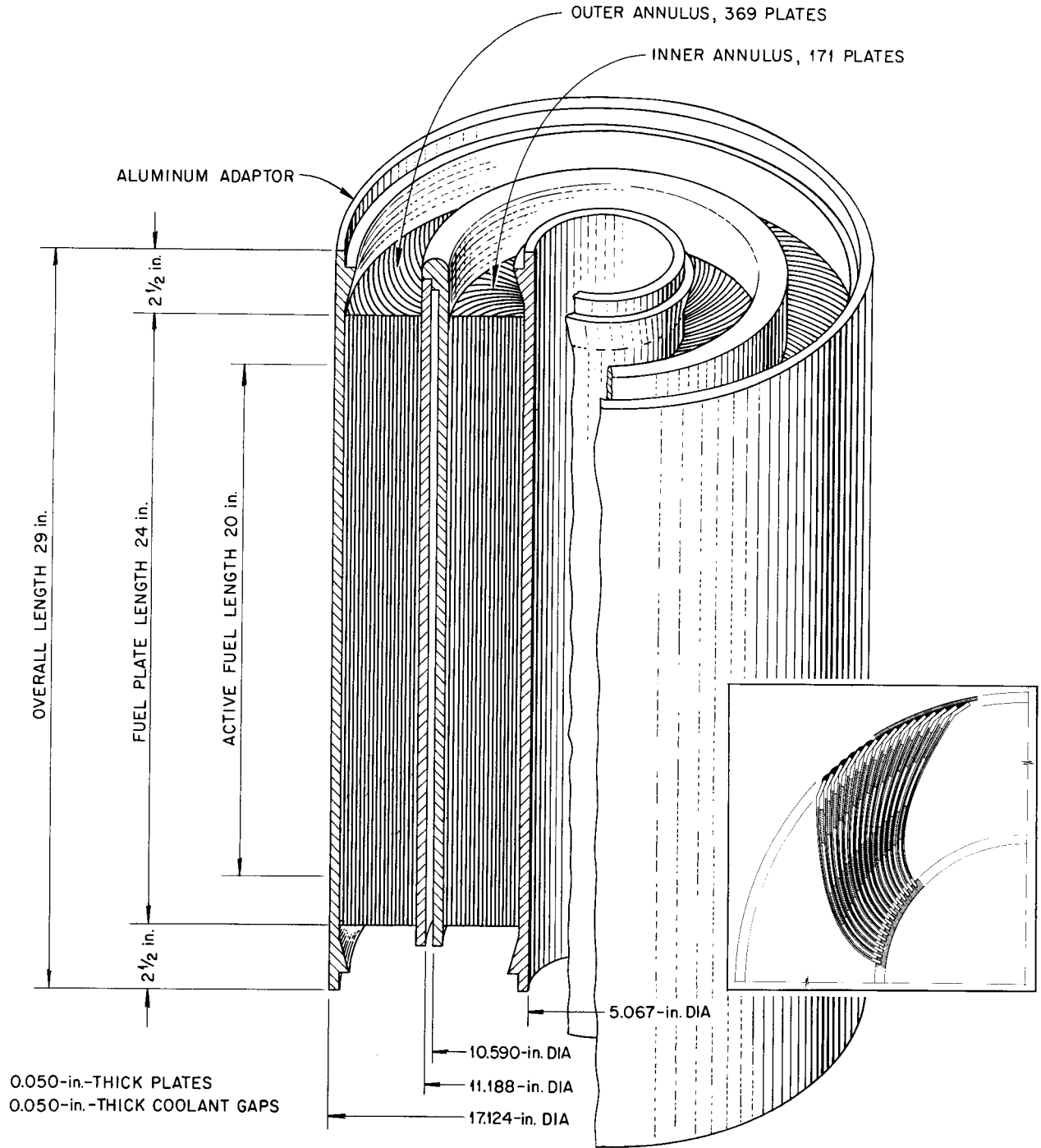


Fig. 18.3. Dimensional Illustration of the Assembled HFIR Fuel Element.

segments basically consists in attaching the inner edge of the formed fuel plates in a tubular side plate by peening and securing the bent-lipped outer edge of the plates by welding.

The conceptual design of a portion of the ATR fuel element array is shown in Fig. 18.4. Design specifications for the individual ATR fuel elements are given in Table 18.2. Since a constant

UNCLASSIFIED  
ORNL-LR-DWG 68039

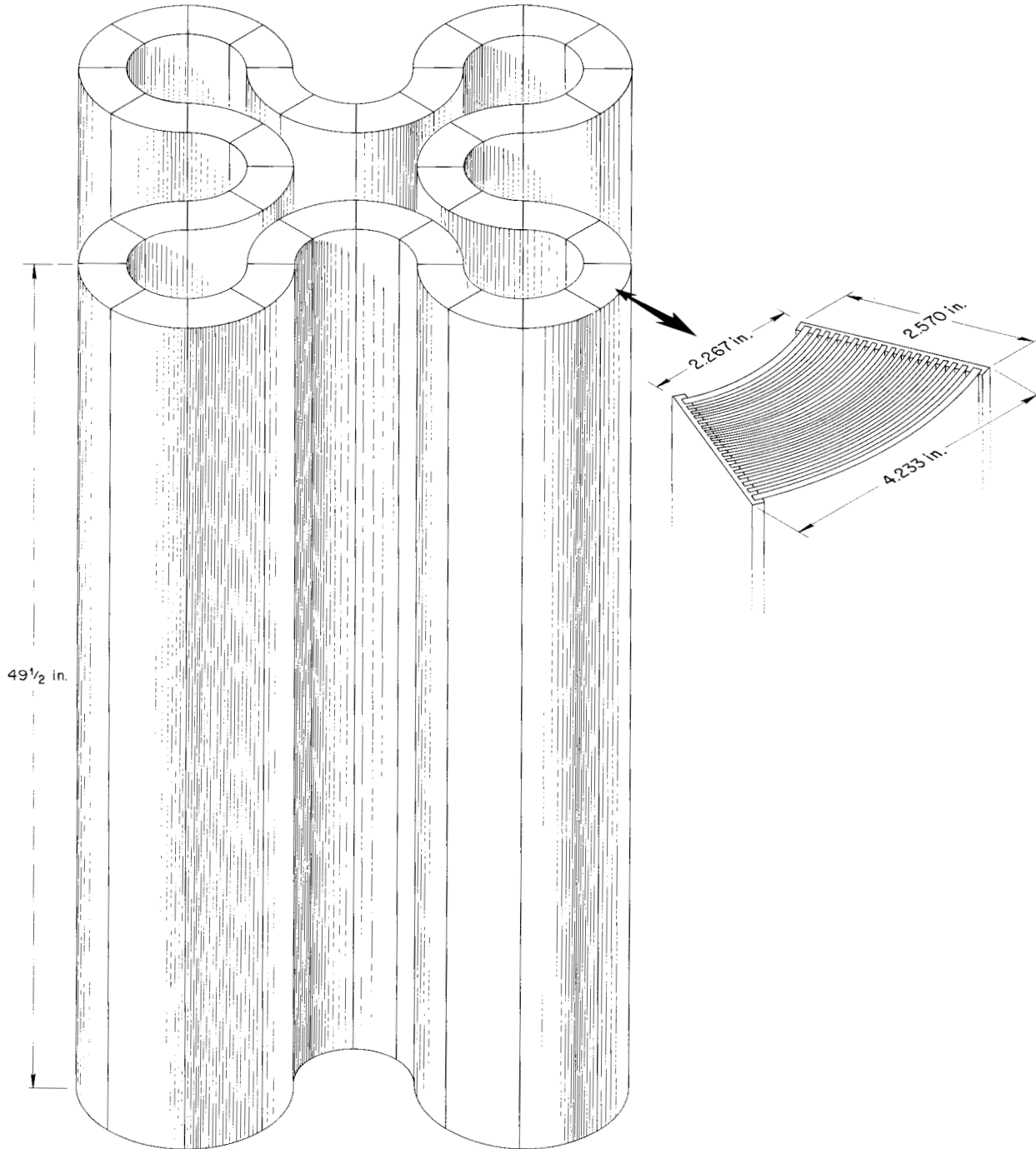


Fig. 18.4. Dimensional Illustration of a Segment of the ATR Fuel Element Array.

Table 18.2. Tentative Design Specifications of the Fuel Element for the ATR

Overall fuel plate size (in.)	
Length	49½
Width	2.221 to 4.055
Thickness	0.050 and 0.080 (outer two plates)
Number of elements	40
Number of plates per element	19
Fuel section size (in.)	
Length	48
Width	1.770 min to 3.60 max
Thickness	0.020
Materials	
Cladding	Type X8001 aluminum
Frame	Type X8001 aluminum
Fuel section	34 wt % U <sub>3</sub> O <sub>8</sub> , 0.15 wt % B <sub>4</sub> C, bal type X8001 aluminum
Side plates	Type 6061-T6 aluminum

plate-to-plate outer channel height,  $0.078 \pm 0.006$  in., must be maintained, each of the 19 fuel plates comprising an element must be accurately formed to a different radius. Mechanical joining techniques are being explored to attach the fuel plates to the side plates in element manufacturing.

#### Fuel Plate Fabrication

M. M. Martin      R. L. Heestand

Development of techniques for fabricating the high-strength type 6061 aluminum-clad fuel plates was continued in support of the HFIR program. As was previously reported,<sup>6</sup> two types of core materials were initially selected for the inner- and outer-annulus fuel plates. A dispersion of 26 wt % U<sub>3</sub>O<sub>8</sub>-0.07 wt % B<sub>4</sub>C in aluminum was selected for the inner-annulus plate, and an alloy of 24 wt % U-bal Al was utilized in the outer-annulus plate. To achieve the required lateral fuel gradient, the fueled cores were hot-forged to a nonuniform curved shape. A complementary filler piece was also forged to provide the rectangular core shape that is more amenable to roll-cladding practices. Boron carbide was dispersed

in the inner-annulus complementary filler piece to provide a uniform boron content throughout the inner-annulus plate.

The prime problem in roll-cladding the forged cores and inserts with type 6061 aluminum was blister formation in the fuel plates. Gas blisters appeared within and between the cladding, core, or filler pieces on nearly all fabricated and annealed plates. Therefore alclad type 6061 aluminum was substituted for the cladding and frame material, the core and filler pieces were degassed by vacuum heat treating at 1095°F, and a maximum fabrication and annealing temperature of 932°F was used for the fuel plates. Alclad type 6061 aluminum provided reliable and continuous metallurgical bonds in the composite plates. Vacuum degassing of the core components greatly enhanced the yield of blister-free fuel plates, which was further improved by limiting the hot-rolling temperature to 932°F. With these improvements, blister-free type 6061 aluminum-clad fuel plates containing either dispersion or alloy cores were fabricated with production yields equivalent to those achieved with type 1100 aluminum.

Although the blistering tendency in type 6061 aluminum-clad fuel plates was decreased by limiting the fabrication temperature to 932°F,

<sup>6</sup>D. T. Bourgette *et al.*, *Met. Div. Ann. Progr. Rept.* May 31, 1961, ORNL-3160, pp 101-3.

further studies are required to more firmly establish the effect of temperature on blistering. As illustrated in Fig. 18.5, a marked change in the surface oxide film occurred on type 6061 aluminum heat-treated above 932°F: the oxide appeared to be porous, thus permitting direct exposure of the aluminum to the atmosphere and the subsequent absorption of hydrogen. This degree of oxide film porosity increases with temperature. Similar studies on the stability of the oxide film on type 1100 aluminum failed to show porosity formation at temperatures as high as 1112°F.

The wide range of requirements for the more corrosion-resistant type X8001 aluminum-clad fuel plates for the ATR has provided a unique opportunity for investigating fabrication variables. The fuel plate length is greater than that normally encountered, and fuel widths vary from 1.77 to 3.60 in. Since considerable cost would result from separate powder compacting dies for the 19

powder-metallurgy core inserts required, fabricating techniques were developed for using only three such dies. This was accomplished by varying the thickness of the initial compacts, using the compacts in tandem, and cross rolling them to obtain the desired fuel width. The feasibility of the procedures was demonstrated in fabricating the required 19 plates for six prototype elements needed for the ATR fuel element test program.

The main problem in fabricating the plates was in determining the core tolerances and fabrication schedules required to minimize bowing of the core within the plate. Studies indicated that variations in the initial compact thickness greater than 0.003 in. would result in core bowing, whereas compacts of uniform thickness could be fabricated without detectable bowing. Core end feathering was initially felt to be a serious problem in fabricating the long dispersion-bearing fuel plates.

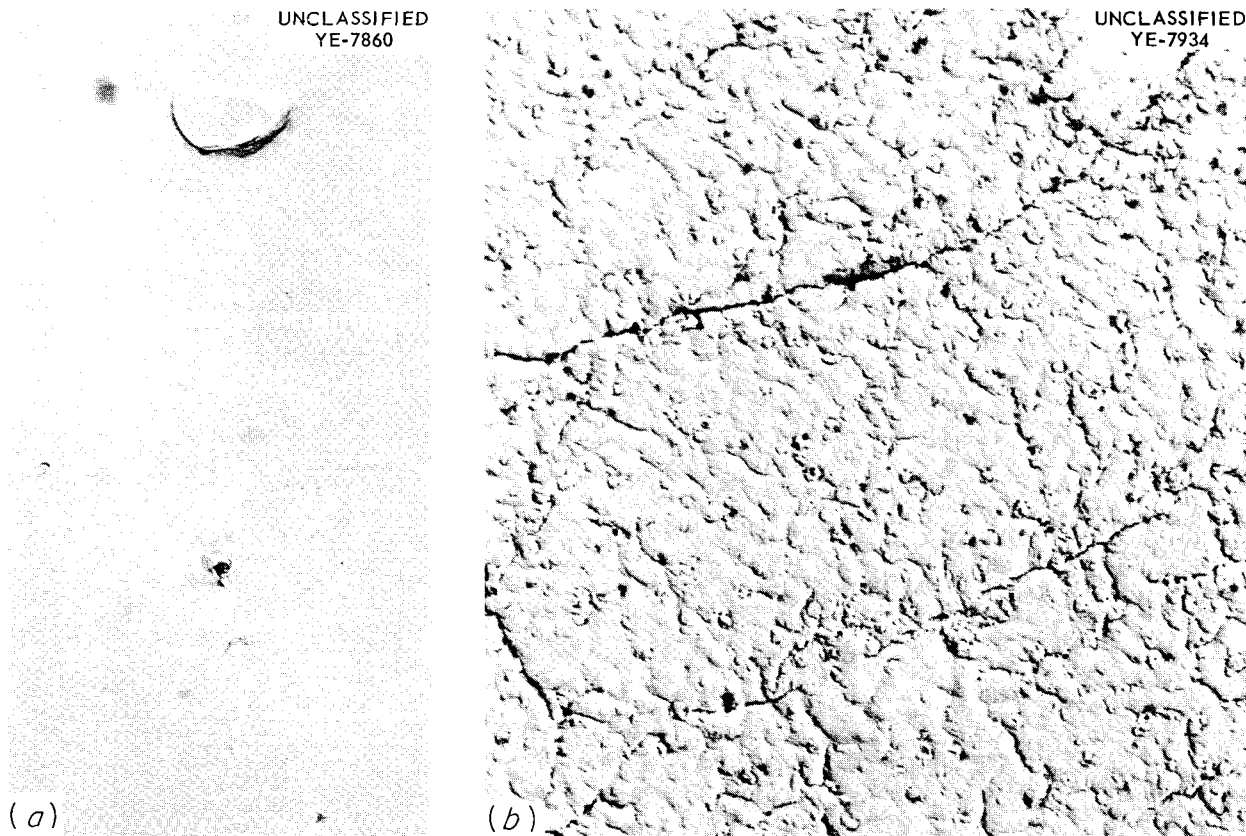


Fig. 18.5. Appearance of Surface Oxide on Type 6061 Aluminum After Annealing in Air for 1 hr at (a) 932°F and (b) 960°F. Carbon replica shadowed with palladium.

However, by sintering the compacts and carefully controlling the initial compact-to-frame thickness variation, fuel plates were fabricated with feathering of the same magnitude as is normally found in fuel plates of half the length. The fuel plates which received cross rolling exhibited considerably less feathering.

### Plate Forming and Assembly

J. H. Erwin      R. W. Knight<sup>7</sup>

An effort was made to improve the reproducibility of the HFIR fuel plate curvature in order to meet the rigid water-channel tolerances. In addition, plate forming and element assembly studies were initiated on the ATR fuel element.

Since the variations encountered in the HFIR fuel plate curvature were believed to be related to the quality of the fabricated composite fuel plate, low-pressure Marforming-type experiments were conducted on composite fuel plates of various qualities, and confirmed the relationship. The

<sup>7</sup>On loan from Engineering and Mechanical Division.

yield of acceptable plates formed by this technique was discouraging, however, since it appears that the involute radii must be duplicated to within  $\pm 0.004$  in. in order to meet the water-channel specifications in the fuel element. Table 18.3 presents a summary of the data obtained from the forming experiments. For comparison, data on the reproducibility of forming commercial type 6061-0 aluminum plate stock are also included. The high-quality composite plates showed a gross improvement over the plates Marformed for the critical experiment. The yield, however, was still considerably below that for the type 6061-0 aluminum plate stock, and consequently that required to economically produce the curved plates. As a result, alternate forming methods coupled with low-pressure Marforming are being explored. Serious consideration is being given to high-pressure Marforming, high-energy electrical discharge forming, and stress relief or creep forming. Data obtained from a limited number of plates which were low-pressure-Marformed and subsequently stress-relieved between mating steel platens of the desired involute curvature indicated sufficient reproducibility to warrant further investigation.

Table 18.3. Summary of Data from Low-Pressure-Marformed HFIR Fuel Plates Showing Degree of Duplication of the Involute Radii

	Inner Annulus		Outer Annulus		
	Type 6061-0 Aluminum	Fuel Plates Utilized in Critical Core	Type 6061-0 Aluminum	Fuel Plates Utilized in Critical Core	Recently Developed Fuel Plates
Number of plates measured	37	18	68	72	101
Maximum spread in plate radius measurements <sup>a</sup> (mils)	9	36	9	18	20
Statistical variance of measurements in the plate group (28 measurements/plate)	1.65	5.03	1.17	3.26	2.75
Percent of acceptable plates (within $\pm 0.004$ in. duplication)	97.3	27.8	98.5	12.5	51.5

<sup>a</sup>Measurements taken at 7 equidistances along the length of each plate at four radii positions (28 measurements/plate).

Similar encouraging results were obtained by employing high-pressure Marforming.

During the past year three fuel elements were assembled in connection with the HFIR fuel element development program. An inner- and outer-annulus element was assembled with type 6061-0 aluminum plate stock to investigate the feasibility of meeting the dimensional tolerances set by the design and to gain experience in assembling this type of element, and an outer-annulus fuel element was constructed from composite fuel plates formed to various curvature tolerances to investigate the possibility of correcting the fuel plate curvature and resulting water-channel spacings by inserting Teflon spacers. The inner- and outer-annulus unfueled elements will be utilized in the HFIR flow test program.

The unfueled type 6061-0 aluminum outer-annulus element was assembled by procedures previously described<sup>6</sup> and welded by procedures described in Chap. 21, this report, and numerous measurements were taken in order to substantiate the effect of the various manufacturing steps on the resulting water-channel spacings. A summary of the critical dimensions is presented in Table 18.4. In the assembled condition all the individual spot and cross-sectional area measurements were within tolerance. Upon completion of the welding, seven

individual spot measurements exceeded the  $\pm 0.010$ -in. tolerance, whereas only one cross-sectional area measurement was greater than the  $\pm 0.006$ -in. tolerance. Modifications to the welding procedures are under study to minimize distortion of the channel spacings.

Although the fabrication of the unfueled inner-annulus element has not been completed, this element in the assembled condition compares favorably with the outer-annulus unfueled element. The only difficulty encountered was the subtle variation in the base angle at the unlippped edge of the formed plates. It appears that this angle must be held to within  $\pm 15$  min in order to facilitate the assembly of the plates into the inner slotted support tube.

The fueled outer-annulus element was constructed from composite plates produced at various stages of the fuel plate fabrication development. In order to correlate the plate quality with the resulting water-channel spacings, the plates were classified according to forming reproducibility and then group-assembled in the element. Variations were noted in the water-channel spacings of the assembled element — depending on this plate classification. By inserting Teflon spacers at the outer edge of the assembly, it was possible to correct, at least temporarily, all out-of-tolerance

Table 18.4. Summary of Plate Spacing Measurements for an HFIR Unfueled Type 6061-0 Outer-Annulus Element

	Element Assembled	Element Completed
Channels		
Number measured	131	369
Percent within $\pm 0.003$ -in. tolerance	100	92.7
Percent within $\pm 0.006$ -in. tolerance	100	99.7
Cross sections <sup>a</sup>		
Numbered measured	917	2583
Percent within $\pm 0.003$ in. tolerance	100	98.9
Percent within $\pm 0.006$ in. tolerance	100	99.96
Number of individual spot measurements	2751	7749
Percent of individual measurements outside $\pm 0.010$ -in. tolerance	0	0.09

<sup>a</sup>Cross section spacing =  $\frac{0.050 + A + B + C}{4}$ .

water-channel spacings in the assembled element. Welding of the element is under way.

In conjunction with the fabrication development of the ATR fuel plates, exploratory experiments were conducted to form the various width plates to their respective radii by the low-pressure Marforming process. Equipment to accommodate the 50-in.-long fuel plates as well as the forming punches for the 19 different radii was constructed. On the basis of a limited number of forming tests, the various punch curvatures were machined with springback allowance increasing from 18% for the narrowest plate to 22% for the widest plate. The plate springback was found to be less on the 0.080-in.-thick plates than on the 0.050-in.-thick fuel plates and to increase by approximately 2% per inch of increase in plate radius, or from 16% at a radius of 3 in. to 20% at a radius of 5 in. The forming results on the prototype  $U_3O_8$  aluminum-bearing fuel plates indicated very erratic duplication of curvatures within any given set of plates. It is hoped that correcting the springback allowances in the punches will eliminate the erratic variation and that satisfactorily formed plates can be obtained by the Marforming process.

Both peening and roll-swaging techniques for mechanically attaching the fuel plates to the side plates were investigated for assembling the ATR fuel element. Joint strengths greater than 200 lb/lin in. were obtained by both techniques. However, two inherent disadvantages were observed in peening: the peened joint consistently feathered where the peening tool struck the side plate, and the vibration of the peening action prevented rigid attachment of the plates and resulted in poor alignment of the fuel plates in the assembly. Guide lands in the side plate between the fuel plate grooves for the swaging roll produced joints with consistently good alignment characteristics and a positive metal-to-metal lock between the fuel plates and side plates. Therefore roll swaging was selected as the mechanical joining technique for assembling ATR fuel elements. The success of the process was further demonstrated by manufacturing prototype assemblies for the ATR fuel element test program.

<sup>8</sup>J. T. Lamartine and W. C. Thurber, *Development of Swaged Stainless Steel Fuel Rods Containing  $UO_2$* , ORNL CF-59-10-8 (Oct. 12, 1959).

## STAINLESS STEEL-BASE FUEL ELEMENT FABRICATION

M. M. Martin      D. O. Hobson

During the past year fabrication studies were continued on stainless steel-base fuel elements. The studies centered on the fabrication of swaged  $UO_2$ -stainless steel fuel rods and the roll cladding of spherical  $UO_2$  dispersions in stainless steel.

In connection with the Maritime Program, 18 swaged  $UO_2$ -stainless steel clad fuel rods were fabricated for a 16-rod element by procedures previously developed.<sup>8</sup> The element is designed for irradiation testing in the Vallecitos Boiling Water Reactor. The rods were prepared by loading stainless steel tubes with fused and ground  $UO_2$ , sealing, and subsequently cold swaging to close diametral tolerances. Fifteen of the rods were swaged to within the  $0.500 \pm 0.001$  in. outer-diameter specification, and the other three within the  $\pm 0.002$ -in. tolerance. Brazing of the fuel rod element is under way by the Welding and Brazing Group.

To facilitate the assembly of the spherical  $UO_2$ -stainless steel fuel plates developed for the Enrico Fermi reactor,<sup>9</sup> an attempt was made to fabricate a fuel plate with sufficient cladding thickness on one side to permit machining integral spacers. Preliminary investigations were thus conducted on roll cladding the type III plate with a 0.058-in.-thick cladding on one side and a standard 0.005-in.-thick cladding on the opposite side. The unsymmetrical cladding thickness coupled with the difference in the coefficient of expansion between the clad and core materials caused the fuel plate to bow during hot rolling. An attempt to anneal out the plate bow by inserting the plate between heavy-gage steel platens was unsuccessful. Machining of the integral spacers and subsequent annealing produced a plate of acceptable flatness. These results suggested that it is feasible to manufacture the type III Fermi fuel plates with integral spacers.

<sup>9</sup>J. H. Cherubini *et al.*, *Fabrication Development of  $UO_2$ -Stainless Steel Composite Fuel Plates for Core B of the Enrico Fermi Fast Breeder Reactor*, ORNL-3077 (Apr. 4, 1961).

## NEUTRON ABSORBER DEVELOPMENT

### Irradiation Behavior of $\text{Eu}_2\text{O}_3$ Dispersions in Stainless Steel

C. F. Leitten, Jr.      A. E. Richt<sup>10</sup>

Irradiation testing results on miniature  $\text{Eu}_2\text{O}_3$  dispersion absorber plates continue to be encouraging.<sup>11</sup> Specimens containing 20, 30, or 40 wt %  $\text{Eu}_2\text{O}_3$  cores were irradiated in the MTR at 170°F to exposures of up to  $2.9 \times 10^{21}$  *nvt* (unperturbed)

<sup>10</sup>Metallography Group.

<sup>11</sup>A. E. Richt, *Army Reactors Program Progress Report*, ORNL-3231, pp 41-43 (Jan. 31, 1962).

<sup>12</sup>C. F. Leitten, Jr., *The Irradiation of Miniature  $\text{Eu}_2\text{O}_3$ -Bearing Absorber Plates*, ORNL CF-59-9-25 (Sept. 8, 1959).

with no evidence of dimensional or structural changes. Four additional specimens remain in-pile for increased exposures.<sup>12</sup>

Postirradiation corrosion tests on sections from these specimens have shown no effect of irradiation upon the corrosion resistance of these dispersion-type absorbers.<sup>13</sup> However, specimens containing 30 and 40 wt %  $\text{Eu}_2\text{O}_3$  cores are susceptible to gross swelling when exposed to water at 570°F and 1200 psi pressure for short periods of time, as illustrated in Table 18.5. Thickness increases of 15 and 30% have been recorded for 30 and 40 wt % specimens, respectively. Specimens containing the 20 wt %  $\text{Eu}_2\text{O}_3$  cores appear to be dimensionally stable under the same conditions.

<sup>13</sup>R. J. Beaver *et al.*, *Met. Div. Ann. Progr. Rept.* May 31, 1961, ORNL-3160, pp 106-9.

Table 18.5. Corrosion Resistance of  $\text{Eu}_2\text{O}_3$ -Stainless Steel  
Dispersions in Water at 570°F and 1200 psi Pressure

Specimen Number	Integrated Unperturbed Dose ( <i>nvt</i> )	Weight Gain	Thickness Gain
<b>20 wt % <math>\text{Eu}_2\text{O}_3</math></b>			
	$\times 10^{20}$		
2A <sup>a</sup> - control		0.03	0
2B <sup>a</sup> - control		0.04	0.91
39-1	7.0	0.01	0.84
39-2	12.1	0.05	2.50
<b>30 wt % <math>\text{Eu}_2\text{O}_3</math></b>			
3 A - control		0.002	0
3B - control		0.01	0.02
39-5	7.6	0.42	13.3
39-6	14.6	0.62	15.4
39-7	27.9	0.71	11.3
<b>40 wt % <math>\text{Eu}_2\text{O}_3</math></b>			
4A - control		2.35	25.5
4B - control		1.53	27.3
39-9	7.2	0.24	34.0
39-10	14.8	1.58	30.5
39-11	28.7	1.51	31.3

<sup>a</sup>A specimens were in cold laboratory; B specimens were run simultaneously with irradiated specimens in hot cell.

### Boron-Gradient Neutron Absorbers

T. D. Watts<sup>14</sup>      R. J. Beaver  
C. F. Leitten, Jr.

Development of the gradient concept for extending the life and burnup of enriched boron-bearing neutron absorbers has been continued. The initial boron gradient was based on the results obtained from the postirradiation examination of a series of stainless steel-clad dispersions of 3 wt % B<sup>10</sup> in iron. These examinations indicated that swelling would occur beyond a B<sup>10</sup> burnup of 4 at. %. More recent refinements in the irradiation program have extended the permissible B<sup>10</sup> burnup to 5 at. %.<sup>13,15</sup> The original gradient profile was therefore recalculated to accommodate this increase in permissible burnup. On the basis of these calculations, an advanced-gradient neutron absorber was designed for service in the SM-1 reactor at Fort Belvoir, Virginia. Increasing the maximum burnup in any increment of thickness resulted in decreasing the number of boron-gradient steps from four to three and increasing the boron concentration in the central portion of the plate from 3 to 6 wt % B<sup>10</sup>. Absorber plates with this boron distribution were fabricated by procedures previously developed for the initial gradient plates.<sup>16</sup>

Paralleling the development of the boron-gradient absorbers, an absorber was designed to utilize both the good irradiation behavior of Eu<sub>2</sub>O<sub>3</sub> dispersions in elemental stainless steel and the economical advantages of boron-bearing dispersions. Such duplex absorbers should also provide long service life. The postirradiation examination of the original SM-1, 3 wt % B<sup>10</sup>-Fe absorber sections, showed that the majority of the burnup along the length of the rod had occurred within the first 6½ in. By utilizing Eu<sub>2</sub>O<sub>3</sub> in only this region and the boron-gradient concept in the remaining portion of the rod, materials costs, as reflected by the price of Eu<sub>2</sub>O<sub>3</sub>, can be significantly reduced.

<sup>14</sup>Powder Metallurgy Group.

<sup>15</sup>A. E. Richt, *Army Reactors Program Progress Report*, ORNL-3231, pp 39-40 (Jan. 31, 1962).

<sup>16</sup>R. J. Beaver and T. D. Watts, *op. cit.*, pp 24-28.

<sup>17</sup>C. F. Leitten, Jr., *et al.*, *Specifications and Fabrication Procedures on Europium-Bearing Absorber Rods for Reactivity Control in Core II of SM-1*, ORNL-2733 (July 29, 1959).

Sample absorber plates with 37 wt % Eu<sub>2</sub>O<sub>3</sub>-elemental stainless steel tips and boron-gradient follower sections were fabricated by techniques developed previously.<sup>16,17</sup> Radiographic examination of the plates showed them to be dimensionally acceptable for irradiation testing in the SM-1 reactor. Metallographic examinations revealed that considerable intermixing of the boron dispersion with the Eu<sub>2</sub>O<sub>3</sub> dispersion had occurred during fabrication at the junction of these two materials. As a result, a slight reaction was observed between the Eu<sub>2</sub>O<sub>3</sub> and the silicon-bearing stainless steel matrix in the boron region. This slight reaction is not felt to be harmful. Fabrication of a full-size absorber section for testing in the SM-1 reactor is in progress.

### BERYLLIUM FABRICATION STUDIES

#### Fabrication of Spiral-Finned Beryllium Tubing

D. O. Hobson

An extrusion process was developed<sup>18</sup> for fabricating economical and reliable spiral-ribbed beryllium tubing as a potential cladding material for advanced gas-cooled reactors. Good quality tubes approximately ½-in.-ID by 0.040-in.-wall thickness and surrounded by 12 equally spaced fins 0.160 in. high were successfully extruded from canned hollow beryllium billets in lengths up to 23 ft.<sup>19</sup>

To evaluate the mechanical properties of the extruded tubing, room-temperature and short-time elevated-temperature tube-burst tests were performed. The room-temperature burst tests showed the tubing to have calculated hoop stresses ranging from 28,000 to 65,000 psi, depending upon the surface finish of the tubes. The higher values corresponded to tubes with a honed surface finish of 4 μin./in. rms. Elevated-temperature short-time burst tests showed the hoop stresses to vary linearly from 27,000 to 10,000 psi at 800 and 1300°F, respectively.

<sup>18</sup>By Nuclear Metals, Inc., subcontract No. 2091.

<sup>19</sup>T. A. Tarpey *et al.*, *Final Report to Union Carbide Nuclear Company, Beryllium Tubing Program, NMI-4971* (Feb. 27, 1962).

## Pressure Bonding of Beryllium

D. O. Hobson

The self-bonding characteristics of beryllium and a beryllium-clad uranium dioxide compartmented fuel element are being investigated.<sup>20</sup> In conjunction with the pressure-bonding studies, the compatibility of beryllium with both coated and uncoated bulk uranium dioxide was studied, as well as the compatibility of beryllium with various bonding container materials.

The pressure-bonding process consists essentially in employing gas pressure at elevated temperatures to achieve solid-state bonding. Self-bonding experiments were conducted at a constant 10,000-psi pressure for 2 to 4 hr at temperatures from 1550 to 1750°F. The surface of the beryllium plates was prepared for bonding by various techniques, which included grit blasting, cold work, hand abrasion, and a variety of pickling treatments. Optimum self-bonding, including grain growth across the interface, was obtained with surfaces which had been grit-blasted with chilled iron shot, acid-leached, and bonded at 10,000 psi pressure for 4 hr at 1650°F.

Beryllium was found to react with  $UO_2$  at 1650°F in times over 1 hr.<sup>21</sup> The compound  $UBe_{13}$  was detected in the reaction zone of a specimen bonded at 1650°F for 4 hr. When the cores were coated with pyrolytic carbon, reaction was not observed until bonding conditions were extended to 4 hr at 1750°F.

## FABRICATION OF REFRACTORY-METAL ALLOYS

D. O. Hobson

Investigations were conducted the past year on the high-temperature capabilities of alloys based on the Nb-V system. The studies have centered around alloys in the 30 to 50 wt % V range, including those modified with small additions of both zirconium and titanium.

Fabrication was limited to cold-rolling operations for ingot breakdown and for production of sheet material for evaluation. The alloys were shown to have two rather unusual properties: they are extremely hard ( $R_C$  25 to 40) compared with other niobium-base alloys, and they appear to initially deform by a twinning mechanism. Neither niobium nor vanadium undergoes deformation twinning at room temperature at slow deformation rates, but Nb-V alloys twin easily at room temperature. This twinning was evidenced by the audible "cracking" sound as the twins were formed during both cold-rolling and hardness testing.

The high hardness value of the Nb-V alloys would indicate that fabrication difficulties might be encountered in this system. The unique twinning ability of the system, however, evidently allows the material to be heavily deformed without fracture. Hardness vs deformation curves were obtained from specimens of various compositions that were cold-rolled in increments of 10% reduction in thickness and with  $R_C$  hardness measurements taken at each increment. It was found that the alloys deformed by twinning up to approximately 20 to 30% reduction in thickness and that thereafter no further twinning was audible. Metallographic examination confirmed the twinning and also indicated that under higher deformations slip is evidently the predominant mechanism. The hardness was found to increase rapidly for the first 20 to 30% of reduction; then, as slip replaced twinning, the hardness increased more slowly at an approximately linear rate.

Specimens from two heats of Nb-40% V-1% Zr and from one heat of Nb-40% V were cold-rolled 90% and annealed for 1 hr at temperatures ranging from 1800 to 2300°F. Preliminary metallographic results showed recrystallization to be initiated at 1800°F in certain bands in all three heats. However, an equiaxed structure was not obtained until approximately 1900°F for the Nb-40% V alloy and not until 2000 to 2100°F for the Nb-40% V-1% Zr alloys. A correlation was observed between the annealing temperature and the twinning in these various alloys. Twinning was "heard" during hardness testing and seen metallographically in specimens of the Nb-40% V alloy annealed at 2000°F and above and in the two Nb-40% V-1% Zr alloys at 2200°F and above. The 1% Zr addition evidently raises the recrystallization temperature and decreases the rate of grain growth.

<sup>20</sup> By Battelle Memorial Institute, subcontract No. 2029.

<sup>21</sup> S. J. Paprocki *et al.*, *Preliminary Studies of Bonding of Beryllium-Clad  $UO_2$  Fuel Elements*, BMI-1545 (Sept. 20, 1961).

## MELTING AND CASTING OF REFRACTORY METALS AND ALLOYS

T. Hikido

In the past year an attempt was made to improve the purification of refractory metals and to grow large single crystals for research studies by zone melting in an electron-beam furnace. The ability of the electron-beam furnace to purify refractory metals, for example, to lower the impurities in niobium to less than 100 ppm total oxygen, nitrogen, and carbon content, was demonstrated previously.<sup>22</sup> The electron-beam furnace was adapted for zone melting by installing the rotatable, water-cooled copper hearth assembly illustrated in Fig. 18.6 and described elsewhere.<sup>23</sup> The material to be purified is contained in an annular cavity approximately 4-in.-ID by 7-in.-OD, and the molten zone is caused to move along the sample by rotating

the hearth beneath the stationary electron beam. The electron beam is shaped in an electromagnet assembly so as to alter the normally circular molten zone to a more rectilinear configuration and thereby provide a straighter liquid-solid interface.

Although only a limited number of experiments have been performed to date, the electron-bombardment, horizontal-zone-melting technique appears promising for producing single crystals of niobium and possibly other refractory metals of sufficient size, purity, and structural quality to be useful for research studies on the mechanisms of corrosion,

<sup>22</sup>D. T. Bourgette and T. Hikido, *Met. Div. Ann. Progr. Rept.* May 31, 1961, ORNL-3160, p 109.

<sup>23</sup>T. Hikido, "Horizontal Zone Melting of Refractory Metals by Remote Gun Electron Bombardment," p 276 in *Proceedings, Fourth Symposium on Electron Beam Technology*, March 29-30, 1962, Boston, Mass. (R. Bakish, ed.), Alloy Electronics Corp., Cambridge, 1962.

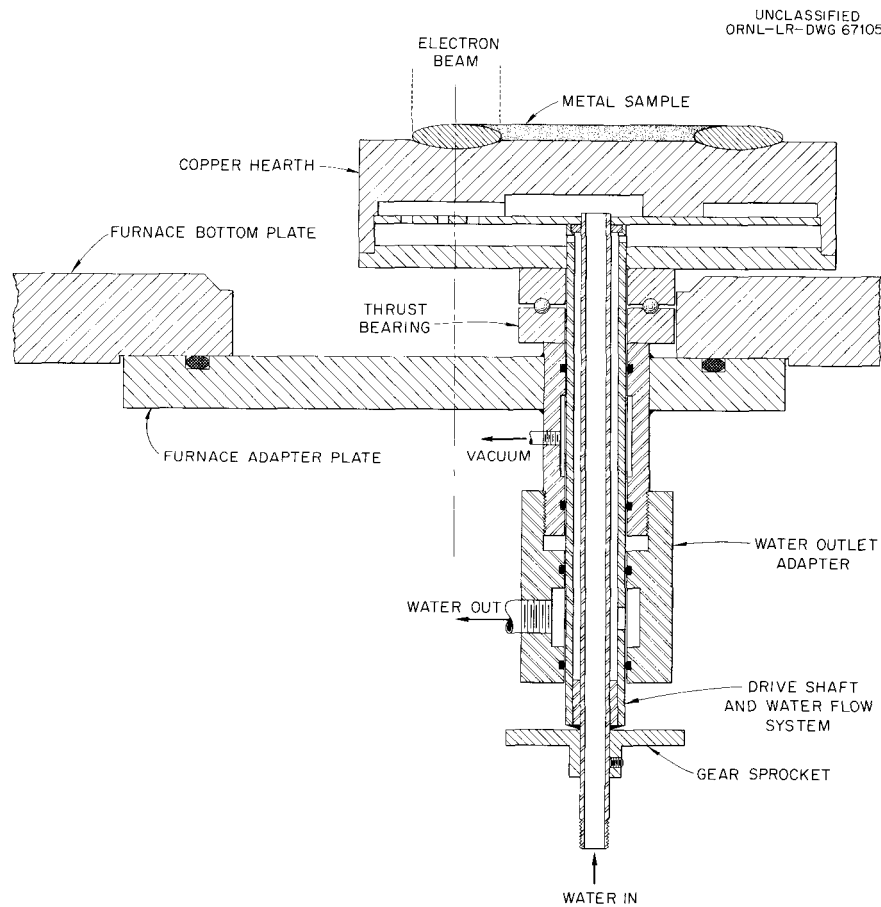


Fig. 18.6. Electron-Beam Furnace Zone Refining Assembly.

oxidation, and deformation. Single crystals cut from zone-melted niobium are illustrated in Fig. 18.7. It has been found possible to prepare several test specimens of selected orientation from a single large crystal. Preliminary x-ray diffraction data indicated the existence of lattice strains in some of these small crystals, which were eliminated by careful polishing of the cut surfaces.

Chemical analyses are available only on the interstitial impurities O<sub>2</sub>, N<sub>2</sub>, H<sub>2</sub>, and C in zone-melted niobium and, as yet, are not sufficient to permit an accurate correlation of purification with zone-melting parameters. However, the data presented in Table 18.6 do indicate that niobium of high purity with respect to the gaseous impurities can be prepared. It is also evident that special steps will be required to remove carbon to the same levels. The similarity of analysis between the first molten zone and the final zone indicates that purification with respect to the gaseous impurities was achieved by volatilization rather than zone refining per se. Additional studies are required

to evaluate the effect of zone melting on the removal of substitutional impurities such as W, Ta, Fe, and Zr.

Table 18.6. Chemical Analysis of Electron-Beam-Melted Niobium

Material	Chemical Analysis (ppm)			
	O <sub>2</sub>	N <sub>2</sub>	H <sub>2</sub>	C
As-received	1800	580	20	100
Electron-beam-melted <sup>a</sup> button (500 g)	36	22	5	29
Zone-melted <sup>b</sup>				
Initial zone	7	<5	2	38
Final zone	9	<5	2	38

<sup>a</sup> Approximately 3½-in.-diam disk, held molten for 12 min.

<sup>b</sup> Zone-melted in three passes.

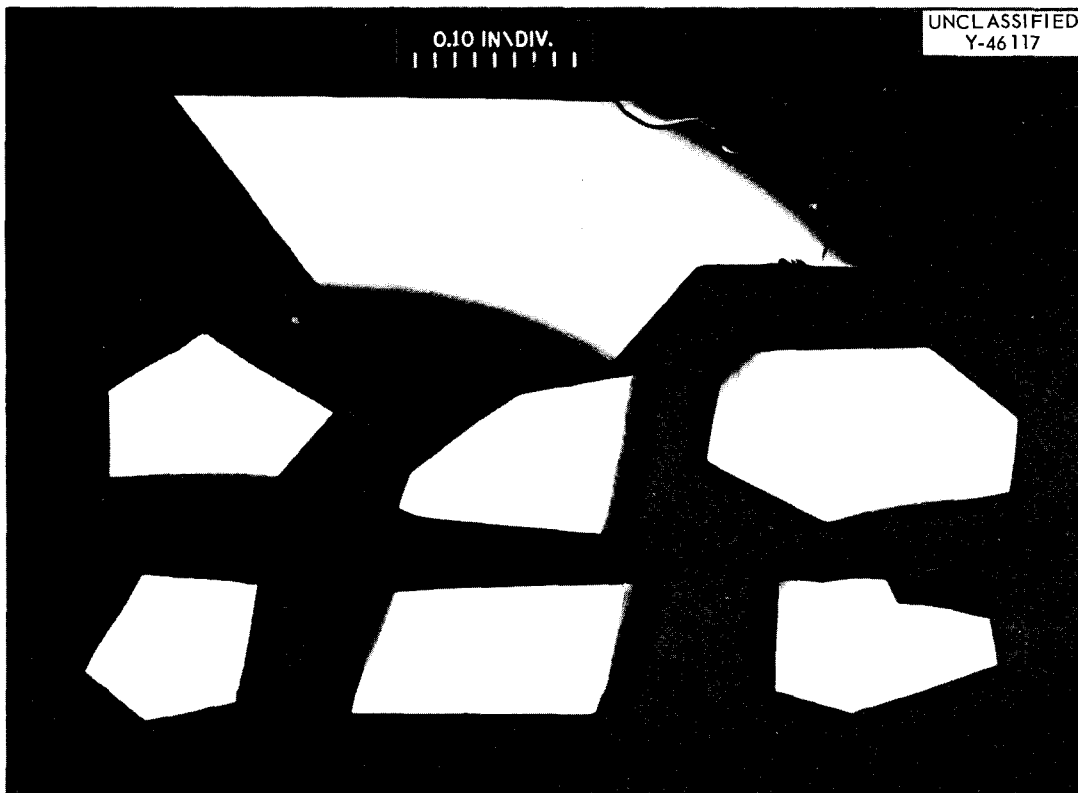


Fig. 18.7. Single Crystals Sectioned from Ingots Zone-Melted in an Electron-Beam Furnace.

Small heats of Nb-V alloys with closely controlled compositions were prepared for screening evaluation tests in a high-temperature-alloy development program. For these initial screening tests a total of 21 Nb-V binary alloys and alloys containing ternary and quaternary additions of zirconium and titanium were prepared. Because of the wide difference in vapor pressure between niobium and vanadium, the argon-atmosphere, tungsten-electrode, arc-melting process was selected to minimize compositional changes during melting. Electron-beam-

purified niobium was used as the melting stock, whereas both electron-beam-purified and as-received crystals were used as the vanadium melting stock. The alloys were prepared in the form of disks approximately 4 in. in diameter by  $\frac{3}{8}$  to  $\frac{1}{2}$  in. thick and weighing about 0.6 kg each. Chemical analyses of the as-cast alloys indicated good control of the alloy composition, although contamination with interstitial impurities was encountered. The cause for this contamination is not presently understood.

## 19. Powder Metallurgy

J. P. Hammond

### FABRICATION OF URANIUM CARBIDE WITH A VOLATILE SINTERING-TEMPERATURE DEPRESSANT

J. P. Hammond

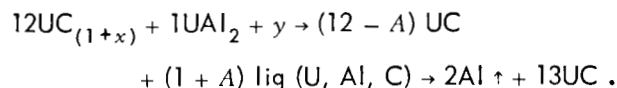
J. D. Sease

Uranium carbide continues to show great promise as a fuel for commercial power reactors, but its fabrication looms as a serious problem. To achieve acceptable densities, sintering temperatures in the range 1800 to 2000°C are required. At such high temperatures, some uranium is usually lost by volatilization, resulting in an undesirable hyperstoichiometric microstructure.

In seeking a solution to this problem, studies were made of liquid-phase sintering as a means of lowering fabrication temperature.<sup>1</sup> In order that the fuel material not be penalized in thermal performance, it was stipulated that the eutectic or other low-melting constituent responsible for the liquid-phase sintering be eliminated during fabrication. By eliminating this constituent, permissible fuel operating temperature and power density are the same as with pure carbide rather than much lower.

From a large number of agents examined for lowering the fabrication temperature,<sup>2</sup> intermetallic  $UAl_2$  was the one selected, as it yielded high densification at temperatures as low as 1200°C. In addition, by taking advantage of high vapor pressure, it proved feasible to remove the aluminum by sintering in a vacuum. The uranium residual from the  $UAl_2$  is combined with carbon introduced in the system as excess carbon ( $x$ ) in the uranium monocarbide and as carbon ( $y$ ) issuing

from the graphite crucible:



Uranium carbide bodies of densities around 93% of theoretical are achieved with sintering at 1300°C. Essentially all the aluminum is removed, and structures virtually free of secondary constituents result.

The effects of the sintering temperature, the amount of  $UAl_2$  used, and the uranium monocarbide carbon level on fabricated density are shown in Fig. 19.1. The designations for the curves refer to the carbon balance of the charging composition. It is seen from the graphs that density improves as both the amount of  $UAl_2$  is increased (from 2 to 10 wt %) and the carbon level of the uranium monocarbide is decreased. Whereas for the 5 and 10 wt % levels of  $UAl_2$ , good densities are obtained with sintering temperatures as low as 1200°C, a temperature of 1300°C or higher was found necessary to assure a monophasic structure and effective removal of the aluminum. Also, as is shown subsequently, excess carbon in the uranium monocarbide proved to inhibit aluminum removal.

Table 19.1 presents the results obtained from sintering UC with 7½ wt %  $UAl_2$ . The compacts were pressed with 2 wt % camphor at 10 to 25 tsi and contained in a closed graphite crucible 2½-in.-OD × 3-in. height with ½-in. sight hole. Firings were made in a tantalum strip-heated furnace at  $10^{-5}$  to  $5 \times 10^{-7}$  torr vacuum. Figure 19.2 shows typical microstructures of the sintering aid. In conformity with the data of Fig. 19.1, it is seen (Table 19.1) that density generally increases with sintering temperature and decreases with uranium

<sup>1</sup>J. D. Sease and J. P. Hammond, *Met. Div. Ann. Progr. Rept. May 31, 1961*, ORNL-3160, p 158.

<sup>2</sup>J. P. Hammond and J. D. Sease, *GCR Quart. Progr. Rept. Dec. 31, 1961*, ORNL-3254, pp 188-91.

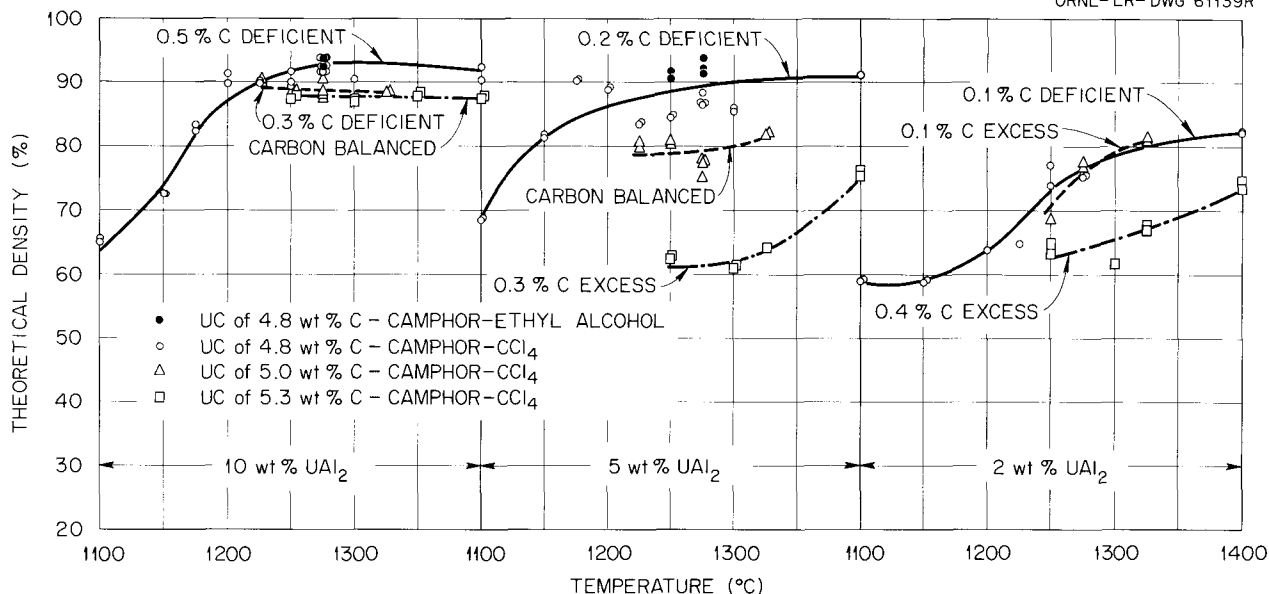


Fig. 19.1. Sintering Characteristics of UC-UAl<sub>2</sub> as a Function of UC Carbon Level and Amount of UAl<sub>2</sub> Compacts Pressed with 2 wt % Camphor at 10 tsi and Fired for 3 hr at Temperature.

monocarbide carbon level. While uranium monocarbide containing 5.1 wt % C resulted in substantially lower density than for stoichiometric uranium monocarbide (compare experiments 8-12 with 1-5), at least some latitude in uranium monocarbide composition is permitted. Results for 4.9 wt % C compare favorably with 4.8 wt % C (experiments 6-7 with 1-5). As a general rule, grain size was found to increase with degree of densification.

The aluminum removal, as reflected by the aluminum analysis and presence of secondary constituents, is not effective at temperatures below 1300°C (experiments 1-5 for 4.8 wt % C material). Whereas sintering at 1300 to 1400°C for 4.8 wt % C-uranium monocarbide resulted in 95% and higher aluminum removal, the UC of 5.1 wt % C showed only 28 to 30% removal for comparable conditions (compare experiments 3-5 with 10-12). Figure 19.2, which shows the corresponding difference in the microstructures, reveals a 93% dense, essentially all-carbide structure for the 4.8 wt % C material as compared with a less dense structure containing 10% secondary constituent for the 5.1 wt % C material.

In a subsequent study to determine why excess carbon adversely affects aluminum removal and

densification, the carbon level of the uranium monocarbide was linked with the wetting behavior of the liquid phase which forms from it. It was found that the excess carbon of the uranium monocarbide is imparted to the liquid phase during or subsequent to the eutectic reaction. For 4.8 wt % C-uranium carbide as the starting material, the liquid phase contains only about 0.5 wt % C; but for 5.1 wt % C-uranium carbide, it can contain higher than 4.5 wt % C. In the sintering process this sharp increase in carbon content of the liquid phase is responsible for a reversal to a completely nonwetting condition. This, in turn, causes premature "skeletonization" of the carbide grains, thus blocking passages for aluminum removal and cutting short the shrinkage process.

#### DEVELOPMENT OF DISPERSION-HARDENED THORIUM AND DISPERSION-TYPE THORIUM FUELS

J. A. Burka      J. P. Hammond

Thorium metal has several unique advantages as a nuclear fuel material: its resistance to radiation damage to high-nuclear burnups at useful operating temperatures, excellent thermal conductivity, and potential for breeding when used in conjunction

Table 19.1. Results for Sintering UC with 7½ wt % UAl<sub>2</sub>

Experiment No.	Carbon Content of UC (wt %)	Sintering Temperature (°C)	Green Density (% of theoretical) <sup>a</sup>	Sintered Density (% of theoretical) <sup>b</sup>	Aluminum Analysis		Microstructure		
					Content <sup>c</sup> (wt %)	Amount Lost (%)	Secondary Constituent		Grain Size (grains/in. <sup>2</sup> )
							Estimated Amount (vol %)	Identity <sup>d</sup>	
1	4.8	1200	68.5	88.5	0.99	29.0	6-7		250
2	4.8	1250	68.0	91.0	0.90	35.0	6	UAl <sub>2</sub> + α-U	128
3	4.8	1300	68.5	93.0	0.07	95.0	< ½	α-U	64
4	4.8	1350	68.5	92.5			< ½	α-U	64
5	4.8	1400	68.5	93.5	0.045	97.0	< ½	α-U	16
6	4.9	1300	67.0	91.0					
7	4.9	1350	67.0	92.5					
8	5.1	1200	66.5	87.0			10	UAl <sub>2</sub> + α-U	> 500
9	5.1	1250	66.5	86.5			10		> 500
10	5.1	1300	66.5	90.0	1.07	28.0	10		500
11	5.1	1350	66.5	89.0	0.97	30.0	10		500
12	5.1	1400	66.5	90.0			8-9	α-U + UAl <sub>2</sub>	250

<sup>a</sup>Based on density of UC-7.5 wt % UAl<sub>2</sub>; values are an average of duplicate tests.

<sup>b</sup>Based on x-ray density of UC (13.63 g/cc); values are an average of duplicate tests.

<sup>c</sup>By wet chemical analysis average of duplicate tests.

<sup>d</sup>By metallographic techniques in conjunction with x-ray diffraction.

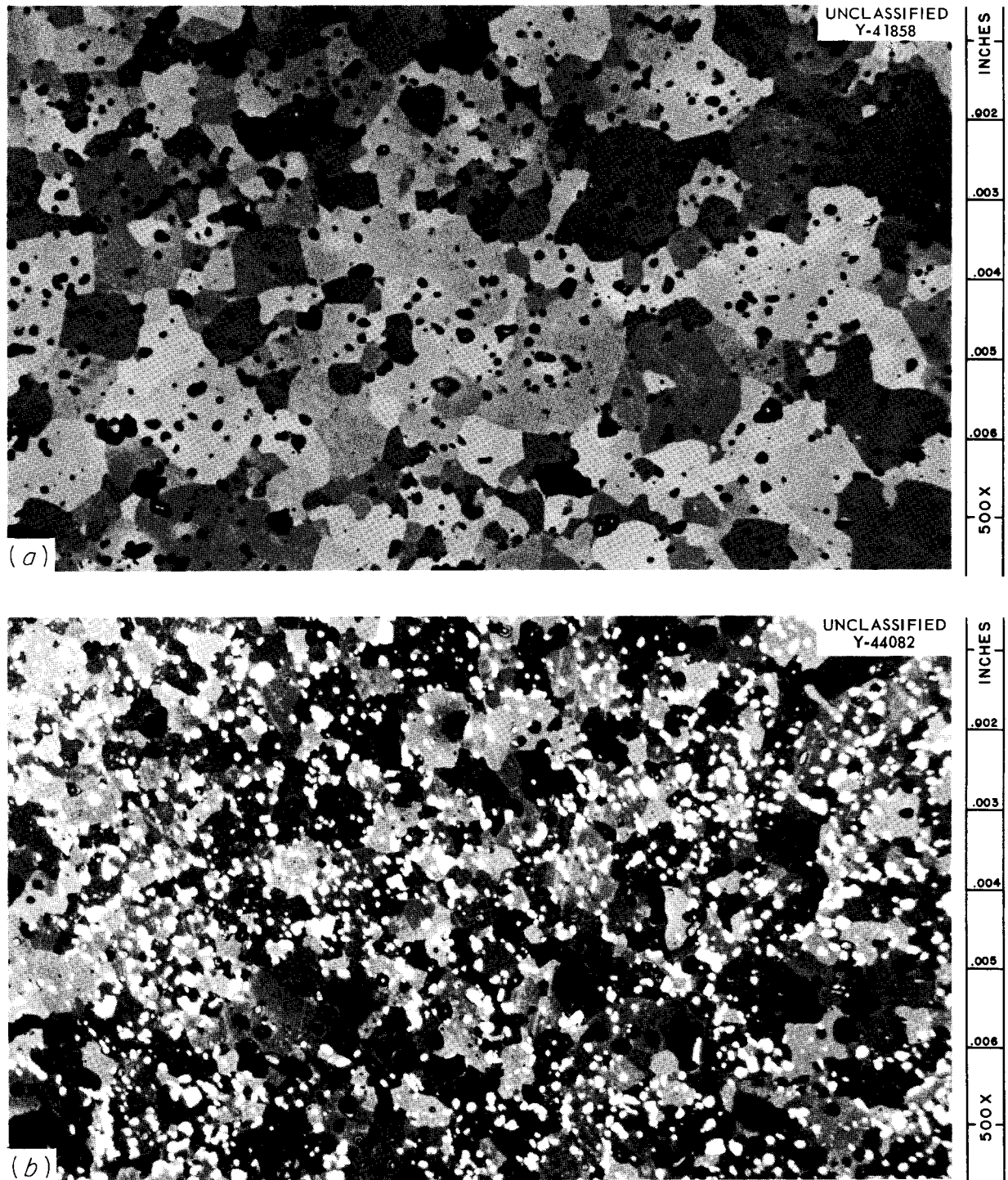


Fig. 19.2. Microstructure of UC-7 $\frac{1}{2}$  wt % UAl<sub>2</sub> as a Function of Carbon Content of the Carbide. Etched with 30 HNO<sub>3</sub>-30 acetic-30 H<sub>2</sub>O. (a) UC of 4.8 wt % C sintered for 3 hr at 1300°C; density is 93% of theoretical; gray matrix is UC; black area, porosity; (b) UC of 5.1 wt % C sintered for 3 hr at 1400°C; density is 90% of theoretical; gray matrix is UC; black area, porosity; and white particles are a mixture of UAl<sub>2</sub> and  $\alpha$ -uranium. 500X.

with  $U^{233}$ . To improve thorium as a fuel material, studies are being made to enhance its high-temperature mechanical properties by alloying<sup>3</sup> and dispersion-hardening. The previous year's work has shown that zirconium and indium are excellent solid-solution strengtheners at elevated temperature. Dispersion-hardening of thorium and Th-Zr alloys is being developed to further improve high-temperature strength, as well as inhibit fission-gas swelling through a process of artificial nucleation and surface tension restraint. Also, work is under way to develop thorium composite fuels with fissile  $UO_2$ , UC, or  $UC_2$  as the dispersoid.

The achievement of dispersion-hardening in thorium has required investigations of techniques for preparing ultrafine powders of thorium, for introducing hard particles, and for consolidating the thorium powders. The present procedure consists of heating thorium metal pieces in a hydrogen atmosphere to produce thorium hydride powder, which is put in a ball mill along with fine oxide powders as the hard-particle dispersant. The powders are simultaneously comminuted and blended by milling, and consolidation is obtained by hot pressing in a graphite die under vacuum. Incident to hot pressing, the hydride is dissociated. Finally, the compacts are extruded in 3-in.-diam copper or iron billets.

Hot-hardness tests on extrusions of Th-10 vol %  $AlO(OH)$  (du Pont F powder), Th-10 vol %  $ZrO_2$  (Monsanta's Micria Zr), and thorium with  $ThO_2$  formed *in situ* during milling are shown in Fig. 19.3, along with results for thorium prepared by arc melting for a reference. On heating,  $AlO(OH)$ , which is added as very small needle-shaped particles, decomposes to  $Al_2O_3$ , which, in turn, reduces to  $ThO_2$  and  $ThAl_2$  (intended dispersants) with fabrication. The  $ThO_2$  introduced by milling resulted from a reaction with the impurities in commercial argon during and subsequent to milling.

The Th-10 vol %  $AlO(OH)$  compact shows the highest hardness values at all temperatures. The curves for the Th-10 vol %  $ZrO_2$  and milled-thorium compacts intersect, with the Th-10 vol %  $ZrO_2$  material displaying excellent resistance to softening to about 500°C. It appears that the milled-thorium compact, as well as the Th-10 vol %  $ZrO_2$ , undergoes a possible drop-off in hardness

with increasing temperature at around 500°C. The thermal stability of the structure and its interrelation with properties are being studied further.

Whereas the dispersion hardening of thorium is in a rudimentary stage of development, clear evidence is shown for strengthening by this mechanism. Present efforts are being devoted to finding more suitable dispersants and refining techniques for rendering and maintaining them in finer form.

Compatibility studies on fissile particles dispersed in thorium indicate a need for coating the particles to reduce the extent of reaction. Uranium oxide and uranium monocarbide, uncoated and coated with niobium or pyrolytic carbon, and  $UC_2$ , coated with pyrolytic carbon, were incorporated in thorium powder by cold pressing followed by cold swaging in Zircaloy-2 tubing. The specimens were then subjected to thermal treatments from 700 to 1300°C.

Particles of UC and  $UC_2$  coated with pyrolytic carbon gave the best results, giving good resistance to reaction at temperatures to 1100°C. The niobium coating proved ineffective. Of the uncoated particles, the  $UO_2$  showed the greatest reaction with the matrix.

Figure 19.4 illustrates the degree of reaction in representative specimens heat-treated at 900°C for 100 hr. Substantial reaction may be observed for both the uncoated uranium monocarbide particles and for the niobium-coated  $UO_2$  particles. The only slight amount of reaction products around the pyrolytic-carbon-coated UC and  $UC_2$  particles attests to the effectiveness of this coating (Fig. 19.4c and d).

## BERYLLIDE FUELS

J. D. Sease

Fuels based on Th-U-Be are attractive for breeder reactors, with gas or organic cooling, both because of the favorable nuclear characteristic of the Th- $U^{233}$  fuel in a thermal system and the surplus neutrons that evolve as a result of fast-neutron reaction with beryllium. While such a fuel is not attractive from a fuel density point of view, its high thermal conductivity would enable a high ratio of surface cooling area to unit amount of

<sup>3</sup>J. A. Burka and J. P. Hammond, *Met. Div. Ann. Progr. Rept. May 31, 1961*, ORNL-3160, pp 158-60.

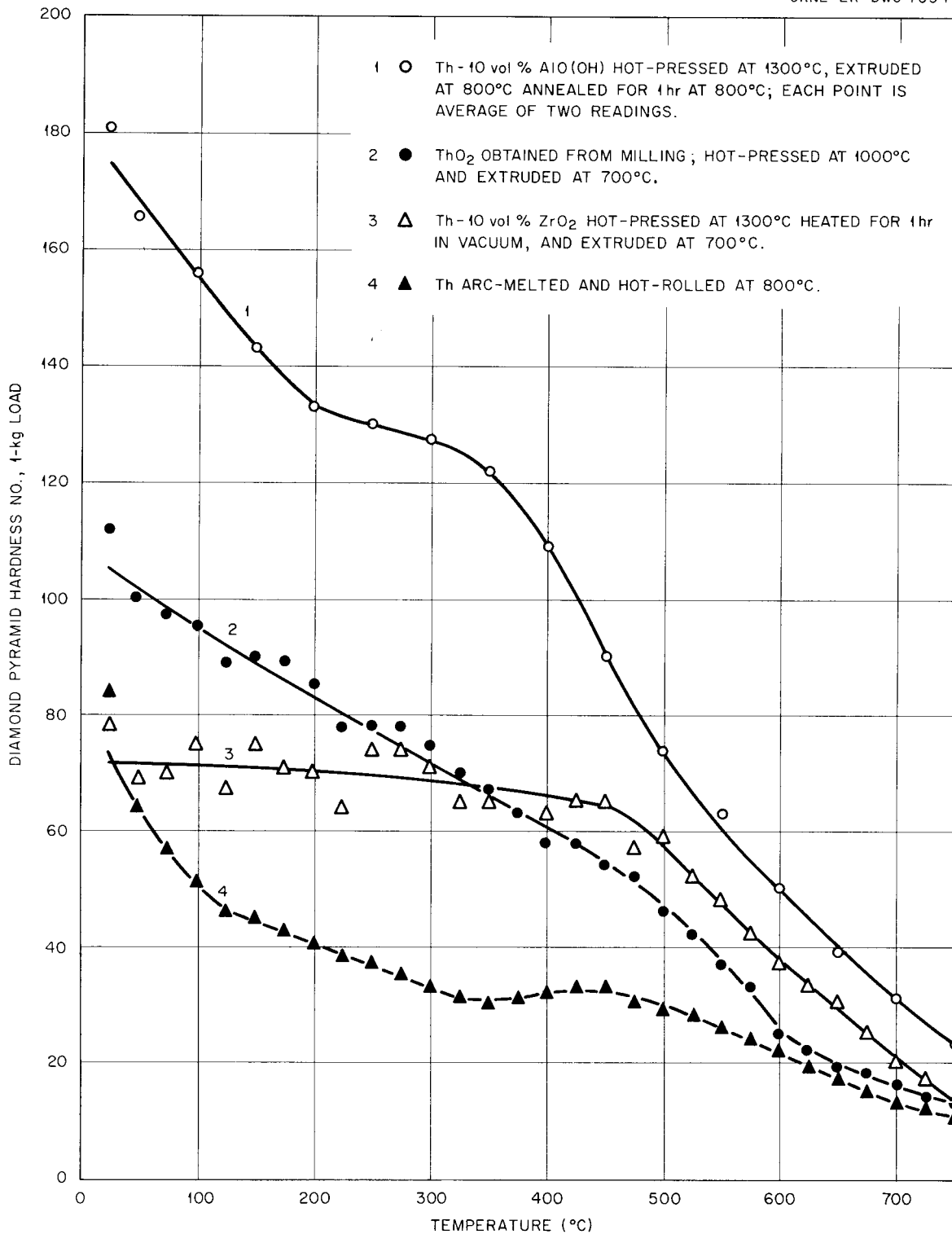


Fig. 19.3. Hot-Hardness Curves of Thorium and Thorium Containing Dispersions of Hard Particles.

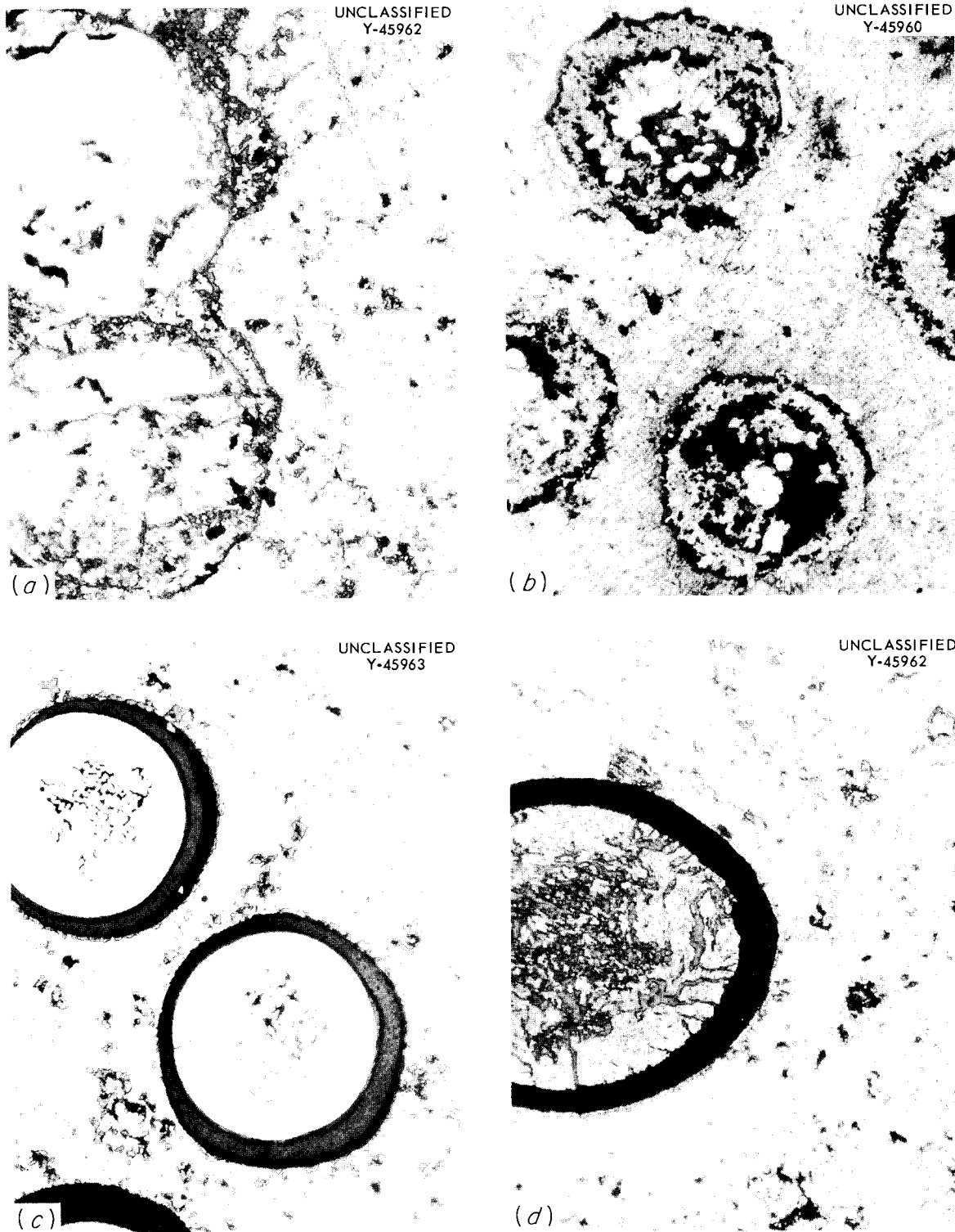


Fig. 19.4. Fissile Particles in a Thorium Matrix Heated at  $900^{\circ}\text{C}$  for 100 hr – (a) Uncoated UC; (b) Niobium-Coated  $\text{UO}_2$ ; (c) Pyrolytic-Carbon-Coated UC; (d) Pyrolytic-Carbon-Coated  $\text{UC}_2$ . Specimens prepared by cold pressing followed by cold swaging. Reaction between dispersoid and matrix is substantial for uncoated UC and niobium-coated  $\text{UO}_2$  (a and b) but is very slight for pyrolytic-carbon-coated UC and  $\text{UC}_2$  (c and d). As-polished. 250X. Reduced 4.5%.

contained fuel, which may be important in gas reactor designs. The question of irradiation stability, however, is the major question unanswered.

A fabrication development program was initiated to produce homogeneous solid-solution fuels of  $(\text{Th}_{19}\text{U}_1)\text{Be}_{13}$ . In the initial phase of the program, beryllide powders were produced by reacting the elemental components in a vacuum with an excess amount of beryllium. Quality hot pressings with densities in excess of 95% of theoretical were produced in  $\text{ThBe}_{13}$ ,  $\text{UBe}_{13}$ , and  $(\text{Th}_{19}\text{U}_1)\text{Be}_{13}$ . Homogeneous solid-solution fuels of  $(\text{Th}_{19}\text{U}_1)\text{Be}_{13}$  with 95% theoretical density were fabricated by the more economical method of mixing separate beryllide powders and sintering them at  $1600^\circ\text{C}$  in argon. The bodies generally contained  $\text{ThO}_2$  in a trace amount. A typical microstructure is shown in Fig. 19.5.

One advantage of the beryllide fuels is that, contrasted to fueled  $\text{BeO}$ , they appear to be very amenable to reprocessing. cursory tests indicated that the beryllides dissolve in the standard 4 M

$\text{HNO}_3$  digestion solution as follows:

Material	Solution	Results
$\text{UBe}_{13}$	Boiling 4 M $\text{HNO}_3$ , $\frac{1}{20}$ M HF	Good
$\text{ThBe}_{13}$	Boiling 4 M $\text{HNO}_3$	Very good
$(\text{Th}_{19}\text{U}_1)\text{Be}_{13}$	Boiling 4 M $\text{HNO}_3$ , $\frac{1}{20}$ M HF	Good

A second advantage is that in reaction tests for 300 hr at  $700^\circ\text{C}$  in flowing dry air,  $\text{ThBe}_{13}$  was shown to have good oxidation resistance ( $+1.5$   $\text{mg}/\text{cm}^2$  for 300 hr).

An irradiation program has been set up to evaluate the beryllide fuels. A capsule of  $\text{UBe}_{13}$  is scheduled to be irradiated in the LITR, starting during the summer of 1962, to a burnup of 12,000 Mwd per metric ton of  $\text{UO}_2$ . When the tests on  $\text{UBe}_{13}$  have been completed,  $(\text{Th}_{19}\text{U}_1)\text{Be}_{13}$  and possibly thorium matrix dispersions will be irradiated.

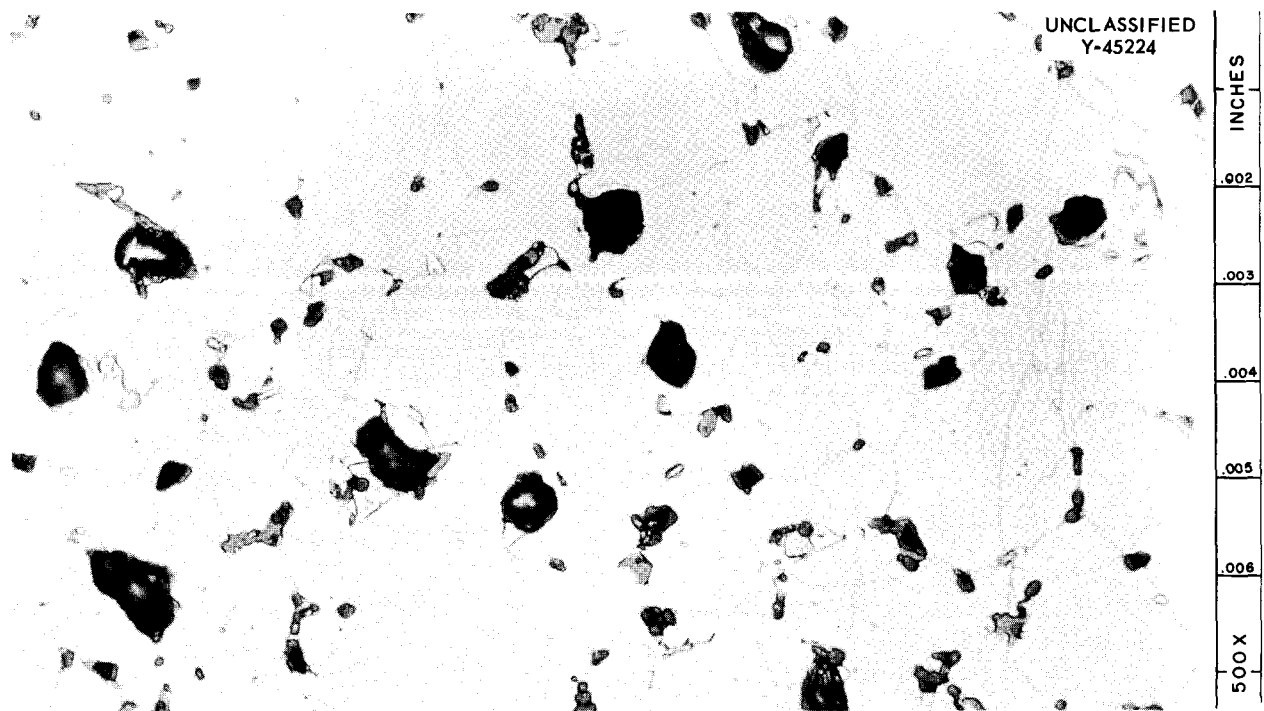


Fig. 19.5. Microstructure of Cold-Pressed  $(\text{Th}_{19}\text{U}_1)\text{Be}_{13}$  Sintered at  $1600^\circ\text{C}$  in 17 psia Argon Atmosphere. Light area is  $(\text{Th}_{19}\text{U}_1)\text{Be}_{13}$ ; gray areas,  $\text{ThO}_2$ ; dark areas, voids. Etched with 20  $\text{HNO}_3$ -1 HF for 10 sec.

## ALUMINUM MATRIX FUELS

T. D. Watts      J. P. Hammond

The function of the Powder Metallurgy laboratory in the joint High-Flux Isotope Reactor (HFIR) and Advanced Test Reactor (ATR) programs is to develop techniques for producing the fuel element cores. Present plans for the HFIR inner annulus call for using the duplex core shown in Fig. 19.6.

In the previous year, a core fabrication procedure involving precision die forging was developed.<sup>4</sup> However, plates prepared with cores made by this method were subject to severe blistering, and the plate rejection was high. This process was modified ("Fuel Plate Fabrication," Chap. 18, this report), and subsequently a large volume of test plates were successfully fabricated without the high degree of blistering formerly experienced.

While the core pieces were being prepared for these plates, a study was begun on a method for fabricating the duplex core component in a single

cold-pressing operation. Such a technique yielded a simpler and cheaper operation and eliminated two major sources of blistering: trapped forging lubricant and occluded air stemming from a misfit between individual core pieces. The method is schematically illustrated in Fig. 19.7.

This method was used to fabricate duplex pressings with a curved interface contour. The dimensional control of the contour was very good. When a square-cornered die was used, the thickness along the width of the fueled section of the core was shown, by metallographic examination, to be controllable to  $\pm 8\%$  at any position and reproducible to  $\pm 5\%$  for the greater area of the pressing. With a die of  $\frac{1}{8}$ -in. radius, this thickness was reproducible to  $\pm 5\%$ . These results were most encouraging when compared with the  $\pm 15\%$  fuel control specified along the width of the rolled plate. Therefore a program was initiated to develop a production process for the HFIR cores using the direct, duplex pressing procedure.

While the ATR cores have simple rectangular cross sections, their fabrication is complicated by the long plate length and the 19 different fuel widths required. To meet the straightness requirements, it has been shown that the thicknesses of

<sup>4</sup>T. D. Watts and A. L. Lotts, *Met. Div. Ann. Progr. Rept.* May 31, 1961, ORNL-3160, pp 165-66.

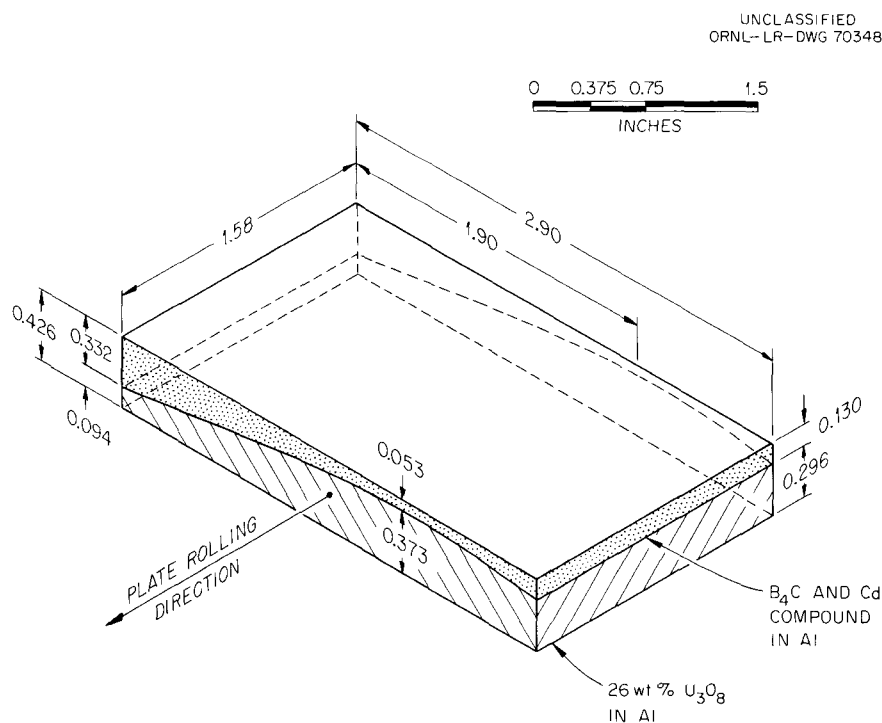


Fig. 19.6. HFIR Inner-Annulus Composite Core Design. As-pressed.

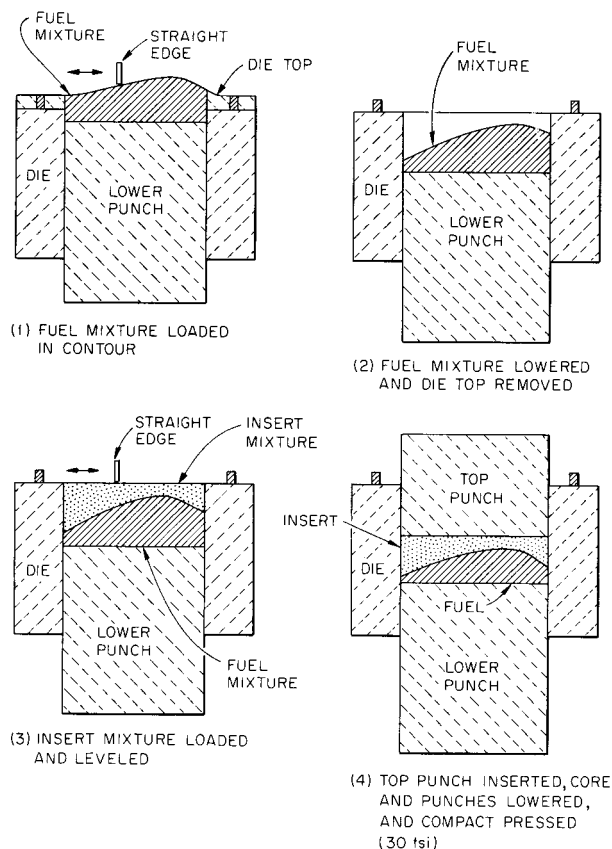
UNCLASSIFIED  
ORNL-LR-DWG 70349

Fig. 19.7. Duplex Pressing of the HFIR Inner Annulus Fuel Core.

the cores have to be controlled to  $\pm 0.0015$  in. This necessitated the use of special powder leveling techniques consisting of hand leveling in two perpendicular directions. The dies and die stand were designed so as to assure their being parallel with the press ram face. With these precautions, the thickness tolerance was met on 95% of the cores produced.

## TRANSURANIUM HFIR TARGET FABRICATION

E. E. Barton      D. M. Hewette II

The conceptual HFIR target design calls for the incorporation of the actinide target elements  $\text{Pu}^{242}$ ,  $\text{Am}^{243}$ , and  $\text{Cm}^{244}$  in the form of an oxide dispersion in aluminum. The proposed fabrication sequence involves the pressing of the actinide oxide-aluminum dispersion in a thin-wall aluminum

tube covered top and bottom with a cap of aluminum powder. Forty of these pellets forming an active length of 20 in. are to be loaded into a finned aluminum tube 35 in. long. Void spaces approximately 6 in. long will be provided at each end of the target rod for collection of fission gases. Reinforcement of these void spaces will be effected by high-strength aluminum alloy tube liners. End caps will be welded on the tube, and the assembled target rod will be hydrostatically pressed to bring the finned tube into intimate contact with the pellets.

Experimental work accomplished during the past year<sup>5</sup> dealt with the establishment of powder blending, pellet pressing techniques, and tube collapsing studies in connection with cladding the target rods. Due to the radiological hazard and limited supply of the actinide materials, stand-in rare-earth oxides were used. Work in progress includes studies of the physical and mechanical properties of the target pellets and a determination of the fission-gas release characteristics of the target pellets.

The stand-in rare-earth oxides, which are supposed to be characteristic of the actinide oxides, have been received in the form of very small particles lying in the micron to submicron range. Blending of these fine oxides with aluminum proved to be very difficult. A satisfactory blending procedure was developed by using aluminum matrix powder of -325 mesh ( $-44 \mu$ ) and a specially designed blending hopper containing small aluminum rods to act as a blending aid. Pellets pressed from powders blended by the above technique resulted in a satisfactory dispersion of the oxide in aluminum, as shown in Fig. 19.8. Mixtures containing 10, 15, 20, and 25 vol % oxide were handled successfully by the above procedures.

The extreme radiological hazards expected with the transuranium elements have forced the development of unusual fabrication procedures. Each dispersion pellet is cold-pressed while being completely enclosed by a pure aluminum cladding. The sides are protected by a thin-walled aluminum cylinder and the top and bottom by aluminum powder. A cross section of the pressed pellet is shown in Fig. 19.9. Final dimensions of the pressed pellet are  $\frac{1}{4}$  in. in diameter by  $\frac{1}{2}$  in. in

<sup>5</sup>Transuranium Quart. Progr. Rept. Feb. 28, 1962, ORNL-3290 (in press).

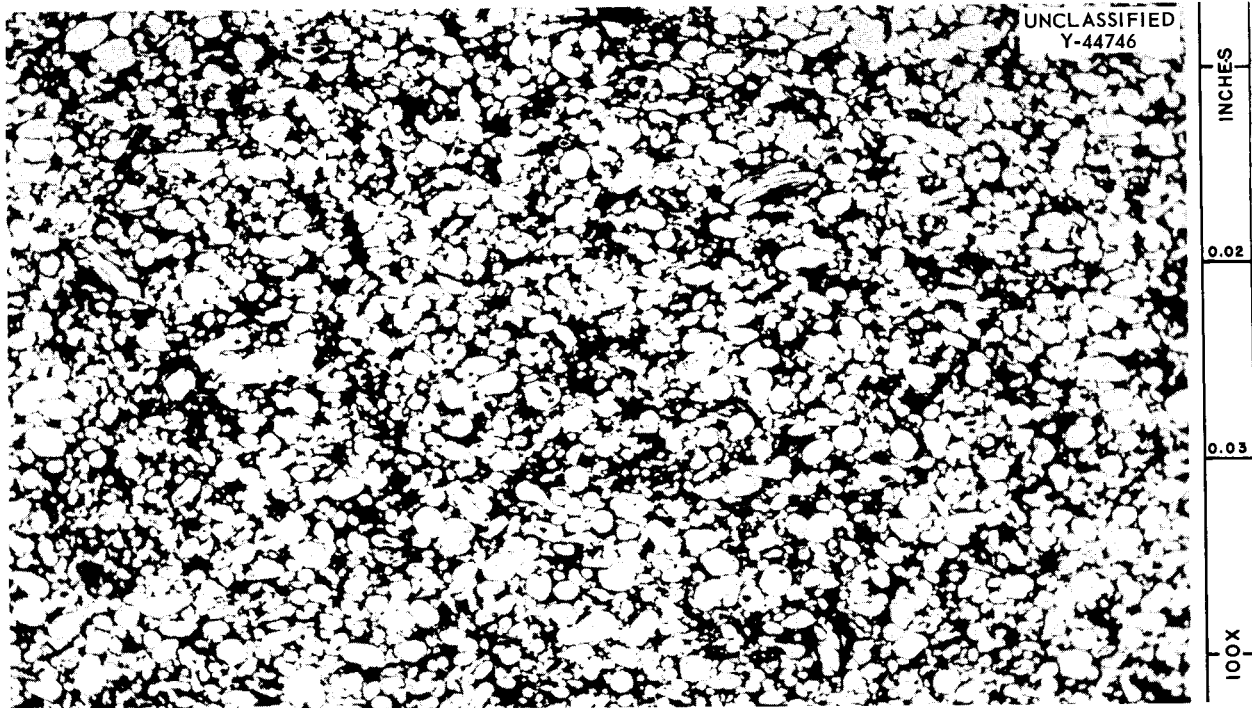


Fig. 19.8. 20 vol % Actinide Oxide-Aluminum Dispersion. Blended in a hopper containing small aluminum rods and pressed at 30 tsi. As-polished.

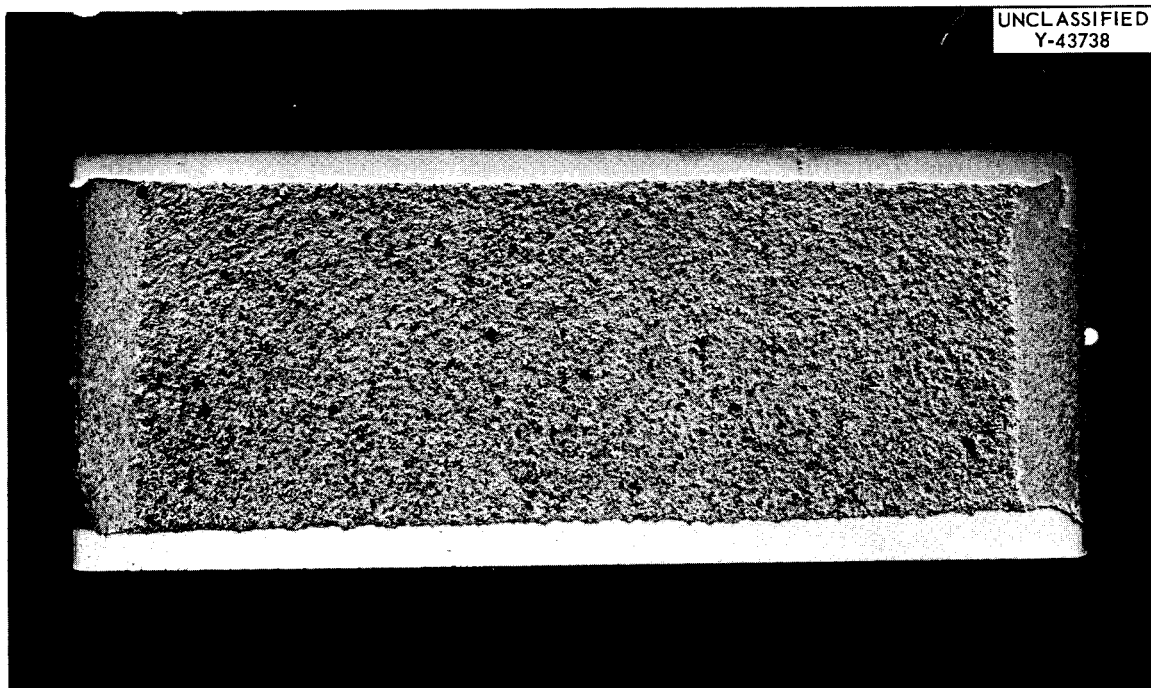


Fig. 19.9. Cross Section of HFIR Target Pellet. As-polished. 9X.

length. As an added precaution in preventing the spread of contamination, drill bushing will be used as the die and will be disposed of after each pressing operation. A wall thickness of 15 mils has been selected for the protective cylinder. Smaller thicknesses were shown to result in excessive folding and buckling during pressing, while thicker tubes consumed too much volume. These procedures, with pressures of 30 tsi and a 2-to-1 compression ratio, yielded pellets with densities of 89 to 91% of theoretical. The powder caps had sufficient density to retain the powders and still permit the escape of the fission gases into the end void volume.

After end caps are welded in place, the aluminum target rod tube will be hydrostatically collapsed around the pellets to improve heat transfer. A collapse experiment was performed with a diametrical clearance of 6 mils between the pellets and the target tube. Pressures on the order of 16,000 psi did not produce intimate contact between the tube and the pellets. Furthermore, the void spaces at the ends of the target rod collapsed in a two-lobe failure at approximately 15,000 psi. Thus, pressures higher than 16,000 psi will be needed to provide intimate mechanical bonding of the tube to the pellets, and a higher strength alloy will be required for the tube liner.

## 20. Remote Fabrication Development

A. L. Lotts

### THORIUM FUEL CYCLE DEVELOPMENT FACILITY

A. R. Irvine<sup>1</sup>      A. L. Lotts

Planning and establishment of criteria for the Thorium Fuel Cycle Development Facility (TFCDF) have continued as a joint program of the Chemical Technology and Metals and Ceramics Divisions. The facility, as proposed, will afford a place where the complete Th-U<sup>233</sup> fuel cycle can be investigated and where the technology now being developed by the ORNL Thorium Utilization Program can be extended and perfected. The detail criteria and basis for the facility are available elsewhere.<sup>2</sup>

At the beginning of the planning, it was recognized that the selection of reference fuel elements would facilitate the establishment of the size of and criteria for the facility. Further, two diverse fuel systems for eventual installation in the facility were considered desirable for assurance of adequate space and design for carrying on a broad range of experimental endeavor. Accordingly, fuel elements with geometries proposed for or being used by various reactors were considered. Fuel elements of the type used for the Consolidated Edison Thorium Reactor (CETR) and the High-Temperature Gas-Cooled Reactor (HTGR) were finally selected as reference for design of the facility. These concepts represent two diverse fuel elements of types anticipated for future reactors utilizing the Th-U<sup>233</sup> fuel cycle. The CETR fuel element is an assembly of stainless

steel tubes containing UO<sub>2</sub>-ThO<sub>2</sub>, and the HTGR fuel element consists of UC<sub>2</sub>-ThC<sub>2</sub>-graphite compacts in a graphite can. In selecting these references, the possibility of working with other materials and geometries was not excluded; the facility will have sufficient flexibility to permit work with other fuel materials such as alloys, dispersion-type fuels, and beryllides.

The processes required for recycling the reference fuel elements were studied from the standpoint of space and services required to accomplish them. It was not intended that these processes represent the exact process steps that might be included, but they did afford a reasonable basis for estimates of the facility parameters. The following conclusions were reached from this analysis.

1. Four large operating cells, as well as supporting cells for equipment storage and decontamination, should be constructed. In the first operating cell, disassembly of fuel elements and reconstitution of fuel would be done; in the second, chemical processing; in the third, fabrication operations involving unclad material having a high potential for contaminating its environment; and in the fourth, final fabrication and inspection operations involving clad fuel having a contamination-free surface.

2. Sufficient shielding should be furnished to provide biological protection from fission-product radiation of sources as large as 35 kg of mixed ThO<sub>2</sub>-UO<sub>2</sub> irradiated to 25,000 Mwd/metric ton and decayed for 90 days.

3. The facility should be capable of handling fuel assemblies up to 12 ft in length provided they can be broken down into or assembled from 6-ft lengths.

<sup>1</sup>Chemical Technology Division.

<sup>2</sup>A. R. Irvine and A. L. Lotts, *Criteria for the Design of the Thorium Fuel Cycle Development Facility*, ORNL-TM-149 (Mar. 2, 1962).

4. Provisions should be made in the facility for future use of an inert-gas blanket in cells which may contain pyrophoric fuels.

5. Suitable provisions should be made for change of process equipment to accommodate new fuels or techniques.

Equipment for accomplishing only the work with oxides will be installed initially in the facility since  $UO_2-ThO_2$  is the only important fuel system in a stage of development to make remote operation of its processing feasible at this time. Although a  $UC_2-ThC_2$ -graphite fuel was selected as the second reference, the processes for fabricating it must be simplified before remote processing can be considered practicable.

The TFCDF is now being conceptionally designed by an architect-engineer firm.

and thorium oxides utilizing sol-gel fuel preparation and vibratory compaction techniques developed under the ORNL Thorium Utilization Program. To implement this program and to provide valuable operating experience with these processes before embarking on the more ambitious program in the proposed TFCDF, a remote fabrication pilot plant is being designed and will be constructed in Cell 4, Building 3019.

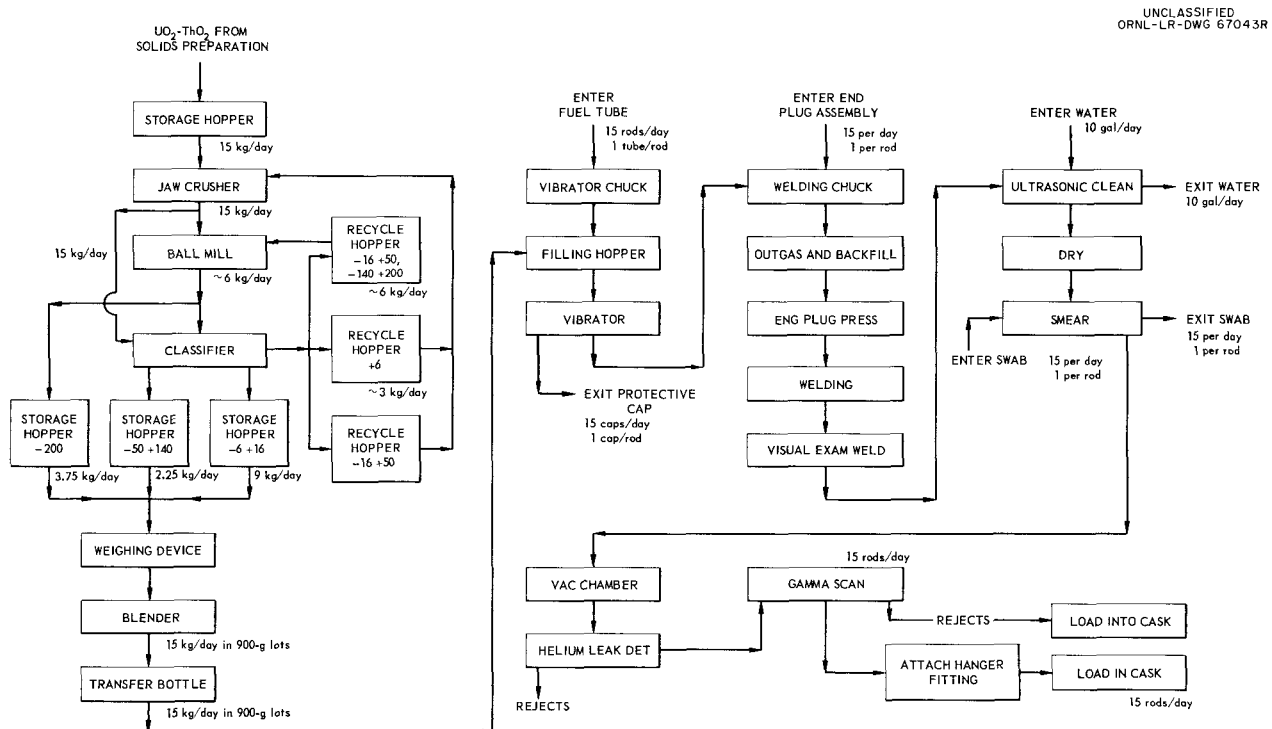
This pilot facility will incorporate all of the equipment for sol-gel preparation of  $Th-U^{233}$  oxide fuel, comminution of the dense fuel chunks to a select blend of three size fractions, fuel rod loading by vibratory compaction, welding of end plugs, and inspection. Because of the radiological hazards of  $U^{233}$  (containing nominally 45 ppm of  $U^{232}$ ) and thorium oxides, these operations will be performed remotely in shielded ( $4\frac{1}{4}$  in. of steel) cubicles hermetically sealed to contain alpha radiation. Tong-like manipulators, mechanical controls, and electrical controls will be used for the remote operations. Cell 4 will be operated by

### Th- $U^{233}$ FUEL ROD FACILITY

J. T. Lamartine<sup>3</sup>

A program is being conducted jointly with the Chemical Technology Division for the development and fabrication of fuel rods containing  $U^{233}$

<sup>3</sup>Now with Metals and Controls, Inc., Attleboro, Mass.



UNCLASSIFIED  
ORNL-LR-DWG 67043R

Fig. 20.1. Th- $U^{233}$  Fuel Rod Facility Process Flow Diagram.

personnel located within the cell and will therefore be used essentially for secondary containment. A process flow diagram for the fuel comminution and fuel rod fabrication and inspection or the metallurgical aspects of the process is presented in Fig. 20.1.

It is planned that, when the facility becomes operational, 100 Zircaloy-2 fuel rods, 0.499-in.-OD  $\times$  0.430-in.-ID  $\times$  45  $\frac{1}{2}$ -in. length and containing Th-3 wt %  $U^{233}$  oxide, will be fabricated for Brookhaven National Laboratory.

Work within the cell on the facility structure is approximately 20% complete. Design of the process equipment is essentially 80% complete, and equipment fabrication and procurement are about 30% complete.

### TRANSURANIUM TARGET FABRICATION EQUIPMENT

M. K. Preston<sup>4</sup>

The design and development of equipment for the fabrication and inspection of the target elements to be used in the production of gram quantities of the transuranic isotopes were initiated. These target elements will be irradiated in the flux trap of the High-Flux Isotope Reactor (HFIR), thereby producing the transuranic elements americium, curium, berkelium, and californium. Periodically, the elements will be removed from the reactor and processed in the Chemical Technology Division portion of the Transuranium Processing Plant (TRU) to remove the desired isotopes. In other portions of TRU the remaining isotopes will be reconstituted as an oxide and fabricated by the Metals and Ceramics Division into new target elements. The design of the HFIR target element has not been firmly determined, but it will most probably consist of a  $\frac{3}{8}$ -in.-OD finned tube with a  $\frac{5}{8}$ -in.-hexagonal can welded to the fins as a spacer. Each target will be approximately 35 in. long, with  $\frac{1}{4}$ -in.-diam  $\times$   $\frac{1}{2}$ -in.-long pellets contained in the 20-in. active length of the target. The pellets will consist of an actinide oxide and aluminum powder mixture pressed to a density approximately 89% of theoretical. During pressing, each pellet will be completely encapsulated in an aluminum can. The remainder of the 35-in. tube will be end caps and void space.

The following is a resumé of the status of the design and development of the target fabrication and inspection equipment for the TRU, these phases of this joint effort being the responsibility of the Metals and Ceramics Division. More detailed information is available in a TRU report.<sup>5</sup>

The fabrication and inspection of HFIR target elements will employ a combination of powder-metallurgical, welding, chemical, and inspection techniques. The operations have been assigned to the three available cubicles (or cells) according to the degree of contamination expected. To minimize recontamination of the target elements, auxiliary enclosures for some items of equipment will be provided within the cubicles. The criteria established for the equipment and fabrication of the transuranium target elements are that equipment should be simple, reliable, small, and capable of producing elements to the specified tolerances with a minimum of maintenance to the equipment. In addition, the equipment must be resistant to damage by radiation, be designed to minimize the spread of contamination, and have components that are easily repaired or replaced.

In accordance with the above criteria, all equipment will be designed to operate semiautomatically, requiring only minimum recourse to the manipulators. To minimize the spread of contamination, special transfer arms and similar devices will be used to effect transfer of components between steps in the process. The manipulators will be used for maintenance, for transfer of components or equipment to and from the intercell conveyor, and for effecting simple and infrequent motions on process equipment. Sensitive parts of the equipment will be of such size that they can be transported by the intercell conveyor for discharge and replacement, and all equipment will be dismountable with an impact wrench and of such size that it can be removed from the cubicle through the 36  $\times$  18-in. equipment transfer hatch located in the cell roof. To assure that the criteria are met, all equipment will be installed, operated, and maintained in cell mock-ups which have been designed and fabricated and are now being installed.

Plan views of the equipment being developed for the cubicles are shown in Figs. 20.2, 20.3, and 20.4 for TRU cubicles Nos. 3, 2, and 1, respectively. The equipment concepts are approximately 40% complete, and detail designs have

<sup>4</sup>On loan from Engineering and Mechanical Division.

<sup>5</sup>*Transuranium Quart. Progr. Rept. Feb. 28, 1962, ORNL-3290 (in press).*

been completed for approximately 12% of the equipment. The completion of conceptual design of equipment by cubicles is as follows: cubicle No. 3, 55%; cubicle No. 2, 45%; and cubicle No. 1,

20%. Detail design of equipment by cubicles is 10% complete for cubicle No. 3 and 25% for cubicle No. 2. Procurement and fabrication of equipment have just commenced.

UNCLASSIFIED  
ORNL-LR-DWG 70350

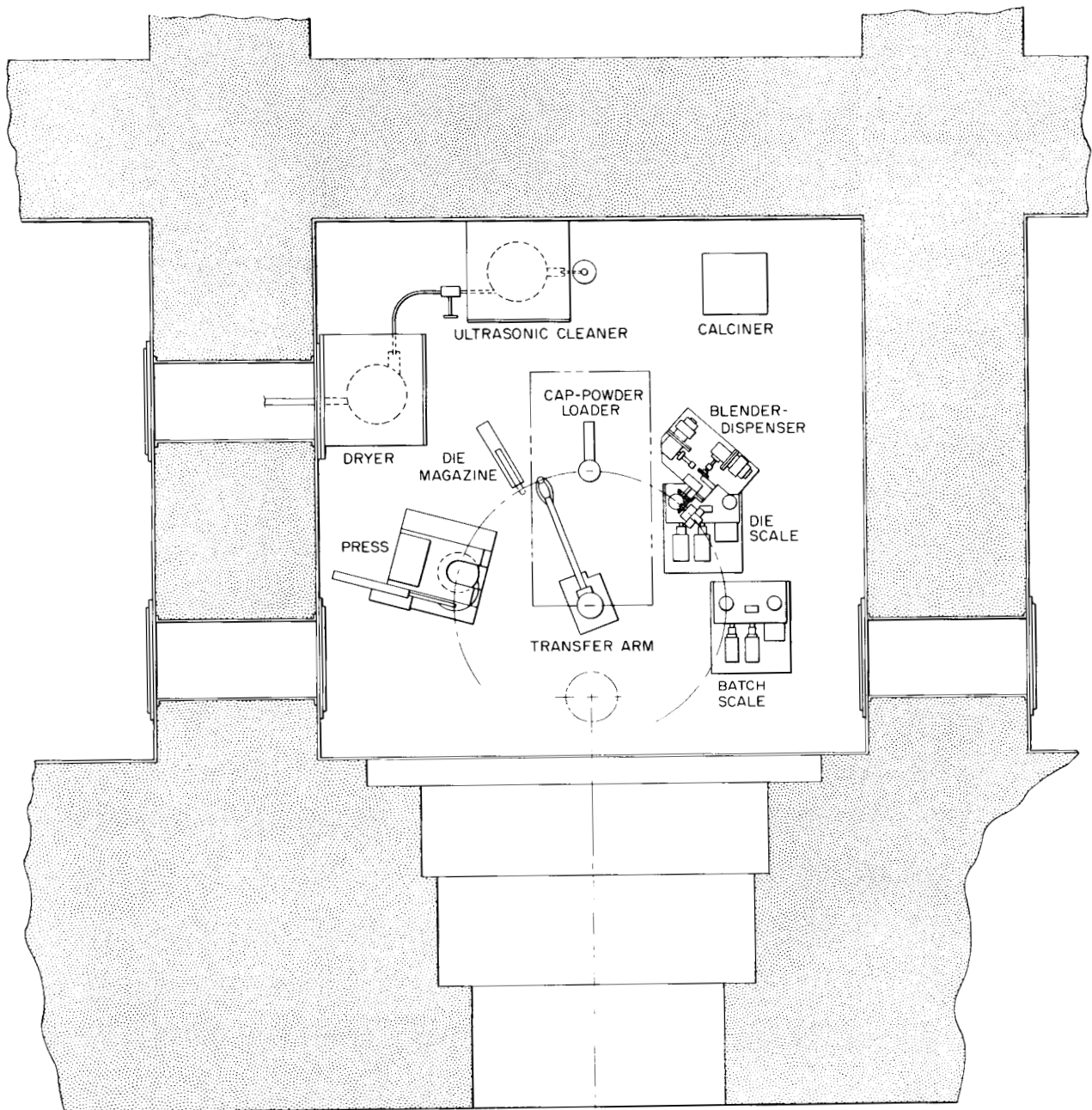


Fig. 20.2. Plan View of Equipment, Cubicle No. 3, TRU Processing Plant.

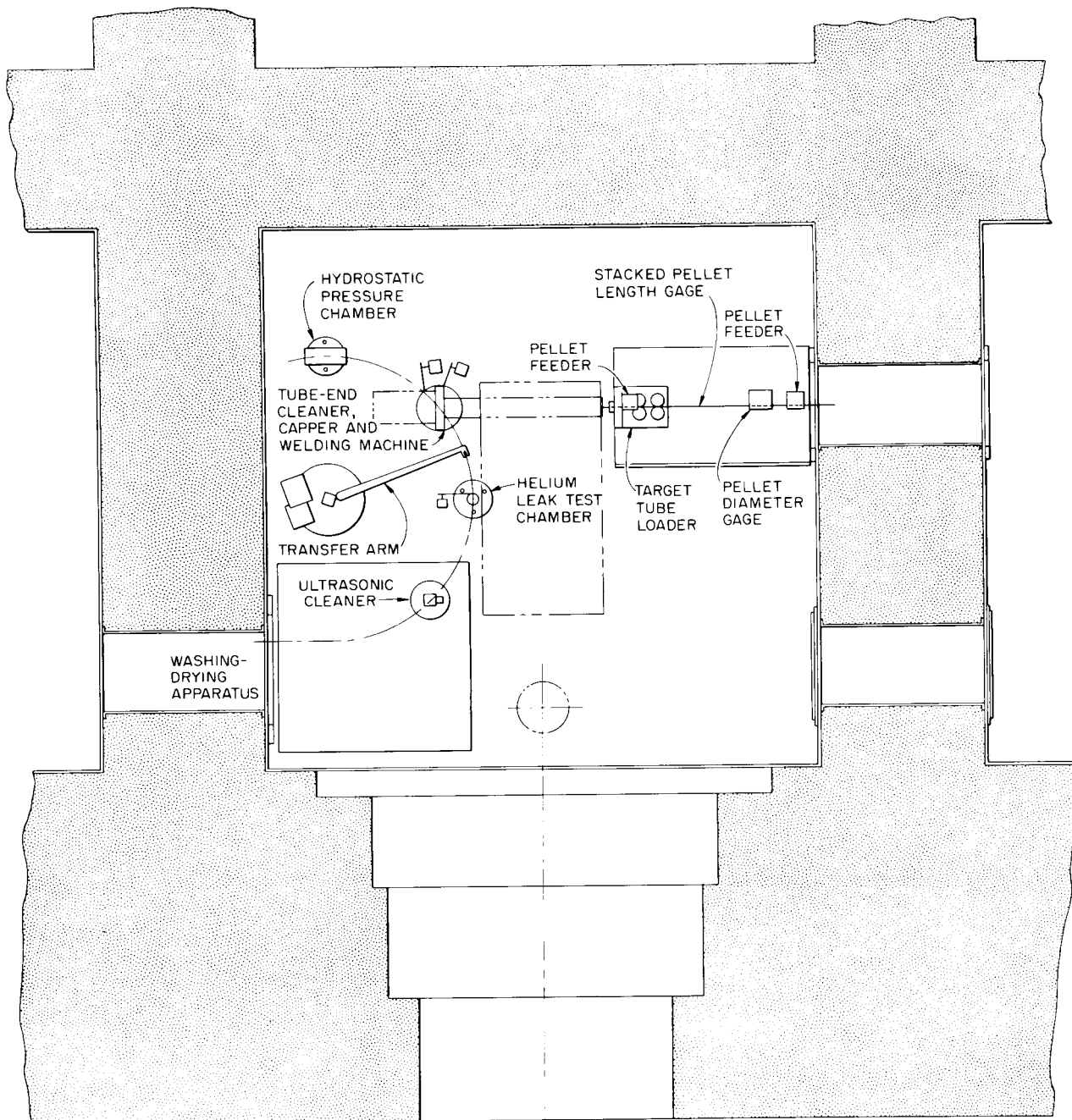


Fig. 20.3. Plan View of Equipment, Cubicle No. 2, TRU Processing Plant.

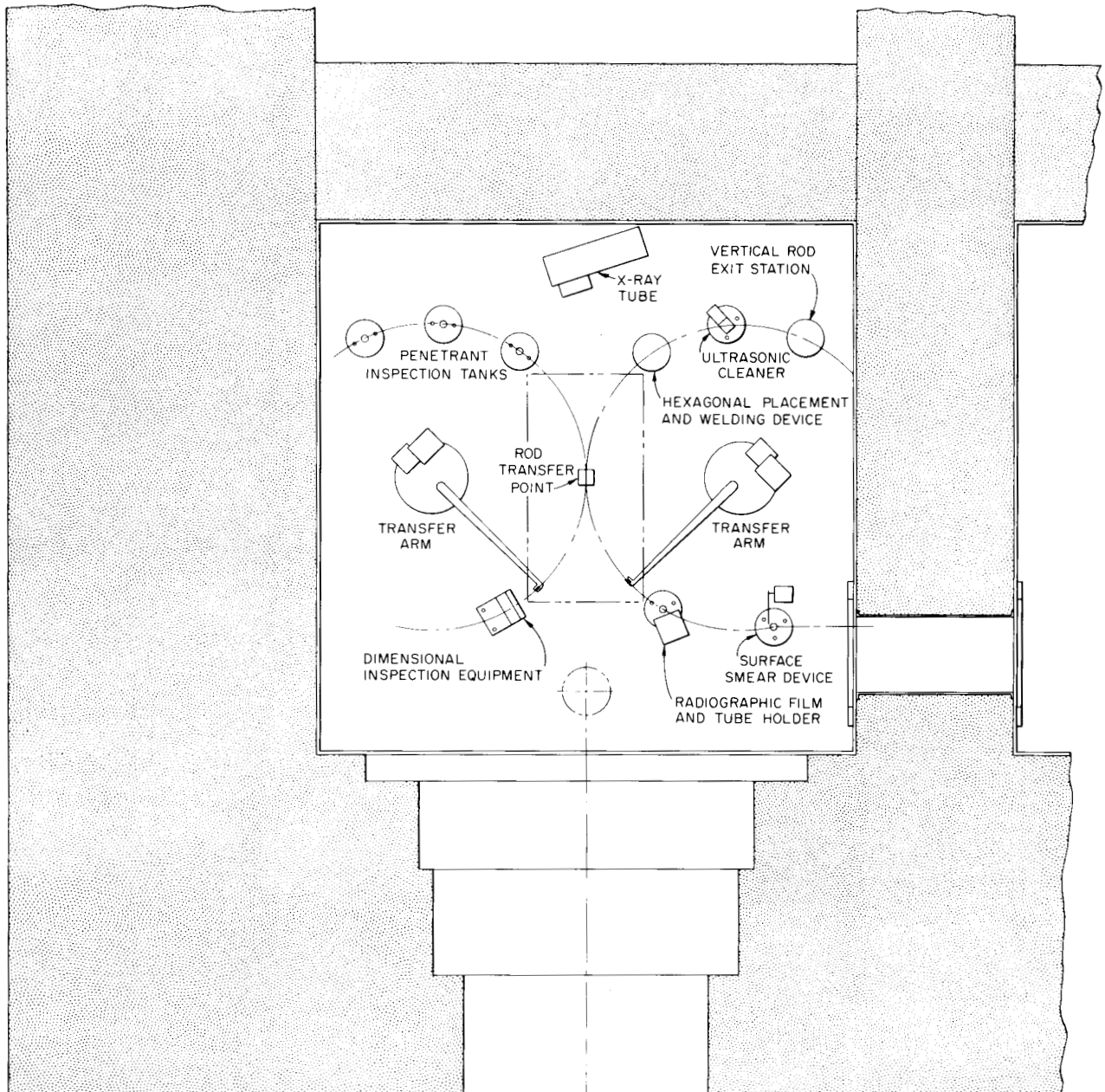


Fig. 20.4. Plan View of Equipment, Cubicle No. 1, TRU Processing Plant.

## PLUTONIUM TARGET FABRICATION EQUIPMENT

A. L. Lotts

Plans were made for installing equipment for the fabrication and inspection of target elements containing  $\text{Pu}^{242}$  and having the same design as that for the target that will contain actinide elements. The  $\text{Pu}^{242}$ -bearing target elements will constitute the first loadings for the flux trap of the HFIR. The principal problem posed by  $\text{Pu}^{242}$

is that it is a strong alpha-radiation emitter and therefore operations involving uncontained  $\text{Pu}^{242}$  must be done in glove boxes.

The flowsheet for the process and the description and location of equipment were established and have been reported elsewhere.<sup>5</sup> Generally, the steps to be employed follow those that are anticipated for the fabrication of target elements in the TRU. Procurement of commercially available equipment and design of special equipment were initiated during the latter part of this reporting period.

## 21. Welding and Brazing

G. M. Slaughter

### COMPONENT FABRICATION DEVELOPMENT

#### Aluminum Alloy Fuel Element Development

J. W. Tackett

The welding development studies over the past year for the High-Flux Isotope Reactor (HFIR) program consisted primarily in improving procedures for fabricating prototype fuel elements. One improvement over the procedure used in fabricating the HFIR critical assembly<sup>1</sup> resulted from making the outer welds circumferentially around the annulus instead of longitudinally along it, which significantly reduced the amount of weld shrinkage. This modified technique can be automated.

The improved welding procedure was utilized to successfully fabricate the outer-annulus flow test assembly described in "Aluminum-Base Fuel Element Fabrication," Chap. 18, this report. One-inch-wide rectangular grooves were machined on the outside-diameter surface of the unit, aluminum bands were installed into the grooves, and the bands were manually tungsten-arc welded to the exposed fuel plate lips. In preparation for welding,  $\frac{3}{16}$ -in.-wide Teflon strips were installed in the channel spacings adjacent to the outer cylindrical surface to provide dimensional control. Figure 21.1a is a photograph of the bands that were circumferentially welded around the element exterior.

During welding, the outside diameter of the unit shrank approximately 100 mils, which caused a slight rotation of the outer surface and a marked reduction (3–5 mils) in the channel spacing measurements obtained adjacent to the outer edge.

The need for additional dimensional control became apparent. Based on the behavior of earlier prototype assemblies, use of additional Teflon in the channels might reduce the diametral shrinkage by a factor of 4 and maintain the channel spacing reduction near the outer edge to within 2 mils. This improved procedure is being used in the fabrication of the prototype element containing cored fuel plates (see Chap. 18, this report).

An improved procedure was developed for attaching the last five fuel plates to the grooved, inner tubular side plates of both the inner and outer annulus. Welding supplemented the peening process utilized to install the first 364 plates in the outer annulus and the first 166 plates in the inner annulus. This plug-welding procedure was successfully demonstrated with both the manual and automatic welding processes and involves the use of short welding grooves machined in the inner side plate at 1-in. intervals. In preparation for welding, additional Teflon spacer strips were preplaced in the channels bordered by these last five plates. Figure 21.1b shows the plug welds on the interior of the outer annulus. Mechanical property tests on mockup specimens demonstrated that these welds possessed strengths ranging from 100 to 175 lb each.

Preliminary experiments indicated the feasibility of an automatic consumable-electrode welding process. Work performed on numerous small mockup samples indicated that good dimensional control can be obtained and that extremely consistent welds can be produced. Suitable welding and positioning equipment is being acquired for future prototype element development.

An alternate fuel element fabrication procedure in which the individual fuel plates are installed between two concentric, grooved tubular side plates and then attached to the grooved side plates

<sup>1</sup>J. W. Tackett, *Met. Div. Ann. Progr. Rept. May 31, 1961*, ORNL-3160, pp 173–74.

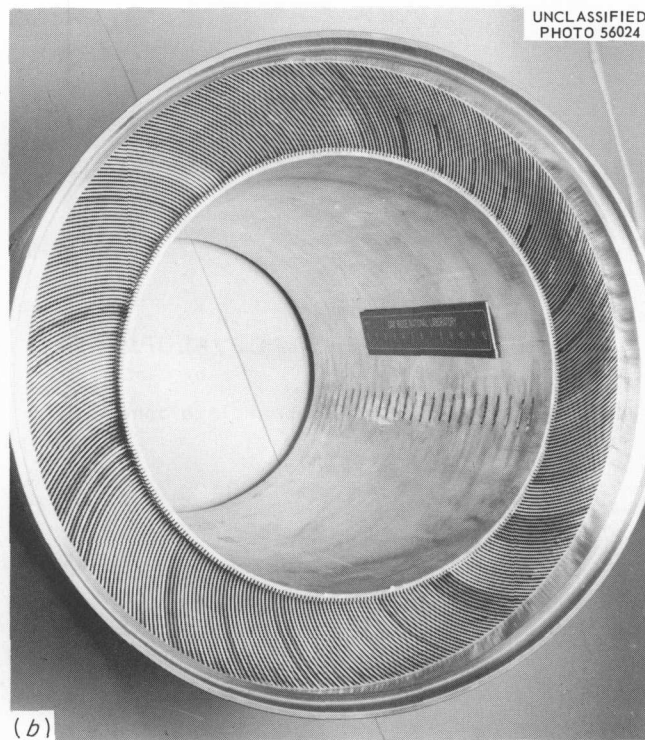


Fig. 21.1. HFIR Flow Test Assembly Showing (a) Circumferential Welded Bands on Element Exterior and (b) Plug Welds on Element Interior.

by circumferential welds is being investigated. Thus far it has been used with some success on both "flat" prototype assemblies and on the inner tubular side of a full-size outer-annulus demonstration assembly containing dummy fuel plates. In each case, the length of the side plate was reduced approximately 0.010 to 0.015 in. during each weld, and a slight upset ridge appeared on the underside of the plate below the weld. However, with the use of proper welding sequence, the overall length of the fuel plate will probably not change appreciably nor will noticeable rippling occur in the individual fuel plates as a result of longitudinal shrinkage in the side plates. The fabrication procedure will be investigated further.

#### Fabrication of Stainless Steel Flat-Plate Fuel Elements

R. G. Donnelly

At the request of the Atomic Power Development Associates (APDA), Detroit, Michigan, this division was given the responsibility for developing fabrication procedures for the Enrico Fermi Reactor core B fuel element. Suitable procedures for assembling the individual fuel plates into a rigid bundle are being determined in the Welding and Brazing laboratory.

A detailed assembly procedure was developed for ensuring the complete and successful brazing

of all 89 individual components in one operation. The low-cross-section Ni-Cr-Si brazing alloy (known as Coast Metals No. 60) was found to provide the best combination of sodium-corrosion resistance and elevated-temperature strength. Brazing is carried out at 2150°F for 1½ hr with carefully scheduled heating, presoaking, and cooling cycles to ensure close dimensional control over the element and adequate flow of alloy throughout the unit.

Several modifications in fixture design have been necessary to meet all the required tolerances and to accommodate the changing demands of the APDA designs. For example, several modifications were required to permit the spacers and plates to be located with reference to the fuel center line instead of to the fuel bundle edge.

The ability to successfully fabricate elements to the required plate-to-plate and stackup height tolerances has been demonstrated, as has the ability to machine the brazed bundle to very stringent dimensional requirements. A photograph showing the machining of a completely brazed assembly is presented in Fig. 21.2. Difficulties are still being encountered in meeting the 0.002-in. tolerance on the spacer-to-spacer width dimension, but are expected to be resolved by the end of the year.

The feasibility of utilizing fuel plates with integral machined spacers is being studied. If suitable rolling and machining procedures can be developed, this concept should eliminate the problems of inexact spacer location and variations in spacer thickness.

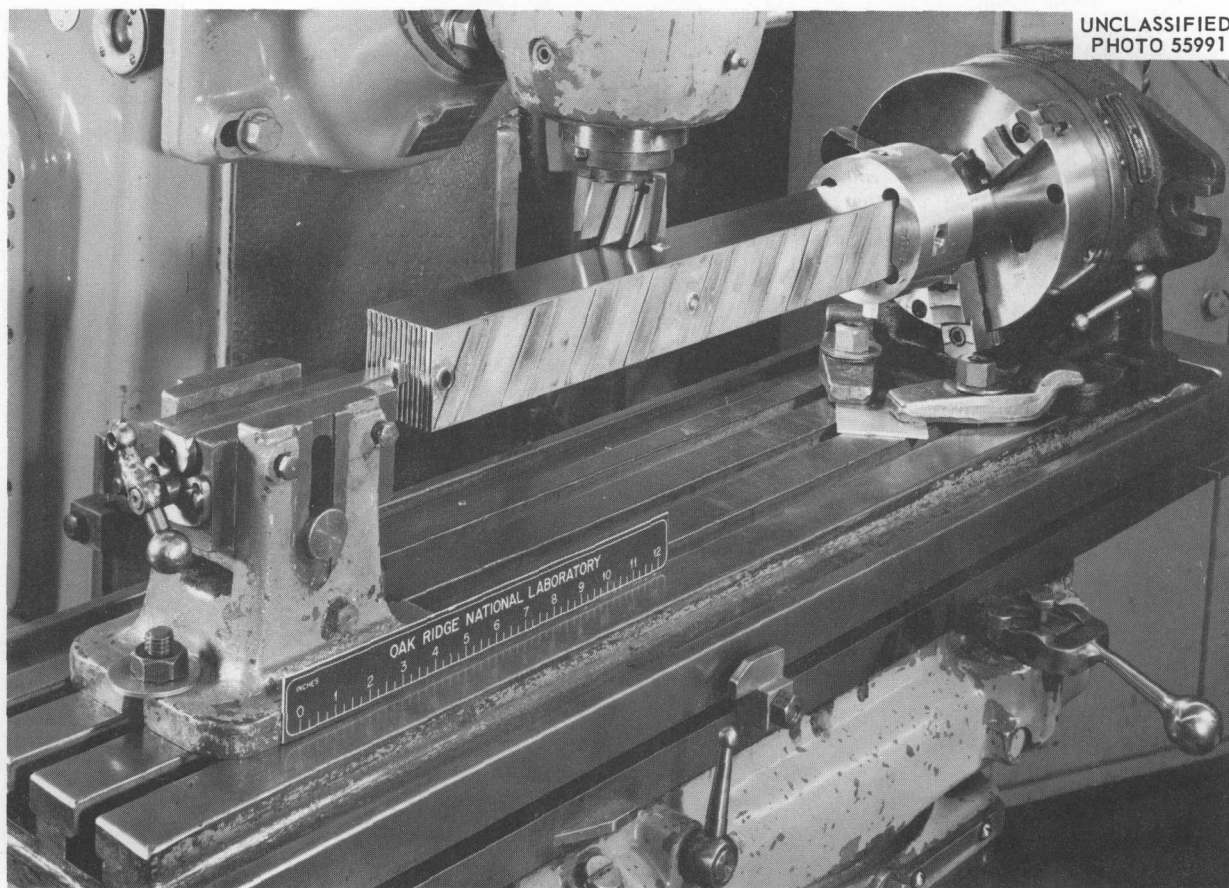


Fig. 21.2. Machining of Enrico Fermi Fuel Element After Brazing.

### Loop Fabrication

E. A. Franco-Ferreira

In order to provide more information on two-phase heat transfer in liquid metals, an experiment was designed by the Heat Transfer and Physical Properties Section of the Reactor Division for determining boiling and condensing coefficients at temperatures up to 1700–1800°F. The Welding and Brazing Group undertook the responsibility for fabricating the 4-ft-long boiler for this loop, which was complicated by the unique geometry of the assembly and the exceptionally high-quality brazes required. This work required an extensive developmental program.

Figure 21.3, a photograph of the boiler during assembly, shows the maze of thermocouples penetrating the copper disks. A slurry of Nicrobraz 50 (Ni-Cr-P) was placed in machined grooves in the copper disks, and all mating surfaces of stainless steel and copper were preplated with a deposit of electroless Ni-P alloy. Vacuum brazing was used since it provided the most reliable means for adequately purging the long and relatively inaccessible capillaries.

Nondestructive inspection of the completed assembly revealed the high degree of success of the operation. In the very critical stainless steel tube to copper-disk joint, bonding of 99% or better was

observed. A complete description of the work has been reported.<sup>2</sup>

### Pressure Vessel Penetrations

G. M. Slaughter      T. R. Housley<sup>3</sup>

Satisfactory methods were developed<sup>4</sup> for penetrating the stainless steel burst-slug-detection tubes and stainless steel-clad thermocouples through the carbon steel pressure shell of the Experimental Gas-Cooled Reactor (EGCR). The burst-slug-detection system permits a channel containing a defective fuel element to be positively identified, while the thermocouples will be used to measure temperatures from numerous points within the reactor. Both types of penetrations require the welding of relatively thin walled components to thicker members under conditions of very limited accessibility, as can be seen in Fig. 21.4.

<sup>2</sup>E. A. Franco-Ferreira, *Fabrication of Boiler Section for Boiling-Liquid-Metal Loop*, ORNL TM-40 (Oct. 16, 1961).

<sup>3</sup>Engineering and Mechanical Division.

<sup>4</sup>G. M. Slaughter and T. R. Housley, *Fabrication and Inspection Procedures for Experimental Gas-Cooled Reactor Burst-Slug-Detection Tube and Thermocouple Penetrations*, ORNL CF-61-8-29 (Aug. 14, 1961).

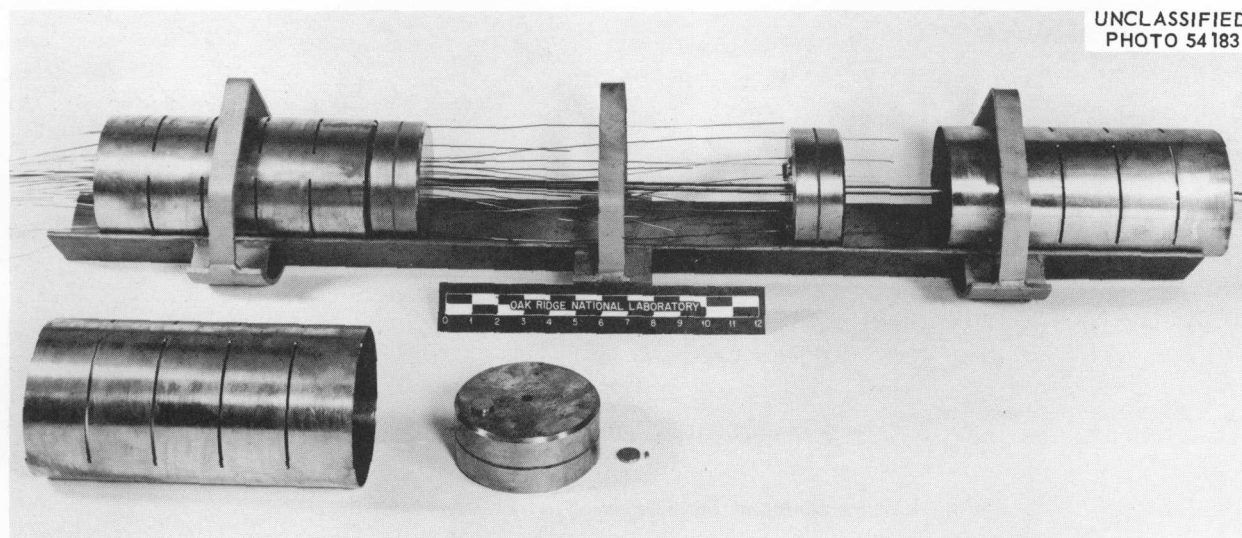


Fig. 21.3. Boiler During Assembly.

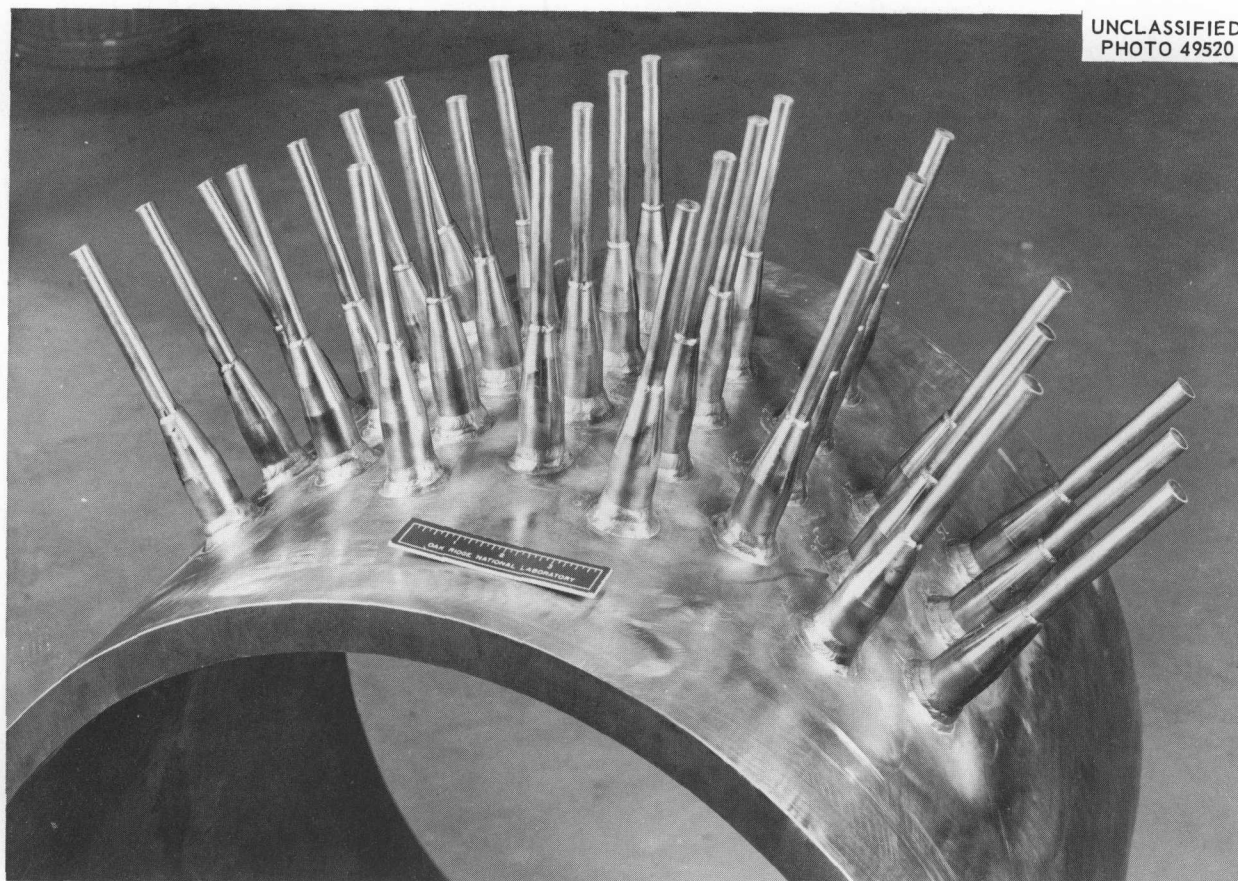


Fig. 21.4. Quadrant of Mockup of EGCR Burst-Slug-Detection Nozzle Assembly.

Suitable joint designs were determined and adequate fabrication and inspection procedures established in the construction of prototype assemblies. Conventional welding and brazing equipment and joining procedures were used throughout. Although accessibility in this application is definitely limited, it appears that welds and brazes of high quality can be made if carefully trained operators are utilized.

#### Instrumented Fuel Capsule Fabrication

E. A. Franco-Ferreira

The effort to improve the methods of attaching thermocouples for measuring temperatures in gas-cooled reactor irradiation test capsules continues.<sup>5,6</sup> This work is also directly applicable to the fabrication of instrumented fuel assemblies for the EGCR.

Typical of the complex capsules required are those for irradiation in GCR-ORR loop No. 1. A sketch of such an instrumented capsule is presented in Fig. 21.5. The cladding thermocouples have insulated junctions and are of 0.060-in.-OD stainless steel-sheathed Chromel-Alumel. The portions of the thermocouples that are inside the capsules are swaged to 0.040-in. OD in order to minimize the size of the slots which must be cut into the  $UO_2$  pellets to accommodate them. The entire length of the thermocouple must be brazed to the tube inner wall with a permissible straightness deviation of only  $3^\circ$ . Copper is used as the brazing material and is preplaced on the thermocouple by electroplating to a thickness of 0.001 in. Brazing is carried out in a hydrogen atmosphere, with an

<sup>5</sup>E. A. Franco-Ferreira, *GCR Quart. Progr. Rept. Sept. 30, 1961*, ORNL-3210, pp 55-58.

<sup>6</sup>E. A. Franco-Ferreira, *GCR Quart. Progr. Rept. Dec. 31, 1961*, ORNL-3254, pp 154-57.

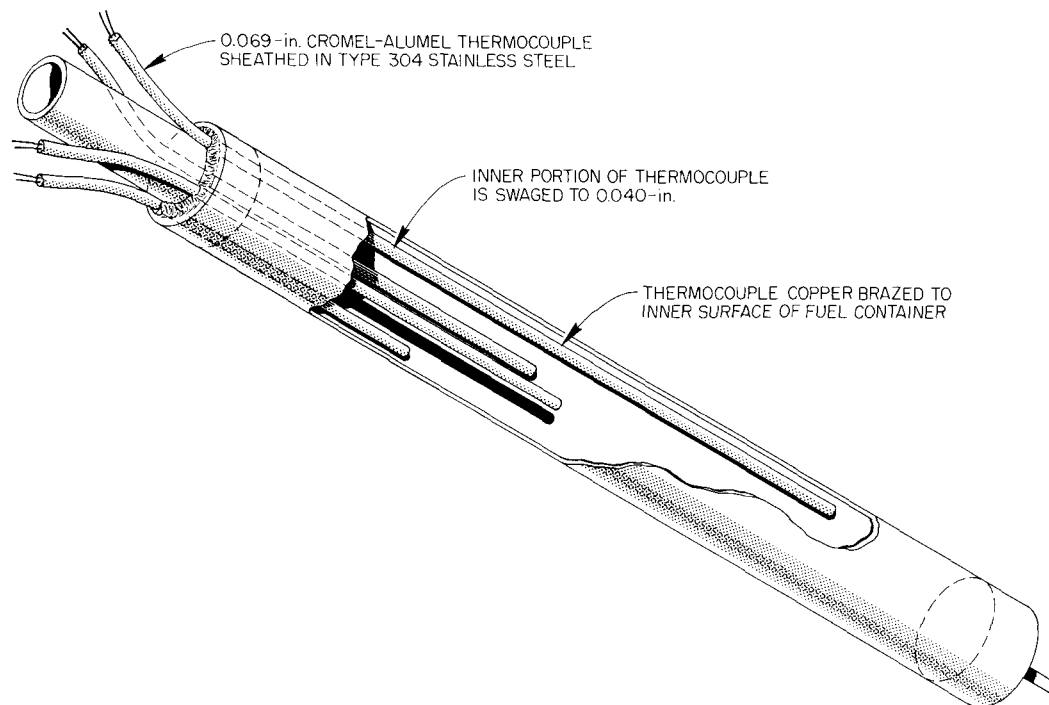


Fig. 21.5. Instrumented Capsule for Irradiation in GCR-ORR Loop No. 1.

Inconel-X jig used to align the thermocouples and hold them in place.

Several of these capsules have been successfully operated in in-pile irradiation experiments, as have a variety of others containing such other miscellaneous instrumentation as pressure transducers.

### Solidified Metal Seal Development

R. G. Donnelly

Preliminary studies on the use of solidified metal seals for elevated-temperature, leaktight, quick-disconnect joints for molten-salt service were reported in the last annual report.<sup>7</sup> These studies were completed, and the feasibility was demonstrated by the successful operation of a small mockup unit.<sup>8</sup>

<sup>7</sup>R. G. Donnelly, *Met. Div. Ann. Progr. Rept. May 31, 1961*, ORNL-3160, pp 175-76.

<sup>8</sup>R. G. Donnelly, *The Development of a Sump-Type Solidified-Metal Seal*, ORNL TM-179 (Mar. 15, 1962).

### Remote Brazing

R. G. Donnelly

The Molten-Salt Reactor Experiment (MSRE) was designed to permit the remote maintenance of all major components such as the heat exchangers and pumps because of radioactive fission products and induced activity. Remote brazing appears to be a very promising means for rejoining some of the necessary pipe connections, and a study is under way, in cooperation with the Reactor Division Remote Maintenance Group, to develop a reliable joint for such applications.<sup>9,10</sup>

The design of such a joint is influenced by both brazing and remote-maintenance requirements. Maintenance procedures are simplified by use of relatively loose fits and a minimum of remote machining, but optimum brazing procedures require relatively tight fits and very clean surfaces. A very

<sup>9</sup>MSRP *Semiann. Progr. Rept. Aug. 31, 1961*, ORNL-3215, pp 109-12.

<sup>10</sup>MSRP *Semiann. Progr. Rept. Feb. 28, 1962*, ORNL-3282 (in press).

promising joint design was developed which provides for the preplacement of brazing alloy on the mating surfaces of the joint and a radial clearance of 0.0025 to 0.0035 in. This clearance is considered optimum in terms of ease of fit-up and reliable brazing alloy flowability.

Several joints of this type were brazed in the laboratory to determine the quality of joint. Ultrasonic inspection of the joints revealed that they undoubtedly were adequate for molten-salt systems. However, the incorporation of a slight taper in the joint appears to be even more advantageous since it makes remote assembly somewhat easier and eliminates nearly all nonbonded areas.

## MATERIALS-JOINING DEVELOPMENT

### Niobium

C. W. Fox

Niobium and its alloys are of continuing interest for a variety of high-temperature reactor applications, and suitable brazing alloys and procedures are being developed. Last year, several corrosion-resistant refractory-metal brazing alloys containing titanium and zirconium were developed which readily flowed on niobium.<sup>11</sup> These alloys melt in the range 1000 to 1300°C and produce very sound braze joints with no evidence of cracking. Mechanical property tests at room and elevated temperatures were done on joints brazed with these alloys and several appeared to be especially attractive. Shear strength determinations were made on Miller-Peaslee type of brazed specimen; some typical room-temperature values are listed in Table 21.1. Table 21.2 illustrates the excellent performance of some of them at 1300°F. It is apparent that such alloys as the 75 Zr-19 Nb-6 Be (wt %) and the 46 Ti-46 Zr-4 V-4 Be compositions exhibit excellent strengths. In addition, aging at 1500°F prior to testing does not appear to impair the room-temperature properties of joints brazed with several of the alloys. The resistance of brazed joints to cracking as a result of thermal cycling also appears to be very good.

<sup>11</sup>C. W. Fox and R. G. Gilliland, *Progress Report on Brazing of Columbium*, ORNL CF-61-7-24 (July 5, 1961).

Table 21.1. Results of Room-Temperature Shear Tests on Brazed Niobium Joints in the Aged and As-Brazed Conditions

Strength of solid niobium specimens: 38,000 psi

Alloy (wt %)	Room-Temperature Shear Strength <sup>a</sup> (psi)	
	As-Brazed	Aged for 100 hr at 1500°F
48 Ti-48 Zr-4 Be	33,300 (6)	24,500 (3)
46 Ti-46 Zr-4 V-4 Be	27,800 (6)	32,500 (4)
75 Zr-19 Nb-6 Be	24,000 (6)	24,800 (4)
67 Zr-29 V-4 Fe	20,200 (5)	14,600 (3)

<sup>a</sup>Number of specimens averaged is given in parentheses.

Table 21.2. Results of Elevated-Temperature Shear Tests on Brazed Niobium Joints in the As-Brazed Condition

Strength of solid niobium specimens: 17,300 psia<sup>a</sup>

Alloy (wt %)	Shear Strength <sup>b</sup> (psi) at 1300°F
75 Zr-19 Nb-6 Be	19,000 (4)
63 Ti-27 Fe-10 Mo	16,500 (4)
48 Ti-48 Zr-4 Be	13,600 (4)
45 Ti-40 Zr-15 Fe	16,000 (4)

<sup>a</sup>This value cannot be considered as the true shear strength since severe bending of the specimen occurred during testing; however, it can be used as a guide in determining joint efficiency.

<sup>b</sup>Number of specimens averaged given in parentheses.

### Beryllium

R. G. Gilliland

Suitable procedures for welding beryllium are being developed to effectively utilize its unique properties for the cladding of advanced fuel elements. The brittle behavior of beryllium welds, together with the frequent occurrence of gross porosity and cracking, has severely limited its applicability up to the present time. Modifications in procedure have been successfully developed previously for producing sound end-closure welds

in tubes made by different vendors by various fabrication processes.<sup>12</sup>

Room- and elevated-temperature shear strengths of tungsten-arc end-closure welds in tubes were determined<sup>13</sup> by placing edge-welded samples in a fixture and pushing the end cap out of the fixed tube. The welds in tubes manufactured by eight different fabrication processes all exhibited similar strengths, even though, as indicated by radiography, the joints in extruded tubing were known to contain some porosity. The room-temperature shear strengths were in the range of 21,000 to 26,000 psi, while the 600°C shear strengths were in the range of 10,000 to 13,000 psi. The only published shear-strength data for pure beryllium list a room-temperature strength of 32,000 psi for type QMV hot-pressed powder.

Efforts to develop high-temperature alloys for brazing beryllium for elevated-temperature service<sup>13</sup> are continuing, but they have been hampered by the generally poor wettability of this material

<sup>12</sup>R. G. Gilliland, *Met. Div. Ann. Progr. Rept. May 31, 1961*, ORNL-3160, p 168.

<sup>13</sup>GCR *Quart. Progr. Rept. Mar. 31, 1962*, ORNL-3302 (in press).

and the rapid formation of brittle intermetallics along the base metal-braze metal interface.

## Ceramics

C. W. Fox

In view of their high strength at very high temperatures and their good corrosion and oxidation resistance, ceramics are exceptionally attractive for advanced high-temperature applications. Their good insulating properties also make them invaluable for components of a variety of experimental apparatus. Since ceramic materials are inherently difficult to join and since suitable methods are not available to attach them to themselves and to other materials for high-integrity, leaktight, high-temperature service, a program is under way to develop techniques for brazing them.

Several experimental brazing alloy compositions have been formulated which readily flow on the oxide ceramics. Typical of the high-quality joints obtained is that shown in Fig. 21.6, a photomicrograph of a Zircaloy-2 to aluminum oxide joint. The brazing alloy composition was 48 Ti-48 Zr-4 Be (wt %). A demonstration mockup assembly of an

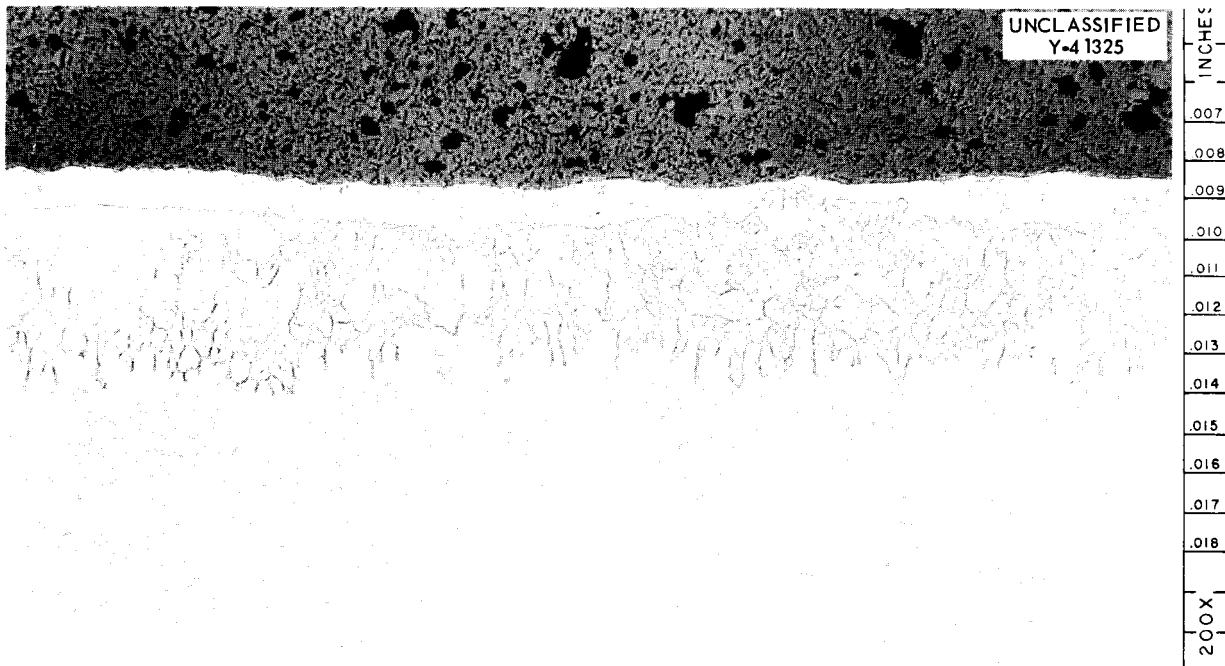


Fig. 21.6. Zircaloy-2 to Aluminum Oxide Joint Brazed with 48 Ti-48 Zr-4 Be (wt %) Alloy. As-Polished.

aluminum oxide compartmented fuel element was fabricated and is shown in Fig. 21.7. Brazing was accomplished at approximately 1950°C in a vacuum muffle furnace, with the time at temperature being approximately 10 min.

In view of the very promising results accomplished to date on this program, the scope will be extended next year to cover the brazing of beryllium oxide and uranium oxide.

### INOR-8

R. G. Gilliland

The Ni-Mo-Cr alloy INOR-8 to be used as the structural material for the Molten Salt Reactor possesses generally good weldability, but some weld-cracking difficulties were encountered on initial welder qualification tests in the shops that will fabricate the actual reactor components. The initial welds were definitely unsatisfactory, as determined by bend tests. ORNL assistance was

provided to the shops to eliminate the trouble, which appeared to be associated with overheating of the metal during welding. A modification of the joint design and strict adherence to the welding procedure provided an apparent solution to the problem.<sup>14</sup> Welds are being produced which exhibit no cracking in bend tests, and several welders have been qualified for component construction.

### Welding of Ferritic Steels to Stainless Steels

G. M. Slaughter

T. R. Housley<sup>15</sup>

Studies were completed to determine the best methods for joining ferritic steels to austenitic stainless steels for such critical applications as the primary coolant piping for the EGCR, and a

<sup>14</sup>MSRP Semiann. Progr. Rept. Feb. 28, 1962, ORNL-3282 (in press).

<sup>15</sup>Engineering and Mechanical Division.

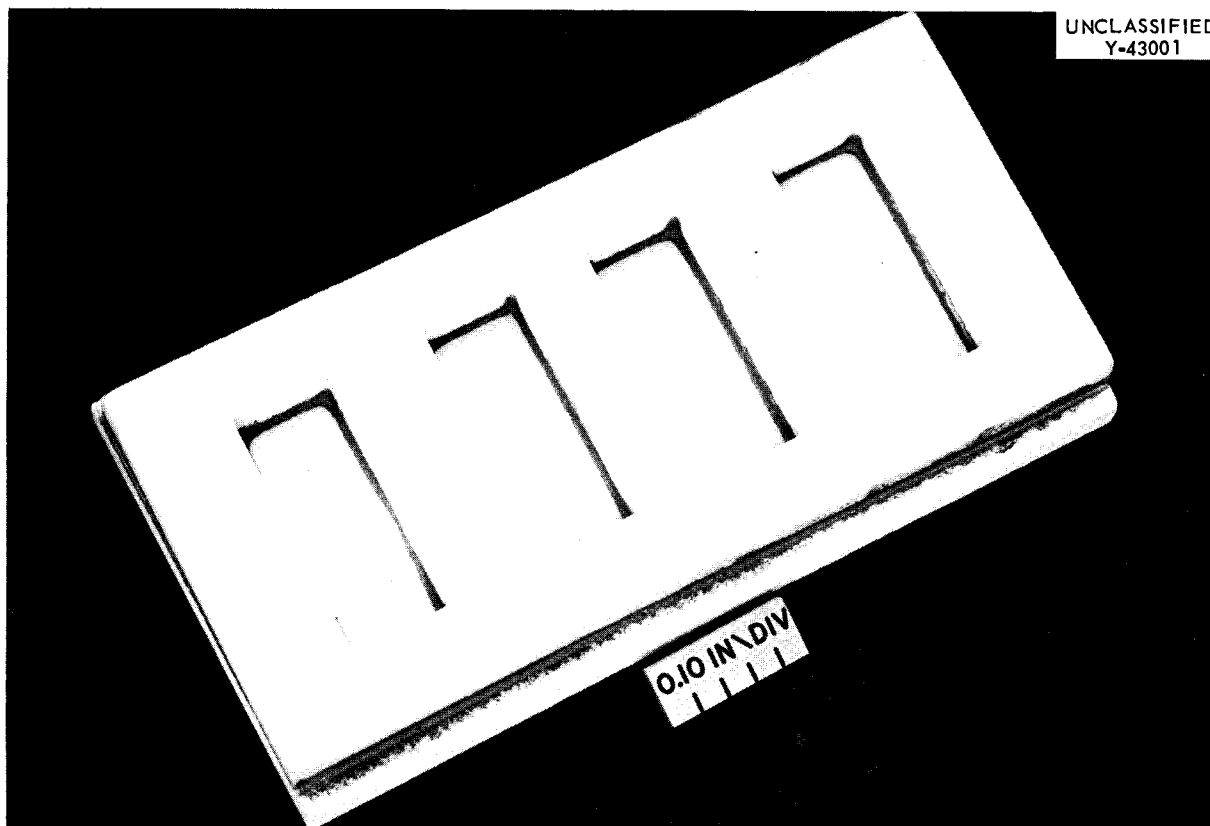


Fig. 21.7. Demonstration Aluminum Oxide, Compartmented Fuel Element, Mockup Assembly.

final report was published.<sup>16</sup> A new nickel-base alloy welding electrode, given the developmental designation BP-85 and now known as Inconel-182, was selected as the most promising weld metal for the application. Welding procedures were developed for joining ASTM A-212, grade B, carbon-silicon steel to type 304 stainless steel and ASTM A-387, grades C and D, low-alloy steels to type 304 stainless steel. The overall deposition characteristics of the electrode were excellent, and the mechanical properties of welds were very good. Thermal-cycling test specimens containing welds

made with Inconel-182 electrode have not revealed any evidence of cracking, in contrast to the specimens containing welds made with the more conventional stainless steel electrodes.

### Graphite

R. G. Donnelly

The development of alloys for brazing graphite and the techniques for successfully fabricating high-integrity graphite-to-graphite and graphite-to-metal joints are described in a final report.<sup>17</sup>

---

<sup>16</sup>G. M. Slaughter and T. R. Housley, *The Welding of Ferritic Steels to Austenitic Stainless Steels*, ORNL TM-98 (Jan. 4, 1962).

---

<sup>17</sup>R. G. Donnelly and G. M. Slaughter, *Welding J.* 41(5), 46-69 (1962).

## 22. Postirradiation Examination

A. R. Olsen

The activities of the Postirradiation Examination (PIE) Group were concerned with service work in support of irradiation test programs for various reactor projects and with the design, construction, and testing of equipment and development of techniques for use in the existing and future hot-cell facilities.

Construction of the new PIE laboratory (previously referred to as the High Radiation Level Examination Laboratory<sup>1-3</sup>) is approximately 90% complete. It now appears certain that the basic facility will be completed late in 1962 and should be in operation early in 1963. Concurrently with the final construction phases, some of the remote experimental equipment will be installed to permit the examination of radioactive experiments early in 1963. A detailed hazard analysis of the new facility now being made will cover operational procedures and effects of possible fire and criticality accidents. J. P. Nichols of the Chemical Technology Division is assisting in this analysis.

The hot-cell facilities in Building 4501 were used continuously during the past year to provide an ever-increasing variety of experimental data. The service requests handled ranged in scope from simple remote transfers to examination of complete in-pile experimental loops. The majority of the work performed by the PIE group is reported directly by project personnel; hence, only a brief account of project support work is presented below.

<sup>1</sup>A. R. Olsen and R. E. McDonald, *Met. Div. Ann. Progr. Rept. July 1, 1960*, ORNL-2988, pp 436-37.

<sup>2</sup>*Technical Function and Operation of the High Radiation Level Examination Laboratory, Bldg. 3525, ORNL CF-61-1-75 (Jan. 31, 1961)*.

<sup>3</sup>A. R. Olsen, "A New Postirradiation Examination Laboratory at the Oak Ridge National Laboratory," p 3 in *Proceedings of the Ninth Conference on Hot Laboratories and Equipment*, American Nuclear Society, Chicago, Ill., 1961.

### REACTOR PROJECT SUPPORT ACTIVITIES

R. E. McDonald

J. R. Parrott

Hot-cell service work was performed in support of the aqueous thermal breeder under study in the Thorium Utilization Program, the Homogeneous Reactor Experiment-2, the Experimental Gas-Cooled Reactor, and the Molten-Salt Reactor Experiment.

#### Thorium Utilization Program

The examination of the first in-pile slurry loop containing thoria in D<sub>2</sub>O was completed during this period. Preliminary examinations were reported last year,<sup>4</sup> including the method of preassembly scanning with a collimated multi-channel gamma-ray spectrometer. The accumulation of slurry in the pressurizer and pump volute areas, indicated by the spectrometer, was confirmed in the dismantling process. After the loop was examined, it was concluded<sup>5</sup> that, under the condition of this experiment, no deleterious effect of radiation on the corrosion of Zircaloy-2 and titanium alloys occurs. However, the 13 mpy maximum corrosion rate for the stainless steel specimens was higher than the rate incurred under similar but unirradiated conditions. All specimens from this loop were remotely replicated by the cellulose-acetate technique for comparison with the preirradiation replicas.<sup>6</sup>

<sup>4</sup>R. E. McDonald, *Met. Div. Ann. Progr. Rept. May 31, 1961*, ORNL-3160, p 149.

<sup>5</sup>E. L. Compere *et al.*, and H. C. Savage *et al.*, *Reactor Chem. Div. Ann. Progr. Rept. Jan. 31, 1962*, ORNL-3262, pp 114-22.

<sup>6</sup>A. R. Olsen and R. E. McDonald, *Met. Div. Ann. Progr. Rept. July 1, 1960*, ORNL-2988, pp 439-42.

During operation of the second in-pile loop, samples of slurry were periodically collected in small stainless steel bombs. These units are dismantled after they have been drained so that all solids that may have settled in the sampler can be recovered for material-balance purpose. A powered pipe cutter<sup>7</sup> and a collet-like fixture with internal gripping teeth have been successfully employed to open conically ended samplers without contamination or loss of the contents.

### Hot-Cell Examination of In-Pile Slurry Autoclaves

A variety of in-pile autoclaves containing various thoria-urania slurries, powders, and pellets were opened, dismantled, and examined.<sup>8-10</sup> The replication techniques developed by the group were extended to obtain total-surface positive replicas of 1/4-in.-diam irradiated pellets (described in "Development of Postirradiation Examination Technique," this chapter) and for obtaining localized-area cellulose-acetate replicas remotely. These replicas were of sufficient quality to permit electron-microscope examination by the palladium-shadowed carbon replica technique. These replicas and similar ones made on an as-fired pellet and an autoclaved-control pellet were examined and photographed at 8000X. Figure 22.1 shows the detail obtained by this replication technique.

### Homogeneous Reactor Experiment

With the cessation of operation of the HRE-2, a number of specimens and corrosion samples from the core and various circulating-line positions have been removed. The results of the examinations will be reported by the experimental groups. In addition to the more normal examination techniques, the replication processes were used to

<sup>7</sup>Technical Function and Operation of the High Radiation Level Examination Laboratory, Bldg. 3525, ORNL CF-61-1-75, p 44 (Jan. 31, 1961).

<sup>8</sup>E. L. Compere et al., and H. C. Savage et al., *Reactor Chem. Div. Ann. Progr. Rept. Jan. 31, 1962*, ORNL-3262, pp 126-30.

<sup>9</sup>J. P. McBride et al., *HRP Progr. Rept. Dec. 1, 1960 to May 31, 1961*, ORNL-3167, pp 73-78.

<sup>10</sup>J. P. McBride, *Radiation Stability of Aqueous Thoria and Thoria-Urania Slurries*, ORNL-3274 (May 18, 1962).

make detailed examinations easier. The core patch and bolt recovered from the reactor core, prior to the final reactor operation cycle, were replicated by the two-step process to provide total-surface positive epoxy replicas before they were sectioned for metallographic examination. Figure 22.2 is a photograph of two of the replicas showing both the core and blanket sides of the patch. This technique is being adapted to the replication of some 58 sections of the actual reactor core wall<sup>11</sup> to permit a full-scale reconstruction and evaluation.

### Experimental Gas-Cooled Reactor

J. R. Parrott      R. E. McDonald

In support of the Experimental Gas-Cooled Reactor Program, a number of irradiated UO<sub>2</sub> powders were prepared for fission-gas release experiments, and five complete beryllium experiments were examined.<sup>12-17</sup> The tube-burst specimens were often scaled and rough and had failed by cracking at relatively high temperatures and pressures in the reactor. It was often impossible to optically locate the cracks even at 30X. The need to locate these failure areas precisely so that the specimens could be properly sectioned for metallographic examination was satisfied by the unusual method of brushing the specimen surfaces with a small stainless steel "toothbrush" and then pressurizing with gas while the specimens were submerged under water. The escaping gas

<sup>11</sup>P. P. Holz, *Description of Manipulator System, Helicarc Underwater Cutting Torch and Procedure for Cutting HRE-2 Core*, ORNL TM-175 (in press).

<sup>12</sup>J. R. Weir, "Effect of High-Temperature Reactor Irradiation on Some Physical and Mechanical Properties of Beryllium," paper presented at the Institute of Metals Conference on the Metallurgy of Beryllium held at the Royal Commonwealth Society, London, October 16-18, 1961; proceedings to be published by the Institute of Metals, London.

<sup>13</sup>J. R. Weir and W. W. Davis, *GCR Quart. Progr. Rept. Mar. 31, 1961*, ORNL-3102, p 203.

<sup>14</sup>J. R. Weir and W. W. Davis, *GCR Quart. Progr. Rept. June 30, 1961*, ORNL-3166, p 164.

<sup>15</sup>J. R. Weir, *GCR Quart. Progr. Rept. Sept. 30, 1961*, ORNL-3210, p 189-92.

<sup>16</sup>J. R. Weir and J. W. Woods, *GCR Quart. Progr. Rept. Dec. 31, 1961*, ORNL-3254, p 225.

<sup>17</sup>*GCR Quart. Progr. Rept. Mar. 31, 1962*, ORNL-3302 (in press).



Fig. 22.1. Surface of Irradiated ThO<sub>2</sub> Pellet Taken at 8000X and Reduced 16%. This electron micrograph was made from a cellulose-acetate replica obtained by remote handling means.

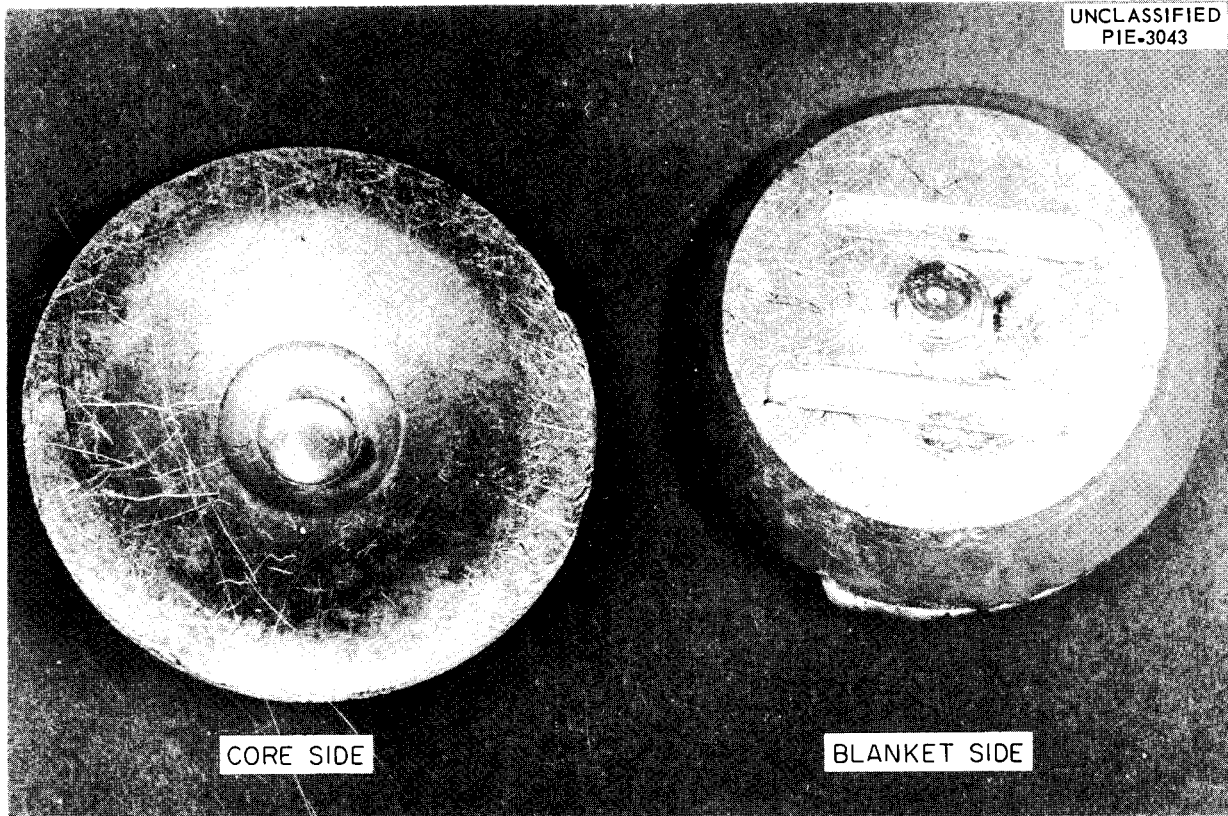


Fig. 22.2. Positive Replicas of HRE-2 Upper Core Patch.

located the leaks, and the area was marked while still under the water. Subsequently, the tube was placed on a small Bodine motor-driven roll positioner under the remote stereomicroscope and the failure region was photographed. Figure 22.3 is a typical photograph of one of the medium-sized cracks located by this technique.

Another unusual method employed in this work involved the use of a modified micrometer to make a series of diameter measurements along the tube after irradiation to determine deformation. The simple motor-driven micrometer used to make these measurements quickly and accurately is shown in Fig. 22.4. A Speedi-Mike micrometer ratchet was attached to a small reversible electric motor, with a piece of surgical rubber tubing used as a collapsible drive-transmission system. This provided quick, reproducible measurements with an accuracy of 0.001 in.

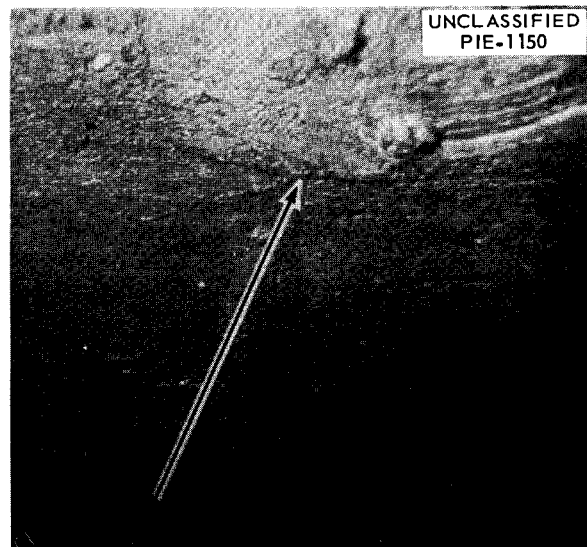


Fig. 22.3. Section of a Beryllium Tube-Burst Specimen Showing Failure Crack. 10X.

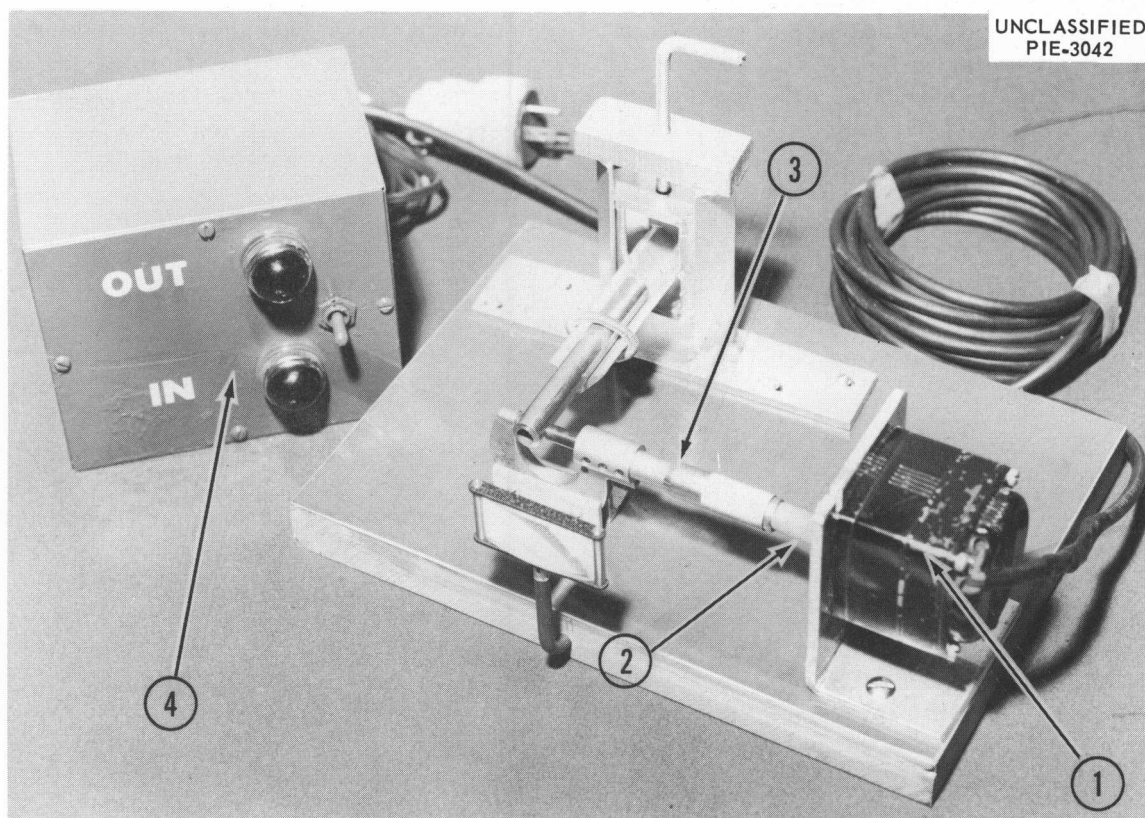


Fig. 22.4. Remotely Operated Micrometer for 0- to 1-in. Measurements. (1) Reversible motor, (2) surgical rubber tubing drive, (3) digital reading micrometer, and (4) control box.

#### Molten-Salt Reactor Experiment

R. E. McDonald      J. R. Parrott

After the bulk of the examinations had been completed in the hot-cell facilities at Battelle Memorial Institute,<sup>18</sup> samples of the salt and all of the corrosion coupons were sent to this group for additional examination. Replicas were made for the examination of the solidified salt surfaces.<sup>19</sup> Additional equipment requirements are being established to permit the complete examination, including the extraction of the fission gas from the next group of capsules in this experimental program.

<sup>18</sup>MSR Program, *Semiann. Progr. Rept.* Feb. 28, 1962, ORNL-3282 (in press).

<sup>19</sup>S. S. Kirslis *et al.*, *Reactor Chem. Div. Ann. Progr. Rept.* Jan. 31, 1962, ORNL-3262, pp 20-26.

#### DEVELOPMENT OF POSTIRRADIATION EXAMINATION TECHNIQUES

R. E. McDonald      A. C. Winther<sup>20</sup>

##### Remote Replication

The remote replication techniques developed by the PIE group are finding a number of applications.<sup>21-23</sup> During the past year the cellulose-

<sup>20</sup>On loan from AEK, Research Establishment, Risø, Denmark.

<sup>21</sup>E. L. Long, Jr., *GCR Quart. Progr. Rept.* Sept. 30, 1961, ORNL-3210, pp 147-52.

<sup>22</sup>A. R. Olsen and R. E. McDonald, *Met. Div. Ann. Progr. Rept.* May 31, 1961, ORNL-3160, pp 150-52.

<sup>23</sup>R. E. McDonald, B. W. McCollum, and G. A. Moore, "Replication of Surface for Hot-Cell Application," p 166 in *Proceedings of the Ninth Conference on Hot Laboratories and Equipment*, American Nuclear Society, Chicago, Ill., 1961.

acetate technique was used to provide replicas of sufficient quality for electron-microscope examinations of irradiated thoria-pellet surfaces and metallographically prepared zirconium microstructures. The total-body replication technique, using room-temperature vulcanizing (RTV) rubber, was extended by backcasting with epoxy resins into the rubber mold replicas. This two-step process provides an epoxy duplicate of the original surface with sufficient detail for optical examination at up to 1000X. The epoxy replicas are decontaminated ultrasonically and then aluminized.

The total-body technique was also used to make positive replications of irradiated P-82 thoria pellets. The pellets were placed in a small dish and covered with liquid rubber. After the rubber vulcanized, a small incision was made at each pellet and the mold flexed to pop out the pellets. The resulting cavities were filled with an epoxy resin from an eyedropper. The pellet replicas were ultrasonically decontaminated, and then aluminized. The surfaces were viewed and photographed at 100 and 200X and then compared with an unirradiated control pellet. This comparison provided the first clue of possible surface changes due to irradiation. This indication prompted an electron-microscope investigation of the surfaces of thoria pellets.

As a result of the demonstrated utility of the RTV rubber technique in examinations of surfaces, a study of the feasibility of replicating large surface areas was begun. A  $3 \times 6$  in. section of a cast aluminum ingot was replicated and viewed at 1000X, the body of a  $3 \times 6 \times \frac{3}{8}$  in. piece of copper was replicated to reproduce five of the six surfaces in a single cast (the sixth surface was the casting riser), and a  $2\frac{1}{2} \times 8 \times \frac{3}{8}$  in. mockup piece of the HRE-2 core vessel was replicated. These results proved, beyond a doubt, that the surfaces could be reproduced in detail. Approximately 50 pieces cut from the HRE-2 core vessel are scheduled for replication. The aim is to reconstruct the vessel from these replicas and then to study the surfaces for defects and the effects of corrosion and erosion on both the core and blanket side. It appears as if the depths of pits, wall-thickness measurements, and other dimensional details can be accurately determined from replicas, if the shrinkage and/or expansion of the RTV and epoxy castings can be better controlled. Some experimental replicas had a dimensional accuracy within 2%. However, this

accuracy seems to be affected by the proportions of diluents, resin-to-catalyst ratios, and the surface area to volume relationships for a particular replica. Preliminary scouting experiments to determine the optimum conditions for some of these variables have been initiated.

### Ultrasonic Cleaning

Four  $\frac{1}{2}$ -gal tanks and 80-w generators, operating at approximately 90,000 cycles, were obtained for both in- and out-of-cell studies in the decontamination of plastic and epoxy replicas. The objects to be cleaned are placed in a glass or stainless steel beaker containing a nonsudsing detergent, a glass-cleaning compound, or one of the various acid solutions. The container is then placed in the tank, which has been half filled with water, and ultrasonically agitated for 2 to 5 min. After each cycle, the object is rinsed in water and the cleaning solution renewed. Many short cycles are better than one long one.

### DEVELOPMENT OF REMOTE EQUIPMENT<sup>24,25</sup>

R. E. McDonald      J. R. Parrott  
J. E. VanCleve

### Positioning Tank for Ultrasonic Testing

J. R. Parrott      R. W. McClung<sup>26</sup>

The remote scanning tank for the ultrasonic inspection of high-level irradiated components in the HRLEL was tested in the Building 4501 mockup.<sup>27,28</sup> Operating techniques and procedures, along with maintenance procedures, were developed and issued in the form of a preliminary operating manual. Minor modifications of the unit to ease maintenance and increase the accuracy and dependability are being made.

<sup>24</sup>J. R. Parrott and J. E. VanCleve, *Met. Div. Ann. Progr. Rept. May 31, 1961*, ORNL-3160, pp 152-57.

<sup>25</sup>*Technical Function and Operation of the High Radiation Level Examination Laboratory, Bldg. 3525*, ORNL CF-61-1-75 (Jan. 31, 1961).

<sup>26</sup>Nondestructive Testing Group.

<sup>27</sup>C. S. Lisser *et al.*, *Instrumentation and Controls Div. Ann. Progr. Rept. July 1, 1961*, ORNL-3191, pp 46-50.

<sup>28</sup>R. W. McClung and K. V. Cook, *Met. Div. Ann. Progr. Rept. May 31, 1961*, ORNL-3160, p 157.

### **Metallography Mounting Equipment**

J. E. VanCleve                      R. E. McDonald

The mounting press with its attendant control panel has been completely fabricated and has been tested in the mockup cell. The operating manual for this unit is 80% complete. It now appears that with simple inexpensive RTV rubber molds accurate epoxy mounts may be made without the heat and pressure associated with the standard mounting techniques. This technique would eliminate the need for a relatively complex machine requiring remote maintenance, making it particularly attractive for hot-cell applications. The technological and economic factors involved are being studied.

### **Kentron Microhardness Tester, Cutoff Saw, and Metallographic Polishing Equipment**

J. E. VanCleve

The Kentron microhardness tester was completely reassembled and then reinstalled in a wooden mockup, including the sample transfer system. The control panel and electrical hookup were completed and most of the testing was finished. The operating manual is 40% complete, but the maintenance section is being delayed pending final installation so that physical surroundings and their effects can be incorporated.

Fabrication of the metallographic cutoff saw was completed, and the unit is undergoing extensive testing in the mockup. All parts are working well and no further modifications are under consideration. A manual covering the operation of the unit is being prepared.

A small commercial surface grinder is being investigated to serve as an inexpensive means of providing the rough grinding required in the metallographic process. Very preliminary results are encouraging. Materials easily ground and polished by conventional methods are also relatively easily handled by the surface grinder and electrolytic polisher without finish grinding. The decision as to whether this unit or another unit is used in the in-cell process for rough grinding will affect the type of polishing cloths and abrasives used for finish polishing. A Disa-Pol electrolytic polisher and etcher unit was set up in the cold

laboratory to evaluate the surfaces produced with the surface grinder and to develop operational procedures. The grinding, polishing, and etching of more difficult materials, such as aluminum and ceramics, will require additional development before reliable procedures are established.

### **Stereomicroscopes and Stages**

J. E. VanCleve                      R. E. McDonald  
J. R. Parrott

All three stereomicroscopes operated well during acceptance tests and produced high-quality 35-mm stereoscopic slides. One unit installed in the mockup is being used with the stage in the development of compatible lighting fixtures to provide the high-intensity controlled light necessary for high-quality color photography. The electrical hookup of the stereomicroscope stage to its control panel was finished and the unit installed in the mockup. Several slight modifications were made on the unit as the result of mockup testing.

### **Master-Slave Manipulators**

J. E. VanCleve

The preproduction prototype model A manipulators and seal tubes in the mockup were exchanged for the production models. Several acceptable arm assemblies were received from the manufacturer, but the plastic boots for the slave arms have not been received for testing as yet. Testing of the manipulators will be continued automatically as other equipment is being tested in the mockup.

### **In-Cell Canner**

R. E. McDonald                      J. R. Parrott

Waste cans (14 in. diam  $\times$  40 in. length) and storage cans (6 in. diam  $\times$  40 in. length) will be sealed and cleaned prior to their removal from the cells in the new facility to prevent the external spread of contamination.

The means considered for remotely sealing the cans included commercial canners, induction brazing, and rolling. Commercial canners of the required size are large, complicated, hard to

remotely maintain, and expensive. Induction brazing was proved to be feasible but is undesirable because of the expensive equipment and the possibility of gas and air in the cans blowing out the braze joint and causing leaks. The method of shape-rolling the edge of the cans to provide a pressure weld has proved effective in the manufacture of fuel rods and for closures on experimental in-pile capsules. Design criteria are being prepared for a unit in which the can will be held vertically and driven by a modified Oster power vise, with the rolls stationed at  $120^\circ$  on the periphery of the can during sealing. The preformed top will have a small groove to match the rollers. This same unit with cutters replacing the formed rolls will be employed to open cans.

Some means had to be found for cleaning the waste cans before they are placed into the air-lock-transfer station. Criteria were established for cleaning the cans ultrasonically in a vertical position in a tank with an equilateral triangular cross section. Three submersible ultrasonic transducers will be mounted vertically on panels forming a triangle. The panels are removable so that the transducers can be removed for replacement. Temperature indicators, liquid-level indicators, and activity meters will be incorporated to safeguard the system. The control panel and generator will be heated at the cell operating face.

### In-Cell Sound Transmission System

R. E. McDonald

A simple in-cell sound transmission system was developed for the new facility to be used for general and local sound pickup. The system consists of a small lavalier microphone potted in rubber, a jumper cord, an amplifier, and a headset. The microphone is coupled directly to a phone plug for plugging into a wall-mounted receptacle for general sound pickup. The jumper cord is used for local pickup of such sounds as the dressing of a grinding wheel. This 30-in. coil cord allows the microphone to be placed anywhere in the cell. The in-cell components are shown in Fig. 22.5. Fifteen of these units will be fabricated for the new facility. This development will be described in a forthcoming technical memorandum.

### X-Ray Diffraction Apparatus

H. L. Yakel<sup>29</sup>

The shielded x-ray diffraction goniometer<sup>30</sup> for the PIE Facility was fabricated and assembled. A general view of the experimental equipment is shown in Fig. 22.6. When attached to the cells, the transfer mechanism of the goniometer will bring metallographically mounted specimens from the operating cell into the center of the diffractometer. The sample will be permanently separated from the exterior environment of the goniometer, but incident and diffracted x-ray beams will be admitted to and from the sample chamber through a beryllium window.

Biological shielding over complete  $4\pi$  geometry is provided except for two narrowly defined apertures through which the incident and diffracted x-ray beams enter and emerge. Operation of the goniometer consists of equal and opposite  $\theta$  movements of the x-ray tube and counter arms. In order for the x-ray-beam apertures to follow the motions of these components, a unique double shield has been devised in which an inner shield containing helical slots moves past an outer shield containing cylindrical slots. The cylindrical slots are in the diffraction plane, and the motion of the inner shield is normal to that plane. These shields are composed of depleted uranium to obtain optimum gamma attenuation per unit length and suitable fabrication properties.

Additional lead shields around the x-ray tube and counter assemblies effectively prevent the emergence of any radiation from the sample along the incident and diffracted beam paths. The sample is shielded with an equivalent of 3.5 in. of uranium or 6 in. of lead at all times (including transit to and from the goniometer). Attenuation factors ranging from  $10^3$  to  $10^4$  for  $\text{Co}^{60}$  gamma radiation are anticipated.<sup>31</sup>

Diffracted x-ray beams are observed with either a side-window proportional counter or a scintillation counter. These devices may be placed in

<sup>29</sup>X-Ray Diffraction Group.

<sup>30</sup>Designed and constructed by Phillips Electronics, Inc.

<sup>31</sup>Oak Ridge National Laboratory, *Radiation Safety and Control Training Manual*, p B-1.

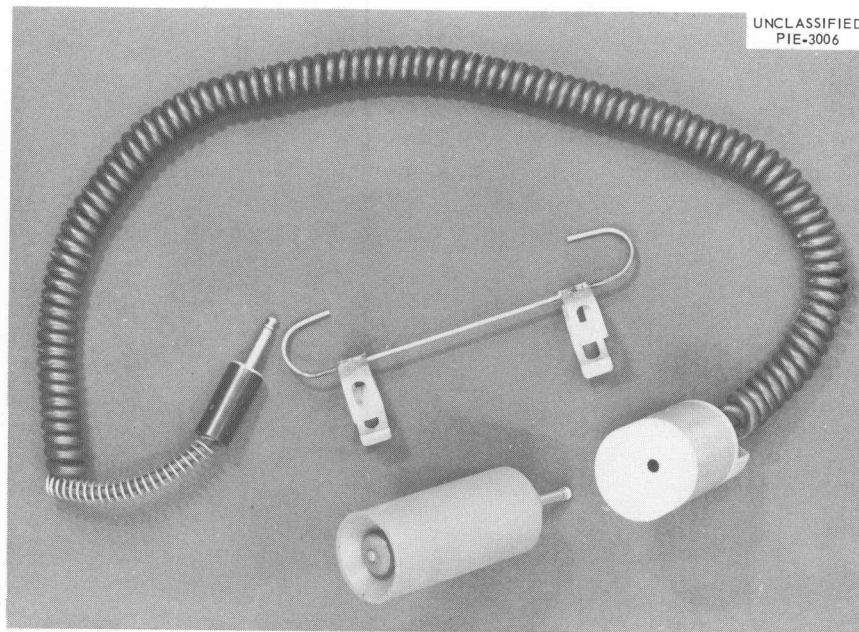


Fig. 22.5. In-Cell Components for Remote Sound System.

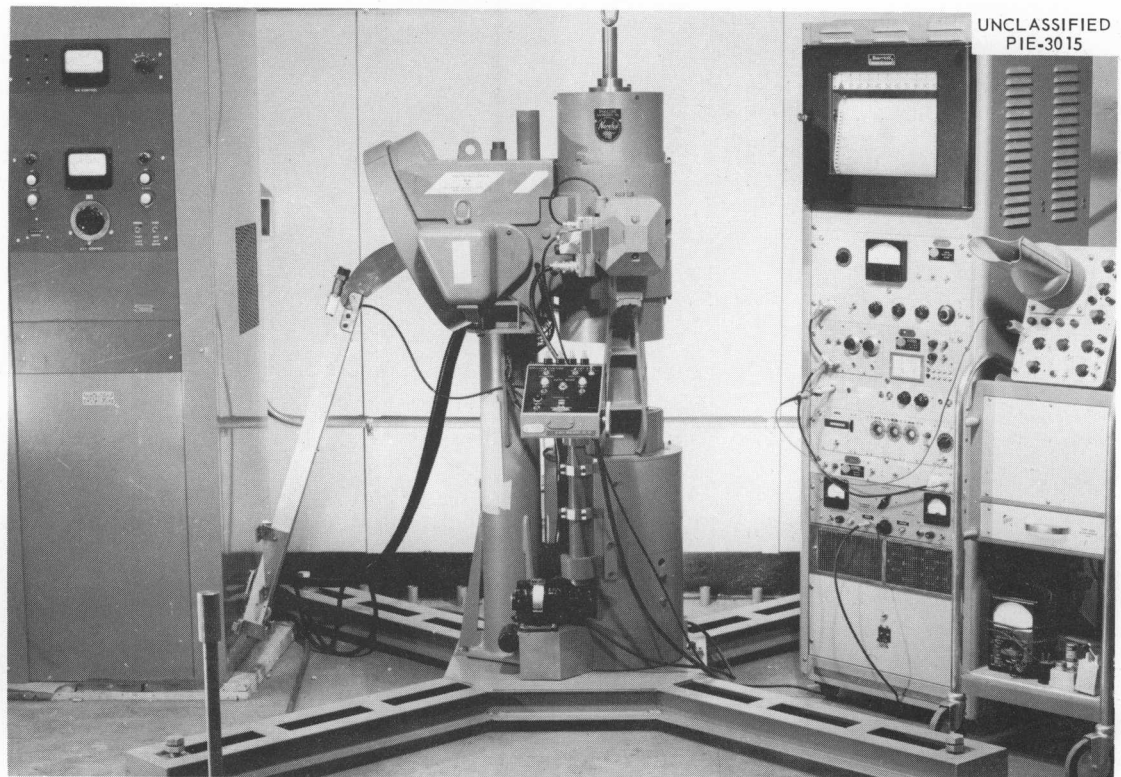


Fig. 22.6. Overall View of PIE X-Ray Diffraction Apparatus. Metallographic specimens are transferred into the shielded goniometer (center). The power supply for the x-ray tube is at left. Signals from the counter are analyzed and displayed through the circuit panel and oscilloscope at right.

the direct diffracted x-ray beam when the sample activity is low or placed so that the beam re-diffracted by a cylindrically bent and ground LiF crystal monochromator can be observed when the sample activity is high.

The output of the preamplifier is fed through a single-channel DD2 linear amplifier whose output

is recorded by a scaler and rate meter. An auxiliary output before pulse-height selection is displayed on an oscilloscope screen. This latter display can also be used to assess the nature and intensity of radioactive background from the sample and to indicate the extent of interference that a counter might find in the directly diffracted beam.

**Part IV**  
**Applied Research**

C. J. McHargue

---



## 23. Physical Properties of Ceramics

D. L. McElroy

T. G. Kollie

W. Fulkerson

The aim of this research is to determine the effects of temperature and physical and chemical variations on the thermal conductivity ( $k$ ) of refractory solids and to evaluate the mechanisms of heat transport operative in these materials. Reproducible and accurate  $k$  data are requisite to this study. To achieve these goals, six methods of measurement were selected for development and intercomparison to span the range  $-100$  to  $2200^{\circ}\text{C}$ , and the initial efforts on three of these methods are described.

### A THERMAL COMPARATOR APPARATUS FOR THERMAL CONDUCTIVITY MEASUREMENTS FROM 40 TO $400^{\circ}\text{C}$ <sup>1</sup>

T. G. Kollie

D. L. McElroy

The thermal comparator developed by Powell to measure thermal conductivity at room temperature was modified to allow measurements to at least  $400^{\circ}\text{C}$  in an inert atmosphere. The detector spheres were made from a hard silver-magnesium alloy which resists flattening and retains the needed high thermal conductivity. The differential response of the detector sphere was shown to be a linear function of the original temperature difference between the spheres and the specimen and to be dependent on the difference in sphere heights, on the sphere load, and on the system atmosphere. The sphere response was correlated with thermal conductivity

to within  $\pm 3\%$  for thermal conductivities ranging from  $1.15$  to  $150 \text{ w m}^{-1}(\text{C})^{-1}$  (Pyrex to molybdenum). Spurious results were obtained on soft materials with high thermal conductivities (aluminum and graphite).

### FURTHER STUDIES ON THE THERMAL COMPARATOR APPARATUS<sup>2</sup>

D. L. McElroy

T. G. Kollie

The thermal comparator allows controlled variables and materials of limited quantity to be tested rapidly because the specimen is only a small disk,  $\frac{1}{4}$  in. thick by 1 in. in diameter. A calibration curve was established at  $75^{\circ}\text{C}$  by using specimens of known  $k$  and by controlling such system variables as the original temperature difference of the spheres and the specimen, difference in sphere heights, sphere load and impact upon contact, sphere flattening, atmosphere of the system, and specimen roughness. Table 23.1 shows the results at  $75^{\circ}\text{C}$  on ten specimens of known  $k$  and the controlled variables of this test. These results, like those of Powell<sup>3</sup>, gave a nearly linear relation between the temperature difference of the detecting spheres at a given time after contact and  $k^{1/2}$ . The results were reproducible to within 1.5% and were within 3% of the average calibration curve for  $k$  values between 1.15 and  $418 \text{ w m}^{-1}(\text{C})^{-1}$ . Measurements were initiated on a series of specimens important to the scope of this program.

<sup>1</sup>Abstract of paper presented at the Conference on Thermal Conductivity Methods Held at Battelle Memorial Institute, October 26-28, 1961.

<sup>2</sup>D. L. McElroy and T. G. Kollie, *Met. Div. Ann. Progr. Rept. May 31, 1961*, ORNL-3160, p 35.

<sup>3</sup>R. W. Powell, *J. Sci. Instr.* 34, 485-92 (1957).

Table 23.1. Thermal Comparator<sup>a</sup> Calibration  
Data at 75°C

Specimen of Known $k$	$k^{1/2}$ at 75°C [ $w\ m^{-1}(\text{°C})^{-1}$ ]	Sphere Response 7 sec After Contact (°C)
Pyrex	1.07	0.75
INOR-8	3.33	1.58
Type 347 stainless steel	3.80	1.69
Steel 17	5.13	1.85
Steel 10	5.96	2.01
Steel 2	7.63	2.28
Iron 1	8.31	2.33
Iron 2	8.38	2.37
Magnox B	11.09	2.93
Ag 99.98%	20.18	4.09

<sup>a</sup>Controlled variables:  $\frac{1}{4}$ -in.-diam Council D spheres; 15-g load; 0.033-in. vertical spacing; helium atmosphere; original sphere-specimen  $\Delta T$ , 8.45°C.

### A RADIAL HEAT FLOW APPARATUS FOR THERMAL CONDUCTIVITY MEASUREMENTS FROM 60 TO 1600°C<sup>4</sup>

T. G. Godfrey<sup>5</sup>

T. G. Kollie      D. L. McElroy

A radial heat flow apparatus operable over the range 60 to 1600°C was developed for measuring the thermal conductivity of refractory materials contemplated for use as nuclear reactor components. The specimen used was a 9-in.-tall stack of 18 disks, 3 in. in outside diameter and  $\frac{5}{8}$  in. in inside diameter; thermocouple holes were machined in some of the disks. The radial temperature gradient was generated by a Pt<sub>90</sub>Rh<sub>10</sub> heater in the center of the specimen and was measured by 12 Pt<sub>90</sub>Rh<sub>10</sub>/Pt thermocouples which entered the specimen stack radially and were turned to assume an axial

<sup>4</sup>Abstract of paper presented at the Conference on Thermal Conductivity Methods Held at Battelle Memorial Institute, October 26-28, 1961.

<sup>5</sup>Ceramics Laboratory.

position. The specimen was heated externally by a muffle heater and end heat losses were prevented by end guard heaters. A procedure was devised which allows an isothermal thermocouple intercalibration to be made prior to each thermal conductivity determination. The effects of thermocouple calibration, core heater power level, and end guard heater control were studied. Measurements on a Ni-Mo alloy to 800°C and on sintered UO<sub>2</sub> to 550°C were reproducible to  $\pm 2\%$ . An error analysis indicated that the results were accurate to  $\pm 3.0\%$ .

### FURTHER STUDIES ON THE RADIAL HEAT FLOW APPARATUS

T. G. Godfrey<sup>5</sup>      T. G. Kollie  
D. L. McElroy

The techniques developed on the Ni-Mo alloy to 800°C<sup>6</sup> in the radial heat flow apparatus were successfully applied to a UO<sub>2</sub> specimen to 875°C before electrical difficulties were encountered. The data obtained on the effects of temperature and on a change in the O/U ratio from 2.012 to 2.006 are described in Chap. 25, this report.<sup>7</sup> Modifications in the equipment may extend the measurements to at least 1400°C, where radiation transmission effects may be observable in UO<sub>2</sub>. Changes receiving study include a noninductively wound muffle heater, a Dauphinee chopper in the temperature control system, and improved thermocouple insulation and placement.

### STUDIES ON A QUENCHING APPARATUS FOR MEASURING THERMAL DIFFUSIVITY

T. G. Godfrey<sup>5</sup>      T. G. Kollie  
D. L. McElroy

The quenching apparatus for measuring thermal diffusivity to 1400°C has been assembled and is being tested. Components of this apparatus include two 1700°C furnaces, equipment for maintaining an

<sup>6</sup>D. L. McElroy and T. G. Godfrey, "The Thermal Conductivity of INOR-8 Between 100 and 800°C," submitted to *American Society of Metals Transactions Quarterly*.

<sup>7</sup>E. E. Stansbury and C. R. Brooks, Department of Chemical and Metallurgical Engineering, University of Tennessee, private communication, Mar. 1, 1961.

inert atmosphere around a cylindrical specimen, and a helium-fluidized bed of  $\text{Al}_2\text{O}_3$  particles. After the specimen attains thermal equilibrium, it is quenched into the fluidized bed, which is approximately  $50^\circ\text{C}$  hotter or colder than the specimen. The time-temperature response of the specimen is measured to obtain the thermal diffusivity ( $\alpha = k/\rho \cdot C_p$ ). The heat transfer coefficient of the fluidized bed was measured as a function of gas flow rates and  $\text{Al}_2\text{O}_3$  particle size. Initial  $\alpha$  measurements will be made on INOR-8 because  $k$  (ref 6) and  $C_p$  (ref 7) have been measured independently, and this will allow an intercomparison of measurement methods. Measurements will be made on  $\text{UO}_2$  when this cross-check is complete.

**TOTAL HEMISPHERICAL EMITTANCE OF Pt,  
Cb-1% Zr, AND POLISHED AND OXIDIZED  
INOR-8 IN THE RANGE 100 to  $1200^\circ\text{C}$ <sup>8</sup>**

T. G. Kollie      D. L. McElroy

The temperature dependence of the total hemispherical emittance was determined for specimens of Pt, Cb-1% Zr, and polished and oxidized INOR-8 by a method which employs an instrumented strip

specimen directly heated electrically in a black-body vacuum chamber held at a constant temperature. A value of 0.24 was found for polished INOR-8 at  $600^\circ\text{C}$ , and this could be increased threefold by a 1-hr oxidation in air at  $1000^\circ\text{C}$ . Oxidation of polished Cb-1% Zr occurred even at an indicated chamber pressure of  $6 \times 10^{-6}$  torr and resulted in unusually high values. An analysis of the platinum specimen heat losses, other than by emission, indicated that this technique might offer a means of measuring the specimen  $k$  if precise specimen dimensions can be obtained. In addition to thermal conductivity values, the strip specimen data yield electrical resistivity values. Tests made with an INOR-8 hollow cylinder specimen, which totally encloses an axial heater, gave comparable total hemispherical emittance values. Specific heat data can be obtained by auxiliary experiments with the hollow cylinder specimen. In addition, it is quite possible that a  $\text{UO}_2$  specimen of this type will yield much needed radiation transmission information.

---

<sup>8</sup> Abstract of paper to be presented at the Symposium on Measurement of Thermal Radiation Properties of Solids, Dayton, Ohio, September 5-7, 1962, sponsored by NBS, NASA, and USAF.

## 24. Sintering Studies

C. S. Morgan

C. S. Yust

Present technology demands high-grade ceramic parts, many of which are produced by sintering. Sintering of ceramics with the fluorite structure is being investigated to gain information on the mechanisms involved in order to produce improved ceramics.

### SINTERING RATES OF FLUORITE-STRUCTURE MATERIALS

The results of sintering-rate studies of fluorite-structure materials are summarized below from a paper to be published.<sup>1</sup>

Sintering rates of powder compacts of materials with the fluorite structure obtained during an initial, rapid densification period gave a definite indication of the sintering mechanism. For example, ThO<sub>2</sub> compacts heated to 1450°C at approximately 3°C/sec and held at 1450°C for 10 min had a density of 7.36 g/cc. Compacts heated similarly but held for an additional 70 sec at 1450°C had a density of 7.38 g/cc, while compacts heated for 10 min at 1450°C and then raised to 1600°C in an additional 70 sec had a density of 7.57 g/cc. The compacts heated to 1450°C and held for 10 min had identical densification rates. The densification rate for compacts held for an additional 70 sec differed by a factor of 10 from the densification rate of compacts taken to 1600°C. Since the diffusion coefficients for thorium in ThO<sub>2</sub> at 1450°C and at 1525°C differed by a factor of 1.6, bulk diffusion cannot be the dominant material transport process. The other known densification mechanism is plastic flow.

Compacts of thoria heated directly to 1600°C and held there for 1 min had higher densities (7.53

g/cc) than those heated at the same rate but held at 1000°C for 205 days before the 1-min treatment at 1600°C (7.31 g/cc). Calcium fluoride compacts heated directly to 1250°C and held there for 2 min had higher densities (2.97 g/cc) than those heated at the same rate but held at 1100°C for 10 min (2.91 g/cc). A plausible explanation of these anomalies assumes that material transport by surface diffusion or evaporation-condensation results in an increase in the radius of curvature of weld necks between particles during the additional time at lower temperature. When the temperature rise is resumed, movement of dislocations contributing to densification by a plastic flow mechanism is reduced because of reduced stresses in the modified geometry of the system.

Maxima and minima such as those found in the densification rate vs time curves<sup>2</sup> for ThO<sub>2</sub> powder compacts heated at a constant rate were also found in densification rate curves for two other materials having the fluorite structure CaF<sub>2</sub> and CeO<sub>2</sub>. The minima occur at approximately the same fraction of the absolute melting point. The minimum was absent from the densification rate curve for powder compacts of ThO<sub>2</sub>-3% ZrO<sub>2</sub>. A minimum was found in the densification curve for Al<sub>2</sub>O<sub>3</sub> (hexagonal structure) but occurred at a temperature corresponding to a different fraction of the melting point.

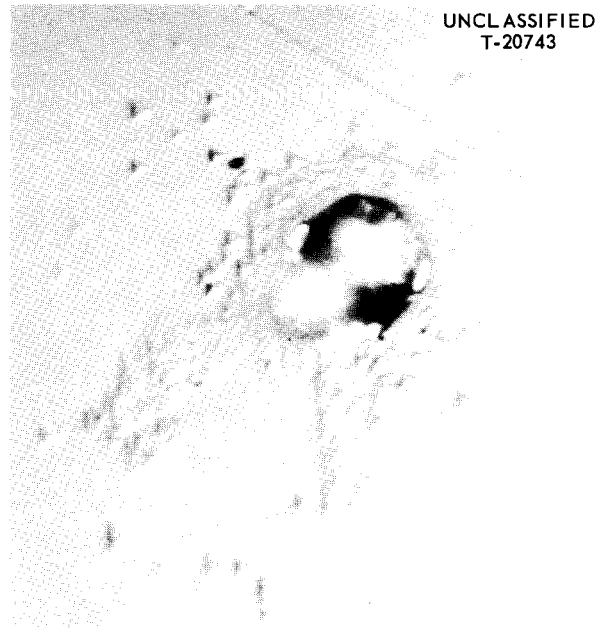
### DISLOCATIONS AROUND WELD NECKS

Evidence for the occurrence of plastic flow during the sintering of calcium fluoride was obtained by observing dislocations by means of an etch-pit technique. Plastic deformation of a crystal requires the generation and motion of dislocations; therefore a high increase in dislocation concentration may be

<sup>1</sup>"Mechanism of Material Transport During Sintering of Fluorite-Structure Material," to be submitted to the *Journal of the American Ceramic Society*.

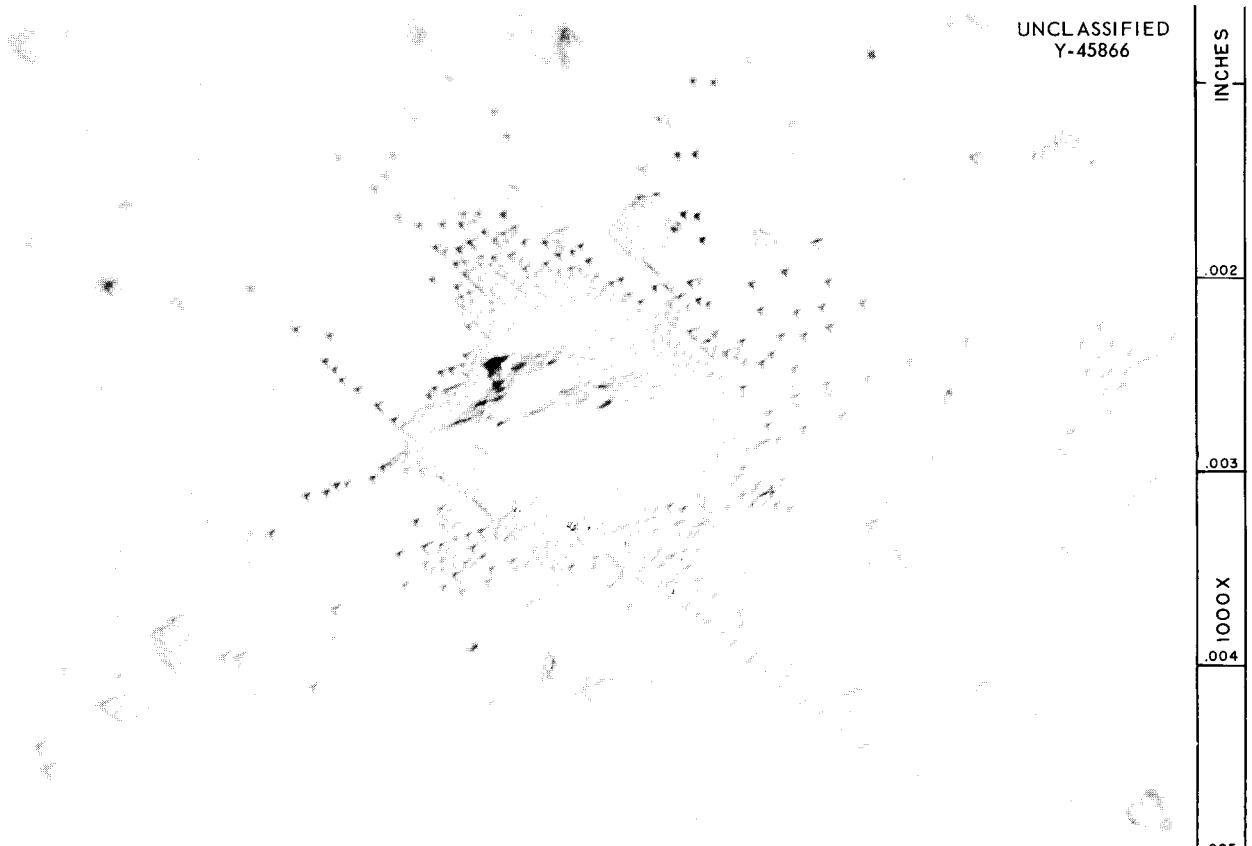
<sup>2</sup>C. S. Morgan and C. S. Yust, *Met. Div. Ann. Progr. Rept.* May 31, 1961, ORNL-3160, p 40.

indicative of plastic flow. Small single crystals of  $\text{CaF}_2$  were placed on a cleaved surface of a larger single crystal, and the specimen was heat-treated to cause a small degree of sintering. The crystals were then etched in sulfamic acid to reveal dislocations. In Fig. 24.1 depicting the surface of a sample sintered for 1 hr at  $1200^\circ\text{C}$  a small  $\text{CaF}_2$  particle is shown sintered to the cleaved crystal with the cleaved surface containing a high density of etch pits in the area of the sintered neck. A cluster of etch pits on a sample sintered for 30 min at  $1200^\circ\text{C}$  is shown in Fig. 24.2 to be located at the point where a small particle was joined to the cleaved surface. The alignment of the etch pits in directions parallel to the sites of the pits is due to slip. Although the slip planes cannot be indexed from their trace in only one surface, the directions present are consistent with the known slip system in calcium fluoride,  $\langle 110 \rangle \{100\}$ . A massive concentration of dislocations in the area of neck formation implies that the mechanism of sintering involves plastic flow, although not necessarily to the exclusion of other processes.



UNCLASSIFIED  
T-20743

Fig. 24.1.  $\text{CaF}_2$  Particle Sintered to Cleaned  $\text{CaF}_2$  Surface. Heated for 1 hr at  $1200^\circ\text{C}$ . Sulfamic acid etch. 1000X.



UNCLASSIFIED  
Y-45866

INCHES

.002

.003

1000X

.004

Fig. 24.2. Cleaned Surface of  $\text{CaF}_2$  Single Crystal at Point Where  $\text{CaF}_2$  Particle Had Started To Join Surface. Heated for 30 min at  $1200^\circ\text{C}$ . Sulfamic acid etch. 1000X.

**MICROSTRUCTURE AROUND HOLE**

A compact prepared from  $\text{CaF}_2$  powder with a small particle size was sintered at  $650^\circ\text{C}$ , and a 13.5-mil hole was drilled in the center. The pellet was then heated for a short time at  $1300^\circ\text{C}$  in an

argon atmosphere, and the face was polished and etched to show grain boundaries. As shown in Fig. 24.3, grains in close proximity to the hole were much smaller, on the average, than other grains. The grains become progressively larger the greater the distance from the hole.

Fig. 24.3. Microstructure Around Hole in Calcium Fluoride Pellet After Sintering. 100X.

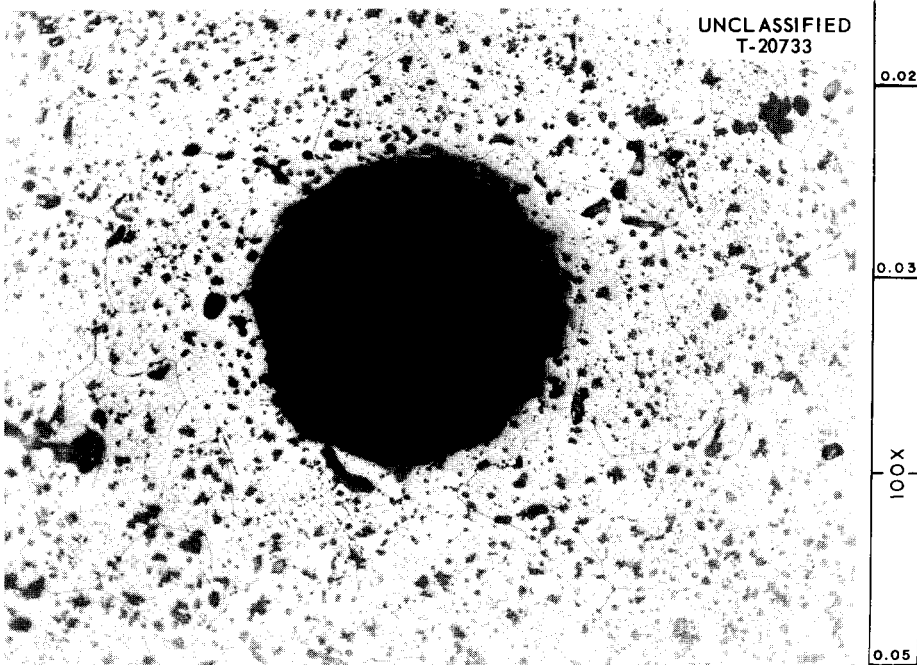
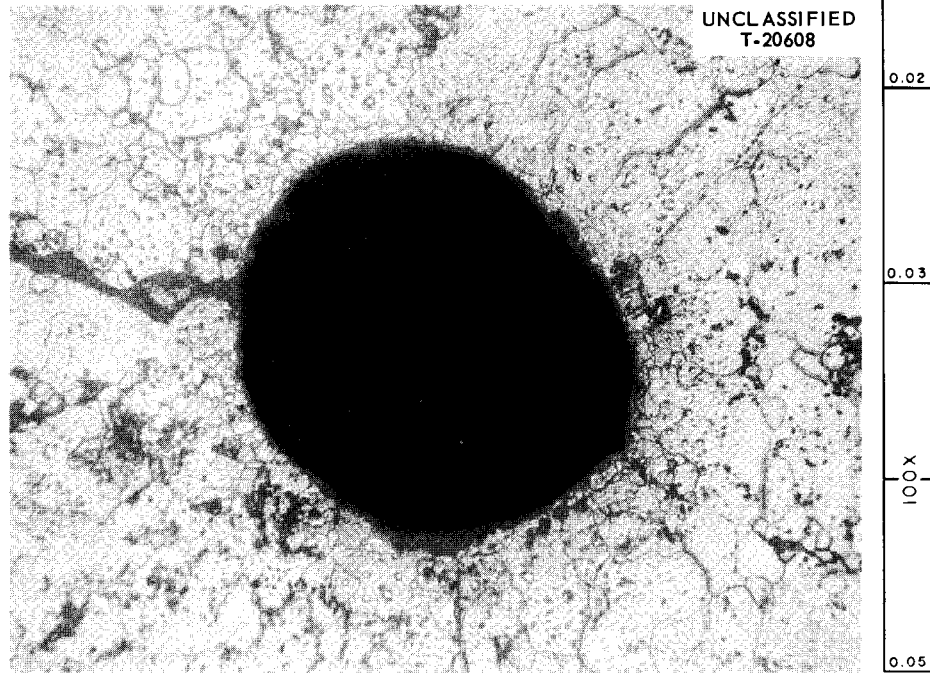


Fig. 24.4. Microstructure After Production of Larger Grains Around Hole by Cooling. 100X.

It was found that if pellets were annealed for longer periods of time at 1250°C and cooled slowly the grains around the hole would grow to sizes approximating those of other grains, as shown in Fig. 24.4. Further firing at 1300°C with more rapid cooling caused smaller grains to again appear in the area surrounding the hole. Drilling the hole near the edge of the CaF<sub>2</sub> pellet did not alter the grain-size behavior.

Formation of smaller grains in the vicinity of the hole suggests that plastic flow is taking place, presumably as the hole shrinks during sintering. After being heated close to the melting point, where the tendency to sinter is greatest, the pellet was allowed to cool rapidly enough to avoid grain growth. Annealing at 1250°C with slow cooling permitted grain growth near the hole as well as in the body of the pellet. Smaller grains around the hole reappeared on subsequent firing and more rapid cooling. The fact that the grains in the vicinity of the hole can be reduced in size after conversion to larger grains suggests that strains caused by drilling of the hole do not account for the differential in grain sizes. Oel has demonstrated a similar grain structure behavior with silver capillaries.<sup>3</sup>

### HOT PRESSING OF THORIUM OXIDE

An investigation of the hot-pressing characteristics of thorium oxide powder compacts is in progress for the purpose of determining the influence of the parameters temperature, pressing time, and applied stress on the hot-pressed density and to interpret the results in terms of a densification mechanism. Thoria powder compacts were placed between graphite rods positioned by a graphite die, the system was heated to the desired temperature, and the appropriate load was applied for a specified period of time. The system was enclosed in an argon atmosphere. An experimental design consisting of 20 hot-pressing experiments covered temperatures ranging from 1000 to 1600°C, pressing times ranging from 20 to 900 sec, and applied stresses ranging from 0 to 3000 psi.

A statistical analysis of the data yielded the density contours depicted in Fig. 24.5.<sup>4</sup> The density at any point within the experimental limits

depicted by the cube may be estimated by the expression

$$Y_c = 6.439 + 0.165X_1 + 0.890X_2 + 0.314X_3 \\ - 0.0306X_1^2 + 0.138X_2^2 + 0.0482X_3^2 + 0.0025X_1X_2 \\ + 0.0425X_1X_3 + 0.195X_2X_3 + 0.260Z,$$

in which  $Y_c$  is the predicted density,  $X_1$ ,  $X_2$ , and  $X_3$  represent time, temperature, and load, transformed as shown below, and  $Z$  is a factor representative of the particular batch of powder used in the experiment and is equal to  $-0.4$  for the Th-3D powder and  $+0.6$  for the Th-3B powder used in the tests. The transformations for  $X_1$ ,  $X_2$ , and  $X_3$  are

$$X_1 = \frac{(\text{time})^{2/3} - 50.29}{26.29}, \\ X_2 = \frac{\text{temperature} - 1300}{184}, \\ X_3 = \frac{\text{load} - 1500}{919}.$$

The expression for estimating the density of a hot-pressed compact is obtained by statistical analysis of the hot-pressing data, and an error is associated with each point within the volume of experimental conditions, the minimum error being at the center of the volume. The increase in error is spherical from the center point, and the errors of the estimates at the vertices of the cube are therefore the largest.

Constant-density contours plotted from Fig. 24.5 are shown in Fig. 24.6. Each point on these curves represents the predicted density of a pellet that had been hot-pressed for 20 sec at the temperature and load corresponding to the coordinates of the point. The family of curves predicts that at above 1200°C any stress will increase the hot-pressed density but that at lower temperatures the applied stress must exceed a certain minimum before significant densification will result. The stress that must be exceeded at any given temperature is indicated on Fig. 24.6 as a dashed line. The apparently anomalous behavior indicated in the lower left corner of Fig. 24.6 of a decrease in

<sup>3</sup>H. J. Oel, *Z. Metallk.* 51(1), 53 (1960).

<sup>4</sup>The experimental design and the statistical analysis were prepared by D. A. Gardiner of the Mathematics Panel.

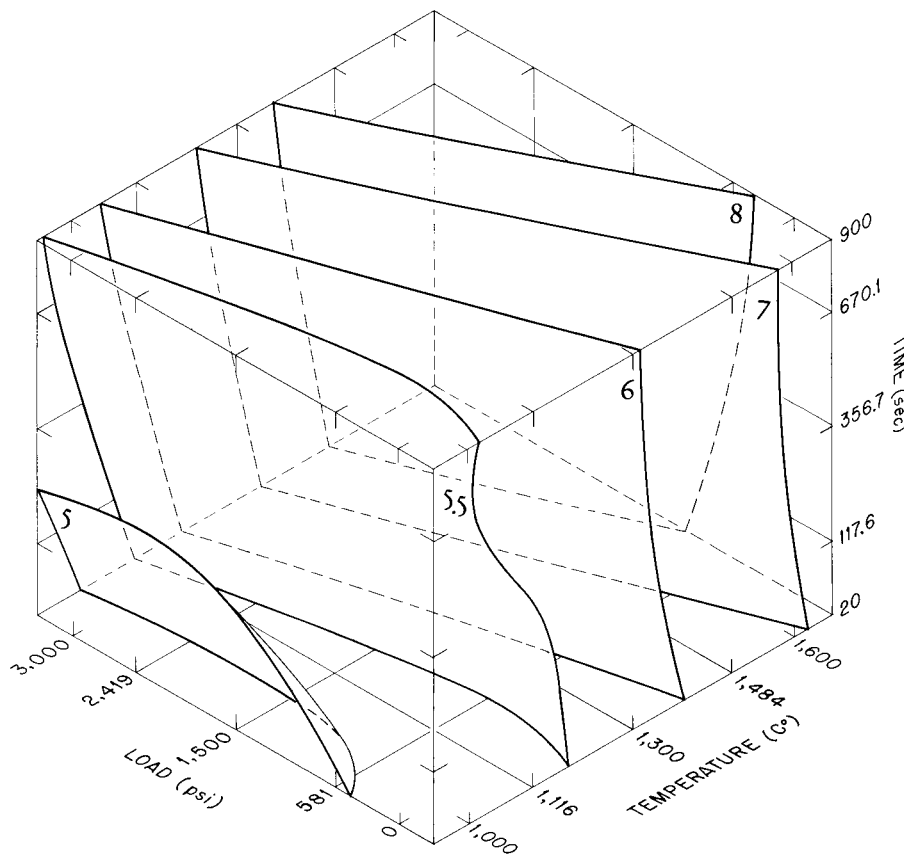


Fig. 24.5. Response Contours of Hot-Pressed Density of  $\text{ThO}_2$ .

the hot-pressed density with increased pressing stress results from the increased error in the calculated density at the vertices of the cube.

Although the data obtained for hot-pressed thorium compacts are limited (Fig. 24.7), they confirm the prediction that stress would increase the density above  $1200^\circ\text{C}$  but not below  $1200^\circ\text{C}$ .

#### DIFFUSION OF THORIUM IN THORIUM OXIDE

The diffusion of thorium in thorium oxide was measured by an isotope-tracer technique. A thin

layer of thorium enriched in  $\text{Th}^{230}$  was deposited on the polished surface of a thorium pellet having 97.5% of theoretical density. After a suitable heat treatment to promote diffusion, the concentration distribution of the isotope was determined by mass spectrographic analysis of thin slices of the pellet.

Typical concentration data are shown in Fig. 24.8. Since the thorium pellet was polycrystalline, the concentration distribution may have been the result of both volume and grain-boundary diffusion

UNCLASSIFIED  
ORNL-LR-DWG 69513

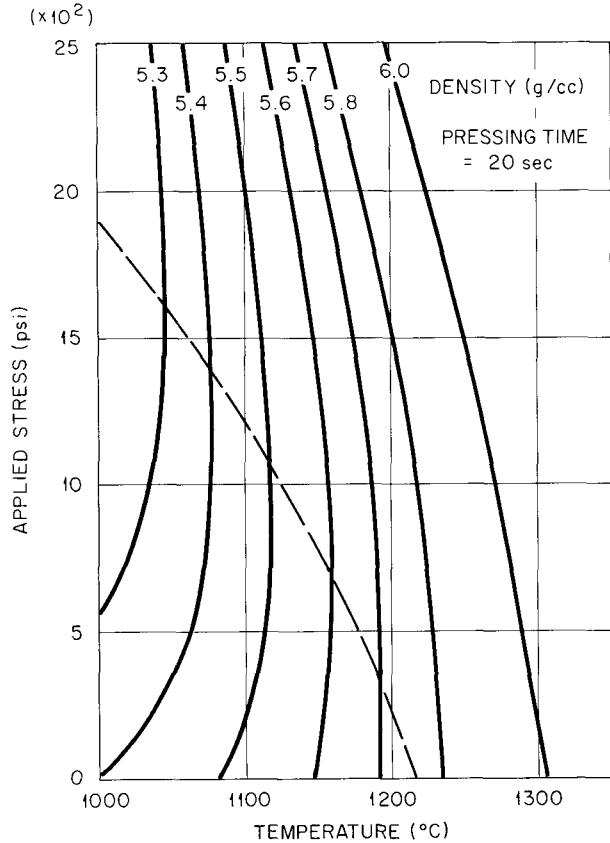


Fig. 24.6. Constant-Density Contours (Plotted from Fig. 24.5) for Hot-Pressed Thoria (Th-3B) Powder.

UNCLASSIFIED  
ORNL-LR-DWG 69514

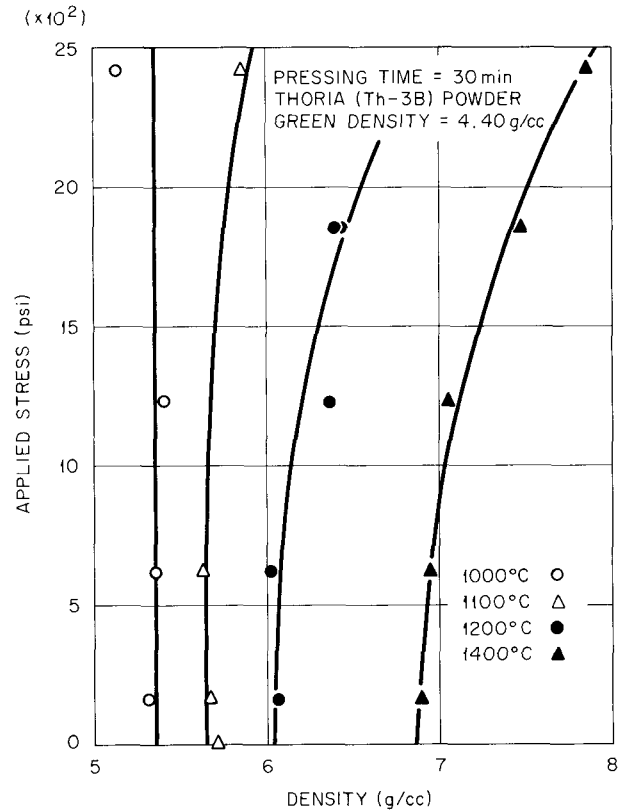


Fig. 24.7. Hot-Pressed Density as a Function of Applied Stress.

processes. Belle<sup>5</sup> treated data of this type by fitting it with two straight lines, one describing the effects of grain boundary diffusion, the other volume diffusion. The lines which fit the data according to Belle's analysis are shown in Fig. 24.8.

The concentration measurements may also be treated according to a procedure devised by Lundy and Federer (Chap. 25, this report), which considers the data to define a continuous curve. The continuous total-concentration curve and its components, as determined by this technique, are also

shown in Fig. 24.8. The excellent agreement between the slopes of the volume diffusion concentration lines obtained by the two methods is apparent.

The activation energy for the diffusion of thorium in thoria was calculated from the data in Fig. 24.9 to be 37.8 kcal/mole. A value of 14.7 kcal/mole for the more rapid process of oxygen diffusion was obtained previously.<sup>6</sup>

<sup>5</sup>J. Belle, *Proc. U.N. Intern. Conf. Peaceful Uses Atomic Energy, 2nd, Geneva, 1958* 6, 569-89 (1959).

<sup>6</sup>C. S. Morgan and C. S. Yust, *Met. Div. Ann. Progr. Rept. May 31, 1961*, ORNL-3160, p 42.

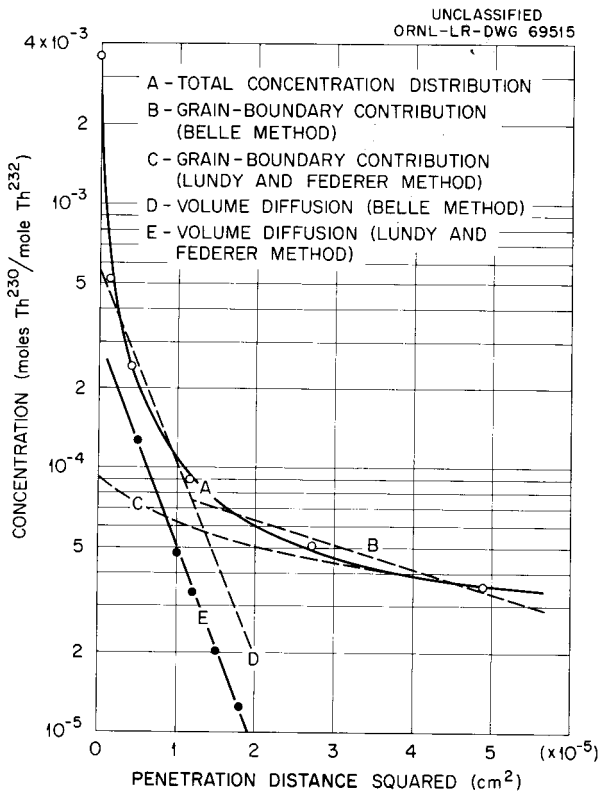


Fig. 24.8. Diffusion of Th<sup>230</sup> in Th<sup>232</sup>O<sub>2</sub>.

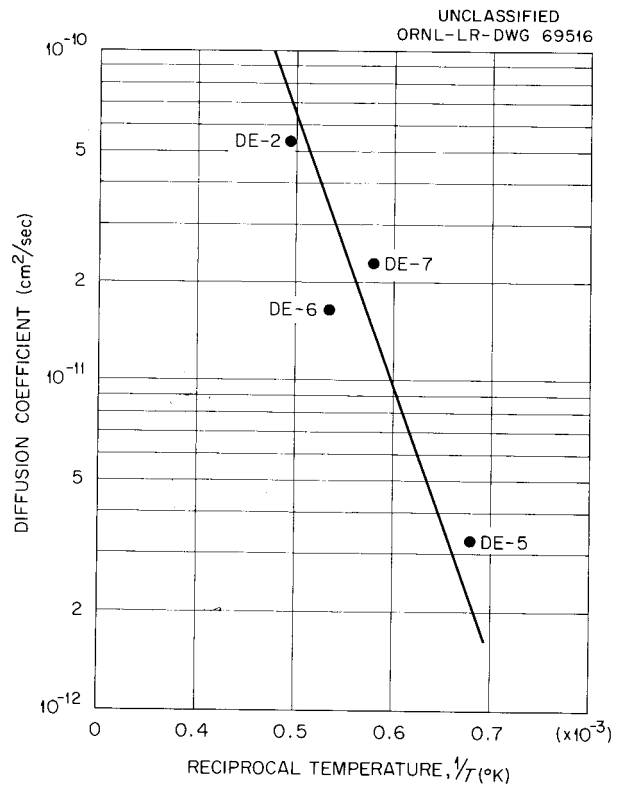


Fig. 24.9. Variation of Diffusion Coefficient of Th<sup>230</sup> in Th<sup>232</sup>O<sub>2</sub> with Temperature.

## 25. Solid Reaction Studies

T. S. Lundy

### DIFFUSION OF Al<sup>26</sup> AND Mn<sup>54</sup> IN ALUMINUM<sup>1</sup>

T. S. Lundy      J. F. Murdock

Diffusion coefficients of Al<sup>26</sup> and Mn<sup>54</sup> in aluminum were determined between 450 and 650°C. Low specific activities of the isotopes necessitated the use of thick-layer technique. The exact solution to Fick's second law for the appropriate boundary conditions was used in treating the data. Temperature dependence of the diffusion coefficients may be expressed by the following equations:

$$D_{Al^{26}} = 1.71e^{-34,000/RT},$$

$$D_{Mn^{54}} = 0.22e^{-28,800/RT}.$$

### REACTION BETWEEN BERYLLIUM AND URANIUM MONOCARBIDE<sup>2</sup>

J. F. Murdock

The reaction between hot-pressed beryllium and arc-melted uranium monocarbide has been studied in the range 700 to 1000°C with diffusion couples. The carbide used was of two compositions: 4.8 and 5.1 wt % C. Reaction occurred throughout the temperature range studied, resulting in a layer of UBe<sub>13</sub> with uniformly dispersed free carbon. The reaction was found to be controlled by the diffusion of beryllium in UBe<sub>13</sub>, with reaction occurring at the UBe<sub>13</sub>-UC interface. An activation energy of 33,000 cal/mole was determined for the process.

<sup>1</sup>Abstract of paper to be published in the *Journal of Applied Physics*.

<sup>2</sup>Abstract of paper to be published in the *Journal of Nuclear Materials*.

### DIFFUSION OF Zr<sup>95</sup> AND Nb<sup>95</sup> IN β-ZIRCONIUM

J. I. Federer      T. S. Lundy      F. G. Arcella<sup>3</sup>

Self-diffusion of Zr<sup>95</sup> in β-zirconium has been studied by other investigators.<sup>4-8</sup> The unusually large differences between their results, the anomalously high diffusion coefficients obtained at low temperatures, and the desire to extend the study over the entire range of temperatures at which β-zirconium is stable prompted this investigation. In addition, the crystal structure of β-zirconium is body-centered cubic, and in general diffusion processes in body-centered cubic materials are less well understood than for face-centered cubic materials. Finally, zirconium possesses properties that recommend its use as a cladding material in some fuel element concepts; therefore the study of diffusion of fission products, such as Zr<sup>95</sup> and Nb<sup>95</sup>, could provide useful information for fuel element design purposes. The zirconium used in this investigation was high-purity iodide material with a coarse grain size. Since Zr<sup>95</sup> cannot be discriminated from its daughter Nb<sup>95</sup> by gamma

<sup>3</sup>Summer employee.

<sup>4</sup>Ye. V. Borisov *et al.*, "Study of Diffusion in Zirconium and in Certain Alloys with a Zirconium Base," pp 196-209 in *Metallurgiya i Metallovedeniye*, Izdatel'stvo Akademii Nauk SSSR, Moscow, 1958 (NP-TR-448, F-TS-9849/V).

<sup>5</sup>G. B. Federov and V. D. Gulyakin, *Met. i Metalloved. Christykh Metal. Sbornik Nauch. Rabot* 1959, No. 1, pp 170-78.

<sup>6</sup>V. S. Lyashenko *et al.*, *Phys. Metals and Metallog.* 8(3), 362-69 (1959).

<sup>7</sup>D. Volokoff *et al.*, *Compt. rend.* 251, 2341-43 (1960).

<sup>8</sup>G. Kidson and J. McGurn, *Can. J. Phys.* 39, 1146-57 (1961).

spectrometry, all the Zr-Zr<sup>95</sup> diffusion anneals were completed within two days from the time that the Zr<sup>95</sup> was purified of Nb<sup>95</sup>; thus the activity of Nb<sup>95</sup> in any of the zirconium self-diffusion experiments did not exceed 3.8% of the total activity.<sup>9</sup>

Diffusion coefficients for Zr<sup>95</sup> and Nb<sup>95</sup> in zirconium were determined over the range 900 to 1750°C. The temperature dependence of the diffusion coefficient for each isotope is shown in the Arrhenius-type plots in Fig. 25.1. Of particular interest is the overall curvature of the Zr<sup>95</sup> plot, which cannot be attributed to experimental scatter. Usually a linear relationship between  $\ln D$  and

<sup>9</sup>The chemical separation was performed by the Isotopes Division.

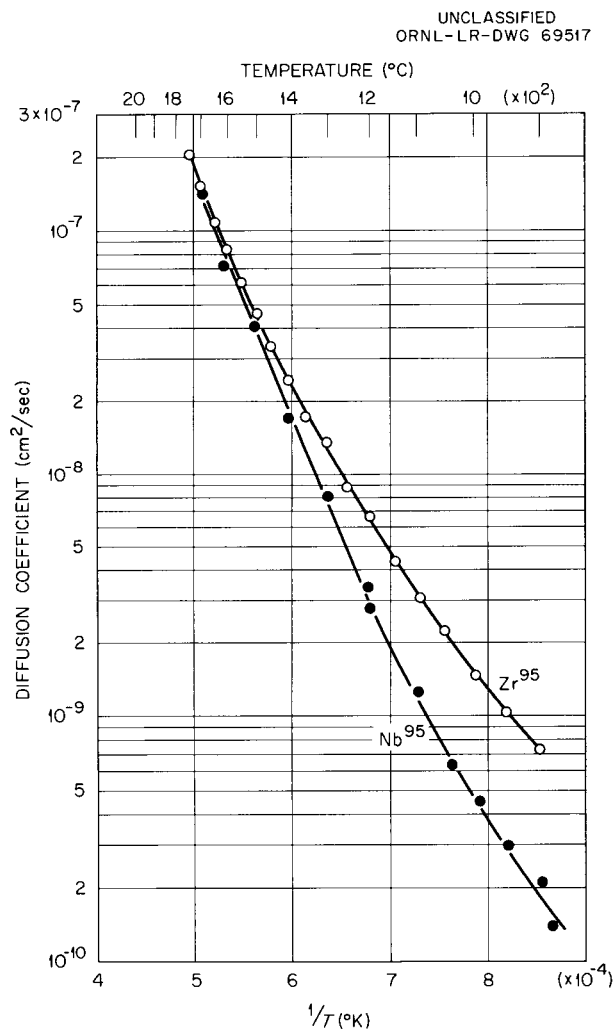


Fig. 25.1. Diffusion of Zr<sup>95</sup> and Nb<sup>95</sup> in  $\beta$ -Zirconium.

reciprocal temperature is taken as evidence of predominantly lattice diffusion, and nonlinearity as evidence of more than one diffusion mechanism operating. An alternate interpretation is that the activation energy for a single mechanism is temperature dependent. The Arrhenius-type plot for Nb<sup>95</sup> may be divided into two segments: above 1150°C,  $\ln D$  plots linearly as a function of reciprocal temperature and the data are expressed by the equation

$$D = 0.024e^{-46,500/RT} \text{ cm}^2/\text{sec};$$

below 1150°C, the observed diffusion coefficients are higher than would be predicted by an extrapolation of the higher temperature data. The apparent activation energies at the lowest and highest temperatures investigated are as follows:

Activation Energy (cal/mole)	Temperature (°C)
Zr-Zr <sup>95</sup>	
21,100	900
46,700	1750
Zr-Nb <sup>95</sup>	
24,500	900
46,500	1150-1700

## DIFFUSION OF FISSION PRODUCTS IN UO<sub>2</sub>

J. I. Federer R. A. Padgett T. S. Lundy

The study of the diffusion of Nb<sup>95</sup> in pressed and sintered UO<sub>2</sub> pellets and in fused single crystals of UO<sub>2</sub> was continued. The techniques of specimen preparation, isotope placement, and treatment of sectioning data were described previously.<sup>10</sup> A method was developed for removing parallel sections as thin as 10<sup>-4</sup> cm by lapping with a suitable abrasive on an optically flat surface. An electronic comparator was used to measure the section thicknesses to an estimated accuracy of  $\pm 5\%$ .

The microstructure of the sintered UO<sub>2</sub> is shown in Fig. 25.2. This material was prepared by cold-pressing UO<sub>2</sub> powder followed by sintering in hydrogen for 2 hr at 1750°C. The resulting bulk density was 10.63 g/cc (97% of theoretical density). Characteristic of this material was the small

<sup>10</sup>T. S. Lundy *et al.*, *Met. Div. Ann. Progr. Rept. May 31, 1961*, ORNL-3160, p 43.

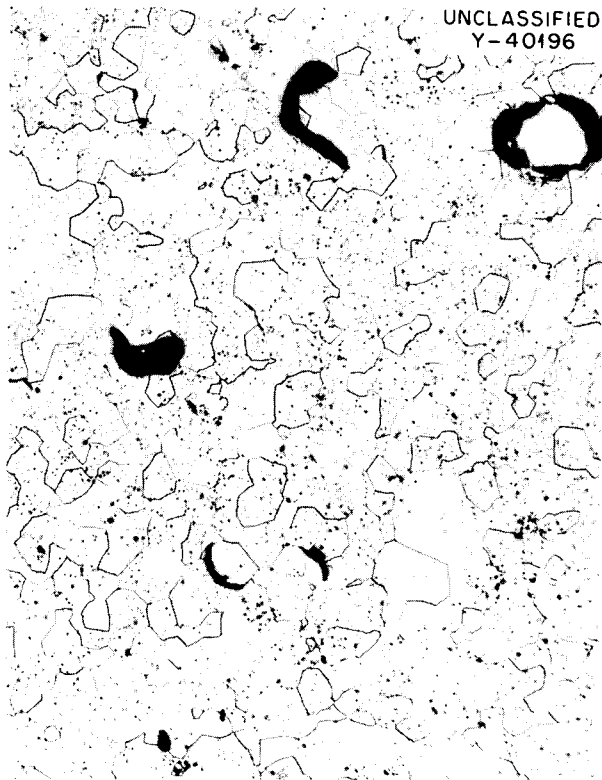


Fig. 25.2.  $\text{UO}_2$  Pellet Prepared by Cold-Pressing  $\text{UO}_2$  Powder Followed by Sintering for 2 hr at  $1750^\circ\text{C}$  in Hydrogen. Etchant: 7:1:2  $-\text{H}_2\text{O}:\text{HNO}_3:\text{H}_2\text{O}_2$  (30%). 200X.

grain size (averaging about ASTM 6) and the abundance of isolated porosity. The microstructure of the fused  $\text{UO}_2$ , shown in Fig. 25.3, exhibits little or no inherent porosity, but a substantial amount of an unidentified second phase can be observed. The material also contained numerous cracks, which caused difficulty in preparing the specimens.

A penetration plot for each type of  $\text{UO}_2$  is shown in Fig. 25.4. The curvature observed for sintered  $\text{UO}_2$  was found to be typical for this material over the temperature range investigated,  $1400\text{--}1950^\circ\text{C}$ , and is an indication that penetration did not occur solely by a lattice diffusion mechanism. A method for subtracting the nonvolume diffusion contributions was developed and will be reported.<sup>11</sup> Application

<sup>11</sup>T. S. Lundy and J. I. Federer, "A Method for Separating Grain Boundary and Lattice Diffusion Effects in Polycrystalline Materials," technical note to be submitted to the *Transactions of the Metallurgical Society of the AIME*.

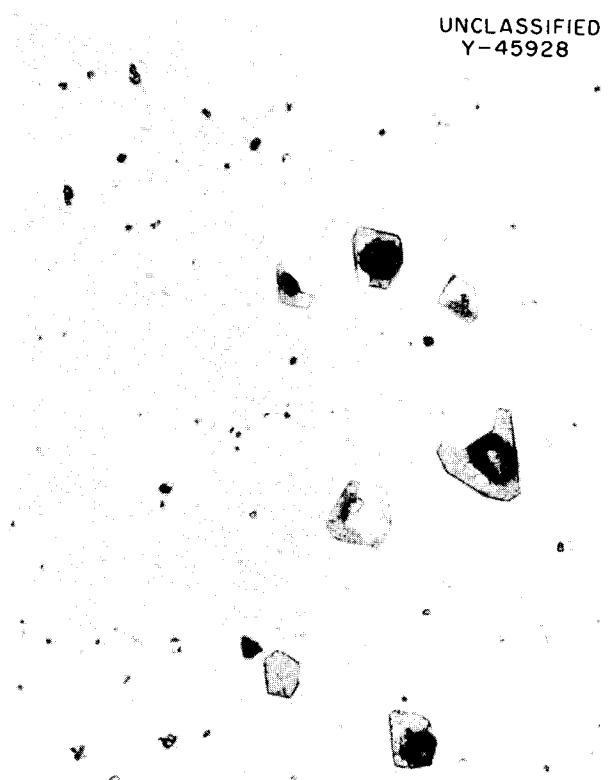


Fig. 25.3. Fused  $\text{UO}_2$  Single Crystal Prepared by Spencer Chemical Company. As-polished. 500X.

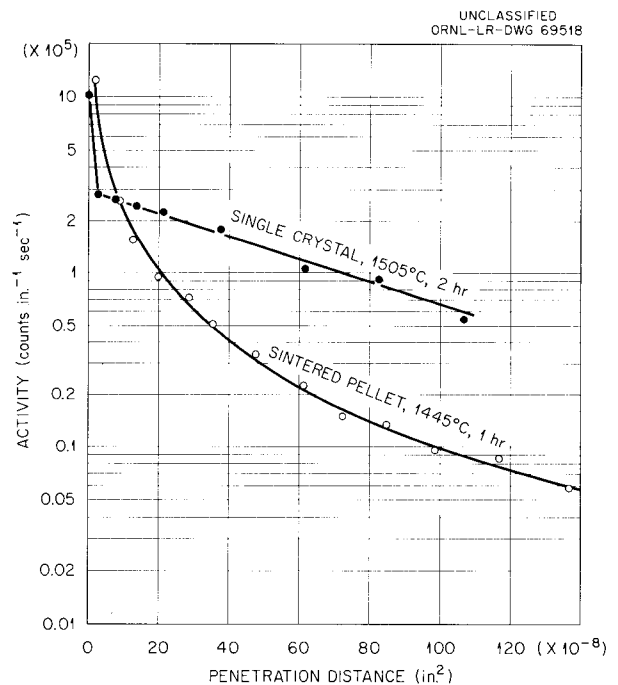


Fig. 25.4. Diffusion of  $\text{Nb}^{95}$  in  $\text{UO}_2$ .

of this technique to the data shown for sintered  $\text{UO}_2$  in Fig. 25.4 resulted in a diffusion coefficient of  $3.4 \times 10^{-11} \text{ cm}^2/\text{sec}$  (1445°C). This technique was also applied to  $\text{Th}^{230}$  diffusion in  $\text{ThO}_2$  (Chap. 24, this report).

The plot for a fused  $\text{UO}_2$  single crystal shown in Fig. 25.4 is linear for depths greater than  $5 \mu$ . The high activity in the first section is attributed to a slow rate of cation interchange between niobium oxide and  $\text{UO}_2$ . The diffusion coefficient calculated from the slope of this plot is  $1.46 \times 10^{-10} \text{ cm}^2/\text{sec}$  (1505°C), which is in reasonable agreement with the value mentioned above for sintered  $\text{UO}_2$  after separating the grain-boundary effects. For comparison, the diffusion coefficient at 1505°C for the self-diffusion of  $\text{U}^{235}$  in  $\text{UO}_2$  is  $6.5 \times 10^{-15} \text{ cm}^2/\text{sec}$  (ref 12) and for  $\text{Xe}^{133}$  in  $\text{UO}_2$  is  $5 \times 10^{-14} \text{ cm}^2/\text{sec}$  (ref 13). These coefficients for self-diffusion and diffusion of  $\text{Nb}^{95}$  in  $\text{UO}_2$  are indicative of the possibly large difference in release rates of fission products from ceramic fuel materials.

### $\text{Ti}^{44}$ DIFFUSION IN TITANIUM

J. F. Murdock      T. S. Lundy

A program was initiated to study the self-diffusion of titanium over the range 700 to 1600°C. Titanium has a low-temperature close-packed hexagonal crystal structure and transforms at 885°C

<sup>12</sup>A. B. Auskern and J. Belle, *J. Nuclear Materials* 3(3), 311 (1961).

to a body-centered cubic crystal structure which is stable to the melting point at 1720°C.

The technique for studying the self-diffusion of titanium involves the following steps: (1) depositing the radioactive isotope on a polished flat end of an inactive right circular cylinder of pure titanium, (2) isothermally annealing the specimen at some temperature, (3) determining the activity profile in the specimen after the anneal, (4) determining diffusion coefficients from these activity profiles, and (5) determining the temperature dependence of the diffusion coefficients from a series of specimens.

The radioisotope being used in this experiment,  $\text{Ti}^{44}$ , was produced<sup>14</sup> by a  $(p,2n)$  reaction with natural  $\text{Sc}^{45}$ . After exposure the target was treated to remove the  $\text{Ti}^{44}$  as a carrier-free isotope contained in a concentrated  $\text{HCl}$  solution.<sup>15</sup> The solution is being used directly by depositing small portions on the inactive titanium and evaporating the solvent to dryness.

The inactive specimens were prepared from arc-melted and cast iodide titanium. Four specimens diffusion-annealed between 900 and 1100°C are being evaluated.

<sup>13</sup>A. H. Booth and G. T. Rymer, *Determination of the Diffusion Constant of Fission Xenon in  $\text{UO}_2$  Crystals and Sintered Compacts*, AECL-692 (Aug. 1958).

<sup>14</sup>The scandium bombardment was performed in the 86-in. ORNL Cyclotron under the direction of J. J. Pina-jian.

<sup>15</sup>The chemical separation was performed by I. Gruverman of Nuclear Science and Engineering Corp., Pittsburgh, Pa.

## 26. Metallurgy of Superconducting Materials

M. L. Picklesimer

E. E. Barton, Jr.

A study<sup>1</sup> of the effects of metallurgical variables on the properties of superconducting materials was started in the past year. The principal effort in the early part of the program will be concentrated on a study of the effects of heat treatment, morphology, impurity content, stoichiometry, and stress state on the critical current-critical field relationships for materials of the Zr-Nb, Nb-Sn, Tc-Zr, Tc-Mo, and Tc-Nb systems. Other alloy systems will be added to the study later.

### NIOBIUM-TIN SYSTEM

Examination of diffusion-couple specimens made from niobium tubing filled with pure tin showed that there are at least three and probably five intermediate phases in the Nb-Sn system, in contradiction to the single Nb<sub>3</sub>Sn phase reported in the literature.<sup>2</sup> The present studies established that the melting points are greater than 1000°C, about 940°C, and about 850°C for the most niobium-rich alloys to the least rich, respectively, of the three phases definitely observed. Microstructural examination in polarized light showed these three phases to have crystal structures with cubic symmetry.

When wire specimens (having a niobium clad over a core of mixed niobium and tin powders in proportion to form Nb<sub>3</sub>Sn) were metallographically sectioned after heat treatment at 1000°C for 16 hr (ref 3), five intermediate phases were found to be

present in the core of the wire in addition to a tin-rich liquid phase and an unreacted niobium powder. The material having this specific composition and heat treatment is reported<sup>3</sup> to have a critical current density of more than 150,000 amp/cm<sup>2</sup> at 4.2°K in a field of 88 kilogauss.

Arc-melted Nb-Sn ingots of five different compositions were obtained and are being sectioned for heat-treatment studies. Differential thermal analysis measurements are being made to establish the melting points accurately. Microstructural examinations of as-cast specimens of the five compositions indicated that there are five intermediate phases in the system, confirming the conclusions of the diffusion couple and wire studies. Two of the phases appeared to have some solubility range. X-ray diffraction measurements of both as-cast and heat-treated specimens are under way.

### ZIRCONIUM-NIOBIUM SYSTEM

Zirconium-niobium alloys in the composition range 25 to 75 wt % Nb have been shown to possess superconducting properties in magnetic field strengths up to 80 to 90 kilogauss.<sup>4</sup> Heat treatment during fabrication has appreciable effects on the critical current density but does not affect appreciably the critical field at low current levels.<sup>5</sup> These compositions lie in the range of the miscibility gap of the body-centered cubic phase over

<sup>1</sup>Jointly with S. T. Sekula of the Solid State Division.

<sup>2</sup>M. I. Agafonova *et al.*, *Akad. Nauk SSSR, Izvest. OTD. Tekh. Nauk, Met. i Toplivo* No. 5, pp 38-41(1959).

<sup>3</sup>J. E. Kunzler *et al.*, *Phys Rev. Letters* 6(3), 89 (1961).

<sup>4</sup>P. R. Aron and H. C. Hitchcock, *Superconductivity of Nb-25 % Zr Alloy in High DC Magnetic Fields*, UCRL-9790 (July 18, 1961).

<sup>5</sup>P. R. Aron and H. C. Hitchcock, *Anomalous Critical Currents in Nb-25 % Zr Wire*, UCRL-10087 (Feb. 16, 1962).

the range 610 to 980°C for pure alloys.<sup>6</sup> Each of these alloys can undergo the solid state reactions  $\beta \rightarrow \beta\text{Zr} + \beta\text{Nb}$  between 610 and 980°C max and  $\beta \rightarrow \alpha\text{Zr} + \beta\text{Nb}$  below 610°C.

Since the transformation structures should strongly influence the superconducting properties, the transformation kinetics and morphologies are being studied. While the alloys studied to date have been too inhomogeneous to permit quantitative measurements, the studies of the alloys containing 60 to 75% Nb have shown that (1) a lamellar structure is produced sluggishly at 800 to 900°C, relatively rapid at 600 and 700°C but too fine to be resolved optically, and not at all at 500°C in 24 hr, (2) the composition (including impurity content) affects the reaction rate appreciably, an increase in zirconium content increasing the rate, (3) reactions at 500 and 600°C do not seem to produce  $\alpha$ -zirconium in the initial reaction, and (4) segregation during freezing is quite severe and an important problem. Chemical etching techniques produced pits too deep to permit satisfactory replication of the structures for electron microscopy. Cathodic etching with ionized argon has not produced the sharpness of structure necessary to resolve the lamellae.

Critical temperatures in zero field and at low current levels were determined (by S. T. Sekula) as a function of composition for the alloy system. The data obtained confirm the results of another study reported before this information could be submitted for publication.<sup>7</sup>

A few tests in high fields were made on both straight-wire and coil specimens of various compositions of the Zr-Nb system to develop the experimental technique. The results in general agreed with the data and experience of others, primarily in that the maximum currents in the coil specimens are only a fraction of the straight-wire values.

Tensile tests (by S. T. Sekula) of commercial 25% Zr-75% Nb 0.010 in. in diameter in the as-fabricated condition showed that the ultimate tensile strength is about 330,000 psi at 4.2°K.

<sup>6</sup>B. A. Rodgers and D. F. Atkins, *Trans. Am. Inst. Mining Met. Engrs.* 203, 1034-41 (1955).

<sup>7</sup>J. K. Hulm and R. D. Blaugher, *Phys. Rev.* 123(5), 1569-80 (1961).

## TECHNETIUM

The critical temperature in zero field of metallic technetium<sup>8</sup> has been reported<sup>9</sup> to be 11.2°K, and to be the highest critical temperature for pure elements. In the interest of determining whether technetium-base alloys also have high field properties so that hypotheses developed from the study of niobium-base alloys can be evaluated on another alloy base, a study of technetium and technetium-base alloys has been incorporated into the present program.

Technetium-99 does not occur naturally and is obtained only as a fission product of uranium. Technetium-99 decays to Ru<sup>99</sup> by beta decay with a 0.29-Mev electron emission and has a specific activity of  $2.08 \times 10^{-2}$  curie/g.<sup>10</sup> This activity level is low enough to permit standard glove-box operations but is difficult to detect and monitor, making the spreading of contamination a hazard. Little is known of the toxicity of technetium compounds with the exception that injected technetium has been reported<sup>11</sup> to be "concentrated by the thyroid gland of rats equally as well as iodine."

The crystal structure of metallic technetium has been reported to be close-packed hexagonal<sup>12</sup> and its melting point<sup>13</sup> to be 2140°C  $\pm$  20. No allotropic transformation has been observed.<sup>14</sup>

Fifty grams of hydrogen-reduced technetium-metal powder was obtained and pressed into 5-g pellets. The first attempts to arc melt the pressed pellets resulted in a 4-g ingot and considerable contamination of the melting furnace because of volatilization of technetium. Later melts were made by induction-melting in high vacuum to reduce the oxygen content and then remelting in an arc furnace. Numerous melts of pure technetium were made

<sup>8</sup>D. M. Hewette, formerly of the Metallography group, developed the techniques for and metallographically prepared the technetium alloy specimens.

<sup>9</sup>J. G. Daubt and J. W. Cobble, *Phys. Rev.* 92, 507 (1953).

<sup>10</sup>G. E. Boyd, *J. Chem. Educ.* 36, 3 (1959).

<sup>11</sup>E. J. Bauman *et al.*, *Am. J. Physiol.* 185, 71 (1956).

<sup>12</sup>R. C. L. Mooney, *Phys. Rev.* 72, 1269 (1947).

<sup>13</sup>G. W. Parker *et al.*, *Chem. Div. Ann. Progr. Rept. Dec. 31, 1951*, ORNL-1260, p 29.

<sup>14</sup>P. W. Bridgman, *Proc. Am. Acad. Arts Sci.* 84, 111 (1955).

in this way without contamination of the arc furnace; the largest single ingot weighed 28 g.

The first attempt at fabricating the arc-melted buttons of technetium was by cold-rolling. The button was reduced approximately 50% in thickness before severe cracking started. All subsequent attempts at fabrication have been by press forging from 900°C after vacuum encapsulation in Inconel capsules, and all have been successful.

As-received technetium-metal powder was examined metallographically and found to be contaminated with both dissolved oxygen and entrapped oxide. The powder had been hydrogen-reduced at 700°C, a temperature apparently too low to completely reduce the oxides to metal.

Metallographic examination of as-cast technetium confirmed the report<sup>14</sup> that there is no allotropic transformation and that the crystal structure is noncubic. Preliminary studies indicated that the recrystallization temperature of severely worked purified technetium is below 700°C and that it is difficult to break up the as-cast grain structure.

A rectangular specimen was cut from one of the cold-rolled sections of purified technetium, platinum leads were attached by spot welding, and the specimen was encased in cellulose acetate, applied from an acetone solution, for contamination control. The critical temperature in zero field was found to be 8.26°K by a resistance measurement (made by S. T. Sekula). This value indicates that the previously reported value of 11.2°K was probably due to the oxygen contamination observed in all metallic powder examined to date.

Attempts to chemically etch metallographic specimens of purified technetium showed the purified metal to be resistant to all common mineral acids, and all combinations of them that were tried, including concentrated HF. Strong oxidizing agents

were tried with and without mineral acids without success. The only successful etchant technique found was 10% oxalic acid used electrolytically.

### TECHNETIUM-ZIRCONIUM SYSTEM

Five alloys of the Tc-Zr system were arc-cast into 10-g buttons. Three of the alloys were so brittle that they cracked into small pieces during press forging from 900°C. Only the terminal alloys were forgeable. Examination of the as-cast microstructure showed the 90 wt % Tc-10 wt % Zr ingot to consist of a primary cubic phase with a small amount of divorced eutectic formed with a second cubic phase, the 82% Tc-18% Zr ingot to contain appreciable volumes of two cubic phases, and the 50% Tc-50% Zr ingot to consist of a major noncubic phase and a very minor amount of a cubic phase. From x-ray diffraction data the first two phases were found to be body-centered cubic and the third phase to be close-packed hexagonal. It seems odd that the addition of 10% Zr to technetium should have resulted in the formation of two cubic phases instead of resulting in a solid solution of zirconium in close-packed hexagonal technetium. Microstructural examination of the Tc-Zr alloys indicated that the phase diagram of this system is likely to be quite complicated.

### TECHNETIUM-MOLYBDENUM SYSTEM

Five 10-g arc castings of the Tc-Mo system were made and press-forged from 900°C in Inconel capsules. Two of the alloys shattered during the forging. All have been removed from their capsules and are being prepared for metallographic examination.

## 27. Zirconium Alloy Research

M. L. Picklesimer

The developmental studies of zirconium-base alloys for use as structural materials in several water-cooled and/or moderated reactor systems are being conducted along three lines of research simultaneously: (1) physical metallurgy, consisting of transformation kinetics and morphologies, mechanical properties, phase diagrams where necessary, heat treatment response, and amounts and compositions of phases present at various temperatures of interest in the oxidation studies; (2) effects of composition, temperature, and environment on the oxidation-corrosion rates in the thin film stages; and (3) effects of alloy composition and oxidation environment on the structural properties of thin oxide films *in situ*.

### PHYSICAL METALLURGY OF ZIRCONIUM ALLOYS

M. L. Picklesimer      P. L. Rittenhouse

The alloy systems under study are Zr-Nb, Zr-Mo, Zr-Pd, and Zr-Cu of hypoeutectoid, hypereutectoid, and eutectoid compositions; Zr-15% Nb-X; and Zircaloy-2. Data on the transformation kinetics, structures, and sequences as determined by hardness measurements, microstructural examination, resistivity measurements, and x-ray diffraction studies have been reported for most of the alloys.<sup>1-3</sup>

<sup>1</sup>M. L. Picklesimer *et al.*, *Met. Div. Ann. Progr. Rept.* Oct. 10, 1957, ORNL-2422, p 117; Oct. 10, 1958, ORNL-2632, pp 67-70 (classified).

<sup>2</sup>G. M. Adamson *et al.*, "Metallurgy," *HRP Quarterly Progress Reports* for periods October 31, 1956, through October 31, 1958.

<sup>3</sup>M. L. Picklesimer *et al.*, *Met. Div. Ann. Progr. Rept.* July 1, 1960, ORNL-2988, pp 167-82; May 31, 1961, ORNL-3160, pp 48-53.

The work during the past year was concentrated on the equilibrium phase boundaries, transformation kinetics, and transformation morphologies occurring in the zirconium-rich end of the Zr-Nb alloy system. Hardness measurements, resistivity-temperature data, aging data by resistivity measurements at temperature, and microstructural examination were used in the study. Additional work was done on refining and understanding the strain-strain analysis<sup>4</sup> for determining the strain anisotropy of  $\alpha$ -zirconium alloys.

### Zr-15% Nb-X

Previous studies of the beta-quench and reheat transformation of the Zr-Nb and Zr-Nb-X alloys showed that the retained  $\beta$  phase transforms to a  $\beta$  phase enriched in niobium and a metastable transition phase poor in niobium ( $\omega$  phase). The principal means of study have been by x-ray diffraction, resistivity measurements, and hardness measurements. The  $\omega$  phase is not detectable by optical or electron microscopy. Several anomalous results in these studies had suggested that the formation of an  $\omega$  phase was appreciably affected by quenching rate, quenching temperature, and time of room-temperature aging before aging at elevated temperatures. The results of investigations completed during the report period confirmed the conclusions reached during the preliminary study.

The aging response at 400°C (the temperature for maximum rate of aging in this set of alloys) for

<sup>4</sup>P. L. Rittenhouse and M. L. Picklesimer, *Metallurgy of Zircaloy-2: Part I - The Effects of Fabrication Variables on the Anisotropy of Mechanical Properties*, ORNL-2944 (Oct. 13, 1960); *Part II - The Effects of Fabrication Variables on the Preferred Orientation and Anisotropy of Strain Behavior*, ORNL-2948 (Jan. 11, 1961).

the Zr-15% Nb-2% Pd alloy after various beta treatments and room-temperature agings is shown in Fig. 27.1. The curves of Fig. 27.1 show that higher "betatizing" temperatures shorten the incubation

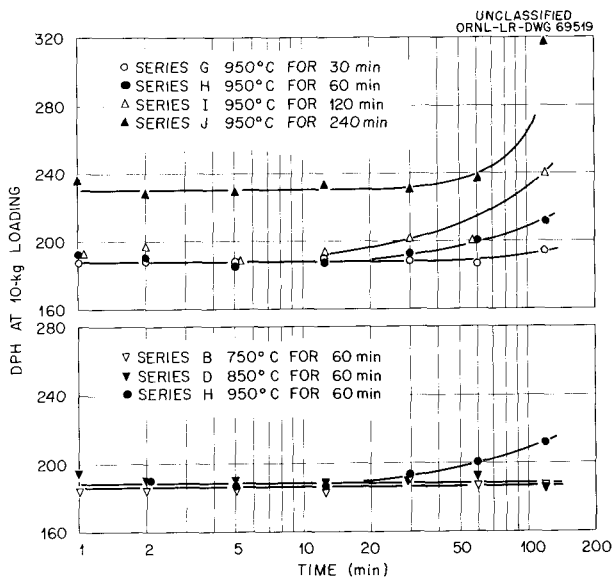


Fig. 27.1. Effect of "Betatizing" Temperature and of Time of "Betatizing" on the 400°C Aging Response of a Zr-15% Nb-2% Pd Alloy. All specimens water-quenched and held at temperature for 16-24 hr before aging.

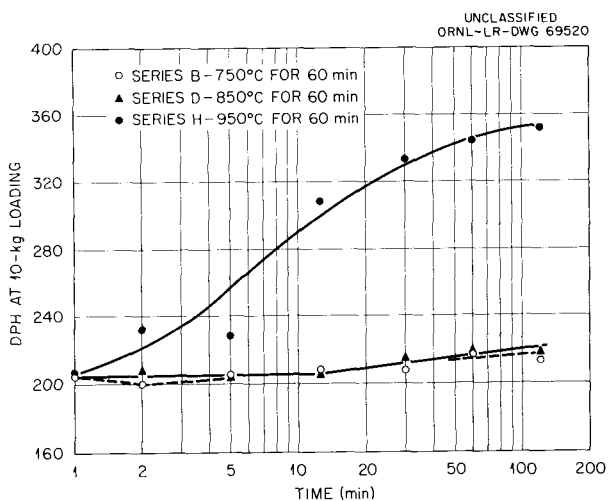


Fig. 27.2. Effect of "Betatizing" Temperature on the 400°C Aging Response of a Zr-15% Nb Binary Alloy.

time, as does increasing the holding time at temperature. The increased hardness level for all aged specimens held for 240 min at 950°C has not yet been accounted for. Increased aging time (0-72 hr) at room temperature after quenching from 750°C did not produce a change in aging response in 2 hr for the Zr-15% Nb-2% Pd alloy in contrast to an increased aging rate with room-temperature aging observed for the Zr-15% Nb binary alloy quenched from 950°C (Fig. 27.2). The effect of adding 2% Pd to the binary Zr-15% Nb alloy can be seen by comparing Figs. 27.1 and 27.2. The effects of room-temperature aging and controlled-cooling rate from various "betatizing" temperatures are still being evaluated. The evidence collected to date verifies that the aging response for the formation of  $\omega$  phase is affected by the vacancy concentration of the alloy at the time of aging at elevated temperature.

Previous studies of the formation of  $\omega$  phase were conducted by measuring hardness values at room temperature after the specimens were quenched from the aging temperature. Since it is possible that such data could be affected by the final quenching, hot-hardness data during aging at 400 and 500°C were determined for a Zr-15% Nb alloy water-quenched from 950°C<sup>5</sup>. The data are presented in Fig. 27.3 and show, when compared with earlier

<sup>5</sup>Data obtained by G. Hallerman, Metallography Section.

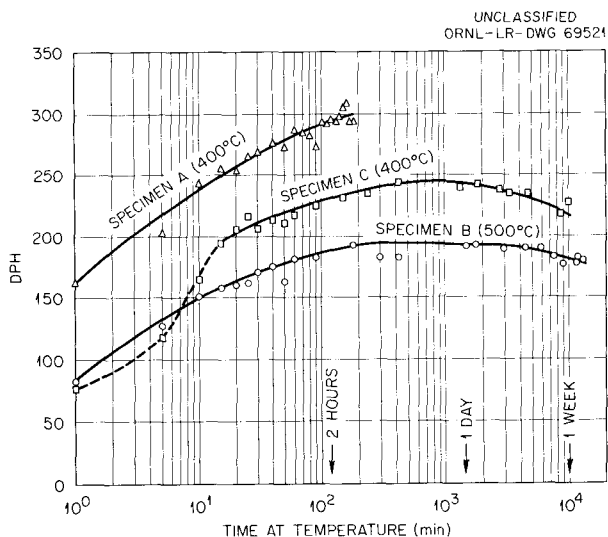


Fig. 27.3. Hot-Hardness Measurements of 400 and 500°C Aging of a Zr-15% Nb Binary Alloy.

data,<sup>6</sup> that for aging times up to one week the temperature at which the hardness measurements are made do not affect the rate data but only the hardness values actually measured (i.e., maximum hardness value at 400°C is 320 DPH, while the maximum hardness value measured at room temperature after aging at 400°C is 400 DPH).

### Solubility of Niobium in $\alpha$ -Zirconium

In the study of the transformation kinetics of alloys of the Zr-Nb system by resistivity measurements, it was necessary to determine the change in the resistivity-temperature relationships with composition. Several features of the resistivity-temperature curves for alloys containing up to 5% Nb seemed anomalous when checked with microstructural examination of control specimens heat-treated at 500 to 900°C. In addition, the increased im-

portance of lean Zr-Nb alloys as possible replacements for Zircaloy-2 and the difficulty of predicting heat-treatment response<sup>7</sup> of the alloys by use of the available diagrams (which are in disagreement as to the solubility limits of niobium in  $\alpha$ -zirconium) led to a reexamination of the  $\alpha$ -zirconium portion of the Zr-Nb phase diagram.

Heating and cooling curves combined with aging curves at various temperatures (using resistivity measurements) were obtained for zirconium alloys containing from 0.5 to 5% Nb. Typical resistivity-temperature curves are presented in Figs. 27.4 – 27.6 and a typical aging curve in the  $\alpha + \beta$  field is given in Fig. 27.7. These curves indicate that use of the temperature point of maximum resistivity may be a valid means of locating the  $\alpha/\alpha + \beta$  temperature for each alloy. If such is the case, the solubility curve so determined is in agreement with

<sup>6</sup>G. M. Adamson *et al.*, *HRP Quar. Progr. Rept.* Jan. 31, 1957, ORNL-2272, p 119.

<sup>7</sup>W. Evans and L. G. Bell, *Progress Report July 1, 1960 to Sept. 30, 1960, Chemistry and Metallurgy Division*, PR-CM-23, Sec. 5.2.5, p 83.

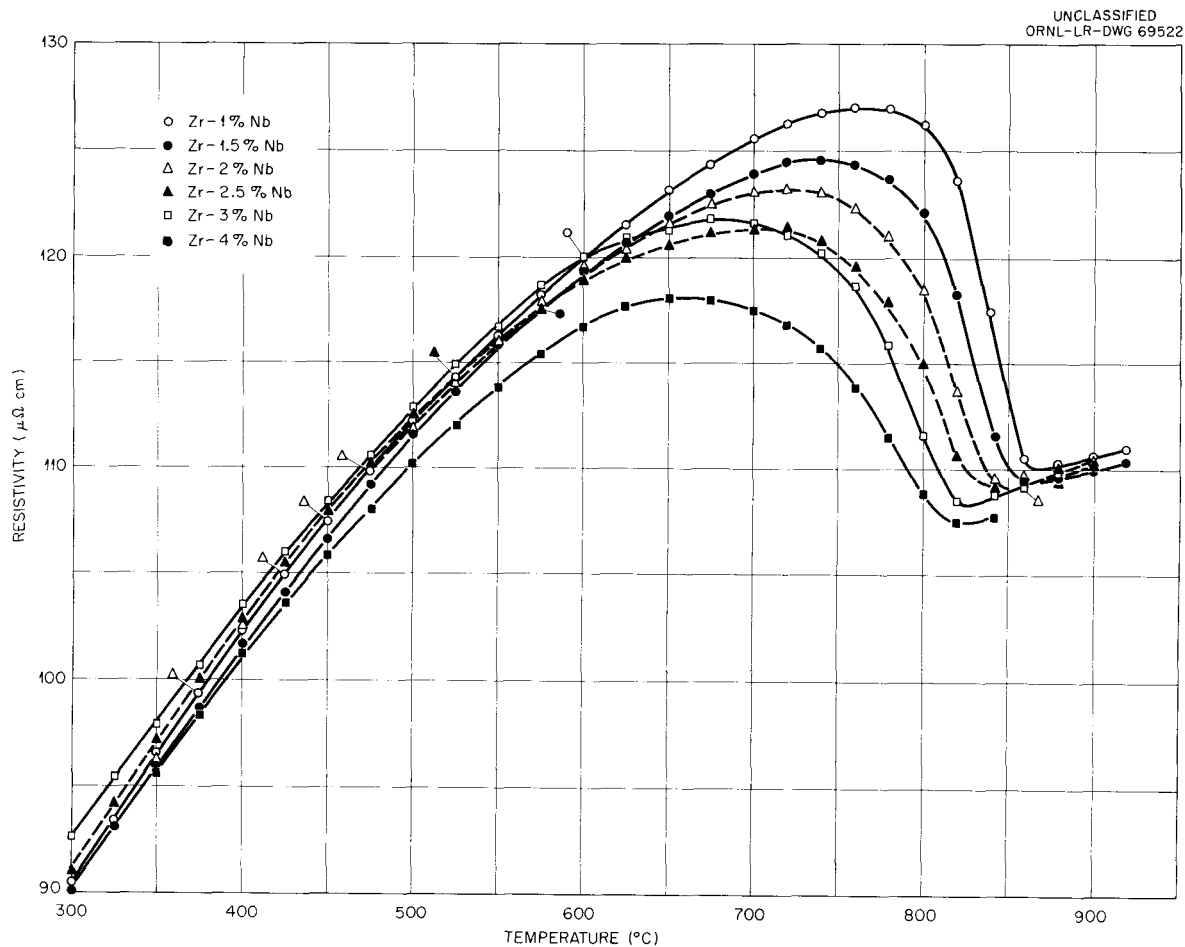


Fig. 27.4. Resistivity-Temperature Curves on Heating for Several Zr-Nb Alloys.

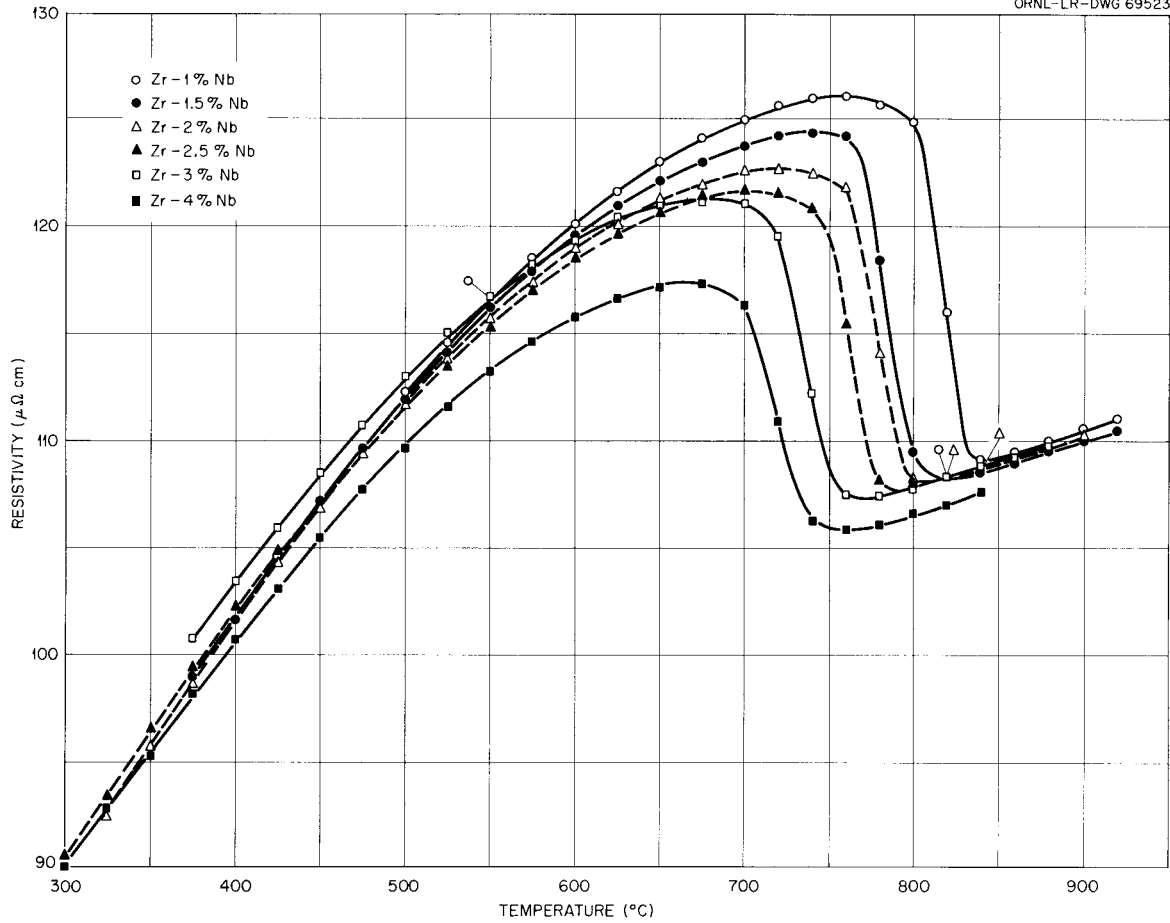


Fig. 27.5. Resistivity-Temperature Curves on Cooling for Several Zr-Nb Alloys.

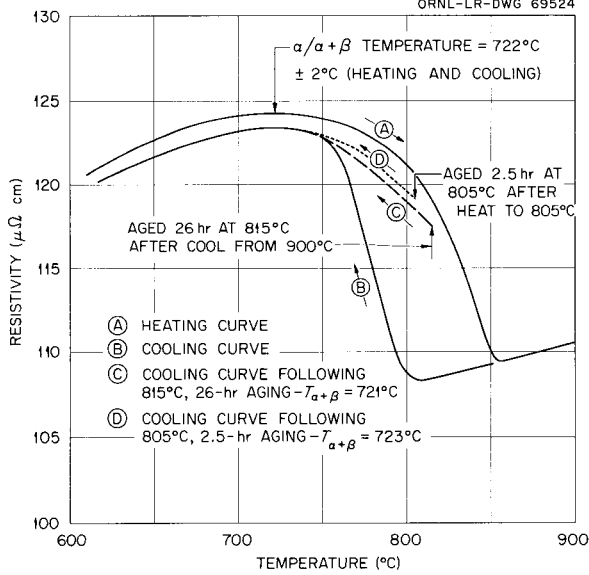


Fig. 27.6. Resistivity-Temperature Curves for a Zr-2% Nb Alloy After Various Agings in the  $\alpha + \beta$  Field.

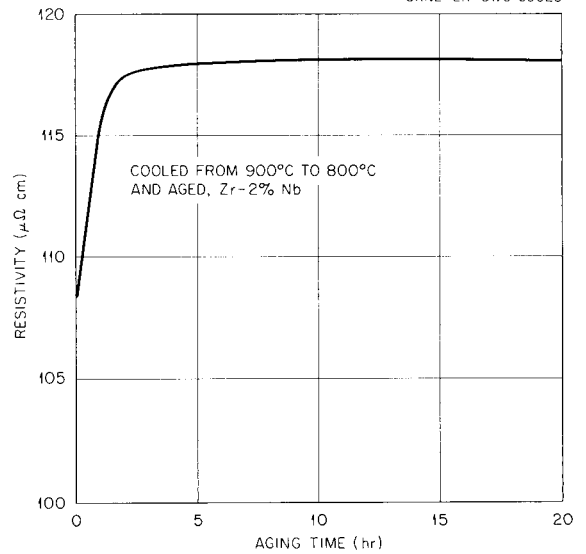


Fig. 27.7. Resistivity-Time Curves for a Zr-2% Nb Alloy Aged at 800°C.

that obtained by Rodgers and Adkins,<sup>8</sup> who report the maximum solubility at the eutectoid temperature to be 6% Nb; a maximum solubility of less than 0.6% Nb was reported by Lundin and Cox.<sup>9</sup>

Microstructural examination of specimens of alloys containing 0.5 to 10% Nb and heat-treated at 20° intervals from 500 to 900°C showed that they were two-phase microstructurally, which contradicts the solubility data determined by resistivity. This also implies that none of the available phase diagrams are correct. While the examination is not yet complete the data available can be explained only by the postulation that an intermediate phase exists between the  $\alpha$  and  $\beta$  phases at temperatures near the eutectoid temperature. The investigation will be continued.

### Zirconium-Palladium System

Since reporting<sup>10</sup> the initial work on the determination of the Zr-Pd phase diagram by resistivity measurements and metallography, additional resistivity measurements were made and the problem of metallographically etching heat-treated specimens was solved. The data determined agree with a phase diagram reported<sup>11</sup> for the system during this period. Further work on alloys of this system has been suspended until the study of the transformation kinetics of the eutectoid can be started.

### Strain Anisotropy of Zircaloy-2

A study of the effects of fabrication variables on the preferred orientation, strain anisotropy, and mechanical properties of Zircaloy-2 has been reported.<sup>12</sup> At that time, however, the validity of

<sup>8</sup>B. A. Rogers and D. F. Adkins, *Trans. Met. Soc. AIME* 203, 1034-41 (1955).

<sup>9</sup>C. E. Lundin and R. H. Cox, *The Determination of the Equilibrium Phase Diagram, Zirconium-Niobium*, TID-11919 (August 1960).

<sup>10</sup>M. L. Picklesimer, *Met. Div. Ann. Progr. Rept.* May 31, 1961, ORNL-3160, p 50.

<sup>11</sup>K. Anderko, *Z. Metallk.* 50(12), 681-86 (1959).

<sup>12</sup>P. L. Rittenhouse and M. L. Picklesimer, *Metallurgy of Zircaloy-2: Part I - The Effects of Fabrication Variables on the Anisotropy of Mechanical Properties*, ORNL-2944 (Oct. 13, 1960); *Part II - The Effects of Fabrication Variables on the Preferred Orientation and Anisotropy of Strain Behavior*, ORNL-2948 (Jan. 11, 1961).

applying Hill's theory of anisotropy<sup>13</sup> to material that is intrinsically anisotropic was not known. The data obtained since those reported in ref 12 show that Hill's theory as developed cannot be applied to Zircaloy-2 and that the strain-strain analysis developed is of more fundamental importance and of wider applicability than had been realized.

Glancing x-ray diffraction photographs of specimens of one schedule (schedule J, Part II of ref 12) have shown that the distribution of the preferred orientation is not symmetric about the fabrication directions and that no axes of anisotropy can be defined for this particular texture. The existence of axes of anisotropy and their location with reference to the principal fabrication directions must be known before Hill's theory can be applied, since both are required by the assumptions of this theory.

The principal components of the textures not previously determined in several schedules of Zircaloy-2 were measured by x-ray diffraction methods and compared with the textures predicted from the strain-strain data determined for these schedules. In every case, the texture predicted from the strain-strain analysis was confirmed by the x-ray diffraction data.

Compression testing of Zircaloy-2 specimens from two schedules of Zircaloy-2 studied showed that the yield strengths in compression and tension are not equal (see Table 27.1). The equality of

<sup>13</sup>R. Hill, *Proc. Roy. Soc. (London)* 193A, 281-97 (1948).

Table 27.1 Room-Temperature Yield Strength of Zircaloy-2 in Tension and Compression

Schedule	Specimen <sup>a</sup> Orientation	Yield Strength (psi)	
		Compression <sup>b</sup>	Tension
		× 10 <sup>3</sup>	
8	RD	66.7	54.9
	TD	62.7	58.3
	ND	122.0	
J	RD	65.6	52.0
	TD	101.3	70.0
	ND	72.5	

<sup>a</sup>RD, rolling direction; TD, transverse direction; ND, normal direction.

<sup>b</sup>Personal communication. S. H. Bush, General Electric, Hanford, Washington, 1961.

yield strengths in compression and in tension is another requirement of Hill's theory of anisotropy.

The  $k$  values, ratio of contractile strain to total or axial strain, measured for specimens stressed in compression are given below (the strain data were determined by the authors; the specimens were tested by S. H. Bush, General Electric, Hanford, Washington):

	Schedule	
	8	J
$k_{xy}$	-0.706	-0.456
$k_{xz}$	-0.294	-0.544
$k_{yx}$	-0.688	-0.514
$k_{yz}$	-0.312	-0.486
$k_{zx}$	-0.480	-0.587
$k_{zy}$	-0.520	-0.413

The second  $k$  equation in ref 14, which was derived from Hill's theory of anisotropy, is experimentally valid since the products of the respective  $k$  values listed above are equal to  $1.00 \pm 0.02$ , an excellent agreement as each  $k$  value can be determined only to an accuracy of  $\pm 0.02$ .

The experimental verification by compression testing of the strain-strain equations<sup>15</sup> developed from Hill's theory of anisotropy and the ability to predict the preferred orientation from a knowledge of the strain-strain data are indicative of the fundamental importance of the strain-strain analysis. They also indicate that the restrictive assumptions of Hill's theory of anisotropy may be unnecessary, allowing wider applicability of his theory.

## OXIDATION-RATE MEASUREMENTS

S. Peterson

The equipment for determination of the oxidation rates of zirconium-base alloys in pure oxygen at 300 to 800°C was rebuilt to permit measurement of the time required to form oxide layers approximately 20 Å thick to an accuracy of 5% or better. The entire apparatus is encased in an air thermostat

<sup>14</sup>P. L. Rittenhouse and M. L. Picklesimer, *Metallurgy of Zircaloy-2: Part II - The Effects of Fabrication Variables on the Preferred Orientation and Anisotropy of Strain Behavior*, p 12, ORNL-2948 (Jan. 11, 1961).

<sup>15</sup>*Ibid.*, pp 11-12.

controlled to 0.1°C or better. Automatic data-plotting instrumentation was designed, built, and installed for the direct plotting of the differential oxidation rate data. The solenoid valve between the oxygen storage system and the specimen chamber was rebuilt for improved operation and sensitivity but still causes a small and slightly variable compression to occur in the specimen system on every closing. It is believed that this error (approx 2%), which is now the limiting error measurement, can be eliminated by use of a valve of different design.

Oxidation-rate measurements were made with the new system on iodide zirconium and Zircaloy-2 in pure oxygen at 10 torr pressure. Data were taken at 450, 500, and 600°C for Zircaloy-2 and at 600°C for iodide zirconium but have not been examined quantitatively because of irregular operating characteristics of the furnace temperature controller. The oxidation-rate data at 600°C are smoother than those at lower temperatures, indicating that the mechanism producing the irregularities is less effective at the higher temperatures. It has been proposed<sup>16</sup> that a defect structure at one of the interfaces of the oxide film periodically builds up and anneals out, causing a pseudocyclic physical compaction of the oxide film and consequently a pseudocyclic change in the instantaneous oxidation rate. The oxidation-rate data obtained to date substantiate the proposed process.

## OXIDE FILM STUDIES

J. C. Banter

A thin-film oxide on a metal substrate may have a different index of refraction from that of the bulk oxide and, if the film is not stoichiometric, may have a defect structure which might change with film thickness, environment, composition of both the oxide and the metal substrate, and strain in the film. Optical measurements may yield information that would characterize the state of the film and reveal the defect structure.

A polarizing spectrometer was obtained for use as an accessory instrument in the optical spectrophotometers to permit a more direct measurement of the optical constants of oxide films *in situ* by reflection techniques. Such determinations require

<sup>16</sup>E. C. Williams and P. C. S. Hayfield, *Inst. Metals (London), Monograph and Rept. Ser. No. 23 (1958)*, pp 131-57.

the measurement of the optical constants of the base metal, free of any film, before the optical constants of the oxide film can be calculated.

Attempts to determine the optical constants of the metal substrate were complicated by the presence of a surface film of finite thickness formed on chemically polished specimens and on a vacuum-annealed specimen exposed to air in the equipment. A high-vacuum capsule for keeping the specimen in the annealing vacuum is being constructed and should permit the desired measurements.

The thin-film oxides *in situ* (produced by anodizing) examined in the polarizing spectrometer appeared to absorb strongly at light wavelengths less than 2500 Å. Optical transmission measurements of thin oxide films (the metal substrate etched away) also indicated this absorption. It has not yet been

shown, however, that the oxide film was not modified by removal of the supporting metal.

A cylindrical lens is being made of a 500-carat strontium titanate boule, which, when used in intimate contact with the oxide films *in situ*, will permit the optical constants of the oxide film to be directly determined by the critical-angle method in the wavelength range 3000 to 6000 Å. With this knowledge, the reflection spectra of the oxide films can be analyzed to determine accurately the film thickness and, hopefully, the defect structure.

X-ray diffraction data showed that the oxide film produced on zirconium alloy specimens by anodization is essentially amorphous (gives no x-ray maxima), but comparison of the optical data for anodized and water-corrosion-produced films *in situ* has shown no optical differences to exist.

## 28. Metallography

R. J. Gray

### SPECIALIZED METALLOGRAPHIC STUDIES AND RELATED EQUIPMENT DEVELOPMENT

#### Electron Metallography

J. O. Stiegler

**Transmission Electron Microscopy Studies of Deformed and Annealed Niobium.** — Preliminary results of a study by transmission electron microscopy of the deformation and annealing behavior of niobium were obtained. Pure niobium containing less than 100 ppm interstitials produced by electron-beam melting and material deliberately doped with several hundred ppm oxygen and carbon were used in the study.

Large single crystals were cut from the electron-beam-melted material and cold-rolled to thicknesses ranging between 0.003 and 0.050 in. They were examined in this state or were annealed, doped, and deformed to the desired level. Foils suitable for transmission-electron microscopy were prepared by chemically polishing the sheet material in solutions varying between 50 ml  $\text{HNO}_3$ –50 ml HF and 90 ml  $\text{HNO}_3$ –10 ml HF, depending on the state of the material. They were then mounted between 75-mesh copper grids and examined directly in the electron microscope. Selected-area-diffraction patterns were obtained of all areas photographed in order to determine their crystallographic orientations. In annealed material, thin areas approximately  $100 \mu$  in diameter were found, while in deformed material, the thin areas were slightly smaller.

During deformation by cold rolling, several different textures develop which are dependent on the orientation of the original crystal with respect to the rolling plane and rolling direction. To date (001) [110],  $(\bar{1}\bar{1}1)$  [110], and  $(\bar{1}\bar{1}3)$  [110] textures have been observed. When all three occur in a

single specimen, they lie in bands 10 to  $100 \mu$  wide and several hundred microns long which run along the rolling direction. All orientations contain a common [110] direction, approximately in the rolling direction; the plane of the foil is rotated about this direction to the (001),  $(\bar{1}\bar{1}1)$ , or  $(\bar{1}\bar{1}3)$  position. Frequently, narrow bands (approx  $1 \mu$  wide), slightly misoriented with respect to one another, are observed in the larger bands. During deformation the small bands rotate about the principal orientation. These orientations are stable in that there is a symmetrical distribution of slip planes in each.

The (001) [110] and  $(\bar{1}\bar{1}1)$  [110] orientations are stable annealing orientations. When a foil is given an intermediate anneal during the deformation, grains having one of these orientations develop and undergo no further change in orientation on subsequent deformation.

Dislocation structures and densities differ among these orientations in a single specimen, as is shown in Figs. 28.1 and 28.2 for the  $(\bar{1}\bar{1}1)$  and (001) areas, respectively, after approximately 95% deformation following an intermediate anneal. The  $(\bar{1}\bar{1}3)$  structure closely resembles that of (001). In all cases the dislocations are arranged in cell walls surrounding regions relatively free of dislocations. In the (001) orientation the cell boundaries are rather diffuse, whereas they are more sharply formed and appear to contain a higher dislocation density in the  $(\bar{1}\bar{1}1)$  orientation. However, the walls appear to lie principally in (110) planes so that the foil is normal to the wall in the (001) orientation and makes a small angle to it in the  $(\bar{1}\bar{1}1)$  orientation, which accentuates the difference. It is not at all surprising that the structures differ, for different combinations of slip systems are operative in the different orientations. In Fig. 28.1 the dislocations in the cell wall are not arranged in dense tangles,

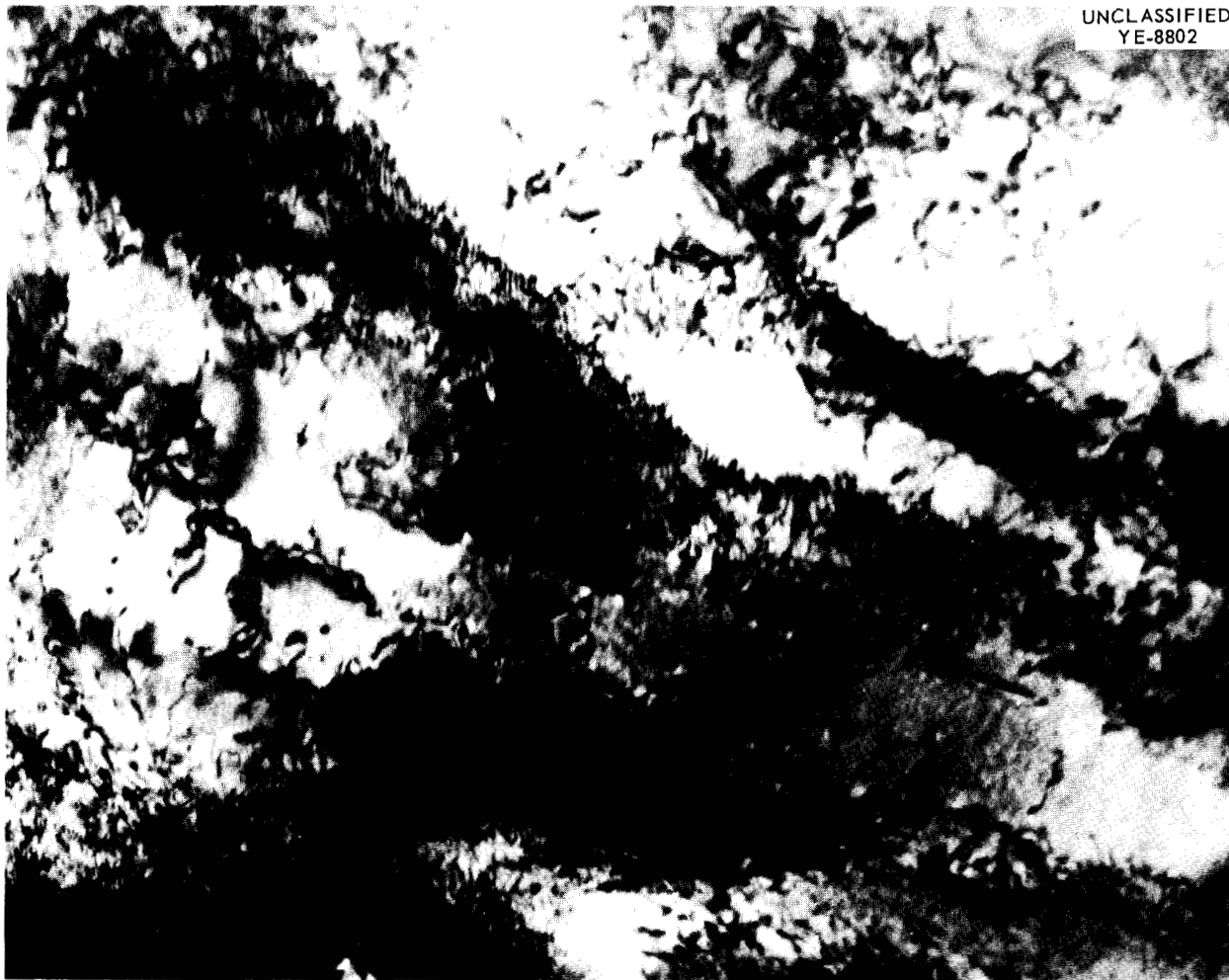


Fig. 28.1. Dislocation Structure in Niobium Having a  $(111) [110]$  Texture Produced by Approximately 95% Deformation by Cold Rolling. 100,000X.

as is commonly observed, but rather in a regular parallel array. This structure is frequently observed in cold-rolled niobium. There is a higher density of dislocations within the cells than in face-centered cubic metals that have high stacking-fault energies and also show well-developed cell structures. The diffraction pattern from the general region of Fig. 28.1 shows spots from cells having  $(111)$  planes parallel to the plane of the foil with their  $(110)$  directions rotated with respect to one another. The cells are too small for a diffraction pattern to be obtained across a single wall to show that neighboring cells are rotated this way, and it is possible that the boundary shown in Fig. 28.1 is a tilt boundary composed of a parallel array of edge dislocations. The cell structure is formed after a few percent deformation. Further deformation does

not change the structure appreciably but does increase the angular misorientation between neighboring cells by increasing the dislocation density in the cell walls.

After a low-temperature anneal (approx  $500^{\circ}\text{C}$  for 1 hr), sharp subgrains are formed in material deformed approximately 95% by cold rolling, and individual dislocations can no longer be observed in the boundaries (Fig. 28.3). A high density of tangled dislocations, however, remains in the subgrains. The fringe structure in a number of the boundaries arises from overlapping grains misoriented with respect to one another.

Annealing for longer times or at a slightly higher temperature ( $600^{\circ}\text{C}$  for 1 hr) results in the beginning of recrystallization, as is shown in Fig. 28.4. The

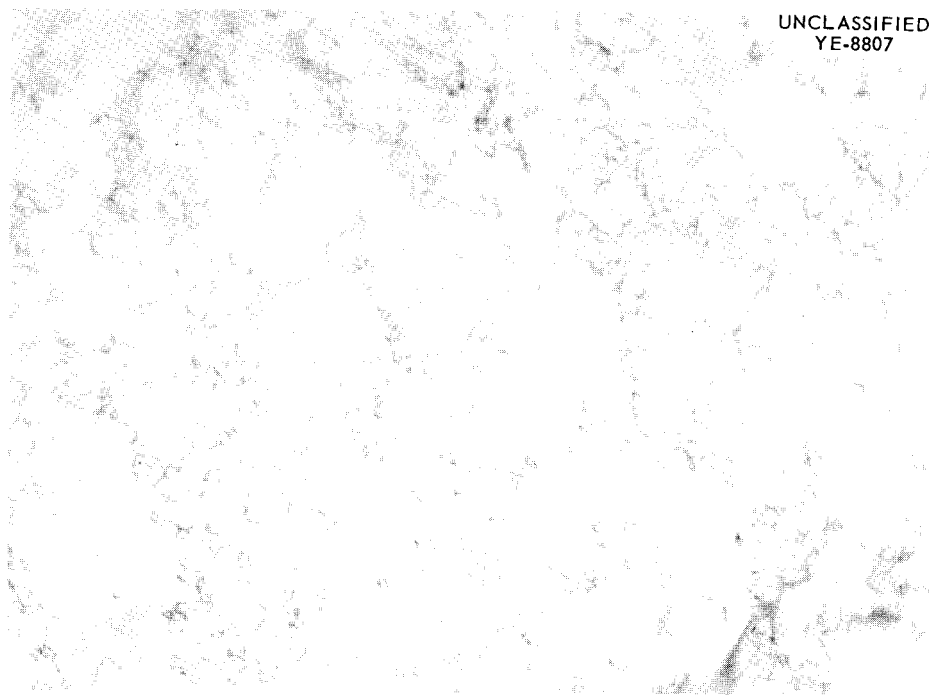


Fig. 28.2. Dislocation Structure in Niobium Having a (001) [110] Texture Produced by Approximately 95% Deformation by Cold Rolling. 35,000X.

recrystallized grains are all small (1 to 2  $\mu$  in diameter) and widely separated at this stage. In addition, they contain a moderately high density of dislocations which are long and straight compared with the short tangles in the polygonized subgrains. The recrystallized grains observed thus far have no orientations not present in the deformed foil. Upon further annealing, the entire foil is filled with recrystallized grains a few microns in diameter. Individual grains grow at the expense of their neighbors and after 1 hr at 1000°C, only a few large grains (approx 1 mm in diameter) are present. In all cases observed to date, these grains have (111) or (001) planes parallel to the plane of the foil; however, they do not appear to contain a common direction.

Complete recrystallization by annealing at 900°C for 1 hr in a vacuum of  $<10^{-6}$  torr reduces the dislocation density considerably over that present in the newly recrystallized grains. In this case, however, the dislocations have a ragged appearance due to precipitation of impurities at them, as is shown in Fig. 28.5. In no case have extended dislocations been observed after this treatment. The impurities appear to be effective in pinning the dislocations.



Fig. 28.3. Subgrain Structure in Niobium Deformed Approximately 95% by Cold Rolling and by Annealing for 1 hr at 500°C. The orientation of this foil is the same as that of Fig. 28.1. 25,000X.

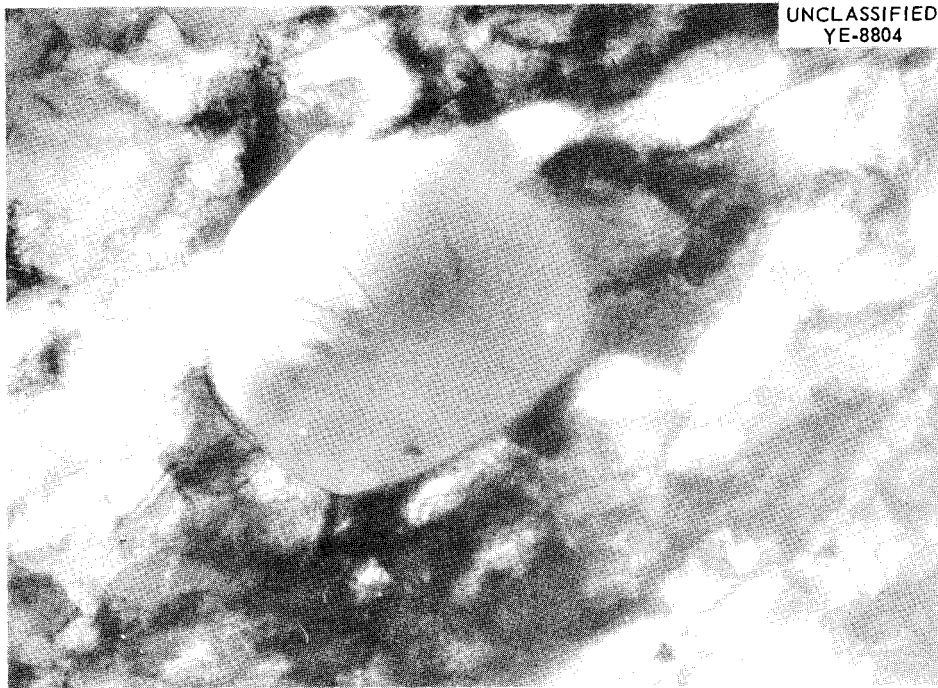


Fig. 28.4. Recrystallized Grain in Niobium Deformed Approximately 95% by Cold Rolling and by Annealing for 1 hr at 600°C. 18,000X.

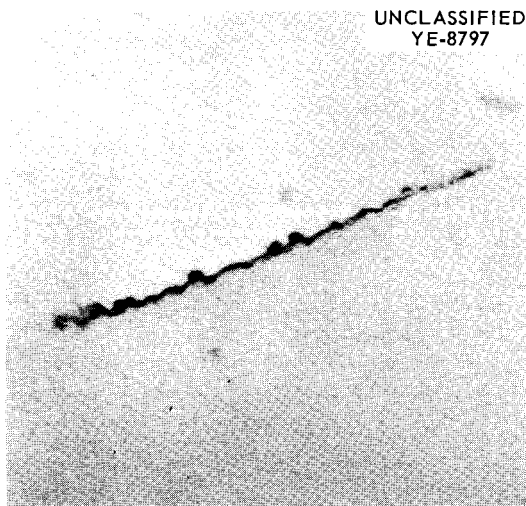
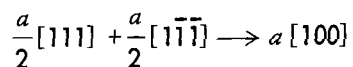


Fig. 28.5. Precipitates at a Dislocation in Niobium Annealed for 1 hr at 900°C. 50,000X.

After high-temperature-annealing treatments, hexagonal-dislocation networks formed by a reaction of the type



are frequently observed, as is shown in Fig. 28.6. The alternating extended and contracted nodes reported by Fourdeux and Berghezan<sup>1</sup> were not observed. Both clean networks produced by short-time, high-temperature anneals and "dirty" ones produced by long-time anneals or in impure material were observed. Presumably, the extended nodes and stacking faults reported previously<sup>1,2</sup> were related to impurities and were either not present in our foils or were too small to be detected.

Foils containing approximately 50, 1000, and 1500 ppm O<sub>2</sub> as determined by weight change have been aged 100 hr at temperatures between 370 and 1040°C. All foils aged at 370°C showed a fine, dot-like precipitate (Figs. 28.6 and 28.7). The density of the precipitate in the specimen containing approximately 1500 ppm O<sub>2</sub> was considerably higher and the size was smaller than in the less contaminated specimens. In all cases, regions near grain boundaries and dislocations were free of precipitate, although the dislocations appeared to be very broad

<sup>1</sup>A. Fourdeux and A. Berghezan, *J. Inst. Metals* 89, 31 (1960).

<sup>2</sup>R. L. Segall, *Acta Met.* 9, 975 (1961).

and contrasty due to enhanced precipitation. Because of this heavy precipitate, it was impossible to determine whether or not the dislocations

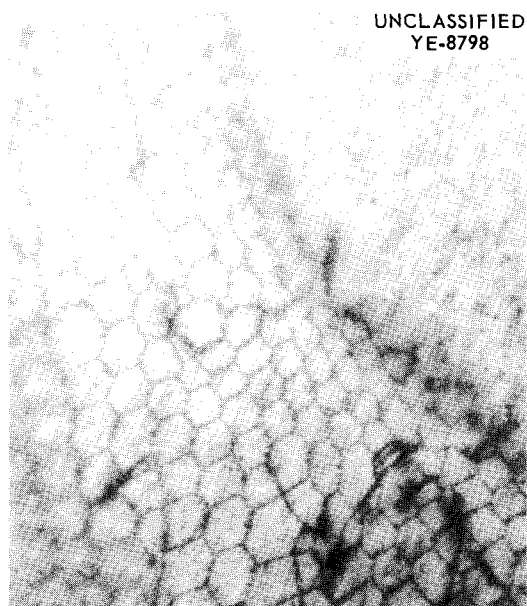


Fig. 28.6. Hexagonal Dislocation Network in Niobium Containing 1500 ppm  $O_2$  Annealed for 1 hr at  $1200^\circ C$  and Aged for 100 hr at Approximately  $370^\circ C$ . 35,000X.

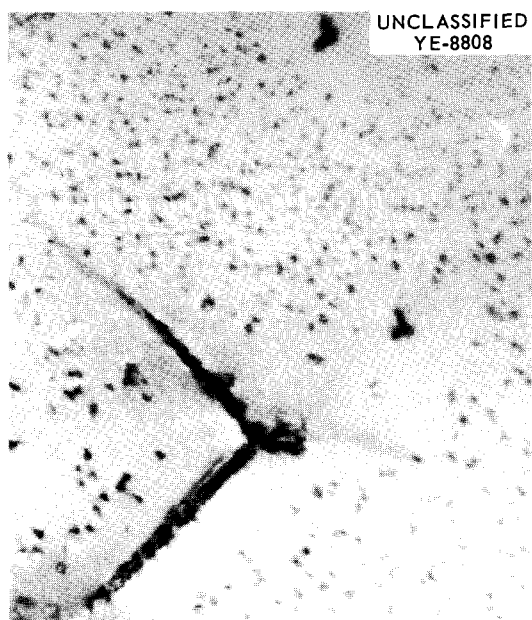


Fig. 28.7. Dot-Like Precipitate in Pure Niobium Treated for 100 hr at Approximately  $370^\circ C$ . 35,000X.

were extended. Aging at temperatures above approximately  $600^\circ C$  produced none of the dot-like precipitate, but did result in "dirty" dislocations.

An oxide of niobium or of an impurity in the electron-beam-melted material evidently precipitates out at less than about  $600^\circ C$ . The appearance of a similar precipitate in the nearly pure foil could be due to slight contamination during the aging process.

Some plate-like precipitates were observed in foils annealed at higher temperatures, but in all such cases the foils had been contaminated, as was evidenced by the appearance of a dark film on the surface.

Specimens containing approximately 500 and 1000 ppm C annealed at  $1000^\circ C$  for 1 hr showed only a few large, isolated precipitates (approx  $0.1 \mu$  in diameter).

#### Elevated-Temperature Hardness Testing

G. Hallerman

Elevated-temperature hardness testing<sup>3</sup> continues to be a useful tool for preliminary evaluation of strength of metals and alloys. In addition, hot hardness has been used in age-hardening studies and in evaluation of high-temperature deformation characteristics for composite plate fabrication of fuel elements. The sensitivity of the hot-hardness testing apparatus was demonstrated by a change in hardness during the allotropic transformation of iron and steel.

**Commercial High-Temperature Alloys.** — Hardness of Haynes alloy No. 25, INOR-8, Inconel, and type 316 stainless steel was determined as a function of temperature to compare their hot-hardness values with those of other high-temperature alloys.

The INOR-8 specimen was annealed at  $2300^\circ F$  for 1 hr, the other specimens at  $2000^\circ F$  for 2 hr prior to hot-hardness testing. Figure 28.8 shows the hardness of these alloys as a function of temperature. A semilogarithmic method of plotting the data resulted in a negative-slope, straight-line plot for each of the specimens tested. The point of deflection of the segments indicates a change in the rate of hardness decrease with temperature for a given alloy. Thus, the points of deflection for

<sup>3</sup>G. Hallerman, *Mel. Div. Ann. Progr. Rept.* May 31, 1961, ORNL-3160, pp 120-24.

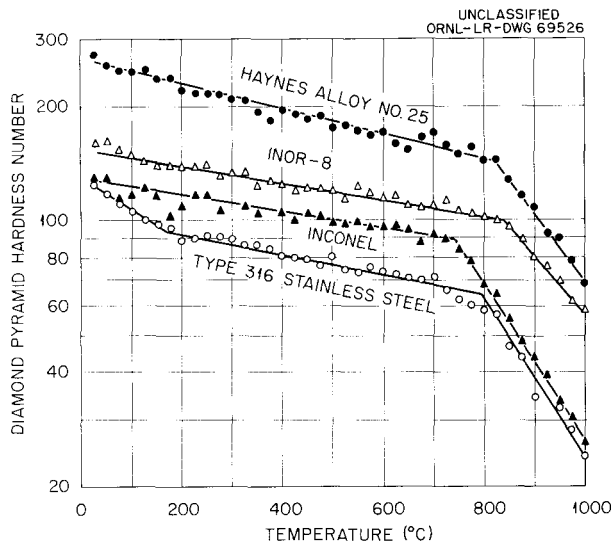


Fig. 28.8. Elevated Temperature Hardness of Haynes Alloy No. 25, INOR-8, Inconel, and Type 316 Stainless Steel.

Haynes alloy No. 25, INOR-8, Inconel, and type 316 stainless steel occur at about 825, 835, 750, and 800°C, respectively.

**Niobium-Vanadium Alloys.** — A series of Nb-V alloys (containing 1, 10, 20, 30, 50, and 60% V) were tested at temperatures up to 1000°C. All specimens were given a prior heat treatment in vacuum for 2 hr at 1200°C. The results are plotted in Fig. 28.9 and show that

1. the hardness decreased relatively little with increase of temperature for all compositions tested,
2. the hardness increased with increase in vanadium content in the entire temperature range for alloys containing up to 30% V,
3. at 1000°C the hardness of Nb-60% V alloy is the same as that of the Nb-10% V and lower than the hardness of the alloys containing 20, 30, or 50% V (hardness vs composition curve, insert in Fig. 28.9).

These results are in good agreement with those obtained at Armour Research Foundation,<sup>4</sup> where it was found that maximum strengthening occurred at about Nb-40% V composition when a vanadium-rich, V-Ni alloy series was tested for ultimate tensile strength at 2000°F.

<sup>4</sup>Paper presented by B. P. Rajala and R. J. Van Thyne at the National Technical Conference on High-Temperature Materials, Cleveland, Ohio, April 26-27, 1961 (AIME).

The usefulness of the hot-hardness tester as a screening tool in alloy development is here again demonstrated, particularly when the simplicity and cost involved are compared with those of elevated-temperature tensile-strength determinations.

**Age Hardening of Haynes Alloy No. 25.** — The customary method of studying age hardening is to interrupt the process of aging by cooling the specimen and measuring its room-temperature hardness. However, the aging process may be conveniently measured while it is occurring at an elevated temperature by making a series of hardness impressions at suitable time intervals. Both methods were used to study age hardening of Haynes alloy No. 25.

Prior to aging, 18 samples of Haynes alloy No. 25 were annealed for 2 hr at 2250°F. Three groups of five specimens were then aged at 1400, 1650, and 1800°F. One specimen from each aging temperature was water-quenched after 4, 16, 32, 64, and 100 hr of aging time. Room-temperature hardness as a function of aging time for these samples is shown in the upper part of Fig. 28.10.

The remaining three samples were used to determine the hardness at the aging temperatures with the aid of the hot-hardness testing equipment. The specimens of this group were heated isothermally — one specimen at 1400°F, one at 1650°F, and one at 1800°F. Hardness impressions were made at various time intervals up to 100 hr. The results of these determinations are shown in the lower part of Fig. 28.10.

Comparison of the two sets of curves shows that the hardness values of the alloy at aging temperatures are lower than the room-temperature hardness of the quenched specimens. Furthermore, overaging is evident in the lower group of curves at all aging temperatures. Finally, the room-temperature hardness curves show that, up to 75 hr of aging time, the 1800°F specimen is the hardest, followed by the 1650 and 1400°F specimens; the reversed order of arrangement of aging curves is seen in Fig. 28.10 for specimens measured at elevated temperatures.

The results show that the hot-hardness method is more suitable than room-temperature hardness measurements for determining the properties of such alloys.

**Aluminum Alloys.** — In composite-plate fabrication of fuel elements both the cladding and the core materials must have similar deformation characteristics so that a uniform cladding thickness and an acceptable metallurgical bond are obtained at hot-rolling temperatures.

UNCLASSIFIED  
ORNL-LR-DWG 69527

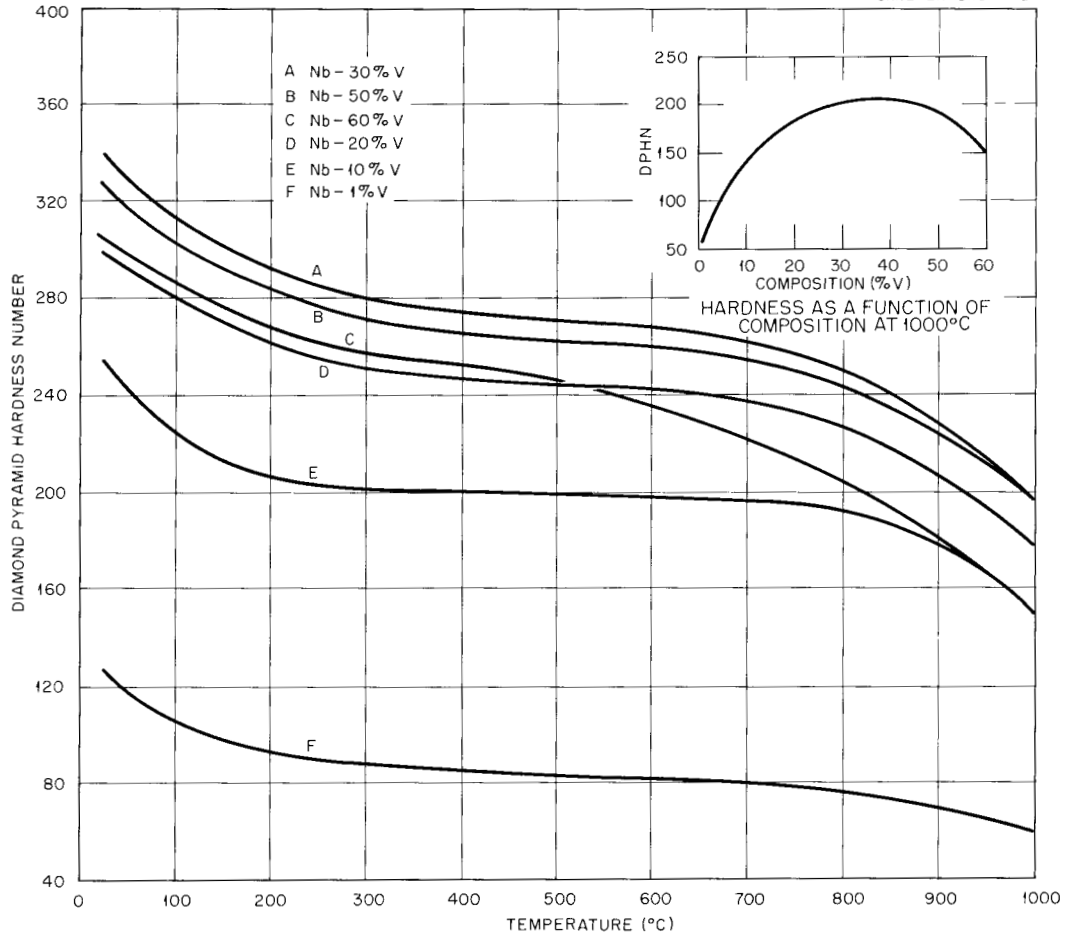


Fig. 28.9. Elevated Temperature Hardness of Nb-V Alloys.

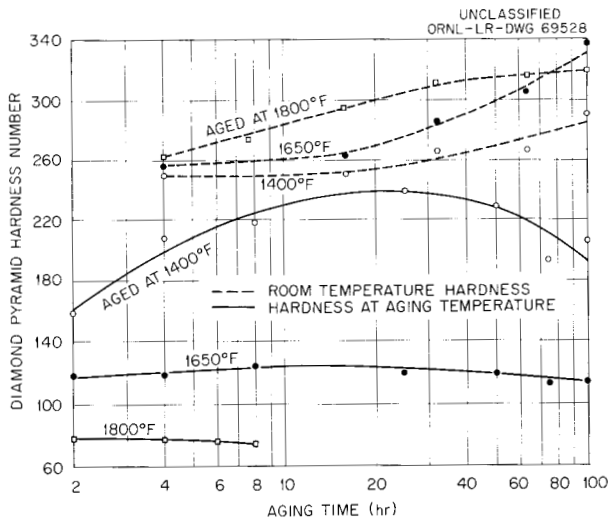


Fig. 28.10. Age-Hardening of Haynes Alloy No. 25.

An evaluation of the high-temperature-deformation characteristics of some aluminum alloys as possible cladding materials for an Al-24% U core has been undertaken. Aluminum alloys 1100, 6061, and 5154 and Al-24% U were tested. All samples were annealed for 3 hr at 500°C and furnace-cooled prior to hot-hardness testing. Results of these determinations are shown in Fig. 28.11. The room-temperature hardness after completion of the hot-hardness runs was essentially the same as that prior to the runs for all alloys examined. Of the commercial alloys, alloy 5154 was the hardest, followed by alloys 6061 and 1100. The same hardness sequence exists at any temperature level. Figure 28.11 also shows that at temperatures above 200 to 250°C the rate of hardness decrease of the three commercial alloys is approximately the same on the semilogarithmic-hardness scale.

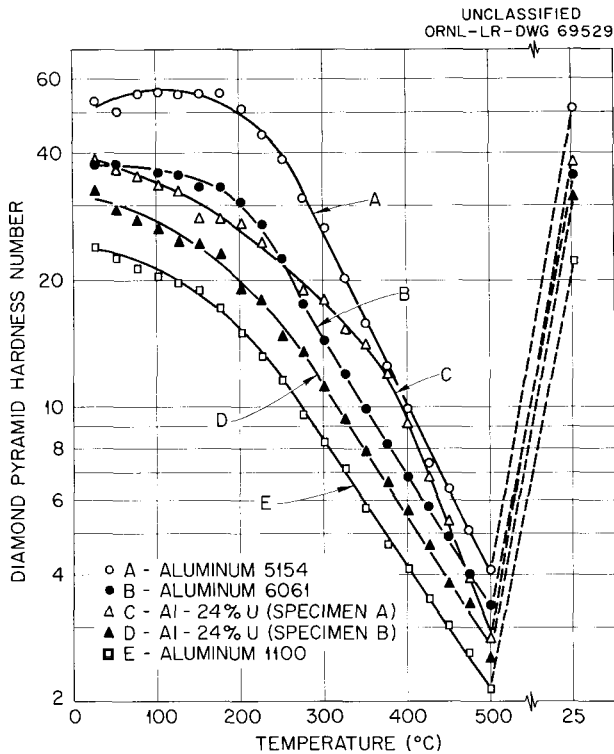


Fig. 28.11. Hardness as a Function of Temperature of Aluminum Alloys.

The difference in hardness of the two aluminum-uranium specimens was explained by a microstructural examination. Although the specimens were prepared from the same casting, the variation in size and distribution of the primary phase ( $UAl_3$ ,  $UAl_4$ , or both) shown in Fig. 28.12 undoubtedly accounts for the hardness difference.

### Instrument for Determining Crushing Strength of Microparticles

G. Hallerman

An instrument for crushing-strength determinations of uncoated and pyrolytic-carbon-coated fuel particles (50 to 500  $\mu$  in diameter) was designed and built in an effort to relate their crushing strength to their fabricability. The tester, shown in Fig. 28.13, consists of a loading mechanism, load cell (dynamometer), and a power-supply-readout unit.

At present, this instrument provides the only means for measuring strength of fuel particles. Such tests combined with metallographic examinations<sup>5</sup> provide the basis for evaluation of various fuel element concepts employing coated particles.

### NEW METALLOGRAPHIC TECHNIQUES

#### Identification of Carbides, Nitrides, and Oxides in Niobium by Electrolytic Staining

R. S. Crouse

Electrolytic staining is a technique that has been used with success in the identification of phases in titanium and zirconium alloys.<sup>6</sup> It has been suggested that the same process might be useful in identifying phases present due to gaseous contamination in niobium.<sup>7</sup> To do this, it was necessary to establish characteristic color standards of each phase.

The metallographic specimen used for standards was taken from other tests in progress.<sup>8,9</sup> The samples had been prepared by heating niobium coupons in controlled individual atmospheres of  $N_2$ ,  $CH_4$ , or air and had been chemically analyzed for nitrogen, carbon, and oxygen content, with the surface layers formed analyzed by x-ray diffraction. By correlating the colors of the phases, as seen after staining, with the chemical and x-ray data,

<sup>5</sup>C. K. H. DuBose and R. J. Gray, *Metallography of Pyrolytic Carbon Coated and Uncoated Uranium Carbide Spheres*, ORNL-TM-91 (Mar. 21, 1962).

<sup>6</sup>E. Ence and H. Margolin, *J. Metals* 6, 346-48 (1954).

<sup>7</sup>Private communication with F. J. Huegel, CANEL, Pratt & Whitney, Middletown, Conn.

<sup>8</sup>H. E. McCoy, Jr., and D. A. Douglas, Jr., "Effect of Various Gaseous Contaminants on Strength and Formability of Columbium," pp 85-118 in *Columbium Metallurgy* (eds., D. L. Douglass and F. W. Kunz), Interscience, New York, 1961.

<sup>9</sup>H. Inouye, "Oxidation of Columbium at Low Oxygen Pressures," pp 649-65 in *Columbium Metallurgy* (eds., D. L. Douglass and F. W. Kunz), Interscience, New York, 1961.

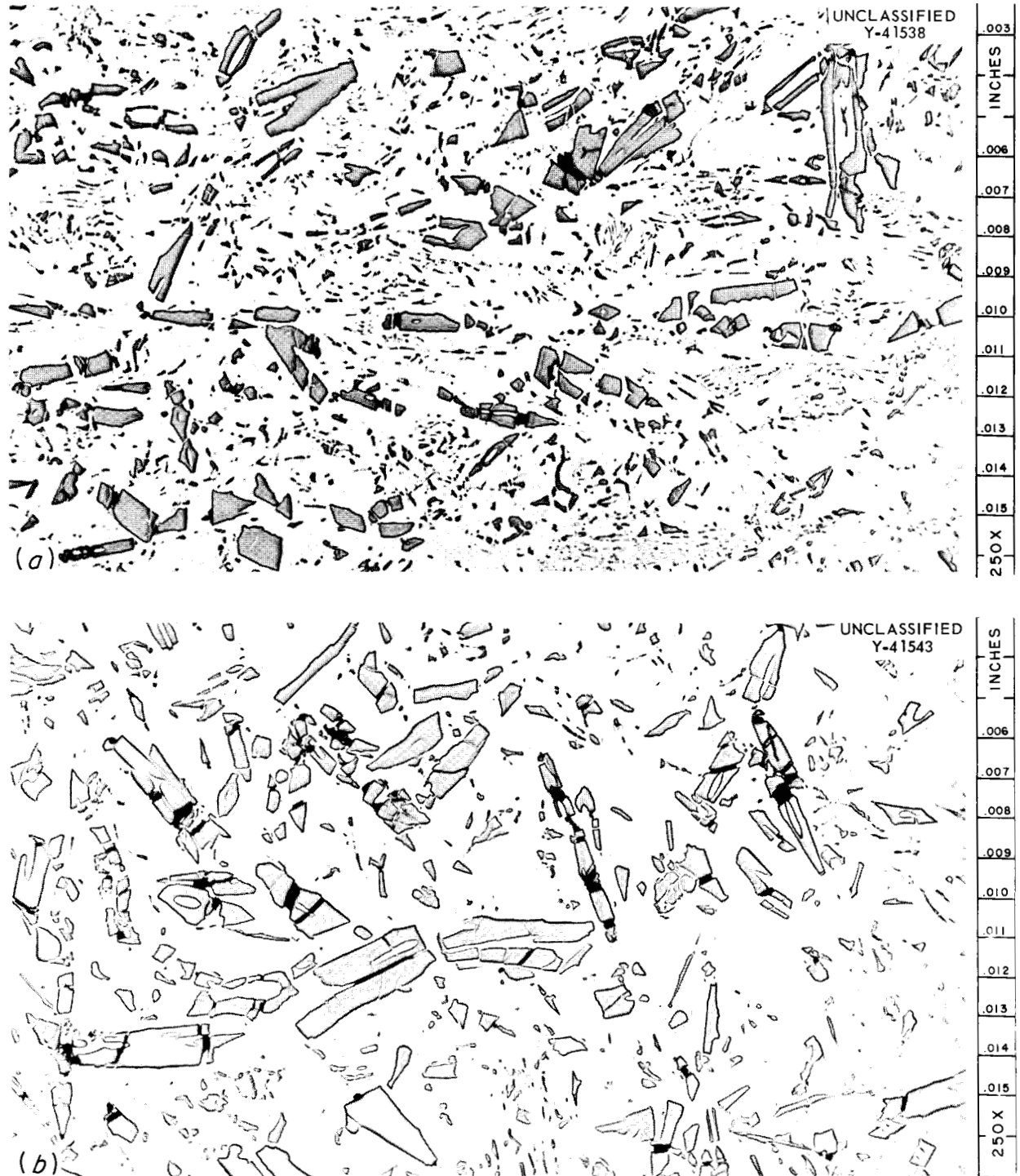


Fig. 28.12. Al-24 wt % U Alloy. Cast, hot-rolled, and annealed. As-polished. (a) Fine dispersion of primary phase and eutectic; (b) coarse primary phase with less eutectic.

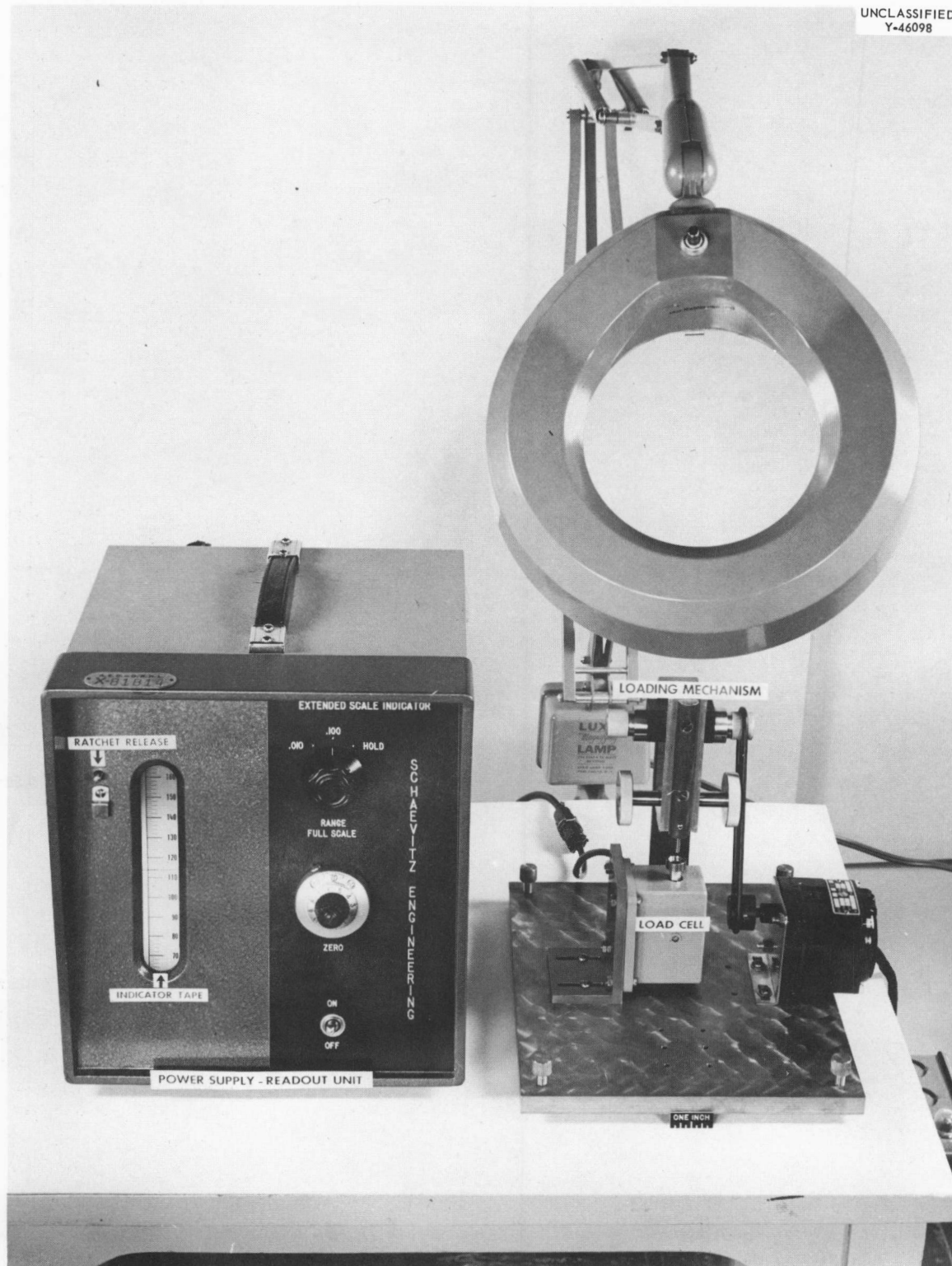
UNCLASSIFIED  
Y-46098

Fig. 28.13. Compression Tester for Microparticles.

characteristic colors were determined and are summarized as follows:

Contaminant	Compound	Color
Carbon	Nb <sub>2</sub> C	Yellow
	NbC	Bright Yellow
Nitrogen	Nb <sub>2</sub> N	Rose-pink
	NbN	Yellow
Oxygen	NbO	Sky blue
	NbO <sub>2</sub>	Gray-green
	Nb <sub>2</sub> O <sub>5</sub>	Red-brown (mottled)

### Etching Behavior of Grain Boundaries in Nickel

T. M. Kegley, Jr.

One characteristic of the corrosion encountered in the fluorine-molten salt environment of the Molten Salt Fluoride Volatility Process<sup>10</sup> is a change in the appearance of grain boundaries at the exposed surfaces. Whether or not this change is revealed depends upon the etching techniques employed. Figure 28.14 shows the effect of two etching techniques on the same "L" nickel specimen. The acetic-nitric acid etchant reveals the grain boundary modification, while the hydrochloric-sulfuric-nitric acid etchant does not. An etching artifact can be discounted since freshly cut surfaces not exposed to the fluoride salt-fluorine environment do not exhibit this behavior.

### REACTOR PROJECT SUPPORT

#### Irradiation Studies on EGCR Prototype Fuel Elements

E. L. Long, Jr.

Metallographic examination of irradiated type 304 stainless steel-clad UO<sub>2</sub> fuel pellets has been reported.<sup>11</sup> Several phenomena were observed that

<sup>10</sup>G. I. Gathers, "Fluoride Volatility Process for High Alloy Fuels," pp 560-73 in *Symposium in the Reprocessing of Irradiated Fuels Held at Brussels, Belgium, May 20-25, 1957*, TID-7534, Book 2.

<sup>11</sup>E. L. Long, Jr., *GCR Quart. Progr. Rept. Mar. 31, 1961*, ORNL-3102, pp 163-74; J. G. Morgan et al., *GCR Quart. Progr. Rept. June 30, 1961*, ORNL-3166, pp 131-36; *Sept. 30, 1961*, ORNL-3210, pp 73-86; *Dec. 31, 1961*, ORNL-3254, pp 70-74.

could reflect on the performance of the EGCR fuel elements. The first group of experimental capsules (ORR Group 1) were loaded with UO<sub>2</sub> pellets that contained various amounts of a second-phase material, later identified by x-ray diffraction as UN<sub>2</sub>. Comparison of metallographic results from the Group 1 capsules with later capsules (ORR Group 2) showed that an acicular second phase present in the UO<sub>2</sub> after irradiation was found only in pellets that originally had contained UN<sub>2</sub>. This acicular structure, which was optically active under polarized light, was identified by x-ray diffraction as U<sub>2</sub>N<sub>3</sub>. A heavy precipitate was found in the inner surface regions of the type 304 stainless steel cladding of all the Group 1 capsules. The precipitate, tentatively identified as a nitride, was believed to have resulted from the disassociation of UN<sub>2</sub> during irradiation. The precipitate resulted in a marked increase in the microhardness, which indicated a decrease in ductility.

Other unexpected microstructural changes deserving additional metallographic investigation were observed. A considerable amount of  $\sigma$  phase was found in the type 304 stainless steel cladding, but is not considered to be directly responsible for any of the capsule failures to date. Intergranular voids were found in areas of clad deformation, primarily opposite pellet-to-pellet interfaces. The nature of the stresses involved is not yet fully understood, and additional examinations are in process.

### Advanced EGCR Irradiation Experiments

E. L. Long, Jr.

This year eight beryllium-clad UO<sub>2</sub>-fueled capsules were examined and reported.<sup>12</sup> Two significant microstructural features were observed. Sub-surface voids were found in the beryllium clad adjacent to the UO<sub>2</sub> fuel. These voids were found to extend through approximately two thirds of the 0.035-in. wall of the cladding in several capsules. A reaction at a UO<sub>2</sub>-Be end plug was observed in one capsule; the reaction product was believed to be primarily UBe<sub>13</sub>.

<sup>12</sup>J. G. Morgan et al., *GCR Quart. Progr. Rept. Dec. 31, 1961*, ORNL-3254, pp 193-215; *Mar. 31, 1962*, ORNL-3302 (in press).

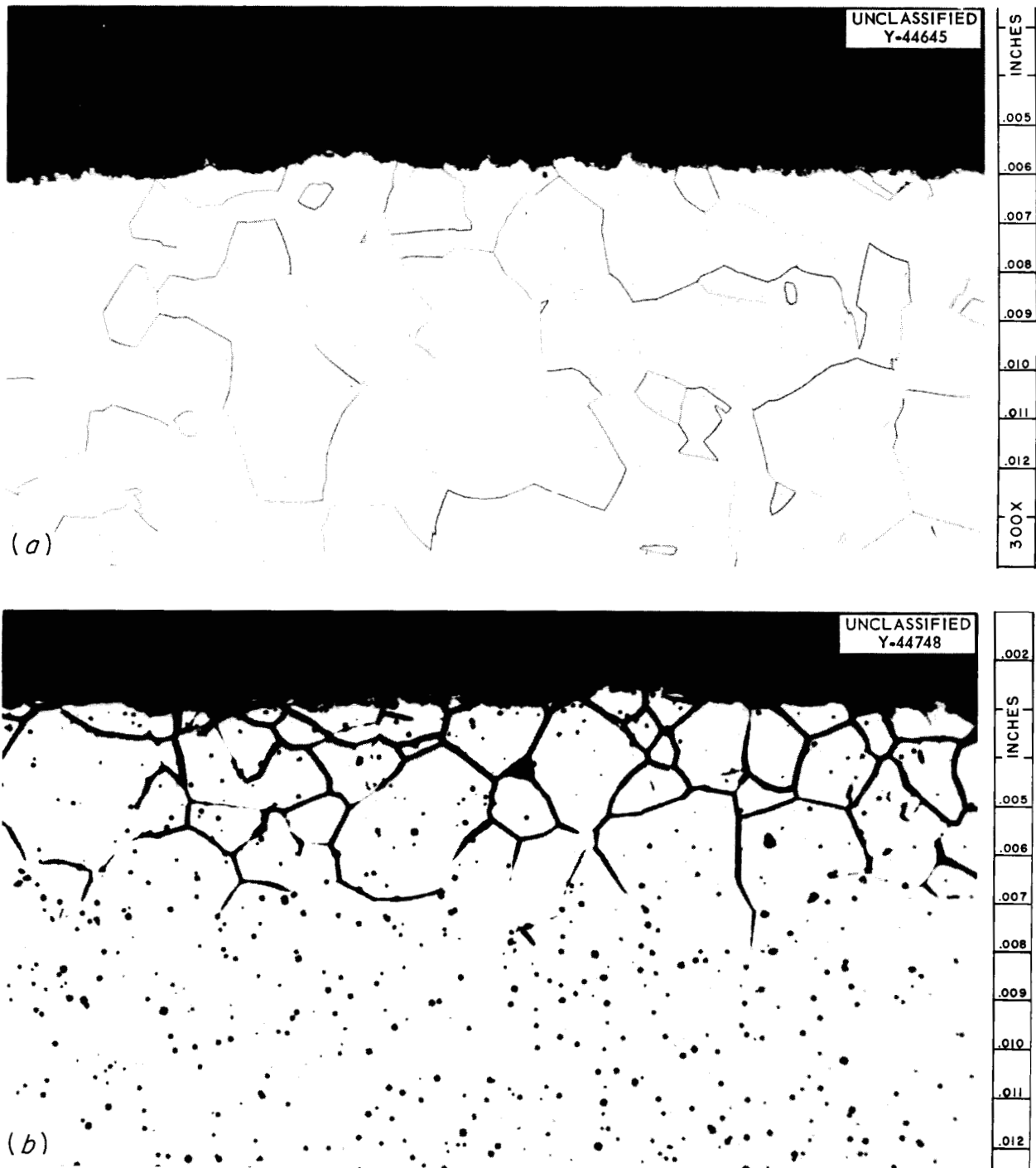


Fig. 28.14. Effect of Different Etching Techniques on the Same "L" Nickel Corrosion Specimen. 300X. (a) Etched with 92 HCl:5 H<sub>2</sub>SO<sub>4</sub>:3 HNO<sub>3</sub>; (b) etched with 3 CH<sub>3</sub>COOH:2 HNO<sub>3</sub> and repolished slightly.

## Examination of Irradiated Advanced Reactor Fuels

E. L. Long, Jr.

**Postirradiation Examination of LITR Uranium Monocarbide Fuel Pellets.** — Metallographic examination of the hollow uranium monocarbide fuel pellets irradiated in the LITR is complete and has been reported.<sup>13</sup> Although in all the experiments the burnup was less than 1 at. %, severe reactions occurred between the tantalum clad and the monocarbide fuel. No additional uranium monocarbide irradiation tests are scheduled.

**Uranium Carbide Particles Dispersed in Graphite.** — Four experimental assemblies irradiated in the MTR were examined and reported.<sup>14</sup> Each assembly contained graphite pellets fueled with uncoated uranium carbide particles. The fuel in the pellets of this series of experiments received burnups ranging from less than 1 at. % to greater than 20 at. %  $U^{235}$ . The first evidence of a microstructural change was observed in the fuel at a burnup of approximately 4 at. %  $U^{235}$ . Numerous small voids were present in the carbide particles that could be associated with the apparent increase in volume. Also, it was impossible to discern any grain structure. The fuel had begun to spheroidize and to migrate into the graphite matrix at approximately 20 at. % burnup. No additional irradiation experiments of this nature are scheduled.

## Examination of EGCR In-Pile Tube-Burst Specimens

E. J. Manthos

Selected in-pile tube-burst specimens of various compositions were examined metallographically. The specimens were irradiated in the ORR at various stresses and temperatures. Operating conditions and test results have been reported.<sup>15-18</sup>

Metallographic examination of submitted Nb-1% Zr and Zircaloy-2 specimens tested in helium and

of INOR-8 specimens tested in air revealed that no microstructural changes had occurred that could be attributed solely to radiation effects.

The first series of Inconel specimens examined was tested in air. A transverse view of a ruptured Inconel specimen is shown in Fig. 28.15. Intergranular failure occurred and, since the specimen remained in the reactor until conclusion of the experiment, the oxide present in the ruptured grain boundaries had ample time to form after failure. It has been postulated that boron, present in grain boundaries, may have caused a decrease in rupture life by transmuted to helium during irradiation.<sup>15</sup> Tube-burst specimens were fabricated from six special heats of Inconel, containing various concentrations of boron, and tested in-pile; the results from this experiment did not show a correlation between boron concentration and rupture life.<sup>16</sup> Metallographic examination of control and in-pile specimens from the special boron heats is now in progress.

In-pile specimens of type 304 and type 304ELC stainless steels were also tested in air. Type 304 stainless steel specimens tested at 1500 or 1600°F exhibited a microstructure similar to that shown in Fig. 28.16. Out-of-pile type 304 stainless steel creep specimens tested in air or nitrogen at 1500 to 1700°F showed a similar precipitate that was identified as CrN or CrN<sub>2</sub> (ref 19). However, the amount of precipitate seen in the creep specimens was not as much as that seen in the in-pile tube-burst specimens. One explanation for the more severe nitriding in the in-pile specimens is that radiation caused disassociation of nitrogen, present in the essentially stagnant air used for pressurizing, to a more reactive form.

All the type 304ELC stainless steel specimens examined were tested at 1500°F. These specimens

<sup>15</sup>O. Sisman *et al.*, *Solid State Div. Ann. Progr. Rept.* Aug. 31, 1960, ORNL-3017, pp 119-24.

<sup>16</sup>O. Sisman *et al.*, *Solid State Div. Ann. Progr. Rept.* Aug. 31, 1961, ORNL-3213, pp 124-33.

<sup>17</sup>N. E. Hinkle *et al.*, *GCR Quart. Progr. Rept.* June 30, 1961, ORNL-3166, pp 160-64.

<sup>18</sup>W. E. Brundage *et al.*, *GCR Quart. Progr. Rept.* Dec. 31, 1961, ORNL-3254, pp 227-29.

<sup>19</sup>H. E. McCoy, Jr., W. R. Martin, and J. R. Weir, "Effect of Environment on the Mechanical Properties of Metals," pp 163-76 in *1961 Proceedings of the Institute of Environmental Sciences National Meeting, April 5-7, 1961, Washington, D. C.*, Institute of Environmental Sciences, Mt. Prospect, Ill., 1961.

<sup>13</sup>J. G. Morgan *et al.*, *GCR Quart. Progr. Rept.* June 30, 1961, ORNL-3166, pp 136-43; *GCR Quart. Progr. Rept.* Mar. 31, 1962, ORNL-3302 (in press).

<sup>14</sup>J. G. Morgan *et al.*, *GCR Quart. Progr. Rept.* June 30, 1961, ORNL-3166, pp 147-48; Dec. 31, 1961, ORNL-3254, pp 157-60; E. L. Long, Jr., *GCR Quart. Progr. Rept.* Sept. 30, 1961, ORNL-3210, pp 147-58; *GCR Quart. Progr. Rept.* Mar. 31, 1962, ORNL-3302 (in press).

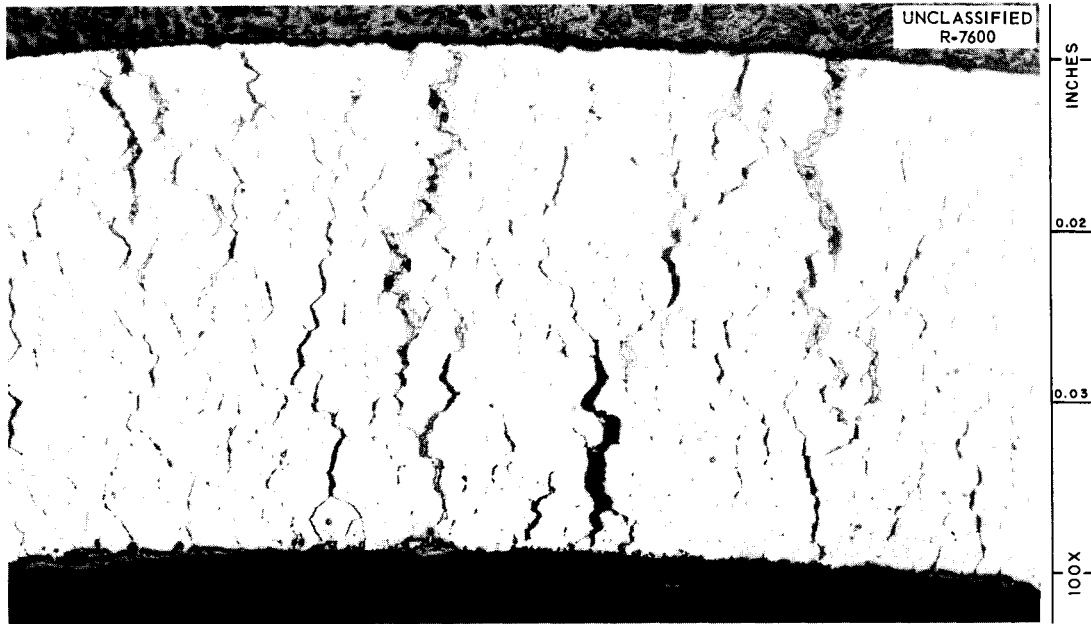


Fig. 28.15. Transverse View of Fractured Area in Inconel In-Pile Tube-Burst Specimen ORR 14-8. Specimen stressed in-pile at 3000 psi and 1500°F; rupture life, 290 hr. Air used for pressurizing and cooling. Gray phase present in fractures is oxide. As-polished. 100X. Reduced 13.5%.

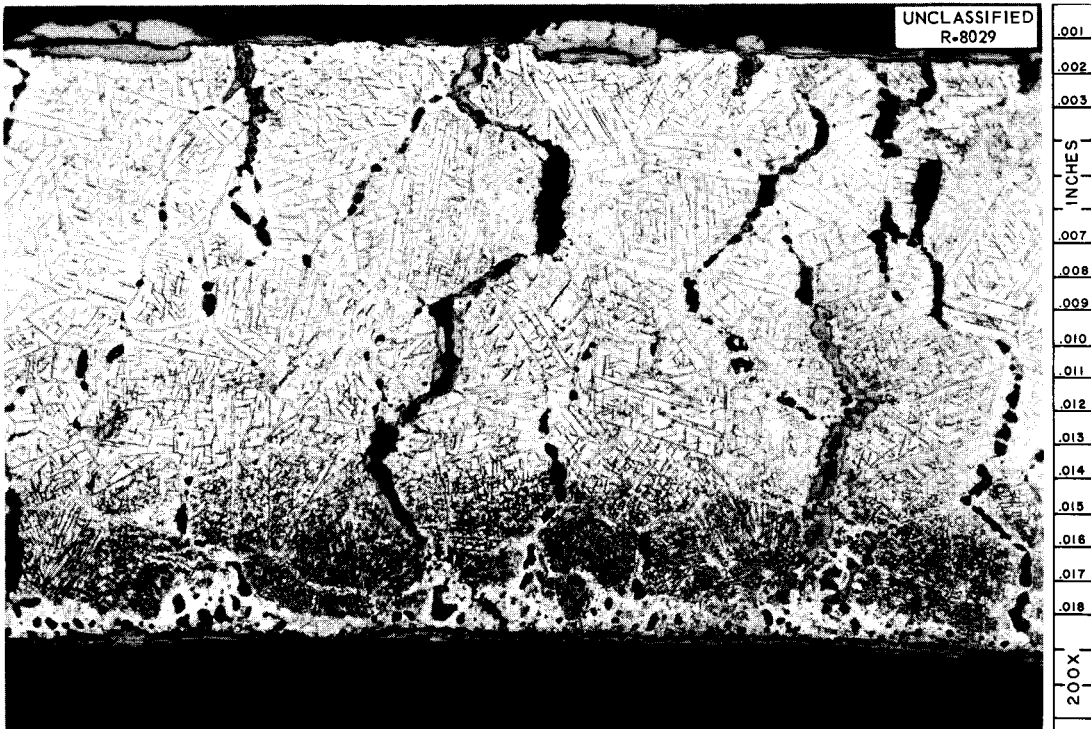


Fig. 28.16. Transverse View of Fractured Area in Type 304 Stainless Steel In-Pile Tube-Burst Specimen ORR 17-6. Rupture life of specimen was 870 hr when stressed in-pile at 2600 psi and 1600°F. Heavy precipitate in specimen believed to be CrN and CrN<sub>2</sub>. Etchant: glyceria regia. 200X. Reduced 13.5%.

also showed nitriding but not to so great an extent as the type 304 stainless steel specimens; nitriding was confined to areas adjacent to fractures, as shown in Fig. 28.17. Specimens of type 304 stainless steel that were tested in-pile with helium as a pressurizing atmosphere and an He-H<sub>2</sub>-O<sub>2</sub> mixture on the outside as a coolant will be examined metallographically in the near future.

### Examination of UO<sub>2</sub> Meltdown Experiment No. 1

E. J. Manthos

An attempt was made to melt a cylindrical UO<sub>2</sub> pellet by inserting it into the ORR and irradiating it at a power level of 60 w/g for 20 min.<sup>20</sup> After irradiation, the top of the pellet was found to be hollow and its exterior surface had a crystalline

<sup>20</sup>W. E. Browning *et al.*, "Release of Fission Products on the In-Pile Melting of Reactor Fuels," paper presented at Second Conference on Nuclear Reactor Chemistry held at Gatlinburg, Tennessee, October 10-12, 1961; proceedings to be published as TID-7622.

appearance. A fragment of the pellet was removed, and its appearance after metallographic preparation is shown in Fig. 28.18. Apparently the interior of the pellet had been heated to such a temperature that sublimation occurred. The dendritic formation seen in Fig. 28.18 was caused by sublimation and deposition of UO<sub>2</sub> on the cooler exterior surface of the pellet.

### Metallography of Pyrolytic Carbon-Coated and Uncoated Uranium Carbide Spheres<sup>21</sup>

C. K. H. DuBose and R. J. Gray

Techniques have been developed for the metallographic preparation and examination of carbon-coated and uncoated uranium carbide particles both in the unsupported condition and as-fabricated into graphite matrices. The particle coatings studied

<sup>21</sup>Abstract of ORNL-TM-91 (Mar. 21, 1962) and of paper to be published in the Proceedings of the 15th AEC Metallography Group Meeting at Savannah River Laboratory, May 17-19, 1961.

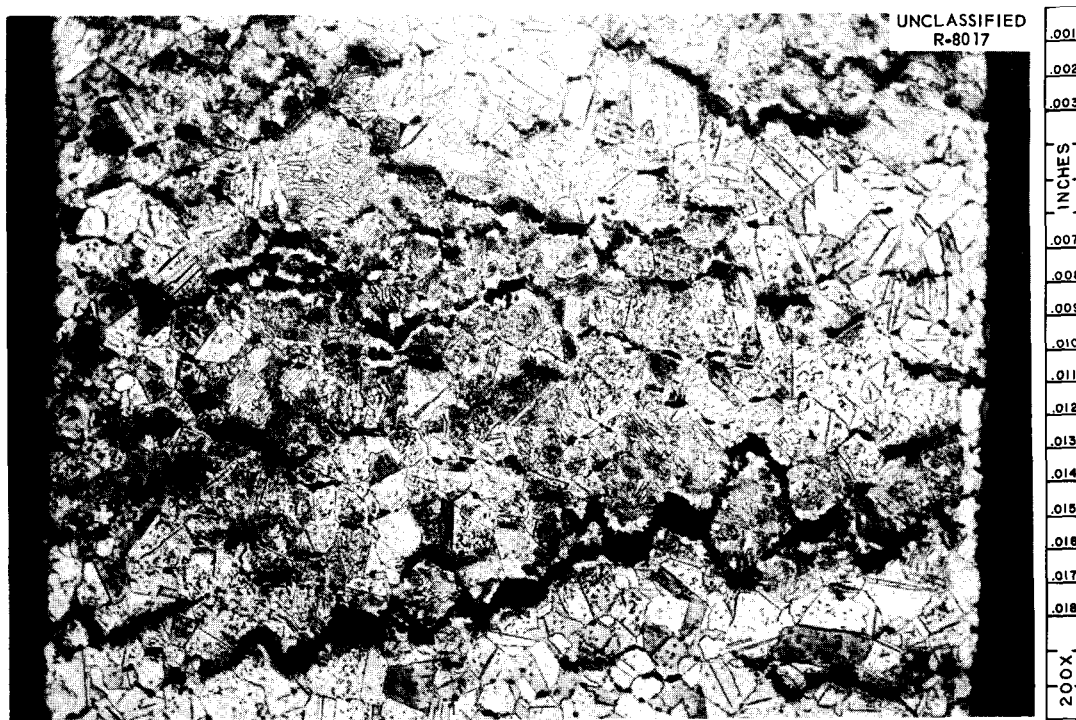


Fig. 28.17. Transverse View of Fractured Area in Type 304ELC Stainless Steel In-Pile Tube-Burst Specimen ORR 11-4. Specimen stressed in-pile at 2500 psi and 1500°F; rupture life, 700 hr. Precipitate around fracture believed to be CrN and Cr<sub>2</sub>N. Etchant: glyceria regia. 200X. Reduced 13.5%.

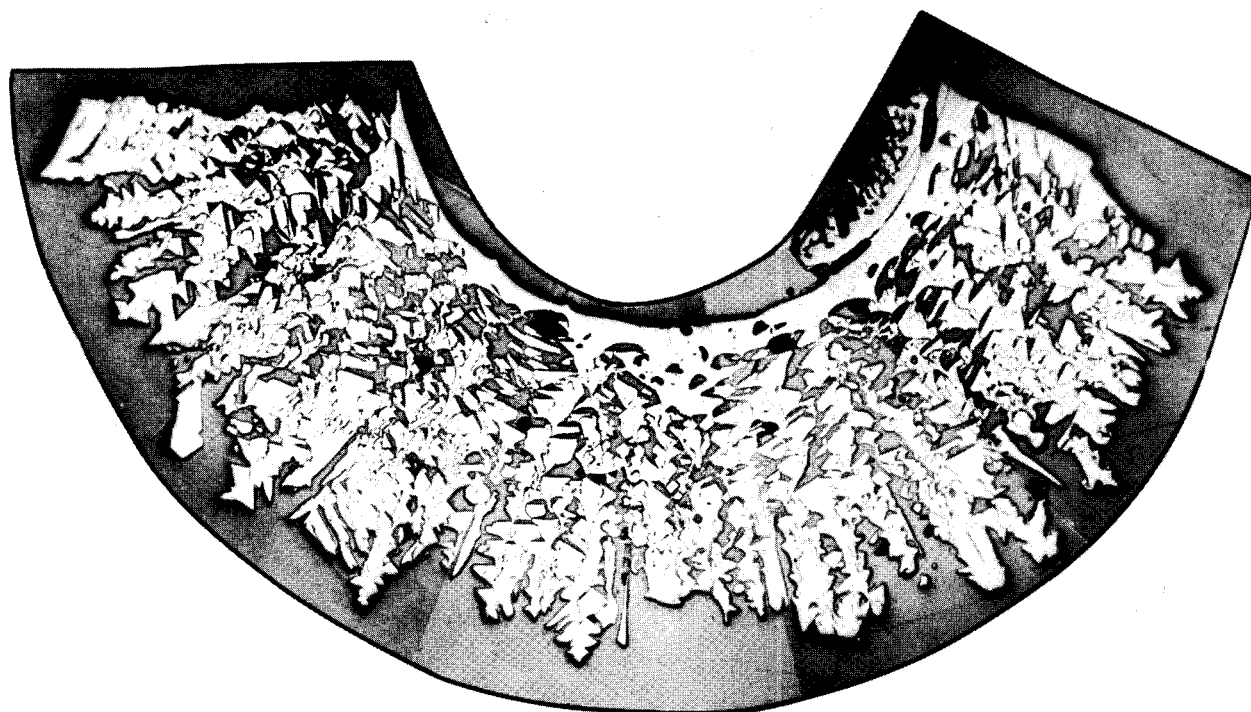


Fig. 28.18. Composite Photomicrograph of  $UO_2$  Fragment Obtained from Top of  $UO_2$  Pellet Irradiated in  $UO_2$  Meltdown Experiment No. 1. As-polished. 23.5X.

were deposited pyrolytically from a hydrocarbon gas, producing two morphological types of pyrolytic-carbon coatings. In one type the coating was smooth on the outer surface and a cross-sectional plane exhibited a laminar onion-ring type of structure; in the other type the surface had a pebble-like finish, with the cross section exhibiting a columnar or conical grain structure. The microstructures of the carbide particles showed variations in the amount of  $UC_2$  and UC with an average ratio of approximately 70:30. Heat treatments above  $1800^\circ C$  may produce uranium oxides at the particle-coating interface.

#### Unusual Etching Characteristics of UC- $UC_2$ Spherical Particles

C. H. K. DuBose

Examination of several batches of commercial pyrolytic carbon-coated spherical UC- $UC_2$  fuel particles revealed some unusual etching effects. The spheres in the as-polished condition were

apparently identical and structurally sound. The polished and chemically etched surfaces of a few particles, however, showed abnormal etching behavior of the UC platelets. These anomalies seemed to fall into three types: the UC platelets were wider than normal in some areas and had a light-gray color, they swelled above the polished surface and had a black coloring, or they became very narrow and had a tendency to coalesce near flakes of free graphite.

Lattice parameters for uranium monocarbide in spheres exhibiting these three anomalies were calculated from x-ray diffraction patterns of crushed UC- $UC_2$  spheres that had been extracted from their coating of pyrolytic carbon.

The first type, light gray, of etching characteristic of some UC platelets is shown in Fig. 28.19a. The gray color associated with these platelets has been encountered in the past when working with uranium carbides in the eutectic compositional range (6.4 wt % C, 50% UC-50%  $UC_2$ ). The lattice parameter calculated for the gray-type UC platelets in the spheres was  $a_0 = 4.948 \text{ \AA}$ , whereas for the UC gray platelets in a slightly hypereutectic arc-melt

button it was 4.958 Å, which is in between the values in the literature.<sup>22,23</sup>

The swelling, or second, type of UC platelets is shown in Fig. 28.19b. The polished surface does not indicate any abnormality, but during the 30-sec etching period the UC platelets turned black and

swelled above the polished surface. As shown in Fig. 28.19, some platelets are out of focus because of their displacement and others have fallen over to one side. Before and after etching, the swelling type of UC platelets had a lattice parameter of  $a_0 = 4.963$  Å, which is only slightly higher than the highest lattice parameter reported for UC.

The third type (Fig. 28.19c) of unusual UC etching behavior – narrow UC platelets coalescing near flakes of graphite – had a parameter of 4.954 Å, which is only slightly lower than normal.

<sup>22</sup>F. A. Rough and A. A. Bauer, *Constitution of Uranium and Thorium Alloys*, BMI-1300 (1958).

<sup>23</sup>ASTM x-ray powder data file No. 9-214.

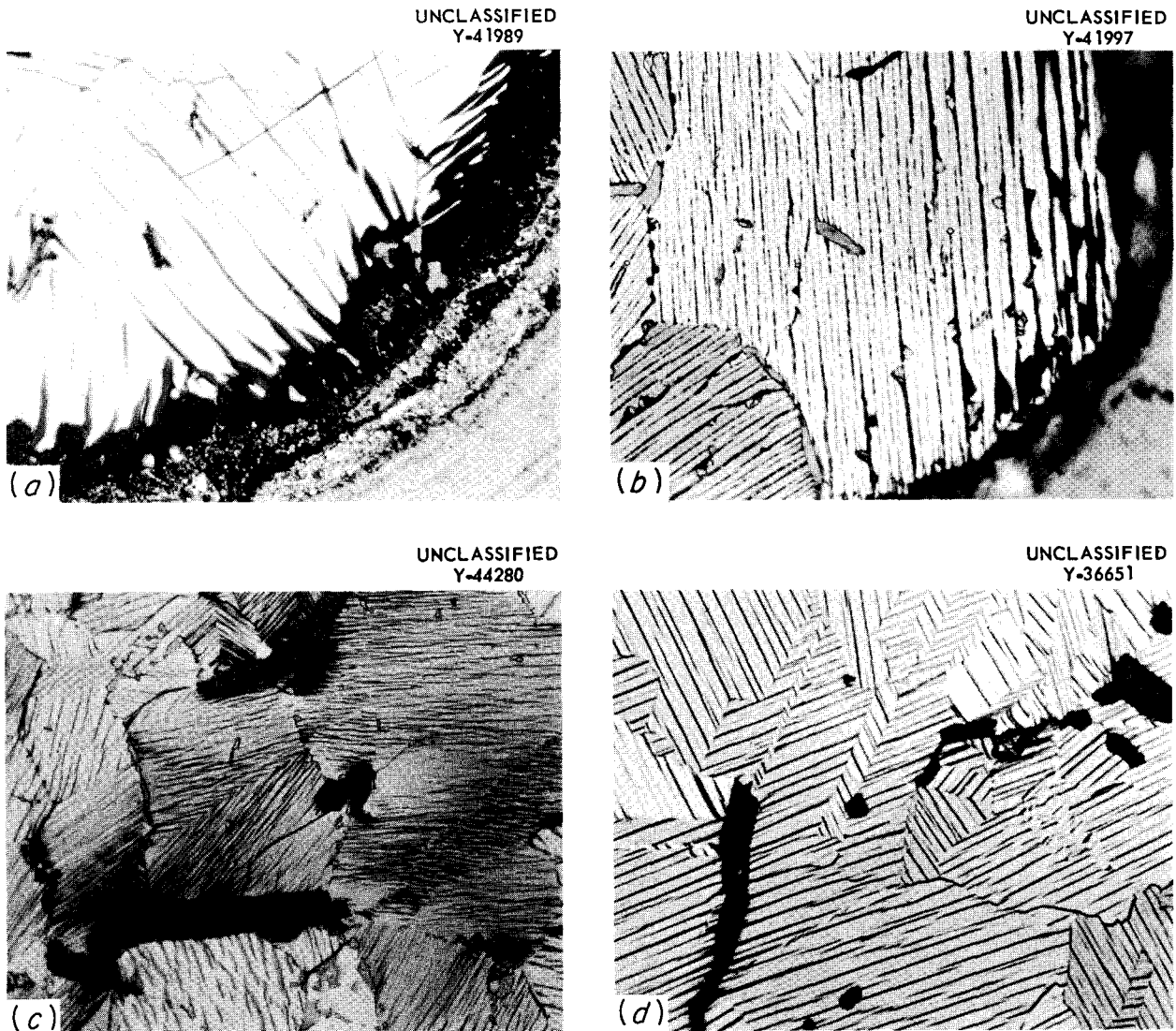


Fig. 28.19. Unusual Etching Behavior of UC Platelets Associated with Shift in UC Lattice Parameter. Etched with 1:1:1  $H_2O$ ,  $CH_3COOH$ ,  $HNO_3$  and immersed for 30 sec. 1000X. (a) Gray-type UC platelets;  $a_0 = 4.948$  Å; (b) swelling-type UC platelets;  $a_0 = 4.963$  Å; (c) narrow UC platelets coalescing at flakes of graphite;  $a_0 = 4.954$  Å; (d) normal structure (with flakes of graphite);  $a_0 = 4.959$  Å.

A structurally sound UC-UC<sub>2</sub> microstructure is shown in Fig. 28.19*d*. A lattice parameter measurement, from x-ray diffraction studies, of the monocarbide in this sample was found to be between the two reported lattice parameters of  $a_0 = 4.955$  and 4.961 Å. The x-ray data are summarized in Table 28.1.

These shifts in lattice parameter for UC do not fully explain why some spheres differ so radically in microstructure from others, but merely point out that there is indeed a variance in at least this one factor. In some instances there was a very slight shift in the UC<sub>2</sub> lattice parameter, but it seemed to be insignificant and unassociated with any corresponding shifts found in the UC lattice parameters. Some question now arises as to the lattice parameter tolerance for UC. The lattice parameters for UC platelets have differed by 0.017 Å from one batch of spheres to another and in some cases for spheres from the same batch. According to observations at Ames,<sup>24</sup> carbon in UC can be replaced by oxygen or nitrogen with a slight decrease in lattice constant to as low as 4.945 Å. A thorough study of a possible shift in UC and/or UC<sub>2</sub> lattice parameters in relation to different carbon-to-uranium ratios across the phase diagram has not been undertaken, at least by this laboratory.

<sup>24</sup>J. J. Katz, *The Chemistry of Uranium*, 1st ed., chap. 9, p 216, McGraw-Hill, New York, 1951.

### Metallographic Examination of Uranium Sesquicarbide Bulk Sample

C. K. H. DuBose      R. J. Gray

An arc-melted button of U-7.04 wt % C was heat-treated for 60 hr at 1600°C to obtain maximum transformation to uranium sesquicarbide.

The reported<sup>25</sup> lattice parameter for uranium sesquicarbide (body-centered cubic) is  $a_0 = 8.088$  Å, whereas that determined in this study was of 8.089 Å. Metallographically, the specimen preparation was identical to that for UC and UC<sub>2</sub>; however, the etching time was found to be intermediate of that required for the other two carbides. The globules at the grain boundaries, Fig. 28.20, are composed of untransformed UC-UC<sub>2</sub> in a matrix of U<sub>2</sub>C<sub>3</sub>. From this experiment and other data reported<sup>25</sup>, it appears that residual stress within an arc-melted button is sufficient to accelerate or induce the formation of U<sub>2</sub>C<sub>3</sub> without any additional external forces.<sup>26</sup> The above-mentioned sample was not subjected to any external stress prior to heat treatment.

<sup>25</sup>M. W. Mallett, A. F. Gerds, and D. A. Vaughn, *J. Electrochem. Soc.* **98**, 505-9 (1951).

<sup>26</sup>Private communication with W. Chubb, Battelle Memorial Institute.

Table 28.1. Some Physical Properties of Uranium Carbide Spheres

Type of Structure	Etching Characteristics	UC-UC <sub>2</sub> Ratio (%) from X-Ray Intensities	UC Lattice Parameter, $a_0$ (Å)
Gray UC platelets	See Fig. 28.19 <i>a</i>	40-60	4.948
Coalescing UC	See Fig. 28.19 <i>c</i>	40-60	4.954 4.955 <sup>a</sup>
Normal UC	See Fig. 28.19 <i>d</i>	40-60	4.959 4.961 <sup>b</sup>
Swelling UC platelets	See Fig. 28.19 <i>b</i>	40-60	4.963

<sup>a</sup>ASTM x-ray powder data file No. 9-214.

<sup>b</sup>F. A. Rough and A. A. Bauer, *Constitution of Uranium and Thorium Alloys*, BMI-1300 (1958).

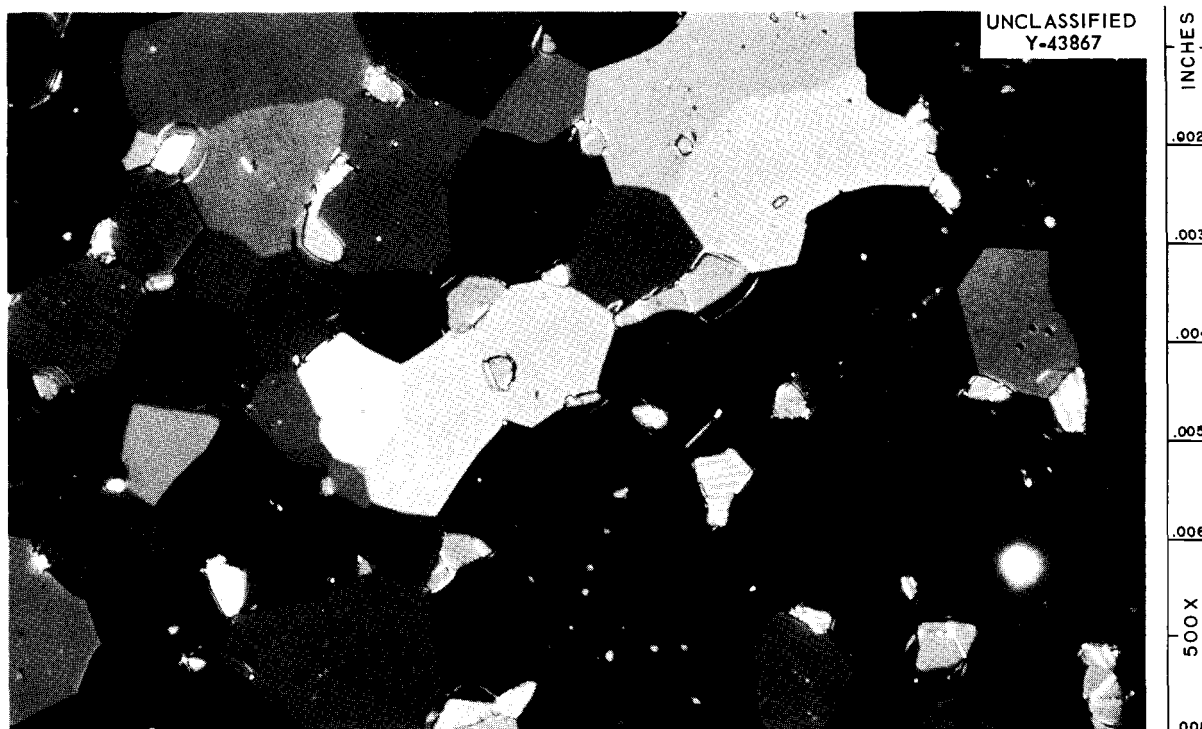


Fig. 28.20. Polarized-Light Illumination of Uranium Sesquicarbide ( $U_2C_3$ ). Globules at grain boundaries composed of UC- $UC_2$ . Etched with 1:1:1,  $H_2O$ ,  $CH_3COOH$ ,  $HNO_3$  and immersed for 15 sec.

### Examination of Heat Flux Corrosion Test Samples

T. M. Kegley, Jr.

Specimens from 12 runs of the Heat Flux Corrosion Test,<sup>27</sup> in which water is circulated through an aluminum flow channel resistance-heated by a

<sup>27</sup>J. C. Griess et al., *Effect of Heat Flux on the Corrosion of Aluminum by Water, Part 1, Experimental Equipment and Preliminary Test Results*, ORNL-2939 (Apr. 29, 1960).

high-amperage current, were examined. One striking result from this test was the difference in corrosion behavior between types 6061 and X8001 aluminum under similar test conditions. The oxide formed in aluminum 6061 was broken up and discontinuous, while that formed in X8001 was continuous. The aluminum 6061 specimen exhibited subsurface attack and void formation not exhibited by the aluminum X8001. Figure 28.21 shows the inner flow surfaces and the corresponding metallographic sections for the aluminum 6061 and X8001 flow channel specimens.

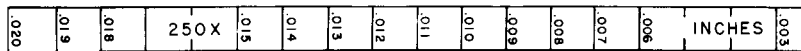
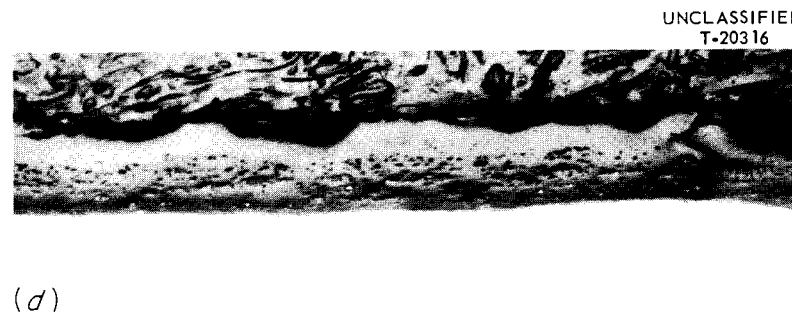
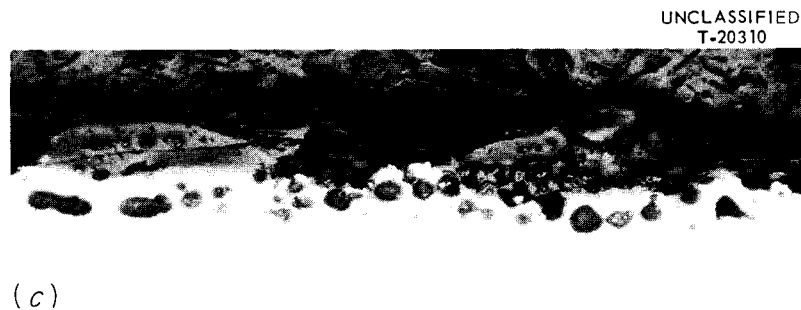
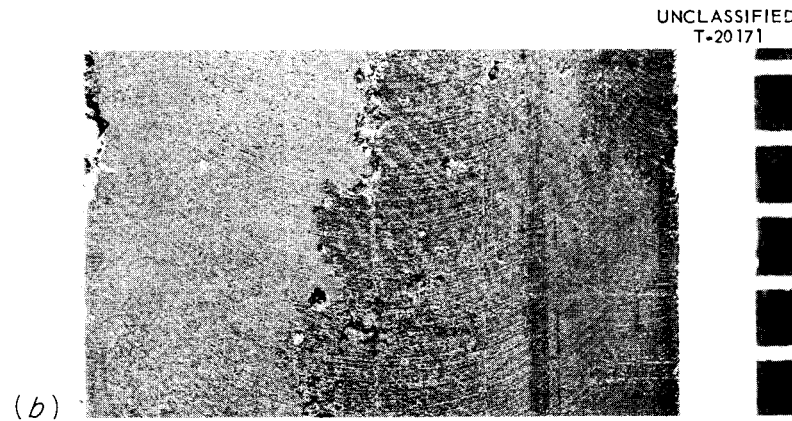
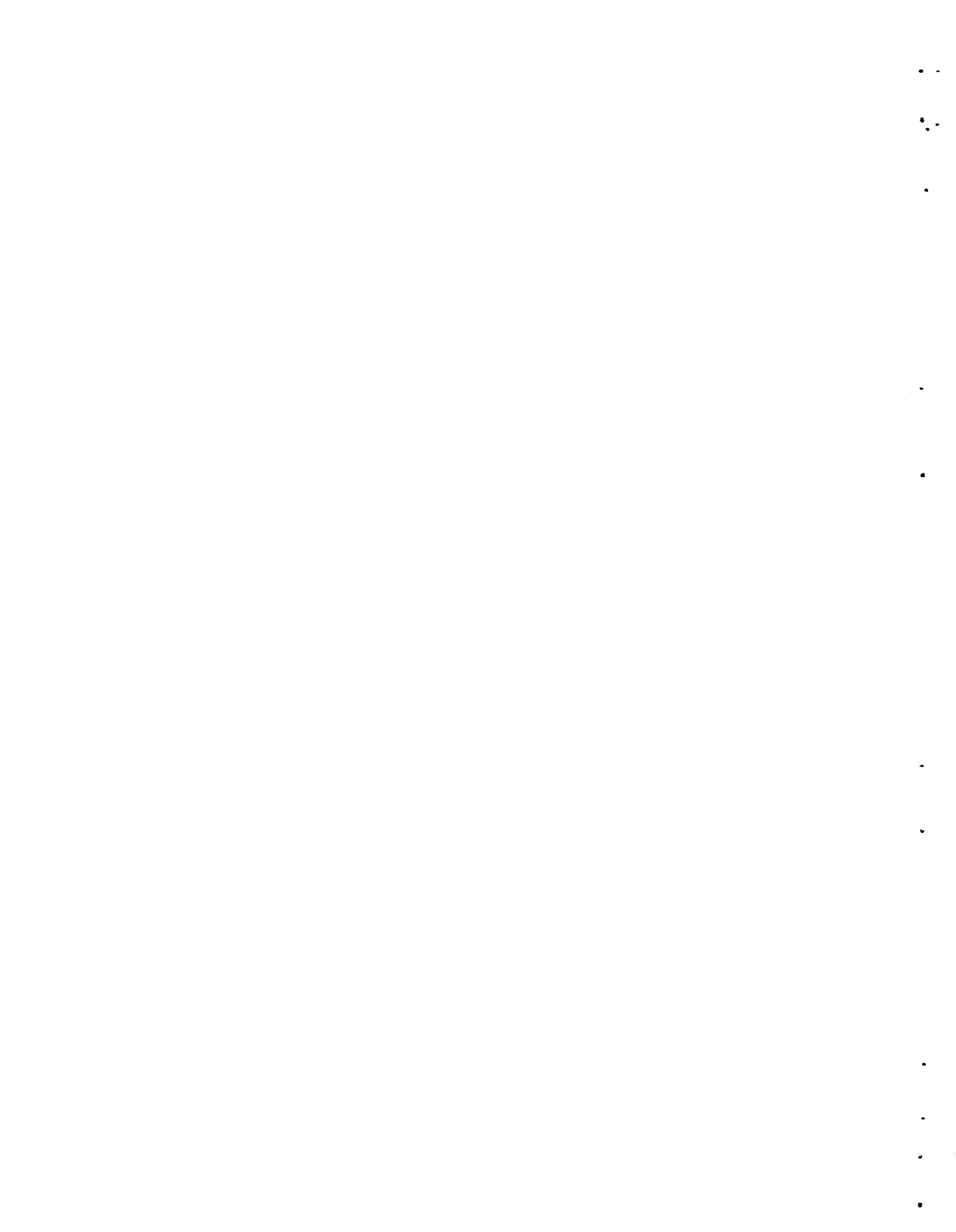


Fig. 28.21. Difference in Corrosion Behavior of Heat-Flux Corrosion Specimens of Aluminum 6061 and X8001. Test conditions: duration, 311 hr (6061), 380 hr (X8001); inlet water temperature: 122°C; outlet water temperature: 138°C; flow rate: 40 fps (6061), 45 fps (X8001); pH 6 water. (a) Inner flow surface of aluminum 6061; 6.7X; (b) inner flow surface of aluminum X8001; 6.7X; (c) metallographic section at flow surface of aluminum 6061 specimen; 250X; (d) metallographic section at flow surface of aluminum X8001 specimen; 250X.

**Part V**  
**Fundamental Research**

B. S. Borie

---



## 29. Crystal Physics

G. W. Clark

J. J. McBride

C. B. Finch

O. C. Kopp

Progress in solid-state research is often dependent upon the availability of single-crystal specimens of high perfection and controlled purity. Many crystalline materials of considerable interest have not been synthesized as large crystals. This program is one of exploring and developing crystal growth processes, of growing quality crystals of controlled purity, of studying the basis of crystallization, and of determining the purity and perfection of grown crystals. The higher quality crystals synthesized are being shared with other groups.

Systems for crystal growth studies include a pressurized Bridgman-Stockbarger furnace, a Czochralski system, autoclave furnaces, flame-fusion furnaces, a direct-current arc torch, a radio-frequency plasma torch, and equipment for growth from molten salts. Compounds included in this crystal growth endeavor are BeO, MgO, ThO<sub>2</sub>, UO<sub>2</sub>, SiO<sub>2</sub>, Cu<sub>2</sub>O, Al<sub>2</sub>O<sub>3</sub>, TiO<sub>2</sub>, ZrO<sub>2</sub>, Y<sub>2</sub>O<sub>3</sub>, Er<sub>2</sub>O<sub>3</sub>, HfO<sub>2</sub>, Fe<sub>3</sub>O<sub>4</sub>, CeO<sub>2</sub>, Zr, Nb<sub>3</sub>Sn, KCl, KBr, and certain rare-earth nitrides, phosphides, and manganese oxides.

The growth of BeO single crystals in an Li<sub>2</sub>MoO<sub>4</sub>-based solvent was previously reported.<sup>1,2</sup> Crystals of BeO, ThO<sub>2</sub>, and CeO<sub>2</sub> are being grown in a less complicated melt system of Li<sub>2</sub>O·2WO<sub>3</sub> at 1000 to 1300°C. The maximum size of BeO and ThO<sub>2</sub> crystals grown was 3 × 3 × 3 mm, while the CeO<sub>2</sub> crystals were somewhat larger. For both BeO and ThO<sub>2</sub> crystals the only known impurity exceeding 0.01 wt % is 0.1 wt % W.

The two crystal-growing techniques utilized rely on the positive temperature dependence of BeO (ThO<sub>2</sub> or CeO<sub>2</sub>) solubility in Li<sub>2</sub>O·2WO<sub>3</sub>. In one, saturated solutions of the desired oxide in Li<sub>2</sub>O·2WO<sub>3</sub> were slowly cooled at rates not exceeding 5°C/hr, and the other involved mass transport from nutrient to seed in saturated solutions having thermal gradients not exceeding 10°C/cm. Larger and better crystals were obtained by successful growth on rotating seed crystals suspended in the solution.

Differential thermal analysis was performed on a number of compositions of the system MgO-Li<sub>2</sub>O·2WO<sub>3</sub>. The study did not define any portion of this system from 10 to 70 mole % MgO that was suitable for growth of MgO.

Supercritical water and ammonia investigations in autoclaves were conducted at temperatures up to 450°C and at pressures up to 30,000 psi. One of the investigations was for the purpose of determining the relative solubility of quartz in the hydroxides of Li, Na, K, Rb, and Cs, and the effect of these solvents on the quality of the resulting grown quartz. As by-products several apparently new compounds were synthesized: Cs<sub>2</sub>O·Fe<sub>2</sub>O<sub>3</sub>·4SiO<sub>2</sub> [an iron analog<sup>3</sup> of the natural mineral pollucite (Cs<sub>2</sub>O·Al<sub>2</sub>O<sub>3</sub>·4SiO<sub>2</sub>)], Rb<sub>2</sub>O·Fe<sub>2</sub>O<sub>3</sub>·4SiO<sub>2</sub>, Cs-, Rb-, and K-iron micas. Considerable attention was directed toward the iron analog; the x-ray structure that was determined is presented in Chapter 36, this report. Among the chemical and physical properties investigated was the tendency for ion exchange. At 1 atm pressure and 100°C no exchange

<sup>1</sup>G. W. Clark, C. B. Finch, and O. C. Kopp, *Met. Div. Ann. Progr. Rept.* May 31, 1961, ORNL-3160, p 15.

<sup>2</sup>S. B. Austerman, *Am. Ceram. Soc. Bull.* 40, 269 (1961).

<sup>3</sup>O. C. Kopp, G. W. Clark, and L. A. Harris, *Hydrothermal Synthesis of an Iron Analog of the Cesium Zeolite, Pollucite*, paper presented at the Annual Meeting of the Geological Society of America, Cincinnati, Ohio, November 2-4, 1961.

with sodium or calcium ions was observed, while at 1500 psi and 275°C in a concentrated NaCl solution a majority of the cesium ions exchanged with the sodium ions. The other compounds are being studied.

Magnetite was grown hydrothermally on seeds in 0.5 M lithium tetraborate at temperatures near 400°C and at 12,000 psi. The growth rate has been slow and spurious nucleation of magnetite has hindered the results. Lithium tetraborate appears to be better than potassium tetraborate<sup>1</sup> as a solvent for magnetite.

Work relating to the pulling of single crystals of salts from a melt<sup>4</sup> was continued, with the main effort concerned with improving the purity and perfection of grown KCl and KBr crystals. A recently grown KCl crystal was quite low in impurities as judged by infrared, visible, and ultraviolet absorption spectra, by emission spectra, by flame photometry, and by the low fluorescence after ultraviolet irradiation. It is expected that the chemical purity and perfection will be improved, and

investigations of the physical perfection by etching techniques are planned.

In general, improved crystal growth techniques are badly needed for materials having melting points above 2500°C. A move in this direction is being made in applying the radio-frequency inductively coupled plasma torch<sup>5</sup> as a modification of the Verneuil<sup>6,7</sup> method of crystal growth. In this system a 3- to 5-Mc/sec, 10-kw induction generator is coupled to a gas contained in a simple fused silica chamber to establish a thermally stable, gaseous plasma at a pressure of 1 atm. This plasma is shaped so as to permit its use as a "flame" in the crystal growth process. This system is believed to offer considerable promise for the growth of crystals of many high-temperature compounds currently unavailable.

In the evaluation of the perfection and growth habits of grown crystals, optical microscopy, absorption spectroscopy, emission spectroscopy, x-ray techniques, and wet chemistry methods were used.

---

<sup>5</sup>T. B. Reed, *J. Appl. Phys.* 32, 821 (1961).

<sup>6</sup>A. Verneuil, *Compt. rend.* 135, 791 (1902).

<sup>7</sup>A. Verneuil, *Ann. chim. et phys.* 3, 20 (1904).

---

<sup>4</sup>J. J. McBride, *Met. Div. Ann. Progr. Rept.* May 31, 1961, ORNL-3160, p 19.

## 30. Deformation of Crystalline Solids

R. O. Williams

J. A. Wheeler, Jr.

Considerable progress was made with measurements on the stored energy of deformation in a series of nickel-base aluminum and copper-base zinc alloys at 77 and 243°K. The principle used for these measurements was described previously.<sup>1</sup> The stored energy is the difference between the mechanical energy (the work) involved in pulling a tensile sample and the heat liberated during deformation. This heat is utilized in vaporizing a suitable fluid ( $\text{CCl}_2\text{F}_2$  at 243°K and liquid nitrogen at 77°K) at its boiling point, the volume of gas being a measure of the quantity of heat. The calorimeter used previously was modified so that the sample could be coated with a film of the liquid instead of being submerged in the liquid; more satisfactory operation resulted from this change. The same fluid is also used externally to provide isothermal conditions.

The work is given as the integral of the force required to deform the sample through the extension, a correction being required for the elastic deformation of the sample, machine, and calorimeter. The heat is calculated from published information on the heats of vaporization. A correction is applied for the background and for the elastic cooling of the system as a result of the applied load. Various problems have been encountered in carrying out these measurements, but at present the results being obtained with liquid nitrogen and  $\text{CCl}_2\text{F}_2$  appear to be reliable. Experimental problems remain to be solved to obtain data at 24°C with  $\text{CCl}_3\text{F}$ .

The results obtained for Cu-2 wt % Zn, Cu-30 wt % Zn, pure nickel, and Ni-5.5 wt % Al at 77 and 243°K are shown in Figs. 30.1-30.4. Figures 30.1 and 30.2 show the stress-strain diagrams, and the corresponding curves for the increase in stored

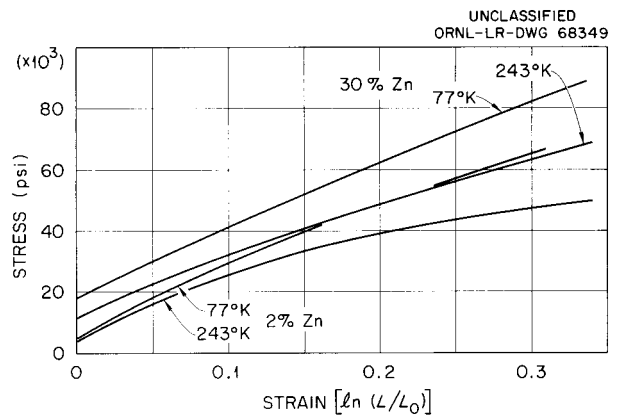


Fig. 30.1. Stress-Strain Curves for Cu-2% Zn and Cu-30% Zn at 77 and 243°K.

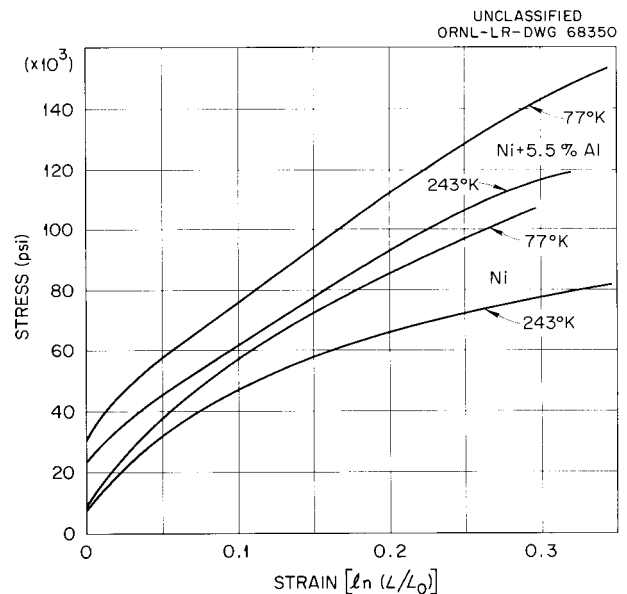


Fig. 30.2. Stress-Strain Curves for Nickel and Ni-5.5% Al at 77 and 243°K.

<sup>1</sup>R. O. Williams and J. A. Wheeler, Jr., *Met. Div. Ann. Progr. Rept. May 31, 1961*, ORNL-3160, p 20.

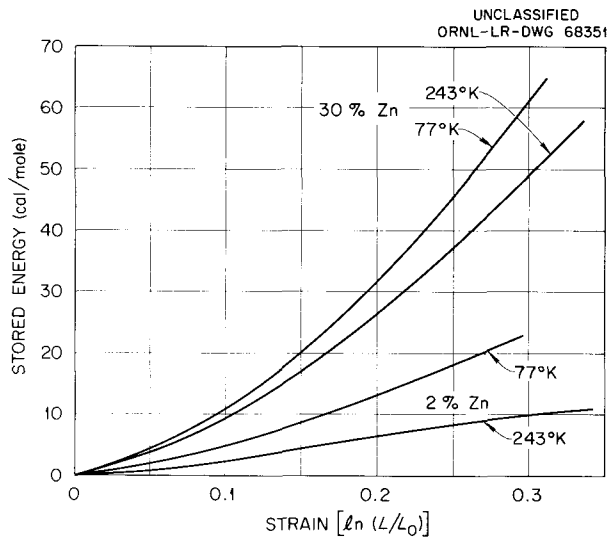


Fig. 30.3. Stored Energy vs Strain for Cu-2% Zn and Cu-30% Zn at 77 and 243°K.

energy are shown in Figs. 30.3 and 30.4. The data for the Ni-5.5% Al alloy may be in error, since it seems somewhat unlikely that the stored energy is so nearly the same at two such widely different temperatures, and are to be checked.

From these experiments, it was possible to determine the fractional part of the mechanical work being stored as a function of strain. The data are plotted in Fig. 30.5 for Ni, Ni-5.5% Al, and Cu-30% Zn.

From these data it is clear that alloying greatly increases the capacity of the metal to store energy while producing a relatively smaller effect on the strength and that reduced temperatures have a large effect on pure metals (pure copper is expected to be very similar to the 2% Zn alloy) while having a lesser effect on the alloys. These conclusions are supported by other measurements of this group and, in some cases, by other published work.

These data will be used in an effort to understand the changes that deformation produces within metals and alloys.

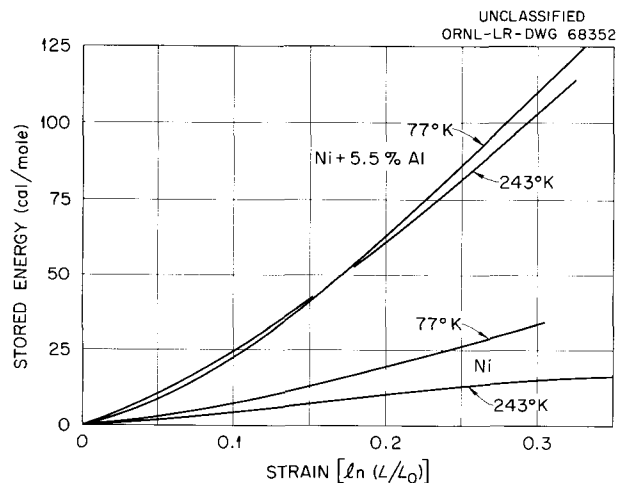


Fig. 30.4. Stored Energy vs Strain for Nickel and Ni-5.5% Al at 77 and 243°K.

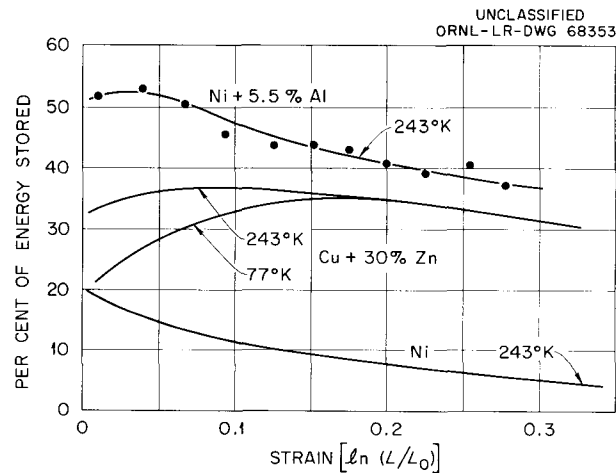


Fig. 30.5. Fractional Rate of Storage of Energy vs Strain for Ni at 243°K, Ni-5.5% Al at 243°K, and Cu-30% Zn at 77 and 243°K.

## 31. Reactions at Metal Surfaces

J. V. Cathcart

B. D. Lichter

R. E. Pawel

G. F. Petersen

It is the purpose of this research to study the factors that control the degree of protectiveness of oxide films on metals. Growing oxide films are subjected to substantial stresses associated with the oxidation process itself, and, although the total energy involved may be small compared with the chemical free energy of the reaction, evidence from previous work<sup>1</sup> indicates that the existence of these mechanical stresses can profoundly influence the rate-determining steps of the oxidation process. The various investigations being carried out by the group are related in that they are directed toward gaining an understanding of the origins of these stresses and evaluating them as factors in controlling the degree of protectiveness of oxide films.

### TANTALUM-GAS REACTIONS

The study<sup>1</sup> of the early stages of the oxidation of tantalum was continued. Only small differences in the rate of oxidation as a function of crystallographic plane were revealed by measurements on tantalum single-crystal specimens with approximately (100) and (320) orientations, as well as by those on several specimens bounded by high-index planes. Single-crystal spheres of tantalum were also oxidized in an effort to establish the relative rates of oxidation as a function of orientation; although small variations in the appearance of the oxide over the surface of the specimens were observed, it was not possible to identify the most rapidly oxidizing orientation. This result was undoubtedly related to the complexity of the oxidation

process, which involves the solution of oxygen in the tantalum followed by a martensitic precipitation of platelets of an oxide phase.

Direct observations with a hot-stage microscope of tantalum specimens during oxidation revealed "preplatelet" surface features resembling deformation lines in the metal. These features were observed primarily on specimens having approximately a (100) surface orientation, and their occurrence suggested the development of large stresses in the tantalum specimens early in the oxidation process.

Insight into the nature of the stresses was provided by measurements of the flexure of tantalum specimens exposed to oxygen on one side only. Preliminary results from this study indicated that surface stresses of the magnitude of 50,000 psi had developed in the specimens as a result of the expansion of the tantalum lattice that accompanies oxygen solution. Plots of maximum bending stress and of maximum surface stress vs time of oxidation are shown in Fig. 31.1. As may be seen, the maximum surface stress was attained in less than 5 min at 500°C. The maximum bending stress was approximately proportional to  $t^{1/2.5}$  and increased smoothly as a function of time even in experiments of longer duration in which the breakaway stage of oxidation was reached. Thus it was concluded that stresses in the oxide film itself, which are responsible for the cracking of the film during breakaway, do not contribute importantly to the stresses producing flexure.

Studies of the nitridation and low-pressure oxidation of tantalum were initiated in a further effort to study the mechanism of the formation of platelets of reaction product in tantalum. Contrary to

<sup>1</sup>J. V. Cathcart, R. E. Pawel, and G. F. Petersen, *Met. Div. Ann. Progr. Rept. May 31, 1961*, ORNL-3160, p 13.

results reported by other investigators,<sup>2</sup> tantalum specimens heated for 500 hr at 750 and 900°C in nitrogen at 1 atm did not exhibit nitride platelet formation; the surfaces of the specimens were, however, badly distorted, probably due to the solution of nitrogen in the tantalum.

Oxidation at 900°C and at pressures of  $10^{-5}$  to  $10^{-3}$  mm Hg resulted in the production of star-shaped features on the surface of tantalum specimens. The composition of the reaction product has not been determined, and the investigation is being continued.

<sup>2</sup>R. Bakish, *J. Electrochem. Soc.* 105, 574 (1958).

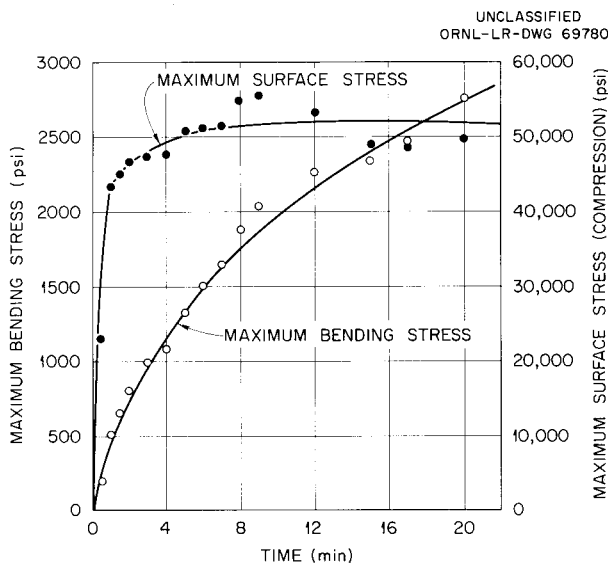


Fig. 31.1. Surface and Bending Stresses Calculated from Flexure Measurements on a Tantalum Specimen Oxidized at 500°C and 0.5 atm  $O_2$ .

Previous results<sup>1</sup> of a study of the sulfidation of tantalum for the purpose of investigating the influence of anion size in gas-tantalum reactions suggested that the mechanism of breakaway in tantalum sulfide films might be different from that occurring during oxidation. This work was extended through further sulfidation rate studies at 700 and 800°C and little difference was observed in the rates of sulfidation, suggesting that the rate of sulfidation of tantalum may pass through a maximum in this temperature range in a manner analogous to that observed during the oxidation of tantalum.<sup>3</sup>

### COPPER OXIDATION STUDIES

Studies of epitaxially induced strains in copper single crystals were continued with the oxidation of a series of crystals with (311) surfaces exposed. The mosaic structure and the state of strain in the films as a function of film thickness are being determined in association with the X-Ray Diffraction Group of this Division.

Progress continues to be made in developing equations suitable for describing the optical properties of  $Cu_2O$  films; equations which take into account the optical absorbancy and the inhomogeneous character of the strains in the films were coded for the IBM 7090 computer. With the assistance of the Central Data Processing Section, these equations are being used in an effort to determine the index of refraction and thickness values for the films from polarizing spectrometer measurements.

<sup>3</sup>R. C. Peterson, W. M. Fassell, Jr., and M. E. Wadsworth, *Trans. Met. Soc., AIME* 200, 1038 (1954).

## 32. Spectroscopy of Ionic Media

G. P. Smith, Jr.

### HIGH-TEMPERATURE SPECTROPHOTOMETER

C. R. Boston      G. P. Smith, Jr.

A spectrophotometer was designed and built to our specifications by Applied Physics Corporation for the study of absorption spectra at the 1000°C level over the wavelength range 186 to 2600 mμ. This instrument, designated the Cary Model 14H, was received this year and placed in operation.

A high-temperature cell compartment was designed and built locally.

### OPTICAL ABSORPTION IN Bi-BiCl<sub>3</sub> MELTS

C. R. Boston      G. P. Smith, Jr.

In the treatment of absorption data to determine the number of light-absorbing species in Bi-BiCl<sub>3</sub> melts, a model has been developed that is more satisfactory than that used in the past. This model is described in a forthcoming publication.<sup>1</sup>

The model for  $N$  light-absorbing species is of the form

$$\left(\frac{A}{b}\right)_0 = \sum_{j=1}^N \gamma_j M_{jj} \epsilon_{jj}$$

where  $(A/b)_0$  is the absorbance per unit path length of the zeroth solution;  $\epsilon_{jj}$  and  $M_{jj}$  are the molar absorptivity and molar concentration, respectively, of the  $j$ th reference solution; and the  $\gamma_j$  are numbers that contain the concentrations of the  $j$  light-absorbing species. Any one  $\gamma_j$  may be eliminated by

<sup>1</sup>C. R. Boston and G. P. Smith, "Spectra of Dilute Solutions of Bismuth Metal in Molten Bismuth Trihalides. Part I. Evidence for Two Solute Species in the System Bi-BiCl<sub>3</sub>," to be published in the *Journal of Physical Chemistry*.

the relation

$$M_{j0} = \sum_{j=1}^N \gamma_j M_{jj}$$

where  $M_{j0}$  is the concentration of the zeroth solution. These equations, which may be derived from the law of additive absorbances, describe the phenomenological behavior of a solution with  $N$  light-absorbing species in terms of the absorbances and concentrations of  $N$  reference solutions.

### WAVE FUNCTION CALCULATIONS

H. W. Joy

Ordinary variational determinations of electronic wave functions for small molecules are based on the requirement that the integral

$$E = \frac{\int \psi^* H \psi \, d\tau}{\int \psi^* \psi \, d\tau}$$

shall be a minimum. Here  $H$  is the "correct" non-relativistic, spin-dependent Hamiltonian operator for the motion of the electrons of a particular molecule in the coulomb field produced by its nuclei held at fixed positions in space; and  $\psi$  is an approximate wave function for a state of the system, having the analytic form of a linear combination of products of one-electron orbital functions ( $\Phi$ ) multiplied by those one-electron spin functions that will combine to produce the desired state, with parameters that can be varied so as to produce a minimum value of  $E$ .

The choice of a set of one-electron orbital ("basis") functions  $\{\Phi\}$  has never been obvious, and the literature shows a significant variety of possibilities. The present work, begun at Stanford

University with F. E. Harris, uses a set of Gaussian exponential functions in spherical polar coordinates based at arbitrary points  $A$  distributed over the space of the molecule:

$$\Phi(r_A, \theta_A, \phi_A) = r_A^l e^{-ar_A^2} Y_l^m(\theta_A, \phi_A).$$

The radial parts  $r_A^l e^{-ar_A^2}$  give the Gaussian property, and the angular parts  $Y_l^m(\theta_A, \phi_A)$  are spherical harmonics,  $P_l^m(\cos \theta_A) e^{im\phi_A}$ . The points  $A$  are located by their coordinates  $(X_A, Y_A, Z_A)$  and have their own cartesian coordinate axes defined by the Euler angles  $(\alpha_A, \beta_A, \gamma_A)$ , all relative to a single fixed-reference cartesian frame.

Harris has reported<sup>2</sup> on the evaluation of the spatial integrals obtained on construction of functions  $\psi$  from the functions  $\Phi$  and their substitution into the equation for  $E$ . A code has been written for the IBM 7090 computer that will construct an

array of all the integrals necessary for a given problem, from input specifying the positions and axis orientations of the points  $A$ , the parameters  $a$ ,  $l$ , and  $m$ , and the locations and charges of the nuclei in a molecule. It will shortly be combined with the Harris code to incorporate the spin functions and to solve the resulting matrix equations,<sup>3</sup> and will then be an almost fully automatic computational system for finding total molecular electronic energies from basic information specifying the molecule.

Since the code is designed to be as generally applicable as possible within the multicenter Gaussian representation, its use in the determination of molecular wave functions will be limited primarily by the size and speed of available computing machinery rather than by a particular molecule or a group of molecules of a particular size and/or shape.

<sup>2</sup>F. E. Harris, *Bull. Am. Phys. Soc.* **6**, Ser II, 345 (1961).

<sup>3</sup>F. E. Harris, *J. Chem. Phys.* **32**, 3 (1960).

## 33. Structure of Metals

C. J. McHargue

### TWINNING IN COLUMBIUM<sup>1</sup>

C. J. McHargue

Mechanical twins were produced in electron-beam-melted columbium by high-speed impact at room temperature and by slow or fast compression at  $-196^{\circ}\text{C}$ . The composition plane of the twins was  $\{112\}$  and the shear direction was  $\langle 111 \rangle$ . Notches in the twin bands often corresponded to traces of  $\{110\}$  of the matrix and appeared to be untwinned regions. Markings within the twin bands were interpreted as having resulted from  $\{110\}$  slip in the twins.

### EFFECT OF INTERSTITIAL ELEMENTS ON TWINNING AND FRACTURE IN COLUMBIUM<sup>2</sup>

C. J. McHargue H. E. McCoy<sup>3</sup>

The effects of additions of oxygen, carbon, nitrogen, and hydrogen on the occurrence of twins and cleavage fracture in single crystals of electron-beam-melted columbium were studied at  $-196^{\circ}\text{C}$ . At slow strain rates all additions of interstitials inhibited twinning. No twins were observed for deformations of 5 to 10% at oxygen contents greater than 2500 ppm, at carbon contents greater than about 160 ppm, or at nitrogen contents above about 550 ppm. A few twins were found after slow compression of specimens containing up to 350 ppm  $\text{H}_2$ .

<sup>1</sup>Abstract of published paper: *Trans. Met. Soc. AIME* 224, 334 (1962).

<sup>2</sup>Abstract of paper to be published in *Transactions of the Metallurgical Society of AIME*.

<sup>3</sup>Mechanical Properties Group.

Impact deformation caused twins to form in all specimens in appreciable amounts; however, many of the twins appeared to be a result of cracking. Extensive cleavage cracking occurred on  $\{100\}$  planes at oxygen contents greater than 1000 ppm, at carbon greater than about 150 ppm, and at nitrogen greater than 130 ppm.

In each crystal more slip lines were observed than had been noted for the base material. The slip lines corresponded to traces of  $\{110\}$  planes only.

### MECHANISM OF BOUNDARY MIGRATION IN RECRYSTALLIZATION<sup>4</sup>

Paul Gordon<sup>5</sup> R. A. Vandermeer

On the basis of a unified concept, theoretical expressions for grain-boundary migration in recrystallization are derived for impurity-controlled and for impurity-independent migration. The expression in the former case is analogous to that proposed by Lücke and Detert and in the latter case is shown to be equivalent to that usually obtained on the basis of absolute reaction rate theory. The equations are tested with quantitative experimental data for boundary migration obtained for the recrystallization of polycrystalline zone-refined aluminum and for binary "alloys" of this aluminum with 0.00021, 0.00043, 0.0017, 0.0034, 0.0068, 0.0124, and 0.0256 at. % Cu. All the essential characteristics of the experimentally determined boundary-migration rates agree both quantitatively and qualitatively with the predictions of the theoretical equations.

<sup>4</sup>Abstract of paper to be published in *Transactions of the Metallurgical Society of AIME*.

<sup>5</sup>Illinois Institute of Technology.

## INFLUENCE OF RECOVERY ON RECRYSTALLIZATION IN ALUMINUM<sup>6</sup>

R. A. Vandermeer    Paul Gordon<sup>5</sup>

A summary is given of earlier metallographic studies in which the nature and mode of recrystallization in polycrystalline zone-refined aluminum containing small quantities of copper were determined from an analysis of the kinetics and geometrical features. During the early stages of recrystallization the isothermal fraction recrystallized at time  $t$  obeys the expression

$$X_v = 1 - \exp(-B t^2),$$

where  $B$  is a constant. The rate of recrystallization tends to be retarded as annealing proceeds and is shown to be due to a decrease in the isothermal grain-boundary migrate rate. The effect is more pronounced the lower the annealing temperature for a specific copper content.

Microcalorimetric studies of the release of stored energy in these aluminum alloys have shown that the decreasing growth rate results from competing recovery processes that lower the available driving energy in unrecrystallized portions of the samples being annealed. The stored-energy-release spectra reveal that there are two distinct recovery stages in the annealing of these alloys.

## EVALUATION OF FIBER TEXTURES FOR CUBIC METALS

G. V. Czigek

Fiber textures are most accurately represented by the distribution of the rod axis,  $T(\phi, \alpha)$ , with respect to the lattice of the grains (inverse pole figure).<sup>7</sup> The experimental determination of textures by x rays gives the pole distribution  $I(\phi)$  of a particular family of planes with respect to the rod or fiber axis. As suggested by Bunge,<sup>8</sup> a con-

venient method of obtaining  $T(\phi, \alpha)$  from  $I(\phi)$  is to expand  $T(\phi, \alpha)$  into a series of cubic functions related to the cubic harmonics:

$$T(\phi, \alpha) = \sum_n K_n S_n(\phi, \alpha), \quad (1)$$

and

$$I(\phi) = I_0 \sum_n K_n S_n^0(\phi), \quad (2)$$

where  $I_0 = \int_0^{\pi/2} I(\phi) \sin \phi d\phi$  (ref 7).

The problem of finding  $T(\phi, \alpha)$  is now reduced to the problem of determining the coefficients  $K_n$ . If it were possible to choose the functions  $S_n^0(\phi)$  normalized and orthogonal (Legendre polynomials), the solution would be

$$K_n = \frac{1}{I_0} \int_0^{\pi/2} I(\phi) S_n^0(\phi) \sin \phi d\phi. \quad (3)$$

Although Bunge assumed that this solution would be sufficient, it is not possible to fulfill both the normalization and orthogonalization for all values of  $n$ . The functions  $S_n^0(\phi_i)$  can be chosen in such a way that all will be orthogonal, but will be equal to zero for some values of  $n$ . The corresponding  $K_n$  coefficients cannot be determined from Eq. (3) but can be found only by using another cubic function referred to another pole figure, that is, another crystallographic axis. A relationship similar to Eq. (1) can be written for the pole distribution,  $J(\psi)$ :

$$T(\psi, \beta) = \sum_m L_m R_m(\psi, \beta) \quad (4)$$

and

$$J(\psi) = J_0 \sum_m L_m R_m^0(\psi). \quad (5)$$

Since there is only one axis distribution, there will be a linear relationship between  $S_n$  and  $R_m$  and, therefore, a relationship between  $L_m$  and  $K_n$ . The particular coefficients  $K_n$  that could not be evaluated from the first expansion can be obtained through this relationship and the second expansion. Additional pole figures may be required for the evaluation of all  $K_n$ 's.

A program for the IBM 7090 is in preparation using 32 functions for the expansion shown by Eq. (1) and the pole figures for {001}, {011}, and {111}.

<sup>6</sup>Abstract of paper to be published in *Recovery and Recrystallization*, Metallurgical Society of the AIME, New York.

<sup>7</sup>L. K. Jetter, C. J. McHargue, and R. O. Williams, *J. Appl. Phys.* 27, 368 (1956).

<sup>8</sup>H. J. Bunge, *Monatsber. deut. Akad. Wiss. Berlin* 1, 400 (1959).

## DEFORMATION STUDIES

C. J. McHargue      R. E. Reed, Jr.

### Stability of $\langle 111 \rangle$ Fiber Texture

It has been reported that the  $\langle 111 \rangle$  fiber texture in aluminum rods did not appear to be stable at high amounts of deformation.<sup>9</sup> Since this observation is contradictory to one of the assumptions characteristic of theories of texture formation, similar data were obtained in a somewhat different manner.

Aluminum rods were cast in such a manner that there were columnar grains parallel to the rod axis. These ingots had a diffuse  $\langle 001 \rangle$  fiber texture. They were swaged at approximately  $-196^\circ\text{C}$ , and samples were taken after reductions in thickness of 23.5, 39.0, 53.0, 61.0, 81.0, 90.0, and 93.5%.

Results of the x-ray study showed that although the rods initially contained no grains in the  $\langle 111 \rangle$  orientation such orientations could be detected after a reduction in area of 23.5%. The amount of material in this orientation increased with the amount of deformation to 53% reduction in area. At higher reductions the amount of the  $\langle 111 \rangle$  texture gradually decreased.

The original observations regarding the stability of the  $\langle 111 \rangle$  orientation were thus confirmed. However, both movements toward and away from this orientation seemed to start at lower respective reductions than in the earlier study, presumably as a result of the lower deformation temperature, which in turn probably resulted in a higher rate of work hardening.

### Inhomogeneous Deformation in Grains of Polycrystalline Aluminum

A study of the influence of neighboring grains on the deformation mechanisms of individual grains is in progress. A Hilger microfocuss x-ray unit with a microscope and camera is being used to examine several areas within individual grains after a tensile elongation of 5, 10, 12, 15, and 20%. The initial studies employed specimens whose grain size

corresponded to the specimen thickness, so that the grains had two free surfaces. The next studies will be of grains with one free surface.

As was expected, much of the behavior was similar to that observed in single crystals; however, the grain-boundary constraints resulted in deviations of the reorientation of the tensile axis from single-crystal behavior and in much more asterism in the Laue spots.

In some cases it was possible to produce an elongation of 20% with little asterism appearing in the spots of the back-reflection Laue photographs; most of the slip occurred only on the slip plane having the highest resolved shear stress. It appears that the orientation of these grains was such that slip on the next favored slip system would not result in formation of Cottrell-Lomer sessile dislocations. In other grains where slip was primarily on one plane but where favored secondary slip would result in Cottrell-Lomer locks, there was considerable asterism in the Laue spots and a deviation from the expected path of reorientation of the tensile axis.

Deformation bands such as those shown in grain A in Fig. 33.1 appeared in grains that contained a  $\{111\}$  plane approximately parallel to the free surface and in which tensile axes were near a  $\langle 111 \rangle$  direction. Moreover, these bands were apparent after 5% extension. The apparently wavy slip lines in the grain on the right side of Fig. 33.1 consisted of short, straight traces of  $\{111\}$  at higher magnification.

A second kind of deformation band is shown in Fig. 33.2. These bands alternate between slip on the primary slip plane (highest resolved shear stress) and the critical slip plane (Hargreaves' terminology).<sup>10</sup> The plane of intersection appears to be the (110) plane perpendicular to the active slip direction for the primary slip plane.

Some grain boundary and neighboring grain effects are illustrated in Fig. 33.3. The bands of clustered slip lines in grain A are rotated 6 to 7° relative to the matrix. This rotation has caused a tilting of the grain boundary and has caused severe local deformation in grain B. These effects are seen to extend approximately halfway across grain B.

<sup>9</sup>C. J. McHargue, *Trans. Met. Soc. AIME* 221, 812 (1961).

<sup>10</sup>L. M. Clarebrough and M. E. Hargreaves, *Progr. in Metal Phys.* 8, 1 (1959).

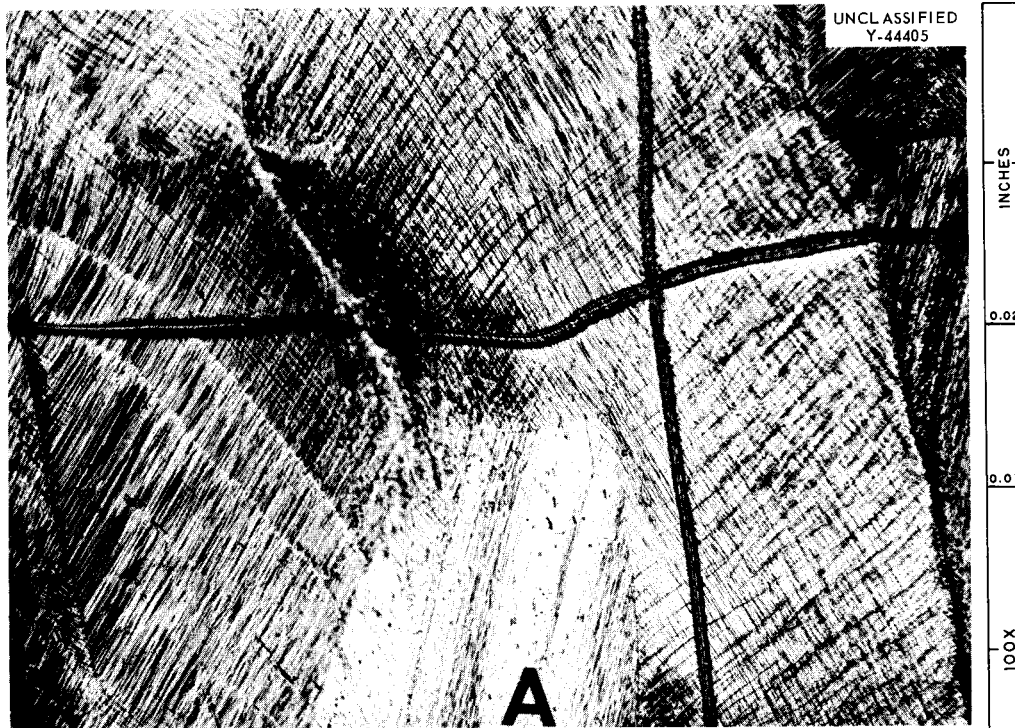


Fig. 33.1. Inhomogeneous Deformation in Polycrystalline Aluminum. The slip lines in grain A have clustered to form a deformation band. 100X. Reduced 18%.



Fig. 33.2. Deformation Bands Caused by Slip on the Primary and Critical Slip Planes in Aluminum. 200X. Reduced 18%.

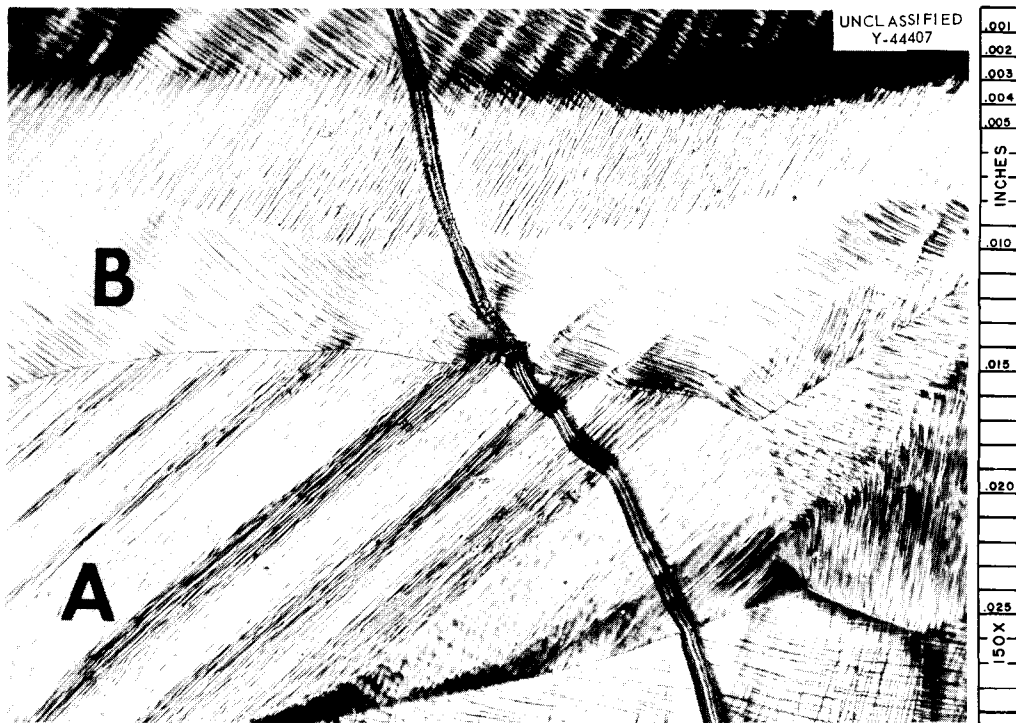


Fig. 33.3. Effects of Grain Boundaries and Neighboring Grains on Deformation of Polycrystalline Aluminum. 150X. Reduced 18%.

### Texture of Irradiated Copper

It is well known that reactor irradiation produces marked changes in the physical and mechanical properties of copper. Among other changes, it has been reported that slip lines in irradiated copper crystals show the pattern typical of copper alloys (e.g.,  $\alpha$ -brass) rather than that characteristic of pure metals.<sup>11,12</sup> Unpublished work by Smallman has been cited as showing that the rolling texture of irradiated copper is the type usually associated with brass.<sup>13</sup> A dose of  $10^{19}$  neutrons/cm<sup>2</sup> was

<sup>11</sup>M. J. Makin, *The Effect of Neutron Irradiation on the Mechanical Properties of Metals. Part III. Copper and Nickel*, AERE M/R-2080 (1956).

<sup>12</sup>R. E. Jamison and T. H. Blewitt, *Phys. Rev.* 86, 641 (1952); 91, 237 (1953).

<sup>13</sup>A. H. Cottrell, "Point Defects and the Mechanical Properties of Metals and Alloys at Low Temperatures," p 3 in *Vacancies and Other Point Defects in Metals and Alloys*, Institute of Metals, London, 1958.

reported to change the texture by the same amount that is produced by a 5% addition of zinc. Since these data have not been published in detail and since a quantitative analysis of such changes as well as of the annealing behavior are important to texture theory, a study of the preferred orientation in irradiated copper has been initiated.

Copper bars with a uniform, fine grain size and a random orientation were irradiated to  $10^{19}$  neutrons/cm<sup>2</sup> in the ORR. The postirradiation treatments included (1) cold-rolling 91%; (2) cold-rolling 91%, annealing for 1/2 hr at 500°C; (3) annealing for 1 hr at 300°C, cold-rolling 91%; (4) annealing for 1 hr at 300°C, cold-rolling 91%, annealing for 1/2 hr at 500°C.

Only a few data have been obtained on the preferred orientation but they show significant differences in the textures of specimens given treatments (1) and (2). It seems that the texture of this irradiated and rolled copper may differ from that of both copper and brass.

## 34. Theory of Alloying

J. C. Betterton, Jr.

### INCREASED CRITICAL CURRENTS IN Nb-Zr SUPERCONDUCTORS FROM PRECIPITATION HEAT TREATMENT<sup>1-4</sup>

G. D. Kneip, Jr.  
D. S. Easton

J. O. Betterton, Jr.  
J. O. Scarbrough

An important principle was discovered in 1961<sup>1</sup> in the study of Nb-Zr superconductors: coherency

or precipitation strains permit large gains in the critical current densities of high-field superconductors. The effect is illustrated in Fig. 34.1, which shows critical current densities of 28% Zr-72% Nb plotted against the transverse magnetic-field strength. Heat treatment at 800°C during or after the cold drawing of the wire increases the amount of current that this superconductor can carry without transforming to the normal state. The effect has been confirmed by Treuting, Wernick, and Hsu<sup>5</sup> at the Bell Telephone Laboratories and by Aron and Hitchcock<sup>6</sup> at the University of California.

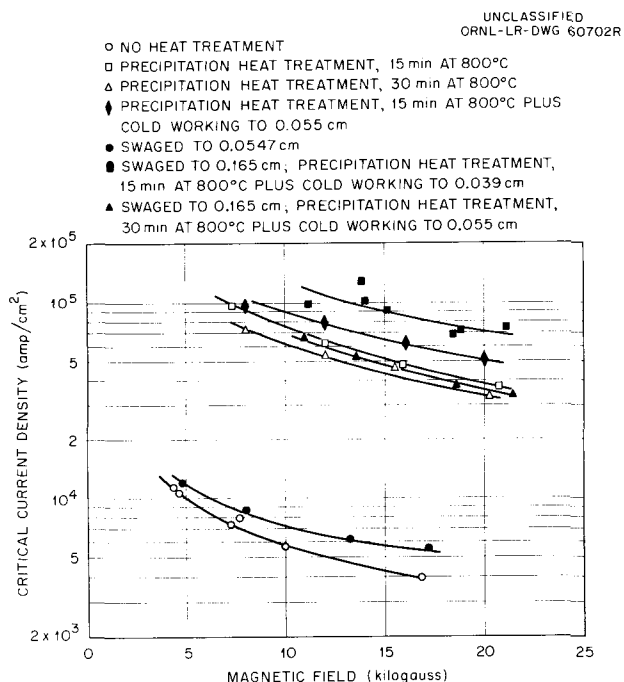


Fig. 34.1. Critical Current Density at 4.2°K for 72% Nb-28% Zr. Open symbols: specimens swaged to 0.0547 cm from as-cast state; closed diamond: specimen swaged to 0.30 cm from as-cast state; other closed symbols: specimens homogenized at 1250°C for 5 days.

<sup>1</sup>G. D. Kneip, Jr., et al., *Superconductivity in Heat-Treated Niobium-Zirconium Alloys*, ORNL CF-61-8-99 (Aug. 10, 1961).

<sup>2</sup>G. D. Kneip, Jr., et al., *J. Appl. Phys.* 33,754 (1962).

<sup>3</sup>G. D. Kneip, Jr., et al., "Increased Critical Currents in Nb-Zr Superconductors from Precipitation Defects," pp 603-8 in *Proceedings of the International Conference on High Magnetic Fields, Cambridge, November 4-7, 1961*, MIT Press, Cambridge, and Wiley, New York, 1962.

<sup>4</sup>Patent application in process.

<sup>5</sup>R. G. Treuting, J. H. Wernick, and F. S. L. Hsu, "Effect of Heat Treatment on Nb-Zr Superconducting Alloys," pp 597-601 in *Proceedings of the International Conference on High Magnetic Fields, Cambridge, November 4-7, 1961*, MIT Press, Cambridge, and Wiley, New York, 1962.

<sup>6</sup>P. R. Aron and H. C. Hitchcock, "Anomalous Critical Currents in Nb-25% Zr Wire," paper presented at the Special Session on Superconducting Materials for Magnets, Annual Meeting of the Metallurgical Society of AIME, February 18-22, 1962; proceedings to be published by Interscience.

## INTERSTITIAL IMPURITIES AND SIZE EFFECTS IN Nb-Zr SUPERCONDUCTORS<sup>7</sup>

J. O. Betterton, Jr.  
D. S. Easton

G. D. Kneip, Jr.  
J. O. Scarbrough

It is known in refractory metal studies<sup>8-11</sup> that alloying with a solute that is more electropositive than the solvent and in the presence of the normal interstitial impurities will produce large effects

<sup>7</sup>J. O. Betterton, Jr., *et al.*, "Size Effect and Interstitial Impurities in Nb<sub>3</sub>Zr Superconductors," Superconducting Solenoids with Metal Insulation," paper presented at the Special Session on Superconducting Materials for Magnets, Annual Meeting of the Metallurgical Society of AIME, February 18-22, 1962; proceedings to be published by Interscience (also to be published as ORNL-3303).

<sup>8</sup>J. W. Martin, *J. Less-Common Metals* 2, 392 (1960).

<sup>9</sup>J. E. McNutt and G. D. Gemmel, "Precipitation Hardening in Columbium Alloys," paper presented at the Fall Meeting of the Metallurgical Society of AIME, Detroit, Michigan, October 23-26, 1961.

<sup>10</sup>W. I. Pollock, "Recent Developments in Columbium Physical Metallurgy," paper presented at the Golden Gate ASM Conference, San Francisco, 1961.

<sup>11</sup>D. O. Hobson, *Aging Phenomena in Columbium-Base Alloys*, ORNL-3245 (Mar. 16, 1962).

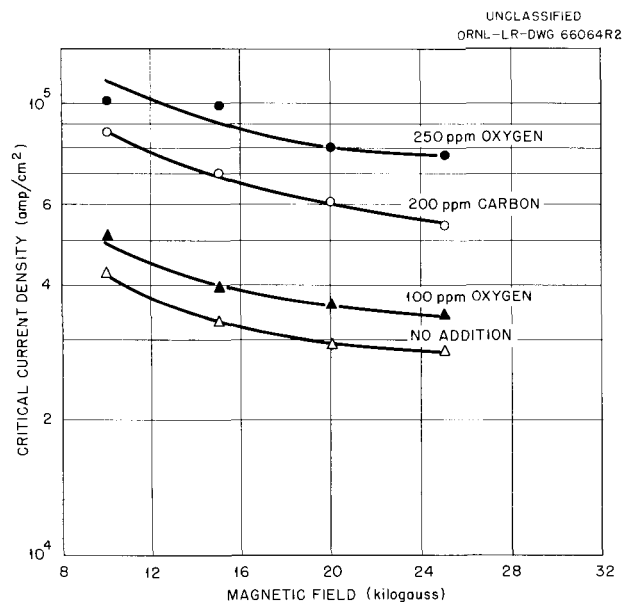


Fig. 34.2. Effect of Adding Interstitial Elements to Nb<sub>3</sub>Zr. Alloy heat-treated at 1500°C for 1 hr at 0.493 cm and cold-swaged 51%; precipitation heat treatment, 15 min at 800°C plus 98.6% cold working; final diameter, 0.040-0.044 cm.

on the mechanical properties and microstructures of these metals. The precipitation which improves the critical current density of Nb-Zr alloys was also found to be associated directly with the interstitial-type elements. This is shown in Fig. 34.2 by the increase in critical current density of Nb<sub>3</sub>Zr that resulted from adding small amounts of oxygen and carbon to the Nb<sub>3</sub>Zr in the precipitated condition. The precipitation heat treatment has a much smaller effect on Nb<sub>3</sub>Zr with no addition of oxygen than when 250 ppm O<sub>2</sub> was added, as is shown in Fig. 34.3. No oxygen effect occurs when the precipitation heat treatment is omitted. In agreement with McNutt,<sup>9</sup> Pollock,<sup>10</sup> and Hobson,<sup>11</sup> the property changes are believed to be caused by additional lattice strain from a coherent precipitation of metastable ZrO or ZrC.

A size effect study<sup>7</sup> in Nb-Zr was made to investigate the distribution of superconducting currents in cold-worked wires of this alloy. Contrary to the usual assumption that critical currents would

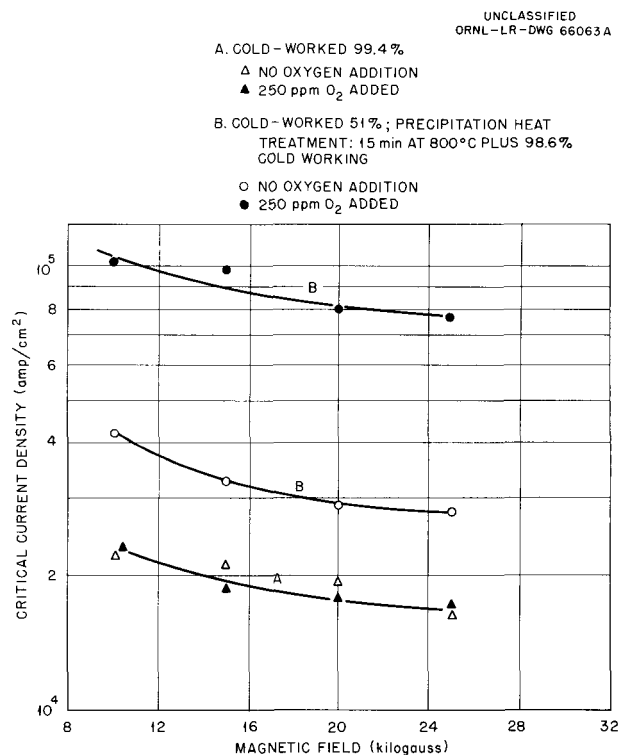


Fig. 34.3. Effect of Oxygen on the Change in Critical Current Density with 800°C Heat Treatment. Final diameter, 0.040-0.044 cm; Nb<sub>3</sub>Zr heat-treated at 0.493 cm for 1 hr at 1500°C.

be proportional to the square of the diameter in a high-field superconductor, the critical currents in this superconductor were found to be proportional to the wire diameter. The effects are illustrated in Fig. 34.4, which shows critical current densities plotted against reciprocal wire diameter. The experimental data follow fairly well the relation

$$\frac{j - j_b}{j_s - j_b} = \frac{4\Delta}{d} \left(1 - \frac{\Delta}{d}\right), \quad \text{for } d > 2\Delta,$$

where  $\Delta$  is the thickness of a surface layer,  $d$  is the diameter of the wire, and  $j_s$  and  $j_b$  are critical

current densities in the surface and bulk regions. This can best be explained by assuming current flow on the surface of the wire either in the normal penetration depth or in a group of filaments that are more densely packed near the surface. The rest of the current is assumed to flow in filaments evenly distributed in the bulk of the wire. The fitting of the curves gave values ranging from  $\Delta = 4 \times 10^{-5}$  cm,  $j_s = 4 \times 10^5$  amp/cm<sup>2</sup>,  $j_b = 0.1 \times 10^5$  amp/cm<sup>2</sup> at 25,000 gauss to  $\Delta = 11 \times 10^{-4}$  cm,  $j_s = 18 \times 10^5$  amp/cm<sup>2</sup>,  $j_b = 0$  at zero applied field. The limiting current densities for very small wires (approx 0.3 mil) were then the values of  $j_s$  obtained. The size effects observed

UNCLASSIFIED  
ORNL-LR-DWG 6774OR2

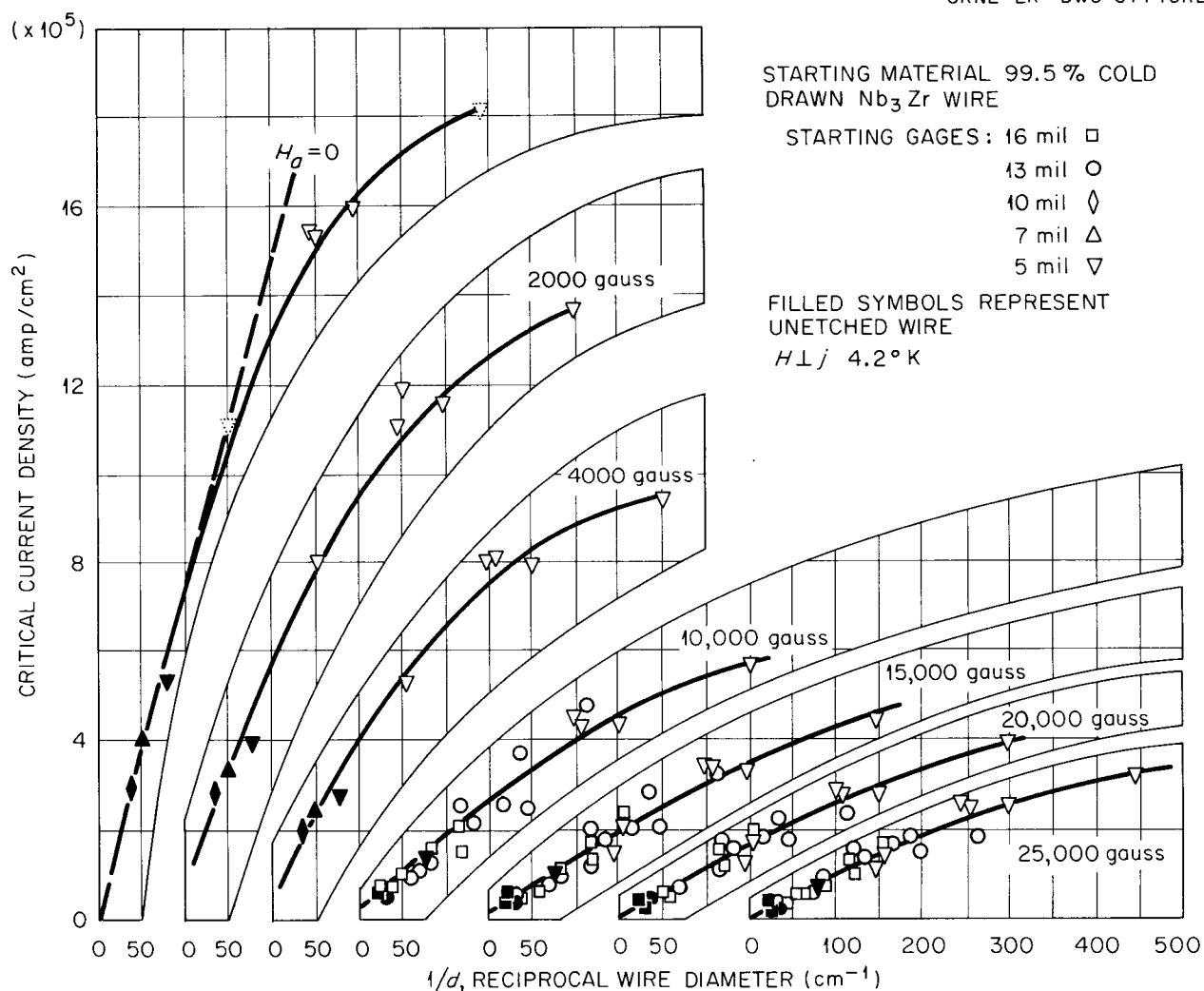


Fig. 34.4. Critical Current Density of Etched Wires vs Reciprocal Wire Diameter.

at higher fields join smoothly with ideal bulk superconducting behavior at zero field, as predicted by Hauser and Buehler,<sup>12</sup> and as shown by the dashed line in Fig. 34.4 corresponding to a bulk critical field of 2230 gauss. This value compares favorably with the 2500-gauss field given by Hulm.<sup>13</sup>

### SUPERCONDUCTING MAGNETS

J. O. Betterton, Jr.      G. D. Kneip, Jr.  
D. S. Easton              J. O. Scarbrough

Magnetic fields of 31,000 gauss have been achieved in a  $0.3 \times 1.2 \times 4.1$  cm volume by means of an iron-core superconducting magnet.<sup>14</sup> Prolonged use of Formvar- or lacquer-insulated coils on this magnet resulted in a decrease of the critical currents of the coils with time. Such behavior would be expected in a dislocation-filament model of the high-field superconductors. Electrical resistance at the breaks in the filaments, as the critical conditions of current and field are exceeded, should raise the temperature of these regions during the dissipation of the field energy. This difficulty was avoided by winding coils with bare wire or Inconel insulation and using pure metal foils between layers. These coils had longer transition times from superconducting to normal states and were used for five months without the critical current decreasing.<sup>7</sup> The 24,000-gauss field decays in about 1.5 sec with this type of coil.

In coils of Nb-Zr superconductors the critical currents are usually smaller than in short sample tests of the same superconductor. A solenoid was made from 0.006-in. ORNL wire heat-treated at 800°C, was insulated with Inconel, and was wound in nearly perfect layers. The critical currents in this coil agreed excellently<sup>7</sup> with the short sample

tests, as shown in Fig. 34.5, possibly because conditioning effects in this wire had been eliminated through pinning of dislocations by the precipitation or because the Inconel screened the currents in adjacent turns induced by shifting of current paths in individual wires as the current was increased.

These magnets are operated with persistent currents. A carbon resistor was wound with an Nb-Zr superconductor and used as a thermal switch between the solenoid leads. Constant fields were achieved quickly by establishing a persistent current without waiting for field equilibrium to be attained.

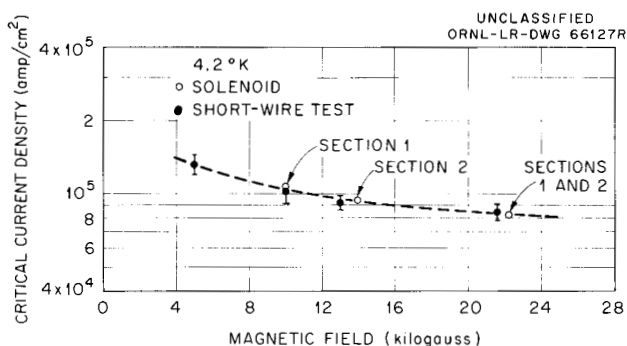


Fig. 34.5. Comparison of Critical Current Densities of Short Wire Tests and in the Inconel-Insulated Solenoids.

### THIN-FOIL ELECTRON TRANSMISSION STUDY OF Nb-Zr SUPERCONDUCTORS

J. O. Stiegler<sup>15</sup>      J. O. Betterton, Jr.

Transmission electron microscopy was used to investigate dislocation configuration and precipitation in severely cold-worked Nb<sub>3</sub>Zr. As shown in Fig. 34.6, the dislocations are tightly packed in walls surrounding regions relatively free of dislocations about 1000 Å in mean dimension. In many instances the dislocations are not tangled but are in a regular, parallel array. The tight packing of dislocations makes it difficult to observe the precipitation in these regions.

<sup>12</sup>J. J. Hauser and E. Buehler, *Phys. Rev.* **125**, 142 (1962).

<sup>13</sup>J. K. Hulm *et al.*, "A High Field Niobium-Zirconium Superconducting Solenoid," pp 332-40 in *Proceedings of the International Conference on High Magnetic Fields, Cambridge, November 4-7, 1961*, MIT Press, Cambridge, and Wiley, New York, 1962.

<sup>14</sup>J. O. Betterton, Jr., and D. S. Easton, "Nb-Nb<sub>3</sub>Sn and Nb-Zr Superconducting Coils in an Iron-Core Magnet," pp 348-57 in *Proceedings of the International Conference on High Magnetic Fields, Cambridge, November 4-7, 1961*, MIT Press, Cambridge, and Wiley, New York, 1962.

<sup>15</sup>Metallography Group.

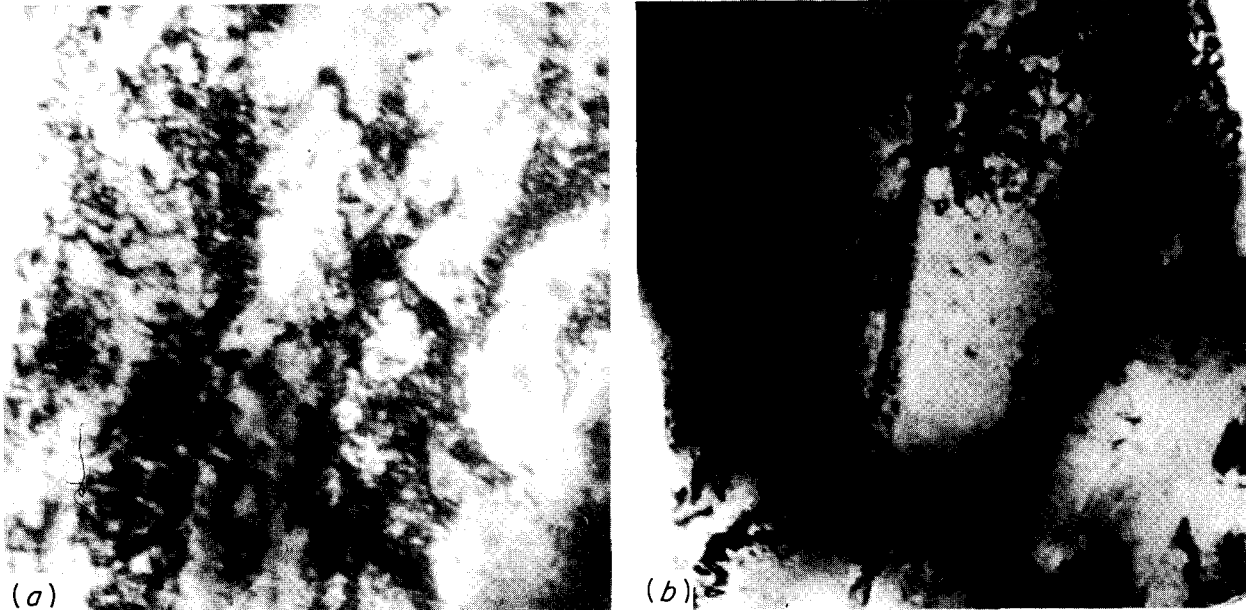
UNCLASSIFIED  
YE-8824UNCLASSIFIED  
YE-8825

Fig. 34.6. Transmission Electron Microstructures of Cold-Worked  $Nb_3Zr$ . 140,000X. Reduced 9%.

The microstructure of  $Nb_3Zr$  resembles that of other cold-worked, body-centered cubic metals, such as iron, which is not a superconductor, and pure niobium ("Transmission Electron Microscopy Studies of Deformed and Annealed Niobium," Chap. 28, this report), which is a relatively soft superconductor. Slight differences do exist in their microstructure, but not to the extent that they exist in the superconducting properties. Large differences in superconducting properties may arise from the capacity of hard superconductors to have more highly stressed regions around dislocations and precipitates than can occur in soft superconductors. These highly stressed regions are on a smaller scale than can be revealed with electron microscopy. Figure 34.6 clearly shows that isolated dislocations are not common in this material. Dislocation walls rather than individual dislocations are probably responsible for the current filaments in hard superconductors.

#### MAGNETORESISTANCE OF TUNGSTEN

J. O. Betterton, Jr.

D. S. Easton

Lifshitz and his co-workers<sup>16,17</sup> relate the transverse magnetoresistance at high fields to open and closed orbits in the Fermi surface. This theory has led to renewed interest in these measurements

for study of topology of Fermi surfaces. The elements V, Nb, Ta, Mo, and W were selected for magnetoresistance study, since they are in that part of the Periodic Table which has been of particular interest in our previous alloy studies and are now available in sufficient purity by electron beam, zone refining so that high field conditions may be approached at 30 kilogauss.

Tungsten crystals of this type, obtained through the courtesy of D. T. Hurd and U. E. Wolff of the General Electric Company, were electromachined into 0.027- to 0.085-in. cylinders and mounted in a rotation holder which fitted with close tolerances in the gap of the iron-core superconducting magnet. O. B. Cavin, X-Ray Diffraction Group, oriented the crystals to within about  $1^\circ$  with Laue x-ray photographs. The crystal with current axis  $\langle 100 \rangle$  was previously reported,<sup>14</sup> and more recently a crystal with the wire axis  $\langle 110 \rangle$  was measured. The magnetoresistance at 4.2°K with magnetic fields in various directions transverse to the wire axis is shown in Figs. 34.7 and 34.8. With currents

<sup>16</sup>1. M. Lifshitz and V. G. Peschanski, *J. Exptl. Theoret. Phys.* **35**, 1251 (1958); translation *Soviet Phys. JETP* **12**, 875 (1959).

<sup>17</sup>1. M. Lifshitz, M. Ia Azbel', and M. I. Kaganov, *J. Exptl. Theoret. Phys.* **31**, 63 (1956); translation *Soviet Phys. JETP* **4**, 41 (1957).

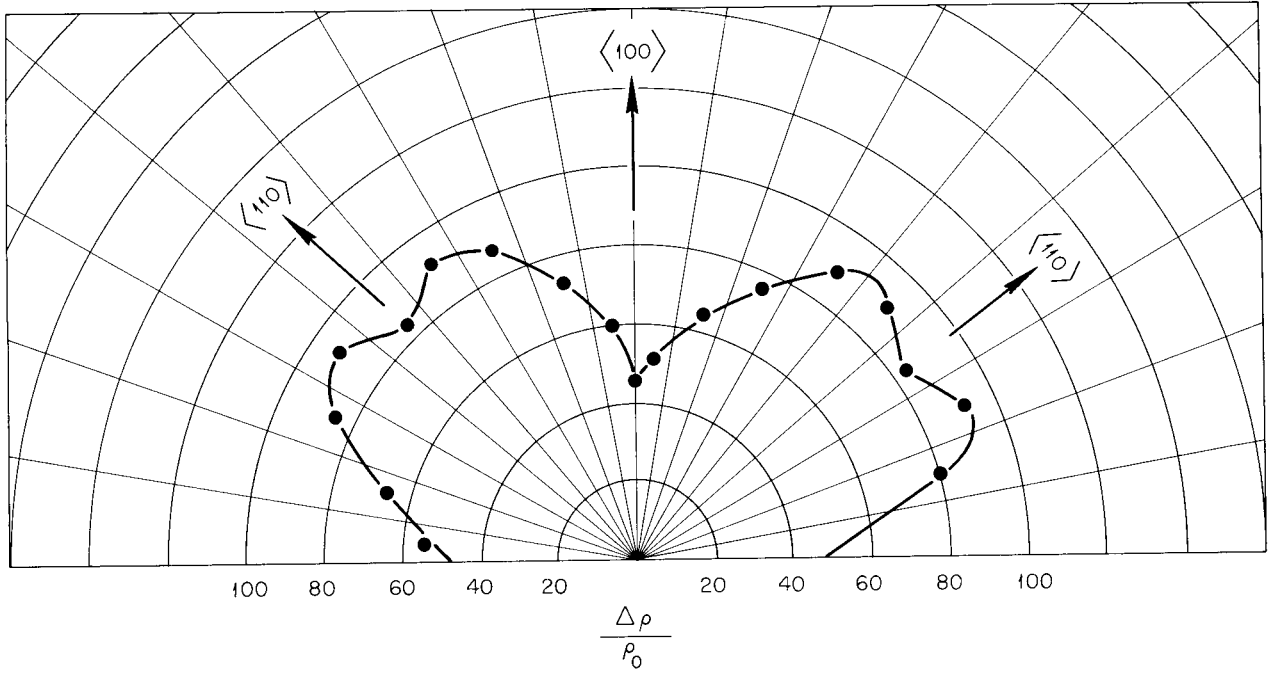


Fig. 34.7. Magnetoresistance of Tungsten Crystal No. 43 vs Different Orientations of Field in a Plane Normal to the Current. Resistivity ratio  $\rho_{317}/\rho_4 = 634$ ; wire and current axis,  $\langle 100 \rangle$ ;  $T = 4.2^\circ\text{K}$ ; field strength = 30 kilogauss;  $\rho_0 = 9.7 \times 10^{-9}$  ohm·cm.

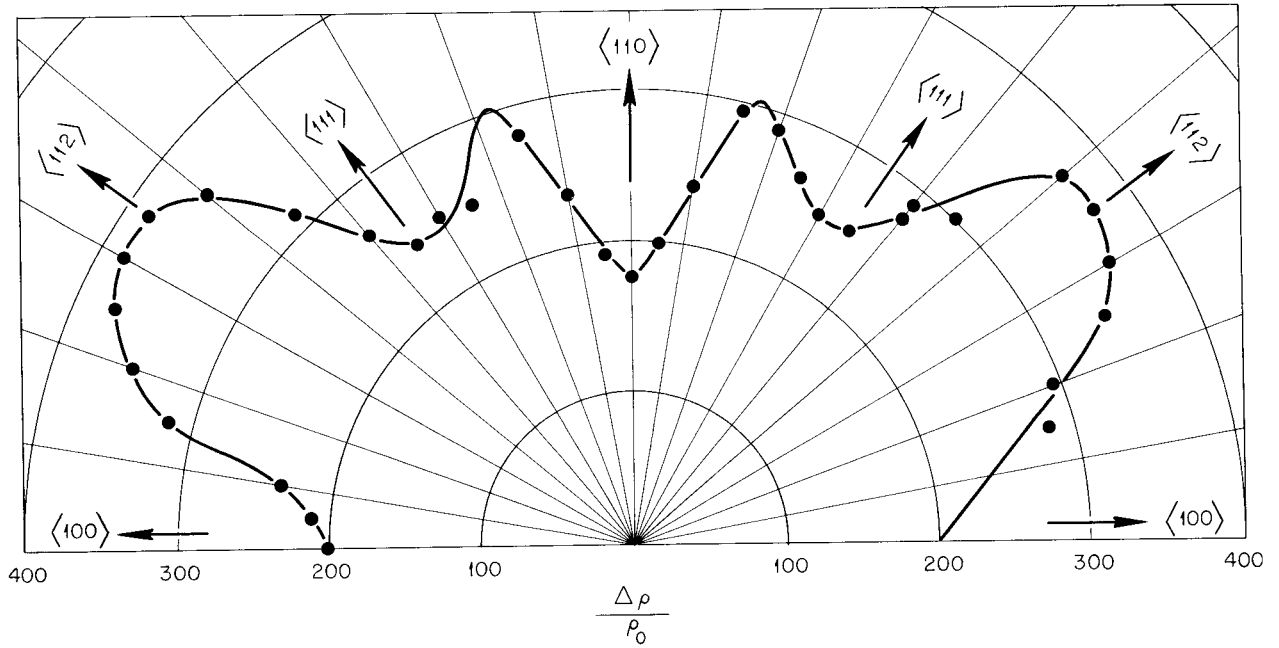


Fig. 34.8. Magnetoresistance of Tungsten Crystal No. 31 vs Different Orientations of Field in a Plane Normal to the Current. Resistivity ratio  $\rho_{317}/\rho_4 = 1229$ ; wire and current axis,  $\langle 110 \rangle$ ;  $T = 4.2^\circ\text{K}$ ; field strength = 30 kilogauss;  $\rho_0 = 4.96 \times 10^{-9}$  ohm·cm.

in the  $\langle 100 \rangle$  direction, broad peaks in the magnetoresistance, with small minima in the center, occur for fields in the  $\langle 110 \rangle$  type of direction. Valleys occur in field directions  $\langle 100 \rangle$ . In the crystal with current direction  $\langle 110 \rangle$ , the largest magnetoresistance occurred in the field direction of type  $\langle 112 \rangle$  with valleys at  $\langle 100 \rangle$  and  $\langle 110 \rangle$ . Our results for the current direction  $\langle 100 \rangle$  agree with earlier measurements<sup>18-20</sup> at liquid-hydrogen temperatures. The transverse magnetoresistance of tungsten was measured by deNoble<sup>19</sup> with the current in the  $\langle 111 \rangle$  direction and found to have very little anisotropy.

In terms of the Lifshitz theory, the valleys would normally refer to saturation effects and directions of closed orbits and the peaks to the occurrence of open orbits and  $H^2$  dependence. However, the magnetoresistance is nearly proportional to  $H^2$  in all directions that have been investigated. The  $H^2$  dependence also occurs in the Lifshitz theory for even-valent metals with closed surfaces and with equal numbers of electrons and holes. Fawcett<sup>21</sup> proposed that this condition also pertains to transition metals with even atomic number such as molybdenum and tungsten and that sheets of Fermi surface are simply connected in these metals. Fawcett<sup>22</sup> extended Lifshitz's theory in the cases of even-valent metals to explain anisotropy in their magnetoresistance. High  $H^2$  type of magnetoresistance would be observed except for minima in those field directions where the current is normal to open orbits or where there are some closed orbits for which high-field conditions are not met; that is, some orbits occur where  $\omega_c T \leq 1$ .

The resistivity ratios,  $\rho_{317}/\rho_4$ , of the present  $\langle 100 \rangle$  and  $\langle 110 \rangle$  crystals were 634 and 1229, respectively. In view of the above, further experiments with still purer crystals and at higher fields are needed to determine whether magnetoresistance anisotropy of tungsten increases or decreases and whether or not saturation effects are encountered at higher effective fields.

## SPECIFIC HEATS OF ZIRCONIUM ALLOYS

G. D. Kneip, Jr.      J. O. Betterton, Jr.  
J. O. Scarbrough

The specific heats of dilute alloys of cadmium and antimony in zirconium were found to consist of an electronic and a vibrational term and to obey Eq. (1) over the range 1.2 to 4.5°K:

$$C = \gamma T + \beta T^3. \quad (1)$$

Both these solutes raise the coefficient of the electronic term and lower the Debye temperature, as do the solutes silver,<sup>23</sup> indium,<sup>24</sup> and tin<sup>24</sup> reported earlier. The rate of increase of the coefficient of the electronic term and hence in the density of states is found experimentally to be a linear function of the solute valence, as shown in Fig. 34.9. This result was discussed previously<sup>23,25,26</sup> in terms of a rigid band model for zirconium in which the  $s$  and  $d$  bands are treated independently and the  $d$  band is assumed not to penetrate into the atomic polyhedra of the solute atoms. The conduction band of the alloy then consists of the interaction of the partially filled zirconium  $s$  band with the  $s$  and  $p$  bands of the solute. The change in the electronic coefficient with solute additions, then, can be shown to be a linear function of the solute concentration and solute valence as observed experimentally. This model, however, leads to a negative number of electrons in the  $s$  band of zirconium.

A better approximation is to assume that the perturbing potential of the solute atom affects the  $s$  and  $d$  bands of zirconium to different extents. The wave function of the  $s$  band should be almost the same in the atomic cells of the solute and solvent atoms. However, a large change in the energy of the  $d$  wave functions should be expected, since, even if they tunnel through the solute cell,

<sup>23</sup>G. D. Kneip, Jr., J. O. Scarbrough, and J. O. Betterton, Jr., *Met. Div. Ann. Progr. Rept. May 31, 1961*, ORNL-3160, pp 4-6.

<sup>24</sup>G. D. Kneip, Jr., and J. O. Betterton, Jr., *Met. Div. Ann. Progr. Rept. Sept. 1, 1959*, ORNL-2839, p 21.

<sup>25</sup>G. D. Kneip, Jr., and J. O. Betterton, Jr., *Met. Div. Ann. Progr. Rept. July 1, 1960*, ORNL-2988, pp 102-7.

<sup>26</sup>G. D. Kneip and J. O. Betterton, Jr., pp 357-58 in *Proceedings of the VII International Conference on Low Temperature Physics* (G. M. Graham and A. C. Hollis Hallett, eds.), University of Toronto Press, 1961.

<sup>18</sup>W. J. DeHaas and J. deNobel, *Physica* 5, 449 (1938).

<sup>19</sup>J. deNobel, *Physica* 15, 532 (1949).

<sup>20</sup>J. deNobel, *Physica* 23, 261, 349 (1957).

<sup>21</sup>E. Fawcett, *Phys. Rev. Letters* 7, 370 (1961).

<sup>22</sup>E. Fawcett, *Phys. Rev. Letters* 6, 534 (1961).

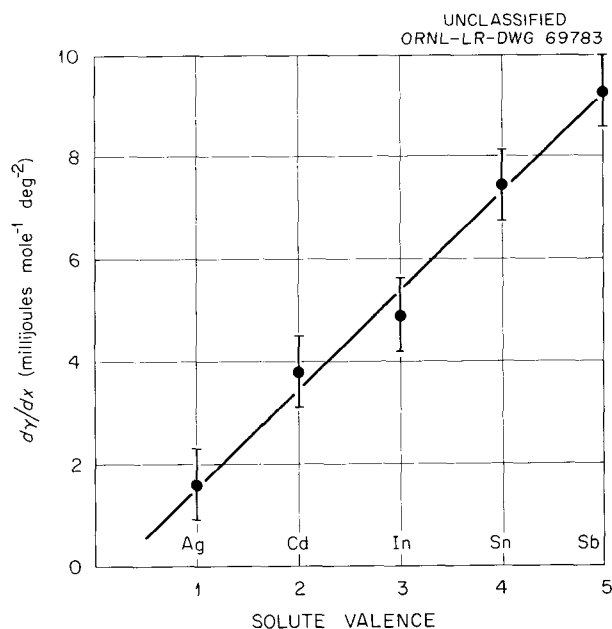


Fig. 34.9. Rate of Change of the Electronic Coefficient,  $dy/dx$ , of the Specific Heat of Zirconium Alloys.

a large number of nodes will be suppressed from the wave functions in the vicinity of the impurity.<sup>27</sup> Assuming then that the bands do not change in shape during alloying but that they may shift with respect to each other, it can be shown that

$$\frac{d}{dx} N(E) = \frac{1}{N(E)} \frac{\partial N(E)}{\partial E} (n - n_s) + \frac{1}{N(E)} \left[ N_d(E) \frac{\partial N_s}{\partial E} - N_s(E) \frac{\partial N_d}{\partial E} \right] \frac{\Delta E_d}{x} - N_d(E);$$

and if the shift in the relative positions is proportional to the solute concentration, then for small  $x$

$$\frac{d}{dx} N(E) \approx \frac{1}{N(E)} \frac{\partial N(E)}{\partial E} (n - n_s) + \frac{A}{N(E)} \left[ N_d(E) \frac{\partial N_s}{\partial E} - N_s(E) \frac{\partial N_d}{\partial E} \right] - N_d(E),$$

where  $A$  is the constant of proportionality,  $n$  the total number of electrons outside closed shells in the

<sup>27</sup>J. Friedel, *Advances in Physics*, vol 3, p 465, Taylor and Francis, London, 1954.

solute, and  $n_s$  the number of zirconium  $s$  electrons. The electronic coefficient of the specific heat is linearly dependent on both the solute concentration and valence, as in the other model, and the slope of the  $dy/dx$  vs solute valence curve is again proportional to the derivative of the density of states with respect to energy. The value of  $d/dx [N(E)]$ , when  $n = n_s$ , however, is now a more complicated function of the densities of states and their derivatives for the two bands. No obvious inconsistencies now exist since the sign of the constant term and thus the direction of the relative movement of the  $s$  and  $d$  bands are determined from the experimental data. The band structure of zirconium then would consist of a low broad  $s$  band overlapping a narrower high  $d$  band. Assuming that the bands are similar to those calculated by Schiff<sup>28</sup> for titanium and in particular that the bottom of the  $s$  band is 5 eV below the bottom of the  $d$  band, there would be about one and three electrons in the  $s$  and  $d$  bands, respectively. For zirconium the  $d$  band must be filled to approximately the minimum in the  $d$  band that arises from the splitting of the crystal potential and the  $d$  atomic orbitals, since the specific heats indicate that the slope of the density of states curve is large and positive at the Fermi surface.

The x-ray emission spectra of zirconium are in agreement with this model. The  $L$  spectra measurements by Shaw and Jossem<sup>29</sup> indicate a very narrow  $d$  band, and the  $M$  spectra studied by Holliday<sup>30</sup> imply that some of the  $4d$  electrons are in a hybridized band with  $p$  symmetry. The magnetic-field dependence of the Hall coefficient and the magnetoresistance of zirconium<sup>31</sup> also indicate an overlapped band structure. A simple two-band model, however, is not adequate to explain the experimental results for these transport properties, as the anisotropy of the Fermi surface must be considered.

The Debye temperatures for each of these alloy series vary linearly with solute concentration. As might be expected, the solvent and solute atoms

<sup>28</sup>B. Schiff, *Proc. Phys. Soc. (London)* A68, 686 (1955).

<sup>29</sup>C. H. Shaw and E. L. Jossem, *Soft X-Ray Spectra of Metals and Alloys, Final Report*, RF Project 471, Ohio State University Research Foundation (December 1959).

<sup>30</sup>J. E. Holliday, *Bull. Am. Phys. Soc. Ser. II*, 6(3), 284 (1961).

<sup>31</sup>T. G. Berlincourt, *Phys. Rev.* 114, 969 (1959).

do not act as independent oscillators in these alloys, and the lattice specific heats do not obey the Kopp rule at low temperatures. At these temperatures, only the long-wavelength phonons are thermally excited so that the lattice specific heat and hence the Debye temperature are determined by elastic waves whose wavelength is several atomic distances. The alloy then behaves as an isotropic solid whose vibrational spectra are similar to those of pure zirconium. The changes in the Debye temperature upon alloying are due to the changes in the average atomic mass and in the elastic constants. As Fig. 34.10 shows, the rate of change in the Debye temperature with concentration is not simply related to the solute valence. Hence, factors other than the electronic energy as reflected by the density of states are apparently important in determining the elastic constants.

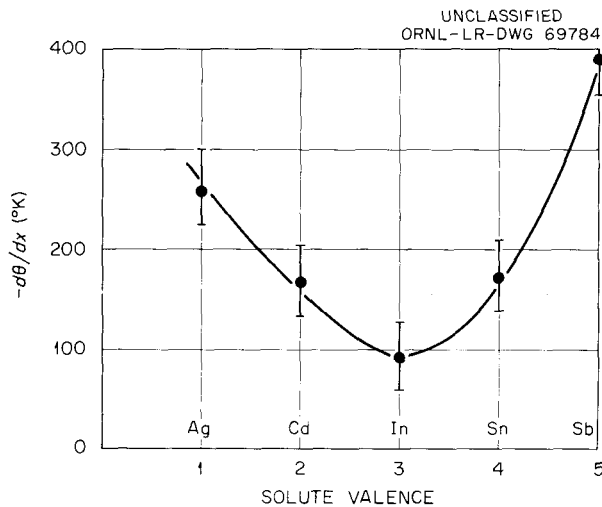


Fig. 34.10. Rate of Change of the Debye Temperature,  $-d\theta/dx$ , of Zirconium Alloys.

### THE Zr-Pb PHASE DIAGRAM

G. D. Kneip, Jr.      J. O. Scarbrough  
J. O. Betterton, Jr.

The zirconium-rich side of the Zr-Pb diagram is being investigated. Lead, like tin, raises the allotropic transformation temperature of zirconium, and preliminary results indicate that there is a

peritectoid reaction,  $\beta + \text{intermediate phase} \rightleftharpoons \alpha$ , at  $890 \pm 10^\circ\text{C}$ . The solubilities of lead in the  $\alpha$  and the  $\beta$  phases at  $890^\circ\text{C}$  are approximately 5 and 4.5 at. %, respectively. The  $\alpha + \beta$  region is unusually narrow in this system.

### THE Zr-Ga PHASE DIAGRAM

D. S. Easton      J. O. Betterton, Jr.

The investigations of the zirconium-rich portion of the Zr-Ga phase diagram<sup>32-34</sup> are now complete. The partial phase diagram is shown in Fig. 34.11.

<sup>32</sup>D. S. Easton and J. O. Betterton, Jr., *Met. Div. Ann. Progr. Rept. Oct. 10, 1958*, ORNL-2632, p 17.

<sup>33</sup>J. O. Betterton, Jr., and D. S. Easton, *Met. Div. Ann. Progr. Rept. Sept. 1, 1959*, ORNL-2839, p 33.

<sup>34</sup>D. S. Easton and J. O. Betterton, Jr., *Met. Div. Ann. Progr. Rept. July 1, 1960*, ORNL-2988, p 110.

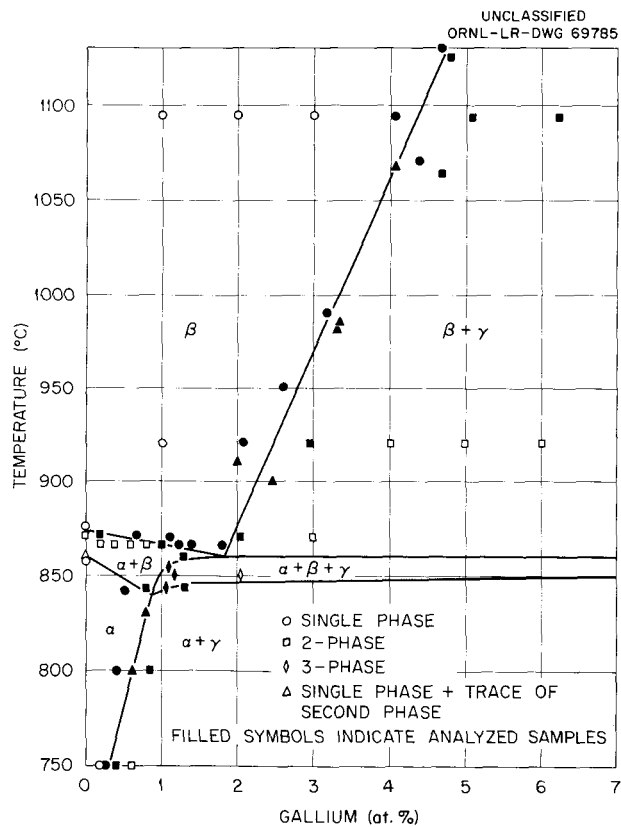


Fig. 34.11. Eutectoid Region of the Zr-Ga Phase Diagram.

A deviation in this diagram from binary equilibrium occurs in the region of the eutectoid reaction  $\beta \rightleftharpoons \alpha + \text{Zr}_3\text{Ga}$ . Similar deviations have been observed in other zirconium-phase diagrams as a result of the very limited solubility of transition elements such as iron and nickel in  $\alpha$ -zirconium. The alloys were quite pure, as they were made from 99.95% Zr and 99.99% Ga and cast and annealed under conditions that do not alter the composition. Neutron-activation and vacuum-fusion analyses show

the following impurities (ppm) in alloys selected from the metallographic specimens: Cu 1-9; Cr 0.8-1.5; Ta 0.02; Mo 0.6-1.7; Fe 39-47; Si 2; W 1-3; Ni 5-6; H 3-4; O 20-33, and N < 5.

The large difference in atomic size of gallium and zirconium restricts the terminal solubility of the  $\alpha$  and  $\beta$  phases and decreases the slope of the  $\alpha/\beta$  boundaries so that  $\beta$  stabilization occurs rather than the  $\alpha$  stabilization observed with the valent solutes indium and aluminum.

## 35. X-Ray Studies of Crystalline Defects

B. S. Borie

### SHORT-RANGE STRUCTURE OF THE ALLOY Cu-16 at. % Al

B. S. Borie      C. J. Sparks

Diffuse intensity measurements on the alloy Cu-16 at. % Al and their interpretation were completed. The measurements were made both at room temperature and at  $-190^{\circ}\text{C}$  in the planes in reciprocal space  $b_3 = 0$  and  $b_1 + b_2 + b_3 = 0$ . A linear extrapolation of the data to absolute zero was performed to minimize contributions of thermal motion to the diffuse scattering. In order to show that the resistivity decrease found by Wechsler and Kernohan<sup>1</sup> for this alloy when exposed in a reactor is caused by a change in short-range order, measurements were made for samples in both irradiated and un-irradiated conditions.

Figure 35.1 is a comparison of the diffuse scattering in the plane  $b_3 = 0$  before and after irradiation. It is clear that reactor irradiation had caused a small increase in the short-range order. However, the general features of the intensity distribution are the same.

In addition to the diffuse scattering caused by ordering, there are modulations of the diffuse intensity associated with small static displacements of atoms from the sites of the average lattice. A method is available<sup>2</sup> for separating the atomic displacement effects from the ordering effects on the diffuse scattering in order that each may be treated separately.

A Fourier transform of the remaining intensity after removal of the atomic displacement effects yields the parameters  $A_{pq}$ , which are related to the

intensity by

$$I(b_1, b_2, 0) = \sum_{pq} A_{pq} \cos 2\pi (b_1 p + b_2 q).$$

The quantities  $b_1, b_2$  are continuous variables defining a point in reciprocal space and take on values equal to one half the Miller indices at the fundamental Bragg reflections. For the distribution shown in Fig. 35.1,  $b_3 = 0$ . The indices  $p$  and  $q$  are integers.

A model for the short-range structure of this alloy was assumed from which values of the  $A_{pq}$ 's could be computed and then compared with those experimentally observed. It was assumed that the aluminum atoms occur in groups of four, arranged in the form of a tetrahedron on the sites of the lattice as shown in Fig. 35.2. All sites that are nearest neighbors of any of the aluminum atoms are assumed to be occupied by copper atoms, so that there are no Al-Al nearest-neighbor pairs. Such tetrahedra are assumed to exist in any one of the six orientations possible on the face-centered cubic lattice. Except for the requirement that no two tetrahedra be so near each other that an Al-Al nearest-neighbor pair is created, the tetrahedra are assumed to be effectively randomly distributed throughout the crystal.

Shown in Table 35.1 are the experimentally observed  $A_{pq}$ 's for both irradiated and unirradiated samples, compared with those computed from the above described model. The comparison is made for both planes in the reciprocal space for which measurements were made.

The atomic displacement modulations are difficult to interpret quantitatively. Qualitatively they appear to be consistent with the assumption that the aluminum atoms composing the above described tetrahedra displace themselves from the sites of the average lattice in such a way that the tetrahedra become more nearly regular.

<sup>1</sup>M. S. Wechsler and R. H. Kernohan, *Solid State Div. Ann. Progr. Rept. Aug. 31, 1958*, ORNL-2614, p 85.

<sup>2</sup>B. S. Borie, *Acta Cryst.* 14, 472 (1961).

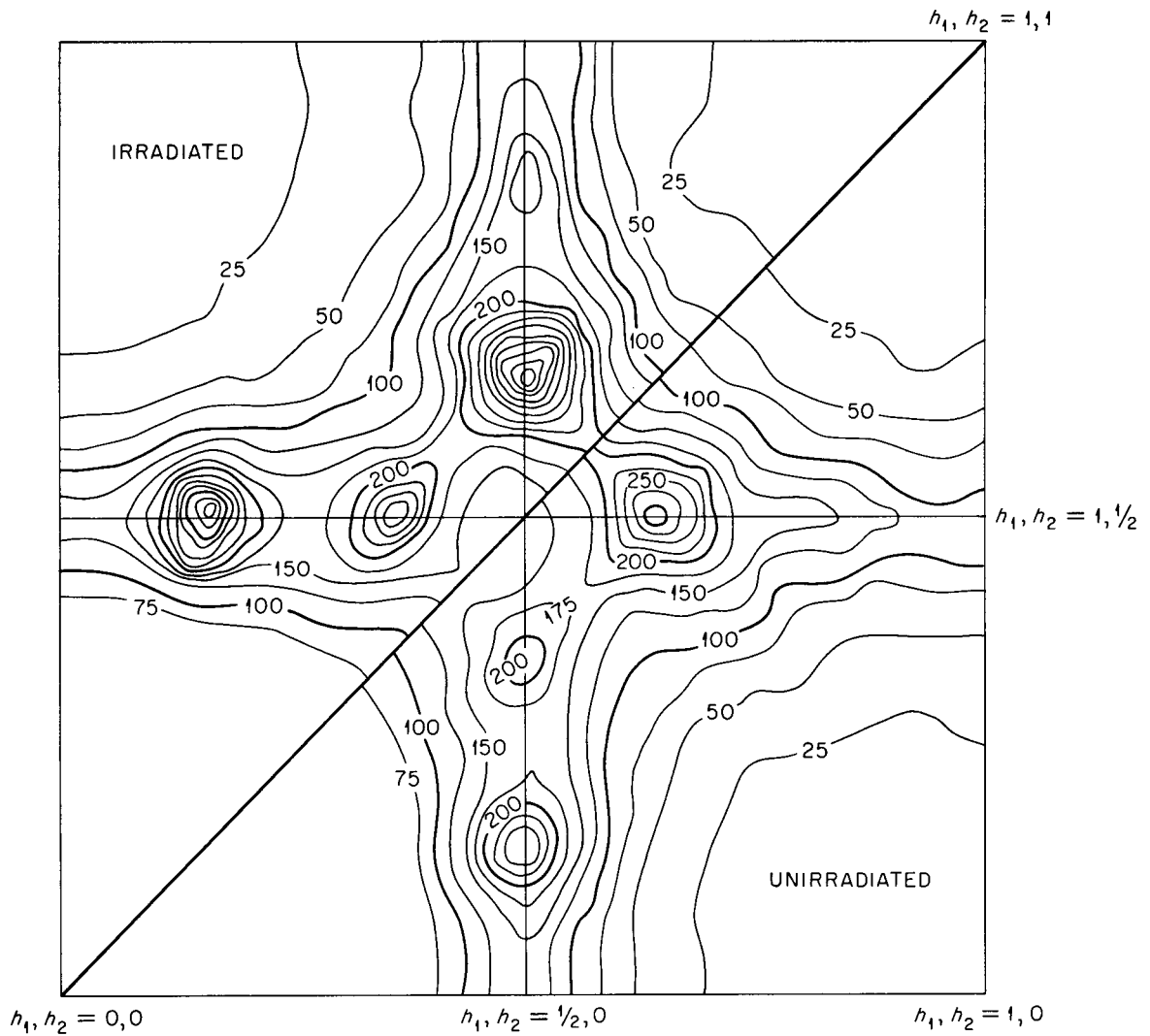


Fig. 35.1. Comparison of the Diffuse Intensity Distribution in the  $h_1, h_2, 0$  Plane of Reciprocal Space for Cu-16 at. % Al Before and After Neutron Irradiation.

Fig. 35.2. Two Face-Centered Cubic Unit Cells Showing Proposed Distorted Tetrahedral Aluminum Array. The face centers are marked by intersections of the dashed lines. Other atomic sites in the vicinity of the four aluminum atoms are presumed to be occupied by copper.

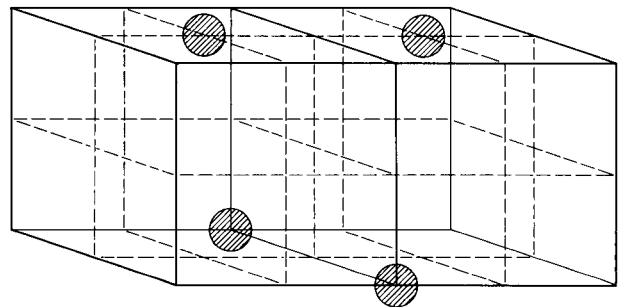


Table 35.1 Comparison of Observed and Computed Short-Range-Order Parameters for Cu-16 at. % Al.

pq	$A_{pq}$ Values for $b_1, b_2, 0$ Plane			pq	$A_{pq}$ Values for $b_1, b_2, b_1 + b_2$ Plane		
	Observed				Observed		
	Irradiated	Unirradiated	Calculated		Irradiated	Unirradiated	Calculated
00	+1.886	+1.732	+1.500	00	+1.209	+1.354	+0.848
10	-0.669	-0.610	-0.564	10	-0.161	-0.139	-0.129
11	-0.024	-0.063	-0.072	21	-0.225	-0.205	-0.184
20	+0.252	+0.254	+0.231	20	+0.171	+0.177	+0.205
21	+0.099	+0.086	+0.100	31	-0.012	-0.015	-0.036
22	-0.124	-0.080	-0.172	30	+0.064	+0.053	+0.055
30	-0.195	-0.168	-0.156	42	+0.036	+0.034	+0.020
31	-0.026	-0.032	-0.077	41	-0.061	-0.063	-0.076
32	+0.050	+0.024	+0.044	40	+0.013	+0.008	-0.034
40	+0.060	+0.072	+0.074	52	+0.030	+0.020	+0.022
41	+0.085	+0.050	+0.028	51	-0.012	-0.012	-0.006
33	-0.009	+0.004	+0.030	50	+0.044	+0.034	+0.033
42	-0.074	-0.040	+0.004	63	-0.019	-0.017	+0.002
43	+0.038	+0.026	-0.002	62	+0.006	+0.003	+0.005
50	-0.064	-0.052	0.000	61	-0.012	-0.012	+0.010
51	-0.023	-0.024	-0.001	60	+0.001	-0.003	-0.001
52	+0.026	+0.018	+0.008	73	+0.003	0.000	+0.002
44	-0.077	-0.045	+0.016	72	+0.010	+0.012	+0.004
53	-0.008	-0.007	+0.011	71	-0.009	-0.007	+0.001
60	+0.076	+0.044	+0.005	84	-0.006	-0.001	+0.008
61	-0.018	-0.006	+0.004	70	+0.013	+0.011	+0.001
62	+0.020	+0.001	+0.001	83	-0.007	-0.005	+0.009
54	+0.041	+0.022	+0.004	82	-0.002	-0.002	+0.005
63	-0.027	-0.002	0.000	81	-0.004	-0.004	+0.002
70	-0.027	-0.011	0.000	94	+0.007	+0.003	+0.002
55	-0.017	-0.010	+0.002	93	-0.001	-0.001	+0.002
71	-0.018	-0.003	0.000	80	+0.004	0.000	0.000

## MONOCHROMATOR DESIGN

C. J. Sparks, Jr.

An extensive study of monochromators and their design and construction was carried out, primarily with the intention of improving our diffuse scattering diffractometer. For this application, high intensity is the important consideration, with resolution of only secondary importance.

A comparison of silicon, germanium, and lithium fluoride showed that LiF is the most desirable of the three for our application. It has the disadvantage of diffracting  $\lambda/2$  as well as  $\lambda$ , which is not the case for diffraction from the (111) reflection of

silicon or germanium. However, this is outweighed by a very considerable intensity gain.

It was found that careful preparation of the LiF wafer before it is doubly bent for focusing yields a gain in intensity of more than a factor of 2 over that of crystals prepared in other ways. Maximum intensity with maximum uniformity of intensity distribution in the diffracted beam was obtained with cleaved wafers polished to a maximum thickness of 10 mils and annealed for about 70 hr at 500°C before bending. Very thin wafers may be bent more uniformly with less plastic distortion, giving a more uniform intensity distribution, and the heat treatment ensures bending success.

## 36. X-Ray Diffraction

H. L. Yakel

### ROUTINE ANALYSES

O. B. Cavin	R. M. Steele
L. A. Harris	H. L. Yakel

Approximately 750 specimens were submitted to the X-Ray Diffraction Group for routine analyses during the period of this report.

Phase identifications and lattice parameter measurements were carried out in the alloy systems Y-Tb, Y-Dy, Y-Ho, Tc-Zr, and Tc-Mo. Quantitative analyses of  $\text{UO}_2:\text{U}_3\text{O}_8:\text{Al}$  compositions in a series of  $\text{Al-U}_3\text{O}_8$  specimens were accomplished through preparation of standard mixtures of the three components.

A diffraction study of the oxygen solubility limit in an Nb-0.88% Zr alloy at 1600°C was completed and is reported elsewhere.<sup>1</sup> X-ray techniques were also successfully used to identify contaminants and reaction products found in UC-UC<sub>2</sub> spheres coated with pyrolytic graphite.<sup>2</sup>

The compounds  $\text{SmScO}_3$  and  $\text{GdScO}_3$  were found to have a distorted perovskite structure. The compound  $\text{Sc}_2\text{TiO}_5$  gives an x-ray diffraction pattern indexable on the basis of a face-centered cubic unit cell with a fluorite-type structure.

Single-crystal x-ray diffraction data<sup>3</sup> for  $\text{CsFeSi}_2\text{O}_6$ , an iron analogue of the mineral pollucite  $\text{CsAlSi}_2\text{O}_6$ , were used to demonstrate random substitution of  $\text{Fe}^{3+}$  for  $\text{Si}^{4+}$  in the crystal

lattice. A similar situation seems probable in pollucite itself ( $\text{Al}^{3+}$  substituting randomly for  $\text{Si}^{4+}$ ).

Single-crystal structure analyses of  $\text{Ca}_2\text{Be}_3\text{O}_5$  and  $\text{Y}_2\text{Be}_2\text{O}_5$  were continued with the collection of complete three-dimensional intensity data for both compounds. A note describing the preliminary x-ray and optical observations on  $\text{Ca}_2\text{Be}_3\text{O}_5$ ,  $\text{Sr}_2\text{Be}_3\text{O}_5$ , and  $\text{Y}_2\text{Be}_2\text{O}_5$  has been accepted for publication.<sup>4</sup> Unit cells were proposed for micaeous phases found in the systems  $\text{RbOH-Fe}_2\text{O}_3\text{-SiO}_2\text{-H}_2\text{O}$  and  $\text{CsOH-Fe}_2\text{O}_3\text{-SiO}_2\text{-H}_2\text{O}$ .

### STRUCTURAL CHANGES IN IRRADIATED BeO (ref 5)

B. S. Borie      H. L. Yakel

X-ray diffraction studies of polycrystalline BeO irradiated to  $1.5 \times 10^{21}$  *nv* ( $E_n > 1$  Mev) at 110°C have shown a selective symmetric or asymmetric broadening of reflections *hk.l* with *l* not zero. Displacements of reflection maxima and centroids to lower scattering angles also occur, but in such a way that unique *c* lattice parameters cannot be defined from spacing measurements. Models of clustered interstitial and vacancy defects in a damaged BeO lattice were proposed, and the predicted x-ray scattering from these models was calculated. Comparison of theoretical and experimental results indicates that the best agreement is obtained for an interstitial-cluster model. Some physical implications of this model are discussed.

<sup>1</sup>D. O. Hobson, *Aging Phenomena in Columbium-Base Alloys*, ORNL-3245 (Mar. 16, 1962).

<sup>2</sup>C. K. H. DuBose and R. J. Gray, *Metallography of Pyrolytic Carbon Coated Uranium Carbide Spheres*, ORNL-TM-91 (Mar. 21, 1962).

<sup>3</sup>O. C. Kopp, G. W. Clark, and L. A. Harris, "Hydrothermal Synthesis of an Iron Analog of the Cesium Zeolite, Pollucite," paper presented at the Annual Meeting of the Geological Society of America, Cincinnati, Ohio, November 2-4, 1961.

<sup>4</sup>L. A. Harris, R. A. Potter, and H. L. Yakel, "Preliminary Observations of Mixed Oxide Compounds Containing BeO," to be published in *Acta Crystallographica*.

<sup>5</sup>Abstract of paper to be submitted to *Acta Crystallographica*.

**HIGH-TEMPERATURE X-RAY DIFFRACTION  
STUDY OF THE ORDER-DISORDER  
TRANSITION IN A Cu-32.2 at. % GOLD  
ALLOY<sup>6</sup>**

H. L. Yakel

The order-disorder transition in a polycrystalline specimen of Cu-32.2 at. % Au has been investigated by means of a high-temperature x-ray diffraction method. The experiment confirmed the existence of an equilibrium  $\text{Cu}_3\text{Au}$  II-type phase in a temperature interval from  $313 \pm 3^\circ\text{C}$  to  $328 \pm 3^\circ\text{C}$ . Diffraction data from this phase are not in conflict with a previously described structure at 31.6 at. % Au based upon an ordered  $\text{Cu}_3\text{Au}$  I-type superlattice in which strictly periodic antiphase domain boundaries occur parallel to any one of the three possible cube faces. Antiphase periods ranging from 18 to 16 are found for the  $\text{Cu}_3\text{Au}$  II-type phase. There is an indication that this period may change as a function of temperature and that periods which are not integral multiples of cubic subcell edges may exist. A two-phase field between the  $\text{Cu}_3\text{Au}$  II-type and disordered

single-phase regions was located on the basis of fundamental reflection broadening. Unambiguous evidence for a similar field was not found between the  $\text{Cu}_3\text{Au}$  I- and II-type single-phase fields.

**ON THE CRYSTAL STRUCTURE OF THE  
ORTHOMANGANITES OF THE HEAVY  
LANTHANIDES AND YTTRIUM<sup>7</sup>**

H. L. Yakel

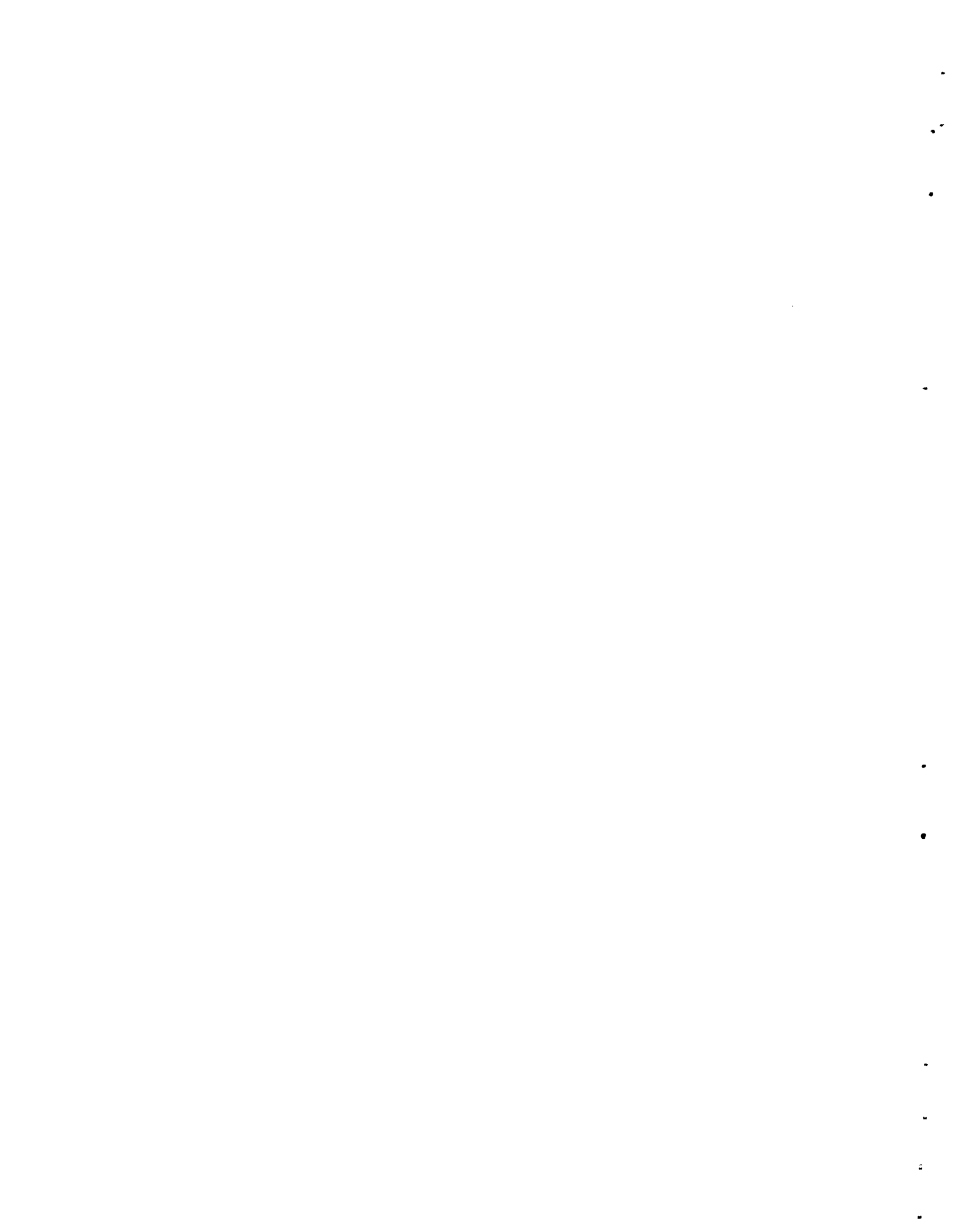
An approximate structure is described for the compounds  $\text{AMnO}_3$ , where A is Ho, Er, Tm, Yb, Lu, or Y. The unit cell is hexagonal, with  $c/a \approx 1.87$ ; the space group is probably  $C_6^3v(P6_3cm)$ . A fivefold coordination of oxygen atoms in the form of a trigonal dipyrmaid surrounds each manganese ion, while the environment of the rare-earth ion resembles that in the hexagonal rare-earth oxides. Refinement of the structure from the x-ray diffraction data was unsatisfactory, due either to least-squares parameter interactions or to basic indeterminate properties.

<sup>6</sup>Abstract of paper to be published in the *Journal of Applied Physics*.

<sup>7</sup>Abstract of paper to be submitted to *Acta Crystallographica*.

# **Papers, Oral Presentations, and Open-Literature Publications**

---



## Papers and Oral Presentations Given at Scientific and Technical Meetings

Research Colloquia, Oxford University, Oxford, England, June 5, 1961

J. O. Betterton, Jr., "Superconductivity of  $Nb_3Sn$ "

American Nuclear Society, National Meeting, Pittsburgh, Pa., June 4-8, 1961

W. R. Martin, "Dimensional Studies of Simulated Experimental Gas-Cooled Reactor Fuel Element at Elevated Temperature"

C. V. Dodd\* and R. W. McClung, "Fuel Element Coolant Channel and Other Spacing Measurements by Eddy-Current Techniques"

R. W. McClung\* and K. V. Cook, "The Development of Ultrasonic Techniques for the Remote Measurement of the HRT Core Vessel Wall Thickness"

Nuclear Congress, 6th, Symposium on Uranium-Thorium Cycle, Rome, Italy, June 13-15, 1961

D. E. Ferguson,\* E. D. Arnold, and W. S. Ernst, Jr., "Preparation and Fabrication of  $ThO_2$  Fuels"

American Physical Society, Mexico City, Mexico, June 22-24, 1961

C. E. Roos,\* J. O. Betterton, Jr., G. D. Kneip, R. W. Boom, and R. E. Worsham, "High Field Studies on  $Nb_3Sn$  Superconductivity"

Plansee Seminar, 4th, Powder Metallurgy in Nuclear Age, Reutte, Austria, June 20-24, 1961

C. S. Morgan, "Influence of Powder Properties in Sintering of Thoria"

American Society for Testing and Materials, 64th Annual Meeting, Atlantic City, N. J., June 25-30, 1961

H. E. McCoy,\* and J. R. Weir, "Discussion of Paper 'Anomalous Fracture in the Creep of Nickel' by T. C. Reuther, P. Shahinian, and M. R. Achter"

D. F. Toner\* and J. L. Scott, "Study of the Factors Controlling the Release of  $Xe^{133}$  from Bulk  $UO_2$ "

Symposium on Ceramics for Nuclear Application, Alfred, N. Y., June 27, 1961

C. E. Curtis, "Technology of the Rare Earth Oxides in Nuclear Applications"

W. O. Harms, "Chemical Elements for Nuclear Ceramics"

---

\*Speaker.

Review of Beryllium Research and Development, Wright-Patterson Air Force Base, Ohio, July 20–21, 1961

R. W. McClung, "Development of Nondestructive Testing Techniques for Thin-Wall Beryllium Tubing"

J. R. Weir, "Mechanical Testing, Corrosion, and Irradiation of Beryllium"

International Nickel Company Power Conference, Estes Park, Colo., Aug. 1–4, 1961

J. H. Coobs, "Fuel Element Cladding Materials for Advanced Nuclear Power Reactors"

H. Inouye, "The Material Problems of the Molten Salt Reactor Equipment"

International Congress of Pure and Applied Chemistry, 18th, Montreal, Canada, Aug. 6–12, 1961

C. R. Boston\* and G. P. Smith, "Visible Absorption Spectra of Solutions of Bismuth Metal in Molten Bismuth Trihalides"

International Calorimetry Conference, Ottawa, Canada, Aug. 14–17, 1961

R. O. Williams and J. A. Wheeler, Jr.,\* "The Use of a Boiling Calorimeter to Measure Changes of Internal Energy During the Deformation of Metals"

Gordon Research Conference, Meriden, N. H., Aug. 28–Sept. 1, 1961

G. P. Smith, "Charge Transfer Spectra in Fused Salts"

Faraday Society, General Discussion on Structure and Properties of Ionic Melts, Liverpool, England, Sept. 5–7, 1961

G. P. Smith\* and C. R. Boston, "Influence of  $Ba^{2+}$ ,  $Sr^{2+}$ ,  $Ca^{2+}$ ,  $Mg^{2+}$ ,  $La^{3+}$ , and  $Y^{3+}$  on the Ultra-Violet Spectrum of  $NO_3^-$  in Ionic Melts"

Atomic Energy Commission Welding Forum, San Antonio, Tex., Sept. 20–22, 1961

W. J. Leonard, "Evaluation of Corrosion Resistance at Various Locations in a Zircaloy-2 Weldment"

G. M. Slaughter\* and T. R. Housley, "Fabrication and Inspection Procedures for EGCR Burst-Slug-Detection Tube and Thermocouple Penetrations"

American Welding Society, Fall Meeting, Dallas, Tex., Sept. 25–28, 1961

R. G. Gilliland\* and G. M. Slaughter, "The Welding of Beryllium"

Electrochemical Society, 120th National Meeting, Detroit, Mich., Oct. 1–5, 1961

J. H. DeVan, "Corrosion Behavior of High Temperature Alloys in Fused Fluoride Mixtures"

A. P. Litman and R. P. Milford,\* "Corrosion Associated with the Oak Ridge National Laboratory Fused Salt Fluoride Volatility Process"

International Conference on the Metallurgy of Beryllium, London, England, Oct. 16–18, 1961

R. W. McClung, "Development of Nondestructive Testing Techniques for Thin-Wall Beryllium Tubing"

J. R. Weir, "The Effect of High-Temperature Reactor Irradiation on Some Physical and Mechanical Properties of Beryllium"

W. J. Werner\* and H. Inouye, "The Reactions of Beryllium with Wet Carbon Dioxide"

---

\*Speaker.

- Society for Nondestructive Testing, 21st National Convention, Detroit, Mich., Oct. 23–27, 1961  
 B. E. Foster\* and J. W. Evans, "X-Ray Mass Attenuation Coefficients in the Range of 50 to 150 kvp"  
 R. W. McClung, "Techniques for Low-Voltage Radiography"
- International Congress on Vacuum Technology, 2nd, Washington, D. C., Oct. 16–19, 1961  
 R. E. Clausing, "A Large-Scale Getter Pumping Experiment Using Vapor Deposited Titanium Films"
- American Society for Metals National Metal Congress and Exposition, 43rd, Detroit, Mich., Oct. 21–27, 1961  
 E. A. Franco-Ferreira, "Electron-Beam Welding"  
 T. S. Lundy\* and J. F. Murdock, "The Diffusion of Al<sup>26</sup> and Mn<sup>54</sup> in Aluminum"  
 H. E. McCoy\* and J. R. Weir, "Effect of Hydrogen on the Creep Properties of Nickel-Base Materials"
- Conference on Thermal Conductivity Measurements, Columbus, Ohio, Oct. 26–28, 1961  
 T. G. Godfrey, T. G. Kollie, and D. L. McElroy,\* "A Radial Heat Flow Apparatus for Thermal Conductivity Measurements from 60 to 1600°C"  
 T. G. Kollie and D. L. McElroy,\* "A Thermal Comparator Apparatus for Thermal Conductivity Measurements from 40 to 400°C"
- Pittsburgh Diffraction Conference, 19th, Pittsburgh, Pa., Nov. 1–3, 1961  
 B. S. Borie,\* C. J. Sparks, and J. V. Cathcart, "X-Ray Diffraction Studies of Cu<sub>2</sub>O Films on Copper"  
 H. L. Yakel,\* B. S. Borie, and R. M. Steele, "Radiation Damage Effects in Beryllium Oxide"
- International Conference on High Magnetic Fields, Cambridge, Mass., Nov. 1–3, 1961  
 J. O. Betterton, Jr.,\* and D. S. Easton, "Nb-Nb<sub>3</sub>Sn and Nb-Zr Superconducting Coils on an Iron-Core Magnet"  
 G. D. Kneip, Jr.,\* J. O. Betterton, Jr., D. S. Easton, and J. O. Scarbrough, "Increased Critical Currents in Nb-Zr Superconductors from Precipitation Induced Defects"
- Geological Society of America, 74th Annual Meeting, Cincinnati, Ohio, Nov. 2–4, 1961  
 O. C. Kopp, G. W. Clark, and L. A. Harris,\* "Hydrothermal Synthesis of an Iron Analog of the Cesium Zeolite, Pollucite"
- American Nuclear Society, Winter Meeting, Chicago, Ill., Nov. 7–10, 1961  
 J. H. DeVan, "Structural Materials for Molten-Salt Reactor Systems"  
 R. E. McDonald, B. W. McCollum, and G. A. Moore, "Replication of Surfaces" (J. E. VanCleve\*)  
 A. R. Olsen, "A New Postirradiation Examination Laboratory at the Oak Ridge National Laboratory"
- Atomic Energy Commission Nondestructive Testing Group, Aiken, S.C., Nov. 15–16, 1961  
 R. W. McClung, "Nondestructive Test Development Program at the Oak Ridge National Laboratory"

---

\*Speaker.

Symposium on Powder Packed Uranium Dioxide Fuel Elements, Windsor, Conn., Nov. 30–Dec. 1, 1961

W. S. Ernst, Jr.,\* and R. L. Beatty, "Vibratory-Compaction Studies at the Oak Ridge National Laboratory"

W. C. Thurber, "Compacted Powder Fuel Irradiation Studies at the Oak Ridge National Laboratory"

High-Temperature Fuels Committee, 13th, Palo Alto, Calif., Dec. 5–7, 1961

J. L. Scott\* and W. C. Thurber,\* "High-Temperature Fuel Work at the Oak Ridge National Laboratory"

Atomic Energy Commission Technical Meeting on Characterization of Uranium Dioxide, Oak Ridge, Tenn., Dec. 12–13, 1961

A. J. Taylor, "Characterization of Uranium Dioxide Powders for Sintering"

A. J. Taylor, M. P. Haydon, J. M. Robbins, and W. O. Harms,\* "Characterization of Spheroidal Uranium Dioxide Particles"

American Society for Metals, Cincinnati Chapter, Cincinnati, Ohio, Feb. 8, 1962

H. Inouye, "Gas-Metal Reactions at High Temperatures"

American Society for Metals Golden Gate Metals Conference, San Francisco, Calif., Feb. 15–17, 1962

G. M. Slaughter,\* C. W. Fox, E. A. Franco-Ferreira, and R. G. Gilliland, "Joining of Refractory Metals for Space Power Applications"

American Institute of Mining, Metallurgical, and Petroleum Engineers, Annual, New York, N.Y., Feb. 18–22, 1962

J. O. Betterton, Jr.,\* G. D. Kneip, Jr., D. S. Easton, and J. O. Scarbrough, "Size Effect and Interstitial Impurities in  $Nb_3Zr$  Superconductors. Superconducting Solenoids with Metal Insulation"

J. R. DiStefano\* and E. E. Hoffman, "Corrosion of Refractory Metals by Lithium"

D. H. Jansen\* and E. E. Hoffman, "Compatibility of Inconel with Boiling Alkali Metals"

A. P. Litman\* and E. E. Hoffman, "Alkali Metal Purification"

R. A. Vandermeer\* and P. Gordon, "The Influence of Recovery on Recrystallization in Aluminum"

National Association of Corrosion Engineers, 18th Annual Meeting, Kansas City, Mo., Mar. 19–23, 1962

H. Inouye, "High-Temperature Reactions of Type 304 Stainless Steel in Low Concentrations of Carbon Dioxide and Carbon Monoxide"

H. E. McCoy, Jr., "The Effects of Various Gaseous Environments on the Mechanical Properties of Austenitic Stainless Steels"

W. J. Werner\* and H. Inouye, "The Reactions of Beryllium with Wet Carbon Dioxide"

Symposium on Electron Beam Technology, 4th, Boston, Mass., Mar. 29–30, 1962

T. Hikido, "Horizontal Zone Melting of Refractory Metals by Remote Gun Electron Bombardment"

---

\*Speaker.

Atomic Energy Commission Metallography Group Meeting, 16th, Richland, Wash., Mar. 28–29, 1962

R. S. Crouse, "Identification of Carbides, Nitrides, and Oxides in Columbium by Anodic Staining"

R. J. Gray,\* R. S. Crouse, and E. L. Long, Jr., "The Organization and Operation of the Metallography at the Oak Ridge National Laboratory"

D. M. Hewette II, "Mounting of Metallographic Samples in Epoxy Resins Using Multiple-Cavity Molds" (R. S. Crouse\*)

American Society for Metals Educational Series, Columbia Basin Chapter, Richland, Wash., Mar. 28–29, 1962

R. S. Crouse, "Metallography in Color"

R. J. Gray, "Metallography Facilities at a National Laboratory, ORNL" and "Light Microscopy"

J. O. Stiegler, "The Electron Probe Microanalyzer and Its Application"

Libby/Cockcroft Symposium on Gas-Coolant Compatibility, Harwell, England, Apr. 2–4, 1962

W. O. Harms, "Compatibility Studies on Ceramic Materials for Gas-Cooled Reactors"

W. R. Martin\* and H. E. McCoy, Jr., "Effect of CO<sub>2</sub> on the Strength and Ductility of Type 304 Stainless Steel at Elevated Temperatures"

US/UK AGR/EGCR Gas-Coolant Compatibility Meeting, Culcheth, England, Apr. 5–6, 1962

J. H. DeVan\* and H. Inouye, "Reactions of Reactor Materials with Gaseous Contaminants in Helium-Cooled Reactor Systems"

B. Fleischer, J. H. DeVan, and J. H. Coobs,\* "Graphite-Stainless Steel Compatibility Studies"

American Welding Society, 43rd Annual, Cleveland, Ohio, Apr. 9–13, 1962

R. G. Donnelly\* and G. M. Slaughter, "Development of Fabrication Procedures for Enrico Fermi Reactor Fuel Elements"

C. W. Fox,\* R. G. Gilliland, and G. M. Slaughter, "Brazing of Columbium"

Physical Metallurgy Colloquia, University of Illinois, Urbana, Ill., Apr. 11, 1962

J. O. Betterton, Jr., "Recent Experiments with High Field Superconductors"

American Nuclear Society National Topical Meeting on High Temperature Materials for Nuclear Applications, San Diego, Calif., Apr. 11–13, 1962

A. T. Chapman, "Fueled BeO and Bulk ThO<sub>2</sub>-UO<sub>2</sub> Fuels"

E. E. Hoffman, "Basic Materials Problems in Liquid-Metal Systems"

American Physical Society, Washington, D.C., Apr. 23–26, 1962

G. D. Kneip, Jr.,\* J. O. Betterton, Jr., D. S. Easton, and J. O. Scarbrough, "Size Effect in Nb-Zr Superconductors"

American Institute of Mining, Metallurgical, and Petroleum Engineers Regional Conference, 16th, Hartford, Conn., Apr. 26–27, 1962

R. J. Gray, "Optical Microscopy"

---

\*Speaker.

American Ceramic Society, 64th Annual, New York, N. Y., Apr. 29–May 3, 1962

A. T. Chapman, "Phase Studies in BeO-Metal Oxide Systems Using the Porous Collector Technique"

Southern Metals Conference, Clemson, S. C., May 3–4, 1962

A. E. Goldman, "Material Problems of Gas-Cooled Reactor Power Plants"

Southeastern Conference on Theoretical and Applied Mechanics, Gatlinburg, Tenn., May 3–6, 1962

C. R. Kennedy and J. T. Venard,\* "Collapse of Tubes by External Pressure"

Atomic Energy Commission Coated Particle Fuels Working Group, 3rd, Oak Ridge, Tenn., May 7–8, 1962

E. S. Bomar,\* F. L. Carlsen, R. L. Beatty, and J. L. Cook, "Specifications, Procurement, and Postirradiation Evaluation"

F. L. Carlsen, "The ORNL Coated Particle Fuels Irradiation Test Program"

F. L. Carlsen\* and V. A. DeCarlo, "Fission-Gas-Release Experiments in the ORR Poolside Sweep Facility"

J. L. Scott, "Release of Fission Products by Neutron-Activation Techniques"

High-Temperature Fuels Committee, 14th, Idaho Falls, Idaho, May 15–17, 1962

J. L. Scott\* and W. C. Thurber,\* "High-Temperature Fuel Work at the Oak Ridge National Laboratory"

American Society of Mechanical Engineers Hydraulic Conference, Worcester, Mass., May 21–23, 1962

P. G. Smith, J. H. DeVan, and A. G. Grindell,\* "Cavitation Damage to Centrifugal Pump Impellers During Operation with Liquid Metals and Molten Salt at 1050–1400°F"

Atomic Energy Commission Annual Corrosion Symposium, Upton, N. Y., May 23–25, 1962

R. E. Pawel\* and J. V. Cathcart, "Oxide Platelet Formation in Tantalum Single Crystals"

---

\*Speaker.

## Publications

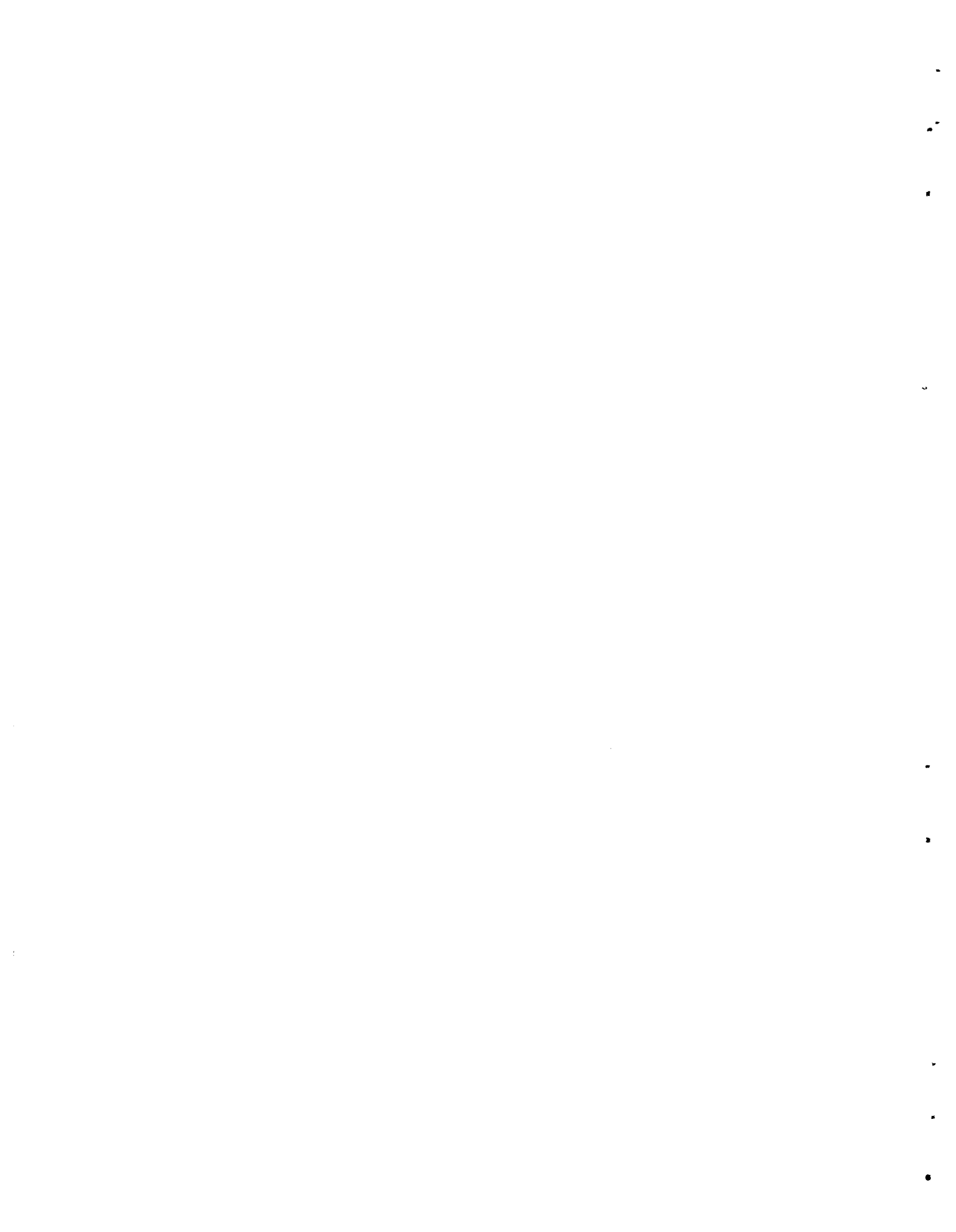
- Beaver, R. J., "Contamination of Fuel Element Surfaces," *Nucl. Safety* 3(1), 61-64 (1961).
- Beaver, R. J., J. E. Cunningham, and R. C. Waugh, "Dispersions in Metals," p 142 in *Uranium Dioxide: Properties and Nuclear Applications* (ed. by J. Belle), Naval Reactors, Division of Reactor Development, USAEC, Washington, 1961.
- Beaver, R. J., C. F. Leitten, Jr., and J. L. English, *An Investigation of the Corrosion Resistance of Brazing Alloys for Austenitic Stainless Steel Fuel Elements for Service in 565°F Pressurized Water*, ORNL-2834 (Mar. 29, 1962).
- Beaver, R. J., J. H. Erwin, and R. S. Mateer, *An Evaluation of the Uranium Contamination on the Surfaces of Alclad Uranium-Aluminum Alloy Research Reactor Fuel Plates*, ORNL-3206 (Mar. 5, 1962).
- Betterton, J. O., Jr., and D. S. Easton, "Nb-Nb<sub>3</sub>-Sn and Nb-Zr Superconducting Coils on an Iron-Core Magnet," pp 348-57 in *Proceedings of the International Conference on High Magnetic Fields, Cambridge, Nov. 4-7, 1961*, MIT Press, Cambridge, and Wiley, New York, 1962.
- Betterton, J. O., Jr., R. W. Boom, G. D. Kneip, R. E. Worsham, and C. E. Roos, "Superconductivity of Nb<sub>3</sub>Sn in a Pulsed Magnetic Field," *Phys. Rev. Letters* 6(10), 532-34 (1961).
- Borie, Bernard, "Temperature Diffuse Scattering for Cubic Powder Patterns," *Acta Cryst.* 14(6), 566-68 (1961).
- Borie, Bernard, and C. J. Sparks, "A Determination of Thin Oxide Film Thickness by Integrated Intensity Measurements," *Acta Cryst.* 14(6), 569-70 (1961).
- Cherubini, J. H., *Determinations of the Kinetics and Mechanisms of Deboronization at 1135°C*, ORNL-3141 (Aug. 31, 1961).
- Cherubini, J. H., C. F. Leitten, Jr., and R. J. Beaver, *Evaluation of the Boron Content in Fuel Plates Fabricated for the First Core Loading of the Army SM-1 Reactor (Formerly APPR-1)*, ORNL-3249 (Feb. 8, 1962).
- Clausing, R. E., *A Large-Scale Getter Pumping Experiment Using Vapor Deposited Titanium Films*, ORNL-3217 (Oct. 24, 1961).
- DeVan, J. H., *Catastrophic Oxidation of High-Temperature Alloys*, ORNL TM-51 (Nov. 10, 1961).
- Dodd, C. V., and R. W. McClung, *Fuel Element Coolant Channel and Other Spacing Measurements by Eddy-Current Techniques*, ORNL TM-129 (Mar. 20, 1962).
- Donnelly, R. G., and G. M. Slaughter, "The Brazing of Graphite," *Welding J.* 41(5), 61-69 (1962).
- Donnelly, R. G., *The Development of a Sump-Type Solidified-Metal Seal*, ORNL TM-179 (Mar. 15, 1962).
- DuBose, C. K. H., and R. J. Gray, *Metallography of Pyrolytic Carbon Coated and Uncoated Uranium Carbide Spheres*, ORNL TM-91 (Mar. 21, 1962).

- Franco-Ferreira, E. A., *Fabrication of Boiler Section for Boiling-Liquid-Metal Loop*, ORNL TM-40 (Oct. 16, 1961).
- Godfrey, T. G., T. G. Kollie, and D. L. McElroy, "A Radial Heat Flow Apparatus for Thermal Conductivity Measurements from 60 to 1600°C," p 179 in *Conference on Thermal Conductivity Methods held at Battelle Memorial Institute Oct. 26, 27, 28, 1961*, BMI, Columbus, 1961.
- Goldman, A. E., and A. P. Litman, *Corrosion Associated with Hydrofluorination in the Oak Ridge National Laboratory Fluoride Volatility Process*, ORNL-2833 (Nov. 1, 1961).
- Gray, R. J., and C. K. H. DuBose, *A Micrographic Study of the Effect of Moisture in the Air on Arc-Cast Uranium Monocarbide and Uranium Dicarbide at Room Temperature Over Extended Periods*, ORNL TM-56 (Nov. 20, 1961).
- Guthrie, P. V., and E. E. Stansbury, *X-Ray and Metallographic Study of the Nickel-Rich Alloys of the Nickel-Molybdenum System. II*, ORNL-3078 (July 3, 1961).
- Hamner, R. L., and L. A. Harris, *The Calcination in Air of Beryllium Oxalate Trihydrate to Beryllium Oxide*, ORNL-3183 (Oct. 5, 1961).
- Harris, L. A., and A. J. Taylor, "A Pressure-Induced Phase Transformation in a  $\text{UO}_3$  Monohydrate," *J. Am. Ceram. Soc.* **45**(1), 25-28 (1962).
- Hikido, T., "Horizontal Zone Melting of Refractory Metals by Remote Gun Electron Bombardment," pp 276-83 in *Proceedings Fourth Symposium on Electron Beam Technology March 29-30, 1962, Boston, Mass.* (ed. by R. Bakish), Alloy Electronics Corporation, Cambridge, 1962.
- Hobson, D. O., *Effect of Alloying Elements on the Strength, Stability, and Corrosion and Oxidation Resistance of Columbium*, ORNL-3212 (Jan. 15, 1962) (classified).
- Hobson, D. O., *Aging Phenomena in Columbium-Base Alloys*, ORNL-3245 (Mar. 16, 1962).
- Hughes, E. W., H. L. Yakel, and H. C. Freeman, "The Crystal Structure of Biuret Hydrate," *Acta Cryst.* **14**, 345-52 (1961).
- Inouye, H., "The Oxidation of Columbium at Low Oxygen Pressure," pp 649-65 in *Columbium Metallurgy* (ed. by D. L. Douglass and F. W. Kunz), Interscience, New York, 1961.
- Irvine, A. R., and A. L. Lotts, *Criteria for the Design of the Thorium Fuel Cycle Development Facility*, ORNL TM-149 (Mar. 2, 1962).
- Kennedy, C. R., *Instantaneous and Time-Dependent Collapse of the OFHC Copper Vessels by External Pressure*, ORNL TM-102 (Jan. 5, 1962).
- Kennedy, C. R., and J. T. Venard, *Collapse of Tubes by External Pressure*, ORNL TM-166 (Apr. 17, 1962).
- Klindt, K. K., A. E. Richt, and W. C. Thurber, *Postirradiation Examination of 17-4 PH Stainless Steel Control Rod Drive Rack from SM-1 Reactor*, ORNL-3218 (Nov. 17, 1961).
- Kollie, T. G., and D. L. McElroy, "Thermal Comparator Apparatus for Thermal Conductivity Measurements from 40 to 400°C," p 289 in *Conference on Thermal Conductivity Methods held at Battelle Memorial Institute Oct. 26, 27, 28, 1961*, BMI, Columbus, 1961.
- Kneip, G. D., Jr., J. O. Betterton, Jr., D. S. Easton, and J. O. Scarbrough, "Superconductivity in Heat-Treated Nb-Zr Alloys," *J. Appl. Phys.* **33**(2), 754-55 (1962); ORNL CF-61-8-99 (Aug. 10, 1961).
- Kneip, G. D., Jr., J. O. Betterton, Jr., D. S. Easton, and J. O. Scarbrough, "Increased Critical Currents in Nb-Zr Superconductors from Precipitation Defects," pp 603-8 in *Proceedings of the International Conference on High Magnetic Fields, Cambridge, Nov. 4-7, 1961*, MIT Press, Cambridge, and Wiley, New York, 1962.

- Kopp, O. C., L. A. Harris, and G. W. Clark, "The Hydrothermal Conversion of Muscovite to Kalsilite and an Iron-Rich Mica," *Am. Mineralogist* **46**, 719-27 (1961).
- Leonard, W. J., "Root-Pass Procedures for Inert-Arc Field Welding of Titanium," *Welding J.* **40**(12), 1246-53 (1961).
- Litman, A. P., *Corrosion of Volatility Pilot Plant Mark I INOR-8 Hydrofluorinator and Mark III L. Nickel Fluorinator After Fourteen Dissolution Runs*, ORNL-3253 (Feb. 9, 1962).
- Lundy, T. S., and J. F. Murdock, "Diffusion of Al<sup>26</sup> and Mn<sup>54</sup> in Aluminum," *J. Appl. Phys.* **33**(5), 1671-73 (1962).
- Martin, W. R., "Dimensional Studies of Simulated Experimental Gas-Cooled Reactor Fuel Elements at Elevated Temperatures" (summary only), *Trans. Am. Nuclear Soc.* **4**(1), 149-50 (1961).
- Martin, W. R., and H. E. McCoy, Jr., *An Investigation of the High-Temperature Properties of the AISI Type 502 Steel*, ORNL-TM-39 (Nov. 28, 1961).
- Martin, W. R., and J. R. Weir, Jr., *Status Report on the Basic Mechanical Properties of Advanced Test Reactor Aluminum Alloys*, ORNL TM-48 (Nov. 10, 1961).
- Martin, W. R., and J. R. Weir, *Dimensional Behavior of the Experimental Gas-Cooled Reactor Fuel Element at Elevated Temperatures*, ORNL-3103 (July 19, 1961).
- McClung, R. W., *Techniques for Low-Voltage Radiography*, ORNL-3252 (Feb. 14, 1962), and *Metals Eng. Quart.* **2**(2), 68-75 (1962).
- McClung, R. W., "Development of Nondestructive Tests for the EGCR Fuel Assembly," *Non-destructive Testing* **19**(5), 352-58 (1961).
- McClung, R. W., *Feasibility Studies - Nondestructive Testing of the Enrico Fermi Reactor Core B Fuel Element*, ORNL-3221 (Dec. 21, 1961).
- McClung, R. W., and K. V. Cook, *Feasibility Studies for the Nondestructive Testing of the EGCR Through-Tube Weldment*, ORNL TM-46 (Nov. 14, 1961).
- McClung, R. W., and K. V. Cook, *Development of Ultrasonic Techniques for the Remote Measurement of the HRT Core Vessel Wall Thickness*, ORNL TM-103 (Mar. 15, 1962); summary only, *Trans. Am. Nuclear Soc.* **4**(1), 140 (1961).
- McCoy, H. E., and D. A. Douglas, "Effect of Various Gaseous Contaminants on the Strength and Formability of Columbium," pp 85-118 in *Columbium Metallurgy* (ed. by D. L. Douglass and F. W. Kunz), Interscience, New York, 1961.
- McDonald, R. E., B. W. McCollum, and G. A. Moore, "Replication of Surfaces for Hot-Cell Application," p 166 in *Proceedings of the Ninth Conference on Hot Laboratories and Equipment*, American Nuclear Society, Chicago, 1961.
- McElroy, D. L., "Discussion of Paper 'Thermal Conductivity of Some Commercial Iron-Nickel Alloys' by T. W. Watson and H. E. Robinson," *J. Heat Transfer* **83**, 407 (1961).
- McHargue, C. J., "The Effect of Initial Orientation on the Fiber Texture of Aluminum Rods," *Trans. Met. Soc. AIME* **221**, 812-19 (1961).
- McHargue, C. J., "Twinning in Columbium," *Trans. Met. Soc. AIME* **224**, 334-39 (1962).
- McHargue, C. J., "Deformation Stacking Faults in Face-Centered Cubic Thorium and Cerium," *Acta Met.* **9**(9), 851-53 (1961).
- McNabb, B., Jr., and H. E. McCoy, Jr., *A Laboratory Gas-Circulating Pump*, ORNL TM-75 (Nov. 30, 1961).
- Olsen, A. R., "A New Postirradiation Examination Laboratory at the Oak Ridge National Laboratory," p3 in *Proceedings of the Ninth Conference on Hot Laboratories and Equipment*, American Nuclear Society, Chicago, 1961.

- Pawel, R. E., J. V. Cathcart, and J. J. Campbell, "Break-Away Phenomena in the Oxidation of Columbium Single Crystals," pp 667-84 in *Columbium Metallurgy* (ed. by D. L. Douglass and F. W. Kunz), Interscience, New York, 1961.
- Pawel, R. E., J. V. Cathcart, and J. J. Campbell, "Oxide Platelet Formation in Tantalum Single Crystals," *Acta Met.* 10(2), 149-60 (1962).
- Petersen, G. F., W. M. Ewing, and G. P. Smith, "Densities of Some Salt Mixtures," *J. Chem. Eng. Data* 6(4), 540 (1961).
- Picklesimer, M. L., "Discussion of Paper 'Effect of Oxygen on the Properties of Zircaloy-2' by L. S. Rubenstein, J. G. Goodwin, and F. L. Shubert," *ASM Trans. Quart.* 54, 703 (1961).
- Picklesimer, M. L., "Discussion of Paper 'Oxidation of Zirconium-Columbium Alloys in Oxygen at 525 and 1090°C' by O. Zmeskel and M. L. Brey," *Trans. Am. Soc. Metals* 53, 932-33 (1961).
- Prados, J. W., "Use of Rate Data in Reactor Hazards Calculations," *Nucl. Safety* 2(4), 12 (1961).
- Prados, J. W., *A Model for Fission-Gas Release from Porous Fuels in Low-Permeability Containers*, ORNL-3168 (Aug. 11, 1961).
- Scott, J. L., *The Release of Kr<sup>85</sup> from UO<sub>2</sub> in ORR Capsules*, ORNL-3195 (Sept. 21, 1961).
- Slaughter, G. M., and T. R. Housley, *The Welding of Ferritic Steels to Austenitic Stainless Steels*, ORNL TM-98 (Jan. 4, 1962).
- Slaughter, G. M., and T. R. Housley, *Fabrication and Inspection Procedures for Experimental Gas-Cooled Reactor Burst-Slug-Detection Tube and Thermocouple Penetrations*, ORNL CF-61-8-29 (Aug. 14, 1961).
- Slaughter, G. M., and P. Patriarca, *Welding and Brazing of High-Temperature Radiators and Heat Exchangers*, ORNL TM-147 (Feb. 20, 1962).
- Smith, G. P., and G. F. Petersen, "Volumetric Properties of the Molten System (Li,K)-(Cl,NO<sub>3</sub>)," *J. Chem. Eng. Data* 6(4), 493-96 (1961).
- Smith, G. P., and C. R. Boston, "Influence of Ba<sup>2+</sup>, Sr<sup>2+</sup>, Ca<sup>2+</sup>, Mg<sup>2+</sup>, La<sup>3+</sup>, and Y<sup>3+</sup> on the Ultra-Violet Spectrum of NO<sub>3</sub><sup>-</sup> in Ionic Melts," *Discussions Faraday Soc.* 32, 14-21 (1962).
- Spruiell, J. E., and D. M. Hewette II, *Surface Preparation of Metallographic Specimens of Zirconium-Base Alloys Containing Copper*, ORNL-3139 (Oct. 13, 1961).
- Stephenson, R. L., and H. E. McCoy, Jr., *Recording Equipment for Internal Friction Measurements*, ORNL-3197 (Oct. 16, 1961), and *J. Sci. Instr.* 39, 54-55 (1962).
- Swindeman, R. W., *Thermal Stresses in Solid Cylinders of Beryllium Oxide*, ORNL TM-123 (Apr. 6, 1962).
- Swindeman, R. W., *Thermal Stresses in Hollow Cylinders of Beryllium Oxide*, ORNL TM-24 (Jan. 9, 1962).
- Swindeman, R. W., *The Strain-Fatigue Properties of Inconel. Part I. General Considerations*, ORNL-3250 (Mar. 29, 1962); *Part II. Isothermal Tests with Constant Hold Time*, ORNL-3250 (Mar. 29, 1962).
- Toner, D. F., and J. L. Scott, "Fission-Product Release from UO<sub>2</sub>," *Nucl. Safety* 3(2), 15-20 (1961).
- Toner, D. F., and J. L. Scott, "Study of Factors Controlling the Release of Xenon-133 from Bulk UO<sub>2</sub>," *Am. Soc. Testing Materials Spec. Tech. Publ. No. 306*, pp 86-99 (1961).
- Tracy, J. W., N. W. Gregory, E. C. Lingafelter, J. D. Dunitz, H. C. Mez, R. E. Rundle, C. Scheringer, H. L. Yakel, Jr., and M. K. Wilkinson, "The Crystal Structure of Chromium(II) Chloride," *Acta Cryst.* 14, 927-29 (1961).

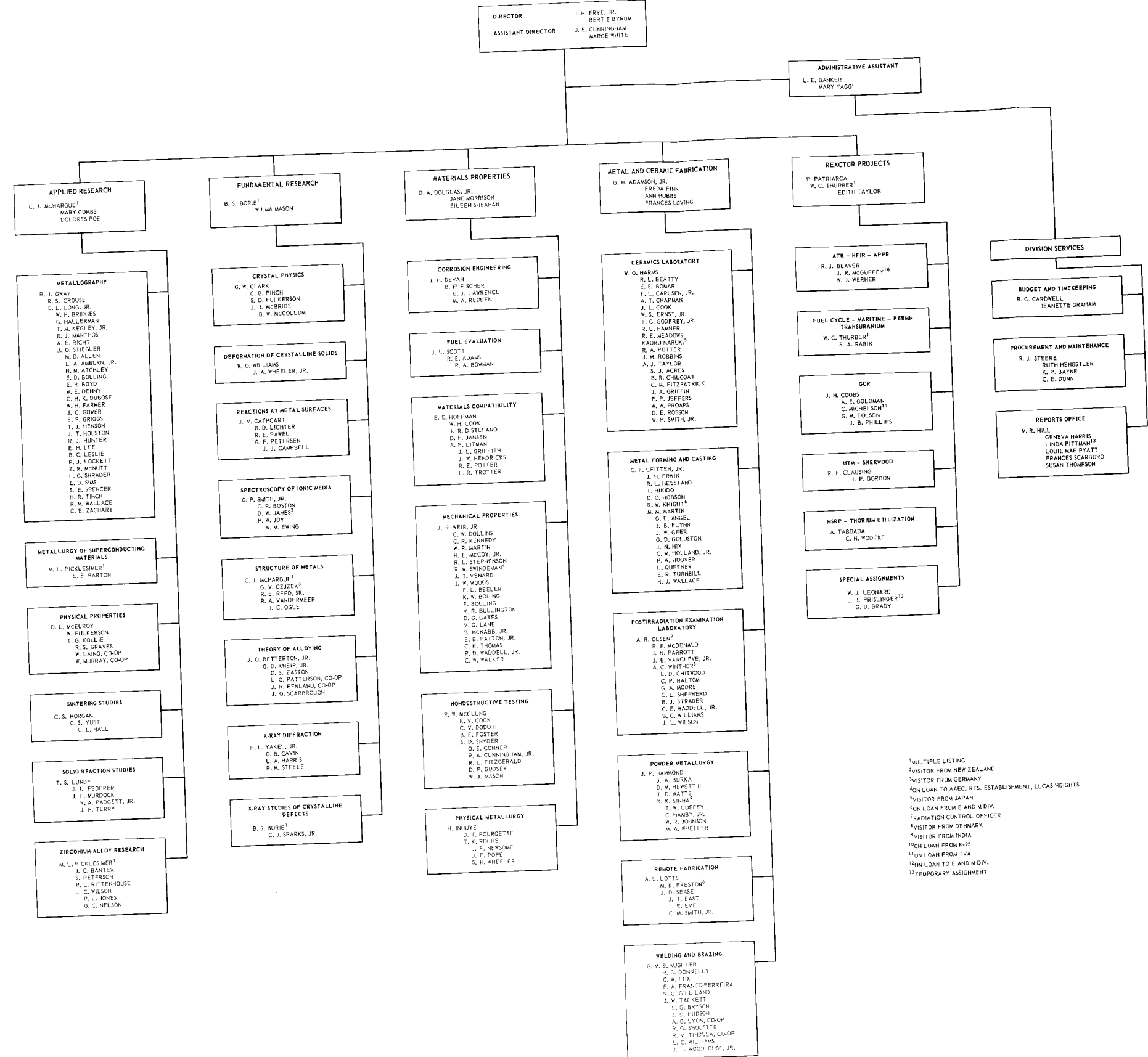
- Waugh, R. C., J. E. Cunningham, and R. J. Beaver, "Aluminum-Uranium Oxide Reaction," p 364 in *Uranium Dioxide: Properties and Nuclear Applications* (ed. by J. Belle), Naval Reactors, Division of Reactor Development, USAEC, Washington, 1961.
- Williams, R. O., "The Stored Energy in Deformed Copper: The Effect of Grain Size and Silver Content," *Acta Met.* **9**, 949-57 (1961).
- Williams, R. O., "Shear Textures in Copper, Brass, Aluminum, Iron, and Zirconium," *Trans. Met. Soc. AIME* **224**, 129-40 (1962).
- Wodtke, C. H., and J. W. Clark, "Torch Cuts Off 'Hot' Plates," *Iron Age* **188**(2), 90 (1961).



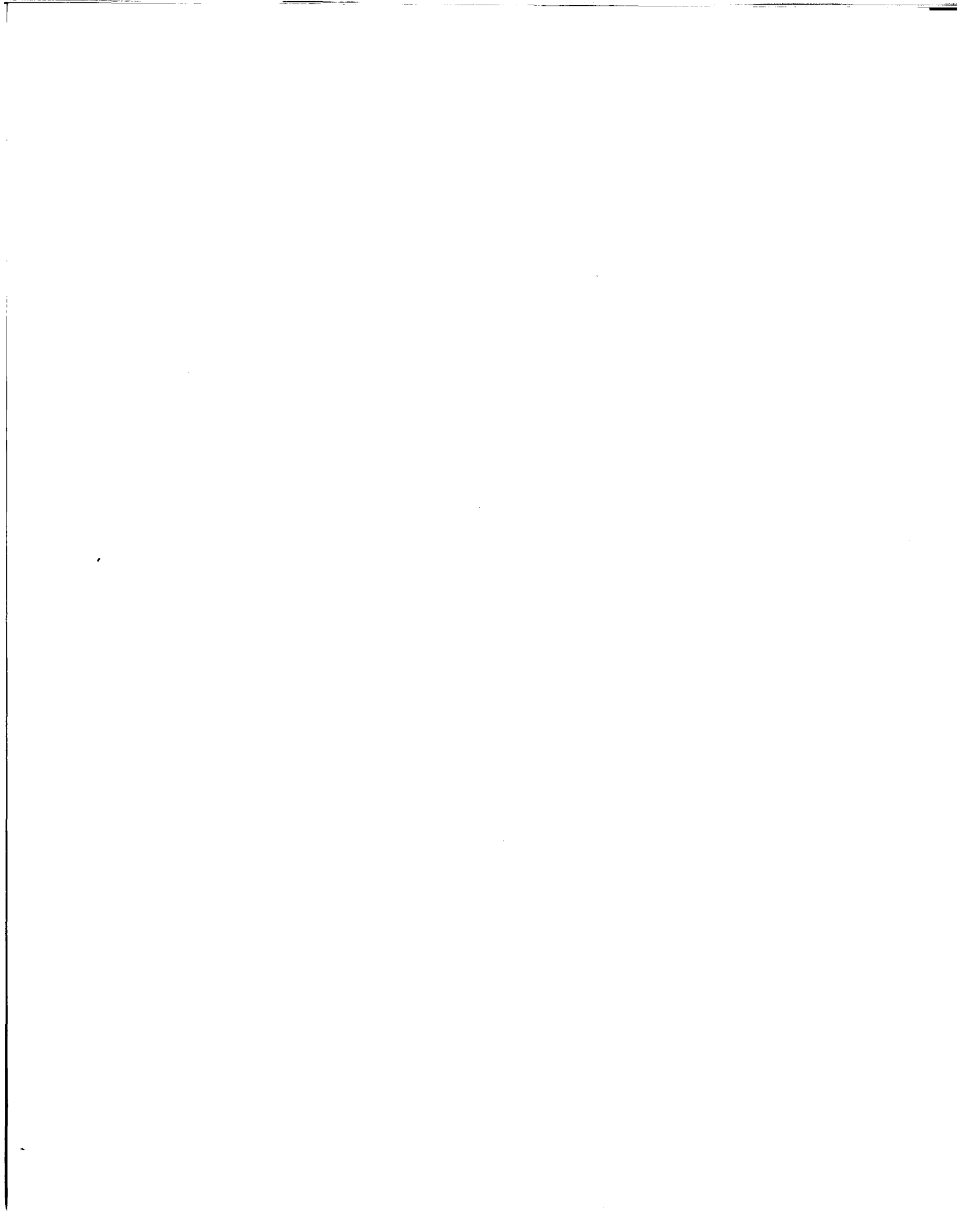
# METALS AND CERAMICS DIVISION

AT  
THE OAK RIDGE NATIONAL LABORATORY

MAY 31, 1962



<sup>1</sup>MULTIPLE LISTING  
<sup>2</sup>VISITOR FROM NEW ZEALAND  
<sup>3</sup>VISITOR FROM GERMANY  
<sup>4</sup>ON LOAN TO AEC, RES. ESTABLISHMENT, LUCAS HEIGHTS  
<sup>5</sup>VISITOR FROM JAPAN  
<sup>6</sup>ON LOAN FROM E AND M DIV.  
<sup>7</sup>RADIATION CONTROL OFFICER  
<sup>8</sup>VISITOR FROM DENMARK  
<sup>9</sup>VISITOR FROM INDIA  
<sup>10</sup>ON LOAN FROM K-25  
<sup>11</sup>ON LOAN FROM TVA  
<sup>12</sup>ON LOAN TO E AND M DIV.  
<sup>13</sup>TEMPORARY ASSIGNMENT



ORNL-3313  
UC-25 – Metals, Ceramics, and Materials  
TID-4500 (17th ed., Rev.)

INTERNAL DISTRIBUTION

- |                                                                 |                                   |
|-----------------------------------------------------------------|-----------------------------------|
| 1. Biology Library                                              | 74. J. A. Lane                    |
| 2-4. Central Research Library                                   | 75. C. E. Larson                  |
| 5. Reactor Division Library                                     | 76. C. F. Leitten, Jr.            |
| 6-7. ORNL-Y-12 Technical Library,<br>Document Reference Section | 77. R. S. Livingston              |
| 8-26. Laboratory Records Department                             | 78. A. L. Lotts                   |
| 27. Laboratory Records, ORNL R.C.                               | 79. T. S. Lundy                   |
| 28. Laboratory Shift Supervisor                                 | 80. H. G. MacPherson              |
| 29. G. M. Adamson, Jr.                                          | 81. W. D. Manly                   |
| 30. R. J. Beaver                                                | 82. R. W. McClung                 |
| 31. J. O. Betterton, Jr.                                        | 83. D. L. McElroy                 |
| 32. D. S. Billington                                            | 84. C. J. McHargue                |
| 33. A. L. Boch                                                  | 85. A. J. Miller                  |
| 34. E. G. Bohlmann                                              | 86. E. C. Miller                  |
| 35. B. S. Borie                                                 | 87. C. S. Morgan                  |
| 36. R. B. Briggs                                                | 88. K. Z. Morgan                  |
| 37. J. V. Cathcart                                              | 89. J. P. Murray (K-25)           |
| 38. G. W. Clark                                                 | 90. M. L. Nelson                  |
| 39. R. E. Clausing                                              | 91. A. R. Olsen                   |
| 40. J. H. Coobs                                                 | 92. P. Patriarca                  |
| 41. J. A. Cox                                                   | 93. M. L. Picklesimer             |
| 42. F. L. Culler                                                | 94. H. W. Savage                  |
| 43. J. E. Cunningham                                            | 95. A. W. Savolainen              |
| 44. J. H. DeVan                                                 | 96. L. D. Schaffer                |
| 45. D. A. Douglas, Jr.                                          | 97. J. L. Scott                   |
| 46. J. H. Erwin                                                 | 98. H. E. Seagren                 |
| 47. J. H. Frye, Jr.                                             | 99. M. J. Skinner                 |
| 48. J. H. Gillette                                              | 100. G. M. Slaughter              |
| 49. R. J. Gray                                                  | 101. C. O. Smith                  |
| 50. B. L. Greenstreet                                           | 102. G. P. Smith, Jr.             |
| 51. W. R. Grimes                                                | 103. J. A. Swartout               |
| 52. J. P. Hammond                                               | 104. A. Taboada                   |
| 53. W. O. Harms                                                 | 105. E. H. Taylor                 |
| 54. C. S. Harrill                                               | 106. W. C. Thurber                |
| 55-64. M. R. Hill                                               | 107. M. S. Wechsler               |
| 65. N. E. Hinkle                                                | 108. A. M. Weinberg               |
| 66. E. E. Hoffman                                               | 109. J. R. Weir, Jr.              |
| 67. A. Hollaender                                               | 110. R. O. Williams               |
| 68. A. S. Householder                                           | 111. J. C. Wilson                 |
| 69. A. Paul Huber (K-25)                                        | 112. H. L. Yakel                  |
| 70. H. Inouye                                                   | 113. A. A. Burr (consultant)      |
| 71. R. G. Jordan (Y-12)                                         | 114. J. R. Johnson (consultant)   |
| 72. M. T. Kelley                                                | 115. C. S. Smith (consultant)     |
| 73. R. B. Korsmeyer                                             | 116. R. Smoluchowski (consultant) |

*EXTERNAL DISTRIBUTION*

- 117. R. W. McNamee, Union Carbide Corporation, New York
- 118. D. E. Baker, General Electric Company, Hanford
- 119-120. David F. Cope, Oak Ridge Operations Office
- 121. Ersel Evans, General Electric Company, Hanford
- 122. J. L. Gregg, Cornell University
- 123. E. G. Haas, Department of the Navy, Washington, D.C.
- 124. J. Simmons, U.S. Atomic Energy Commission, Washington, D.C.
- 125. Lawrence M. Slifkin, University of North Carolina
- 126. E. E. Stansbury, University of Tennessee
- 127. Nathaniel Stetson, Savannah River Operations Office
- 128. D. K. Stevens, U.S. Atomic Energy Commission, Washington, D.C.
- 129. Dorothy Smith, Division of Research, U.S. Atomic Energy Commission, Washington, D.C.
- 130. Watt Webb, Union Carbide Metals
- 131. Division of Research and Development, AEC, ORO
- 132-705. Given distribution as shown in TID-4500 (17th ed., Rev.) under Metals, Ceramics, and Materials category (75 copies - OTS)

Reports previously issued in this series are as follows:

ORNL-28	Period Ending March 1, 1948
ORNL-69	Period Ending May 31, 1948
ORNL-407	Period Ending July 31, 1949
ORNL-511	Period Ending October 31, 1949
ORNL-583	Period Ending January 31, 1950
ORNL-754	Period Ending April 30, 1950
ORNL-827	Period Ending July 31, 1950
ORNL-910	Period Ending October 31, 1950
ORNL-987	Period Ending January 31, 1951
ORNL-1033	Period Ending April 30, 1951
ORNL-1108	Period Ending July 31, 1951
ORNL-1161	Period Ending October 31, 1951
ORNL-1267	Period Ending January 31, 1952
ORNL-1302	Period Ending April 30, 1952
ORNL-1366	Period Ending July 31, 1952
ORNL-1437	Period Ending October 31, 1952
ORNL-1503	Period Ending January 31, 1953
ORNL-1551	Period Ending April 10, 1953
ORNL-1625	Period Ending October 10, 1953
ORNL-1727	Period Ending April 10, 1954
ORNL-1875	Period Ending October 10, 1954
ORNL-1911	Period Ending April 10, 1955
ORNL-1988	Period Ending October 10, 1955
ORNL-2080	Period Ending April 10, 1956
ORNL-2217	Period Ending October 10, 1956
ORNL-2422	Period Ending October 10, 1957
ORNL-2632	Period Ending October 10, 1958
ORNL-2839	Period Ending September 1, 1959
ORNL-2988	Period Ending July 1, 1960
ORNL-3160	Period Ending May 31, 1961